DOE/ER/75388--T1

OSTI copy

DOE/ER/75388-F

Final Report
Grant No. DE-FG05-88ER75388
03

HEU TO LEU FUEL CONVERSION

Submitted to:

Ms. Barbara J. Jackson
Environmental Acquisitions Branch, AD-423
U. S. Department of Energy
P.O. Box 2001
Oak Ridge, TN 37831-8758

Submitted by:

Robert U. Mulder
Associate Professor
Director of Reactor Facility

Report No. UVA/527367/MANE95/101
October 1994

DEPARTMENT OF MECHANICAL, AEROSPACE AND NUCLEAR ENGINEERING

SCHOOL OF
ENGINEERING
& APPLIED SCIENCE

University of Virginia
Thornton Hall
Charlottesville, VA 22903

MASTER

DISTRIBUTION OF THIS DOCUMENT IS UNLIMITED

Original

T1

UNIVERSITY OF VIRGINIA
School of Engineering and Applied Science

The University of Virginia's School of Engineering and Applied Science has an undergraduate enrollment of approximately 1,500 students with a graduate enrollment of approximately 600. There are 160 faculty members, a majority of whom conduct research in addition to teaching.

Research is a vital part of the educational program and interests parallel academic specialties. These range from the classical engineering disciplines of Chemical, Civil, Electrical, and Mechanical and Aerospace to newer, more specialized fields of Applied Mechanics, Biomedical Engineering, Systems Engineering, Materials Science, Nuclear Engineering and Engineering Physics, Applied Mathematics and Computer Science. Within these disciplines there are well equipped laboratories for conducting highly specialized research. All departments offer the doctorate; Biomedical and Materials Science grant only graduate degrees. In addition, courses in the humanities are offered within the School.

The University of Virginia (which includes approximately 2,000 faculty and a total of full-time student enrollment of about 17,000), also offers professional degrees under the schools of Architecture, Law, Medicine, Nursing, Commerce, Business Administration, and Education. In addition, the College of Arts and Sciences houses departments of Mathematics, Physics, Chemistry and others relevant to the engineering research program. The School of Engineering and Applied Science is an integral part of this University community which provides opportunities for interdisciplinary work in pursuit of the basic goals of education, research, and public service.

12:49 p
DEC 21

DISCLAIMER

This report was prepared as an account of work sponsored by an agency of the United States Government. Neither the United States Government nor any agency thereof, nor any of their employees, makes any warranty, express or implied, or assumes any legal liability or responsibility for the accuracy, completeness, or usefulness of any information, apparatus, product, or process disclosed, or represents that its use would not infringe privately owned rights. Reference herein to any specific commercial product, process, or service by trade name, trademark, manufacturer, or otherwise does not necessarily constitute or imply its endorsement, recommendation, or favoring by the United States Government or any agency thereof. The views and opinions of authors expressed herein do not necessarily state or reflect those of the United States Government or any agency thereof.

DISCLAIMER

Portions of this document may be illegible in electronic image products. Images are produced from the best available original document.

Table of Contents

		Page
I.	Introduction	1
II.	Order to Convert	1
III.	Receipt of LEU Fuel	2
IV.	Initial Loading of LEU Fuel	2
	a) Initial Criticality (LEU-1 Core)	2
	b) Flow Coastdown Measurements	8
	c) Void Coefficient Measurements	8
V.	Loading of Operational Core	13
	a) Initial Criticality (LEU-2 Core)	13
	b) Experimental Facilities	19
	c) Approach to Full Power	19
	d) Power Coefficient Measurement	19
	e) Moderator Temperature Coefficient Measurement	20
VI.	Comparison between LEU and HEU Cores	21
VII.	Shipment of All HEU Fuel Elements From Facility	22
VIII.	Pool Water Analysis	23
IX.	Summary	23
	Attachment 1: LEU Fuel Conversion Test Program	25

List of Figures

Figure		Page
1.	LEU-1, Approach to Critical	4
2.	LEU-1 Core Loading Diagram	5
3.	Integral Rod Worth, LEU-1 Shim Rods #1, #2, and #3	6
4.	Integral Rod Worth, LEU-1 Regulating Rod	7
5.	LEU-1 Flow Coastdown	9
6.	Void Swords	10
7.	LEU-2 Approach to Critical	14
8.	LEU-2 Approach to Critical (Expanded Scale)	15
9.	LEU-2 Core Loading Diagram	16
10.	Integral Rod Worth, LEU-2 Shim Rods #1, #2, and #3	17
11.	Integral Rod Worth, LEU-2 Regulating Rod	18

APPENDICIES

Appendix I - Thesis - Design Optimization of a Low Enrichment University of Virginia Nuclear Reactor. (Mary Katherine Fehr)

Appendix II - Thesis - Neutronic Analysis For The UVAR Reactor HEU to LEU Conversion Project. (David W. Freeman)

Appendix III - Thesis - Effective Diffusion Theory Cross Sections for UVAR Control Rods. (Stuart Wasserman)

Appendix IV - Safety Analysis Report For The Low-Enriched Uranium Fueled University of Virginia Reactor.

Appendix V - Procedures for Loading UVAR fuel Assemblies into the BMI-1 Shipping Cask for Transfer to Savannah River.

List of Commonly Used Acronyms

CAVALIER - Cooperatively Assembled Virginia Low Intensity Educational Reactor

CIF - Cannister Irradiation Facility

EPI RAB - Epi-Thermal Rabbit Facility

HEU - High Enriched Uranium

H.T. - Hot Thimble Facility

HYD RAB - Hydraulic Rabbit Facility

LEU - Low Enriched Uranium

LSSS - Limiting Safety System Setting

MIF - Mineral Irradiation Facility

Reg - Stainless Steel Regulating Rod

SAR - Safety Analysis Report

SHIM - Boron-Stainless Steel Control Rod

THER RAB - Thermal Rabbit Facility

UVAR - University of Virginia Reactor

HEU TO LEU FUEL CONVERSION REPORT

I. Introduction

The Nuclear Regulatory Commission issued a ruling, effective March 27, 1986, that all U.S. non-power reactors convert from HEU fuel to LEU fuel. A Reduced Enrichment for Research and Test Reactors (RERTR) Program was conducted by the Department of Energy at Argonne National Laboratory to coordinate the development of the high density LEU fuel and assist in the development of Safety Analysis Reports for the smaller non-power reactors. Several meetings were held at Argonne in 1987 with the non-power reactor community to discuss the conversion and to set up a conversion schedule for university reactors. EG&G at Idaho was asssigned the coordination of the fuel element redesigns. The fuel elements were manufactured by the Babcock & Wilcox Company in Lynchburg, Virginia.

The University of Virginia was awarded a grant (DE-FG05-88ER75388) by the DOE Idaho Operations Office in 1988 to perform safety analysis studies for the LEU conversion for its 2 MW UVAR and 100 Watt CAVALIER reactors. The University subsequently decided to shut down the CAVALIER reactor. A preliminary SAR on the UVAR, along with Technical Specification changes, was submitted to the NRC in November, 1990. An updated SAR was approved by the NRC in January, 1991.

In September, 1992, representatives from the fuel manufacturer (B&W) and the fuel designer (EG&G, Idaho) came to the UVAR facility to observe trial fittings of new 22 plate LEU mock fuel elements. B&W fabricated two non-fuel bearing elements, a regular 22 plate element and a control rod element. The elements were dimensionally checked against the drawings and test fitted in the UVAR grid plate. The dimensions were acceptable and the elements fit in the grid plate with no problems. The staff made several suggestions for minor construction changes to the end pieces on the elements, which were incorporated into the final design of the actual fuel elements. The "dummy" elements were kept by the facility and are on display for visiting tour groups. The manufacture of the UVAR LEU core was completed in late 1993.

II. Order to Convert

An "Order to Convert", along with Technical Specification changes pertinent to the fuel conversion was issued by the NRC on April 29, 1993. An attachment to the NRC order specified that a maximum limit of 5 kg of U-235 in the form of HEU fuel could be stored at the facility after receipt of LEU fuel until the HEU

fuel was shipped off site. Prior to the time of the conversion order the facility had 6.17 kg of U-235 in the form of HEU fuel so a fuel shipment of 12 fuel elements with a U-235 content of 1.72 kg was made on July 28, 1993 to Savannah River, to reduce the HEU inventory to below the 5 kg limit.
The UVAR reactor operated with HEU fuel until December, 1993 to finish ongoing experiments. The last operation with HEU fuel was on December 22, 1993 and the reactor was then unloaded.

III. Receipt of LEU Fuel

An attachment to the "Order to Convert" modifying License R-66 allows up to 11 kg of U-235 to be possessed by the licensee in the form of LEU fuel.
Procedures for the receipt of LEU fuel were developed by the reactor staff and approved by the U.Va. Reactor Safety Committee. On January 11, 1994, the facility received 8.1 kg of LEU fuel from the Babcock & Wilcox Company in the form of 5 control elements, 26 regular elements, and 2 partial elements. The LEU Technical Specifications were put into effect upon receipt of the fuel.

IV. Initial Loading of LEU Fuel

A detailed LEU Test Program developed by the reactor staff was reviewed by the Reactor Safety Committee at four different meetings and approved. The final version of the Test Program was issued on February 15, 1994 (see Appendix 1). The first planned core loading was a 4 x 4 fuel array surrounded by graphite to compare it with a similar HEU configuration operated in 1975.

a) Initial Criticality (LEU-1 Core)

Initial loading of the LEU fuel began on April 19, 1994. Graphite elements were placed in the grid plate surrounding the proposed location of the fuel. A Sb-Be startup source was placed in grid position 14 opposite the installed Source Range fission chamber, located at the top of the graphite element in grid plate position 85. An auxillary fission chamber was placed in grid position 36, with a Pu-Be source opposite the core on top of the graphite element in grid position 42.

The control rods and associated fuel elements were first loaded in the reactor in grid positions 25, 34, 45, and 54. The rod drive mechanisms were attached and checked out for proper operation. Rod drop measurements were made with the following results:

Rod	Response Time (msec)	Drop Time (msec)	Total (msec)
1	14.1	488.9	503
2	34.3	466.7	501
3	34.3	474.7	509

The Regulating Rod is not scrammable.
These measurements were well within the Technical Specification limits of 50 msec (response time) and 700 msec (drop time).

The fuel elements were loaded in the reactor with the control rods positioned at 10 inches. Count rate data was obtained with the rods first at 10 inches and then 26 inches and a reciprocal multiplication curve was plotted. After the addition of the first two elements, in positions 44 and 35, the auxillary fission chamber was discovered not functioning properly. This problem was corrected and the core loading was accomplished with no further problems. When the count rate data indicated that criticality might be achieved with the addition of one more element a partial element was loaded first to check rod positions. Figure 1 shows a plot of the reciprocal multiplication data taken with the auxillary fission chamber.
The reactor first achieved criticality with the four control rod elements and 10 regular elements in the core at 3:38 P.M. on April 20, 1994 with the Regulating Rod and Shim Rods 1 and 2 fully withdrawn and Shim Rod 3 at 22.5 inches. The final configuration (LEU-1) is shown in Figure 2. A 4x4 loading was established with partial fuel elements in grid positions 23 and 26.

The critical rod positions for the LEU-1 configuration were:

Shim Rod 1 @ 12.66 inches Shim Rod 3 @ 12.71 inches
Shim Rod 2 @ 12.68 inches Reg. Rod @ 12.54 inches

The rods were then calibrated and yielded the following worths:

Shim Rod 1 = 3.46 %Δk/k Shim Rod 3 = 2.41 %Δk/k
Shim Rod 2 = 3.86 %Δk/k Reg. Rod = 0.375 %Δk/k

Integral rod worth curves for LEU-1 are shown in Figures 3 and 4.

The shutdown margin with the highest worth Rod 2 and the non-scrammable Reg Rod fully withdrawn was experimentally determined to be - 1.21 % Δk/k, which is well above the Technical Specification minimum of - 0.4 % Δk/k.
The excess reactivity was experimentally determined to be + 4.66 % Δk/k, which is below the Technical Specification limit of + 5.0 % Δk/k.

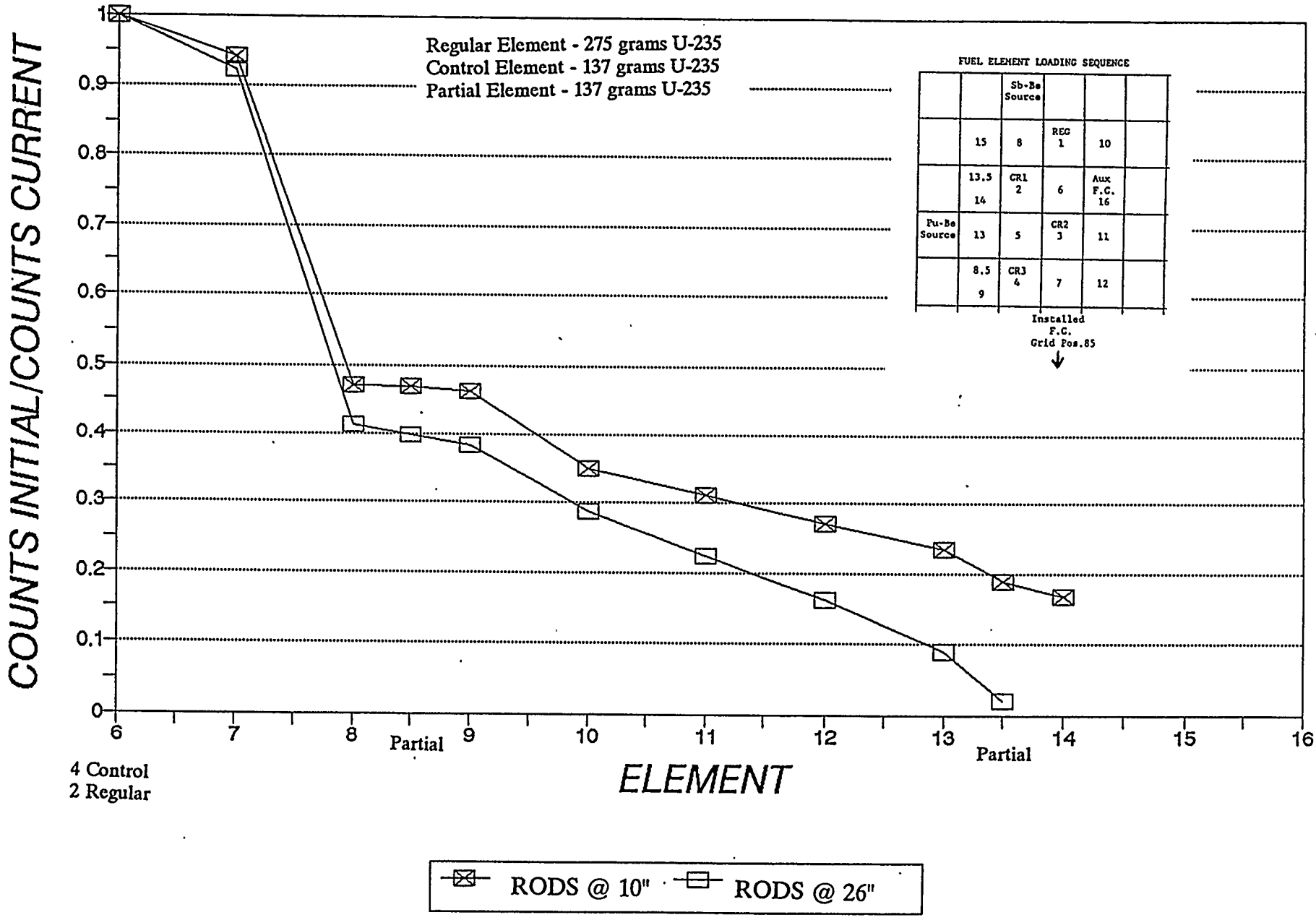


Figure 1. LEU-1, Approach to Critical

CORE LOADING LEU-1 SHUTDOWN MARGIN - 1.21 % delta k/k

Date April 21, 1994 EXCESS REACTIVITY + 4.66 % delta k/k

U-235 3571 GRAMS EXPERIMENT WORTH None % delta k/k

F - Normal Fuel Element
PF - Partial Fuel Element
CR - Control Rod Fuel Element
G - Graphite Element
S - Graphite Source Element
REG - Control Rod Fuel Element with Regulating Rod
P - Grid Plate Plug
HYD RAB - Hydraulic Rabbit
THER RAB - Thermal Pneumatic Rabbit
EPI RAB - Epithermal Pneumatic Rabbit
RB - Radiation Basket

Rod Worths #1 - 3.46 % #2 - 3.86 % #3 - 2.41 % Reg - 0.375 %

G 11	G 12	G 13	S 14	G 15	G 16	G 17	G 18
G 21	G 22	PF VP-002 23	F VS-002 24	F- REG VC-001 25	PF VP-001 26	G 27	G 28
G 31	G 32	F VS-004 33	F-CR1 VC-002 34	F VS-005 35	F VS-003 36	G 37	G 38
G 41	G 42	F VS-007 43	F VS-008 44	F-CR2 VC-003 45	F VS-009 46	G 47	G 48
G 51	G 52	F VS-010 53	F-CR3 VC-004 54	F VS-011 55	F VS-012 56	G 57	G 58
G 61	G 62	G 63	G 64	G 65	G 66	G 67	G 68
G 71	G 72	G 73	G 74	G 75	G 76	G 77	G 78
G 81	G 82	G 83	G 84	G 85	G 86	G 87	G 88

Figure 2. LEU-1 Core Loading Diagram

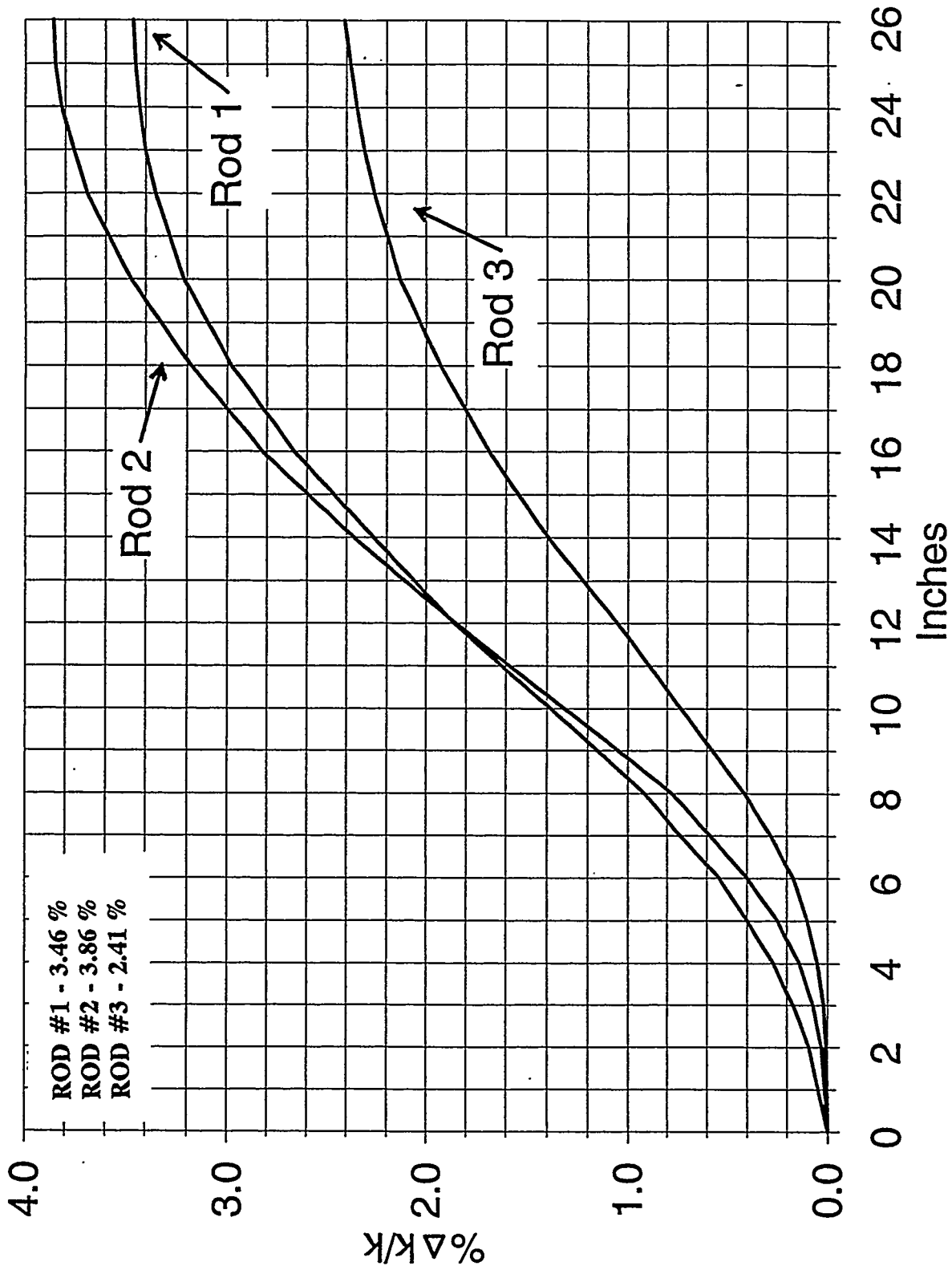


Figure 3. Integral Rod Worth, LEU-1 Shim Rods #1, #2, and #3

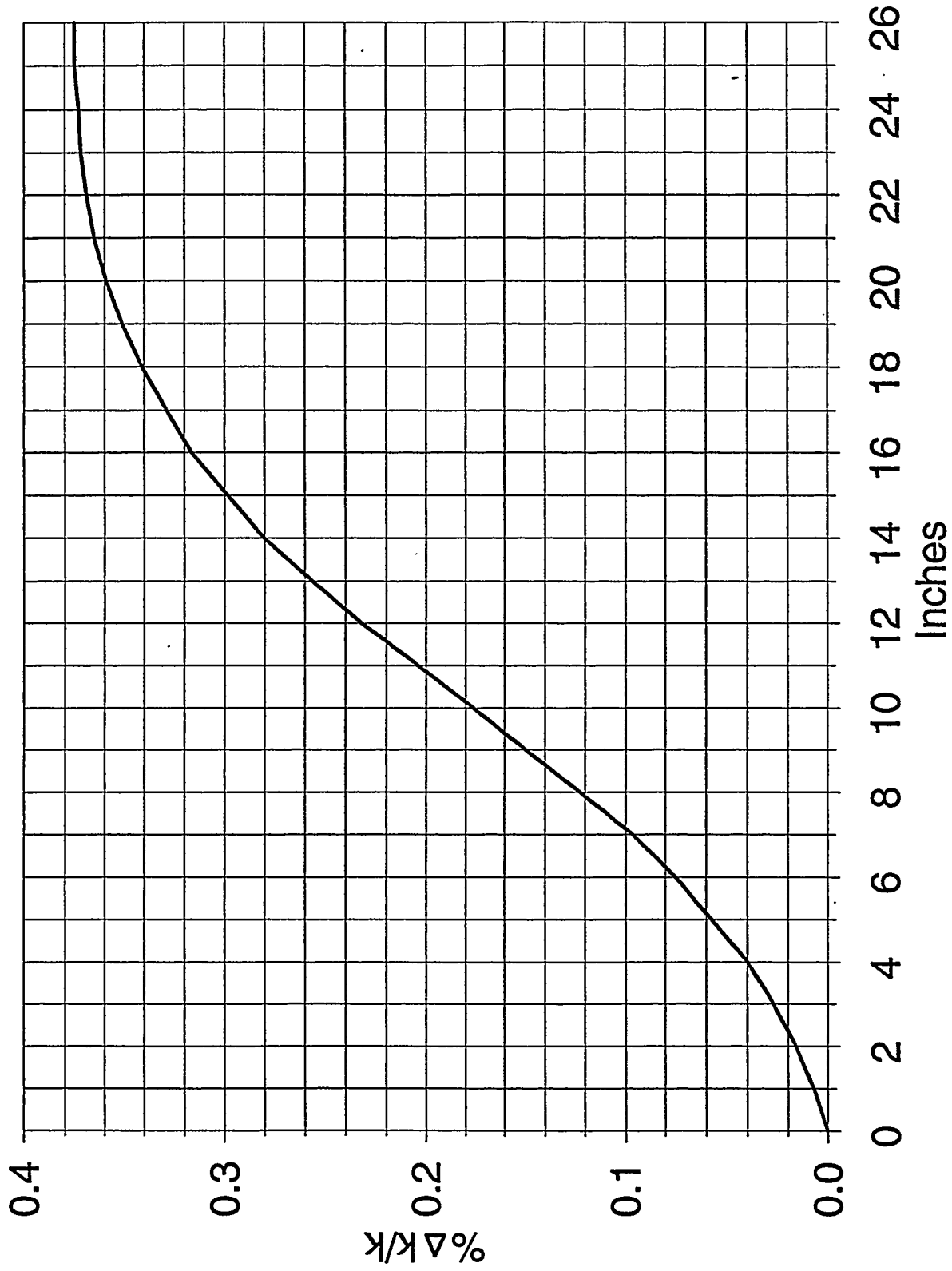


Figure 4. Integral Rod Worth, LEU-1 Regulating Rod

During the final adjustments to the core loading, determinations were made of the reactivity worth of a normal fuel element and a partial fuel element. The results were:

Partial fuel element in grid position 23 = + 1.43 %Δk/k, and
Normal fuel element in grid position 23 = + 2.03 %Δk/k

b) Flow Coastdown Measurements

Primary flow coastdown measurements were made on April 26, 1994 with the reactor core LEU-1 loaded and the reactor shut down. Figure 5 shows a graph of the measurement and comparison with SAR calculations. The slope of the measured coastdown very closely matches that predicted by the SAR. SAR calculations were performed with the header stuck up.

c) Void Coefficient Measurements

A set of two identical swords (see Figure 6) were constructed of acrylic that had voids built into them that extended uniformly over the length of the active fuel region of the core when inserted into a coolant channel of a fuel element. After measuring the volume of the void in the swords at the pressure associated with the depth of water at the core, one sword had vents cut into it to allow it to flood with water when immersed. These swords were placed in turn into three coolant channels in the LEU-1 core and the critical rod positions were noted for the six conditions (flooded sword in channel x, voided sword in channel x,...). The swords were located in the eighth fuel channel from the east side of the core in the following fuel elements: Element VS-007 in grid position 43, Element VS-008 in grid position 44, and Element VS-010 in grid position 53. To assure accuracy in the rod position measurements, the three shim rods were always placed in the same position after traveling in the same direction in all of the startups in the series performed for this experiment. The regulating rod was always moved in the inward direction for the final criticality adjustment. By paying particular care to the final direction of the rod motion, backlash in the gear train should not affect the rod position indication for a particular rod position. All rod positions were repeatable to within +/- 0.01 inches. The change in regulating rod position between when the flooded sword and the voided sword were in a given channel represents the worth of the void in that channel. To reduce the change in regulating rod position to reactivity, a divided difference interpolation of the regulating rod calibration data was performed.

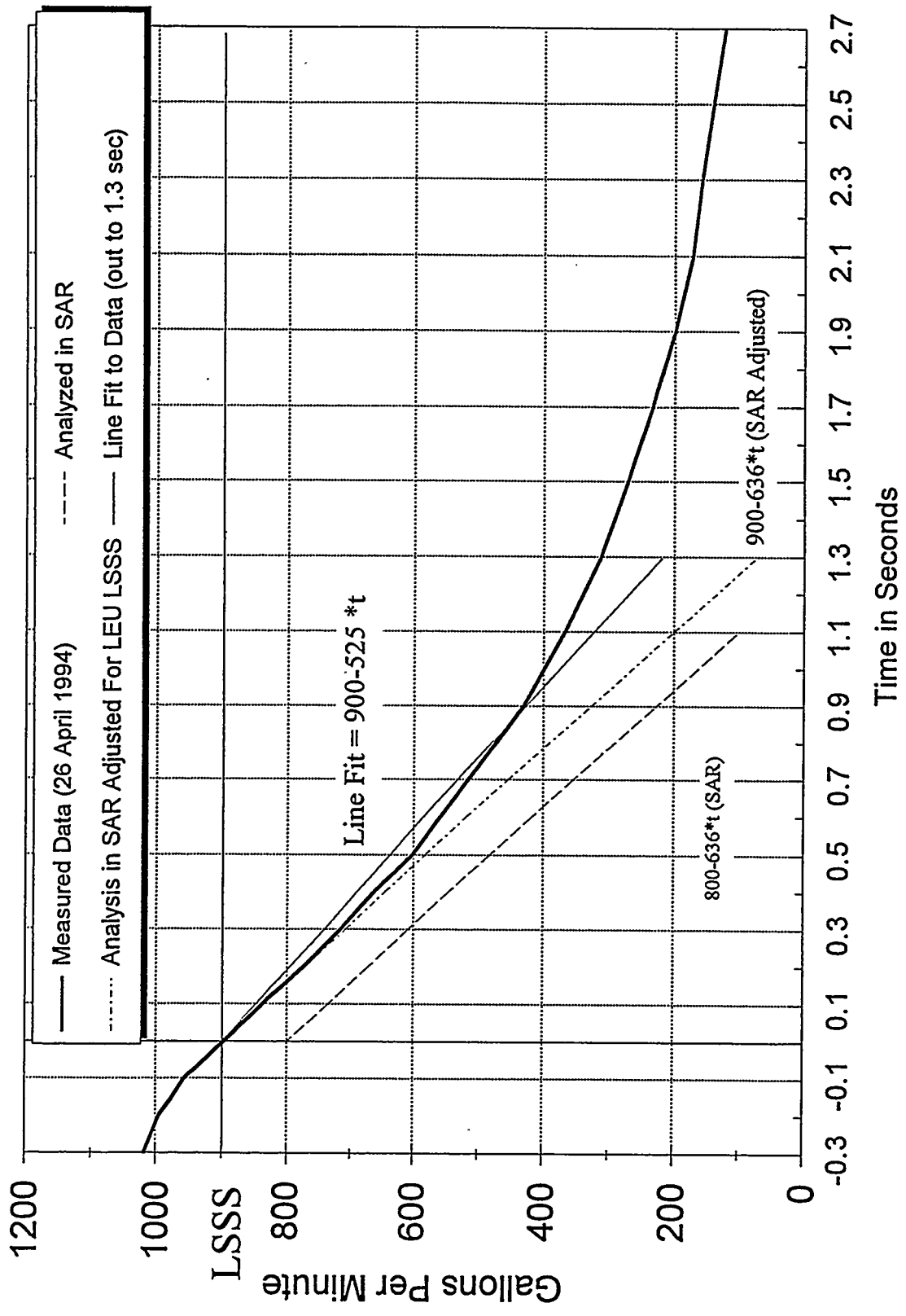


Figure 5. LEU-1 FLOW COASTDOWN, HEADER UP

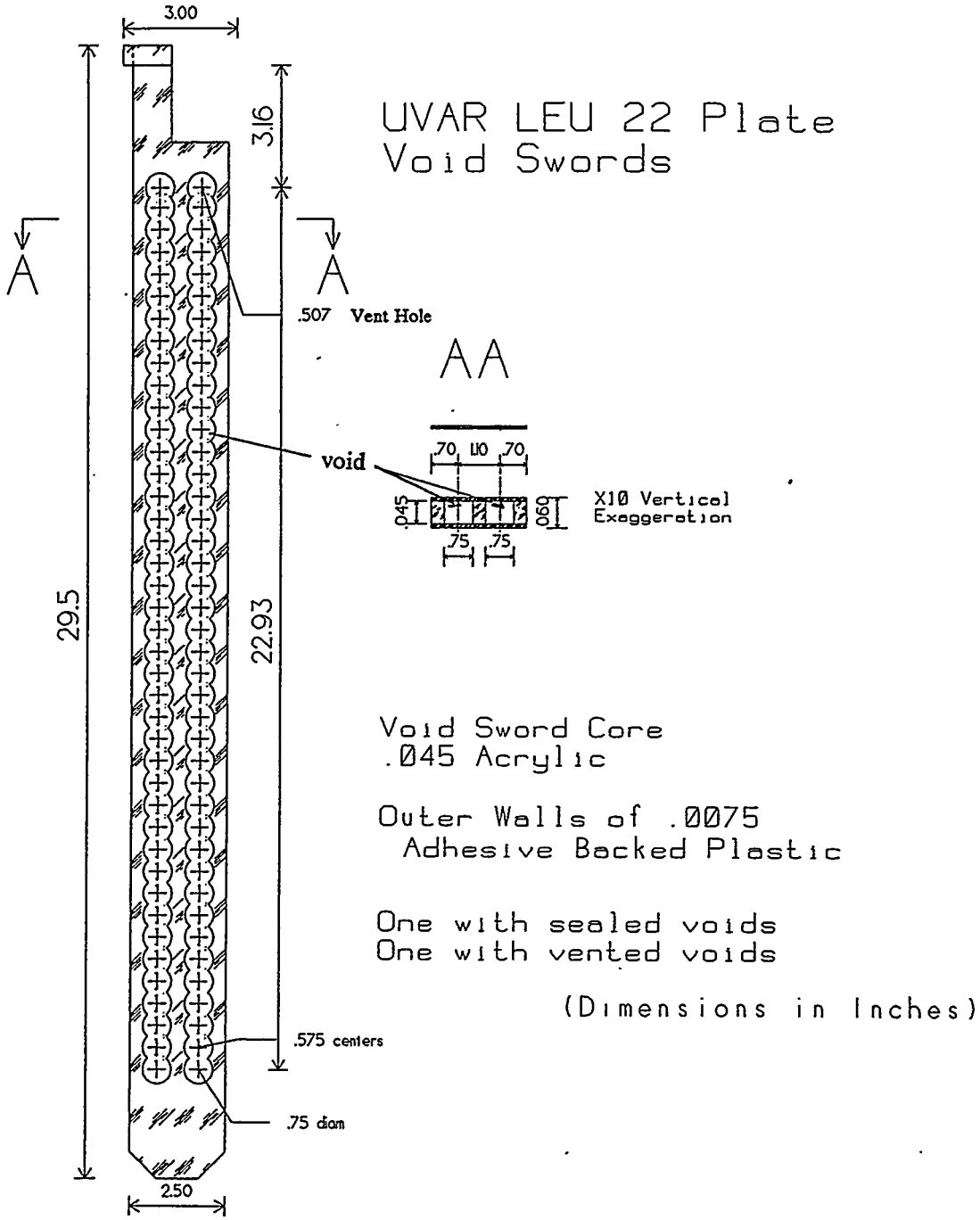


Figure 6. VOID SWORDS

A discussion on the vertical extent of the active core is in order. With the rods at about 12.5 inches from the bottom, the core should not be considered to be a full 24 inches tall. This could be important when considering the volume of the core and the volume of the void in the sword. By designing the swords so that the void was distributed uniformly over the vertical length of the fuel, any arbitrarily chosen height of the core affects the volume of the void to the same extent as the volume of the core.

The calculation of the relative size of the void in the sword to the volume of the core is reduced to a two dimensional problem in the xy plane. To express the size of the void as a percent of voidable volume of the core, the water areas in the xy plane were calculated by defining the total area of the core from the pitch of the grid of holes in the grid plate (4x4 elements) and subtracting out the area occupied by metal. Included in the metal were the side plates, fuel plates, and rod guide plates. Some of the water area thus defined is in the rod channels. The staff does not think the rod channels are voidable. They are defined by solid 0.125 inch aluminum guide plates that are separated from the fuel by coolant channels and are thus not directly heated. There would be no voiding in the rod channels during a nucleate boiling condition and the adjacent cooling channel would have to be essentially empty before the water in the rod channel would start to boil. Therefore, the staff carried through a calculation for the area of the water in the core excluding the rod channels as well as one including the rod channels. Similar calculations for the water area in the xy plane of an individual element were performed, again defining the total area from the pitch of the grid plate. The void in the experiment was then expressed as the ratio of the applicable water area to the effective area of the void in the void sword. The effective area of the void is the measured void volume (at pressure) divided by the length of the void in the sword. This gives the percent of the voidable volume in the core (both with and without the rod channels) or an individual element represented by the actual void in the sword.

By dividing the reactivity measured for the void in the sword at a particular location in the core by the percent voidable area (or volume by considering an arbitrary dimension in z) represented by the sword we get the results in units of % $\Delta k/k$ per % void for the various voidable volumes considered above. The experiment was performed in three distinct locations in the core chosen so that by applying four fold symmetry, a representative value for all of the non-rodded elements in the core was obtained. The regulating rod, being different from the shim rod in composition, prevents full symmetry from being achieved.

The data reported here should not be construed to be valid for uniform voiding of the core or for voiding in the heat generation pattern resulting from boiling (nucleate or bulk boiling) that would occur in an overpower transient. Rather, the results are from an experiment that could be feasibly performed within the

operating restrictions of the UVAR reactor.

The following measurements were made:

	Reg Rod (inches)	Reactivity Worth (% Δk/k))	Worth of Void (% Δk/k)
Flood in VS-008	11.78	0.228	
Void in VS-008	12.31	0.242	-0.014
Flood in VS-007	11.88	0.231	
Void in VS-007	12.23	0.240	-0.009
Flood in VS-010	11.65	0.225	
Void in VS-010	12.15	0.238	-0.013
Clean	11.11	0.210	

The results of the void coefficient measurement are as follows:

	VS-008	VS-007	VS-010
(% Δk/k/%Void Core) With Rod Channels	-.192	-.126	-.178
(% Δk/k/%Void Core) Without Rod Channels	-.163	-.111	-.155
(% Δk/k/%Void Element)	-.009	-.006	-.008

The LEU-1 reference reactor core was then unloaded.

V. Loading of Operational Core

a) Initial Criticality (LEU-2 Core)

The control rods were repositioned in the grid plate on April 29, 1994 to establish a configuration for routine operation to accommodate planned experiments. Rod drop measurements were repeated with the following results.

Rod	Response Time (msec)	Drop Time (msec)	Total (msec)
1	13.1	486.9	500
2	28.3	469.7	498
3	20.2	469.7	489.9

The Regulating Rod is not scrammable.
These measurement results were also well below the Technical Specification maximum limits for rod response and drop times (see page 3).

Fuel was added to the core, one element at a time, with the rods held at 10 inches. Reciprocal multiplication data was taken with the rods at 10 inches and 26 inches. Figure 7 shows a plot of the reciprocal multiplication curve and Figure 8 provides an expanded scale for the reciprocal multiplication data corresponding to the last few elements.

Criticality was achieved on May 6, 1994 and the final configuration (LEU-2) was established on May 10, 1994. A diagram of the loading is shown in Figure 9. This loading is a 4 x 5 array of fuel with a partial element in grid position 24. Hot Thimble experiments were loaded in grid positions 53 and 55 and the critical rod positions for this configuration were:

Shim Rod 1 @ 25.65 inches
Shim Rod 2 @ 12.52 inches
Shim Rod 3 @ 0.00 inches
Reg Rod @ 17.60 inches

The rods were then calibrated, yielding the following worths:

Rod 1 = 2.80 %Δk/k
Rod 2 = 2.63 %Δk/k
Rod 3 = 1.84 %Δk/k
Reg Rod = 0.401 %Δk/k

Integral rod worth curves for LEU-2 are shown in Figures 10 and 11.
The shutdown margin with Rod 1 and the Regulating Rod fully withdrawn was experimentally determined to be - 1.2 %Δk/k, well above the minimum of - 0.4 % Δk/k required by the Technical Specifications.

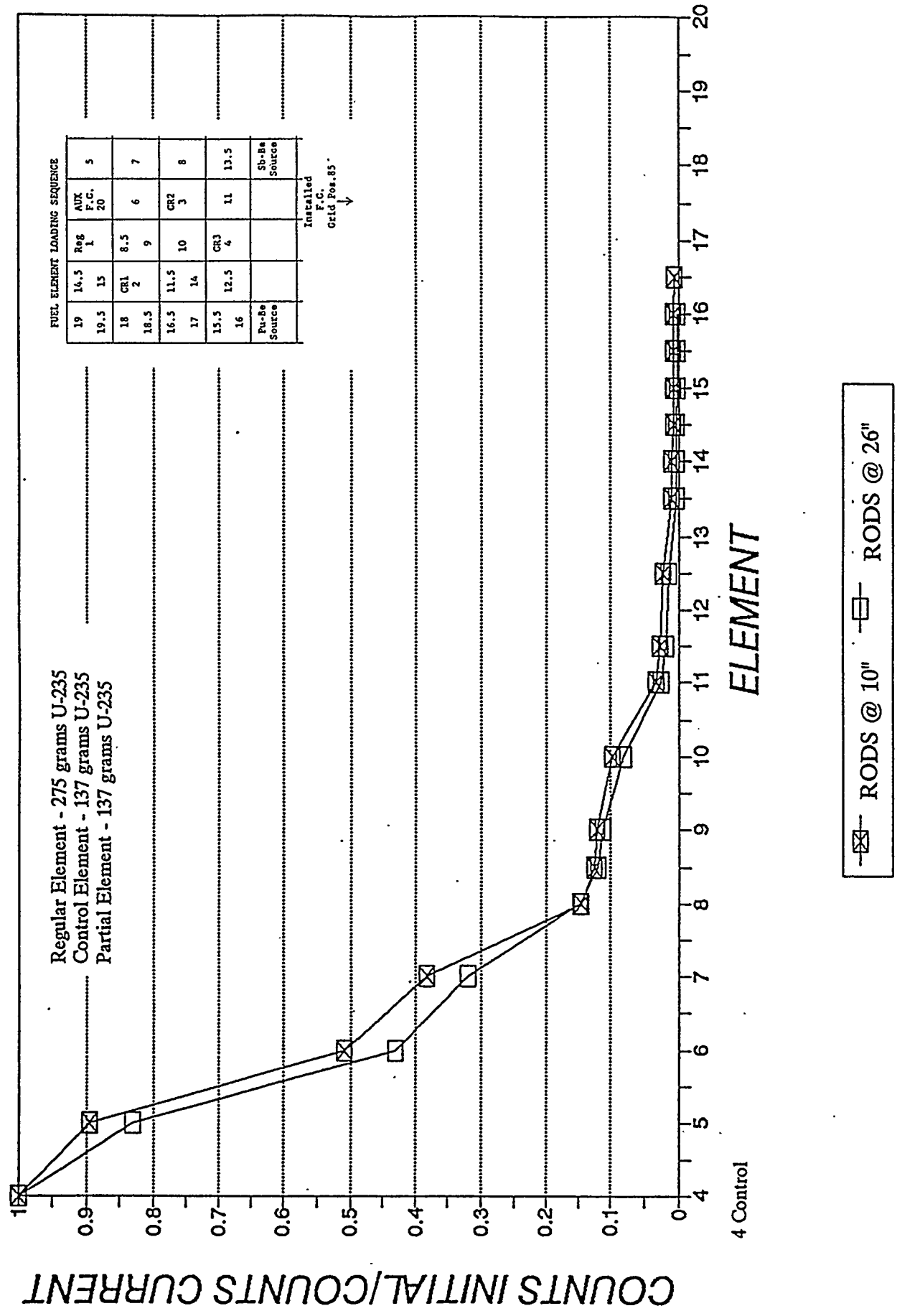


Figure 7. LEU-2 Approach to Critical

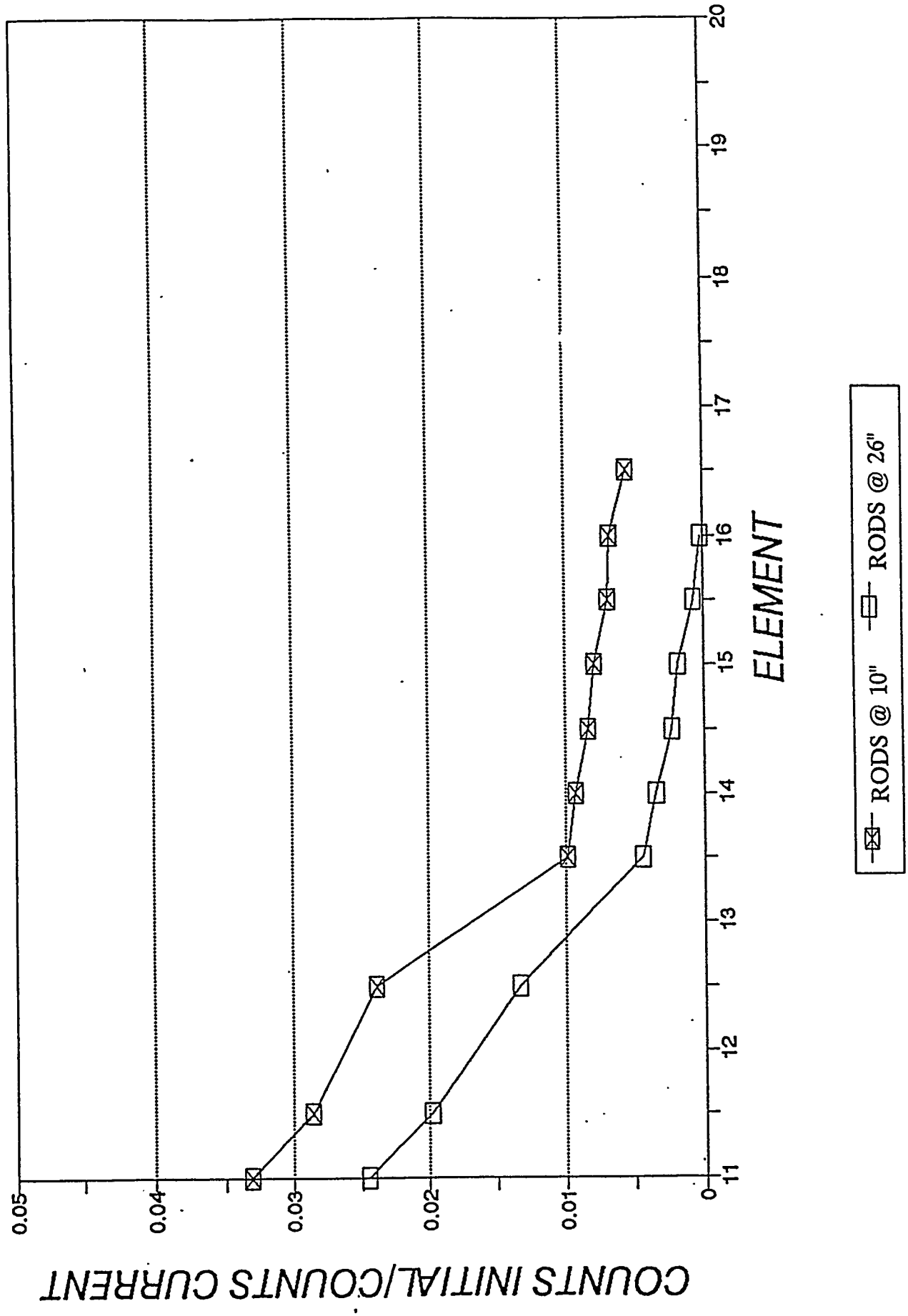


Figure 8. LEU-2 Approach to Critical (Expanded Scale)

CORE LOADING LEU-2 SHUTDOWN MARGIN - 1.2 % delta k/k

Date June 13, 1994 EXCESS REACTIVITY + 3.27 % delta k/k

U-235 4807 GRAMS EXPERIMENT WORTH 1.63 % delta k/k

F - Normal Fuel Element
PF - Partial Fuel Element
CR - Control Rod Fuel Element
G - Graphite Element
S - Graphite Source Element
REG - Control Rod Fuel Element with Regulating Rod
P - Grid Plate Plug
HYD RAB - Hydraulic Rabbit
THER RAB - Thermal Pneumatic Rabbit
EPI RAB - Epithermal Pneumatic Rabbit
RB - Radiation Basket

Rod Worths #1 - 2.80 % #2 - 2.63 % #3 - 1.84 % Reg - 0.401 %

MINERAL IRRADIATION FACILITY

P 11	F VS-015 12	F VS-009 13	F-REG VC-001 14	F VS-013 15	F VS-004 16	17	P 18
P 21	F VS-006 22	F-CR1 VC-002 23	PF VP-001 24	F VS-007 25	F VS-008 26	27	P 28
G 31	F VS-001 32	F VS-010 33	F. VS-011 34	F-CR2 VC-003 35	F VS-012 36	37	P 38
G 41	F VS-014 42	F VS-003 43	F-CR3 VC-004 44	F VS-002 45	F VS-005 46	47	P 48
G 51	G 52	HT-1 53	G 54	HT-3 55	S 56	57	P 58
G 61	G 62	G 63	EPI RAB 64	G 65	G 66	G 67	G 68
G 71	G 72	THER RAB 73	G 74	G 75	HYD RAB 76	G 77	G 78
G 81	G 82	G 83	G 84	G 85	G 86	G 87	G 88

CANISTER IRR. FAC.

Figure 9. LEU-2 Core Loading Diagram

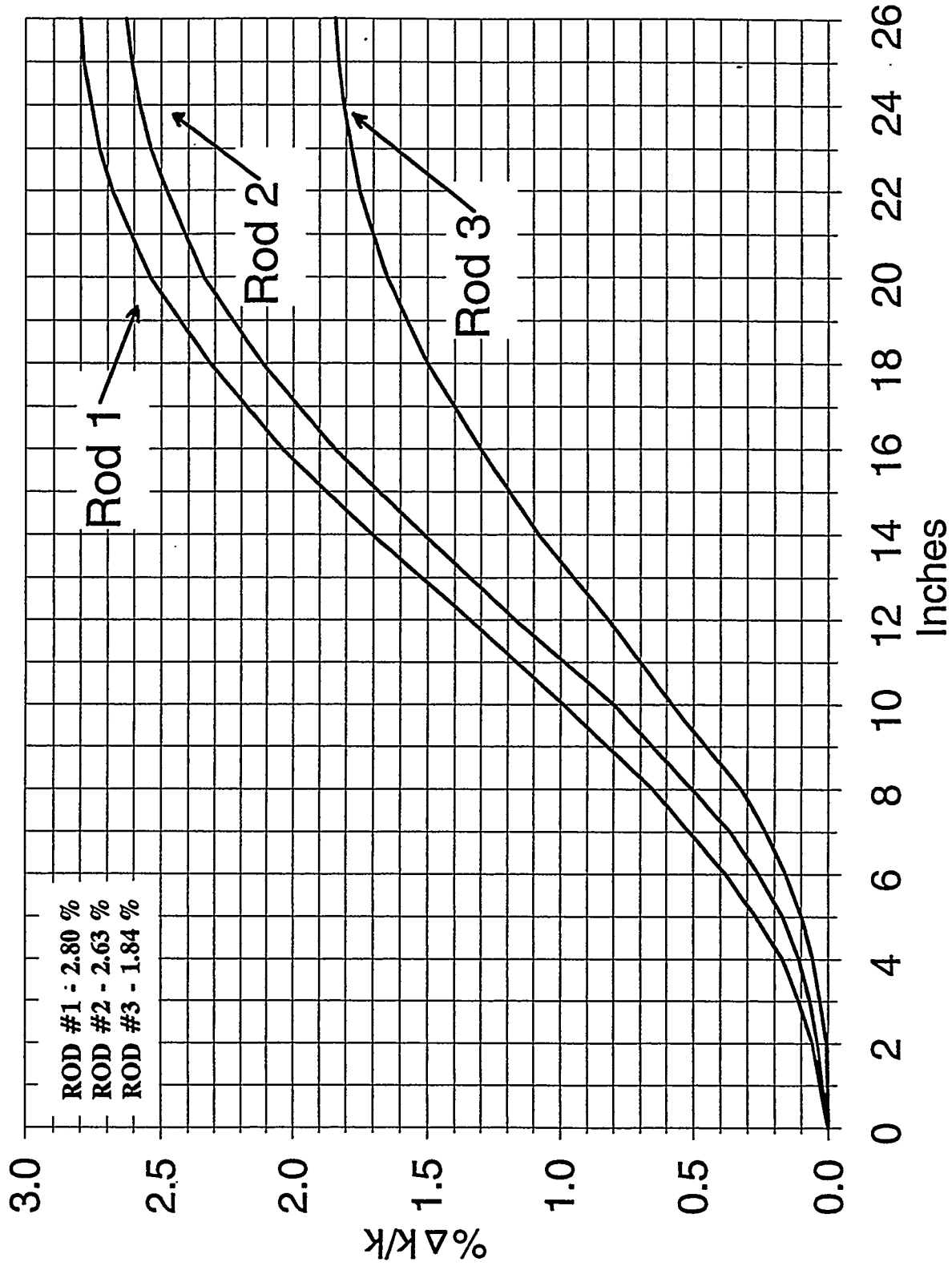


Figure 10. Integral Rod Worth, LEU-2 Shim Rods #1, #2, and #3

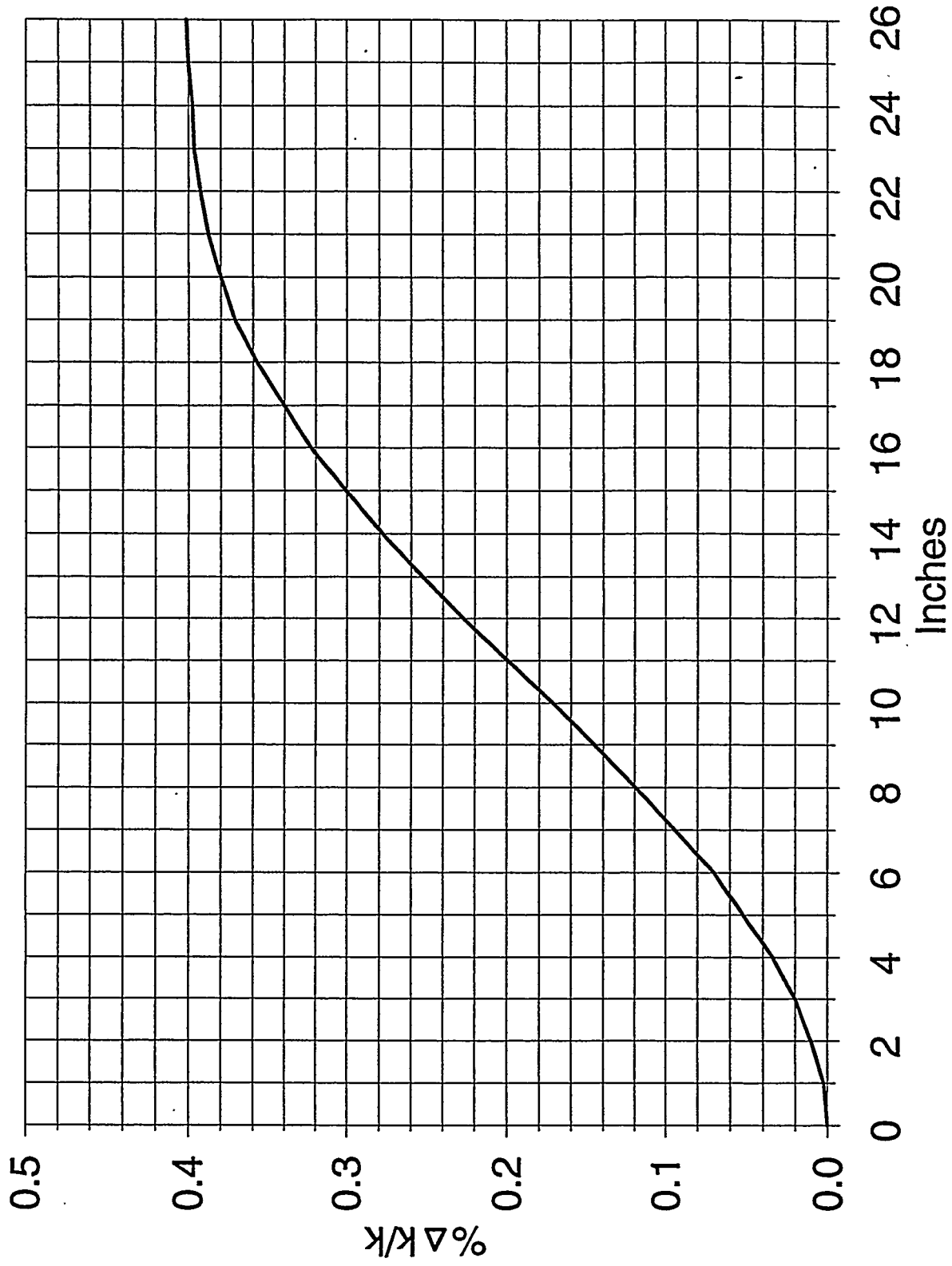


Figure 11. Integral Rod Worth, LEU-2 Regulating Rod

The excess reactivity of LEU-2 was measured experimentally to be + 3.27 % Δk/k, well below the + 5.0 % Δk/k limit required by the Technical Specifications.

b) Experimental Facilities

Before operating at any appreciable power, various experimental facilities were installed in the reactor and the reactivity worth of each facility was determined with the following results:

Experimental Facility	Worth (%Δk/k)
Epi-Thermal Rabbit, grid position 64	- 0.01
Thermal Rabbit, grid position 73	- 0.01
Hot Thimble #1, with specimens, grid position 53	- 0.28
Hot Thimble #3, without specimens, grid position 55	- 0.54
Canister Irradiation Facility, east side of core	- 0.04

The sum of the absolute worth of the experimental facilities is 0.88 %Δk/k, well below the 2 %Δk/k limit for all experiments required by the Technical Specifications.

c) Approach to Full Power

The initial approach to power with the LEU-2 core was begun on the afternoon of May 12, 1994. The power was leveled out at 200 kW, 500 kW, 1 MW, and finally 2 MW to check instrument response and to perform radiation surveys. Full power of 2 MW was achieved at about 5:20 P.M. Radiation surveys at the reactor bridge and around experimental areas showed no increase in radiation levels as compared to the HEU core.

d) Power Coefficient Measurement

The reactor was taken critical at low power in a xenon-free condition and the critical rod positions were noted. Rod #2 was withdrawn about 0.5 inch to put the reactor on a positive period. Doubling times were measured with a stop watch using the linear instrument. The power was allowed to rise until it leveled off at 870 kW due to negative temperature effects. The average temperature rise across the core was noted. The doubling times were converted to reactivity and matched almost exactly with the reactivity worth of rod #2 when it was withdrawn as determined from the rod worth curve. The power coefficient was experimentally verified to be -0.139 %Δk/k/MW or in terms of the change in average core temperature - 0.0275 %Δk/k/^{0}F. It is noted that this measurement includes several effects such as the fuel doppler, fuel expansion, and moderator temperature coefficients. The moderator temperature coefficient was measured separately.

e) Moderator Temperature Coefficient Measurement

The reactor was operated all day at full power on May 13, 1994 and the pool temperature was 97.9 °F when the reactor was shut down. The cooling systems were secured and the reactor remained shut down for three days to allow Xenon to decay. The reactor was taken critical at low power on May 16, 1994. The pool temperature was 86.9 °F and the ΔT was 0.0 °F. The secondary cooling system was energized and the pool was allowed to cool down. The power level was maintained by adjusting Rod #2. The pool was cooled for 1.5 hours. The Core outlet temperature changed by 11.24 °F. Rod #2 moved from 14.39 inches at the beginning of the test to a final position of 14.16 inches. The reactivity associated with this change was obtained from the rod worth curves and determined to be 0.05 % Δk/k.

Rod #2 was then moved back to it's original position of 14.39 and doubling times were taken to determine the reactivity associated with the rod movement as a check against the rod curves. The reactivity associated with the doubling times was 0.039 % Δk/k. Due to incomplete mixing from the cooldown the moderator temperature increased 2.06 °F during this measurement giving a temperature differential 9.18 °F as compared with the original temperature. An average of these measurements yielded a value of - 0.0044 %Δk/k/°F for the moderator temperature coefficient.

f) Experimental Facilities

Between May 23, 1994 and June 10, 1994, several other experiments were loaded in the reactor, giving the following experiments and experimental facilities now in the reactor.

		Worth (% Δk/k)
1.	Epi-Thermal Rabbit, grid position 64	- 0.01
2.	Thermal Rabbit, grid position 73	- 0.01
3.	Hot Thimble #1, with specimens, grid position 53	- 0.28
4.	Hot Thimble #3, without specimens, grid position 55	- 0.54
5.	1.2 kg of Fe samples in H.T. #3	+ 0.05
6.	Cannister Irradiation Facility (East side of core)	- 0.04
7.	MIF Stand, front of core on pool floor	0.00
8.	MIF Lead Shield, front of core on MIF stand	+ 0.33
9.	MIF Box, Model 3, #2 (Gas cooled), North side of core	- 0.37

The sum of the absolute worth of the experimental facilities is 1.63 %Δk/k, which is below the Technical Specification limit of 2.0 % for all experiments..

VI. Comparison Between LEU and HEU Cores

The LEU-1 core was similar to an HEU core operated in 1975. They were both 4x4 configurations surrounded by graphite. Due to the increased U-235 content of the LEU fuel, with changes from 18 to 22 plates per element, partial elements were loaded in grid positions 23 and 26 in the LEU core. Comparisions of the two cores are as follows:

	HEU Core (2.73 kg U-235)	LEU-1 Core (3.57 kg U-235)
Rod Worth (% Δk/k)		
Rod #1	3.56	3.46
Rod #2	3.75	3.86
Rod #3	2.30	2.41
Reg Rod	0.428	0.375
Shutdown Margin (% Δk/k) (Rod #2 and Reg withdrawn)	- 2.7	- 1.21
Excess Reactivity (% Δk/k)	+ 3.35	+ 4.66

The control rod worths that were computed for both the HEU and LEU-1 cores were in good agreement with these measured values.

A comparison of the measurements made with the LEU fuel and predictions in the LEU SAR, and HEU comparisons, where available, are presented below.

The "Power" temperature coefficient was measured during a core-heat-up experiment. It is expressed as the change in Δk/k per average change in core temperature. This is not the same conceptually as the isothermal moderator temperature coefficient, which was measured during a pool-cool-down experiment at low power.

	LEU Core	LEU-SAR	HEU Core
Power Coeff. (% Δk/k/MW)	- 0.139	NA	NA
"Power" Temperature Coefficient (% Δk/k/°F)(LEU-2)	-.0275	NA	-.0288
Moderator Temp. Coefficient (% Δk/k/°F) (LEU-2)	-.0044	-.0082	NA
Void Coefficient (uniform) (% Δk/k/% void) (LEU-1)	- 0.19	- 0.22	NA

The most significant observation is that the "Power" temperature coefficients for the old HEU and new LEU-2 cores are almost identical, signifying that the safety characteristics of the two cores are essentially the same.

The isothermal moderator temperature coefficient value is clearly different from the "Power" temperature coefficient value, but it was not expected to be comparable. The measured isothermal moderator temperature coefficient is about a factor of 2 smaller than the value calculated for an ideal unrodded LEU core model. Considering experimental uncertainties in the measurement, and the lack of partially inserted control rods in the computational model, the agreement is judged to be acceptable.

The void coefficient measurements lie in the range of the calculated void coefficients. Local experimental differences are expected to be caused by the presence of partially inserted control rods in the core.

VII. Shipment of All HEU Fuel Elements From Facility

All HEU fuel (32 elements) was shipped to Savannah River in the BMI-1 shipping cask in three shipments made on May 4, 1994, June 6, 1994, and July 8, 1994, respectively.

VIII. Pool Water Analysis

During the month after the UVAR reactor had been operated at full power with LEU fuel, daily samples were taken of the reactor pool water and analyzed for specific isotopes. There was no indication of fission product activity in the pool water, attesting to the integrity of the new LEU fuel. The most predominant isotope found in the pool water was Na-24 from the activation of aluminum. This is normally found in the water since Al makes up most of the structural material in and around the reactor. A tabulation of the analysis is shown in Table 1.

Normal weekly pool water samples after operating for over three months have shown no increase in activity in the pool.

IX. Summary

The UVAR has been successfully converted from HEU to LEU fuel. The initial criticality predictions for 4-by-4 and 4-by-5 LEU core configurations were qualitatively correct, leading to a practical LEU-2 core configuration that meets all Technical Specification requirements. The prediction that control rod worths would not be very different between HEU and LEU cores was borne out. Void coefficient measurements agree reasonably well with prior predictions. Temperature coefficient measurements are fairly comparable between HEU and LEU cores. And finally, flow coastdown measurements confirm that adequate cooling is available.

Additional core-specific computational work is in progress to resolve minor uncertainties. Otherwise, the experimental verification tests are essentially finished and the UVAR is back in routine full-time operation.

X. Acknowledgement

The University of Virginia would like to thank the U.S. Department of Energy for its support of this project under Grant # DE-FG05-88ER75388. Three Masters Degree Theses were produced as a result of this work.

Design Optimization of a Low Enrichment University of Virginia Nuclear Reactor, by Mary Katherine Fehr.

Neutronic Analysis For The UVAR Reactor HEU to LEU Conversion Project, by David W. Freeman.

Effective Diffusion Theory Cross Sections for UVAR Control Rods, by Stuart Wasserman.

Table 1. UVAR Pool Water Analysis

UVAR Reactor Pool Water Analyses with LEU Fuel (μCi/ml)													
Isotope	Na-24	Mn-54	Mn-56	Mg-27	Cl-38	Cr-51	W-187	Sb-122	Ar-41	Xe-135	Xe-133	I-131	Co-60
½ life	15.0h	312d	2.6h	9.5m	37.3m	27.7d	23.9h	2.7d	1.8h	9.1h	5.3d	8.0d	5.3y
EC **	5.0E-5	3.0E-5	7.0E-5	—	—	5.0E-4	3.0E-5	1.0E-5	—	—	—	1.0E-6	3.0E-6
5/12	1.0E-4		5.5E-6	2.9E-3	1.5E-5				6.1E-4				
5/13	5.5E-4		1.5E-5	1.3E-4	9.7E-6	<4.3E-6	<2.3E-6	<9.1E-7	7.0E-4	<4.7E-7	<1.1E-6	<5.3E-7	<8.3E-7
5/16	2.2E-4		5.7E-6	1.8E-3	1.9E-5	<3.5E-6	<1.9E-6	<7.5E-7	7.2E-4	<3.9E-7	<9.0E-7	<4.3E-7	<5.3E-7
5/17	2.6E-4		5.2E-6	2.9E-3	2.3E-5	<4.2E-6	<2.2E-6	<9.0E-7	6.2E-4	<4.5E-7	<1.0E-6	<5.1E-7	<6.0E-7
5/18	6.4E-4		9.7E-6	4.1E-3	1.8E-5	<5.1E-6	<2.8E-6	<1.1E-6	8.5E-4	<5.6E-7	<1.3E-6	<6.3E-7	<9.1E-7
5/19	3.9E-4		1.1E-6	<1.2E-4	<7.5E-6	<2.8E-6	1.5E-6	5.7E-7	5.6E-5	<3.1E-7	<7.2E-7	<3.5E-7	<6.7E-7
5/20	9.8E-5		<4.2E-7	<4.9E-5	<3.6E-6	1.0E-6	8.9E-7	<3.2E-7	<5.3E-7	<1.6E-7	<4.2E-7	<1.8E-7	<3.5E-7
5/23	1.5E-6	<5.4E-8	<1.1E-7	<1.6E-2	<2.9E-6	2.6E-7	1.8E-7	<6.8E-8	<1.8E-7	<4.7E-8	<1.5E-7	<4.2E-8	<6.2E-8
5/24	9.4E-7	<3.0E-8	<2.5E-7		<4.3E-4	2.0E-7	<1.2E-7	4.8E-8	6.1E-7	<3.9E-8	<9.1E-8	<2.4E-8	3.8E-8
5/25	3.3E-4		6.1E-6	<1.4E-4	<7.1E-6	<3.1E-6	<1.7E-6	<6.8E-7	3.5E-4	<3.5E-7	<8.0E-7	<3.8E-7	<6.4E-7
5/26	6.1E-4		1.8E-5	2.5E-3	1.2E-5	<2.9E-6	1.1E-6	<6.3E-7	8.8E-4	2.6E-7	<7.4E-7	<3.6E-7	<5.9E-7
5/27	5.5E-4	<6.0E-8	8.4E-6	<1.7E-2	<2.2E-5	1.1E-6	1.1E-6	3.0E-7	4.4E-4	2.6E-7	<1.2E-7	<3.4E-8	<4.8E-8
5/31	5.8E-4		1.3E-5	8.8E-4	7.0E-6	<4.5E-6		<9.6E-7	8.0E-4	<5.0E-7	<1.1E-6	<5.5E-7	<8.5E-7
6/1	6.4E-4		2.6E-4	3.3E-3	1.9E-5	<5.2E-6		<1.1E-6	8.3E-4	<5.7E-7	<1.3E-6	<6.4E-7	<9.2E-7
6/2	6.5E-4		1.1E-5	3.5E-4	5.7E-6	<4.7E-6	<2.5E-6	<1.0E-6	7.2E-4	<5.1E-7	<1.2E-6	<5.8E-7	<9.3E-7
6/3	7.4E-4		1.6E-5	5.3E-4	<1.1E-5	<4.9E-6	1.9E-6	<1.1E-6	8.2E-4	<5.4E-7	<1.2E-6	<6.1E-7	<9.7E-7
6/6	9.7E-6	6.7E-8	<3.3E-7		<6.9E-4	6.7E-7	2.1E-7	1.1E-7	<9.2-7	<5.0E-8	<1.1E-7	<3.0E-8	<4.7E-8
6/7	2.7E-6	1.8E-8	<5.5E-7		<2.1E-2	5.5E-7	1.0E-7	8.7E-8	<2.3E-6	<4.3E-8	<7.8E-8	<2.1E-8	<2.9E-8
6/8	5.1E-7	<3.1E-8	<2.2E-7		<2.8E-4	4.6E-7	<1.2E-7	5.7E-8	<6.3E-7	<3.9E-8	<9.1E-8	<2.4E-8	<3.5E-8
6/9	1.1E-7	<2.8E-8	<2.7E-7		<6.6E-4	2.2E-7	<1.1E-7	4.5E-8	<8.1E-7	<3.9E-8	<8.9E-8	<2.3E-8	<3.1E-8
6/10	4.5E-5	<7.6E-7	2.3E-4	2.6E-3	7.7E-6	<4.3E-6	<2.4E-6	<1E-6	2.0E-4	<4.6E-7	<1.1E-6	<5.3E-7	<3.9E-7
Isotope	Na-24	Mn-54	Mn-56	Mg-27	Cl-38	Cr-51	W-187	Sb-122	Ar-41	Xe-135	Xe-133	I-131	Co-60

** Effluent Concentration limit from 10CFR20, App B, Table 2, Column 2, μCi/ml

Attachment 1

LEU FUEL CONVERSION TEST PROGRAM

Low Enriched Uranium Fuel Core Conversion Program

University of Virginia Nuclear Research Reactor

15 February 1994

License No. R - 66

Docket No. 50 - 62

University of Virginia
School of Engineering and Applied Science
Department of Mechanical, Aerospace, and Nuclear Engineering
Nuclear Reactor Facility
Charlottesville, Virginia
22903-2442

Table of Contents

PAGE

Introduction 1

LEU conversion time line 3

Prerequisites 6
Checklist 6
Preparations for Void Measurements 7
Construction of Swords and Test Chamber 7
Testing the Swords 7
Preparations for Measuring Flow Coast Down Measurement 10

LEU Core 1 Procedure 12
Description 12
Preliminary 12
Loading 12
Partial Element Worth Measurement 13
Primary Pump Flow Coast Down Measurements 14
Void Measurements 15
Attachment 1: Core 1 map 16
Attachment 2: Worksheet for calculating Critical Mass 17

Measuring Flow Coast Down 19
Figure 1: Amplifier 21

Measuring Void Coefficient with Void Swords 23
Void Coefficient Measurement Data Table 25
Figure 1: The essential features of the swords 27
Figure 2: A test chamber 28

LEU Core 2 Procedure 30
Description 30
Preliminary 30
Loading 30
Power ascension 32
Power reactivity coefficient measurement 33
Attachment 1: Core 2 map 34
Attachment 2: Worksheet for calculating Critical Mass 35

Measuring the Power Reactivity Coefficient of UVAR 37

Measuring the Temperature Reactivity Coefficient of UVAR 41

Introduction

This program is the Low Enrichment Uranium (LEU) core conversion program for the University of Virginia Nuclear Reactor Facility mandated by the NRC. The Nuclear Regulatory Commission (NRC) requires ("to the extent that measurements are possible") a number of measurements to verify core operability and safety. In this test program measurements or calculations will be made for the following items:

1. Initial loading measurements;
2. Critical mass;
3. Excess (operational) reactivity;
4. Shut-down margin;
5. Control Rod worths;
6. Partial fuel element worths;
7. Void coefficient;
8. Primary pump flow coast-down;
9. Primary flow;
10. Experimental facility and experiment worths;
11. Temperature and Power coefficients;
12. Reactor power calibration;
13. Reactor pool water fission product activities.

A report will be made, within six months of initial core loading, compiling all data and comparing all results against available HEU core measurements and LEU predictions. The report will also include explanations of any significant differences found during comparisons that could affect both normal operation and possible accidents with the reactor.

The measurement of the effective delayed neutron fraction ($\overline{\beta}_{eff}$) will not be undertaken during the initial conversion period. It is felt that the cost in time and money to undertake this measurement is too great. Extensive computer calculations of $\overline{\beta}_{eff}$ have been made[1]. These calculated values of $\overline{\beta}_{eff}$ show no difference from the HEU $\overline{\beta}_{eff}$ of 0.0074. The $\overline{\beta}_{eff}$ of 0.0074 will be used for the UVAR LEU fuel.

Thermal neutron flux distribution will not be measured since correlations with calculated data could not be made without much more time and experimentation. If interest and funding become available these two measurements may be considered for graduate research.

Relative flux measurements at the experimental facilities will be done after the conversion process only as necessary for specific experimental requirements.

---

[1] Freeman, D., Neutronic Analysis for the UVAR Reactor HEU to LEU Conversion Project, Masters Thesis, University of Virginia, January 1990.

Procedures for this program which do not utilize the UVAR Standard Operating Procedures have been written specifically for the test they control. They are approved only for the duration of the conversion program (until the UVAR is returned to normal (unrestricted) operations).

As with all procedures, these are structured and cannot cover all contingencies. The UVAR LEU Conversion Program is an experimental test program and situations may arise where other steps or methods may be more appropriate. Therefore, these procedures may be deviated from by approval of the Facility Director when the deviation does not change the original intent of the existing procedure. Deviations which change procedure intent must have prior approval of the Reactor Safety Committee. All deviations must be documented.

LEU conversion time line

Time (week)	Priority 1 item	Priority 2 item	Priority 3 item
-2	1. Construct void swords.	1. Construct/gather necessary additional electronic equipment.	
-1	1. Trial fit swords in new fuel. 2. Pressure test void swords.	1. Op check additional electronic equipment/ready for installation.	1. Install second fission chamber in core grid plate & source check.
0	1. Load the referenced/ calculated core.	1. Obtain subcritical mult. data; 2. Obtain critical mass data; 3. Determine rod worths.	1. Calculate operational shut-down margin; 2. Calculate excess reactivity.
+1	Referenced core in place.	1. Measure partial element reactivity; 2. Measure core flow and flow coast-down.	1. Calculate partial element worth.
+2	Referenced core in place.	1. Measure void reactivity.	
	Establish working core configuration.	1. Obtain subcritical mult. data; 2. Obtain critical mass data.	
+3	Working core in place.	1. Determine rod worths; 2. Load non-fixed experiments; 3. Measure reactivity of non-fixed experiments.	1. Calculate operational shut-down margin; 2. Calculate excess reactivity.
+4	1. Ramp to 500 kW. 2. Ramp to 1.0 MW. 3. Ramp to 1.5 MW. 4. Ramp to 2.0 MW. 5. Ramp to 2.0 MW.	1. Perform power calibrations (each pwr level); 2. Measure power & temperature coefficient reactivity, ramp from 200 kW - 2.0 MW.	1. Calculate temperature coefficient.
+5	1. Resume normal operations.	1. Obtain and analyze pool water samples daily.	1. Compare & correlate LEU/HEU data as applicable - start writing report.

Time (week)	Priority 1 item	Priority 2 item	Priority 3 item
+6	Normal operations.	1. Obtain and analyze pool water samples daily.	1. Compare & correlate LEU/HEU data as applicable - continue writing report.
+7	Normal operations.	1. Obtain and analyze pool water samples daily.	
+8	Normal operations.	1. Obtain and analyze pool water samples daily.	

Month 4 - send preliminary report to ReSC (circulate for staff review prior to all submittals)

Month 5.5 - send final report to ReSC and NRC

Prerequisites for LEU Conversion

I. Prerequisites Checklist

The steps of this checklist may be completed in any order. It is to be used as a quick indication of which Prerequisite sections have been or have yet to be completed.

____ Void swords have been manufactured and tested as per *Preparations for Void Measurements*, pg. 7,.

Date: _____ by: _____

____ Void Constants are:

$Void_{fp}$ = _____

Voidable Volume of reactor = _____

% Void = _____

Date: _____ by: _____

____ Primary Flow coastdown amplifier has been manufactured and tested as per *Preparations for Coastdown Measurements*, pg. 10.

Date: _____ by: _____

____ Additional source range instrumentation and detector has been tested and is ready for installation and source check.

Date: _____ by: _____

III. Preparations for Void Measurements

A. Construction of Swords and Test Chamber

1. The swords will be made of three layers of plastic with the middle layer cut in a pattern that allows a reasonable compromise between amount of void and support of the voided area. Both swords will be constructed with the same pattern and the flooded sword will have flood and vent holes at the top and bottom to allow water to flood the entire open area in the pattern. At least one of the side layers should be clear plastic so that flooding can be observed when testing the sword. The voided portion of the sword should span the entire length of the fueled region. A sketch that shows the essential features of the swords is given in Figure 1 of the *Procedure for Measuring Void Coefficient with Void Swords* (see page 27).

2. A test chamber consisting of a rigid cylinder capable of holding the entire sword that has a cap with a graduated sight glass penetrating it will be needed. This chamber and cap must be capable of withstanding 10 psi pressure. A sketch of a possible chamber is included as Figure 2 of the *Procedure for Measuring Void Coefficient with Void Swords* (see page 28).

B. Testing the Swords

1. Flooded Sword

   Immerse the flooded sword in water and visually check that water fills all of the voids

2. Void Sword

   A. Calculate the outline volume of the sword.

   B. Measure the density of a sample of the material used to make the sword.

   C. Measure the mass of the sword. This will yield the nominal void volume of the sword.

III.B.2. Testing the Void Sword (cont.)

NOTE:

$Void_{zp} = (V_t * \rho_p - M_m) / \rho_p$ where

$Void_{zp}$ =	Void in cc of sword under zero pressure
V_t =	Calculated volume of sword
ρ_p =	Measured density of plastic used for sword
M_m =	Measured mass of sword

D. Measure the actual volume of the void sword when immersed vertically in water by measuring the volume of the displaced water.

NOTE:

$Void_{im} = (V_{im} * \rho_p - M_m) / \rho_p$ where

$Void_{im}$ =	Void in cc of sword under water
V_{im} =	Measured displacement of sword
ρ_p =	Measured density of plastic used for sword
M_m =	Measured mass of sword

E. Measure the change in volume of the chamber when subjected to the hydrostatic pressure of the core.

i. Place the cap on the test chamber and fill the test chamber until there is a reasonable level in the graduated sight glass at its top.

ii. Agitate the test chamber to assure that all of the air has escaped.

iii. Note the level of the graduated sight glass and attach a pressure hose to the top of the cylinder.

iv. Pressurize the cylinder with gas to a pressure of 19'4.5" water head. DO NOT OVER PRESSURIZE. Use appropriate precautions to avoid flying glass.

v. Note the change (drop) in level of the water in the graduated sight glass. This is the change in volume of the chamber as the walls expand (bow) as a result of the gas pressure.

III.B.2. Testing the Void Sword (cont.)

F. Measure the change in displacement of the sword when subjected to the hydrostatic pressure of the core.

i. Place the cap on the test chamber and fill the test chamber until there is a reasonable level in the graduated sight glass at its top.

ii. Agitate the test chamber to assure that all of the air has escaped.

iii. Note the level of the graduated sight glass and attach a pressure hose to the top of the cylinder.

iv. Pressurize the cylinder with gas to a pressure of 19'4.5" water head. DO NOT OVER PRESSURIZE. Use appropriate precautions to avoid flying glass.

v. Note the change (drop) in level of the water in the graduated sight glass. This is the change in volume of the air filled portion of the sword as the sides partially collapse plus that of the chamber expansion.

G. Adjusting the measured void of the sword with the change in displacement due to pressurizing the sword will yield the actual void volume produced by the sword when it is inserted in the core. Record this on pg. 6 of this procedure.

NOTE:

$Void_{fp} = Void_{im} - \Delta V$ where

$Void_{fp}$ = Void in cc of sword under full pressure
$Void_{im}$ = Void in cc of sword under water
ΔV = Drop in level of graduated sight glass when pressurizing test chamber w/sword minus the drop in level when pressurizing test chamber w/o sword.

3. Calculate the voidable portion of the reactor. This is the fuel channels and inter-element gap over the length of the actual fuel. This will yield the percent void represented by the insertion of the voided sword. Record this on pg. 6 of this procedure

NOTE:

$\%Void = Void_{fp} / Voidable\ Volume * 100$

IV. Preparations for Measuring Flow Coast Down Measurement:

Amplifier construction

_____ Ensure a simple amplifier such as the one shown in Figure 1 of the *Procedure For Measuring Flow Coast Down*, pg. 21, is constructed to connect the Visicorder to the normal flow instrument current loop. The amplifier may be built on a bread board.

Procedure
for
Establishing LEU Core 1

LEU Core 1 Procedure

I. Description:

4 x 4 - graphite reflected (to the extent possible). Referenced to High Enrichment Uranium (HEU) Texas element core 4 x 4 - graphite reflected. (see Attachment 1 for core loading map, page 16).

II. Preliminary:

_____ A. HEU fuel removed from core as per SOP 5.4.2.B, grid plate bare with exception of source/source holder, graphite reflectors, plugs, and detectors.

_____ B. Auxiliary source range detector installed.

_____ C. Control rod inspection completed satisfactorily in accordance with (IAW) SOP 7.5.

_____ D. Limit maximum power level to 10^6 cps on main source range with fission chamber completely inserted (approximately 250 watts).

III. Loading:

NOTE
Ensure the Daily Checklist is completed prior to the first reactor startup each day that the reactor is to be taken critical from a secured condition.

A. Initial and date each major component of the checklist (part B), listed below, as the step is completed.

B. Load LEU fuel IAW SOP 5.4 and Attachment 1 (core 1 loading map, page 16).

_____ 1. Desired graphite reflectors and plugs in place.

_____ 2. Control rods installed IAW SOP 5.4.2.D.

_____ 3. Control rod drop times completed satisfactorily IAW SOP 7.3.

_____ 4. Subcritical multiplication (1/M) data obtained.

III.B. Loading (cont.)

_____ 5. Completely banked initial critical rod configuration rod heights obtained (for critical mass measurement, see Attachment 2, page 17).

_____ 6. Core loaded to desired configuration.

_____ 7. Integral & differential rod worths obtained IAW SOP 7.4.

_____ 8. Core excess reactivity calculated IAW SOP 5.5.

Excess reactivity is _____ % Δk/k (< 5.0 % Δk/k).

_____ 9. Core shutdown margin calculated IAW SOP 5.5.

Shutdown margin is _____ % Δk/k (> 0.4 % Δk/k).

IV. Partial Element Worth Measurement:

NOTE
Ensure the Daily Checklist is completed prior to the first reactor startup each day that the reactor is to be taken critical from a secured condition.

A. Bring the reactor critical, at power less than 10^6 cps, IAW SOP 5.1

_____ 1. Measure banked critical rod heights

Rod 1: _____ ; Rod 2: _____ ; Rod 3: _____ ; Reg Rod: _____

_____ 2. Note pool temperature: (_____ ° F)

_____ 3. Shut down the reactor.

B. Remove the designated fuel element IAW SOP 5.4.2.C.3.

IV. Partial Element Worth Measurement (cont.)

C. Add the designated partial fuel element IAW SOP 5.4.2.C.2.

D. Bring the reactor critical, at power less than 10^6 cps, IAW SOP 5.1.

_____ 1. Measure critical rod heights:

Rod 1: _____ ; Rod 2: _____ ; Rod 3: _____ ; Reg Rod: _____.

_____ 2. Note pool temperature: (_____ ° F).

_____ 3. Shut down the reactor.

E. Return core to initial reference core configuration (see pg. 16) IAW SOP 5.4.2.C.

V. Primary Pump Flow Coast Down Measurements

A. Initial Conditions

_____ 1. The reactor is shut down.

_____ 2. The amplifier has been installed on the flow instrument IAW the *Procedure for Measuring Flow Coast Down*, pg. 19.

B. Perform flow coast down measurements IAW the *Procedure for Measuring Flow Coast Down*, pg. 19.

_____ 1. The Flow Coast-down measurement is complete.

_____ 2. The amplifier installed for the measurement has been removed from the flow instrument.

_____ 3. The flow instrument has been returned to normal operation.

VI. Void Measurements

NOTE
Ensure the Daily Checklist is completed prior to the first reactor startup each day that the reactor is to be taken critical from a secured condition.

A. Limit maximum power level to 10^6 cps on main source range with fission chamber completely inserted (approximately 250 watts).

B. Record critical rod height positions in provided data table (pg. 25).

C. Measure the Void coefficient IAW the *Procedure for Measuring Void Coefficient with Void Swords*, pg. 23.

_____ Void measurements completed.

Attachment 1: Core 1 map

Core Loading: LEU - 1; Date: _____; U - 235: 3846 Grams;

F	Normal Fuel Element	**P**	Grid Plate Plug
PF	Partial Fuel Element	**HYD RAB**	Hydraulic Rabbit
CR	Control Rod Fuel Element	**THER RAB**	Thermal Pneumatic Rabbit
G	Graphite Element	**EPI RAB**	Epithermal Pneumatic Rabbit
S	Graphite Source Element	**RB**	Radiation Basket

REG Control Rod Fuel Element with Regulating Rod

North ⇑

G 11	G 12	G 13	S 14	G 15	G 16	G 17	G 18
G 21	G 22	F VS-001 23	F VS-002 24	F-REG VC 001 25	F VS-003 26	G 27	G 28
G 31	G 32	F VS-004 33	F-CR1 VC-002 34	F VS-005 35	F VS-006 36	G 37	G 38
G 41	G 42	F VS-007 43	F VS-008 44	F-CR2 VC-003 45	F VS-009 46	G 47	G 48
G 51	G 52	F VS-010 53	F-CR3 VC-004 54	F VS-011 55	F VS-012 56	G 57	G 58
G 61	G 62	G 63	G 64	G 65	G 66	G 67	G 68
G 71	G 72	G 73	G 74	G 75	G 76	G 77	G 78
G 81	G 82	G 83	G 84	G 85	G 86	G 87	G 88

Loading Approved By: _____ Date: _____

Attachment 2: Worksheet for calculating Critical Mass

List each fuel element placed in core and associated U-235 content (in grams)

Element	Mass	Σ Mass	Banked Rod heights	Banked Height %	C/C_o mass prediction	est. Critical Mass
VC-001						
VC-002						
VC-003						
VC-004						

Banked Height % = Banked rod height/26

Estimated Critical Mass = Σ Mass of the n-1 elements + [mass of the n^{th} element * banked rod height %] (note: valid only when criticality is achieved.

Procedure
for
Measuring Flow Coast Down

Procedure For
Measuring Flow Coast Down

I. Prerequisite

The UVAR must be shut-down to perform this measurement.

II. Set Up/Calibration

A. Ensure a simple amplifier such as the one shown in Figure 1 (page 21) has been constructed.

B. De-energize the 35 volt power supply for the flow instrument and install the amplifier into the GROUNDED END of the current loop as shown in Figure 1 (page 21). Re-energize the 35 volt power supply.

C. Connect the amplifier to one channel of the Visicorder and check that the Visicorder is working. This will be the Flow Channel of the Visicorder.

D. Thoroughly vent the differential pressure cell and apply a differential pressure corresponding to 100% flow using the manometer bottles in a manner similar to that used in the normal calibration of the flow meter.

E. Set one of the unused galvanometers of the Visicorder to coincide with the position of the Flow Channel. This will record a line at 100% throughout the measurement.

F. Connect the Header up position indicator to the unused galvanometer of the Visicorder, check that indication is given when header position is changed.

G. Apply a zero differential pressure to the cell and set the other unused galvanometer to correspond with the Flow Channel. This will record a line at zero throughout the measurement.

H. If the distance from the zero line to the 100% line is not appropriate adjust the voltage on the collector of the transistor of the amplifier depicted in Figure 1.

I. Run the Visicorder at a slow speed while setting the bottles to zero, 1/4, 1/2, 3/4 and full scale. Pause for several centimeters of paper travel at each point to make a permanent record of the relationship of Visicorder position and differential pressure. Annotate the chart for future reference. The head of water for these points are given in SOP 7.7.

J. Isolate the manometer bottles and place the differential pressure cell in service.

III. Measurement

A. Establish the nominal flow condition for the coast down measurement. This will normally be with the header up, both primary isolation valves fully open, and all positions in the grid plate filled.

B. Set the Visicorder for 25 inches per second and check that it is working properly.

C. Start the Visicorder and turn off the primary pump. Stop the Visicorder soon after flow indications fall to zero.

IV. Disassembly

A. De-energize the 35 volt power supply for the flow instrument.

B. Disconnect the amplifier from the channel of the Visicorder.

C. Remove the amplifier from the GROUNDED END of the current loop as shown in Figure 1 (page 21).

D. Re-energize the 35 volt power supply.

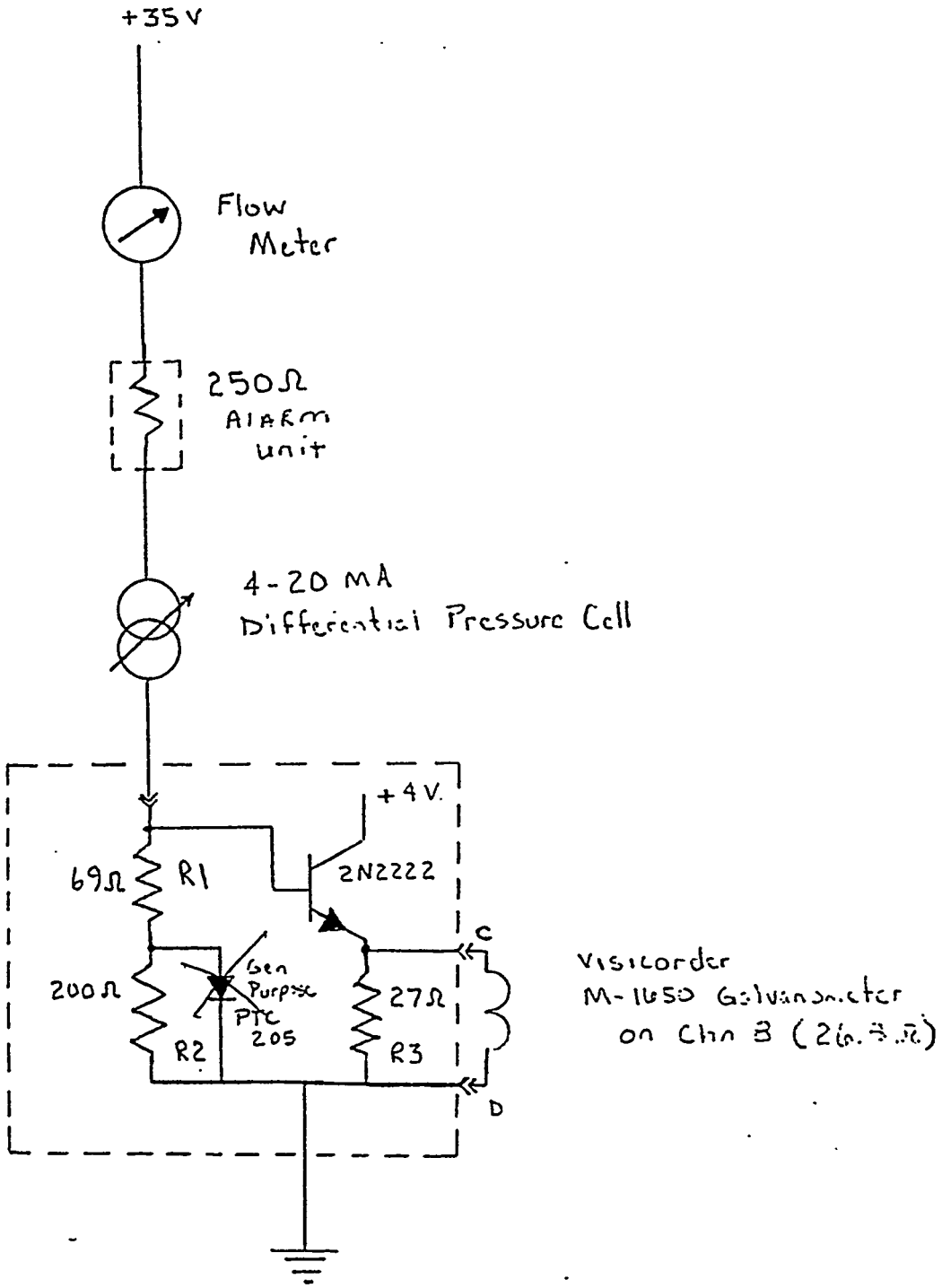
V. Data Reduction

A. Measure the relationship between differential pressure and position on the Visicorder trace with a scale (ruler) and the trace from step II.H. The actual flow rate is proportional to the square root of the differential pressure. Thus, for example, the position 3/4 of the way from the Zero Line to the 100% Line is 86.6% of full flow. Full flow on the indicator is normally set to 1200 gpm so this point would correspond to 1040 gpm.

B. Mark the trace at several convenient flow rates such as 1000, 900, 800, ..., 100 gpm. One of these marks should be at the Limiting Safety System Setting (LSSS) for primary flow.

C. Using the LSSS as the zero time point, plot the flow rate vs. time for the transient. This is the flow coast down curve to compare with the one in the Safety Analysis Report (SAR). A favorable flow coast down condition is one where this line is always above the line in the SAR.

Figure 1: Amplifier



Procedure
for
Measuring Void Coefficient with Void Swords

Procedure For
Measuring Void Coefficient with Void Swords

I. Introduction

This procedure utilizes a pair of swords of identical construction with the exception that one of them is flooded while the other is sealed to contain air. It is the difference in reactivity between the flooded volume of one sword and the air filled volume of the other sword that constitutes an individual void coefficient measurement. Several of these measurements must be performed at representative locations throughout the core to get a core average void coefficient.

It may not be possible to manipulate the swords into the core from the bridge in which case the fuel elements will have to be brought close to the surface to insert the swords. The fuel elements may be removed with the control rods either inserted or at ten inches but the rods must be at ten inches when replacing the fuel element, see SOP 5.4.2. parts B and C. If the elements are brought near the surface, monitor the dose rate carefully as the element is brought up. An element can be quite radioactive when pulled from a core that has recently been operating for just a short time at low power.

The procedures in SOP 5.4.2.c. are to be followed for any fuel manipulations. SOP 5.1.A, 5.1.B, or 5.1.C. are to be followed for bringing the reactor critical for each measurement. SOP 2.F. is to be followed when bringing either the sword or fuel element near the surface.

II. Equipment Setup

A. Obtain the $Void_{fp}$ value calculated in the prerequisite section: *Preparations for void measurements* (tabulated on pg. 6).

B. Obtain the voidable portion of the reactor calculated in the prerequisite section: *Preparations for void measurements* (tabulated on pg. 6).

C. Determine the percent void represented by the insertion of the voided sword calculated in the prerequisite section: *Preparations for void measurements* (tabulated on pg. 6).

III. Individual Measurement.

A. Position the rods either at the bottom or banked at 10 inches.

III. B. Insert the Flooded Sword into a channel of a normal fuel element noting the position of the sword in the element and the element in the core. If the fuel element was removed for this operation, reinsert the fuel element with the rods at 10 inches.

C. Take the reactor critical at low power with the control rods banked and note the rod positions on the Void Coefficent Measurement Data Table pg 25.

D. Position the rods either at the bottom or banked at 10 inches.

E. Remove the Flooded Sword and insert the Voided Sword in the same location. If the fuel element was removed for this operation, reinsert the fuel element with the rods at 10 inches.

F. Take the reactor Critical with 3 of the four rods in the same position as in step C and the remaining rod (the regulating rod if the reactivity change is very small) at the position required for criticality. Note the rod positions on the Void Coefficent Measurement Data Table pg 25.

G. The Void Coefficient for that position is the change in reactivity from the change in rod position divided by the voidable volume represented by the sword.

H. Position the rods either on the bottom of the core or banked at 10 inches

I. Remove the Voided Sword from the element. If the fuel element was removed for this operation, reinsert the fuel element with the rods at 10 inches.

J. Repeat steps A through I for several representative positions in the core.

Void Coefficient Measurement
Data Table

Voidable Volume of reactor = _____

$Void_{fp}$ = _____ % Void = _____

Element # & sword postion	Pool temp	Rod Positions - flooded sword				Rod Position - dry sword			
		Rod 1	Rod 2	Rod 3	Reg	Rod 1	Rod 2	Rod 3	Reg

IV. Data Considerations

From section III, local void coefficients are measured in several locations in the core. To get an idea of the void coefficient at other locations, the core's symmetry will be used. The core established from core 1 map (page 16), can be made approximately symmetric by establishing a critical banked rod height on rods 1 and 2, with the Regulating rod and rod 3 in their full out positions.

Other reactor facilities have gone to great lengths to determine the volume of the void and voidable volume below the rods and used that number when calculating the void coefficient. By making the void length identical to the fuel length and having the void in the sword aligned with the fuel, the active length of the core will always match the active void volume and no adjustment will be needed.

There is no technical specification limit on void coefficient nor a prescribed manner of reporting it.

Figure 1: The essential features of the swords

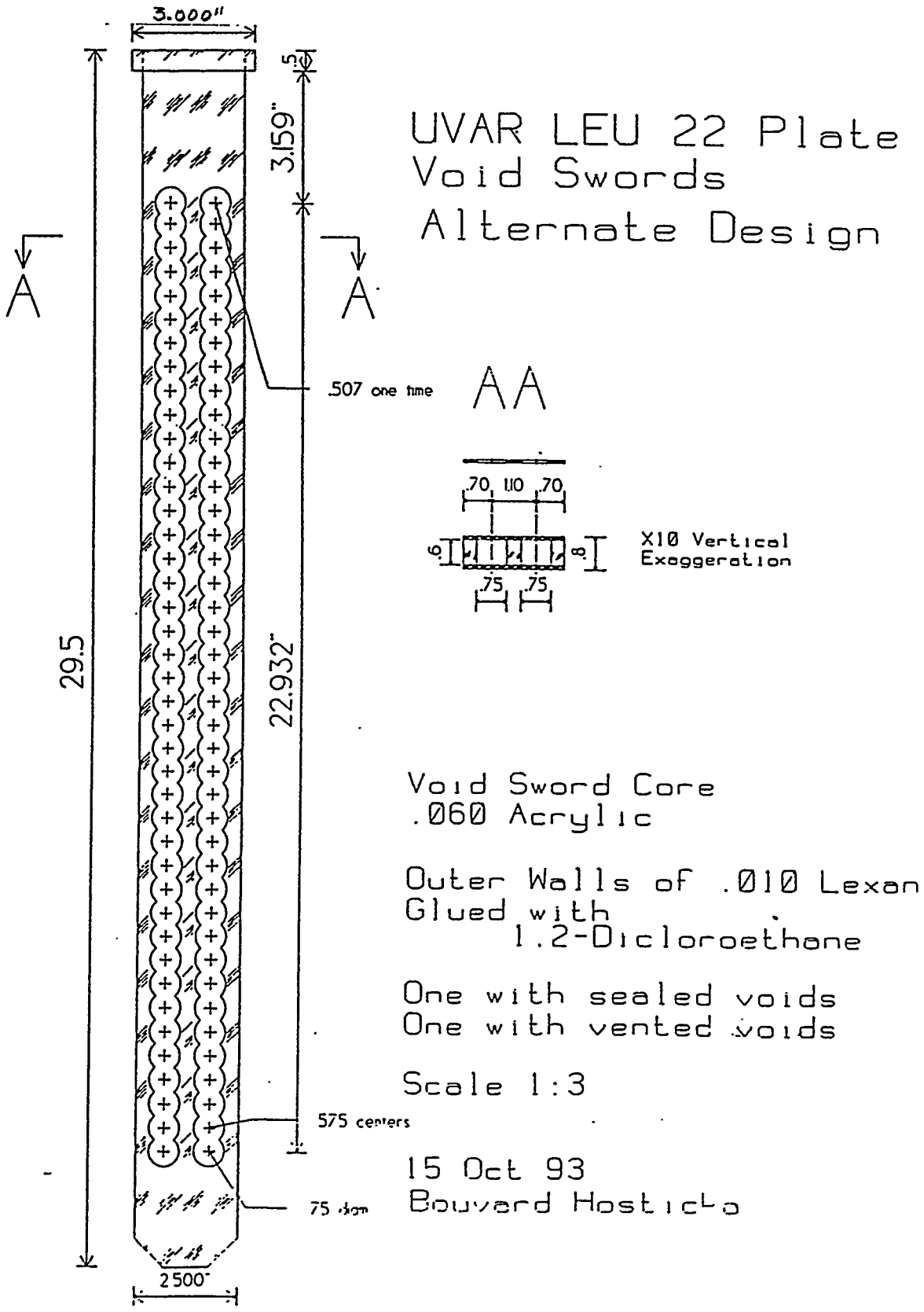
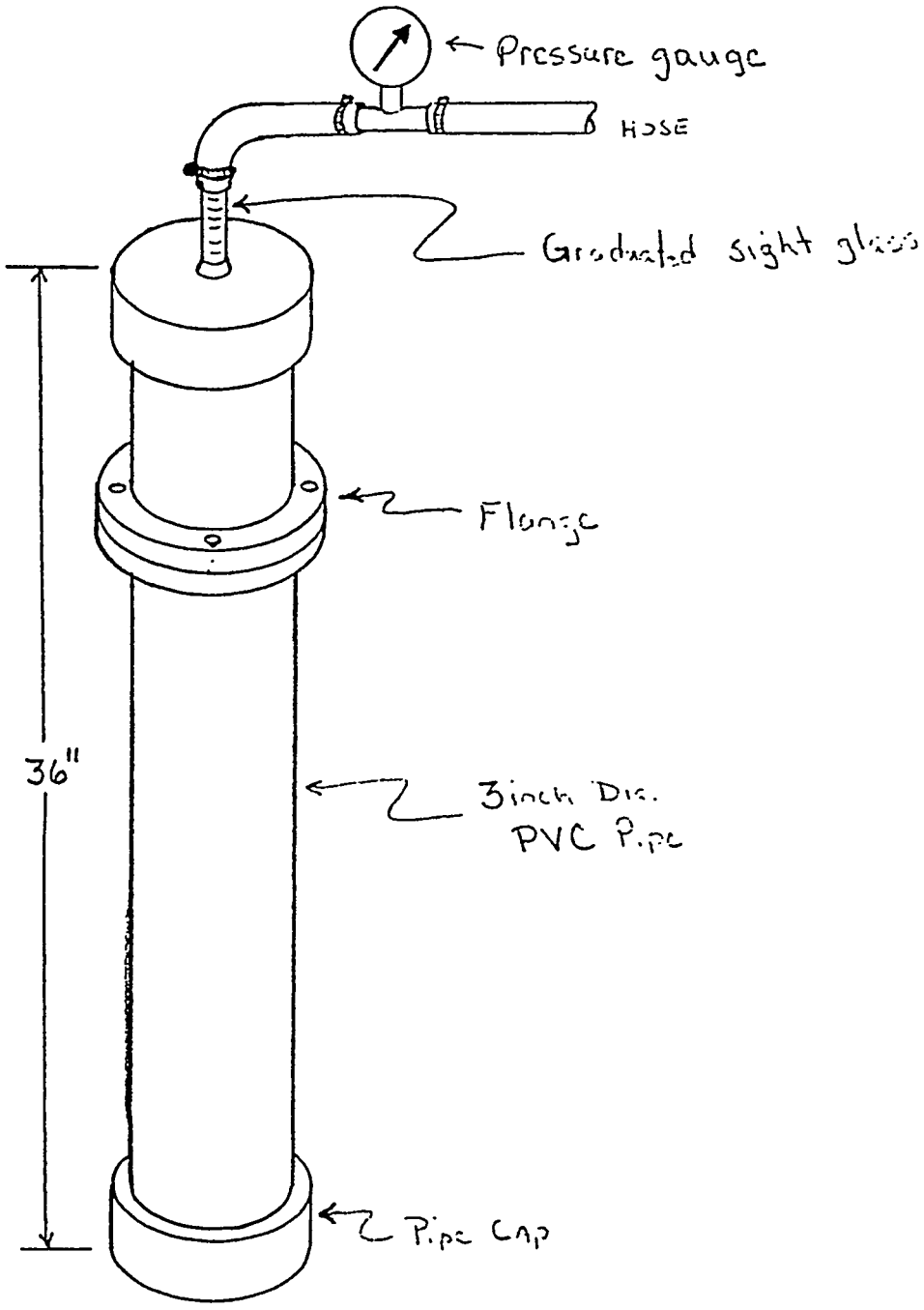


Figure 2: A test chamber



Procedure
for
Establishing LEU Core 2

LEU Core 2 Procedure

I. Description:

Partially graphite reflected (South-west corner). Non-referenced - Operational (see Attachment 2 for core loading map, page 34).

II. Preliminary (data from LEU Core 1 Procedure):

_____ A. Subcritical multiplication data obtained.

_____ B. Critical mass data obtained.

_____ C. Control rod reactivity worth data obtained.

_____ D. Excess reactivity and shutdown margin calculated.

_____ E. Partial element reactivity worth obtained.

_____ F. Primary flow and pump coastdown data obtained.

_____ G. Void measurements completed.

III. Loading

NOTE
Ensure the Daily Checklist is completed prior to the first reactor startup each day that the reactor is to be taken critical from a secured condition.

A. Initial and date each major component listed below as the step is completed.

B. Limit maximum power level to 10^6 cps on main source range with fission chamber completely inserted (approximately 250 watts).

C. Shuffle LEU fuel IAW SOP 5.4.2.C and Attachment 1 (core 2 loading map, page 34).

_____ 1. Desired graphite reflectors and plugs in place.

_____ 2. Control rods moved IAW SOP 5.4.2.D. (if necessary)

III. C. Loading (cont.)

_____ 3. Control rod drop times completed satisfactorily IAW SOP 7.3 (as necessary).

_____ 4. Subcritical multiplication (1/M) data obtained.

_____ 5. Banked initial critical rod configuration rod heights obtained (for critical mass measurement, see Attachment 2, page 35).

_____ 6. Core loaded in desired configuration.

_____ 7. Integral & differential rod worths obtained IAW SOP 7.4.

_____ 8. Core base excess reactivity calculated IAW SOP 5.5.

Base excess reactivity is _____ % Δk/k (< 5.0 % Δk/k).

_____ 9. Core base shutdown margin calculated IAW SOP 5.5.

Base shutdown margin is _____ % Δk/k (> 0.4 % Δk/k).

_____ 10. Non-fixed experiment reactivity values measured IAW SOP 6.5.

_____ 11. Core working shutdown margin calculated IAW SOP 5.5.

Working shutdown margin is _____ % Δk/k (> 0.4 % Δk/k).

_____ 12. Core working excess reactivity calculated IAW SOP 5.5.

Working excess reactivity is _____ % Δk/k (< 5.0 % Δk/k).

_____ 13. Total experimental reactivity worth calculated.

Total experimental worth is _____ % Δk/k (< 2.0 % Δk/k).

_____ 14. Minimum permissible critical rod positions established.

_____ 15. Operational working core established.

IV. Power ascension

NOTE
Ensure the Daily Checklist for **FORCED CONVECTION** is completed prior to the first reactor startup each day that the reactor is to be taken critical from a secured condition.

A. Perform SOP 7.1.5., Primary Heat Balance Calibration.

1. At the low power critical point, less than 10^6 cps, record the following:

_____ a. Critical rod heights

Rod 1: _____ ; Rod 2: _____ ; Rod 3: _____ ; Reg Rod: _____

_____ b. Pool temperature: (_____ ° F)

_____ c. Core Delta-T: (_____ ° F)

2. After reaching 200 kW, increment reactor power increases in 500 kW steps to approximately 2 MW IAW SOP 7.1.5.d

Adjust nuclear instrumentation detector position at each step, so to have nuclear instrumentation agree (-5% to +15%) with calculated heat balance power (see Table 1).

Table 1
Power vs Instrument reading

Power level	Delta T (°F)	Power Range (%)	Intermediate Range (nV)	Linear Range (μA)	Core Gamma (μA)
200 kW	1.285	100**	4 E7	2 E-6	1.85 E-10
500 kW	3.21	25	1 E8	5 E-6	4.62 E-10
1.0 MW	6.22	50	2 E8	1 E-5	9.25 E-10
1.5 MW	9.63	75	3 E8	1.5 E-5	1.39 E-9
2.0 MW	12.85	100	4 E8	2 E-5	1.85 E-9

** in 200 kW position on the Range Switch

B. Shut down the reactor IAW SOP 5.3

V. Power reactivity coefficient measurement

NOTE
Ensure the Daily Checklist for **FORCED CONVECTION** is completed prior to the first reactor startup each day that the reactor is to be taken critical from a secured condition.

A. Perform Power reactivity coefficient measurement IAW *Procedure for Measuring Power Reactivity Coefficient of UVAR*, pg. 37.

VI. Temperature reactivity coefficient measurement

NOTE
Ensure the Daily Checklist for **FORCED CONVECTION** is completed prior to the first reactor startup each day that the reactor is to be taken critical from a secured condition.

A. Perform Temperature reactivity coefficient measurement IAW *Procedure for Measuring Temperature Reactivity Coefficient of UVAR*, pg. 41.

Attachment 1: Core 2 map (example)

Core Loading: LEU-2 ; Date: _____; U - 235: 4944 Grams;

F	Normal Fuel Element	**P**	Grid Plate Plug
PF	Partial Fuel Element	**HYD RAB**	Hydraulic Rabbit
CR	Control Rod Fuel Element	**THER RAB**	Thermal Pneumatic Rabbit
G	Graphite Element	**EPI RAB**	Epithermal Pneumatic Rabbit
S	Graphite Source Element	**RB**	Radiation Basket

REG Control Rod Fuel Element with Regulating Rod

North ⇑

G 11	F VS-001 12	F VS-002 13	F-REG VC 001 14	F VS-003 15	F VS-004 16	P 17	P 18
G 21	F VS-005 22	F-CR1 VC-002 23	F VS-006 24	F VS-007 25	F VS-008 26	P 27	P 28
G 31	F VS-009 32	F VS-010 33	F VS-011 34	F-CR2 VC-003 35	F VS-012 36	P 37	P 38
G 41	F VS-013 42	F VS-014 43	F-CR3 VC-004 44	F VS-015 45	F VS-016 46	P 47	P 48
G 51	G 52	HT 53	G 54	HT 55	S 56	P 57	P 58
G 61	G 62	G 63	EPI RAB 64	G 65	G 66	G 67	G 68
G 71	G 72	THER RAB 73	G 74	G 75	HYD RAB 76	G 77	G 78
G 81	G 82	G 83	G 84	G 85	G 86	G 87	G 88

Loading Approved By: _____ Date: _____

Attachment 2: Worksheet for calculating Critical Mass (Core 2)

List each fuel element placed in core and associated U-235 content (in grams)

Element	Mass	Σ Mass	Banked Rod heights	Banked Height %	C/C_o mass prediction	est. Critical Mass
VC-001						
VC-002						
VC-003						
VC-004						

Banked Height % = Banked rod height/26

Estimated Critical Mass = Σ Mass of the n-1 elements + [mass of the n^{th} element * banked rod height %] (note: valid only when criticality is achieved.

Procedure for Measuring the Power Reactivity Coefficient

Procedure for Measuring the Power Reactivity Coefficient of UVAR

I. Prerequisites

A. This procedure is to be done in conjunction with the normal start up procedure of SOP 5.1.A. Nothing in this procedure requires, or allows for, a deviation from SOP 5.1.A.

B. The UVAR reactor must be in a condition to be brought to full power with no restrictions other than stated in SOP 5.1.A.

C. The UVAR core must not be in a noticeable xenon transient.

D. Reactor pool temperature and Delta-T instruments must be in a valid state of calibration. If other temperature indications are used such as the Systemteknik Temperature system, they must also be in a state of valid calibration.

II. Measurements

A. Take the reactor critical in forced convection with the power low in the indicating range of the Linear Power instrument.

B. Set the critical rod position such that one rod is well into the linear portion of its integral rod worth curve (flat part of its differential rod worth curve) such that an addition of up to 0.222% $\Delta k/k$ (30 cents) of reactivity can be calculated from the linear slope of the rod worth curve.

C. Record the core inlet temperature (pool temperature) and outlet temperature (Pool temperature Plus Delta T). They should be the same temperature. The average core temperature is defined as the average of the inlet and outlet temperatures.

Temperatures: _____ ° F (Pool) _____ ° F (Delta-T)

II. D. Record the critical rod positions and determine which rod is to be used for the rest of this procedure.

Critical rod heights

Rod 1: _____ ; Rod 2: _____ ; Rod 3: _____ ; Reg Rod: _____

E. Establish a period of about 40 to 60 seconds using the selected rod in the linear portion of its integral rod worth curve. Record the rods new position.

Rod heights

Rod 1: _____ ; Rod 2: _____ ; Rod 3: _____ ; Reg Rod: _____

F. Measure the doubling time as if this were a rod calibration. If it is less than 21 seconds (Period less than 30 seconds), insert the rod and return to a low power and try again with a shorter rod pull.

G. If the period is acceptable allow power to rise to the power range. Continue measuring doubling times as power rises until it is apparent that significant negative reactivity is being added to the core as a result of the rise in power.

H. If power reaches 1.8 MW, insert the one rod pulled in step E. as necessary to level power at or below 2 MW.

I. If it is apparent that the power rise will be stopped at less than 2 MW without further rod motion, allow the reactor to come to a steady level power at whatever power results from the negative temperature reactivity balancing the reactivity added by the initial rod withdrawal.

J. Once power is level, record the rod positions, the core inlet temperature (Pool Temperature) and the core outlet temperature (Pool temperature plus Delta-T).

Note:
If final power is not at least 1.5 MW, repeat with somewhat larger reactivity insertion as calculated by using the previously determined power coefficient value.

1. Final power level was _____ ($\leq$ 2 MW).

2. Doubling time was _____ seconds ($>$ 21 sec).

II.D. 3. Final critical rod heights:

Rod 1: _____ ; Rod 2: _____ ; Rod 3: _____ ; Reg Rod: _____

4. Final temperatures: _____ ° F (Pool) _____ ° F (Delta-T)

K. Continue operating the reactor in accordance with SOP 5.2. or shut down the reactor in accordance with SOP 5.3. as the operation schedule dictates.

III. Calculations

A. Determine the amount of positive reactivity added to the core at the beginning of the approach to power by either noting the difference in rod position and using the rod worth curves (either directly reading curves or using slope of curve), or the reactivity vs. doubling time relation (if no rod motion was required to stop the transient.)

B. Determine the average core temperature at the beginning and end of the transient. The average core temperature is the inlet temperature plus outlet temperature divided by two, or the pool temperature plus one half Delta T.

C. The Power coefficient includes moderator and fuel temperature coefficients and treats the entire UVAR core as a unit. The Power coefficient is the change in reactivity divided by change in power. This should be a negative quantity since the temperature rise should add negative reactivity to balance the positive reactivity added by the rod initial rod withdrawal.

Procedure for Measuring the Temperature Reactivity Coefficient

Procedure for Measuring the Temperature Reactivity Coefficient of UVAR

I. Prerequisites

A. This procedure is to be accomplished in conjunction with the normal reactor start up and operating procedures in the Standard Operating Procedures (SOP). Nothing in this procedure allows a deviation from any SOP.

B. The UVAR reactor must be in a condition to be operated at full power with no restrictions other than stated in the SOPs.

C. Reactor pool temperature must be in a valid state of calibration. If other temperature indications are used, such as the Systemteknik Temperature system, they must also be in a state of valid calibration.

D. This measurement should be scheduled for a time when the reactor is not needed at power for several days.

E. The pool temperature at the beginning of section III must be high enough to allow cooling the pool at about 10° F per hour over a temperature span of 10 or 15° F without cooling it below 60° F or more than 20° F. Pre-heating the pool with section II may not be necessary if the pool is already at a sufficiently high temperature to perform section III.

II. Pool Heat-Up (If necessary)

A. Operate the reactor at power in forced convection with the cooling tower fan off long enough to raise the pool temperature to about 100° F. The nominal heat-up rate of the pool is about 10° F per hour. Do not challenge the Pool Temperature Scram at 105° F.

B. Shut down the reactor or reduce power to less than one kilowatt after the heat-up to allow xenon (and iodine) to decay.

C. Avoid operating the cooling system over the next few days. The desired conditions for the next phase of the measurement is to have the pool at a temperature sufficiently high after any xenon transient is over to allow cooling the pool at about 10° F per hour over a temperature span of 10 or 15° F without cooling it below 60° F or more than 20° F.

III. Temperature Coefficient Measurement

A. Allow sufficient time following previous power operations to allow xenon to decay to the point where there will be no significant change in xenon reactivity over the course of a two hour operation. It is anticipated that a shut down over a weekend from a few hour operation should be sufficient, but if longer operations were recently performed, a longer decay period may be warranted.

B. Turn off the secondary pump to prevent cooling the pool until the actual reactivity measurement is performed.

C. Run the primary pump for at least an hour to eliminate any stratification in the pool.

D. Take the reactor critical in forced convection with- the power low in the indicating range of the Linear Power instrument with at least one rod in the level part of its differential rod worth curve.

E. Maintain the reactor critical for 30 minutes, noting any rod motion and pool temperature changes to verify that xenon or other effects are not changing core reactivity

F. Record the pool temperature and rod positions.

Temperatures: _____ ° F (Pool) _____ ° F (Delta-T)

Critical rod heights

Rod 1: _____ ; Rod 2: _____ ; Rod 3: _____ ; Reg Rod: _____

G. Start the secondary pump. After the cooling tower basin has refilled, start the cooling tower fan.

H. Maintain the reactor critical as the pool cools by inserting the rod selected in step D.

III. I. Record pool temperature and rod position as the pool cools and the reactor is maintained critical. If possible allow the pool to cool through at least 10 °F. The nominal cool-down rate of the pool is about 10 °F per hour.

1. Critical rod heights:

   Rod 1: _____ ; Rod 2: _____ ; Rod 3: _____ ; Reg Rod: _____

2. Temperature: _____ ° F
   Pool

3. Critical rod heights:

   Rod 1: _____ ; Rod 2: _____ ; Rod 3: _____ ; Reg Rod: _____

4. Temperature: _____ ° F
   Pool

5. Critical rod heights:

   Rod 1: _____ ; Rod 2: _____ ; Rod 3: _____ ; Reg Rod: _____

6. Temperature: _____ ° F
   Pool

7. Critical rod heights:

   Rod 1: _____ ; Rod 2: _____ ; Rod 3: _____ ; Reg Rod: _____

8. Temperature: _____ ° F
   Pool

9. Final critical rod heights:

   Rod 1: _____ ; Rod 2: _____ ; Rod 3: _____ ; Reg Rod: _____

10. Final temperature: _____ ° F
    Pool

J. Turn off the secondary pump to prevent further cooling of the pool.

K. Shut down the reactor in accordance with SOP 5.3.

L. Turn off the primary pump.

III. M. Turn on the secondary pump.

N. Measure the reactivity worth of the reduction in the pool temperature by measuring the doubling times associated with moving the rod(s) moved in step III.I to their positions in step III.F. in accordance with SOP 7.4.

1. Determine the sequence of rod movement to minimize the use of adjacent rods when making the measurement using data obtained in step III.F and III.I of this procedure.

Note
Rod positions and movement sequence will be different than that suggested in SOP 7.4.B.1.d

2. SOP 7.4.B.3 steps d, e, f, and g are not applicable for this use.

IV. Calculations

A. Determine the amount of reactivity added by the rod during the cooling by noting the difference in rod position and using the rod worth curves (verify with reactivity calculated by doubling time measurements).

B. Determine the drop in pool temperature associated with the rod insertion.

C. The temperature coefficient is the change in reactivity divided by change in pool temperature.

APPENDIX I

HEU TO LEU FUEL CONVERSION REPORT

Design Optimization of a Low Enrichment University of Virginia Nuclear Reactor

A Thesis

Presented to

the Faculty of the School of Engineering and Applied Science

University of Virginia

In Partial Fulfillment

of the Requirements for the Degree

Master of Science (Nuclear Engineering)

by

Mary Katherine Fehr

January 1989

APPROVAL SHEET

This thesis is submitted in partial fulfillment of the requirements for the degree of Master of Science (Nuclear Engineering)

Mary Fahr
AUTHOR

This thesis has been read and approved by the Examining Committee:

Roger A Rydin
Thesis adviser

Albert B Reynolds
Committee Chairman

Kenneth K. Lawless

Accepted for the School of Engineering and Applied Science:

Dean, School of Engineering and Applied Science

January, 1989

ACKNOWLEDGEMENTS

The author would like to acknowledge the contributions of UVAR staff member Dave Freeman whose follow up and support calculations provided much confidence in the work presented here. Many thanks are also due to all of the people who have provided assistance and guidance along the way including (but not limited to): Dr. Roger Rydin, Dr. Robert Mulder, Stuart Wasserman, Bo Hosticka, Pres Farrar, and Vance Hampton (for keeping the Genicom printer going through all of the computer runs done). A very special "no thanks" goes to Roger Johnson for the continual reminder of all of the trees that were sacrificed for this project.

ABSTRACT

The HEU-LEU fuel conversion effort at the University of Virginia for the 2 MWT UVAR reactor was divided into several areas of concentration. This portion was concerned primarily with scoping studies for the neutronics calculations and design. Computer models were created and tested to determine the capabilities of the codes being used with respect to the objectives sought for the UVAR. Three fuel configurations (HEU 18 plate/element curved plate fuel, LEU 18 plate/element fuel, and LEU 22 plate/element fuel) were studied in depth. These studies included the testing of each fuel configuration in each of three core configuration models (4 x 4, 4 x 5, and 5 x 5 arrays of fuel elements). Control rod worths were determined for each fuel configuration for the beginning of life 4 x 4 core, and these compared very favorably with experimental measurements made of the HEU BOL core in 1975. Depletion studies done follow trends set at other institutions, and indicated that the LEU 18 plate/element fuel is nominally a direct replacement for the existing HEU fuel in the UVAR for the 4 x 5 core array, although it maintains a lower excess reactivity throughout its life than does the HEU fueled core. These studies also showed that the use of 22 plates/element in the 4 x 5 array would provide a

considerably longer core life time as well as a generally higher thermal flux than either the existing HEU elements or the LEU with 18 plates/element.

TABLE OF CONTENTS

1. INTRODUCTION 1

1.1 BACKGROUND OF STUDY 1

1.1.1 Purpose of Conversion and Study . . . 1

1.1.2 Characteristics of the UVAR 2

1.1.3 Goals of the Conversion 4

1.2 CODES TO BE USED 7

1.3 VERIFICATION 8

2. PROCEDURE 10

2.1 OBTAINING BENCHMARK CALCULATIONS 10

2.1.1 Documents 10

2.1.2 LEOPARD Model 10

2.1.3 2DB Cell Model 16

2.1.4 2DB Core Model 21

2.1.5 Other Variables 23

2.1.6 Mesh Spacing 24

2.1.7 "Card read" Cross Sections 27

2.1.8 Fine Tuning 28

2.1.9 Verification 31

2.2 THE LEU MODEL 33

2.2.1 Fuel Specifications 33

2.2.2 LEU LEOPARD and 2DB Models 34

2.2.3 Boron impurities 35

2.2.4 22 Plate Elements 37
2.2.5 Results 39
2.3 OBTAINING CORE LIFE CALCULATIONS 39
2.3.1 Methods of Burnup 40
2.3.2 Depletion Cross Sections 41
2.3.3 Control Region Cross Sections 42
2.3.4 Calculation of Uniformly Shuffled Depletion 43
2.3.5 Calculation of Unshuffled Depletion . 44
2.4 CALCULATIONS FOR INCREASED CORE SIZES 45
2.4.1 4 x 5 Core Model 46
2.4.2 Depletion and Results 47
2.4.3 5 x 5 Core Model 48

3. RESULTS AND DISCUSSION 50
3.1 BENCHMARK CALCULATIONS 50
3.1.1 Basic Data 50
3.1.2 Control Rod Worths 51
3.1.3 Beginning of Life k_{eff} 53
3.2 4 x 4 CALCULATIONAL RESULTS 55
3.3 4 X 5 CALCULATIONAL RESULTS 57
3.3.1 Depletion Methods 57
3.3.2 Axial Buckling Trials 59
3.4 5 x 5 CALCULATIONAL RESULTS 62
3.5 ADDITIONAL HEU TO LEU COMPARISONS 63

4. CONCLUSIONS AND RECOMMENDATIONS 68

4.1 CONCLUSIONS 68

4.2 RECOMMENDATIONS 72

5. FUTURE WORK ON THIS PROJECT 74

APPENDIX 77

REFERENCES 80

LIST OF FIGURES

Figure 1. Standard Fuel Element for LEOPARD Input 12

Figure 2. Control Fuel Element for LEOPARD Input, by Region. 13

Figure 3. Control Fuel Element for LEOPARD Input with Lattice and Non-lattice Regions. 15

Figure 4. Standard Fuel Element with Curved Fuel Plates. 16

Figure 5. Control Fuel Element with Curved Fuel Plates. 16

Figure 6. Grid Plate Measurements of Fuel Cell. . . . 20

Figure 7. Standard Curved Plate Fuel Element. 20

Figure 8. Standard Fuel Cell in 2DB. 20

Figure 9. 4 x 4 Core Model. 21

Figure 10. 2DB Fuel Cell with Mesh Spacing. 26

Figure 11. The Effect of Mesh Spacing in the Reflector Region on k_{eff}. 30

Figure 12. 4 x 5 Core Model. 47

Figure 13. 5 x 5 Core Model. 48

Figure 14. Reactivity of 4 x 4 Cores Over Time 56

Figure 15. Reactivity Over Time for 4 x 5 Uniformly Shuffled Cores. 58

Figure 16. Reactivity Over Time for 4 x 5 Unshuffled Cores. 58

Figure 17. Reactivity Over Time for 4 x 5 Cores Using 1st Buckling Approximation. 60

Figure 18. Reactivity Over Time for 4 x 5 Cores Using 2nd Buckling Approximation. 60

Figure 19. Reactivity Over Time for 4 x 5 Cores Using 3rd Buckling Approximation. 60

Figure 20. Reactivity Over Time for 4 x 5 Cores as Calculated by ANL. 60

Figure 21. Reactivity of 5 x 5 Cores Over Time. . . . 63

Figure 22. Thermal Flux Traverse in the Direction Through the Fuel Plates and Through the Peak Flux Value in the Fueled Region. . . . 64

Figure 23. Reactivity of 4 x 4 Cores Scaled to the Life Time of 4 x 5 Cores. 65

Figure 24. Reactivity of 4 x 5 Cores. 66

Figure 25. Reactivity of 5 x 5 Cores Scaled to the Life Time of 4 x 5 Cores. 67

Figure 26. Long Core Experiment. 77

Figure 27. Sample EPRI Core. 78

Figure 28. Ground Floor View of Reactor Face, Pool, and Approximate Position of Core. 79

LIST OF TABLES

Table I. Basic Fuel Element Data. 35

Table II. Control Rod Worths for the 4 x 4 Texas A&M Core and Replacements. 52

Table III. Beginning of life Unrodded k_{eff} for 4 x 4 Texas A&M Core and Replacements. 54

1. INTRODUCTION

1.1 BACKGROUND OF STUDY

1.1.1 Purpose of Conversion and Study The University of Virginia, with support from the Department of Energy (DOE) and assistance from Argonne National Laboratory (ANL), is studying the effects of converting the university's two megawatt swimming pool research reactor, UVAR, to low enrichment fuel. The conversion of almost all domestic, non-power reactors to low enriched uranium (LEU) is part of a U.S. policy [1] geared toward reducing the risk of nuclear weapons proliferation. One of the goals of the Reduced Enrichment Research and Test Reactors (RERTR) program was to develop, test, and promote the utilization of a fuel that had a much lower enrichment of uranium than the standard 90% to 93%. A second goal was to develop a fuel that would be almost a direct replacement, from both a thermal-hydraulic and a reactivity point of view, for the high enriched uranium (HEU) fuel.

The LEU fuel element which resulted from the various goals was one which had a lower enrichment (about 20% U-235), a 15% higher loading of U-235 per element (225 g versus 195 g), a much higher uranium density per element (3.47 g/cc versus 0.69 g/cc), and approximately the same dimensions as the HEU fuel element. The dimensions and

loading of the University of Virginia's fuel plates were chosen to serve as the standard plate for all U.S. research reactors [2]. It should be noted that while all institutions choosing the plate-type LEU fuel will be using the same standardized fuel plate, the number and spacing of these plates within the fuel element will vary between these institutions since their element specifications are different. (Two other options open to U.S. research reactors seeking to convert to LEU are to make use of the SPERT fuel pin or to convert to a TRIGA reactor core, however these options were not studied by Virginia).

1.1.2 Characteristics of the UVAR Throughout the past 28 years, the UVAR has been strictly an experimentally operated reactor. This means that the shape and size of the core as well as the core loading pattern and boundary conditions were easily varied over time as the need arose. Some examples of past core configurations may be found in the Appendix. Each time a new core configuration was loaded, it had to be tested to assure compliance with the Safety Analysis Report (SAR) and Technical Specifications (Tech. Specs.) with respect to excess reactivity and shutdown margin. The number of fuel elements used in a given core would vary between 16 and 27 as the core depleted. Partial elements, those in which every other fueled plate is removed and replaced with an aluminum plate,

were also used. In addition to the standard 18-plate curved plate elements, the UVAR grid plate has been loaded with 12-plate flat plate element cores. Complete cores (of either 18 or 12 plates per element) would have to alternate in some fashion between these two types of elements so that all elements would remain self-protecting. (An element is considered to be self-protecting if it measures 100 R/hr at 1 meter in air.) Given all of this, there has never been a set core loading scheme. The cores were always loaded to meet all of these types of needs, with an attempt to start each new configuration with approximately uniform burnup. Rough burnup records for each element were maintained, and from this, judgement was used to determine which elements would be placed in any given position.

Control is maintained in the core by the use of three boron stainless steel shim rods and one stainless steel regulating rod. Each rod is located within a control rod element. The control elements are positioned in a staggered pattern throughout the central portion of the core so as to allow the emergency core spray system uniform flow access to the entire core, without interference from the control rod drive mechanisms.

The UVAR core is comprised of elements positioned on a grid plate suspended near the floor of the reactor pool.

The grid plate has 64 positions available for fuel elements, graphite elements, and various experimental facilities. These 64 positions are arranged in an 8 x 8 array. The core is moderated by water and reflected by water and/or graphite. Graphite elements are approximately the same size as standard fuel elements, and fit into the grid plate holes in the same way that all the other elements do. Thus, the amount and the arrangement of the graphite around the core is limited by the position, size, and shape of the core, as well as by the capacity of the grid plate. The amount of graphite may also vary as the core burns and new elements are added to the core so that the core will remain within Tech. Spec. limits of operation.

In addition to having water and/or graphite surrounding the core, a variety of experimental equipment might also be placed next to or inside the core at various times and for varying durations over the life of the core. At this time, one face of the core can be used for fixed or removable experimental facilities. Different experimental facilities that have been used over time may be found in core diagrams located in the Appendix.

1.1.3 Goals of the Conversion In addition to the order to convert to LEU fuel, all affected facilities were also asked by the Nuclear Regulatory Commission (NRC) to avoid

making any changes to the reactor, outside of direct replacement of the core, to a minimum. For this reason, the University of Virginia decided to study the new fuel type, and determine whether a simple direct substitution of fuel elements would maintain, reduce, or improve the current level of operation of the UVAR experimental facility. The primary interest was to maintain, as a minimum, the current level of experimental flexibility. If greater flexibility could be gained, that would be desirable, however a loss of flexibility would not be looked upon in a favorable manner by the experimenters at the UVAR facility.

A second point of concern was the (reactor) staff practice of increasing the size of the UVAR core as it burned. At the beginning of core life (BOL), the core consisted of sixteen elements (four of which were control elements), arranged in a 4 x 4 pattern. As the core burned, in order to keep sufficient excess reactivity, full or partial elements would be added. At the present time, the core has 26 elements (including the four control elements). By increasing the core size in order to extend core life, the higher leakages associated with smaller cores and higher average thermal fluxes were sacrificed. Obviously this is not desirable for an experimental facility which relies very heavily on leaked neutrons for its livelihood. It is for this reason that additional studies were done toward

maintaining a more compact core. A 4 x 5 core seemed to be the most reasonably maintainable core, and so this core was studied in detail.

The final major interest for the LEU fuel conversion study was that the new core should be able to accept a wide range of experiments placed on its boundary. These boundaries include conditions that have been utilized with past cores, as well as various potential experimental upgrades. Some of these boundary conditions include: one, two, or three open beam ports at a time; a rotated core allowing for symmetrical control rod placement, with two faces open for removable experimental facilities; and an experimental flux trap within the core.

Since all computations to be done required the use of computer codes for modeling the UVAR core, the computational models had to be benchmarked with experimental measurements. Benchmarking was done by modeling the first 18 curved plate element core utilized in the UVAR (referred to hereafter as the Texas A&M core or just the Texas core), and comparing the modeling results to actual measured results. The Texas core was chosen for benchmarking purposes since it was the only core configuration for which exact values were known for the weights of the individual elements, for the loading of these elements, and for the burnup of these elements.

The Texas core was also probably one of the best documented cores in terms of experimental measurements taken for the purpose of licensing requirements. One final plus for the Texas core was that it was perhaps the "nicest" core that could be used from a symmetry point of view.

1.2 CODES TO BE USED

All modeling was to be done using computer codes that were operational on the University's CDC Cyber 855 mainframe computer. Codes already in operation at UVA included THERMOS, GAMTEC, EXTERMINATOR, and RETRAN. THERMOS is a one-dimensional thermalization code utilizing transport theory for its calculations. It has available slab and cylindrical geometries for description of the cell. GAMTEC is a one-dimensional transport code that is a combination of the GAM slowing down code and the TEMPEST thermalization code. GAMTEC is separable in energy and cylindrical space. EXTERMINATOR is a two-dimensional few-group diffusion theory code. While it does not have the capability of performing depletion calculations, it does have the ability to do modeling of a single element without leakage creating a numerical convergence problem. RETRAN is a thermal-hydraulic analysis code for an entire reactor system.

Computer codes which were received from ANL through the University of Michigan included LEOPARD, LINX, 2DB-UM, and

the PARET package. LEOPARD is a zero-dimensional, slowing down and thermalization, cross-section generating code that has the ability to do cell depletion calculations to obtain these cross sections. Calculations may be done using either two or four energy groups. (At UVA, two energy groups were used in calculations. It was later announced [20] that when using LEOPARD as the cross section generator, the two group calculations were found to be more accurate at predicting the behavior of several small university reactor cores than the four group calculations were.) LINX is a convenient means of transferring the cross sections generated in LEOPARD to 2DB. 2DB, the final neutronics code in the package, is a two dimensional, diffusion theory code used to model the core itself. It allows for input point depletions to be done directly from the LEOPARD table, or it will carry out spatial depletions for the user once given the starting point of the depletion study and the time steps to be taken. It will calculate almost all neutronics parameters of interest. The PARET package is a collection of thermal hydraulics codes.

1.3 VERIFICATION

The verification of the methods used in this part of the project was restricted to the comparison of the effective multiplication factor k_{eff}, and the rod worths for the calculated versus measured benchmark case. Some degree

of verification was also available by demonstrating that the LEU fuel would follow certain established trends. The only trend worthy of note here was that the LEU should be roughly equivalent to the HEU by the end of the core life (EOL) [3]. It is important to note at this time that EOL for the UVAR is not a very specifically defined term because as the core depletes and excess reactivity and flux levels are no longer high enough to support experimental work, more fuel elements are added to the core to keep it going for a longer period of time. It was later determined that the fuel developers considered the EOL for the UVAR to be the point at which a 4 x 5 core no longer had sufficient excess reactivity.

2. PROCEDURE

2.1 OBTAINING BENCHMARK CALCULATIONS

2.1.1 Documents In order to properly model the Texas core, all of the original data for the Texas fuel needed to be found. Since the Texas core was first put into operation in 1975, most of the data was found in files labeled "Texas '75" or "Texas A&M" core and fuel [4]. Almost all of the required blueprints of the fuel plates and elements were found in the blueprint file [5-7], however any that were missing that contained necessary information were replaced by blueprints from the next generation of fuel, known more commonly as TRTR-2 fuel [8-10]. This TRTR-2 fuel was essentially the same as the Texas fuel, so only where necessary, important data was taken from these documents and used as Texas data.

2.1.2 LEOPARD Model Once all of the basic pertinent data (dimensions, weights, loadings, etc.) were obtained, it was possible to create a LEOPARD model [11]. Since LEOPARD is a zero-dimensional code, all of the information that was input to describe the model was done with respect to a basic cell. This basic cell is comprised of everything that a standard element is comprised of, and yet all information about this cell is given in relative values. For instance, in describing the fuel meat itself, all values are given as

either number densities or volume fractions. The cell composition part of the input to the code is broken into four parts. The first part is the description of the fuel meat, the second describes the clad material, the third the moderating agent, and the fourth describes everything else (primarily the structure of the element and anything "extra" in the basic fuel-clad-moderator cell). The first three parts are lumped together and called the lattice region, while the fourth part is referred to as the non-lattice region. The meat region must contain a fissionable isotope, and cross sections are generated for the lattice region using the spectra of this fissionable material. Cross sections are generated for the non-lattice region by using a "borrowed spectrum" from the lattice region. The relative strength of this borrowed spectrum is directly dependent on an input factor referred to as the non-lattice fraction, i.e., the fraction of the basic cell that is in the non-lattice region.

There are two basic types of fueled elements which are dealt with in this study, standard elements and control rod elements (known hereafter as control elements). Thus there are two sets of LEOPARD input decks that are needed to properly describe each different region. First, the input for the standard element will be described, followed by that for the control element.

The composition input is broken up into fuel, clad, moderator, and extra regions. The fuel is made up of either UAl_x-Al alloy or U_3Si_2-Al (in the case of the LEU fuel), and its dimensions set the basic size limits for the rest of the regions. The clad is defined as the aluminum that is immediately on either side of the fuel; it does not include any aluminum that extends beyond the meat edges. The moderator is the water immediately on the outer sides of the clad. Any other water or clad material that extends beyond the edges of the meat, as well as any additional water or box structure on any of the ends, is considered to be in the extra region. Figure 1 gives an idea of the way the model is defined, with region 1 being the fuel-clad-moderator region, and region 2 being the non-lattice region.

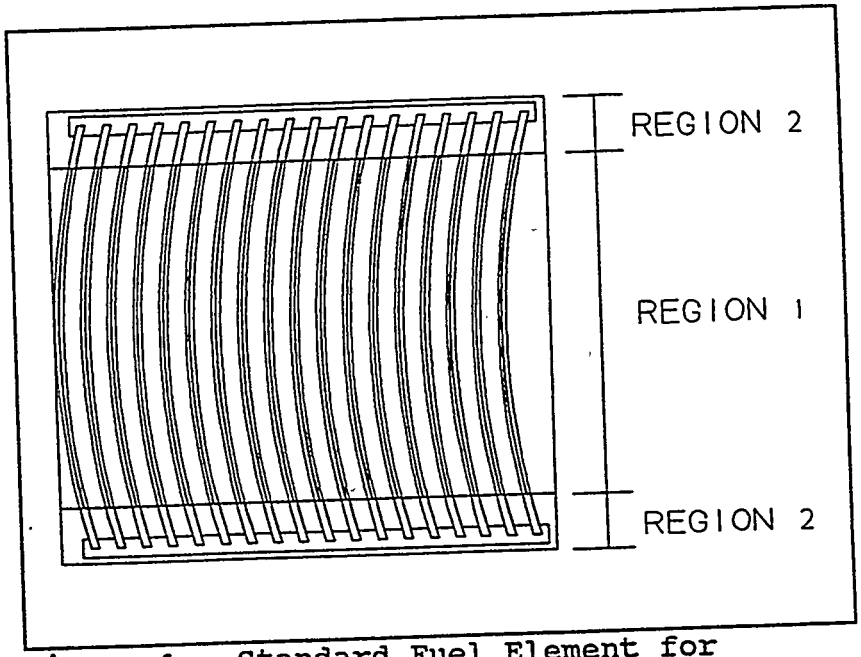


Figure 1. Standard Fuel Element for LEOPARD Input

The control element is the same as the standard element except that half of the total number of fuel plates are removed from the center of the element to make room for the control rod and its guide plates. For this type of element, there are four basic regions (see Figures 2 and 3). The first two of these regions, the fuel and its associated clad and moderator (region 1), and the edge and box structure extra region (region 2) are defined as above for the standard element. The cross sections used are the same as those used above. The other two regions (regions 3 and 4), those corresponding to the first two regions but in the center of the cell, are somewhat different because the fuel plates are now replaced by guide plates, water, and either control rod or control rod water. (Control rod water is taken to be that water which replaces the control rod when the rod is removed.)

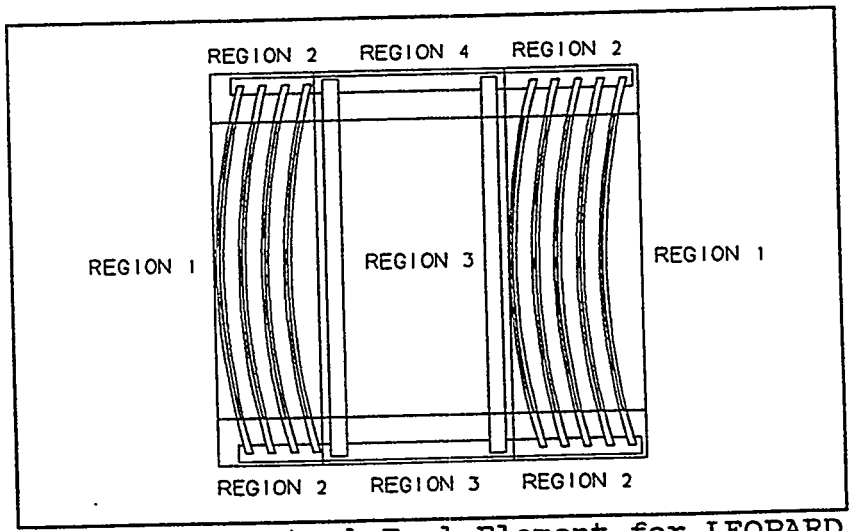


Figure 2. Control Fuel Element for LEOPARD Input, by Region.

Since neither of these two regions, (3 and 4) contains fissionable material, "borrowed" spectra must be used, and thus these are also considered to be non-lattice regions. The size of region 3, the control box, is that which is vacated by the removal of half of the fuel plates, i.e., it extends out to the edges of the meat and is the width of the removed plates with their associated water moderator. This region contains the control rod guide plates and water. (Effective cross sections for this region for the case of a control rod or regulating rod are calculated elsewhere by Wasserman and Freeman [12,13].) The lattice region is as defined above for a standard element, while the non-lattice region is defined by the control box. The non-lattice fraction is thus 50%. The final region of interest, the edges of the control box (region 4), includes the edges of the guide plates and the water between the control box and the side plates of the element, as well as the side plates and extra water within the boundaries as determined by the remaining fuel plates. The aluminum and water volume fractions within this region are very close to those found within the corresponding region for the standard element, and since both must use borrowed spectra, it was decided to use the region 2 non-lattice cross sections generated for the standard element for this region as well.

In summary, the control element is subdivided into

three regions requiring different sets of cross sections. The non-lattice region (region 2) of the standard element corresponds in both size and approximate volume fractions to the edge region of the control element. The fuel regions (region 1) in the two types of element use the same number densities and configuration, and thus both have the same cross sections. The control box (region 3) must be treated separately, and it is designated as the non-lattice region in the control rod LEOPARD calculation. The input buckling was taken to be that value valid for the entire core, and was obtained using an estimated reflector savings based on the transport extrapolation length. The active volume and power, required for depletion calculations, were taken on a per full fuel element basis to give the correct average power density of the core.

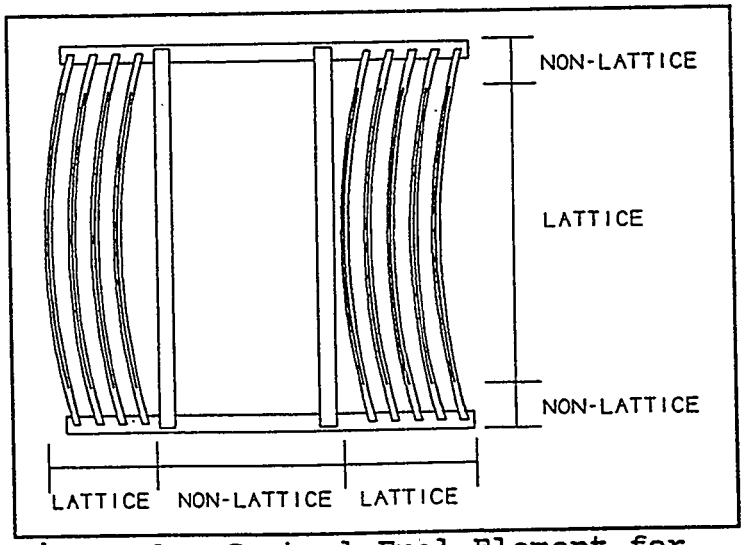


Figure 3. Control Fuel Element for LEOPARD Input with Lattice and Non-lattice Regions.

2.1.3 2DB Cell Model In modeling the fuel cell for the 2DB code [14,15], special care needed to be taken since the 18 plate fuel element was made using curved plates rather than flat plates. (Compare Figures 4 and 5 below with Figures 1 and 2 or 3.)

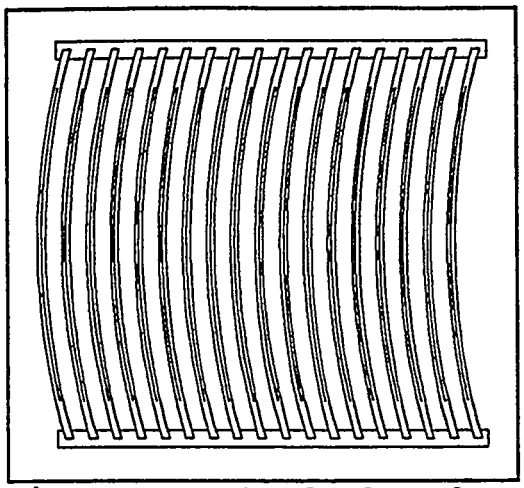


Figure 4. Standard Fuel Element with Curved Fuel Plates.

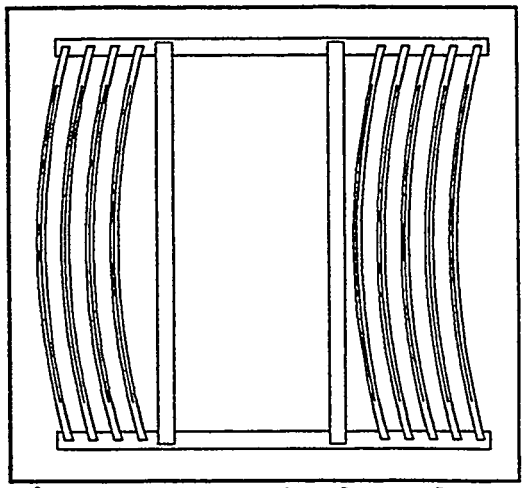


Figure 5. Control Fuel Element with Curved Fuel Plates.

The procedure developed to design the 2DB cell is illustrated below and is based on conservation of area in the two-dimensional cell.

As a starting point, the outer size of the element, and thus the size of the 2DB cell, is given by the "center-to-center" dimensions of the holes in the grid plate which holds the elements. These dimensions were taken from blueprints of the grid plate and subsequently confirmed by actual measurements performed by reactor staff members [16].

In Figures 6, 7, and 8 as well as in the discussion that follows, these dimensions will be referred to as G_x, for the direction through the plates, and G_y, for the direction along the fuel plates (refer to Figure 6). (The axial, or "z" direction is not explicitly used in these calculations.) The area found when G_x is multiplied by G_y is given by A_G. The second "fixed" dimension was taken to be the width of a fuel-clad-moderator ensemble. This is the width of the lattice region in LEOPARD and is the pitch of the fuel plate; it is referred to as L_x in Figure 7 below. The width (L_x) and length, L_y, of the lattice region of the fuel plate may be combined to give A_L, the area subtended by the fuel-clad-moderator ensemble of a plate in the standard fuel element.

The fueled (fuel-clad moderator) region of the element is the single most important region in the model of the cell and core in 2DB, so care is taken to maintain it as unmodified as possible in the model. For a standard, 18 plate element, the lattice region in LEOPARD is given by 18 times the area A_L. Recall that the non-lattice region is defined as everything else in the cell that is not specifically defined as lattice. Thus, the area of the non-lattice region is that which remains when the 18 A_L is subtracted from the area subtended by the grid plate dimensions, A_G. The non-lattice area is given the

designation A_{NL}. (Refer to the equations next to Figure 7.) This area is also maintained in the 2DB cell. (See Figure 8.)

When actual numbers are applied to the above description, it is found that G_x is slightly larger than 18 times L_x. This is due to a small amount of water surrounding each element, and allows for easier movement of an element in or out of the core (as opposed to the fit being "skin tight"). Since it is not practical to actually place water in this very small space in the 2DB model, the concept of conservation of area was used to take care of the problem. To achieve this, the length G_x was divided into 18 equal lengths, each of which was designated L_x'. The area, A_L was then divided by L_x' to give a new length L_y' for the lattice region. Since each L_x' represents the width of one "plate", in order break up the standard cell model so that it might also be used as the control cell model, the plates were grouped into three groupings, one for the control box, and one for the block of fuel plates on each side of the control box. Thus, from the leftmost part of the cell, the divisions are 4 L_x', 9 L_x', and 5 L_x' accordingly.

With the new dimensions now defined (L_x' and L_y') for the 2DB cell fueled region, only the non-lattice structure region of the cell remains undefined. Again, area is

conserved, as the area A_{NL} is divided by G_x to give the width of the modified structure region. This width is then divided by two (one for each side plate structure region). This value is then labeled NL_y' in Figure 8 below.

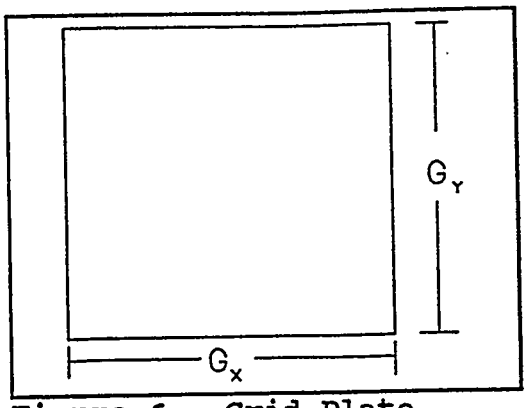


Figure 6. Grid Plate Measurements of Fuel Cell.

$$A_G = G_X * G_Y$$

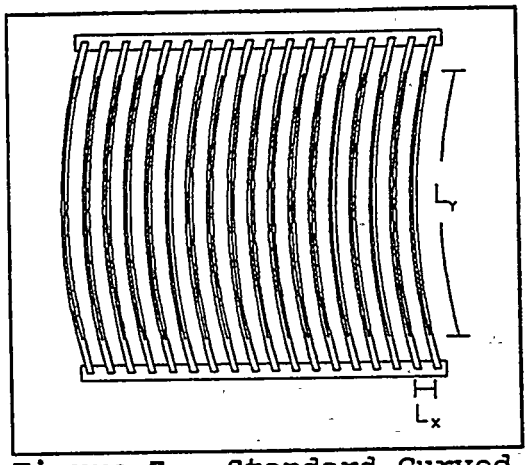


Figure 7. Standard Curved Plate Fuel Element.

$$A_L = L_X * L_Y$$

$$A_{NL} = A_G - 18A_L$$

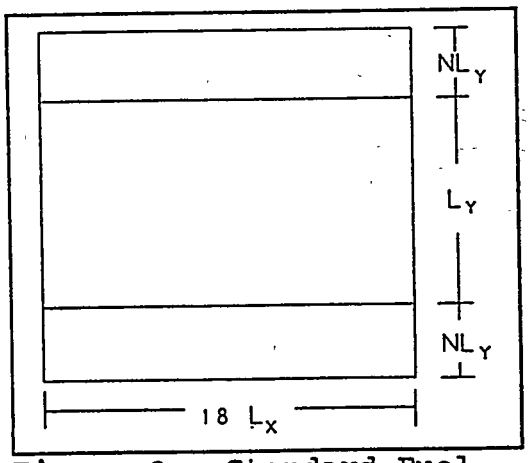


Figure 8. Standard Fuel Cell in 2DB.

$$L_X' = G_X/18$$

$$L_Y' = A_L/L_X'$$

$$2NL_Y' = A_{NL}/G_X$$

2.1.4 2DB Core Model The 2DB core model is made up of reflector material and the appropriate number of basic cells which were developed in detail above. The core itself is comprised of 16 basic cells in a 4 x 4 array. This is then surrounded on all sides by the equivalent of three cells of reflector material. This reflector material is water on the outside of the model, and "canned" graphite [7] on the inner part of the reflector immediately next to the core itself. Figure 9 illustrates the basic configuration of the Texas core model including the relative thicknesses of the two types of reflector material.

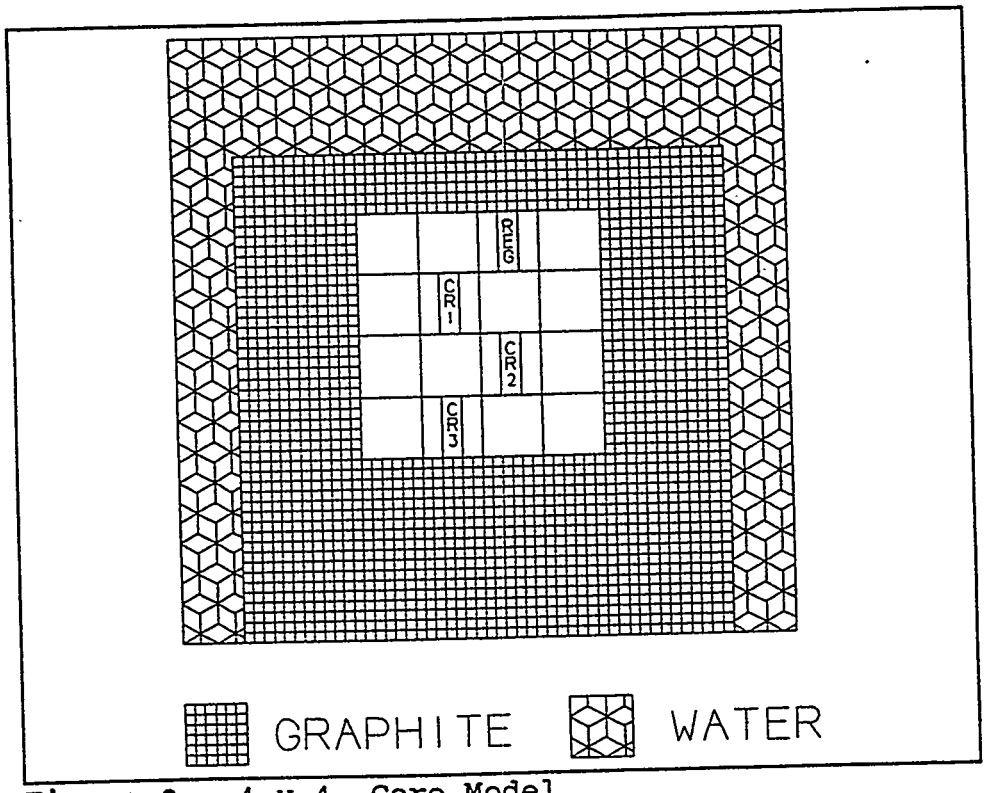


Figure 9. 4 x 4 Core Model.

Since the grid plate on which the core and graphite elements are loaded is an 8 x 8 element unit square, the amount and positioning of the graphite reflector about the core is limited. Of course, less graphite than the maximum amount possible may be used, however this decision is based on the needs of the facility at the time as well as on operational regulations. A lesser amount of graphite around the core may be considered a change in core boundary conditions and thus is not dealt with in this study.

The Texas core is made up of 16 basic cells. A cell is considered to be a squared-up version of an element; the cell takes up the same area as the element, however it is slightly modified so that x-y geometry might be easily used. The fuel cells are divided as indicated above in Figure 8, while an explanation of the mesh spacing appears in Section 2.1.6. All structure regions use the non-lattice cross sections calculated with the standard element in LEOPARD. All fueled regions in both the full fuel element and the control element use the lattice cross sections from the standard element. The center section of the element might contain fuel, a control rod, a regulating rod, or a water hole representing the absence of a rod. Fuel cross sections are obtained from the lattice region of the standard fuel element. Effective control and "reg" rod cross sections were obtained from work done by Wasserman [12] and Freeman

[13]. Cross sections used for the water hole were those obtained as non-lattice cross sections in the control fuel element.

2.1.5 Other Variables The majority of the input into the 2DB code either describes the model of the core or gives instructions to the code about the types of calculations and output that are desired. Exceptions to this include such information as the power modifier, the volume involved, and the axial buckling of the core. Most of these are simply basic calculations that require nothing more than plugging in the appropriate numerical values when required. An exception to this statement is the case of the axial buckling. For this, as a first approximation, an extrapolation distance of 4.5 cm was added to each end of the active core, and the axial buckling calculated as usual. The value of 4.5 cm may most correctly be referred to as a judgement call since there are no well documented values to be used in this case. This value was found to be approximately what was required for the 2DB results to match experimental results, and it seemed to be approximately that determined by J. L. Meem in his two-group calculations for the original UVAR [17]. It was later determined that use of an incorrect definition of reflector savings contributed to this (mis)matchup between Meem's value of 8.65 cm_2 for reflector savings to be added to the height of the core at

both ends and the value of 4.5 cm used in the calculations. Sensitivity studies were done using a variety of values for the axial buckling, and it was determined that there was essentially a linear relationship between axial buckling and k_{eff}. Thus it may be used as something of a scaling factor.

The second axial buckling approximation took into consideration the problems discovered with the first approximation, and thus a value of 7.8 cm reflector savings was used. This value agrees fairly well with values determined by ANL using three-dimensional analysis of the UVAR [3], as well as with the value obtained at UVA using an RZ model of the core, and it is not too far off from Meem's "basic principles" hand calculations.

2.1.6 Mesh Spacing Determination of the mesh spacing to be used in the 2DB model was rather simplified by the original design of the basic cell. Since 2DB is a diffusion theory code, it was not desirable to have the mesh spacing be widely varying in nature. As an upper limit, the mesh sizing needed to be internally consistent in the x and y directions, and it needed to follow the various boundaries imposed by the basic cell (e.g., the non-lattice region and the control rod region). As a lower limit, ultimately, practicality of calculation time was the only limiting factor.

The decision of mesh space sizing was made fairly early in the modelling process. Since it was decided that at a later time it would be desirable to be able to move the control elements to other positions in the core model, the mesh spacing for the standard elements was chosen to be the same as that for the control elements to ease this modification. For this reason, the spacing utilized will be described in terms of the control element, with the standard element being a subset of this.

In the "y-direction" (along the plates of the element), six mesh spaces describe the element. Two of these spaces are for the non-lattice region (one at each end of the cell). The remaining part of the element (the lattice region) is divided equally between the other four mesh spaces. This is illustrated in Figure 10 below.

In the "x-direction" (through the plates of the element), eight mesh spaces were used. Since the control rod and its structure take up half of the element in this direction, half of the mesh spaces are devoted to it. (In the case of the standard element, these spaces are occupied by fueled plates.) The remaining four mesh spaces are divided between the plates on either side of the control region, two on each side. Given the physical description of the element in the x-direction, it is easily seen why the

decision was made to have the number of mesh spaces for this region be a multiple of four. Four mesh spaces seemed too few (especially in light of the fact that there would be only two describing that direction in the control region), and eight mesh spaces made the dimensions of a square mesh space a lot more compatible with the dimensions describing this region in the y-direction. (In this way, the spacing was relatively similar in the x and y directions. Any great differences would have been inconsistent with the basic requirements of diffusion theory.)

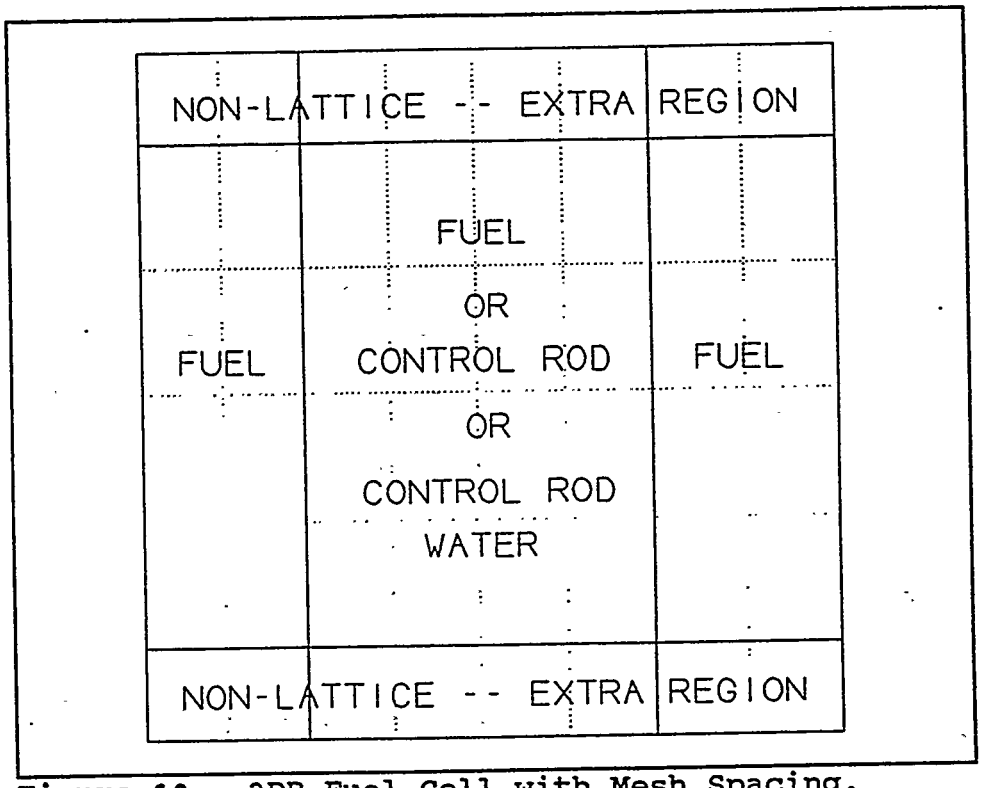


Figure 10. 2DB Fuel Cell with Mesh Spacing.

Since the cross sections for the control rodded region were determined using a combination of transport and

diffusion theory codes, and in general were calculated in a much different manner than the other cross sections used in the 2DB code, great care had to be taken to assure that the mesh spaces were comparable in each case. This was perhaps one of the strongest reasons for the choice of mesh spacing.

2.1.7 "Card read" Cross Sections Cross section values that were not able to be transferred to 2DB via LINX were required to be input by hand as "card" input. Most of the card read cross sections were not able to be calculated in LEOPARD due to the lack of any fissionable isotopes in the region of interest (the exception to this being the calculation of the cross sections in the control box region done as a non-lattice region in the control element run of LEOPARD). There are five sets of card read cross sections in the 2DB input. The five sets are comprised of reflector water, reflector graphite, control box water, control rod, and regulating rod cross sections.

Four of the sets of cross sections had to be calculated using methods other than LEOPARD for their generation. The two types of reflector material were in this category due to the lack of fissionable isotopes present within them, while the two types of rod material required transport theory to appropriately model the strong absorber. For the canned graphite (a graphite block placed in a sealed aluminum

container), appropriate proportions of graphite, air, aluminum, and water (between the elements) were determined, and this information was used as input into the code GAMTEC. The output cross sections from GAMTEC were then used in the 2DB core model. Cross sections for the reflector water might have been similarly obtained, however they were instead received from ANL [18]. These water cross sections were calculated using the code EPRICELL. The calculations for the rods were done at UVA using THERMOS, GAMTEC, and EXTERMINATOR by Wasserman and Freeman. Canned graphite cross sections for the reflector region were also available from EPRICELL [19], but were not used in these calculations since they were essentially the same as those obtained and already in use at UVA.

2.1.8 Fine Tuning The number of cells of reflector material surrounding the core was chosen to be three on all sides, and this decision was based initially on a judicious guess. Having approximately nine inches of reflector surrounding a core that was approximately twelve inches wide in each direction seemed adequate at the time. It was later learned that other people involved in these same calculations at other institutions were using similar thicknesses of reflector material for comparable sized cores, and therefore the decision was upheld [20]. Of course the final decision lay in whether the addition of any

additional amount of reflector material would change the output results of the code. (If the k_{eff} calculated by 2DB with the original thickness of reflector material was the same, or approximately so, as that calculated using a larger thickness of reflector material, then the original amount was taken to be adequate.)

Once the reflector thickness to be used in calculations was finally decided, the mesh spacing in those reflector cells needed to be determined. Since there was no real idea as to what the appropriate spacing should be, it was decided to model a basic core and run several cases of this same model, altering only the size of the reflector mesh in each case. The resulting k_{eff} was then plotted against the number of spaces in the reflector region in the outward direction. This plot is presented below in Figure 11.

As can easily be seen from the plot, the value of k_{eff} is affected very strongly by the size of the mesh spacing when that spacing is very large. The mesh spacing was chosen to be that spacing at which point k_{eff} was no longer appreciably affected by changes in the spacing. According to the plot, k_{eff} is not affected much by using more than six or seven equal sized mesh spaces in the reflector region. Since the three reflector cells could most conveniently be divided into six mesh spaces (two spaces per direction per

reflector cell), this option was chosen over the seven meshes per reflector distance.

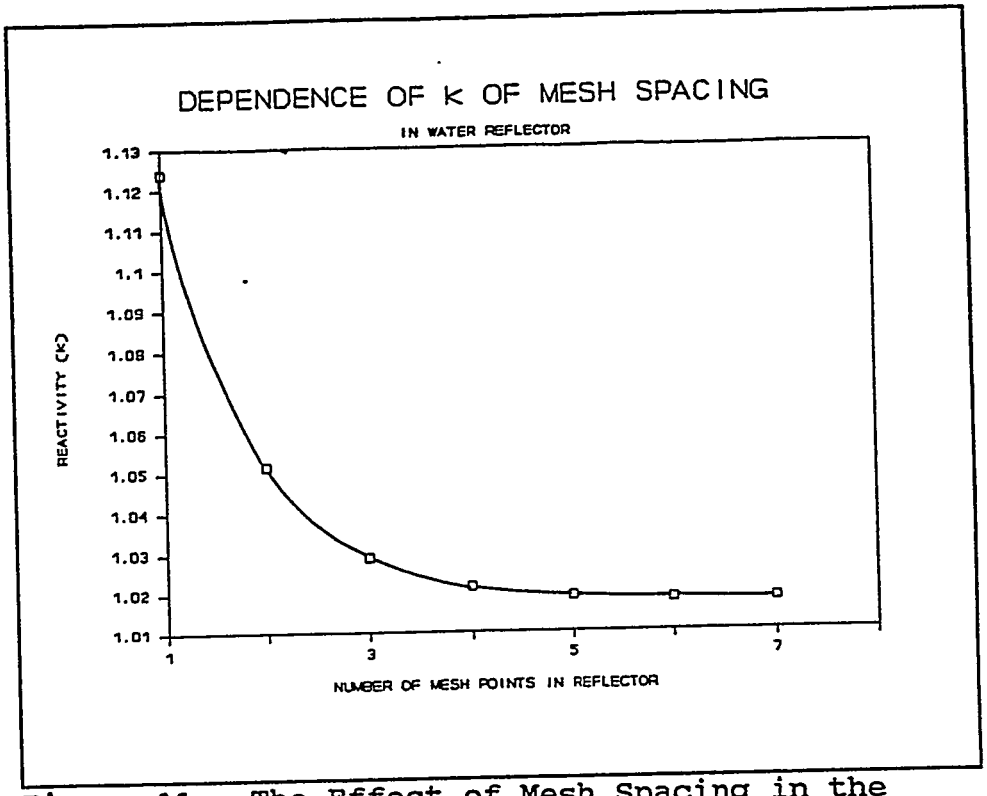


Figure 11. The Effect of Mesh Spacing in the Reflector Region on k_{eff}.

As discussed in the preceding paragraph, it was determined that, for any given direction, two mesh spaces per reflector cell (total of six for the region) were sufficient to describe the reflector region. Due to a misunderstanding between two of the project participants, a model was made utilizing six mesh spaces per cell (rather than per region). Since this smaller spacing allowed for more accurate mapping of the flux in the reflector region (where the thermal flux peak was assumed to occur due to the high amount of leakage from this small core), and yet did

not significantly increase the cost of the calculations, it was permitted to remain throughout the remainder of the study. (Ultimately, due to sheer amount of calculations being done by the code, and since it had already been determined that two mesh spaces per cell were sufficient, the reflector region was modelled such that the inner two reflector cells were split into six mesh spaces each, while the remaining (outer) cell had three mesh spaces. This decision was also justified since the reflector in the rows farthest from the core has relatively very little effect on what happens in the core, and thus, mesh spacing there is not so critical.)

2.1.9 Verification In order to verify the benchmarked case, it was determined that delta k (the difference in k between the all rods in and the all rods out cases) and rod worths (delta k for each rod) would be calculated and compared with measured values. Since 2DB deals only with a two dimensional core model, a control rod may be considered to be either in or out of the core, and partial insertions cannot be accurately calculated. Given these restrictions, delta k and rod worths could not be calculated in even approximately the same way as obtained experimentally with an actual core, yet they have the same meaning as the values obtained by measurement and thus may be compared.

The radial peaking factor is the final item to be found

and used for verification purposes. This factor is calculated in this study, but is not utilized here. Rather, it is used as input into the thermal-hydraulics study. The thermal flux radial peaking factor is defined as the highest flux found in the fueled region of the core divided by the average flux in the fueled region of the core.

Of actual interest is the power production peaking factor, however this value is not directly available from 2DB while the thermal flux peaking factor is. In order to obtain the appropriate peaking factor value for later calculations, an assumption was made that the macroscopic fission cross-section is constant, or approximately so, over the entire core and that power is directly proportional to this macroscopic cross section times the thermal flux. Thus, thermal flux is proportional to power, and the power production peaking factor is equal to the thermal flux peaking factor.

This definition of thermal flux peaking factor is careful not to include any fluxes found in the control regions, the structure regions, or the reflector regions since power is not generated there and thus inclusion of these regions would not produce an accurate power factor. 2DB automatically calculates a flux map of the entire core, providing a flux value for each mesh space. A careful study

of this map, including outlining regions to be avoided, gives the peak flux value for the core.

The average value for the core is obtained through the use of an edit. An edit provides a relatively large amount of information including fluxes for each region in its definition. Since it is desired to obtain an average flux over all of the fuel in the core, an edit is required such that all of the fuel in the core is in one region, and nothing else is included in that region. The remaining regions of the edit may be designed to include other sections of the core as reason dictates, the only restraint is that the entire core model must be included within the edit.

2.2 THE LEU MODEL

2.2.1 Fuel Specifications Following the completion of the benchmarking process, the next core to be modeled was essentially a duplicate of the Texas core, only the new core used LEU fuel instead of the HEU fuel of the Texas core. (It should be noted here that all of the LEU models described in this study at UVA use curved plate elements so that a direct comparison might be made with the 18-plate curved plate HEU elements.) The LEU fuel was composed of U_3Si_2, with the uranium content being 19.75% enriched uranium-235. The LEU fuel plate is the standard plate

adopted for this conversion effort by all facilities choosing to convert to plate type fuel. The standard plate is based on, and has the same outer dimensions as the UVAR HEU plate that was considered in the benchmark calculation. The information regarding the dimensions of both the fuel and the plate as well as the actual loading of the plate was all determined at a meeting at ANL attended by many of the facilities involved in the conversion and the ANL representatives of the RERTR program [2]. Other required information was obtained from TRTR documents, and again, Texas core blueprints were used as needed.

2.2.2 LEU LEOPARD and 2DB Models The LEOPARD cell model and the 2DB core model were defined in the same manner as was used for the Texas core. Some modifications to input values were required due to the different fuel type and the slightly different meat dimensions. The meat thickness remained the same, however the length and width changed slightly. Table I [2,5,6,8-10,21-23] gives all pertinent basic information for both the HEU and the LEU fuels. The change in the width of the meat affected the size of the lattice and the non-lattice regions, and the change in the length of the meat in the plate had its strongest effect on the axial buckling in 2DB.

Table I. Basic Fuel Element Data.

DESCRIPTION	HEU-18	LEU-18	LEU-22
Dimensions (inches)			
Active Length	23.5	23.25	23.25
Width	2.375	2.395	2.395
Depth	0.02	0.02	0.02
Plate Length	24.625	24.625	24.625
Depth	0.05	0.05	0.05
Active Volume($in.^3$)	1.116	1.114	1.114
U-235/element (g)	192.3*	225	275
U-235/plate (g)	10.68	12.5	12.5
U-238/plate (g)	0.81	49.84	49.84
U-234/plate (g)	0.0	0.317	0.317
U-236/plate (g)	0.0	0.633	0.633
U-235 loading (%)	92.92	19.75	19.75
Water Gap (in.)	0.122	0.122	0.091

* NOTE: This is the actual value for the approximately 1% burned fuel as reported by and received from Texas A&M in 1975.

2.2.3 Boron impurities Much of the aluminum used in the fuel elements is not considered to be pure aluminum [21-24]. In general, the two types of aluminum used are

classified as Al-1100 and Al-6061, with the 1100 being essentially pure aluminum and the 6061 having a variety of impurities. (For the purposes of this project, any substance present in the Al-6061 that is not pure aluminum is considered to be an "impurity", even if its presence is intentional.) Some of the "impurities" are actually alloying materials added to the aluminum, while others of the impurities are the result of the fabrication processes used. For calculational and design purposes, the impurities are combined to give a "boron equivalent" impurity. This is done when dealing with reactors since boron acts as a poison and will thus have an effect on the operation of the reactor. By referring to the impurities by their boron equivalent, their effect on operation may be fairly accurately determined.

For calculational purposes, aluminum 1100 is considered to have no boron equivalent impurities, while the level of impurities in the 6061 varies according to when and under what conditions it was manufactured. For these calculations, the 6061 in the HEU elements is considered to be more pure than that in the LEU elements. For the HEU elements, a value of 10 parts per million (ppm) was used. This value is considered to be an upper limit, however a more accurate value could not be easily obtained since it is difficult to accurately measure amounts less than this. For

the LEU elements, a value was difficult to obtain since the manufacturers were only given an upper limit of 30 ppm. Based on studies done, ANL suggested a value of 20 ppm be used for these calculations [3]. Even a value such as this is probably higher than what is actually found in the aluminum, however it was suggested as a fairly intermediate value between the probable and the upper tolerable limit.

Referring now to the LEOPARD cell description in section 2.1.2, for the HEU element, all aluminum in the fuel meat as well as all clad material is taken to be aluminum 1100, while all of the structure material (that in the extra, non-lattice, region) is considered to be 6061 aluminum with 10 ppm boron equivalent impurities [5,6]. The LEU element is similar, however, instead of the clad material being 1100 as for the HEU element, it is 6061 aluminum [3]. All 6061 aluminum in the LEU element is considered to have a boron equivalent impurity of 20 ppm.

2.2.4 22 Plate Elements In order to realize one of the goals of this conversion (that of maintaining a smaller core), something other than a direct replacement with the 18 plate per element LEU fuel had to be pursued. Two basic options lay open: increasing the amount of LEU in some of the plates in an element, or increasing the number of plates in each element. This latter approach was opted for after

the manufacturers announced that they would not make available fuel plates with a higher LEU loading. Since the Europeans were using elements with 24 plates each, it was determined that it might be feasible to add to the number of plates in the elements for the UVAR [3]. ANL suggested that 23 plates per element was the most that should be attempted, so for primarily symmetry reasons (wanting to maintain an even number of plates), a 22 plate per element configuration was chosen for study.

In the early stages of this study, a 20 plate per element configuration was also studied to see if it might be a viable alternative to the 18 or 22 plate options. This option was subsequently dropped in favor of the 22 plate per element option with the reasoning that with more plates in the element, the element would have a longer lifetime. Longer element lifetime preserves the experimentally desirable more compact core, while also requiring a lesser number of elements for a set time period. This latter reason is an economics one which should appeal to the Department of Energy, who pays the fuel bill.

The models for the 22 plate per element cell were similar to those using 18 plates. The only difference as far as the codes were concerned between the 18 an 22 plate elements was that in increasing the number of plates, the

amount of water between the plates was decreased. This difference manifested itself only in the LEOPARD models, since it affected the pitch of the plates and the water to aluminum ratio in the extra (non-lattice) region. Since it was not known exactly how the plates and moderator would be divided about the control rod in the control elements, the 2DB cell remained divided the same way as it had been for the 18 plate case. This lack of exactness is irrelevant once the control cell is placed in the core model along with standard cells.

2.2.5 Results The attainable results for these models include the k_{eff} (or % $\Delta k/k$, where this is equal to $(k_{eff}-1)/k_{eff} * 100$) for the case of no control rods, the delta k (rods in to rods out cases) using control rods, the worths of the control rods, and the radial peaking factors for the rodded and unrodded cases. LEU rodded cores were not calculated in this section of this project, thus these results will not be given here. Radial peaking factors were determined for some of the cases run, however since determination of these was not an objective of this part of the study, they shall not be presented here. The unrodded k_{eff} values and plots will be presented for both the 18 and 22 plate per element core models.

2.3 OBTAINING CORE LIFE CALCULATIONS

2.3.1 Methods of Burnup Throughout the life of the UVAR, attempts were made to build cores in which each of the elements had been burned to approximately the same degree. Weight factors were assigned to each of the positions in the core. These factors, when combined with the records of how long and when each element was actually in the core, were used to determine the burnup of each element. None of this was very exact since the weighting factors were only estimated and the cores were actually built and added on to until a reasonable excess reactivity was obtained using the elements available.

The best approximate method of calculating the burnup history of the UVAR up to this time may be referred to as a perfectly (uniformly) shuffled burn. In this method, the elements are shuffled such that they all have the same burnup at the start of a time step. This shuffle is externally forced on the system rather than allowing 2DB to do the shuffle itself. Using this method, 2DB is run for each time step, and each run is totally independent of all of the others.

A second method used for calculating core lifetime did not utilize any shuffling at all. This method used the capabilities within 2DB to determine depletion and burnup. Although no effort was made to approximate the actual burnup

patterns of the UVAR using this method, it was done so that a more accurate idea could be obtained of how the HEU fuel compared with the LEU-18 and LEU-22 elements.

2.3.2 Depletion Cross Sections The first step in doing depletion calculations was to determine how many time steps were desired and how big each of these steps should be. The rationale for the limits that were actually chosen shall be presented below. Once the desired time steps were determined, this information was entered into the LEOPARD input deck as per the LEOPARD input manual instructions. LEOPARD calculated cross sections for each time step, and at the end of each, reported the time that had passed and the amount of burnup that had occurred by the time of that step. The amount of burnup was given in three forms, megawatt days per metric ton uranium (MWD/MTU), percent of uranium burned, and percent uranium-235 burned. Since the primary idea at this point was to compare the lifetimes of the HEU, LEU-18, and LEU-22 fueled cores, when depletion was plotted over time, the burnup amount in MWD/MTU had to be used due to the differing amounts of uranium present from the outset of the core life. (Note that this was only important for the perfectly shuffled cores as will be explained further in section 2.3.4.)

Once cross sections were calculated for each desired

depletion step, they were transferred to 2DB via LINX. Methods for using LINX for the transfer of cross sections which were not depletion oriented were not found. When calculations of an undepleted core were desired, a small number of time steps was designated and a run of 2DB was made using the method of perfectly shuffled burn for the single (initial) time step. When approached from this manner, the LINX program could be used to transfer cross sections to 2DB. A second means for attaining the same end is discussed in the following section.

2.3.3 Control Region Cross Sections At this time it is important to point out that only the fueled regions and their non-lattice regions were permitted to deplete, i.e., the cross sections for the control water remained constant throughout the life of the core. This policy was followed since burnup cross sections were not attainable for the control rods as obtained by Wasserman and Freeman, and thus it would have been inconsistent to use burned values for the control water and not for the control rods. It was for this reason that the control region cross sections were chosen to be "card read cross sections" as discussed in section 2.1.7, as this was the only means of permitting the rest of the core to burn while the control rod region (non-lattice region 3 in Figure 2) remained unchanged over time.

2.3.4 Calculation of Uniformly Shuffled Depletion The uniform shuffle technique relies entirely on the LEOPARD generated cross sections for its depletion. For this method a separate 2DB run was made for each time step desired, and each run differed only in the initial amount of burnup entered in the input deck. (This value was that MWD/MTU value discussed previously.) One of the options within 2DB is a choice of what type of search and output is desired. For core life calculations, the desired calculation was a determination of k_{eff} for the given set of input parameters and situation. Therefore, at the end of each run the corresponding calculated k_{eff} was given. This value was tabulated for each burnup step and for each type of core, and then plotted over time to allow comparison of the cores. (These plots are presented later along with the other results of this study.)

When determining the size of time step to take for this burnup method, a bit of foresight was called for. The goal was to compare plots of k_{eff} over time for the three types of cores (HEU, LEU-18, and LEU-22), thus each time step chosen could represent a point on the plot. Since the core lifetime (for a fixed size core) is determined by how long it can remain critical ($k_{eff}>1$), it was this limit that was used to determine how long the core was permitted to burn.

Additional output that was requested from the 2DB runs was a mapping of the (thermal and epithermal) flux values throughout the core. Comparison of two dimensional plots of this data for the different cores over time would indicate how the flux and power levels changed. Another useful bit of information from this data was the determination of the radial peaking factor for each core.

2.3.5 Calculation of Unshuffled Depletion The method of unshuffled depletion relies on a combination of LEOPARD and 2DB for depletion calculations. As with the uniformly shuffled depletion method, LEOPARD calculates depletion cross sections. That however is where the similarities end. For this method 2DB relies on the number and size of time steps put in its input deck, as well as the initial amount of burnup present at the start of the run. One run will generate calculations for each burnup step requested in the input deck. The only restriction is that since 2DB gets the required cross section values from LEOPARD (interpolating for values that were not specifically calculated), the values generated in LEOPARD must be able to support the complete depletion requirements of 2DB. The primary requirement is that enough values be calculated to cover the amount of depletion time over the entire core in 2DB. A practice followed in this study, while not required, but which allowed for less error in interpolation, was to make

the time steps within LEOPARD very similar in size to those requested by 2DB. This practice also came in handy when the two depletion methods were compared (for this purpose, the depletion steps in 2DB were made identical to those in the perfectly shuffled depletion steps of LEOPARD).

As with the uniformly shuffled model, cross sections were transferred via LINX (with the exception of the afore mentioned "card read cross sections"), and similar 2DB output was requested. Also, tables and plots of k_{eff} over time were made and these in turn were compared with each other as well as with corresponding data from the other depletion method.

2.4 CALCULATIONS FOR INCREASED CORE SIZES

All of the core models described up to this point have been cores that are four elements wide by four elements long (4 x 4). Since UVAR cores tend to grow in size as they are depleted up to and beyond a 5 x 5 core, these larger cores needed to be considered in following core lifetimes. Two basic larger core designs were made, these were a 4 x 5 model and a 5 x 5 model. It is important to note that while the 4 x 4 core model was based on the original Texas A & M design of 1975, the larger core designs are not based on any particular former core configuration, rather, they are sort

of idealized cores generated only for the purpose of these comparison calculations.

2.4.1 4 x 5 Core Model The 4 x 5 core model (Figure 12) is a basic takeoff from the 4 x 4 core model; it was generated by modifying the existing 4 x 4 model in LEOPARD and in 2DB. In LEOPARD, the modifications were limited to the new total buckling value, a larger value for the active volume of the element, and a lower power per element factor. These latter two values are used when the code calculates depletion.

The modifications in 2DB were a good bit more detailed. In the model of the core itself, a row of graphite had to be removed so that the new row of elements could be added. (Since there are only a given number of positions on the grid plate in the core, and each of these positions is considered to be occupied by either elements or graphite in the models, in order to add something, something else must be removed.) Also, to maintain the three cell amount of reflector surrounding the core in the model, an extra row of reflector water had to be added to the core model.

The dimensions, mesh numbers, and region number designations all had to be modified to generate the larger core model from the basic 4 x 4 model. Cross sections and

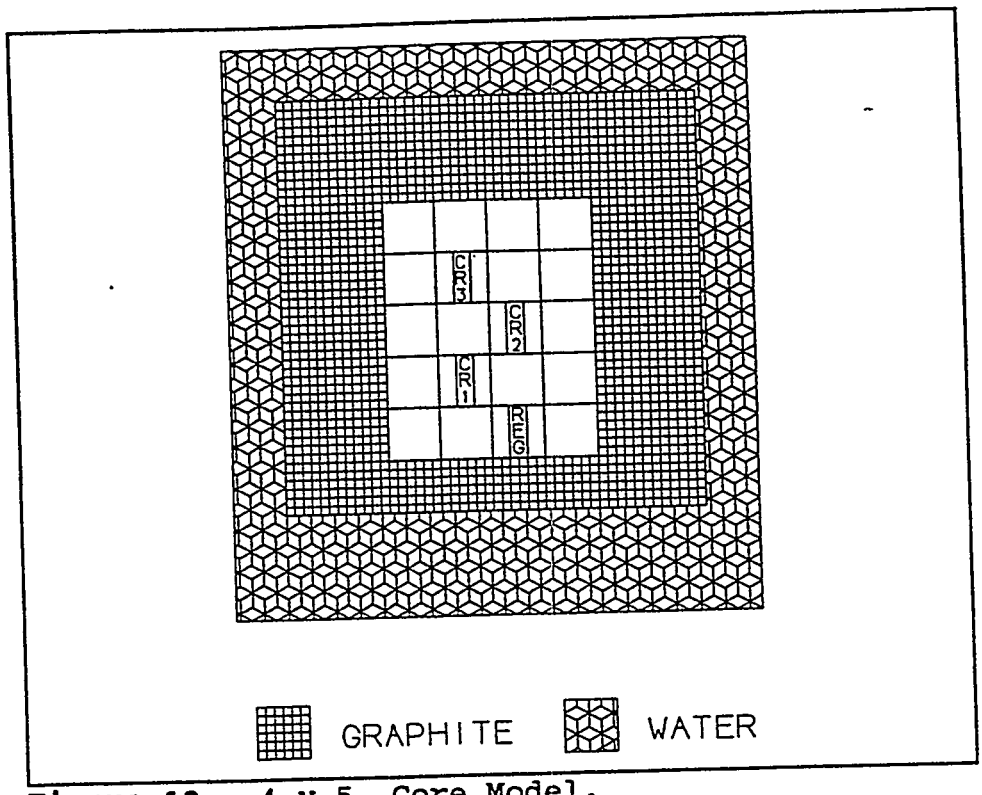


Figure 12. 4 x 5 Core Model.

burnup data (for the uniformly shuffled cores) were also in need of modification for the new core size. (These values needed to be modified since the increased core size affected the power density in the core, which in turn directly influenced the burnup calculations for the cross sections.)

2.4.2 Depletion and Results Burnup calculations were carried out utilizing both of the depletion methods used in the smaller core study. As before, plots were made (and will be presented) indicating the trends of the excess reactivity throughout the life of the core, and core flux maps were obtained through 2DB output.

2.4.3 5 x 5 Core Model The 5 x 5 core model (Figure 13) was developed in the same way as the 4 x 5 model, with the exception that it used the 4 x 5 model as a base case (as opposed to the 4 x 4 model). Again, a row of graphite was removed and replaced with a row of standard fuel elements such that the core was a 5 x 5 array of fueled elements. An additional row of reflector water was added to the side from which the graphite was removed to maintain the same thickness of reflector around the core.

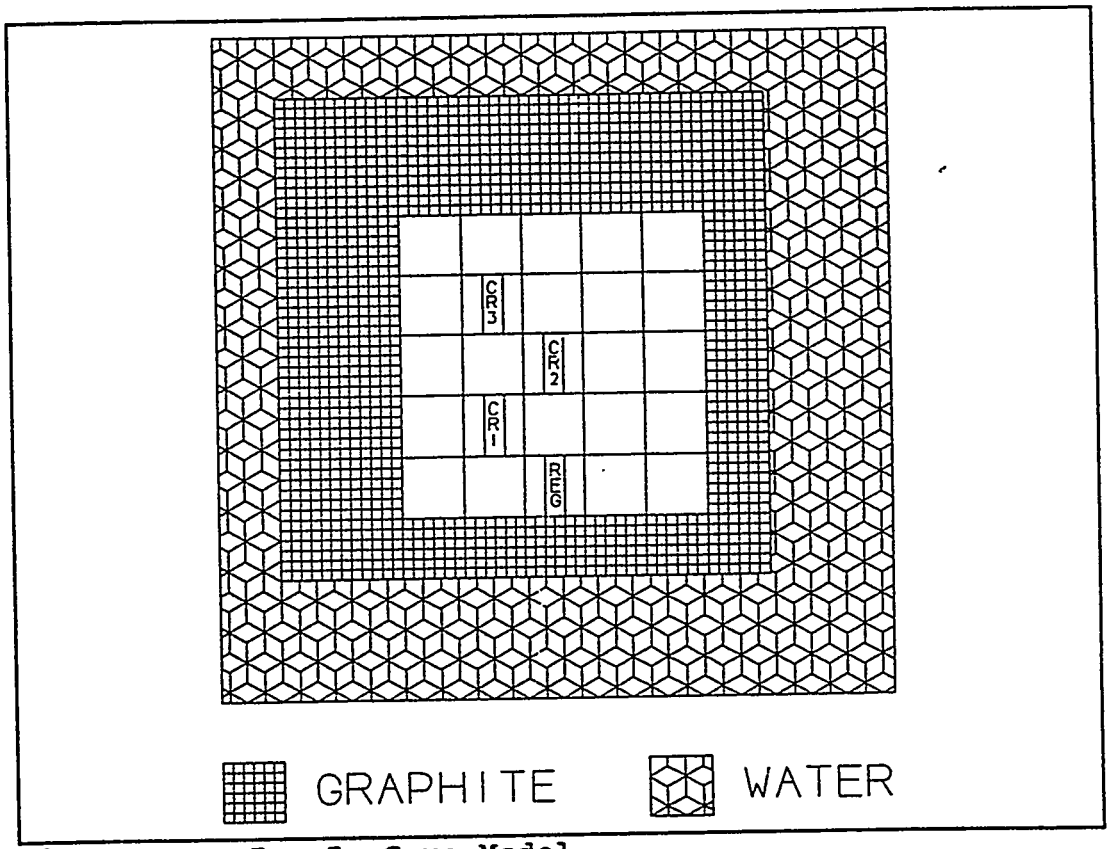


Figure 13. 5 x 5 Core Model.

Modifications to LEOPARD and 2DB were along a similar vein as those done in creating the 4 x 5 model. All depletion calculations were performed and output obtained according to now established routines.

3. RESULTS AND DISCUSSION

3.1 BENCHMARK CALCULATIONS

3.1.1 Basic Data The first thing that had to be done was to determine exactly what experimental data was available to be matched with the calculations which were to be done. For this information, the records of the Texas 75 core were looked at and compared with the types of output able to be obtained from the codes. For the neutronics part of the calculations to be done (this project), the only things that could be compared with measured values were the effective multiplication factors (k_{eff}) with and without the control rods. The HEU calculations could be compared with the LEU calculations, and the basic trends through life could be compared with generally expected trends for these types of fuels.

The axial buckling of the various cores was something that presented a number of problems. In many of the original runs of 2DB, an axial buckling consistent with what was required for the calculational model to match to experimental data was used. The next approximation was a single appropriate value for the core under consideration. This value was about two times as large as the original value used. As will be noted later, this change did not change the lifetime excess reactivity curves, but merely

shifted them upward on the graph. These approximations were necessary since the tools for properly determining the axial buckling (three-dimensional codes) were not directly available to UVA at the time. The final approximation used was spatially dependent buckling values as obtained from ANL [25-27].

3.1.2 Control Rod Worths The first core to be modeled and studied was the first UVAR core having 18 curved plates/element fuel elements, the Texas '75 core. The model number of this benchmarking core shall be denoted as the HEU-18 (HEU fuel, 18 plates per element) core. The core model is a two-dimensional representation of the active region of the Texas '75 core. The control rods in the model are considered to be either fully inserted, or fully withdrawn. The control rods in the model are independent of each other and thus some may be inserted while others remain withdrawn. The next two cores to be calculated also used the model established for the Texas '75 core, however they were done using the LEU fuel (18 and 22 plates/element). These two core calculations are referred to hereafter as LEU-18 and LEU-22 respectively. The results of the control rod worths for each of these cases are given below in Table II.

In the examination and comparison of these and other

results, it is important to realize that the experimentally determined values were found using an operating core and not the idealized situation found with the computer codes. Thus, the computer model may be accurate even though its results do not exactly match those of experiment.

Table II. Control Rod Worths for the 4 x 4 Texas A&M Core and Replacements.

Core	Rod 1* ($)	Rod 2* ($)	Rod 3* ($)	Rod 4* ($)
Texas '75 (Expt.)	4.75	5.00	3.06	0.57
HEU-18	4.75	4.89	2.79	0.71
LEU-18	4.73	4.87	2.84	0.75
LEU-22	4.79	4.92	2.96	0.83

* Experimental and Computational Uncertainties are ±5%

The computationally determined rod worths were found by finding the difference in k_{eff} for each rod between the inserted case and the removed case. A conversion factor, β_{eff}, was then used to present the worth in dollars.

The experimental rod worths were determined using the standard means available (hold three rods in a fixed position and move the fourth). The total worths of the

three shim rods (containing boron) were all predicted by the codes to within the experimental accuracy of the measurements. Experimental uncertainty is taken to be ±5%. One source of this uncertainty is considered to be the inaccuracies involved in the measurement of the period. Another source of uncertainty is introduced when the conversion factor beta-effective is used to determine the worth in dollars. A value of β_{eff}= 0.0080 was used since this was the value typically used at the UVAR at the time of operation of the Texas '75 core.

The table above also indicates that the control rods will be worth approximately the same with the LEU fuel as they have been with the HEU fuel.

3.1.3 Beginning of Life k_{eff} A second viable comparison (between the HEU-18 computer core model and the actual Texas '75 core) was the k_{eff} value in the xenon-free beginning of life (BOL) core situation. Table III below reports these findings for an unrodded (all rods removed) core configuration. The calculated values were taken directly from the 2DB output information, while the value reported for the experimental case could not be directly determined. (To determine the value directly, the core would have had to be operated with all rods fully withdrawn, which is not allowable for any reason.) Instead, the excess

reactivity for the unrodded core was determined by entering the critical rod positions into the measured integral rod worth curves.

Table III. Beginning of life Unrodded k_{eff} for 4 x 4 Texas A&M Core and Replacements.

DESCRIPTION	B^2	k_{eff}
Experimental*		1.036 ± 0.005
2DB Calculations**		
HEU-18	0.0017	1.062
LEU-18	0.0018	1.039
LEU-22	0.0018	1.051

* Implied from Control Rod Worth Curves
** All calculation models use an extrapolation length of 7.8 cm.

The axial buckling value used in the determination of the calculated k_{eff} was that from the second approximation as described above. This value (indicated in the table above as B^2) is considered to be fairly accurate (for a single buckling value) and is consistent with that obtained by ANL [3], Meem [17], and an RZ model of the core.

A difference of about 0.02 is seen between the values for k_{eff} for the calculated and the experimental cores. This

the difference between the calculated value of k_{eff} and the critical value of 1.) The Figure plots excess reactivity (in % $\Delta k/k$) versus burnup (in megawatt days [MWD]). This is a standard means of expressing such information.

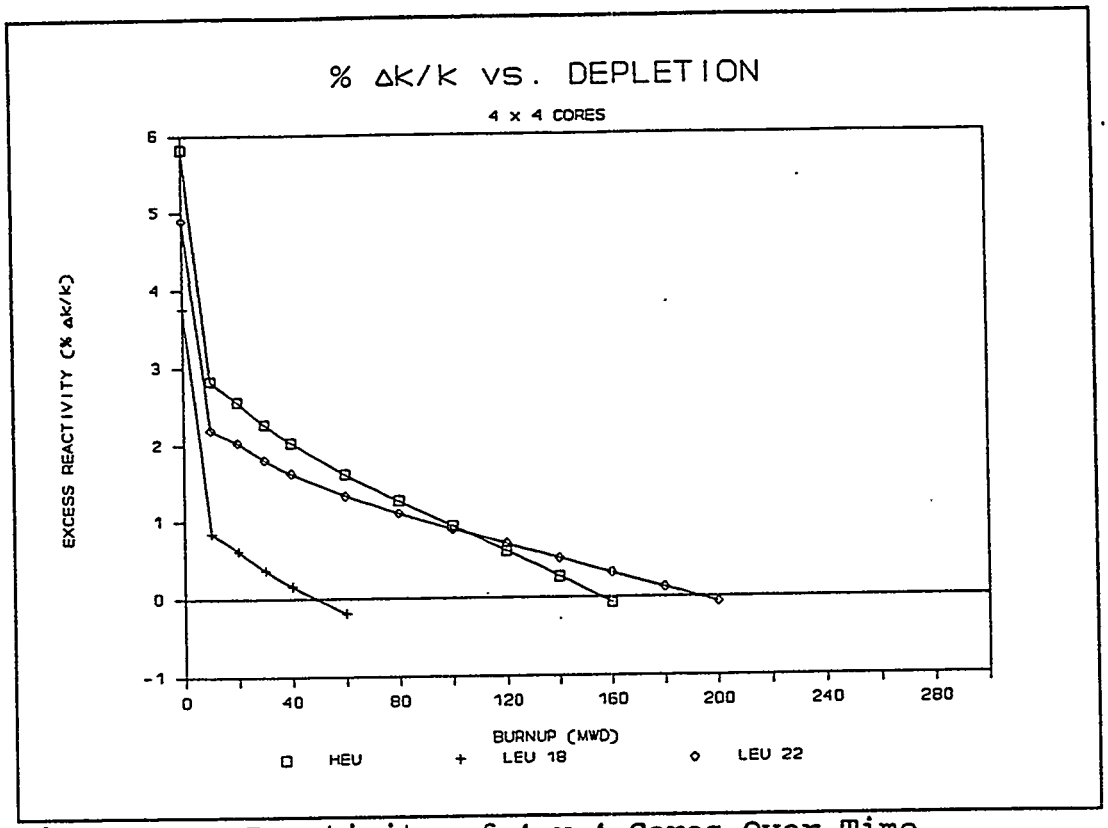


Figure 14. Reactivity of 4 x 4 Cores Over Time

From the graph, it is seen that for a 4 x 4 core model, the LEU-18 core has a much shorter life than does the HEU core, while the LEU-22 is seen to have a slightly longer life than its HEU counterpart. Since traditionally, the UVAR has been operated starting with a 4 x 4 core arrangement and allowing the core size to expand as the core burns, this plot indicates that for an LEU-18 core, such an

option would not be practical, and a bigger core might have to be used at the start.

3.3 4 X 5 CALCULATIONAL RESULTS

3.3.1 Depletion Methods There were originally two methods of depletion used for part of this study. Both methods were applied to each of the different core sizes; however, since the results of these methods for each core size were comparable between the core sizes, only the comparison for the 4 x 5 model will be presented here. Figures 15 and 16 compare the two burnup methods quite well. In doing the calculations to obtain these Figures, the models were identical in every way except those that pertained directly to the depletion calculation itself.

It should be noted that these figures are presented only to illustrate the difference between the depletion methods. Many modifications were made to the models after these graphs were generated and therefore they should not be accepted as final results. Some of the modifications include: upgrading the axial buckling to the second and finally the third approximations, changing the fuel meat from U_3Si_2 to U_3Si_2-Al to include the small amount of Al used as the "glue" for the U_3Si_2 powder, and modifying the boron equivalent content of the aluminum in the elements.

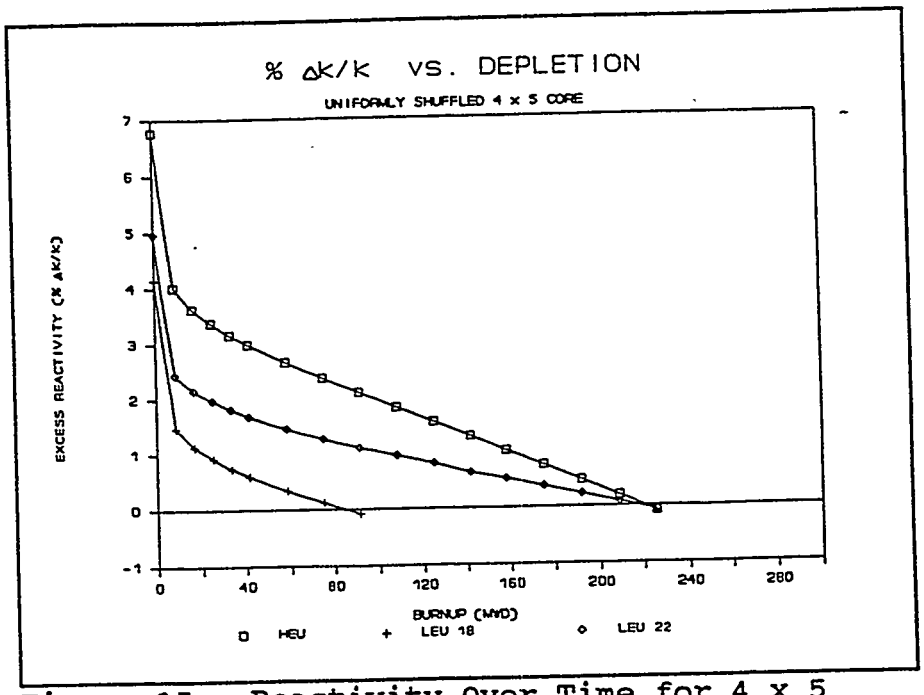


Figure 15. Reactivity Over Time for 4 x 5 Uniformly Shuffled Cores.

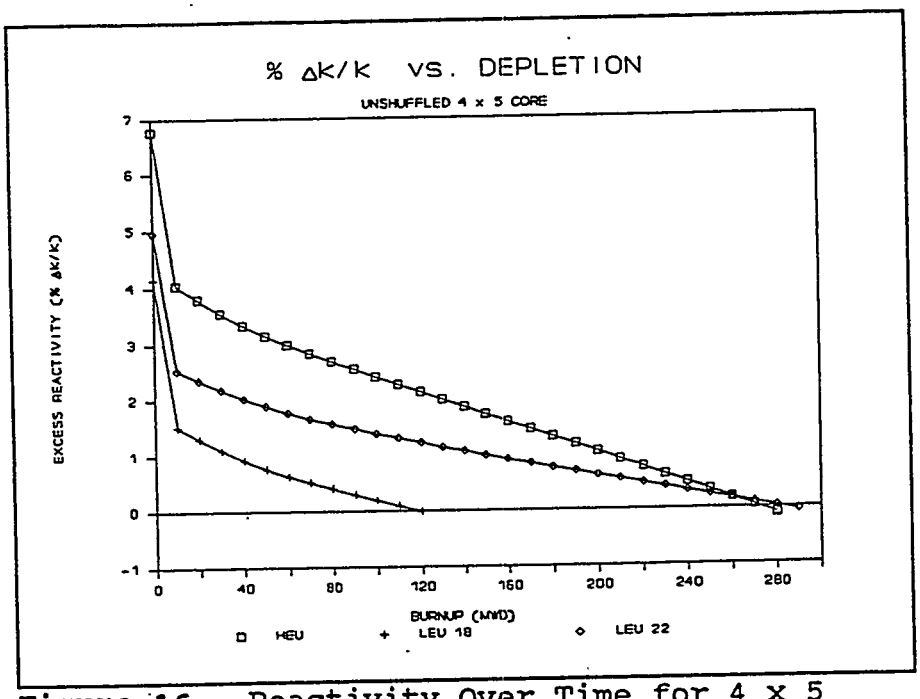


Figure 16. Reactivity Over Time for 4 x 5 Unshuffled Cores.

The figures clearly indicate that the uniform shuffling practice attempted for the UVAR was counterproductive. The unshuffled cores in Figure 16 tended to last up to 50% longer than their "perfectly shuffled" counterparts of Figure 15 because of a certain amount of natural power flattening. Having demonstrated that these results held true for each different core size as well as for cores with many different modifications, it was decided to recommend that the idea of the uniformly shuffled core be abandoned.

3.3.2 Axial Buckling Trials As discussed above, three approximations have been made for axial buckling. A comparison of the effects of each on the 4 x 5 core model is made here. The figures below illustrate this comparison. Figure 17 uses the first approximation for buckling, with an extrapolation length, d = 4.5 cm. This graph is the same as Figure 16 above, and thus several modifications were made after this graph was obtained. Figure 18 uses the second approximation for the buckling, with d = 7.8 cm. All modifications previously discussed (appearing immediately before Figure 15) had been made at the time of the generation of this graph. Figure 19 is considered to be the most up-to-date representation of the core calculations done at UVA up to this writing. This graph uses the third approximation for buckling (spatially dependent), and is in all other respects identical (computationally) to Figure 18.

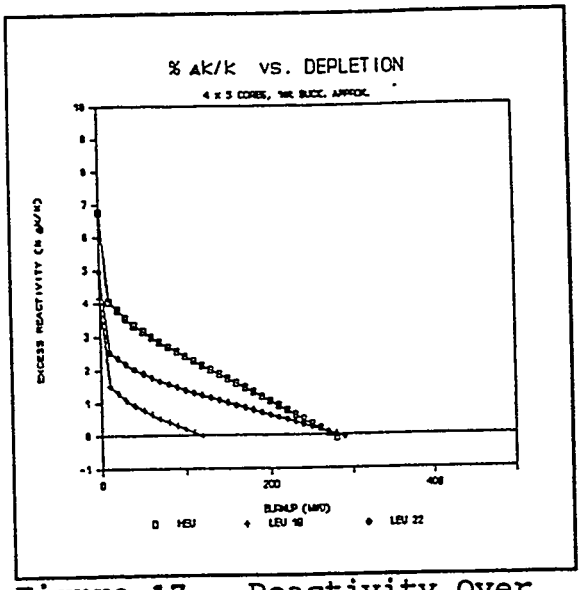


Figure 17. Reactivity Over Time for 4 x 5 Cores Using 1st Buckling Approximation.

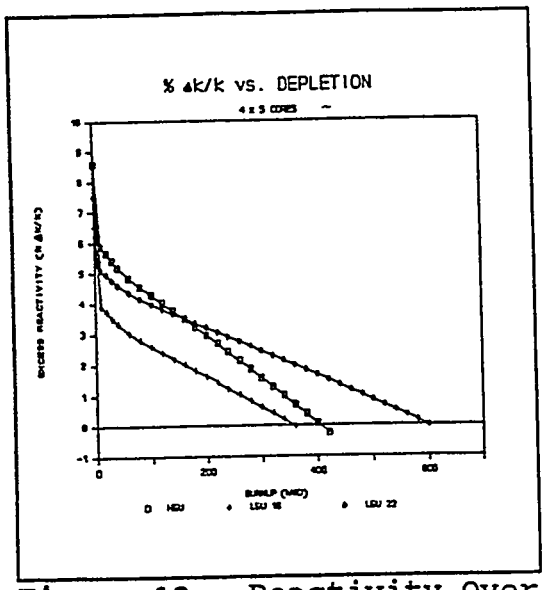


Figure 18. Reactivity Over Time for 4 x 5 Cores Using 2nd Buckling Approximation.

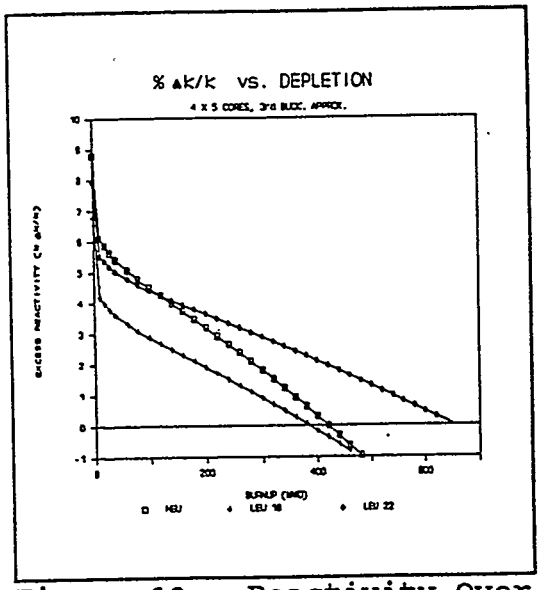


Figure 19. Reactivity Over Time for 4 x 5 Cores Using 3rd Buckling Approximation.

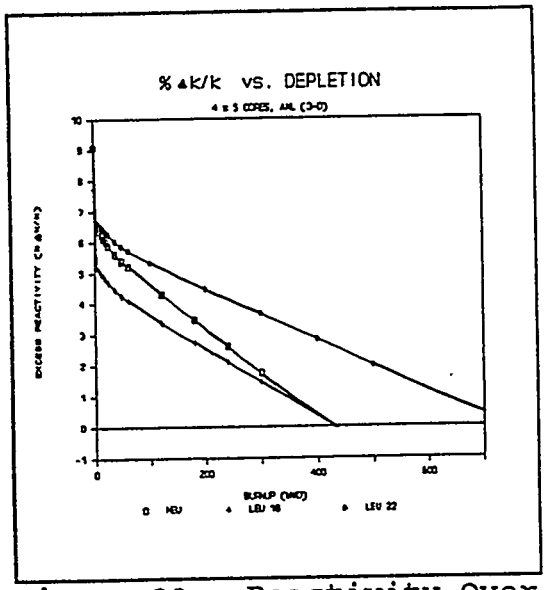


Figure 20. Reactivity Over Time for 4 x 5 Cores as Calculated by ANL.

The final graph, Figure 20, represents calculations done by ANL [27] of the 4 x 5 UVAR core. ANL has independently calculated each of the 4 x 5 cases using both a three-dimensional model and a two-dimensional model with appropriate spatial axial buckling values. These two models reported similar results upon comparison. This graph was generated using the three-dimensional analysis of the core in seven energy groups. (Computations done at UVA were done using a two-dimensional core with only two energy groups.)

General examination (due to modifications made between Figures 17 and 18) indicates that the change to the second axial buckling approximation (from the first approximation) tended to lengthen the lives of the core by a factor of about two. The change then to the spatially dependent axial buckling induced very little change to the curves, though the slopes are seen to change a small amount. Comparing Figures 19 and 20 indicates that UVA and ANL predict the HEU cores essentially identically, while for the LEU curves UVA predicts % $\Delta k/k$ values that are consistently about 1% lower than those predicted by ANL. Reasons for this small discrepancy seem to be based on differences in description of the LEU meat (UVA uses U-235, U-238, U-234, and U-236 per Table I while ANL lumps all uranium which is not U-235 together as U-238). UVA also considers the extra water on the outer sides of the two end fuel plates to be part of the

non-lattice region (see Figures 6, 7, and 8), while ANL increases the amount of water between each fuel plate to make up the difference.

Referring specifically to Figure 19, it is seen that the HEU and the LEU-18 cores had approximately the same length of core life, while the LEU-22 core has about a 50% longer life. This was to be expected, since the LEU fuel (when using 18 plates per element) was designed to be an approximate replacement for the HEU fuel for a standard 18 plate element. Therefore, the confirmation of similar lifetimes for the HEU-18 and LEU-18 cores was another verification of the methods used by UVA in this study.

3.4 5 x 5 CALCULATIONAL RESULTS

Figure 21 below illustrates the effects of the different fuel element types on core life. From this graph, it is seen that (as was true for the 4 x 5 case) the HEU-18 and the LEU-18 have similar lifetimes, assuming no shuffling is done. In addition, the graph indicates that the LEU-22 core gives approximately an additional 50% longer life for the core than either the HEU-18 or the LEU-18 cores, at a cost of 20% more fuel.

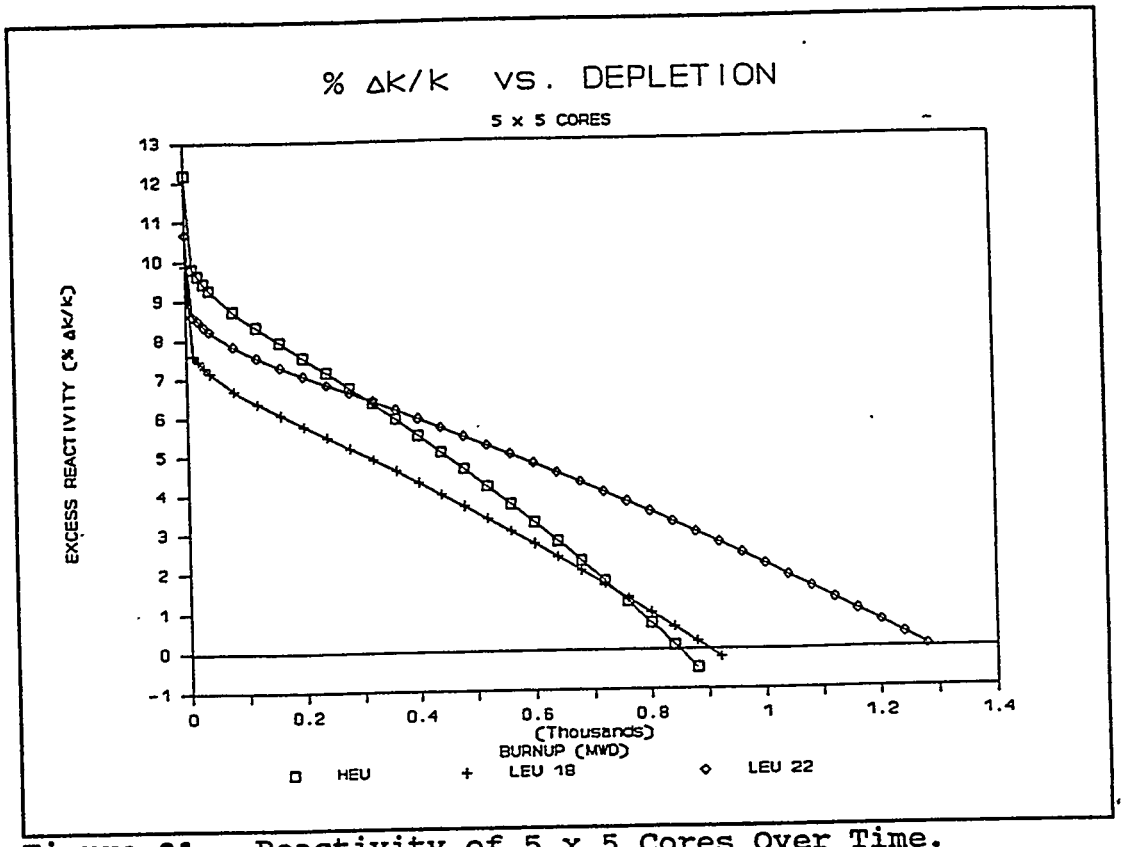


Figure 21. Reactivity of 5 x 5 Cores Over Time.

3.5 ADDITIONAL HEU TO LEU COMPARISONS

Referring to Figures 23, 24, and 25 below, it should be noted that in all cases, as well as for all core sizes, the HEU core starts out with a higher k_{eff} than do its LEU counterparts. This is because the LEU cores have a harder neutron spectrum and tend to rely more on neutrons leaked back into the core more than the HEU core does. This was expected, and can be seen in Figure 22 below. At the core-reflector boundary of the thermal flux traverse, a much steeper slope is seen for the LEU-22 case, while the least

steep slope is seen for the HEU case. A negative slope (as seen in this Figure) indicates that neutrons are leaked into the core, while a positive slope would indicate that neutrons are leaking out of the core.

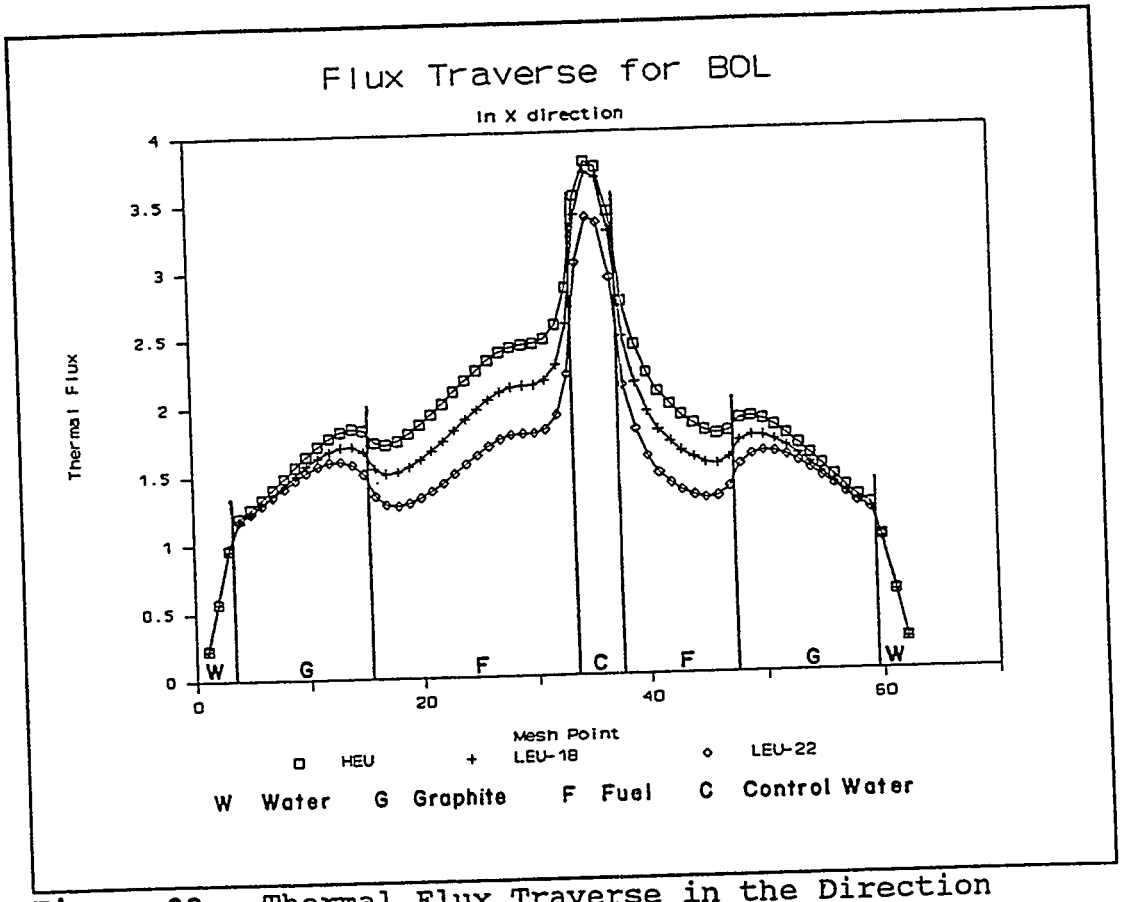


Figure 22. Thermal Flux Traverse in the Direction Through the Fuel Plates and Through the Peak Flux Value in the Fueled Region.

It should be noted that changing the boundary will affect the leakage of the neutrons (exchanging graphite for water would decrease the slope, thus indicating that fewer neutrons are leaking into the core, or even that the neutrons are now primarily leaking out of the core).

It also should noted (from Figures 23, 24, and 25) that the burnup curves for LEU are less steep than are those for HEU. Thus, as the cores are depleted, the LEU cores (18 and 22 plates/element) tend to have larger amounts of excess reactivity than the HEU-18 cores. This cross-over occurs at different times in the core life as determined by the core size and number of plates. In the case of the 4 x 4 cores, the cross-over never occurs for the LEU-18 core, while it occurs at about the halfway point in the life of the LEU-22 core. For the case of the 4 x 5 cores, the HEU and LEU-18 cores do not

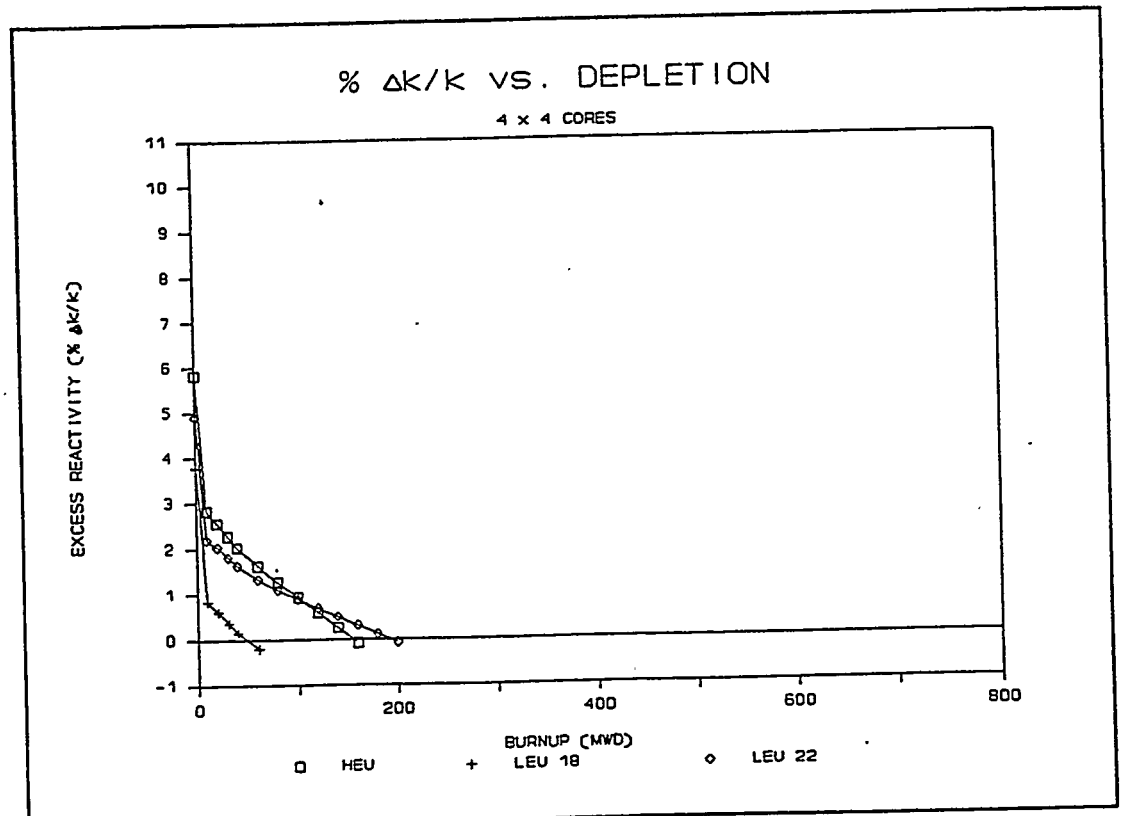


Figure 23. Reactivity of 4 x 4 Cores Scaled to the Life Time of 4 x 5 Cores.

meet until somewhere near the end of life (exactly where is still being debated, however UVA's best guess puts it a bit beyond the end of life). The LEU-22 crosses over the HEU very early in its life at about one fourth of the LEU-22 core life, thus it has about a 50% longer life than the HEU core.

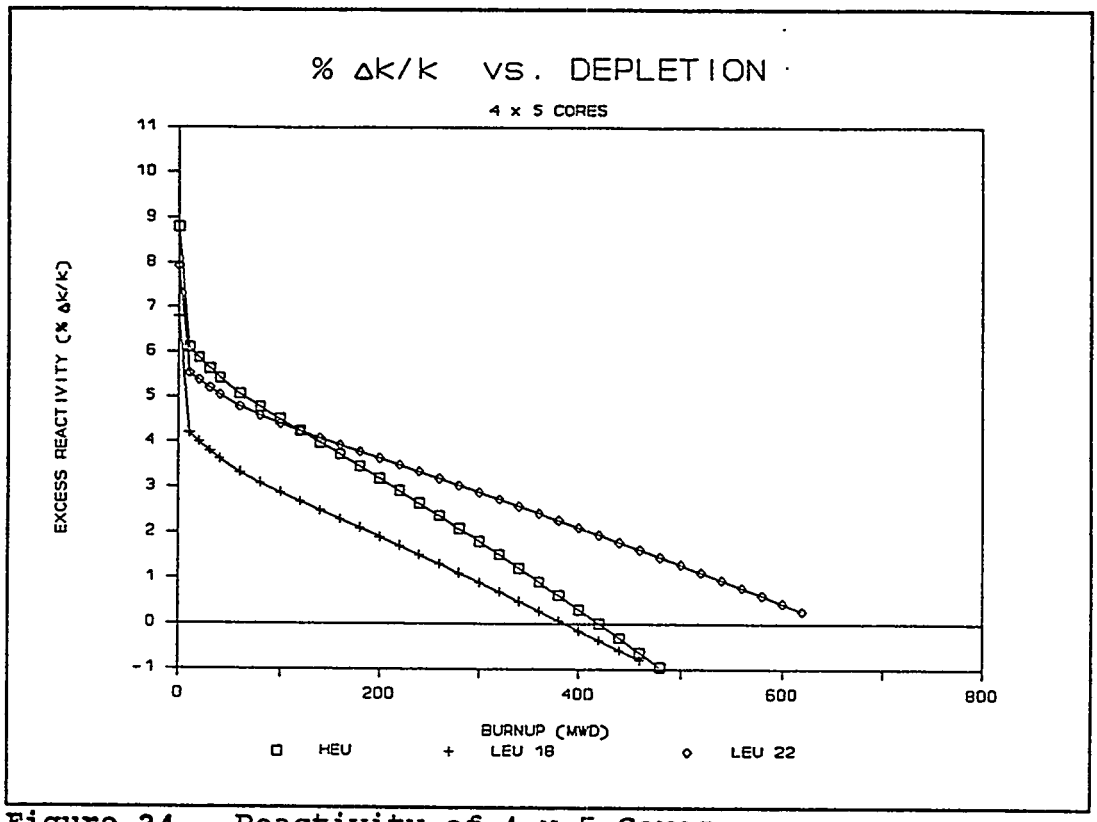


Figure 24. Reactivity of 4 x 5 Cores.

The 5 x 5 cores show a continuation of this trend, with the HEU/LEU-18 cross-over occurring shortly before the end of core life, and the HEU/LEU-22 cross-over occurring near the beginning of core life.

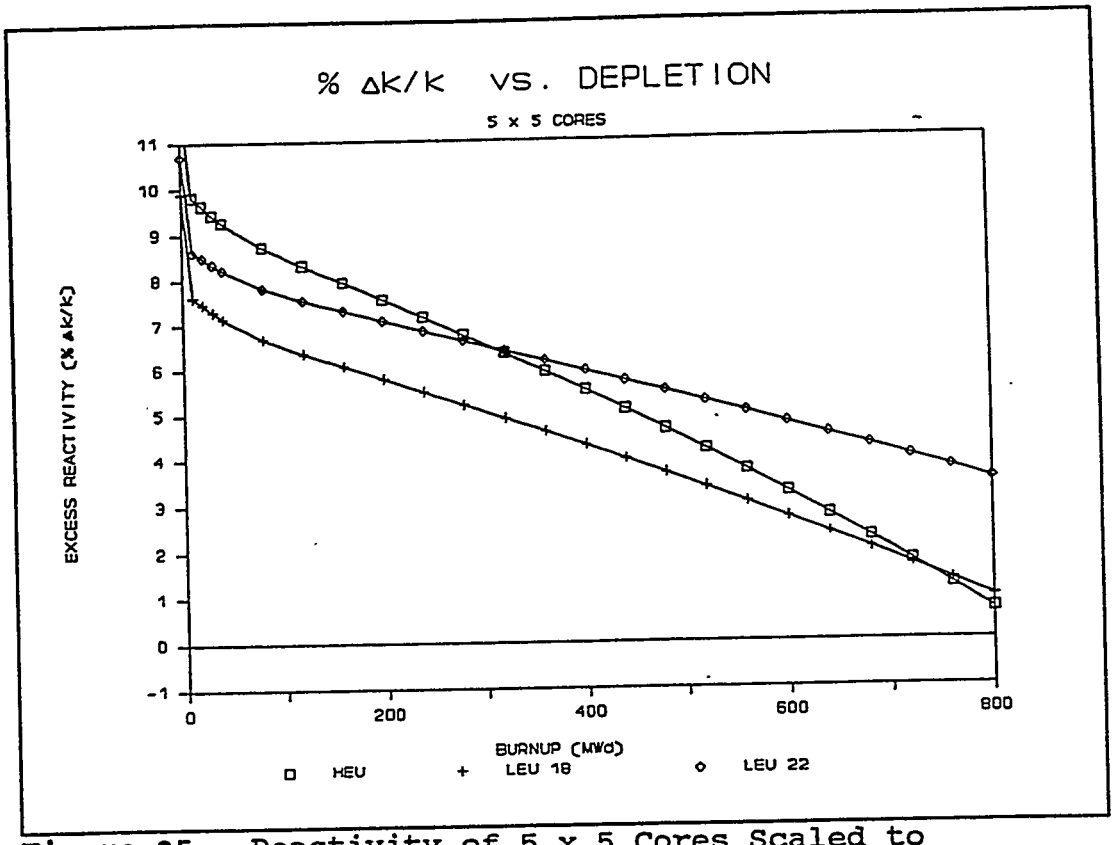


Figure 25. Reactivity of 5 x 5 Cores Scaled to the Life Time of 4 x 5 Cores.

4. CONCLUSIONS AND RECOMMENDATIONS

4.1 CONCLUSIONS

This study had as its purpose the benchmarking of the HEU 18 plate per element 4 x 4 core, the calculational comparison of the HEU-18, LEU-18, and LEU-22 fueled cores for different sized arrays, and the determination of the optimum LEU fueled basic UVAR core. A basic model of the benchmark (4 x 4) core was developed and was compared with the experimental results obtained in 1975. The worths of the three control rods were predicted almost exactly, while the prediction of the far less important stainless steel regulating rod was not quite as accurate. The control rod worths for the LEU fueled cores were also predicted, and it was concluded that the conversion to the LEU fuel will not significantly change the control rod worths.

The k_{eff} values for each of the unrodded 4 x 4 calculated cores and for the benchmark core were compared for the beginning of life case. The difference of 2% between the HEU-18 model and the experimentally inferred benchmark case indicates a real need for calculations to be done using a three-dimensional model so that the effects of the control rods being partially inserted might be properly included. The comparison of these initial k_{eff} values between the calculated cores showed that there is a fairly

considerable difference between the HEU-18 and the LEU-18 from the very beginning, with the LEU-18 starting out its life with a k_{eff} 2.3% lower than the HEU-18. The LEU-22 core should start out with about a 1% lower k_{eff} than the HEU-18.

From the study of the unrodded 4 x 4 cores, the conclusion was reached that, given the relatively low initial value of k_{eff} followed by the sharp drop in k over a very short period of time due to xenon poisoning, the LEU-18 fuel arranged in a 4 x 4 core would have such a relatively short operational life that it is not to be considered an acceptable option for use in the UVAR.

Depletion studies were conducted, examining the trends of k_{eff} over the course of the life of the core. Based on these results, it was determined that the shuffling method followed in the past for the UVAR was counterproductive and should be abandoned in favor of no shuffling or some other improved shuffling pattern.

Comparison of k_{eff} trends over core life for different values of axial buckling (in 2DB) indicates a very strong relationship exists between k and the axial buckling. This is illustrated in the comparison between the first and the second buckling approximations used with the 4 x 5 cores where the axial buckling was almost doubled in size, and the

effect on % $\Delta k/k$ was almost a 2% increase. When the buckling was allowed to vary spatially over the core rather than maintain a single value for the core, essentially no change in % $\Delta k/k$ was noted. This leads to the conclusion that while the spatially dependent buckling may be "more correct", the single value approach used for the axial buckling was quite a good approximation, and may be used when other "better" values are not to be had.

It is well known that a smaller core will produce a higher experimental flux at the same total power than a larger core will, and it is for this reason that UVA would like to be able to maintain cores of the size of a 4 x 5 core for a longer period of time. After studying the excess reactivity trends over core life for the 4 x 5 and 5 x 5 cores (and with the unshuffled and the uniformly shuffled depletion methods), it was found that the LEU-22 fuel in the 4 x 5 core had only a slightly shorter life than did the HEU-18 in the 5 x 5 core with no shuffling used in either case. (It was also found, though not explicitly presented here, that the LEU-22 in the 4 x 5 core [unshuffled] had approximately the same life time as the HEU-18 in the 5 x 5 core using the shuffling methods in practice for the UVAR [uniform shuffling].) Therefore it seems to be strongly to the benefit of the UVAR experimenters that the LEU-22 fuel be adopted so that a smaller core size might be maintained

for a longer period of time.

The LEU-22 fuel not only has a longer life than the HEU-18 fuel does, but it maintains a higher level of excess reactivity for a longer period of time. This converts to a smaller amount of change in the core over time for the LEU-22 fueled core. Traditionally, since various parameters of the core (control rod worths) must be recalibrated as time goes by due to such changes in the core, a core that changes less over time would be very desirable since it hopefully would not require recalibration as often. Another benefit of the slower changing core would be that the fuel elements would not have to be shuffled as often to maintain a "good" core.

For the case of the 4 x 5 core, the LEU-22 fuel was predicted to give about a 50% longer core life than the LEU-18 would be able to give. This increased core life is especially impressive when it is considered that a 50% increase is obtained for only an increase of 20% more fuel. From this it is seen that adoption of the LEU-22 fuel would require a slightly higher initial expense per fuel element on the part of DOE for the purchase of the new fuel, but this would be more than repaid by the fewer number of fuel elements that would have to be purchased, and in the fewer number of used fuel shipments that would have to be made.

The final comment to be made is that while all of these calculations were done at UVA, and all of these conclusions were reached as a result of work done there, the 4 x 5 UVAR core was also calculated at ANL. A comparison of the results shows that the calculations done at UVA using the tools and computer codes available, are quite acceptable.

4.2 RECOMMENDATIONS

The recommendation made based on these studies is that the University of Virginia should adopt 22 plates per element LEU fuel rather than the 18 plate per element standard. A relatively small initial higher fuel fabrication cost is incurred (production costs for the structure of the element and the individual plates remain the same, however more plates means more cost per element), but the use of the LEU-22 fuel easily offsets the cost of replacing all of the elements at a much earlier time than would be required for the LEU-22 core, and leads to a cost savings in the end.

A second recommendation to the UVAR facility itself would be to abandon the shuffling pattern used thus far for the UVAR, and adopt a more beneficial one. To this end, ANL has recommended the adoption of an equilibrium-cycle shuffling pattern based on the adoption of a fixed 4 x 5

core. This shuffling pattern, while potentially being a great boon to the facility, should not be permitted to limit core size and configuration as the experimental need arises.

5. FUTURE WORK ON THIS PROJECT

This part of the HEU to LEU fuel conversion effort was concerned primarily with the determination of the appropriate methods with which to proceed with more in-depth studies for the UVAR. Several of these studies were mentioned previously; however, to complete the calculations required for NRC licensing approval, many more studies are required.

All calculations presented here for the LEU fuel were done based on modifications to the Texas A&M fuel elements. Very simply stated, the LEU-18 elements were treated as if the fuel plates were removed from the HEU elements and replaced with LEU fueled plates. The LEU-22 elements were treated by taking eighteen times the pitch of a single LEU-18 plate/moderator section and dividing it equally twenty-two ways. This was done since at the time no better information was available as to the actual element configuration. As "official" LEU element drawings become available, the LEOPARD and 2DB cells will have to be modified accordingly. The changes to be made are very slight and should only affect the water gap between the plates. The new elements will be designed such that (for the case of the UVAR) 18 (or 22) times the pitch of a fuel plate will be equal to the width of the element as dictated

by the grid plate. This is made possible when the plates in the element are flat rather than curved as they are for the HEU fuel in the UVAR.

Since, based on this study, UVA will only be actively interested in the 4 x 5 core array fueled with the LEU-22 fuel, this is the only case that need be studied in more depth. The studies should take into consideration the range of core boundaries that have been used, are planned to be used, or are even as yet unplanned conditions. Some of these boundaries would include: permanent experimental facilities on one and two faces of the core; open beam ports on one, two, and three sides of the core; and the addition of a D_2O tank on one face of the core.

Other boundary changes that need to be studied involve specifically the reflector region of the core. For the calculations done in this study, the maximum amount of graphite allowed by the grid plate was used. As evidenced by the high excess reactivities calculated under these conditions, these were not "true to life cores". Graphite should be removed and replaced by water in various arrangements around the core.

Finally, the positions of the control rod elements are not fixed and may be moved if it is considered beneficial to

do so, thus it is important to determine the effects computationally of several possible control rod configurations.

APPENDIX

The Figures 26 and 27 illustrate, to some extent, the variety of core configurations that have been used in the UVAR in the past several years.

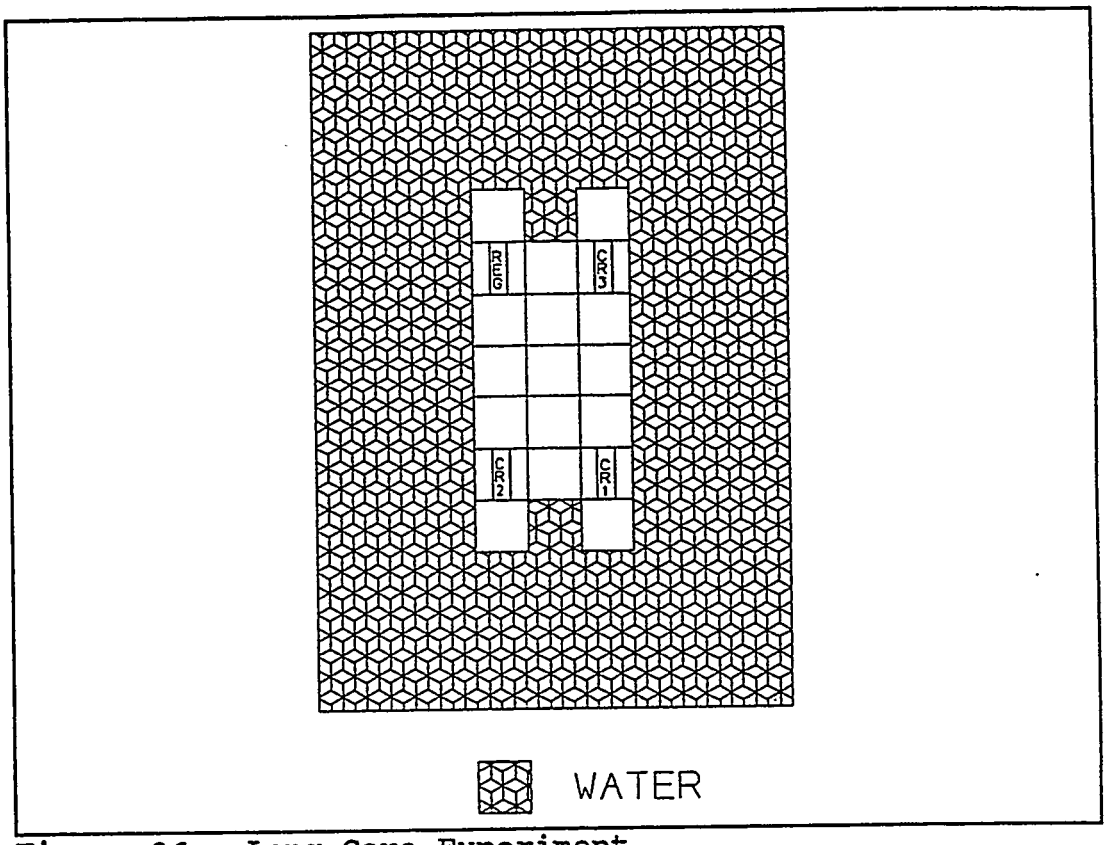


Figure 26. Long Core Experiment.

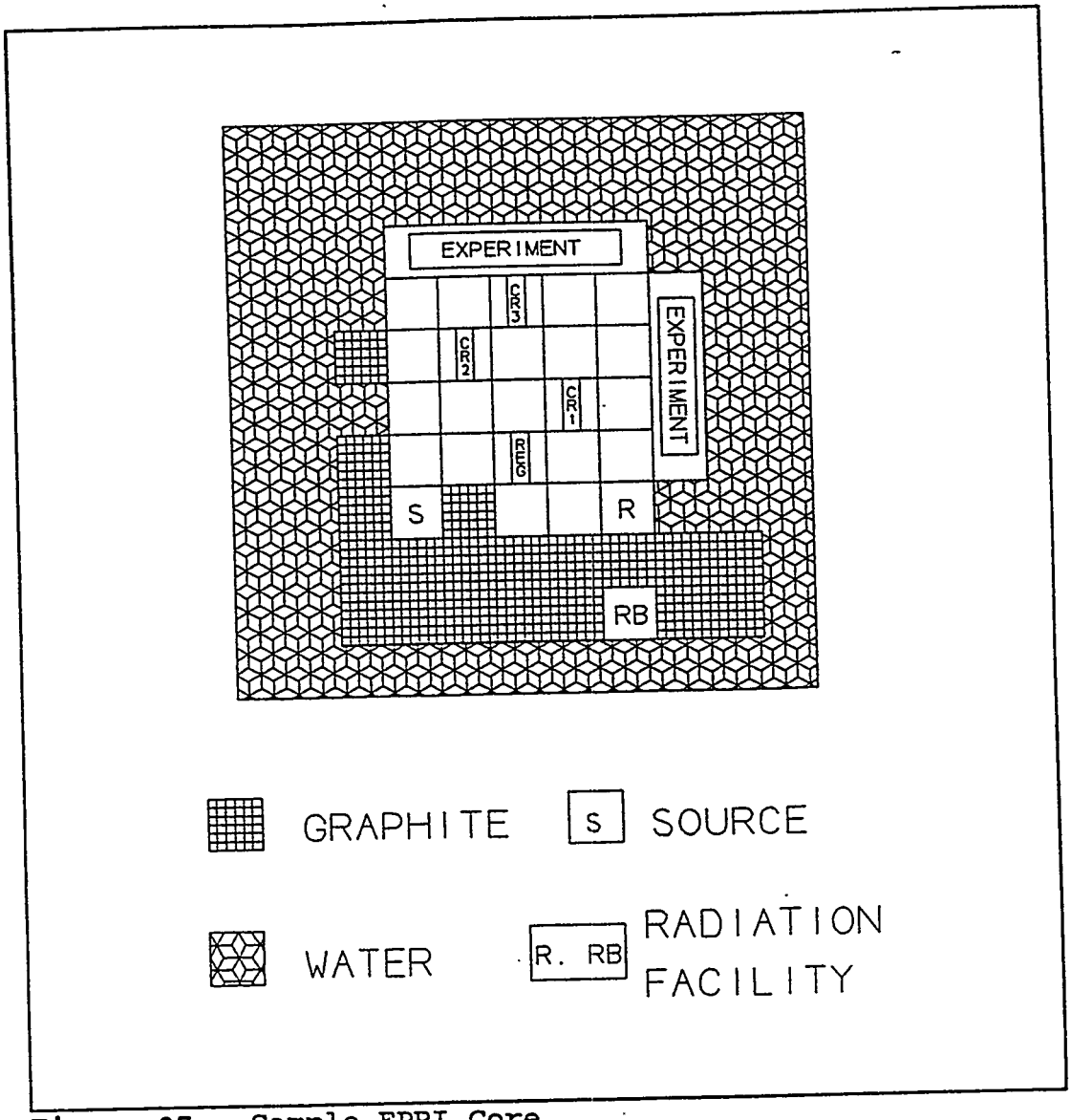


Figure 27. Sample EPRI Core.

The Figure 28 illustrates the current appearance of the reactor core, the reactor pool, and some of the surrounding facility.

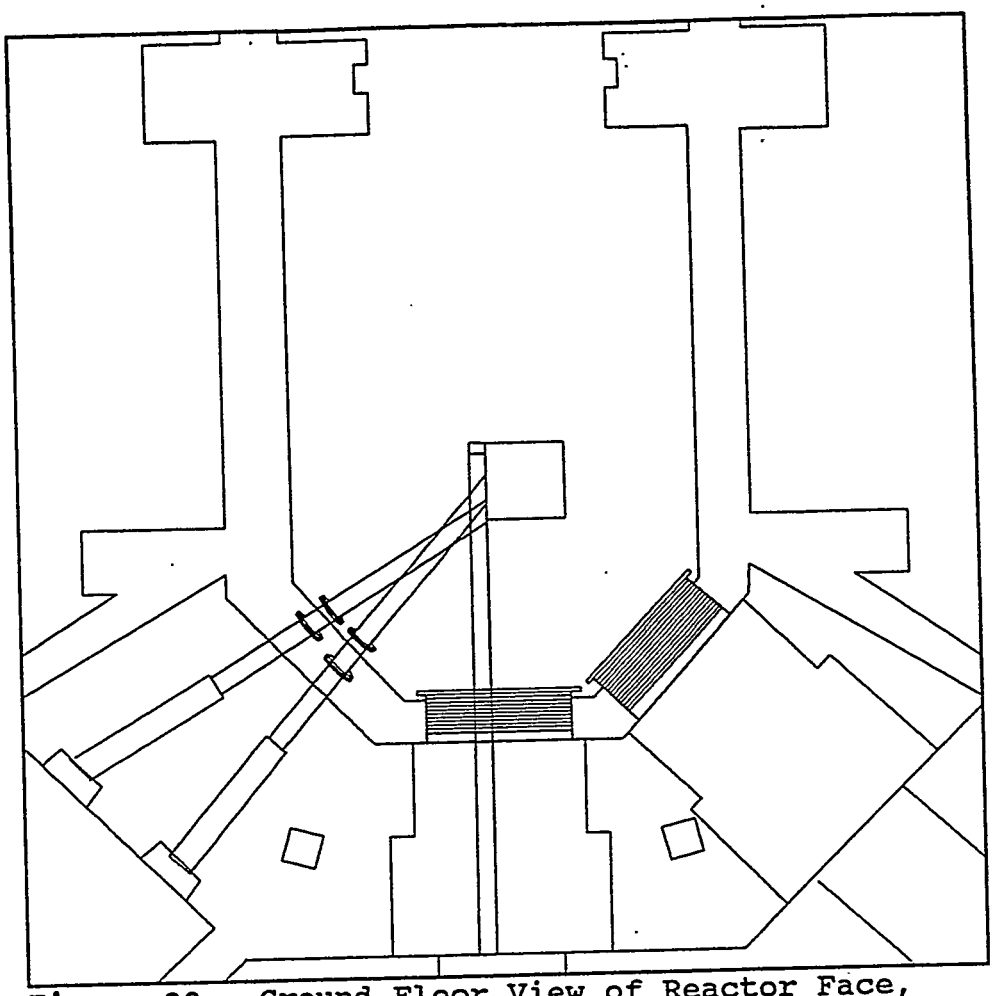


Figure 28. Ground Floor View of Reactor Face, Pool, and Approximate Position of Core.

REFERENCES

[1] "Limitations on the Use of Highly Enriched Uranium (HEU) in Domestic Non-power Reactors," 10 CFR 50.64, Jan. 1, 1987 Ed.

[2] "University Plate-type Reactors LEU Fuel Options," copied page sent to all project participants by ANL.

[3] Private communications with J. Matos (ANL) throughout project's duration.

[4] "MTR Fuel Shipped to University of Virginia on 10-23-73," document on file with UVAR reactor Administrator.

[5] "Fuel Element - Standard," blueprint # NE-33, Nuclear Science Center; A&M College of Texas, Department of Nuclear Engineering, Sept. 6, 1960.

[6] "Fuel Element - Control Rod," blueprint # NE-34, Nuclear Science Center; A&M College of Texas, Department of Nuclear Engineering, Sept. 6, 1960.

[7] "Modified Reflector Element," blueprint # UVAR 1002, University of Virginia Reactor Facility.

[8] "University of Virginia Test Research and Training Reactor 2 - Fuel Plate," blueprint # 409337, EG&G Idaho, Inc., Aug. 5, 1980.

[9] "University of Virginia Test Research and Training Reactor 2 - Standard Fuel Element Assembly," blueprint # 409338, EG&G Idaho, Inc., Aug. 8, 1980.

[10] "University of Virginia Test Research and Training Reactor 2 - Control Fuel Element Assembly," blueprint # 409339, EG&G Idaho, Inc., Aug. 6, 1980.

[11] "LEOPARD Manual," (summary of the LEOPARD input description contained in WCAP-3269-26, Sept. 1963.), May 29, 1981.

[12] Wasserman, S., MS thesis, University of Virginia, 1989, in process.

[13] "QA Package for Control Rod Worth, Shutdown Margin, and Excess Reactivity Study," D. Freeman, August 1988.

[14] "2DBUM," (input manual for 2DBUM, Version # 6, 5/9/80).

[15] "2DBUM (APOLLO VERSION)," (input manual for 2DBUM, Version # 10, JULY86), Sept. 1986.

[16] "Dimensions of the Grid Plate," Memorandum, University of Virginia Department of Nuclear Engineering and Engineering Physics, Reactor Facility, (to: The LEU Conversion Participants), B. Hosticka, Apr. 29, 1988.

[17] Meem, J. L., Two Group Reactor Theory. New York:Gordon and Breach Science Publishers, 1964.

[18] Personal Correspondence from ANL (Woodruff), reflector water cross sections.

[19] Personal Correspondence from ANL (Woodruff), reflector graphite cross sections.

[20] Meeting of all university participants in conversion project. RERTR mtg. at ANL, July, 1987.

[21] "Specification for Test Research Training Reactor LEU Silicide U_3Si_2 Fuel Plates," TRTR - 6, EG&G Idaho, Inc., Rev. 3. Apr. 5 1988.

[22] "Specification for Low Enriched U Metal for Reactor Fuel Plates," TRTR - 11, EG&G Idaho, Inc., Rev. 1. Apr.1, 1987.

[23] "Specification for Reactor Grade Uranium Silicide U_3Si_2 Powder," TRTR - 14, EG&G Idaho, Inc., Rev. 2. July 1, 1987.

[24] "Specification for Aluminum for Fuel Plate Core Matrix," TRTR - 15, EG&G Idaho, Inc., Rev. 2. July 1, 1987.

[25] "Regionwise Extrapolation Lengths for UVAR 4X5 HEU Reference Core (cm.)," FAX copy from ANL (Matos) to UVA (Fehr). Sept. 2, 1988.

[26] "Regionwise Extrapolation Lengths for UVAR 4X5 LEU-18 Reference Core (cm.)," FAX copy from ANL (Matos) to UVA (Rydin). Sept. 9, 1988.

[27] "Regionwise Extrapolation Lengths for UVAR 4X5 LEU-22 Reference Core (cm.)," FAX copy from ANL (Matos) to UVA (Rydin). Sept. 13, 1988.

APPENDIX II

HEU TO LEU FUEL CONVERSION REPORT

NEUTRONIC ANALYSIS FOR THE UVAR REACTOR HEU TO LEU CONVERSION PROJECT

A Thesis

Presented to

the Faculty of the School Engineering and Applied Science

University of Virginia

In Partial Fulfillment

of the Requirements for the Degree

Master of Science

by

David W. Freeman

January, 1990

ABSTRACT

The University of Virginia Research Reactor is currently in the process of converting from high-enriched uranium (HEU) fuel to low-enriched uranium (LEU) fuel. The conversion is in response to a mandate from the Nuclear Regulatory Commission. This thesis addresses several neutronics concerns associated with the conversion project including: 1) control rod worths; 2) radial peaking factors; 3) temperature feedback effects; 4) moderator void feedback effects; 5) reflector worth effects; 6) delayed neutron fractions; and 7) prompt neutron lifetimes.

Control rod reactivity worths for LEU fueled cores were found to be essentially the same as for the HEU fueled cores. Radial peaking factors for the LEU fuel were found to be slightly higher than for HEU fuel due to the harder flux spectrum associated with the LEU fuel. Temperature and moderator void reactivity feedback effects for both the LEU and HEU fueled cores were found to be very similar except for the doppler effect which was significantly higher in the LEU fuel due to the higher uranium-238 loading.

Reflector worths for several different water and graphite reflector options were quantified for the LEU fueled cores, and heavy water reflector tanks were analyzed. An effective delayed neutron fraction of 0.0074 was determined for both the HEU and LEU fueled cores. A prompt neutron lifetime of 67 micro-seconds was determined for the LEU core which was about 15 percent lower than

that determined for the HEU core.

The overall thesis results show that the LEU-fueled core will behave very similarly to the HEU core currently being used.

ACKNOWLEDGEMENTS

This report is dedicated to my wife, Donna, and my daughters, Sarah and Jodi, who constantly supported me throughout the project.

Thanks go to Dr. Rydin for providing guidance and keeping the project on track. A special thanks goes to Vicki Thomas who typed this thesis and helped with the format.

Thanks go to Press Farrar who provided historical background and documentation for the reactor.

Finally, thanks are owed to Mary Fehr and Stuart Wasserman for laying the strong foundation of computer models which I inherited.

TABLE OF CONTENTS

	Page
Abstract	i
Acknowledgements	iii
List of Figures	vii
List of Tables	viii
1.0 INTRODUCTION	1
2.0 BACKGROUND INFORMATION	5
2.1 Description of UVAR	5
2.2 Control Rods	8
2.3 HEU Fuel	9
2.4 LEU Fuel	11
3.0 METHODOLOGY	16
3.1 Methodology for Developing Neutron Cross Sections	17
3.1.1 Core Region Cross Sections	17
3.1.2 Control Rod Cross Sections	19
3.1.3 Reflector Cross Sections	21
3.2 Diffusion Theory Modeling of the UVAR Core	21
4.0 CONTROL ROD WORTH STUDY	26
4.1 4-by-4 Cores and 4-by-5 Cores	26
4.2 Core-Life Effects on Control Rod Worths	29
4.3 Reflector Effects on Control Rod Worths	30
4.4 Control Rod Position Effects	32
4.5 Control Rod Worth Study Summary	34

5.0 RADIAL PEAKING FACTORS 36

5.1 Radial Peaking Factors for UVAR 4-by-4 and 4-by-5 Cores 38

5.2 Control Rod Element Rotation Effects on Radial Peaking Factors 40

5.3 Control Rod Insertion Effects on Radial Peaking Factors 43

5.4 Core-Life Effects on Radial Peaking Factors 44

5.5 Core-Reflector Effects on Radial Peaking Factors . . 47

5.6 Radial Peaking Factor Summary 48

6.0 TEMPERATURE AND VOID EFFECTS STUDY 49

6.1 Temperature Effects 49

6.1.1 Doppler Effects. 50

6.1.2 Moderator Temperature Effects. 54

6.1.3 Power Defects. 54

6.1.4 Gross System Heating Effects 55

6.2 MODERATOR VOID EFFECTS. 55

6.2.1 Uniform Core Void Effects. 55

6.2.2 Local Core Void Effects. 59

6.3 Temperature and Moderator Effects Summary 62

7.0 REFLECTOR WORTH STUDY. 63

7.1 Graphite and Water Reflector Options. 63

7.2 Deuterium Tank Reflectors 69

7.3 Black Boundary Reflectors 72

7.4 Reflector Worth Study Summary. 72

8.0 DELAYED NEUTRON AND PROMPT NEUTRON LIFETIME STUDY. . . 74

8.1 Methodology 74

8.2 Model Verification. 75

8.3 Prompt Neutron Lifetimes. 76

8.4 Effective Delayed Neutron Fractions 79

8.5 Summary of Delayed Neutron and Prompt Neutron Lifetime Study 83

9.0 SUMMARY. 84

REFERENCES. 87

APPENDIX A MATERIAL CROSS SECTIONS FOR UVAR 2-D CORE MODEL

LIST OF FIGURES

		Page
Figure 2-1.	UVAR Grid Plate	7
Figure 2-2.	HEU-18 Fuel and Control Rod Elements.	10
Figure 2-3.	LEU-22 UVAR Fuel Element and Control Rod Element Designs	14
Figure 2-4.	LEU-18 UVAR Fuel Element and Control Rod Element Designs	15
Figure 3-1.	UVAR 4-by-4 Core Model.	24
Figure 3-2.	UVAR 4-by-5 Core Model.	25
Figure 4-1.	Alternate Control Rod Locations for UVAR 4-by-5 Core.	33
Figure 6-1.	Void Coefficient as a Function of Void Percent.	58
Figure 7-1.	Reflector Options 1 through 6	65
Figure 7-2.	Reflector Options 7 through 13.	66

LIST OF TABLES

		Page
Table 4.1.	Control Rod Worths for the UVAR 4-by-4 and 4-by-5 Cores.	27
Table 4.2.	Comparison of Experimentally Determined and Calculated Rod Worths for the 4-by-4 HEU-18 Core.	28
Table 4.3.	Core-Life Effects On Control Rods.	29
Table 4.4.	Reflector Effects on Control Rod Worths. . . .	31
Table 4.5.	Control Rod Worths for Alternate Rod Locations in a UVAR 4-by-5 Core	32
Table 5.1.	Radial Peaking Factors for UVAR 4-by-4 and 4-by-5 Core Configurations with Various Fuel Options	39
Table 5.2.	Radial Peaking Factors for Control Rod Orientation Scenarios.	42
Table 5.3.	Radial Peaking Factors for LEU-22 4-by-4 Graphite Reflected Core with Various Rod Insertions	44
Table 5.4.	Core-Life Effects on Radial Peaking Factors for the LEU-22 4-by-5 Graphite Reflected Core.	46
Table 5.5.	Core Reflector Effects on Radial Peaking Factors	47
Table 6.1.	Doppler Effects for the UVAR Reactor	51
Table 6.2.	Moderator Temperature Effects for the UVAR Reactor	53
Table 6.3.	Power Defects For 4-by-4 UVAR Cores.	54
Table 6.4.	Reactivity Effects Associated with Uniform Moderator Void Conditions With LEU-22, LEU-18, and HEU-18 Fuel Loadings	56

Table 6.5. Uniform Moderator Void Coefficients for LEU-22, LEU-18, and HEU-18 Fuels 57

Table 6.6. Local Void Reactivity Effects for Void Scenarios 1 Through 4. 60

Table 6.7. Local Moderator Void Coefficients. 61

Table 7.1. Reactivity Effects Associated With Variations of a Full Graphite Reflected 4-by-5 Core. . . 67

Table 7.2. Reactivity Effects Associated with Variations of a Single Graphite Reflector Row Surrounding the 4-by-5 Core 68

Table 7.3. Core-Life Effects on Relative Worth of Reflector Option 2 Using LEU-18 Fuel. 69

Table 7.4. Representative D_2O Tanks 70

Table 7.5. Reactivity Effects Associated with Different-Sized D_2O Tanks Bordering the West UVAR Core Face. 71

Table 8.1. Energy Group Structure Used for the EXTERMINATOR Analysis. 75

Table 8.2. Delayed Neutron Fractions 75

Table 8.3. Comparison of k-effective Values Calculated by the EXTERMINATOR and 2DB codes. 76

Table 8.4. Prompt Neutron Lifetimes for the UVAR Core. . . 78

Table 8.5. Total Effective Delayed Neutron Fractions for LEU-22 Fueled Core 81

APPENDIX A

Table A.1 Core Region Cross Sections for LEU-22 Fuel. . . 91

Table A.2 Core Region Cross Sections for LEU-18 Fuel. . . 92

Table A.3 Core Region Cross Sections for HEU-18 Fuel. . . 93

Table A.4 Control Rod Region Cross Sections. 94

Table A.5 ANL Developed Water and Graphite Reflector Cross Sections. 95

Table A.6 UVA Developed Graphite Reflector Cross Sections. 96

CHAPTER 1. INTRODUCTION

This report presents several studies designed to address neutronics issues and concerns associated with converting the University Of Virginia Research Reactor (UVAR) from highly-enriched uranium (HEU) fuel to low-enriched uranium (LEU) fuel. The neutronics studies were performed using advanced neutronics computer modeling techniques. Studies presented in this report address the following topics: 1) control rod worths; 2) radial peaking factors; 3) temperature and moderator feedback effects; 4) reflector worths; and 5) delayed neutron and prompt neutron lifetimes. Background information used to build the computer models and study methodologies are also addressed.

Several research reactor facilities in the United States use HEU fuel. The Nuclear Regulatory Commission (NRC) has directed all research facilities using HEU fuel to convert to LEU fuel. HEU fuels are often enriched in excess of 90 percent uranium-235 while LEU fuels have an enrichment limit of 20 percent. The order to convert to LEU fuel was in response to security and safeguards issues raised over the HEU fuel.

Currently, the UVAR is in the process of being converted from HEU to LEU fuel. The conversion process is being performed by the UVAR staff and is non-trivial. The process includes: 1) a revision of the Safety Analysis Report; 2) Technical

Specifications changes; and 3) other, as yet undefined, analyses deemed necessary by NRC.

To date, much work has been performed on the project by both UVAR staff and graduate students. This work is well summarized in the facility Progress Report [1] to the Department of Energy (DOE). The work has focused on the operating performance of the LEU fuel as compared to the currently used HEU fuel.

LEU fuel elements considered for use in the UVAR will use generic LEU fuel plates described in Chapter 2. LEU fuel elements using 18 plates (LEU-18), 20 plates (LEU-20), and 22 plates (LEU-22) have been considered as potential replacements for the current 18 plate HEU fuel elements (HEU-18). The neutronics analyses have not addressed LEU-20 fuel elements and have assumed that their characteristics were bounded by the LEU-18 and LEU-22 fuel element characteristics.

In the fall of 1988, The University of Virginia (UVA) Reactor Safety Committee tentatively approved the use of either the LEU-18, LEU-20, or LEU-22 fuel elements. Work performed by Fehr [2] showed that the LEU-22 fuel element would be a superior replacement for the current fuel in terms of core lifetime. Based on this information, the UVAR staff decided to choose LEU-22 fuel as the preferred replacement element. For this reason, several of the studies presented in this analysis address only the LEU-22 fuel option.

A key issue of concern was whether or not the UVAR control rods would provide an adequate reactivity insertion in LEU cores for safe operation and whether their associated reactivity effects would be significantly altered from those in HEU cores. This issue is addressed in Chapter 4 of this thesis and in Reference [3].

The focus of the HEU to LEU conversion safety analysis is the thermal hydraulics analysis [4]. This effort is supported by information presented in the peaking factor study presented in Chapter 5.

Chapter 6 presents a study which addresses temperature and moderator feedback effects for the LEU fuel, and Chapter 7 addresses reflector worth behavior for the various fuel options.

NRC informally requested, via a guidance handout at the 1988 National Organization of Test, Research, and Training Reactors (TRTR) meeting, that delayed neutron fractions and prompt neutron lifetimes be calculated as part of the license renewal process. The study presented in Chapter 8 addresses this issue.

It should be noted that no simple mechanism exists for quantifying errors associated with the computer modeling techniques used throughout this thesis. Errors may be incurred in the modeling process, computer computations, and input data. A default error value of plus or minus 5 percent has been chosen as representing what is believed to be a reasonable estimate of the

error involved with values presented in this thesis. Higher error estimates are quoted in this thesis when deemed appropriate. As discussed in Chapter 9, the computer models can be "fine-tuned" when experimental data from the new LEU core becomes available. This process should eventually provide information allowing a better estimate of computational errors to be made.

The current schedule for the conversion project includes the submission of a revised Safety Analysis Report (in which the author will be heavily involved) in August, 1989. LEU fuel element fabrication is projected for completion by the end of 1989. Assuming that NRC licensing concerns can be addressed in a timely fashion, it should be possible to convert the UVAR to LEU fuel in early 1990.

2.0 BACKGROUND INFORMATION

This chapter presents background information which forms the basis for the UVAR neutronics models developed for analyses presented in this report. Presented below are descriptions of: 1) the UVAR reactor; 2) control rods; 3) HEU fuel; and 4) LEU fuel.

2.1 Description of the UVAR Reactor

The UVAR reactor is a pool type research reactor constructed in 1959. Currently licensed to operate at 2 megawatts, the UVAR is used primarily as a research tool. Research activities, such as neutron activation analysis and neutron radiography, use the reactor core as a powerful neutron source. The reactor assembly is comprised of fuel elements, control rod fuel elements, control rods, and graphite reflector elements; all of which sit in the reactor grid plate. The grid plate assembly is supported by an aluminum framework which is suspended from a movable bridge. Pool water (light water) serves as moderator, coolant, reflector, and radiation shielding.

The reactor sits under about 20 feet of water at the bottom of a 75,000 gallon pool. The reactor is cooled by pool water downflow through the core elements in excess of 1000 gallons per minute. This water passes through a tube-in-shell heat exchanger and is returned to the pool. Heat is transferred to the atmosphere via a cooling tower mounted on the facility roof.

A full description of the UVAR is presented in the facility Safety Analysis Report [5]. Certain key features of the UVAR, such as the grid plate and core components, are discussed below.

Grid Plate

The UVAR reactor is located on the reactor grid plate. The reactor is "built" by loading various core components into the grid plate to achieve a desired core configuration. Core configurations are widely varied and are limited only by shutdown margin and excess reactivity requirements.

The UVAR grid plate, shown in Figure 2-1, contains an 8-by-8 array of holes, approximately 2 1/2 inches in diameter, for positioning reactor components. For the purposes of this analysis, the grid plate has been subdivided into 64 equal grid cells measuring 3.189 inches by 3.031 inches [6]. The grid cells are depicted in Figure 2-1 with dotted lines.

Reactor Core Components

Reactor components include fuel elements, control rod fuel elements, graphite elements, and grid plate plugs. Reactor components are designed to fit into the grid plate holes and extend no further than the grid cell boundaries.

Fuel elements, control rod elements, and graphite elements all have similar dimensions of about 3 inches in length and width, and 35 inches in height. The bottom of each element consists of a cylindrical tapered nozzle which fits snugly into the grid plate

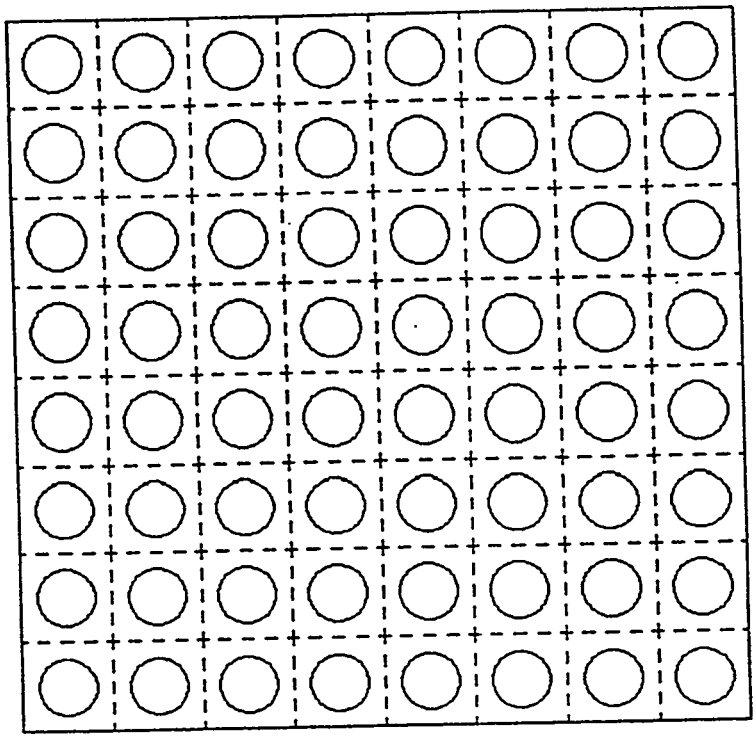


Figure 2-1. UVAR Grid Plate

holes. Graphite elements, used as reflectors, are generally placed on the outside faces of the fuel that makes up the core to enhance core reactivity.

Grid plugs are used to prevent water flow through empty grid locations. UVAR Standard Operating Procedures (SOPs) require all unused grid locations to be plugged in order to minimize non-element by-pass flow. A grid plug is a short metal cylinder, approximately 3 inches in diameter, mounted on a tapered nozzle. When inserted in the grid plate, the plug extends only a few inches above the grid plate, which is below the active fuel region.

2.2 Control Rods

The UVAR uses four control rods; 3 safety rods and 1 regulating rod. Safety rod reactivity worths range from 3 to 5% $\Delta\rho$ and are used to scram the reactor. The regulating rod has a relatively low worth (0.3-1% $\Delta\rho$) and is used primarily to compensate for small changes in reactivity. The control rods are oval and fit into the center hole of the control rod element. Each type of rod is discussed below.

Safety Rods

The UVAR safety rods are made of boron-stainless steel, clad in aluminum, and are about 1.5% natural boron by volume. The rods are about 25 inches long and have an oval cross section geometry with approximate dimensions of 2 1/4 by 7/8 inches. The rods are

vertically grooved to increase surface area. The safety rods are magnetically coupled to their drive mechanisms and drop by gravity into the core on a scram signal.

Regulating Rod

The regulating rod, commonly referred to as the "reg rod", is made of stainless steel, clad in aluminum. It has the same dimensions as the safety rods but is not grooved. The rod is permanently attached to its drive mechanism and, therefore, does not drop on a scram signal. The reg rod has a relatively low worth and is generally located in the outer portions of the core, with the primary purpose of compensating for small reactivity changes associated with normal operations.

2.3 HEU Fuel

The UVAR is currently fueled with highly enriched uranium (HEU) fuel elements, shown in Figure 2-2. Each fuel element contains 18 curved fuel plates and is referred to as "HEU-18" fuel throughout this analysis. Each element initially contained 195 grams of U-235; however, the HEU fuel used in this analysis was partially burned, having an estimated 192.3 grams of U-235 per element. The element has approximate cross sectional dimensions of 3-by-3 inches, with an active fuel length of about 24 inches.

HEU control rod fuel elements are similar to the regular fuel elements except that the center 9 fuel plates have been removed to allow room for the control rod to move up and down. The HEU control rod element is shown in Figure 2-2.

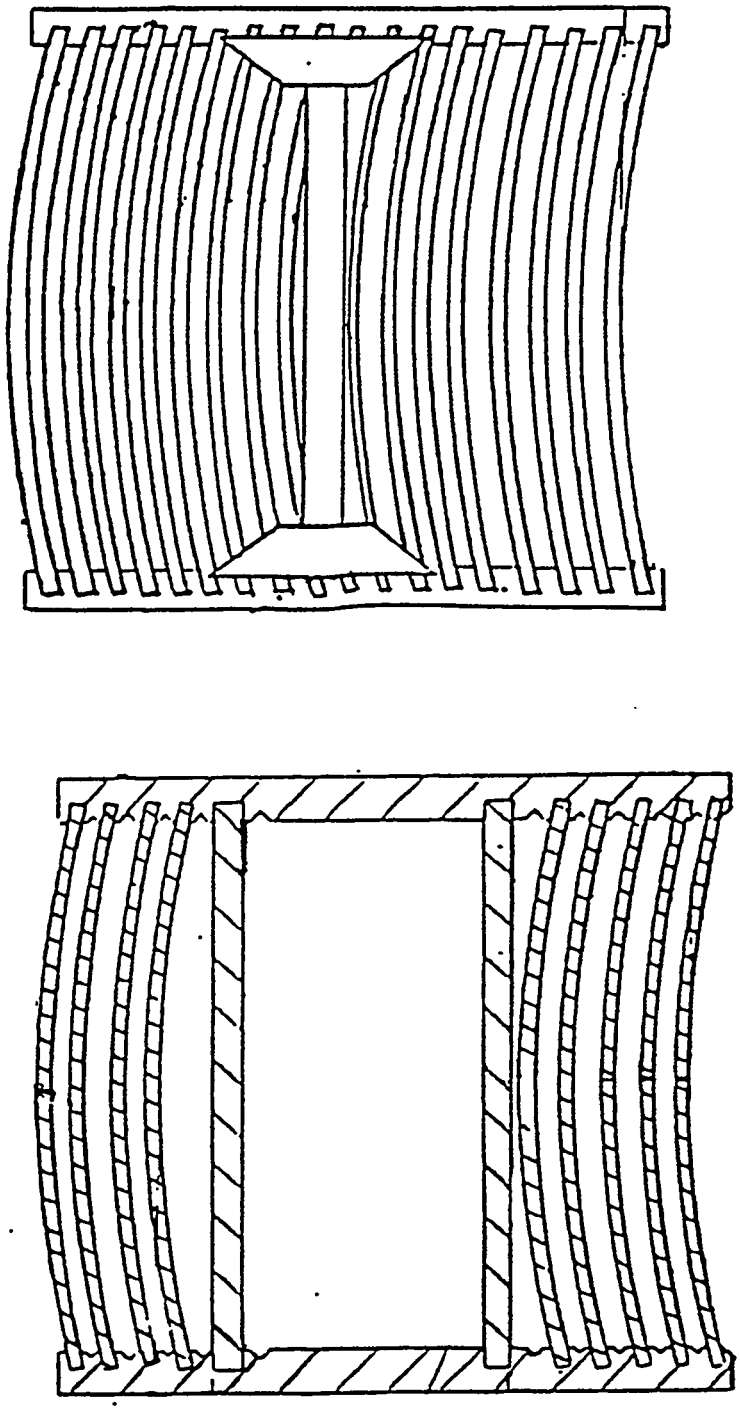


Figure 2-2 HEU-18 Fuel and Control Rod Elements [5].

Important parameters associated with the HEU-18 fuel elements are presented below:

Parameter	Value
1. HEU Fuel Meat	
a. width	0.02 inch
b. length	2.375 inch
c. height	23.5 inch
2. Clad Thickness	0.015 inch
3. Plate Thickness	0.05 inch
4. Water Gap	0.122 inch
5. U-235/plate	10.7 gram
6. U-235/element	192.3 gram

2.4 LEU Fuel

Generic LEU fuel plates have been designed by EG&G Idaho (in cooperation with DOE) and fabricated by Babcock and Wilcox in Lynchburg, Virginia. The plate is made oversized so that it can be "trimmed" to fit different fuel element designs.

Detailed requirements for LEU fuel meat and fuel plates have been published in TRTR specifications [7 - 11]. This information has been reviewed for applicability to the UVAR neutronics work effort [12] and is incorporated in the LEU neutronics analyses presented in this report.

The LEU fuel plate and fuel meat will have dimensions almost identical to the HEU fuel. The LEU fuel meat is 19.75 percent enriched uranium silicide powder (U_3Si_2) dispersed in aluminum powder which is "hot-rolled" to form the fuel core matrix, commonly referred to as the fuel meat. The fuel meat is bonded with, and encased in, an aluminum clad to form the fuel plate.

Specifications for the Generic LEU fuel plate are presented below[13]:

	PARAMETER	VALUE
1.	Type of Fuel	U_3Si_2
2.	Fuel Meat Density	3.47 gram/cm3
3.	U-235 Per Plate	12.5 gram
4.	Plate Thickness	0.050 inch
5.	Plate Width	2.775 inch
6.	Clad Thickness	0.015 inch
7.	Fuel Meat Thickness	0.020 inch
8.	Fuel Meat Width	2.395 inch
9.	Fuel Meat Length	23.25 inch

Generic LEU fuel element designs do not exist because facility-specific elements are generally required. In response to the need for an element design to form a consistent basis for the thermal-hydraulic and neutronics analyses, preliminary UVAR element designs were developed. These designs are presented in

references [13] and [14], and have been distributed to LEU Project Principals at both UVA and EG&G Idaho.

The UVAR LEU elements use the generic LEU fuel plate described earlier. The elements will use flat plate fuel and will have the same outer dimensions as previously-used UVAR 12-plate elements. The LEU element designs are based on blueprints for previous HEU elements [15,16]. The element designs currently address only two dimensions. The axial dimension in both the neutronics and thermal-hydraulics analyses is accounted for by an axial dimension function.

Figures 2-3 and 2-4 present the UVAR LEU fuel element and control rod element designs for 22-plate elements (LEU-22) and-18 plate elements (LEU-18). Applicable dimensions for the LEU fuel and control rod elements are presented in the figures.

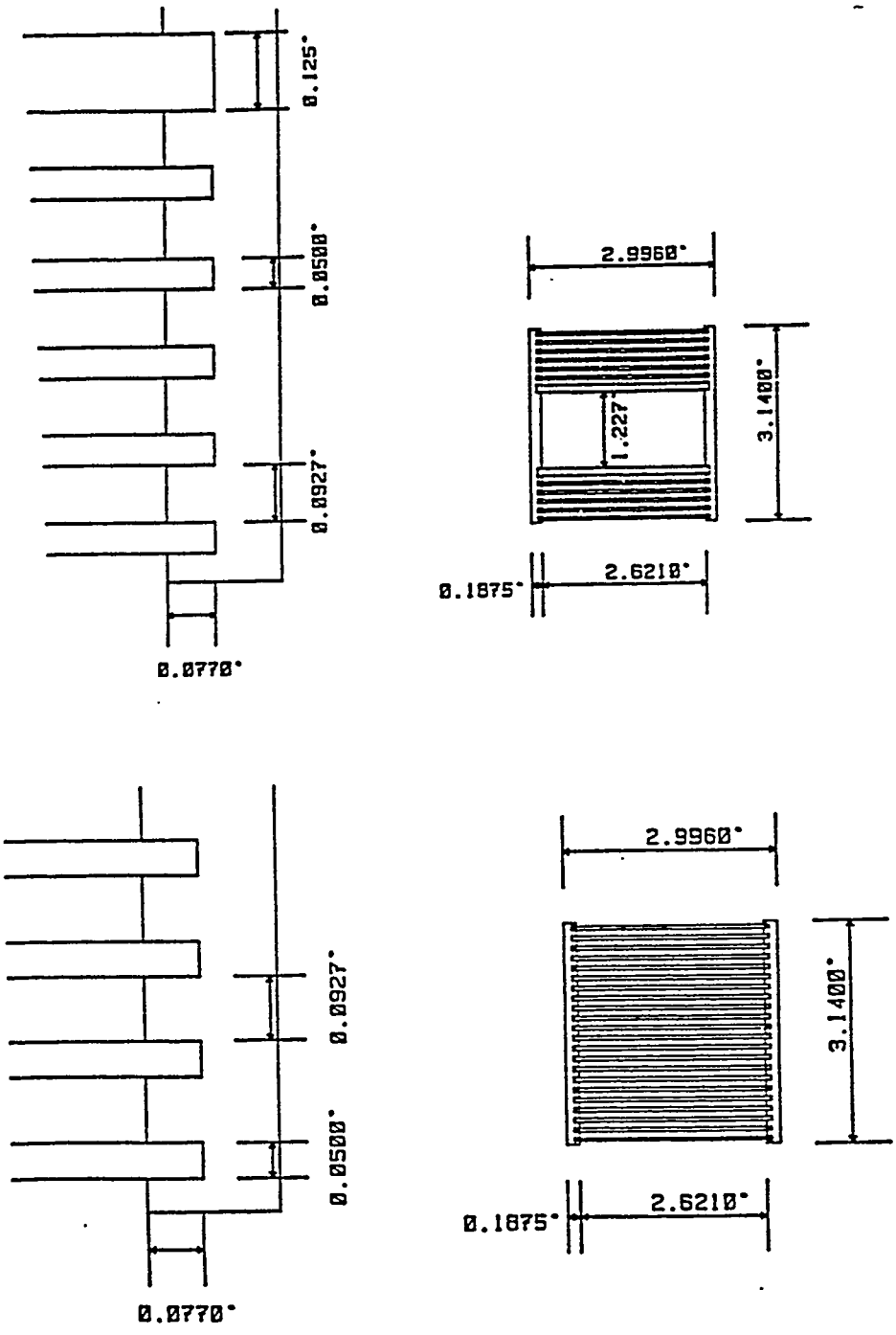


Figure 2-3. LEU-22 UVAR Fuel Element and Control Rod Fuel Element Designs. (Figures by B. Hosticka, April 1988).

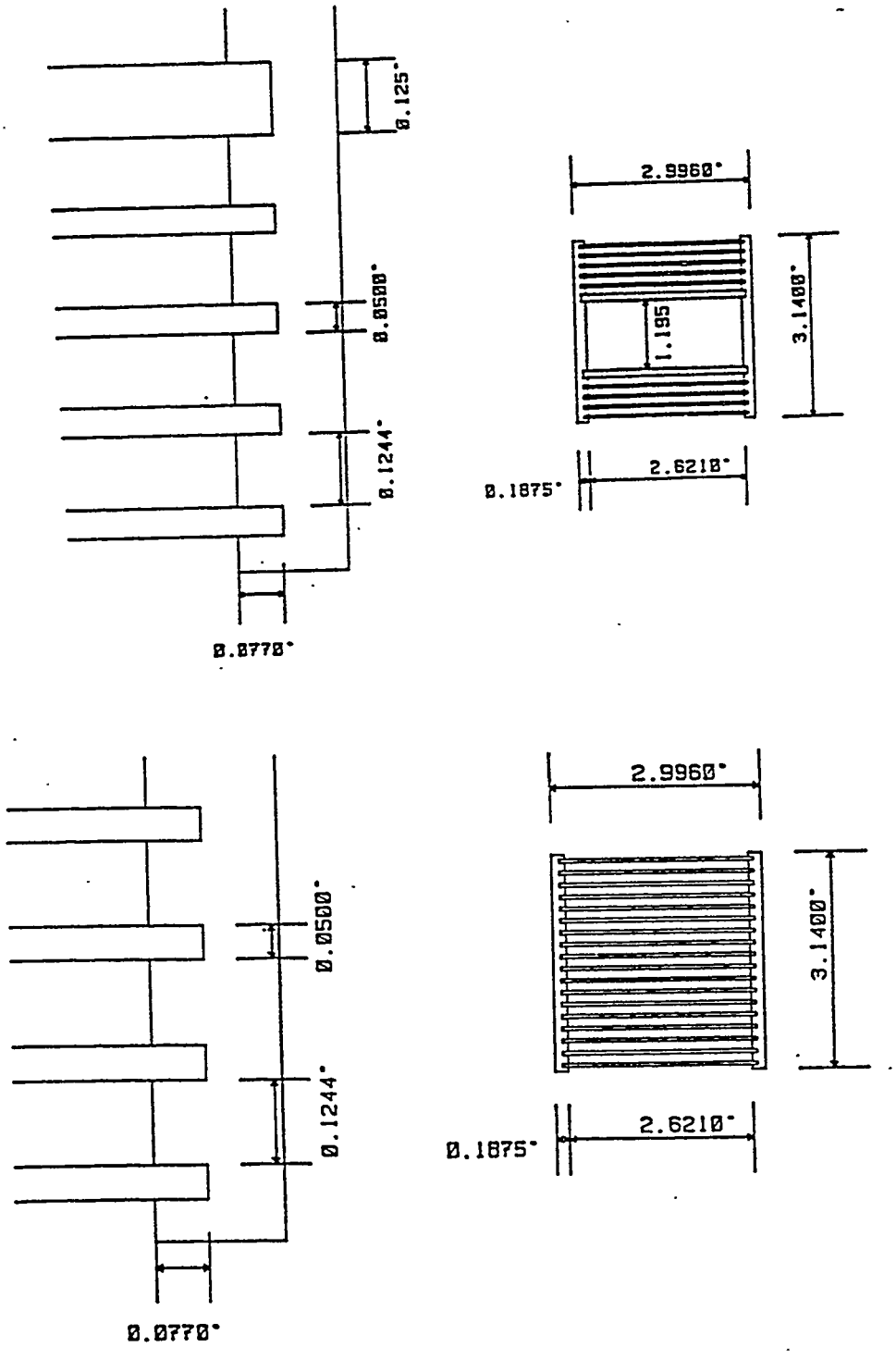


Figure 2-4. LEU-18 UVAR Fuel Element and Control Rod Element Designs (Figures by B. Hosticka, April, 1988).

3.0 METHODOLOGY

Studies presented in this report were performed using several combinations of various main-frame computer codes. The basic methodologies supporting the studies are presented here. Study specific methodologies are presented, as appropriate, in the sections addressing the studies. Computer codes used in the analyses included: 1) LEOPARD; 2)THERMOS; 3) GAMTEC; 4) EXTERMINATOR; and 5) 2DB.

The LEOPARD[17], THERMOS[18], and GAMTEC[19] codes are neutron interaction cross section generator codes and were used to develop energy-dependent cross sections for the analyses. Additionally, the EXTERMINATOR [20] 2-D diffusion theory code was used to help develop control rod cross sections. The methodologies for cross section development are presented in Section 3.1.

2-D diffusion theory codes, 2DB and EXTERMINATOR, were used to develop detailed UVAR core models. The 2DB core model, as modified by the University of Michigan (referred to as 2DB-UM), was used for the bulk of the analyses. The EXTERMINATOR code was used to model the UVAR core for the purposes of calculating delayed neutron fractions and prompt neutron lifetimes. The 2-D diffusion theory codes are described in Section 3.2.

3.1 Methodology For Developing Neutron Cross Sections

Cross sections used in this analysis can be classified as follows:

1. Core-region cross sections
2. Control rod cross sections
3. Reflector cross sections

A different methodology was employed to develop each type of cross section. These methodologies are discussed below.

3.1.1 Core-Region Cross Sections

The LEOPARD computer code was used to develop multi-group cross sections for the UVAR core region. Variations in LEOPARD input parameters were employed to develop temperature and void dependent cross sections used in the temperature and moderator void study presented in Chapter 6. Additionally, the code calculates cross sections associated with fuel depletion at discrete burnup steps.

The LEOPARD code computes two and four group spectrum weighted macroscopic cross sections for an infinitely repeating unit fuel cell in slab geometry. The code allows both lattice and non-lattice portions of the unit fuel cell to be defined. The lattice region is defined as the fuel/clad/moderator repeating array. The non-lattice region contains any materials, such as structure and water spaces, which are not in the lattice. The

UVAR fuel cell model defines the fuel meat, clad, and water gap array of the element to be the lattice region. The non-lattice region contains the element side plates, non-fuel bearing fuel plate edges, control rod guide plates, and control rod water holes. The fuel and control rod elements are slightly smaller than the grid cell dimensions shown in Figure 2-1, thus when loaded in the gridplate, a small amount of water exists between the edges of adjacent elements in all directions. This water is considered non-lattice.

The LEOPARD models "distort" the actual fuel and control rod element dimensions somewhat while conserving materials and surface area. The distortion consists of "compressing" the cell in the y direction and correspondingly "stretching" the cell in the x direction. This distortion was performed so that the lattice region of the cell extends completely across the grid cell in the x direction, thus eliminating the small amount of water that actually lies between each element in the x direction. This distortion technique, developed by Fehr [2], allows for an uninterrupted fuel lattice region when several elements are loaded together in the 2-D core models.

Burn-up cross sections account for fuel depletion, xenon and samarium buildup, and other fission products.

Two and four group cross sections calculated for the fuel lattice, non-lattice and control rod non-lattice regions are

presented in Appendix A.

3.1.2 Control Rod Cross Sections

Two group control rod cross sections were developed using a combination of various features provided in the THERMOS, GAMTEC, and EXTERMINATOR codes. The method of developing control rod cross sections is quite involved and time consuming to perform. Several different modeling techniques were investigated by Wasserman [22]. The Wasserman study yielded methodologies for control rod modeling that produced results consistent with experimental data. The Wasserman study specifically addressed control rods in the UVAR HEU-18 fueled core. An analogous methodology was developed to calculate control rod cross sections for the LEU fuel. Control rod cross sections were used to calculate control rod worths (Section 4). A brief description of the methodology is presented here; however, the reader is referred to Wasserman (and Reference [3]) for a detailed presentation.

Control rods are difficult to model using diffusion theory computer codes because the control rod is a strong absorber and creates a steep local flux gradient. Diffusion theory cannot adequately handle the steep gradient, thus transport theory is required. The methodology developed to model the control rod region consists of calculating cross sections for that region which, when used in a full 2-D diffusion core model, produce the correct results. These cross sections are called "effective"

diffusion theory cross sections because they help the diffusion theory code "effectively" handle the local rod transport problem.

The effective cross sections were developed by first calculating transport thermal microscopic cross sections for the control rod region. A 1-D THERMOS slab transport model of a control rod fuel element with control rod material in the central region was developed. The THERMOS model calculated region-smeared microscopic cross sections and region-dependent neutron absorption fractions.

Fast group microscopic cross sections were developed with a cylindrical GAMTEC model control rod fuel element. GAMTEC calculates fast group cross sections using a P-1 approximation. GAMTEC also calculates resonance absorption fractions for the cell model.

The thermal and fast microscopic cross sections were input into a 2-D EXTERMINATOR model of a rodded control rod element using x-y geometry. The area of the control rod region in the EXTERMINATOR model corresponds to the area used for the control rod water hole region of the 2DB models.

The thermal absorption cross sections were manually adjusted in the EXTERMINATOR model until the thermal absorption fractions in the fuel and control rod regions matched those predicted by the THERMOS model. The fast absorption cross sections in the EXTERMINATOR model were also manually adjusted such that the

fraction of neutrons reaching thermal energies matched the resonance escape probability predicted by the GAMTEC P-1 approximation.

The methodology described above was applied to each fuel type (i.e., HEU-18, LEU-18, LEU-22). Resulting macroscopic cross sections are presented in Appendix A.

3.1.3 Reflector Cross Sections

Graphite and water are the predominant reflector materials for the UVAR reactor. Other reflector materials are addressed in Section 7.

Two and four group water and graphite reflector cross sections were provided by Argonne National Laboratory (ANL) EPRI-CELL computer models. These cross sections are presented in Appendix A.

Two group graphite reflector cross sections were developed by Wasserman at UVA using the GAMTEC code. The UVA cross sections were used in the 2DB core models and are presented in Appendix A. The UVA graphite cross sections were found to be consistent with the ANL cross sections.

3.2 Diffusion Theory Modeling Of The UVAR Core

The 2DB code was used to model the UVAR core for the purposes of calculating the k-effective eigenvalue solutions. Studies presented in this report focus on reactivity effects associated with various core changes as determined from changes in the 2DB calculated k-effective. The EXTERMINATOR code was used to develop

2-D UVAR core models for the purpose of calculating delayed neutron fractions and prompt neutron lifetimes. The EXTERMINATOR model is analogous to the 2DB model and is addressed in Section 8.

Fehr [2] developed the basic 2DB core model for HEU-18 and for LEU fuels. The Fehr models were revised and updated somewhat to be consistent with the UVA LEU element designs described in Section 2. The reader is referred to Fehr for detailed modeling descriptions.

The 2DB core model consists of a 60-by-62 mesh in x-y geometry. The model extends about 10 to 15 cm beyond the UVAR grid plate in both directions. The outer boundaries were defined with a zero flux condition. The axial direction is accounted for by spatially-dependent axial buckling terms developed from ANL 3-D UVAR core models.

Cross sections described in Section 3.1 were used as input into the code. LEOPARD-developed cross sections were input directly through the LINX computer code while other cross sections were input by hand.

Two basic core models were considered in this analysis; the 4-by-4 and 4-by-5 core model. The 4-by-4 core model, presented in Figure 3-1, consists of 12 fuel and 4 control rod elements in a 4-by-4 array. Figure 3-2 presents the 4-by-5 core model which consists of 16 fuel elements and 4 control rod elements in an 4-by-5 array. Individual fuel elements are identified by the number

appearing in the lower left hand corner of the fuel element cells shown in Figures 3-1 and 3-2. The cores are shown with an optional full graphite reflector, which means that each grid plate location surrounding the core is loaded with a graphite element.

Core models shown in Figures 3-1 and 3-2 use "staggered" control rod locations. Staggered control rod locations are necessary because the emergency core cooling system sprays from the east and west directions. If the control rod locations were not staggered, spray water to adjacent elements would be impeded.

The models are built with unit cells, each with dimensions corresponding to the grid cells described in Section 3.1.

The core model was "built" by placing appropriate material cross sections in desired model cells. Fuel region cross sections developed with the LEOPARD code were input in cells to simulate fuel elements. LEOPARD control rod element cross sections were input into cells to simulate control rod elements. Control rod cross sections and reflector cross sections were utilized in the same manner.

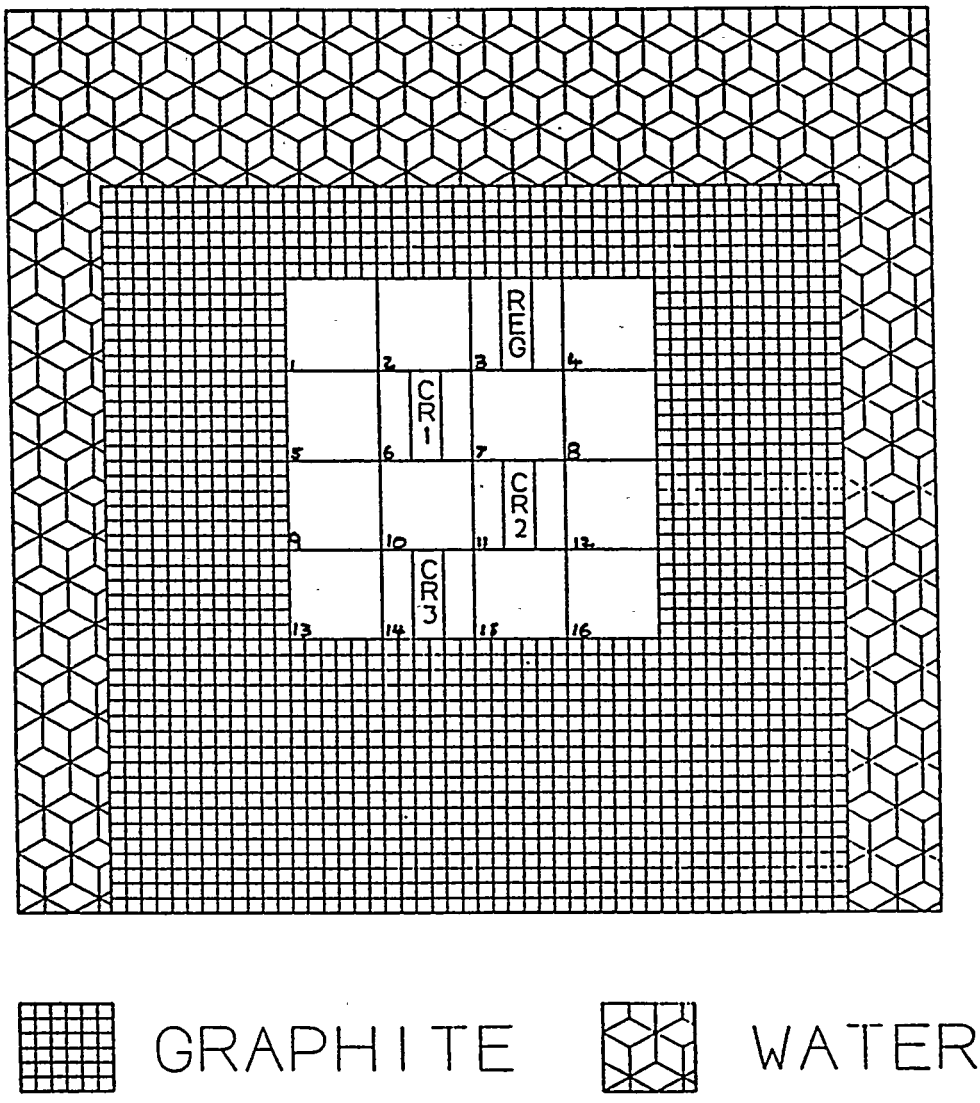


Figure 3-1. UVAR 4-by-4 Core Model. (Figure by M. Fehr, January, 1989)

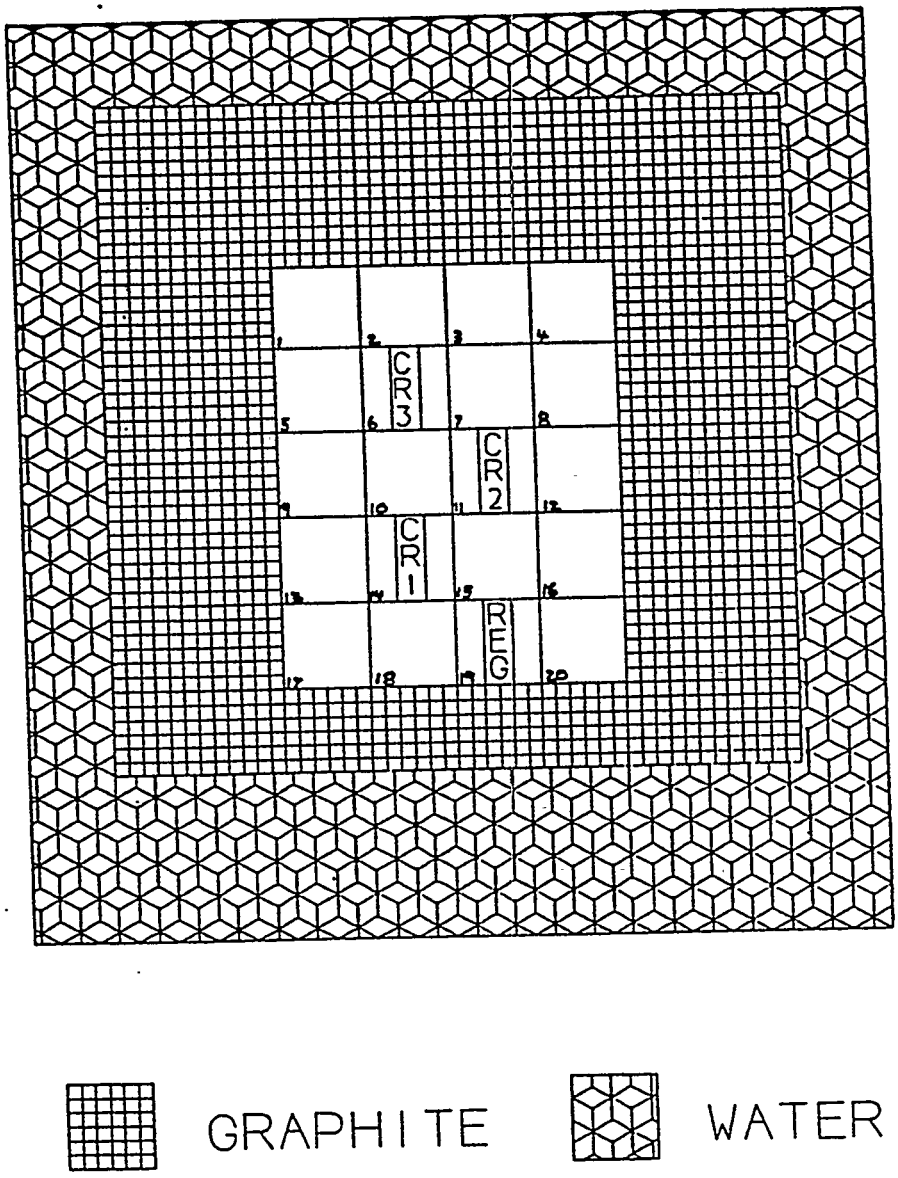


Figure 3-2. UVAR 4-by-5 Core Model. (Figure by M. Fehr, January, 1989)

CHAPTER 4.0 CONTROL ROD WORTH STUDY

Control rod worths have been determined for 4-by-4 and 4-by-5 UVAR cores constructed with the LEU-22, LEU-18, and HEU-18 fuel options. The term "control rod" encompasses both the safety rods (Rods 1, 2, and 3) and the regulating rod as described in Section 2. The effects of core life and core reflector material on control rod worth have also been determined. Additionally, control rod worth as a function of the positioning of the rods in the core has been investigated.

4.1 Rod Worths In 4-by-4 and 4-by-5 UVAR Cores

Control rod worths have been determined for both the 4-by-4 and 4-by-5 graphite reflected UVAR core models for each fuel option. Rod worths were determined by replacing control rod water hole cross sections by the control rod cross sections presented in Appendix A. Control rod locations are shown in Figures 3-1 and 3-2 (See Chapter 3) for the 4-by-4 and 4-by-5 cores, respectively. Control rod worths were initially developed in the Spring of 1988 and were documented in a UVA internal memorandum [23]. The neutronics models have since been revised and the rod study has consequently been updated. Results of the updated study, not significantly different from the original study, are presented here.

Table 4.1 presents calculated control rod worths for the UVAR 4-by-4 and 4-by-5 cores for each fuel option. Rod worths

presented in Table 4.1 have an estimated computational error of the order of five percent.

Table 4.1 Control Rod Worths For the UVAR 4-by-4 and 4-by-5 Cores.

Rod Inserted	- Rod Worths (%$\Delta\rho$) - LEU-22	LEU-18	HEU-18
I. 4-by-4 UVAR Core			
a) Reg. Rod	0.67	0.66	0.58
b) Rod 1	3.75	3.69	3.77
c) Rod 2	3.93	3.89	3.97
d) Rod 3	2.32	2.23	2.25
II. 4-by-5 UVAR Core			
a) Reg. Rod	0.39	0.39	0.33
b) Rod 1	2.46	2.38	2.47
c) Rod 2	3.21	3.18	3.21
d) Rod 3	2.79	2.75	2.79

Information provided in Table 4.1 shows that rod worths are not significantly affected by the different fuel types.

The maximum control rod worth is that of Safety Rod 2. This is expected because Rod 2 is the most centrally located rod and is consequently exposed to higher flux and carries a higher adjoint importance than the other rods. This is also consistent with the fact the peak flux value (determined in Section 5) is also found in the same region.

Experimentally determined control rod worths for the 4-by-4 HEU-18 core are available [24] and are compared with the calculated worths in Table 4.2. Experimentally determined worths

were converted from dollars to % $\Delta\rho$ using an effective delayed neutron fraction of 0.0074. (Information presented in Chapter 8 shows that an effective delayed neutron fraction of 0.0074 is appropriate for the HEU core.)

Table 4.2 Comparison of Experimentally Determined and Calculated Rod Worths for the 4-by-4 HEU-18 UVAR Core.

Rod ID	Experimentally Determined Worth (%$\Delta\rho$)	Calculated Worth (%$\Delta\rho$)	Difference
Reg. Rod	0.43	0.58	35%
Rod 1	3.52	3.77	7%
Rod 2	3.70	3.97	7%
Rod 3	2.27	2.25	<1%

The calculated control rod worths presented in Table 4.2 match well with the experimental values. It should be noted that an estimated 10 percent absolute error is considered appropriate for the experimental values. The calculated worth of the regulating rod is a bit high; however, because of the minor role that the regulating rod plays in core safety (the regulating rod is non-scramable), no further calculational refinement was considered necessary. (ANL has privately stated [25] that they also over-calculate the worth of the regulating rod. The reason for this is not readily apparent, but may indicated a need to examine the cell boundary conditions or the cross section library for iron and other stainless steel constituents.)

4.2 Core-Life Effects On Control Rod Worth

Core-life effects on control rod worth were determined for the single case of a 4-by-5 graphite reflected core using LEU-22 fuel. The results of this study are generally applicable to other control rods and fuel options.

The worth of control rod 1 was determined at four different stages of core burnup: 1) 0 MW-days; 2) 4 MW-days; 3) 194 MW-days; and 4) 394 MW-days. The control rod worths calculated at each stage of core burnup are presented in Table 4.3.

Table 4.3 Core-Life Effects on Control Rod Worth

Core Burnup (MW-day)	Worth (%$\Delta\rho$)
0	2.46
4	2.51
194	2.57
394	2.62

The results above show that control rod worth tends to increase slightly over core life. The worth associated with 0 MW-day burnup is calculated for a "clean" xenon-free core. Experiments have shown that the UVAR reaches equilibrium xenon conditions after about 40 hours of continuous 2 Megawatt operation (i.e., 80 MW-hrs). This corresponds roughly to the first burnup step of 4 MW-days (96 MW-hrs). The difference in rod worth between the 0 MW-day and 4 MW-day cases is most likely a result of changes in spatial flux shape due to xenon rather than as a result

of fuel burnup. Control rod worth changes for the longer time steps (all at equilibrium xenon conditions) are due to fuel burnup.

Because control rod worths tend to increase with core burnup (and with xenon buildup), the shutdown (safety) margin also increases in the direction of conservatism - a favorable trait. Control rod worth curves form the basis for demonstrating compliance with NRC requirements and determining the worth of experiments. Because control rod worths change with core burnup, the rods should be periodically recalibrated to account for the burnup effect. Currently, UVAR procedures require rod recalibration every 1200 Mw-hours (50 Mw-days) for just this reason. As discussed earlier, control rod worths may change due to xenon buildup over operations extending over several days; however, no method exists to account for this change. Because rod worths swing in the conservative direction (i.e., greater shutdown margins) this effect is not deleterious to safe operation.

4.3 Reflector Effects On Control Rod Worths

Reflector effects on control rod worth were determined for three representative reflector options for the LEU-22 4-by-5 UVAR core. The reactivity worth of control rod 1 was determined for the UVAR using Reflector Options 1, 5, and 13 as described in Section 7.1.

Reflector Option 1 consists of a full grid plate of graphite surrounding the centrally-located 4-by-5 core. Reflector Option 5 is similar to Option 1 except that the entire East core face is reflected by water. Reflector Option 13 consists of a full water reflector surrounding the 4-by-5 core.

The reactivity worths of control rod 1, calculated for the UVAR core using the various reflector options are presented in Table 4.4. Control rod worths were calculated relative to the unrodded core.

Table 4.4 Reflector Effects on Control Rod Worth

Reflector Option	Control Rod 1 Worth (%$\Delta\rho$)
1	2.47
5	2.75
13	2.84

The results presented above show that control rod worth tends to increase as the core graphite reflector is replaced by water reflector. The rod worth for the all-water reflector (Option 13) is about 15 percent higher than for the all-graphite reflector (Option 1). This implies that control rod worths should be reexamined (recalibrated) following significant changes in core reflector. UVAR procedures address this effect by requiring control rod recalibration with removal or insertion of one or more graphite elements next to the core.

4.4 Control Rod Position Effects

Control rod worths for control rods in the alternate locations shown in Figure 4-1 have been calculated for LEU-22 fuel.

It has been suggested that rotating the UVAR core by 45 degrees would lead to higher neutron fluxes in certain experimental facilities. As discussed in Chapter 3, the UVAR core models used staggered rod positions to prevent interfering with the emergency core cooling system (ECCS). If the core is rotated the rod pattern shown in Figure 4-1 is proposed to prevent interference with the ECCS.

Reactivity worths of the control rods in the alternate positions shown in Figure 4-1 for LEU-22 fuel are presented in Table 4.5

Table 4.5. Control Rod Worths For Alternate Rod Locations In UVAR 4-by-5 Core.

Rod Inserted	Rod Worth (% $\Delta\rho$)
Reg Rod	0.80
Rod 1	2.56
Rod 2	2.74
Rod 3	2.70

Information provided in Table 4.5 shows that the safety rod worths (Rods 1,2, and 3) show little variation, as expected, due to the symmetrical nature of their locations.

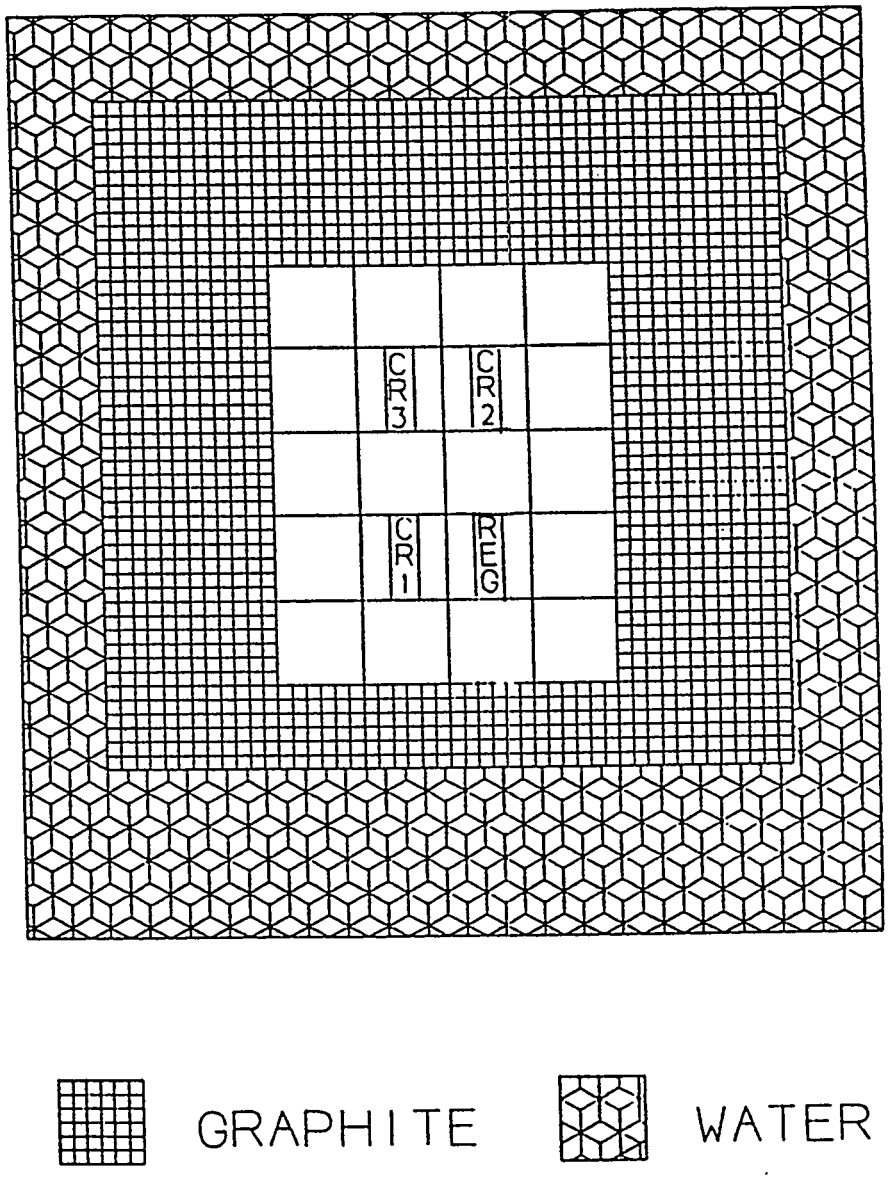


Figure 4-1. Alternate Control Rod Locations for UVAR 4-by-5 Core.

Rod worths for Rods 1 and 3 in the alternate locations are about the same as calculated in the staggered-rod positions (Table 4.1) because their relative core locations are similar. Rod 2 in the alternate-location model has about 1/2% $\Delta\rho$ less worth than in the staggered-location model. This is because Rod 2 is more centrally located in the staggered model resulting in higher importance. By the same argument, the regulating rod worth in the alternate model is more than twice that calculated in the staggered model.

The sum of all control rod worths in the alternate model is about the same as for the staggered model.

4.5 Control Rod Worth Study Summary

Based on the results presented above, the following summary statements can be made:

1. Control rod worths are not significantly affected by the choice of fuel option.
2. Control rod worths are dependent on the rod position in the core with centrally-located rods having the highest worths.
3. Good agreement was found between experimentally determined and calculated rod worths.

4. Control rod worths change with xenon build-up and core burn-up implying that control rods should be periodically recalibrated.
5. Control rod worths change with core reflector changes implying the need to recalibrate rods following core reflector changes.
6. Control rod worths vary for the alternate-rod-position model considered; however, the sum of the rod worths was almost identical to that calculated for the staggered-rod-position model.

5.0 RADIAL PEAKING FACTORS

Radial peaking factors have been determined for the UVAR core for the purpose of supporting the Thermal Hydraulics Analysis portion of the HEU to LEU Conversion effort. The sensitivity of radial peaking factors to variations in core configuration, control rod element orientation, control rod insertion, core burnup, and core reflector options have been evaluated. Axial peaking factors are not addressed in this analysis; however, experimental data pertaining to axial peaking factors for the HEU UVAR are available [26].

Peaking factors were determined using the 2DB computer code described in Section 3. The 2DB code provides a mesh-centered flux map (and optional edge-centered fluxes) for each energy group. The 2DB code also provides average group flux values for specified edit regions. The "active" or "lattice" fuel region of the reactor core, where heat production occurs, was defined as a single edit region. Peaking factors were calculated by taking the peak-to-average thermal flux ratio found in the active fuel region of the reactor core.

Thermal flux peaking factors are considered representative of power peaking factors. Neglecting fast fission effects, power production can be considered proportional to $\Sigma_f \phi_{th}$, where Σ_f is the thermal macroscopic fission cross section and ϕ_{th} is the thermal neutron flux. If Σ_f is considered constant, power

production is proportional to ϕ_{th}. For all beginning-of-life (BOL) unburned UVAR core models, Σ_f was indeed constant over the fuel region. All analyses presented below use a BOL core model except for the core burnup analysis presented in Section 5.5. (The core burnup analysis accounts for a non-uniform Σ_f distribution.)

Thermal flux peaking factors were used in the original HEU UVAR thermal-hydraulic safety analysis and in the UVAR 2 megawatt upgrade safety analysis, and are considered appropriate for use in the LEU thermal-hydraulic analysis. The thermal-hydraulic analysis focuses on a single "hot-channel" and relies on peaking factors to relate the hot channel to the nominal channel which is normalized to core size and average power.

The calculated peak thermal flux in the fuel region was found to occur immediately adjacent to a control rod element water hole. The model mesh boundary between the water hole and fuel region is located between the control rod guide plate and the first adjacent fuel plate (see Figures 2-3 and 2-4). Consequently, the flux at the mesh-edge boundary between the fuel region and water hole is higher than the flux at the center of the first fuel region mesh. Although the mesh edge flux is higher, the channel between the first adjacent fuel plate and the control rod guide plate is not considered the "hot-channel" because it only receives heat from the single fuel plate. The next adjacent channel is the "hot-

channel", receiving the maximum heat flux from the two surrounding fuel plates. Mesh-centered flux values for the computer models are located in the "hot-channel" and are therefore considered more appropriate than edge-centered values. Mesh-centered fluxes have been used throughout this analysis.

The LEU peaking factor analysis focused on the four areas of study described below:

1) 4-by-4 and 4-by-5 graphite reflected core;

2) control rod element rotation effects;

3) control rod insertion effects;

4) core burnup effects; and

5) core reflector effects.

The results of these studies are presented below.

5.1 Radial Peaking Factors for 4-by-4 and 4-by-5 UVAR Cores

Radial peaking factors have been determined for the UVAR reactor in 4-by-4 and 4-by-5 graphite-reflected, unrodded BOL core configurations. Peaking factors for LEU-22, LEU-18, and HEU-18 fuel options have been evaluated for each core configuration.

Radial peaking factors determined for the above-defined core configurations and fuel options are presented in Table 5.1.

Information presented in Table 5.1 shows that peaking factors are slightly higher in LEU fuel than in HEU fuel. This is primarily due to a harder flux spectrum downscattering in the control

rod water holes. The LEU-18 peaking factors are about 4 to 6 percent higher than the HEU-18 peaking factor.

Table 5.1. Radial Peaking Factors for UVAR 4-by-4 And 4-by-5 Core Configurations With Various Fuel Options.

Core Configuration/Fuel Option	Radial Peaking Factor
1. 4-by-4 Core Configuration	
a) LEU-22	1.72
b) LEU-18	1.67
c) HEU-18	1.61
2. 4-by-5 Core Configuration	
a) LEU-22	1.81
b) LEU-18	1.76
c) HEU-18	1.66

Peaking factors increase with core size and with the number of plates per fuel element. Peaking factors for the 4-by-5 cores are about 3 to 5 percent higher than for the 4-by-4 cores. The peaking factor for LEU-22 fuel is also about 3 percent higher than for LEU-18 fuel.

Peak thermal flux values were found in locations immediately to the left of the Control Rod 2 water hole (see Figures 2.3 and 2.4). This location is consistent with the measured peak flux found by Sternberg [26].

Limited experimental data is available on UVAR HEU radial

peaking factors. A radial peaking factor of 1.37 was experimentally determined for a partially-burned UVAR 4-by-4 HEU-12 (12 flat plates per element) core via foil flux mapping [5]. An estimated experimental error of 10 percent is considered appropriate for this value.

This experimental value was subsequently "corrected" [5] using a 1-D neutronics code to predict a value of 1.45 for the HEU-18 core. The value of 1.45 is about 10 percent lower than the value of 1.61 estimated in this analysis, which appears to be within the experimental and computational uncertainty.

The 4-by-4 core configurations are the limiting core configurations (for each fuel type) for the Thermal Hydraulic Analysis [4]. This is primarily due to the higher average power density and non-element bypass flow rate associated with the small cores. These factors outweigh the importance of the slight increase in peaking factors associated with the larger cores. No core larger than 4-by-5 was considered in this analysis.

5.2 Control Rod Element Rotation Effects on Radial Peaking Factors

The control rod elements are asymmetrical in that there is one more fuel plate on one side of the control rod hole than on the other side (see Section 2). Because the LEU fuel elements will use flat plate fuel, it should be possible to load the control rod elements (and fuel elements) into the grid plate in

two different orientations, each 180 degrees rotated from the other.

The curved plate HEU-18 fuel, currently used in the UVAR, cannot be rotated. This is due to the physical nature of the HEU-18 curved plate elements which interlock and consequently must all be loaded in the same orientation.

Radial peaking factors presented in Section 5.1 were calculated for cores in which all control rod elements were loaded with the extra plate on the left side of the element. To characterize the effect of different control rod orientations on peaking factors, three different control rod orientation scenarios were analyzed:

Scenario 1. All control rods loaded with the extra plate on the right side of the element.

Scenario 2. Rods 1 and 3 loaded with the extra plate on the right side of the element; Reg Rod and Rod 2 loaded with the extra plate on the left side of the element.

Scenario 3. All control rods loaded with the extra plate on the left side of the element.

Control rod locations are shown in Figures 3-1 and 3-2.

Table 5.2 presents radial peaking factors determined for the different control rod element orientation scenarios. It should be noted that values presented for the HEU-18 fuel option in Scenario

2 are fictitious because the curved plate fuel cannot be physically loaded in opposing orientations. HEU-18 peaking factors for Scenario 2 are presented for comparison purposes only.

Table 5.2 Radial Peaking Factors For Control Rod Orientation Scenarios

Core Configuration/ Fuel Loading	Radial Peaking Factors		
	Scenario 1	Scenario 2	Scenario 3*
1) 4-by-4 Core Configuration			
a) LEU-22	1.72	1.66	1.72
b) LEU-18	1.67	1.62	1.67
c) HEU-18	1.61	1.57	1.61
2) 4-by-5 Core Configuration			
a) LEU-22	1.81	1.75	-
b) LEU-18	1.76	1.70	-
c) HEU-18	1.66	1.62	-

* Peaking factors for Scenario 3 were calculated for the 4-by-4 core configuration only.

Information presented in Table 5.2 shows that radial peaking factors for Scenario 2 are about 2.4 to 3.5 percent lower than those presented in Scenario 1. Scenario 3 values are virtually identical to Scenario 1 values. This is reasonable because of the near symmetry of the core and the fact that all elements have the same orientation in Scenarios 1 and 3.

The differences in values can be taken as an estimate of the overall precision associated with calculated peaking factors.

5.3 Control Rod Insertion Effects on Radial Peaking Factors

The peaking factors presented in Sections 5.1 and 5.2 were calculated for unrodded cores. In order to gain insight into the effect of control rod insertion on peaking factors, the LEU-22 4-by-4 graphite reflected BOL core was analyzed with various control rod insertion scenarios. This analysis is not completely rigorous due to the limitations on diffusion theory when handling interfaces at control rod boundaries and the approximations involved in developing cross sections for the control rod regions (see Section 4). None the less, this analysis provides insight into the general behavior of peaking factors with control rod insertion.

Table 5.3 presents the radial peaking factors associated with the LEU-22 4-by-4 BOL graphite reflected core with various control rod insertions.

Information provided in Table 5.3 shows that radial peaking factors increase by as much as 3 percent with single rod insertions except for Rod 2. Because the peak flux location of the unrodded core is adjacent to Control Rod 2, insertion of rods other than Rod 2 push the flux up in the Rod 2 region causing an increased peak. Similarly, insertion of Rod 2 depresses the flux in that region and "pushes" the peak location towards the Rod 1

water hole. Consequently, the flux shape is flattened and the peaking factor decreases by about 2 percent.

Table 5.3. Radial Peaking Factors for LEU-22 4-by-4 Graphite Reflected Core With Various Rod Insertions.

Core Status	Peaking Factor	Peak Location
1. Unrodded Core (No rods inserted)	1.72	Adjacent left side of Rod 2
2. Rod 1 Inserted Only	1.77	Adjacent left side of Rod 2
3. Rod 2 Inserted Only	1.69	Adjacent Right Side of Rod 1
4. Rod 3 Inserted Only	1.75	Adjacent Left side of Rod 2
5. Reg Rod Inserted Only	1.76	Adjacent Left side of Rod 2

The Peaking Factors presented in Table 5.3 vary from 1.69 to 1.77 (about 5%) depending on which rod is inserted. Combinations of more than one rod inserted at a time were not evaluated because the UVAR cannot be taken critical with more than one rod fully inserted due to regulatory restrictions on shutdown margin and excess reactivity.

5.4 Core-Life Effects on Radial Peaking Factors

The peaking factors presented in Sections 5.1, 5.2, and 5.3 were calculated for beginning of life (BOL), unburned cores. During reactor operation, the core is slowly "burned" resulting in

less U-235 and a buildup of fission products and poisons. The effect of core burnup on peaking factors was determined by analyzing a 4-by-5 LEU-22 graphite-reflected core at various burnup times. Burnup times evaluated were: 1) no burnup; 2) 194 MW-days burnup; and 3) 394 MW-days burnup.

As discussed earlier, the validity of the thermal flux peaking factor is tied to the assumption that Σ_f remains constant over the fuel region. This assumption is valid for BOL cores; however, because cores burn unevenly, Σ_f is not constant throughout the fuel region in a burned core. In order to account for the non-uniform Σ_f distribution in the core, the following approximation scheme was used to calculate peaking factors for burned cores:

1. The peak value of $(\Sigma_f \phi_{th})_{local}$ was determined by multiplying the local Σ_f determined for each fuel element by the associated mesh thermal fluxes. In each case the location of the peak value of $(\Sigma_f \phi_{th})_{local}$ coincided with the location of the peak thermal flux.
2. An average value $\bar{\Sigma}_f$ was determined by simply summing element specific Σ_f's over the 20 elements and then dividing by the 20 elements. The average thermal flux $(\bar{\phi}_{th})$ in the active fuel region was provided as output by the 2DB code.
3. The peaking factor was then estimated as follows:

$$\text{peaking factor} = \frac{(\Sigma_f \phi_{th})_{local}^{peak}}{\bar{\Sigma}_f \, \bar{\phi}_{th}}$$

Ideally, the denominator would be a flux-weighted average of Σ_f over each fuel region mesh point. Unfortunately, this value is not readily available from the information provided in the 2DB output*. The above described weighting scheme provides an adequate approximation for determining the general behavior of peaking factors with core burnup.

Table 5.4 presents radial peaking factors for the UVAR 4-by-5 LEU-22 graphite reflected core with 0, 194, and 394 Mw-days burnup. Also presented in Table 5.4 is the min-to-max variation in Σ_f over the core region for each burnup step.

Table 5.4. Core Life Effects on Radial Peaking Factors for the LEU-22 4-by-5 Graphite Reflected Core.

Burnup (MW-day)	Peaking Factor	Σ_f variation
0	1.81	0%
194	1.77	3%
394	1.73	6%

*Certain edits were added to the 2DB code by the University of Michigan that appear to address power peaking factors; however, there are unresolved inconsistencies in these edits. Preference was given to the original code edits for flux values which were used throughout the peaking factor analysis.

Information presented in Table 5.4 shows that peaking factors decrease with core life. This is consistent with the fact that there is more local burnup in the peak flux region than in the rest of the core resulting in a flattened flux distribution.

5.5 Core-Reflector Effects on Radial Peaking Factors

Reflector options for the UVAR core were analyzed for the LEU-22 and LEU-18 fuel options as discussed in Chapter 7. Peaking factors associated with the various reflector options have been determined. Table 5.5 presents peaking factors associated with three representative reflector options for LEU-22 and LEU-18 fuel.

Table 5.5. Core-Reflector Effects on Radial Peaking Factors

	--- $\Delta\rho$(%Δk/k) ---	
Reflector Option	LEU-22	LEU-18
1. All-Graphite Reflector	1.73	1.67
2. Single Row of Graphite Surrounding Core	1.75	1.69
3. All-Water Reflector	1.76	1.73

Peaking factors were found to be relatively insensitive to the various reflector options and showed a maximum variability of about 3 percent.

5.6 Radial Peaking Factor Summary

Peaking factors for various core configurations, control rod orientations, rod insertions, core burnup, and reflector options have been obtained. Based on information presented above, the following conclusions have been made:

1. Radial peaking factors for LEU fuel are slightly higher than for HEU fuel. Peaking factors increase with core size and with the number of fuel plates per element.
2. Radial peaking factors may vary by as much as 3.5 percent depending on control rod orientations.
3. Insertion of a single control rod can produce a change in peaking factor ranging from a 2 percent decrease to a 3 percent increase.
4. Peaking factors decrease somewhat with core life due to the higher burnup occurring in the peak flux region.
5. Peaking factors are relatively insensitive to the core-reflector option, showing a maximum variability of about 3 percent.

CHAPTER 6.0 TEMPERATURE AND MODERATOR EFFECTS STUDY

Temperature and moderator void effects have been characterized for the UVAR reactor. Section 6.1 addresses temperature effects and Section 6.2 addresses moderator void effects.

6.1 Temperature Effects

Temperature effects have been determined for the UVAR reactor for both a 4-by-4 and 4-by-5 graphite reflected core configuration. Temperature effects on core reactivity have been quantified separately in terms of: 1) doppler effect; 2) moderator temperature effect; 3) power defects; and 4) gross system heating effect. Temperature effects for the 4-by-4 core configuration were determined in the Spring of 1988 and were documented via a UVA internal memorandum [27]. The temperature-effects analysis for the 4-by-5 core configuration was performed in early 1989 and incorporates the latest revised core models.

Temperature effects presented in the following sections are determined from the change in core reactivity associated with that effect relative to the reactivity associated with a "reference" core condition. Reference core conditions were determined from a review of information used in the UVAR HEU-to-LEU thermal hydraulics work, where the fuel-plate-to-moderator-temperature differential was determined to be about $9^{o}C$ for 22 plate elements and about $12^{o}C$ for 18 plate elements. The temperature gradient

across the thin fuel plate was assumed to be negligible. Temperatures used for the reference cores are provided below:

Element Type	Fuel Plate Temperature (°C)	Moderator Temperature (°C)
22 plate	30	21
18 plate	33	21

Temperature effects for the 4-by-4 cores were determined for LEU-22, LEU-18, and HEU-18 fuel options. Temperature effects for the 4-by-5 cores were determined for LEU-22 and HEU-18 fuel options only.

6.1.1 Doppler Effects

Doppler effects for the UVAR core were determined by adjusting the resonance temperature parameter in the LEOPARD code. Table 6.1 presents reactivity worths and doppler coefficients associated with resonance temperatures of 75, 100, and 200 degrees celsius. Differential reactivity worths were determined from the change in k-effective associated with each resonance temperature relative to the reference case k-effective. Doppler coefficients were determined by dividing reactivity worths by the associated change in resonance temperature.

Doppler coefficients for each fuel option remain relatively stable over the 75°C to 200°C temperature range. Doppler coefficients for LEU are about an order of magnitude greater than

for HEU fuel. This is consistent with the fact that LEU fuel has a much higher uranium-238 loading and is thus more sensitive to resonance effects. Similarly, LEU-22 fuel has a slightly higher doppler coefficient than LEU-18 because of the higher U-238 loading per element. It should be noted that the values presented in Table 6-1 neglect doppler broadening of the uranium-235 fission cross section.

Recommended values of doppler coefficients for the UVAR reactor are:

1) LEU-22: -1.1×10^{-5} % $\Delta\rho$ per ^{o}C
2) LEU-18: -1.0×10^{-5} % $\Delta\rho$ per ^{o}C
3) HEU-18: -1.3×10^{-6} % $\Delta\rho$ per ^{o}C

As estimated absolute error of 10 percent is believed to be associated with each of the above values.

6.1.2 Moderator Temperature Effects

Moderator temperature effects were determined by adjusting the moderator temperature parameter of the LEOPARD code. Table 6.2 presents reactivity worths and moderator temperature coefficients for the UVAR core. Reactivity worths were calculated based on changes in k-effective relative to the reference case (moderator temperature = $21^{o}C$).

Moderator temperature coefficients are relatively stable over the temperature range of interest and do not vary significantly between fuel types. Recommended moderator temperature

coefficients for the UVAR are the values presented for the 50°C case for the 4-by-5 core because the UVAR normally operates with moderator temperatures below 50°C. An estimated 10% absolute error is considered appropriate for the recommended coefficients.

Table 6.2 Moderator Temperature Effects for the UVAR Reactor

Moderator Temperature (°C)	Reactivity Worth ($\Delta\rho$)	Moderator Temperature Coeff ($\Delta\rho$ per °C)
I. UVAR 4-by-4 Core Configuration (1988 Study)		
	LEU-22 Fuel	
50	-5.0×10^{-3}	-1.7×10^{-4}
75	-1.1×10^{-2}	-2.0×10^{-4}
	LEU-18 Fuel	
50	-5.3×10^{-3}	-1.8×10^{-4}
75	-1.1×10^{-2}	-2.0×10^{-4}
	HEU-18 Fuel	
50	-5.4×10^{-3}	-1.8×10^{-4}
75	-1.1×10^{-2}	-2.0×10^{-4}
II. UVAR 4-by-5 Core Configuration (1989 Study)		
	LEU-22 Fuel	
50	-3.9×10^{-3}	-1.4×10^{-4}
75	-8.5×10^{-3}	-1.6×10^{-4}
95	-1.3×10^{-2}	-1.7×10^{-4}
	HEU-18 Fuel	
50	-4.2×10^{-3}	-1.5×10^{-4}
75	-8.8×10^{-3}	-1.6×10^{-4}
95	-1.3×10^{-2}	-1.8×10^{-4}

6.1.4 Gross System Heating Effects

Reactivity effects associated with gross system heating have been determined for a 20°C rise in all reactor components and moderator. This is consistent with actual operating conditions on hot humid days when the bulk temperature of the pool can swing from 68°F (20°C) to 104°F (40°C) during a single day of operation. Gross system heating coefficients are presented below for the 4-by-5 core configuration with LEU-22 and HEU-18 fuel.

Fuel Type	Temperature Coeff ($\Delta\rho$/°C)
LEU-22	-1.11×10^{-4}
HEU-18	-1.13×10^{-4}

The gross system heating coefficients for each fuel type are similar and have an estimated absolute error of about 10 percent.

6.2 Moderator Void Effects

6.2.1 Uniform Core Void Effects

Uniform moderator void effects on core reactivity, and void coefficients, have been determined for UVAR 4-by-5 graphite reflected cores with LEU-22, LEU-18, and HEU-18 fuel loadings. Uniform moderator voids ranging from 1 to 95 percent were analyzed.

Uniform voids in the core-moderator region were simulated by adjusting core-water densities in the LEOPARD fuel and control rod element models. Cross sections generated by the LEOPARD code were

then used in the 2DB diffusion theory code eigenvalue calculation. Reactivity worths ($\Delta\rho$) associated with uniform core voids were determined by the change in k-effective relative to the no-void core condition.

Table 6.4 presents reactivity worths associated with different void fractions for LEU-22, LEU-18 and HEU-18 fuels. The core moderator densities used to simulate the uniform core voids are also presented.

Table 6.4 Reactivity Effects Associated With Uniform Moderator Void Conditions With LEU-22, LEU-18, and HEU-18 Fuel Loadings.

% Void	Moderator Density(g/cm^3)	LEU-22 (%$\Delta\rho$)	LEU-18 (%$\Delta\rho$)	HEU-18 (%$\Delta\rho$)
1	0.99	-0.193	-0.173	-0.152
2	0.98	-0.386	-0.348	-0.307
5	0.95	-1.16	-1.00	-0.887
10	0.90	-2.48	-2.18	-1.94
20	0.80	-5.77	-5.16	-4.66
50	0.50	-24.7	-23.3	-24.3
90	0.10	-150.	-161.	-165.
95	0.05	-211.	-236.	-253.

Uniform moderator void coefficients were determined by dividing the reactivity worths presented in Table 6.4 by their associated percent void. Void coefficients calculated in this manner are presented in Table 6.5.

Table 6.5 Uniform Moderator Void Coefficients for LEU-22, LEU-18, and HEU-18 Fuels.

	Void Coefficients (%$\Delta\rho$/% Void)		
% Void	LEU-22	LEU-18	HEU-18
1	-0.193	-0.172	-0.152
2	-0.193	-0.174	-0.154
5	-0.231	-0.201	-0.177
10	-0.248	-0.218	-0.194
20	-0.289	-0.258	-0.233
50	-0.493	-0.466	-0.486
90	-1.67	-1.79	-1.83
95	-2.22	-2.48	-2.66

Figure 6-1 presents a plot of the void coefficient versus percent void for each fuel option.

Information provided above shows that in the 1 to 20 percent void region, the void coefficient for the LEU-18 fuel is higher than in the HEU-18 fuel. This is as expected because the harder flux spectrum associated with LEU fuel is more sensitive to moderator changes. Similarly, void coefficients for LEU-22 fuel are higher than for LEU-18 fuel due to the smaller water gaps associated with LEU-22 (and consequently a harder spectrum).

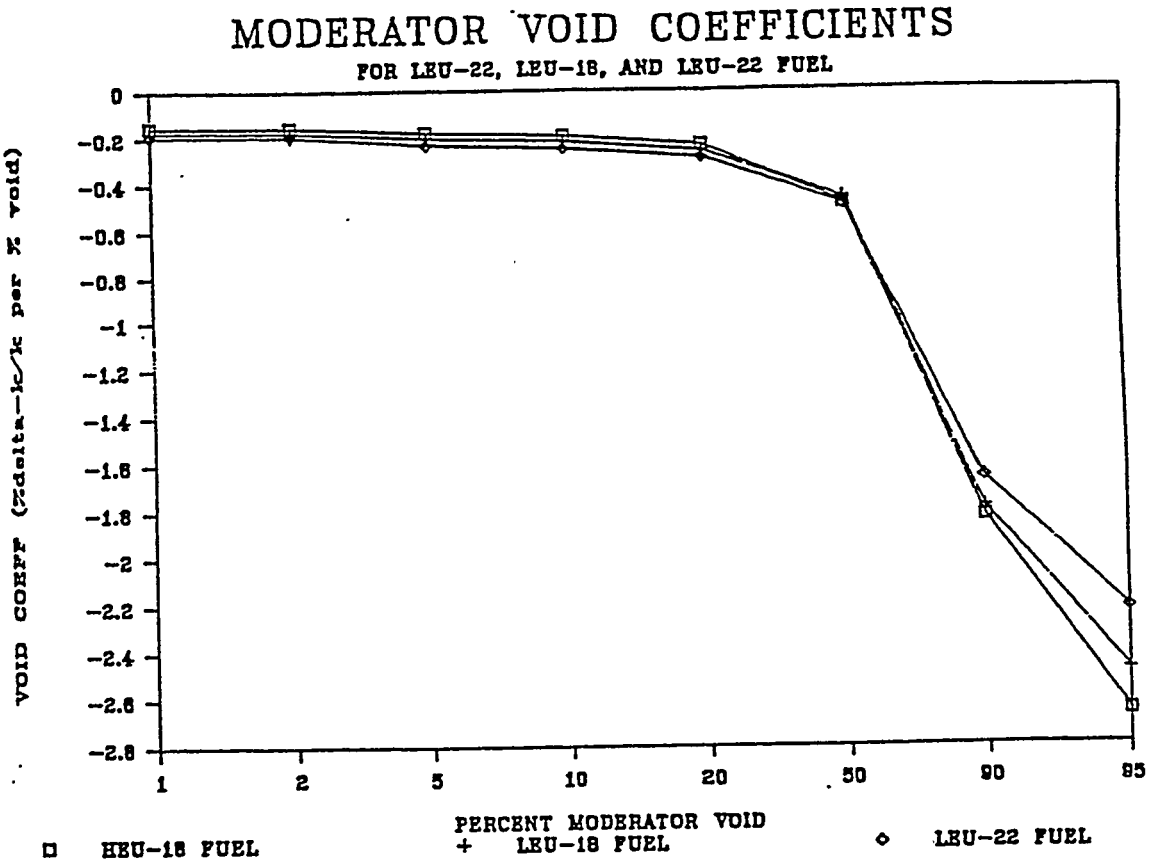


Figure 6-1. Void Coefficient As A Function Of Void Percent

A 20 percent total core void is significant and is considered a reasonable upper limit for void-effect studies. Void effects in this analysis were also considered for higher void fractions of 50, 90 and 95 percent. It should be noted that analyzing these higher void fractions "pushes" our current neutronics computer modeling capabilities due to limited data libraries and the breakdown of diffusion theory with increasing void fractions. Therefore, results presented above for the higher void fractions are not considered rigorous but are presented to provide insight into the general nature of void effects in severely voided cores.

6.2.2 Local Core Void Effects

Local void effects were analyzed for a UVAR 4-by-5 graphite reflected core with LEU-22, LEU-18, and HEU-18 fuels. Local void effects were determined by voiding 99 percent of the core moderator in local fuel element regions. As mentioned earlier, severe void conditions are difficult to model with diffusion theory modeling techniques. On the other hand, neutrons that stream across a local void are not lost to the system, so that the predicted void effects may indeed be meaningful.

Four different local void scenarios were considered. Each scenario consists of voiding 99 percent of the core moderator in particular regions. The locations of the voided regions (see Figure 3-2) considered are as follows:

Scenario 1 - West region of Element 11.

Scenario 2 - East regions of Elements 10 and 6, and West regions of Elements 11 and 7.

Scenario 3 - West region of Element 11 and entire Element 10 fuel region.

Scenario 4 - Fuel regions of Elements 10, 11, 6, and 7.

Each scenario includes voiding the west region of Element 11. This is where the "hot-channel" is located (determined by the Peaking Factor study in Chapter 5) and is therefore the most likely region to void.

Table 6.6 presents reactivity effects associated with the different void cases for LEU-22, LEU-18, and HEU-18 fuels. Reactivity worths are calculated relative to the unvoided core.

Table 6.6 Local Void Reactivity Effects for Void Scenarios 1 Through 4

Case	LEU-22 (%Δρ)	LEU-18 (%Δρ)	HEU-18 (%Δρ)
1	-0.678	-0.730	-0.834
2	-2.88	-3.16	-3.59
3	-3.49	-3.77	-4.23
4	-8.67	-9.50	-10.7

Unlike the uniform-moderator void effects discussed in Section 1, local void reactivity effects appear to be greater for the HEU fuel option which has a softer spectrum.

Local void coefficients have been developed by dividing the reactivity worths presented in Table 6.6 by the percent core water void. The percent core water void represents the ratio of the void volume to the total moderator volume of the unvoided core. Table 6.7 presents local void coefficient and percent core voids associated with each scenario for LEU-22, LEU-18, and HEU-18 fuel.

Table 6.7 Local Moderator Void Coefficients ($\%\Delta\rho/\%$ void)

Scenario	% of Core Voided	LEU-22	LEU-18	HEU-18
1	-1.3	-0.52	-0.56	-0.64
2	-4.6	-0.63	-0.69	-0.78
3	-5.9	-0.59	-0.64	-0.72
4	-14	-0.62	-0.68	-0.76

Local moderator void coefficients appear to be relatively constant over the scenarios considered. Unlike the uniform void cases, higher void coefficients were consistently determined for the HEU soft-spectrum fuel option because these voids occurred in regions of high importance.

6.3 Temperature and Moderator Effects Summary

Temperature and moderator effects were analyzed for the UVAR reactor. Based on the results presented above, the following summary statements can be made.

1. Doppler effects in the LEU fuel were found to be about an order of magnitude greater than in the HEU fuel due to the higher U-238 loading.
2. Moderator temperature coefficients were about the same for the different fuel types and were larger than the doppler coefficients by an order of magnitude for the LEU fuel and by two orders of magnitude for the HEU fuel.
3. The power defects and gross system heating effects calculated for the different fuel types were similar to each other and appeared to be dominated by moderator temperature effects.
4. Uniform moderator void coefficients were slightly higher in the LEU fuels than in the HEU fuel due to harder flux spectra as expected. This trend faltered as void fractions were increased past 50 percent.
5. Local moderator void coefficients appear to be relatively constant for the various scenarios and, unlike the uniform void coefficients, higher coefficients were found for the soft-flux spectrum cases (HEU-18) than for the LEU cases.

CHAPTER 7.0 REFLECTOR WORTH STUDY

Reflector worths were determined for several different reflector materials and thicknesses placed on different faces of the UVAR reactor in a 4-by-5 core configuration. Reflector materials analyzed include graphite, water, deuterium tanks, and black boundaries (total absorbers). LEU-22, LEU-18, and HEU-18 fuel options were considered. The results of this study were first presented via a UVA internal memorandum [28]. Due to model revisions incorporated after the completion of that study, reflector worths presented here have an estimated uncertainty of approximately 10 percent.

7.1 Graphite And Water Reflector Options

The UVAR reactor fuel and control rod elements are positioned on the UVAR grid plate, which has an 8-by-8 array of grid locations. Grid locations may be occupied by a fuel element, control rod fuel element, graphite element, or grid plug.

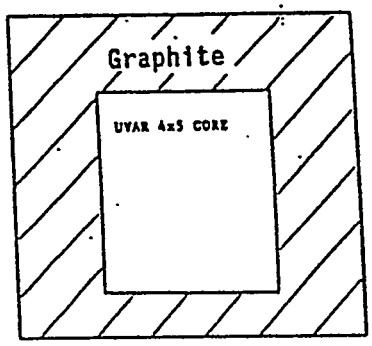
For the purposes of this analysis, the 4-by-5 core configuration was assumed to be centrally located on the grid plate. Remaining grid locations, surrounding the core, were assumed to contain either graphite elements or grid plugs. Grid plugs are short devices that do not extend into the active fuel region of the core, thus a grid location with a grid plug provides pool water reflector for the core in that location. The entire grid plate assembly is, of course, surrounded by pool water.

Several different reflector options were developed using graphite and water reflectors. Reflector Options 1 through 6 are variations of a full graphite reflector as shown in Figure 7.1.

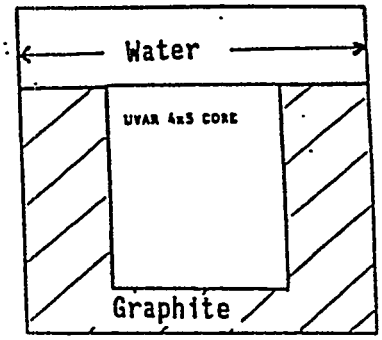
Option 1 consists of two full rows of graphite on the north, west, and east core faces, and a single row of graphite on the south core face. Reflector Options 2 through 6 were created by replacing graphite with water reflector on one or more of the core faces. Option 7, shown in Figure 7.2, consists of a single row of graphite surrounding the core. Options 8 through 12 are variations of Option 7 as shown in Figure 7.2. Option 13 (not shown) is the all-water reflector option. Reactivity worths associated with Options 2 through 6, and Options 7 and 13, calculated relative to Option 1, are presented in Table 7.1.

The reactivity worth associated with going from a full graphite reflector (Option 1) to a single row of graphite surrounding the core (Option 7) is only about 1.5%, while the reactivity swing from Option 1 to the full water reflector (Option 13) is over 7 percent. This shows that the importance of the first row of graphite reflector far outweighs the outermost second row.

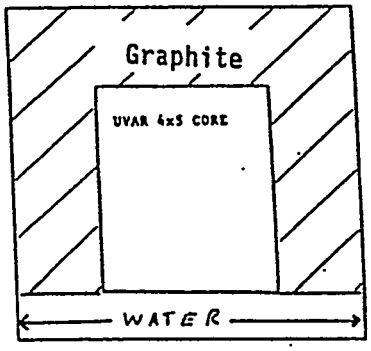
Table 7.2 presents reactivity effects associated with Options 8 through 13. Reactivity worths are calculated relative to Option 7.



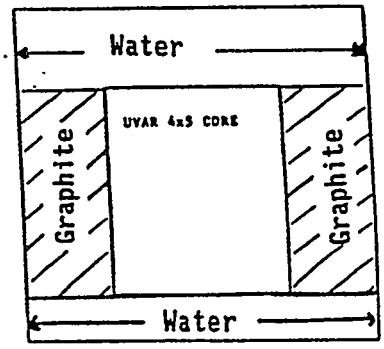
Option 1



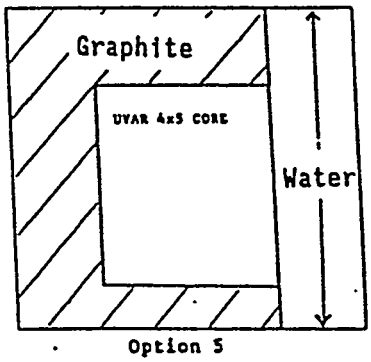
Option 2



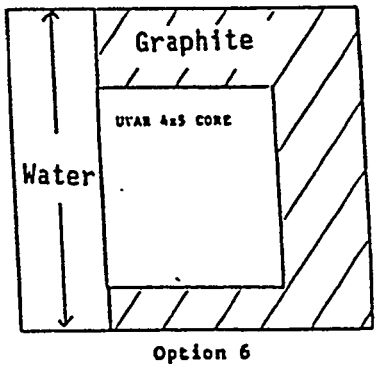
Option 3



Option 4



Option 5



Option 6

Figure 7-1. Reflector Options 1 through 6.

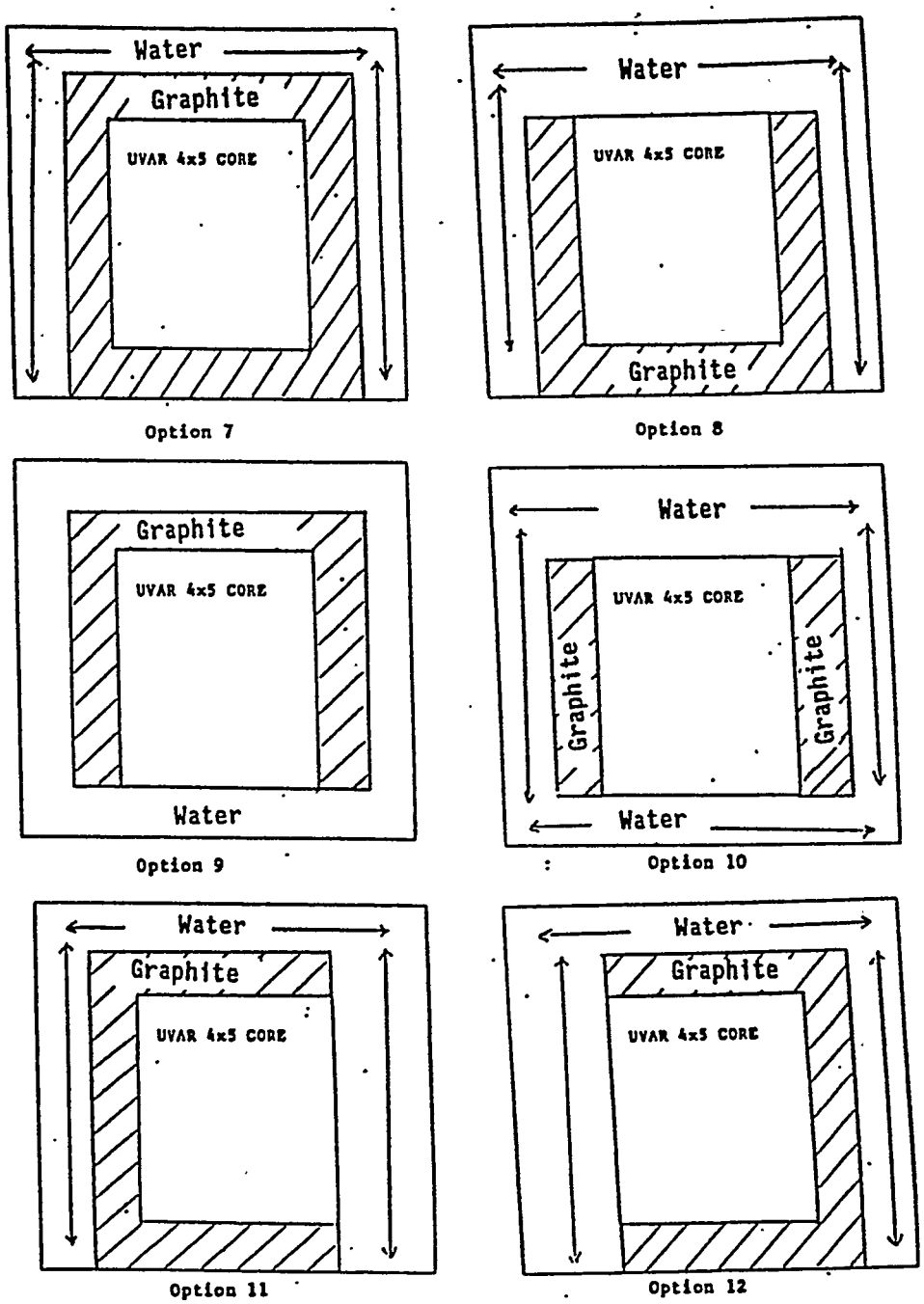


Figure 7-2. Reflector Options 7 through 12.

Table 7.1. Reactivity Effects Associated With Variations Of A Full Graphite Reflected 4-by-5 Core

Option	Reflector Description	LEU 18 FUEL (%Δρ)*	LEU-22 FUEL (%Δρ)*
1	Full graphite reflector: two rows of graphite on the east, north, and west face; and one row of graphite on the south face.	Reference Core	
2	Same as Option 1 with north face graphite replaced by water.	-1.96	-1.99
3	Same as Option 1 with south face graphite replaced by water.	-1.17	-1.24
4	Same as Option 1 with north and south face graphite replaced by water.	-3.35	-3.45
5	Same as Option 1 with east face graphite replaced by water.	-2.27	-2.33
6	Same as Option 1 with west face graphite replaced by water.	-2.19	-2.28
7	Single row of graphite surrounding entire core.	-1.48	-1.55
13	All-water reflector.	-7.23	-7.42

*Reactivity worths calculated relative to Option 1.

Table 7.2 Reactivity Effects Associated With Variations Of A Single Graphite Reflector Row Surrounding the 4-by-5 Core.

Option	Reflector Description	LEU 18 FUEL (%Δρ)*	LEU-22 FUEL (%Δρ)*
7	Single row of graphite surrounding entire core.	Reference Core	
8	Same as Option 7 with north face graphite replaced by water.	-1.36	-1.38
9	Same as Option 7 with south face graphite replaced by water.	-1.12	-1.18
10	Same as Option 7 with north and south face graphite replaced by water.	-2.64	-2.71
11	Same as Option 7 with east face graphite replaced by water.	-1.74	-1.78
12	Same as Option 7 with west face graphite replaced by water.	-1.69	-1.74
13	All-water reflector.	-5.75	-5.87

*Reactivity worths calculated relative to Option 7.

Information in Tables 7.1 and 7.2 shows that reflector reactivity effects are slightly greater for LEU-22 fuel than for LEU-18 fuel due to the harder leakage spectrum of the latter.

The effect of burnup on the relative worth of a reflector variant was determined for Option 2 using LEU-18 fuel. Four time steps were considered ranging from 0 to 384 megawatt-days. The results of this analysis show that the relative worth increases on the order of 10 percent over core life. Reflector worth increases with burnup because as the core burns, the flux shape is flattened resulting in higher leakage. These results are considered to be representative of the behavior of reflector worths with burnup in general. The results of the analysis are shown in Table 7.3.

Table 7.3 Core-Life Effects On Relative Worth of Reflector Option 2 Using LEU-18 Fuel.

Core Burnup Status	Relative Worth $\Delta\rho$
0 Mw-days	-1.96%
4 Mw-days	-2.02%
194 Mw-days	-2.09%
394 MW-days	-2.16%

7.2 Deuterium Reflector Tanks

Reactivity effects associated with various-sized deuterium tanks were analyzed in response to current plans to install an experimental D_2O tank between the core and the neutron beamport facilities. Preliminary designs have not yet been developed, so a

wide range of D_2O tank sizes were analyzed. All D_2O tanks were assumed to be fabricated of one-quarter inch pure aluminum plate. Two group microscopic cross sections were developed for each tank using the GAMTEC code described in Section 3.

The tanks were assumed to be 59 cm high, consistent with the active fuel length, due to the 2-D limitations of our codes. It should be noted that the actual tank heights will probably be significantly shorter than the assumed 59 cm. Thus, results presented here are conservative. Tank sizes were consistent with integer grid plate spacings. 2-D Tank dimensions are specified in Table 7.4.

Table 7.4 Representative D_2O Tanks

D_2O Tank ID	2-D Physical Dimensions
Tank 1	8.1 cm x 7.7 cm
Tank 2	8.1 cm x 15.4 cm
Tank 3	16.2 cm x 15.4 cm
Tank 4	24.3 cm x 15.4 cm
Tank 5	24.3 cm x 23.1 cm
Tank 6	8.1 cm x 30.8 cm
Tank 7	16.2 cm x 38.5 cm
Tank 8	16.2 cm x 80.8 cm

Reflector Option 6 was used as the reference core to determine D_2O tank reactivity effects. Option 6 consists of a full graphite reflector on the north, east, and south core faces and water reflector on the west core face. Core reactivities associated with the D_2O tanks were determined by placing the tanks on the west core face (thus replacing water reflector). Table 7.5 presents reactivity worths associated with each tank.

Table 7.5 Reactivity Effects Associated With Different Sized D_2O Tanks Bordering West UVAR Core Face.

Tank	Reactivity Worth (%$\Delta\rho$)
1	0.38
2	0.77
3	0.89
4	1.4
5	1.3
6	1.4
7	1.8
8	2.1

Information presented in Table 7.5 shows that a D_2O Tank may produce a significant positive reactivity effect when replacing water reflector. To determine how this compares with graphite reflector material, graphite reflector was placed in the Tank 8

location. The reactivity associated with the graphite was 1.9% $\Delta\rho$, which is only slightly lower than the 2.1% $\Delta\rho$ associated with Tank 8. Therefore, while the D_2O tanks are significantly better reflectors than light water, they are only marginally better than graphite.

7.3 Black Boundary Reflectors

A single case, using a 4-by-5 core model with LEU-22 fuel, was analyzed with a black (vacuum) boundary on the east face of the core. The associated reactivity worth was determined to be about -8% $\Delta\rho$ relative to replacing graphite, and about -5 to -6% $\Delta\rho$ relative to replacing water. It should be noted that diffusion theory codes cannot really handle black boundaries properly so that the worths presented are only approximations that are likely to be overestimates of the true situation.

7.4 Reflector Worth Study Summary

Based on the information presented in the sections above the following summary conclusions can be made.

1. Reflector effects are slightly more pronounced in the LEU-22 fuel than in the LEU-18 fuel due to the higher leakage associated with the harder flux spectrum.
2. The calculated k-effectives associated with the BOL LEU-22 and LEU-18 full-water-reflected cores are 1.03 and 1.02 respectively. It may be reasonable to initially load the new core with a full water reflector and

subsequently add graphite with burnup, as appropriate. This should minimize core handling operations, core configuration changes and rod calibrations. It is hoped that reflector worths determined in this study will provide input for such decisions.

3. Replacing water with a D_2O tank can lead to a significant positive reactivity insertion depending on the tank size. Replacing graphite with a D_2O tank results in a relatively small positive reactivity insertion.
4. Replacing an entire core face graphite reflector with a heavily absorbent medium or vacuum results in a negative reactivity swing on the order of 8 percent.

CHAPTER 8.0 DELAYED NEUTRON AND PROMPT NEUTRON LIFETIME STUDY

Effective delayed neutron fractions and prompt neutron lifetimes have been calculated for the UVAR 4-by-5 graphite and water-reflected core models using both LEU-22 and HEU-18 fuel options. Calculation of these parameters is in response to NRC guidance received at the TRTR-88 meeting in Oregon. A summary of methodology and results are presented below.

8.1 METHODOLOGY

Effective delayed neutron fractions (βeff) and prompt neutron lifetimes (ℓ) were calculated using the EXTERMINATOR[20] 2-D diffusion theory code. A 60-by-62 x-y mesh, identical to the mesh used in the 2DB models, was used.

Four group cross sections for the core region were calculated from LEOPARD models for the fuel and control rod elements. Four group reflector cross sections for water and graphite were taken from ANL EPRI-CELL models. Composition-dependent axial buckling terms were developed based on ANL 3-D modeling of the UVAR core.

The EXTERMINATOR code requires average reciprocal velocities for each energy group. The group structure for the LEOPARD code is not explicitly defined. Fortunately, the ANL EPRI-CELL models do specify a group structure consistent with the LEOPARD code. This group structure is presented in Table 8.1.

Table 8.1. Energy Group Structure Used for the EXTERMINATOR Analysis.

Energy Group	E-max(eV)	<v> (m/s)	χ_p
1	1.0 E7	1.8 E9	0.739
2	8.2 E5	3.4 E8	0.261
3	5.5 E3	4.9 E6	0.00018
4	0.62	2.6 E5	0.0

Delayed neutron fractions used in the analysis were based on delayed neutron yields presented by Brady, et al [29] for six precursor groups. Information was available for nine and twelve precursor groups; however, EXTERMINATOR is limited to eight groups. The delayed neutron yields from Brady were normalized to a delayed neutron fraction of 0.0065. The delayed fractions (β_i) are presented in Table 8.2.

Table 8.2. Delayed Neutron Fractions

Group	% Yield	β_i
1	0.0351	0.0002282
2	0.1809	0.001176
3	0.1778	0.001156
4	0.3837	0.002494
5	0.1565	0.001017
6	0.0659	0.0004284
	Total	0.0065

8.2 MODEL VERIFICATION

The EXTERMINATOR UVAR model was verified by: 1) checking model inputs; and 2) comparing calculated k-effective values with

those calculated by our existing two group 2DB models.

Both two and four energy group EXTERMINATOR models were developed for the LEU-22 fuel core. A four group EXTERMINATOR model for HEU-18 fuel was also developed. Table 8.3 presents a comparison of k-effective values calculated by the EXTERMINATOR and 2DB codes. As stated earlier, the model core is a 4-by-5 graphite reflected core.

Table 8.3. Comparison of k-effective Values Calculated By the EXTERMINATOR and 2DB Codes.

Model	k-eff EXTERMINATOR	k-eff 2DB
1. 4 Group LEU-22	1.115	-
2 Group LEU-22	1.110	1.109
2. 4 Group HEU-18	1.118	-
2 Group HEU-18	-	1.115

Information provided in Table 8.3 shows that the EXTERMINATOR and 2DB calculated values of k-effective agree closely. This provides confidence that the EXTERMINATOR models are properly set up.

8.3 PROMPT NEUTRON LIFETIMES

Prompt neutron lifetimes were calculated by the EXTERMINATOR code using first-order perturbation theory. The prompt neutron lifetime is the weighted integral time that the average neutron lives before being captured or leaked from the core. EXTERMINATOR

computes the prompt neutron lifetime by numerically solving the following equation:

$$\ell = \frac{\int_{core}[\phi^*(r,E)\frac{1}{v(E)}\phi(r,E)dE]dV}{\frac{1}{k_{eff}}\int_{core}[\int_0^\infty \phi^*(r,E')\chi_p(E')dE'\int_0^\infty \nu\Sigma_f(r,E)\phi(r,E)]dV}$$

where $\phi^*(r,E)$ = adjoint flux at location r and energy E,

$\frac{1}{v(E)}$ = reciprocal neutron velocity at energy E,

$\phi(r,E)$ = neutron flux at location r and energy E,

$\chi_p(E')$ = fraction of prompt neutrons born at energy E',

ν = prompt neutron production factor for uranium-235, and

$\Sigma_f(r,E)$ = macroscopic fission cross section at location r and energy E.

Prompt neutron lifetimes have been calculated for both LEU-22 and HEU-18 fuels. Both graphite and water reflected cores were evaluated. The prompt neutron lifetimes associated with the LEU-22 4-by-5 graphite reflected core with control rod insertion were also evaluated. The results of the prompt neutron lifetime analysis are presented in Table 8.4.

Table 8.4 shows that the prompt neutron lifetime for the LEU-22 core is about 15% lower than that of the HEU-18 core. This is as expected because of the significantly higher U-238 loading of the LEU fuel. Calculated prompt neutron lifetimes for the water

reflected cores are about 20 percent lower than for the graphite reflected cores. This is due to the higher leakage and absorption associated with the water reflector.

Table 8.4. Prompt Neutron Lifetimes for the UVAR Core.

Core Description	ℓ (μsecs)
1. All-Graphite Reflector	
a) LEU-22	67.0
b) HEU-18	78.8
2. Water Reflected	
a) LEU-22	53.0
b) HEU-18	64.4
3. Graphite Reflected LEU-22 Single Rod Inserted	67.0
4. Graphite Reflected LEU-22 All Rods Inserted	66.5

Rod effects were determined by inserting two group rod cross sections into the rod hole locations. The two group cross sections were input as EXTERMINATOR groups 3 and 4. Although using two group cross sections in a 4 group model is not completely rigorous, this method does provide insight into the general behavior of prompt neutron lifetime with control rod

insertion. The prompt neutron lifetime is not significantly affected by rod insertion.

8.4 EFFECTIVE DELAYED NEUTRON FRACTIONS

The EXTERMINATOR code calculates effective delayed neutron fractions based on input delayed-group neutron energy spectra. The effective delayed neutron fraction represents the importance weighted production rate of delayed neutrons divided by the total importance weighted production rate of all neutrons. The EXTERMINATOR code computes the delayed neutron fraction using the following equation:

$$\beta_{eff} = \sum_{i=1}^{6} \frac{\int_{core}[\int_0^\infty \chi_{di}(E')\phi^*(r,E')dE' \int_0^\infty \beta_i \nu\Sigma_f(r,E)\phi(r,E)dE]dV}{\int_{core}[\int_0^\infty \chi_p(E')\phi^*(r,E')dE' \int_0^\infty \nu\Sigma_f(r,E)\phi(r,E)dE]dV}$$

where $\chi_{di}(E')$ = fraction of delayed neutrons in the ith precursor group born at energy E', and

β_i = delayed neutron fraction for the ith precursor group.

Other terms in the above equation are as defined in Section 8.3.

Several references were consulted to determine the delayed neutron energy spectra. Most references (e.g. [30], [31], and [32]) agree that delayed neutrons are born at energies between 200 and 650 keV. This range is clearly bounded by EXTERMINATOR group

2 (5.5 keV to 820 keV). Duderstadt [33] presents information that implies that some delayed neutrons may be born at energies in EXTERMINATOR group 1. In order to check the sensitivity of the calculation to reasonable assumptions of the delayed neutron spectrum, the following delayed neutron spectra were evaluated:

$$\chi 1 = \begin{bmatrix} 0 \\ 1 \\ 0 \\ 0 \end{bmatrix}, \quad \chi 2 = \begin{bmatrix} 0.1 \\ 0.9 \\ 0 \\ 0 \end{bmatrix}, \quad \chi 3 = \begin{bmatrix} 0.2 \\ 0.8 \\ 0 \\ 0 \end{bmatrix}$$

The above energy spectra are believed to bound the actual situation.

Four other delayed neutron energy spectra were also evaluated to provide insight into the behavior of neutrons born at different energies. It should be noted that these spectra are not considered representative of the physical situation and were evaluated for purely academic purposes. These spectra are defined below:

$$\chi 4 = \begin{bmatrix} 1 \\ 0 \\ 0 \\ 0 \end{bmatrix}, \quad \chi 5 = \begin{bmatrix} 0 \\ 0 \\ 1 \\ 0 \end{bmatrix}, \quad \chi 6 = \begin{bmatrix} 0 \\ 0 \\ 0 \\ 1 \end{bmatrix}, \quad \chi 7 = \begin{bmatrix} 0.739 \\ 0.261 \\ 0.0002 \\ 0 \end{bmatrix}$$

The $\chi 1$ spectrum is identical to the fission spectrum presented in Table 8.1.

Table 8.5 presents total effective delayed neutron fractions associated with each energy spectrum.

Table 8.5. Total Effective Delayed Neutron Fractions for LEU-22 Fueled Core

Energy Spectrum	βeff
1. Reasonable Spectrum Approximations	
a) χ_1	0.00736
b) χ_2	0.00724
c) χ_3	0.00713
2. "Academic" Spectrum Approximations	
a) χ_4	0.00620
b) χ_5	0.00807
c) χ_6	0.00949
c) χ_7	0.00650

The effective delayed neutron fraction appears to be relatively insensitive to reasonable spectrum approximations. A shift of about 3% is associated with allowing twenty percent of the delayed neutrons to be born in group 1. Because the χ_1 spectrum was consistently supported in the literature, it was chosen as the preferred spectrum. Based on information provided in Table 8.5, a value of βeff = 0.0074 is recommended for use with the LEU-22 fuel. An estimated absolute error of about 5% is considered appropriate; however, it should be noted that the precision is of the order of 1%.

The academic spectrum assumptions show that βeff increases as the energy of the delayed neutrons decreases, as expected. A maximum value of βeff = 0.00949 is obtained when all of the delayed neutrons are born in the thermal group. The χ_7 spectrum, which is identical to the fission spectrum (see Table 8.1), produced βeff = β = 0.0065, as expected.

To gain insight into the leakage effect, βeff was calculated for the LEU-22 fuel using an all-water reflector and a χ_1 spectrum. βeff associated with this case was 0.00752 which is about 2% higher than that calculated for the graphite-reflected case. This is reasonable considering that more prompt neutron leakage and absorption occurs with a water reflector. It should be noted that this value is well within the estimated 5% error associated with the above-recommended value of βeff.

The calculated value of βeff with a single rod inserted was 0.00738 which is not significantly different from the recommended value. The calculated value of βeff with all rods inserted is 0.00741, which is also very close to the recommended value.

Finally, βeff was calculated for the HEU-18 fuel core. The calculated value is βeff = 0.00738, which is not significantly different from the recommended value for the LEU core.

8.5 Summary of Delayed Neutron and Prompt Neutron Lifetime Study

In summary, the following conclusions have been made based on the information presented above:

1. The prompt neutron lifetime associated with the LEU-22 core is 67 μsecs, which is about 15% lower than the value calculated for the HEU core.
2. Prompt neutron lifetimes in the water reflected cores are about 20 percent lower than in the graphite reflected cores.
3. Prompt neutron lifetime is not significantly affected by control rod insertion.
4. A value of βeff = 0.0074 ± 5% is recommended for use with the LEU-22 core. Additionally, βeff appears to be relatively insensitive to reasonable assumptions in the delayed neutron spectrum.
5. The value of βeff does not change significantly with reflector options or insertion of control rods.
6. The βeff value associated with the HEU core is slightly higher, but not significantly different from the value associated with the LEU core.

9.0 CONCLUSIONS

Several key neutronics issues have been addressed by the studies presented in this thesis. Study-specific summaries have been presented with each study.

RESULTS

Control rod reactivity worths for the LEU fueled cores were found to be essentially the same as for HEU fueled cores. Control rod worths were also found to change slightly with core burn-up and core reflector changes implying the need to re-evaluate control rod worths periodically with burn-up and following reflector changes.

Peaking factors associated with LEU fuel were somewhat higher than for HEU fuel. Higher peaking factors and the relatively small water gap associated with the LEU-22 fuel have led Hosticka [4] to recommend adopting more conservative UVAR Limiting Safety System Settings.

Temperature and moderator void feedback effects for both the LEU and HEU fueled cores were found to be very similar except for the doppler effect which was significantly higher in the LEU fuel due to the higher uranium-238 loading.

Reflector worths for several different water and graphite reflector options were quantified for the LEU fueled cores. The reactivity worths of deuterium tank reflectors were found to be

similar to graphite reflectors.

An effective delayed neutron fraction of 0.0074 was determined for both the LEU and HEU fueled cores. A prompt neutron lifetime of 67 micro-seconds was determined for the LEU fueled core which was about 15 percent lower than in the HEU fueled core.

CONCLUSION AND FUTURE WORK

The overall study results show that the LEU-fueled core will behave very similarly to the HEU core currently being used.

Future work on the project will include preparation and submission of a revised Safety Analysis Report and UVAR Technical Specifications to NRC, plus responding to NRC licensing concerns.

After the license renewal process is complete, an experimental data collection phase is envisioned for the initially loaded LEU core. Experimental data collected during this phase will provide information needed to "fine-tune" the UVAR neutronics models and will also address possible safety concerns such as verifying bypass flow rates, fuel element flow distributions, and radial and axial flux maps. Additional experimental data to be collected on the clean core are recommended by Meem [34].

Additional investigation of radial peaking factors using transport theory models may be useful in verifying the values presented in this thesis which were predicted by diffusion theory codes. Further investigations into the experimentally determined and calculated reactivity worth discrepancy for the regulating rod

may be warranted and should include an evaluation of rod region boundary conditions. New measurements of moderator temperature coefficients and quantification of the corresponding effective core temperature rise are also warranted.

REFERENCES

1. Rydin, R.A., D. Freeman, M. Fehr, B. Hosticka, R. Mulder, Conversion of the University of Virginia Reactor to Low Enrichment Fuel, Second Year Progress Report, University of Virginia Department of Nuclear Engineering and Engineering Physics, February, 1989.

2. Fehr, M.K., Design Optimization of a Low Enrichment University of Virginia Nuclear Reactor, Masters Thesis, University of Virginia, School of Engineering and Applied Science, January 1989.

3. Freeman, D., QA Package For Control Rod Worth, Shutdown Margin and Excess Reactivity Study, Draft 3, University of Virginia Internal Report, August 9, 1988.

4. Hosticka, B., "Thermal and Hydraulic Analysis of LEU-18 and 22 Plate Fuel" Memo to the University of Virginia Reactor Safety Committee, October, 1988.

5. UVAR Design and Analysis Handbook, University of Virginia Department of Nuclear Engineering and Engineering Physics, Edited by J.P. Farrar, December 1983.

6. UVAR Gridplate blueprint.

7. National Organization Of Test, Research, And Training Reactors, Specification for Test Research Training Reactor LEU Silicide U3Si2 Fuel Plates,TRTR-6, Revision 4, May 20, 1988.

8. National Organization Of Test, Research, And Training Reactors, Specification for Low Enriched U Metal For Reactor Fuel Plates,TRTR-11, March 12, 1987.

9. National Organization Of Test, Research, And Training Reactors, Specification For Reactor Grade Uranium Silicide U3Si2 Powder,TRTR-14, Revision 2, July 1, 1987.

10. National Organization Of Test, Research, And Training Reactors, Specification For Aluminum Powder For Fuel Plate Core Matrix,TRTR-15, Revision 2, July 1, 1987.

11. EG&G Drawing 42264, Test Research Training Reactor LEU Fuel for UVAR 22-Plate Element, Revision B, Dec. 5, 1986.

12. Freeman, D., "Review of Literature Provided by L.K. Seymour's Letter of January 10, 1989", UVA Internal Memorandum, February 23, 1989.

13. Freeman, D., "Preliminary Design of 18 and 22 Plate Fuel Elements," Memo to the University Of Virginia Reactor Safety Committee, April 20, 1988.

14. Freeman, D., "Preliminary Design of 18 and 22 Plate LEU Control Rod Fuel Elements," Memo to the University Of Virginia Reactor Safety Committee, May 6, 1988.

15. United Nuclear Corporation, "UVAR Fuel Element" Blue Print #D-401580, July, 1969.

16. EG&G, "UVAR Control Rod Element" Blue Print #409339, October, 1978.

17. Barry, R.F., LEOPARD-A Spectrum Dependent Non-Spatial Depletion Code," WCAP-3269-26, Westinghouse Electric Corporation, September, 1963.

18. Bennett, C. L., Purcell, W. L., BRT: Battelle-Revised-Thermos, Battelle Memorial Instiute, Reactor Physics Department, June, 1970.

19. Carter, L.L., C. Richey, C. Hughey, GAMTECII: A Code for Generating Consistent Multigroup Constants Utilized in Diffusion and Transport Theory Calculations, Pacific Northwest Laboratory, March, 1965.

20. ORNL-4078, EXTERMINATOR-2: A Fortran IV Code For Solving Multigroup Neutron Diffusion Equations In Two Dimensions, Oak Ridge National Laboratories, 1978.

21. University of Michigan, 2DB-UM APOLLO VERSION (Based largely on 2DB Code), Version #10, September, 1986.

22. Wasserman, S., Effective Diffusion Theory Cross Sections For UVAR Control Rods, Masters Thesis, University of Virginia, School of Engineering and Applied Science, June, 1989.

23. Freeman, D., "Review Documentation of S. Wasserman's Work", University of Virginia Internal Memorandum, April 12, 1988.

24. Farrar, J.P., "Results of Testing For 18 Plate Texas A&M Fuel Elements In UVAR Reactor," Letter to Nuclear Regulatory Commission, June 17, 1975.

25. Private Communications with J. Matos, Argonne National Laboratories, Winter, 1988.

26. Sternberg, H.I., Thermal Power Calculation and Correlation of UVAR by Foil Irradiation and Heat Balance, Masters Thesis, University of Virginia, November 1981.

27. Freeman, D., "Temperature and Moderator Effects for the UVAR Core." University of Virginia Internal Memorandum, May 31, 1988.

28. Freeman, D., "Reactivity Effects Associated With Various UVAR Core Reflector Options", University of Virginia Internal Memorandum, March 16, 1989.

29. Brady, M.C., R. Talmadge, W. Wilson, "Few-Group Analysis of Current Delayed Neutron Data", ANS Transactions, Volume 53, 1988.

30. Argonne National Laboratories, Reactor Physics Constants, ANL-5800, Second Edition, 1963.

31. LaMarsh, J. R., Introduction To Nuclear Reactor Theory, Addison-Wesley Publishing Company, 1965.

32. Keepin, G.R., Physics Of Nuclear Kinetics, Addison-Wesley Publishing Company, 1965.

33. Duderstadt, J.J., L.J. Hamilton, Nuclear Reactor Analysis, John Wiley and Sons, Inc., New York, 1976.

34. Meem, J.L., "Possible Experiments On the New LEU Core", Memo to University of Virginia Reactor Safety Committee, October 20, 1988.

APPENDIX A. MATERIAL CROSS SECTIONS FOR UVAR 2-D CORE MODEL

This Appendix presents material cross sections for the UVAR 2-D Core model. Tables A-1 through A-3 present core region cross sections developed with the LEOPARD code. Table A-4 presents control rod cross sections for both the safety and regulating rods using the various fuel options. Table A-5 presents ANL calculated water and graphite reflector cross sections and Table A-6 presents UVA developed graphite reflector cross sections.

Table A-1. Core Region Cross Sections for LEU-22 Fuel (cm^{-1}).

Description	Group	Σ_f	Σ_a	$\nu\Sigma_f$	Σ_{tr}	$\Sigma_{g,g}$	$\Sigma_{(g-1),g}$
I. Two Group Cross Sections							
1. Fuel Lattice	1	2.32×10^{-3}	6.22×10^{-3}	5.71×10^{-3}	2.54×10^{-1}	2.22×10^{-1}	0.0
	2	9.32×10^{-2}	1.26×10^{-1}	2.25×10^{-1}	1.26×10^{0}	1.13×10^{0}	2.57×10^{-2}
2. Fuel Non-Lattice	1	0.0	3.83×10^{-4}	0.0	1.89×10^{-1}	1.75×10^{-1}	0.0
	2	0.0	1.31×10^{-2}	0.0	6.15×10^{-1}	6.02×10^{-1}	1.38×10^{-2}
3. Control Rod Element Non-Lattice	1	0.0	4.08×10^{-4}	0.0	2.70×10^{-1}	2.32×10^{-1}	0.0
	2	0.0	1.67×10^{-2}	0.0	1.61×10^{0}	1.59×10^{0}	3.76×10^{-2}
II. Four Group Cross Sections							
1. Fuel Lattice	1	6.91×10^{-4}	1.11×10^{-3}	1.91×10^{-3}	1.68×10^{-1}	8.46×10^{-2}	0.0
	2	4.05×10^{-4}	8.83×10^{-4}	9.89×10^{-4}	3.04×10^{-1}	2.09×10^{-1}	8.21×10^{-2}
	3	6.47×10^{-3}	1.84×10^{-2}	1.57×10^{-2}	4.09×10^{-1}	3.05×10^{-1}	9.44×10^{-2}
	4	9.32×10^{-2}	1.26×10^{-1}	2.25×10^{-1}	1.26×10^{0}	1.13×10^{0}	8.57×10^{-2}
2. Fuel Non-Lattice	1	0.0	3.47×10^{-4}	0.0	1.42×10^{-1}	1.00×10^{-1}	0.0
	2	0.0	1.25×10^{-4}	0.0	2.28×10^{-1}	1.80×10^{-1}	4.15×10^{-2}
	3	0.0	7.35×10^{-4}	0.0	2.26×10^{-1}	1.79×10^{-1}	4.77×10^{-2}
	4	0.0	1.31×10^{-2}	0.0	6.15×10^{-1}	6.02×10^{-1}	4.58×10^{-2}
3. Control Rod Non-Lattice	1	0.0	3.77×10^{-4}	0.0	1.76×10^{-1}	7.69×10^{-2}	0.0
	2	0.0	3.88×10^{-5}	0.0	3.16×10^{-1}	1.93×10^{-1}	9.89×10^{-2}
	3	0.0	8.67×10^{-4}	0.0	4.77×10^{-1}	3.53×10^{0}	1.22×10^{-1}
	4	0.0	1.67×10^{-2}	0.0	1.61×10^{0}	1.59×10^{0}	1.23×10^{-1}

Table A-2. Core Region Cross Sections For LEU-18 Fuel (cm^{-1}).

Description	Group	Σ_f	Σ_a	$\nu\Sigma_f$	Σ_{tr}	$\Sigma_{g,g}$	$\Sigma_{(g-1),g}$
I. Two Group Cross Sections							
1. Fuel Lattice	1	1.93×10^{-3}	5.41×10^{-3}	4.75×10^{-3}	2.61×10^{-1}	2.26×10^{-1}	0.0
	2	7.90×10^{-2}	1.09×10^{-1}	1.91×10^{-1}	1.40×10^{0}	1.29×10^{0}	2.92×10^{-2}
2. Fuel Non-Lattice	1	0.0	3.92×10^{-4}	0.0	1.93×10^{-1}	1.77×10^{-1}	0.0
	2	0.0	1.37×10^{-2}	0.0	6.81×10^{-1}	6.67×10^{-1}	1.51×10^{-2}
3. Control Rod Element Non-Lattice	1	0.0	4.15×10^{-4}	0.0	2.67×10^{-1}	2.29×10^{-1}	0.0
	2	0.0	1.70×10^{-2}	0.0	1.65×10^{0}	1.63×10^{0}	3.81×10^{-2}
II. Four Group Cross Sections							
1. Fuel Lattice	1	5.68×10^{-4}	9.80×10^{-4}	1.57×10^{-3}	1.71×10^{-1}	8.23×10^{-2}	0.0
	2	3.31×10^{-4}	6.87×10^{-4}	8.09×10^{-4}	3.09×10^{-1}	2.05×10^{-1}	8.76×10^{-2}
	3	5.36×10^{-3}	1.59×10^{-2}	1.30×10^{-2}	4.38×10^{-1}	3.25×10^{-1}	1.04×10^{-1}
	4	7.90×10^{-2}	1.09×10^{-1}	1.91×10^{-1}	1.40×10^{0}	1.29×10^{0}	9.65×10^{-2}
2. Fuel Non-Lattice	1	0.0	3.57×10^{-4}	0.0	1.44×10^{-1}	9.99×10^{-2}	0.0
	2	0.0	1.22×10^{-4}	0.0	2.30×10^{-1}	1.78×10^{-1}	4.34×10^{-2}
	3	0.0	7.52×10^{-2}	0.0	2.39×10^{-1}	1.89×10^{-1}	5.13×10^{-2}
	4	0.0	1.37×10^{-2}	0.0	6.81×10^{-1}	6.67×10^{-1}	4.97×10^{-2}
3. Control Rod Non-Lattice	1	0.0	3.23×10^{-4}	0.0	1.74×10^{-1}	7.59×10^{-2}	0.0
	2	0.0	3.89×10^{-5}	0.0	3.12×10^{-1}	1.89×10^{-1}	9.76×10^{-2}
	3	0.0	8.75×10^{-4}	0.0	4.79×10^{-1}	3.54×10^{-1}	1.23×10^{-1}
	4	0.0	1.70×10^{-2}	0.0	1.65×10^{0}	1.63×10^{0}	1.24×10^{-1}

Table A-3. Core Region Cross Sections for HEU-18 Fuel (cm^{-1})

Description	Group	Σ_f	Σ_a	$\nu\Sigma_f$	Σ_{tr}	$\Sigma_{g,g}$	$\Sigma_{(g-1),g}$
I. Two Group Cross Sections							
1. Fuel Lattice	1	1.60×10^{-3}	3.01×10^{-3}	3.90×10^{-3}	2.58×10^{-1}	2.42×10^{-1}	0.0
	2	6.96×10^{-2}	9.64×10^{-2}	1.68×10^{-1}	1.40×10^{0}	1.30×10^{0}	3.03×10^{-2}
2. Fuel Non-Lattice	1	0.0	3.89×10^{-4}	0.0	1.98×10^{-1}	1.81×10^{-1}	0.0
	2	0.0	1.34×10^{-2}	0.0	7.21×10^{-1}	7.08×10^{-1}	1.60×10^{-2}
3. Control Rod Element Non-Lattice	1	0.0	4.13×10^{-4}	0.0	2.58×10^{-1}	2.22×10^{-1}	0.0
	2	0.0	1.63×10^{-2}	0.0	1.50×10^{0}	1.48×10^{0}	3.47×10^{-2}
II. Four Group Cross Sections							
1. Fuel Lattice	1	2.21×10^{-4}	5.87×10^{-4}	6.02×10^{-4}	1.69×10^{-1}	8.23×10^{-2}	0.0
	2	2.85×10^{-4}	4.24×10^{-4}	6.96×10^{-4}	3.05×10^{-1}	2.02×10^{-1}	8.63×10^{-2}
	3	4.65×10^{-3}	8.68×10^{-3}	1.12×10^{-2}	4.29×10^{-1}	3.21×10^{-1}	1.03×10^{-1}
	4	6.96×10^{-2}	9.64×10^{-2}	1.68×10^{-1}	1.40×10^{0}	1.30×10^{0}	9.89×10^{-2}
2. Fuel Non-Lattice	1	0.0	3.55×10^{-4}	0.0	1.46×10^{-1}	1.00×10^{-1}	0.0
	2	0.0	1.18×10^{-4}	0.0	2.34×10^{-1}	1.80×10^{-1}	4.51×10^{-2}
	3	0.0	7.40×10^{-4}	0.0	2.52×10^{-1}	1.99×10^{-1}	5.37×10^{-2}
	4	0.0	1.34×10^{-2}	0.0	7.21×10^{-1}	7.08×10^{-1}	5.21×10^{-2}
3. Control Rod Non-Lattice	1	0.0	3.76×10^{-4}	0.0	1.69×10^{-1}	7.96×10^{-2}	0.0
	2	0.0	5.26×10^{-5}	0.0	3.01×10^{-1}	1.90×10^{-1}	8.86×10^{-2}
	3	0.0	8.55×10^{-4}	0.0	4.44×10^{-1}	3.32×10^{-1}	1.11×10^{-1}
	4	0.0	1.63×10^{-2}	0.0	1.50×10^{0}	1.48×10^{0}	1.11×10^{-1}

Table A.4 Control Rod Region Cross Sections

Rod/Fuel	Group	Σ_a	Σ_{tr}	Σ_{g-g}	$\Sigma_{(g-1)-g}$
I. Safety Rods					
1. LEU-22	1	0.0182	0.270	0.573	0.0
	2	0.0171	2.00	1.53	0.0229
2. LEU-18	1	0.0186	0.271	0.577	0.0
	2	0.166	2.05	1.57	0.0233
3. HEU-18	1	0.0178	0.270	0.573	0.0
	2	0.171	2.06	1.56	0.0229
II. Regulating Rod					
1. LEU-22	1	0.00268	0.284	0.552	0.0
	2	0.0384	1.23	1.37	0.0163
2. LEU-18	1	0.00220	0.284	0.552	0.0
	2	0.0425	1.25	1.39	0.0164
3. HEU-18	1	0.00234	0.281	0.546	0.0
	2	0.0368	1.24	1.37	0.0160

[1] g-g represents in-group scattering

[2] (g-1)-g represents one group downscatter

Table A.5. ANL Developed Water and Graphite Reflector Cross Sections (cm^{-1}).

Description	Group	Σ_a	Σ_{tr}	Σ_{g-g}	$\Sigma_{(g-1)-g}$
I. Water Reflector					
1. Two Group	1	4.58×10^{-4}	2.65×10^{-1}	8.39×10^{-1}	0.0
	2	1.97×10^{-2}	2.30×10^{0}	2.63×10^{-0}	4.91×10^{-2}
2. Four Group	1	3.60×10^{-4}	1.59×10^{-1}	2.70×10^{-1}	0.0
	2	9.68×10^{-6}	3.12×10^{-1}	8.83×10^{-1}	1.07×10^{-1}
	3	1.00×10^{-3}	5.69×10^{-1}	1.38×10^{0}	1.50×10^{-1}
	4	1.97×10^{-2}	2.30×10^{0}	2.63×10^{0}	1.48×10^{-1}
II. Graphite Reflector					
1. Two Group	1	1.06×10^{-4}	2.69×10^{-1}	3.64×10^{-1}	0.0
	2	3.28×10^{-3}	4.93×10^{-1}	5.21×10^{-1}	7.23×10^{-3}
2. Four Group	1	8.90×10^{-5}	1.44×10^{-1}	1.85×10^{-1}	0.0
	2	2.73×10^{-5}	3.06×10^{-1}	3.75×10^{-1}	3.10×10^{-2}
	3	1.75×10^{-4}	3.51×10^{-1}	4.24×10^{-1}	1.99×10^{-2}
	4	3.28×10^{-3}	4.93×10^{-1}	5.21×10^{-1}	1.58×10^{-2}

Table A.6. UVA Developed Graphite Reflector Cross Sections (cm^{-1})

Description	Group	Σ_a	Σ_{tr}	Σ_{g-g}	$\Sigma_{(g-1)-g}$
Graphite Reflector	1	1.04×10^{-4}	2.63×10^{-1}	4.26×10^{-1}	0.0
	2	3.44×10^{-3}	6.25×10^{-1}	7.26×10^{-1}	5.92×10^{-3}

APPENDIX III

HEU TO LEU FUEL CONVERSION REPORT

Effective Diffusion Theory Cross Sections for UVAR Control-Rods

A Thesis

Presented to

the Faculty of the School of Engineering and Applied Science

University of Virginia

In Partial Fulfillment

of the Requirements for the Degree

Master of Science (Engineering Physics)

by

Stuart Wasserman

January 1990

APPROVAL SHEET

This thesis is submitted in partial fulfillment of the

requirements for the degree of

Master of Science (Engineering Physics)

AUTHOR

This thesis has been read and approved by the Examining Committee:

Thesis adviser

Committee Chairman

Accepted for the School of Engineering and Applied Science:

Dean, School of Engineering
and Applied Science

January 1990

TABLE OF CONTENTS

1. Introduction 1

1.1 Background 1

1.2 The Problem 2

1.3 The Solution 3

1.4 Outline 5

2. Diffusion Theory Versus Transport Theory 7

2.1 The Transport Equation 7

2.2 The Diffusion Equation 8

2.3 Validity of the Diffusion Approximation . . . 10

3. Description of the Computer Codes 15

3.1 GAMTEC 15

3.1A GAM 16

3.1B TEMPEST 21

3.2 BRT 25

3.3 Comparison of GAMTEC and 2DB-UM 26

3.4 EXTERMINATOR and 2DB-UM 26

4. The Transport Computer Models 29

4.1 The Problem 29

4.2 The Solution 30

4.3 The Actual Control-Rod Cell 32

4.4 Preliminary Calculations 32

4.5 The Models 35
4.5.1 Modelling Limitations of the Codes . . 35
4.5.2 Trial Case Constants 41
4.5.3 Trial Case A - Slab Model 44
4.5.4 Trial Case B - Slab Model 47
4.5.5 Trial Case C - Slab Model 50
4.5.6 Trial Case D - Slab Model 52
4.5.7 Trial Case E - Slab Model 54
4.5.8 Trial Case F - Slab Model 56
4.5.9 Trial Case G - Slab Model 58
4.5.10 The Cylindrical Models 59
4.6 The Output Parameters 61
4.6.1 The Thermal Group 61
4.6.2 The Fast Group 62
4.7 Transport Code Output 63
4.7.1 Slab vs. Cylindrical Models 63
4.7.2 The Composition of the Rod Region . . 70
4.7.3 Modelling the Grooves 73
4.7.4 The Fast Group 76
4.7.5 The Final Transport Representation . . 77
5. The Diffusion and Effective Diffusion Models . . . 79
5.1 The 2DB-UM Model 79
5.2 The EXTERMINATOR Cell Model 83
5.3 Effective Cross Sections 85
5.4 Effects of the Diffusion Approximation 88
6. The Regulating-Rod 95

7. Results 97
7.1 The Experimental Data 97
7.2 Calculated Control-Rod Worths 98
7.3 Conclusions 100
7.4 Recommendations 100
8. Appendix 103

LIST OF FIGURES

Figure 2-1	Modelling Approximations	9
Figure 4-1	The Fuel Elements	33
Figure 4-2	The Control and Regulating Rods . .	34
Figure 4-3	Computer Code Limitations	38
Figure 4-4	Slab Model A vs. the Actual Cell .	39
Figure 4-5	Conversion of a Slab Model into a Cylindrical Model	40
Figure 4-6	Slab Model A vs. Slab Model B . . .	49
Figure 4-7	Slab Model B vs. Slab Model C . . .	51
Figure 4-8	Slab Model B vs. Slab Model D . . .	53
Figure 4-9	Slab Models E and G	57
Figure 4-10	Comparison of the Fluxes Generated by Cylindrical Model D	68
Figure 5-1	Complete TWODB-UM Model	81
Figure 5-2	TWODB-UM Control-Rod Cell Model . .	82
Figure 5-3	BRT vs. EXTERMINATOR	91
Figure 5-4	BRT Predictions vs. TWODB-UM Predictions	93

LIST OF TABLES

Table I	A Hypothetical Boundary	13
Table II	Summary of Initial Calculations . .	35
Table III	Transport Output Parameters	65
Table IV	Model B vs. Model D	72
Table V	Model D vs. Model G	75
Table VI	Comparison of the Cylindrical Models	78
Table VII	Effective Cross Sections for Different Transport Models	89
Table VIII	Experimental Rod Worths	97
Table IX	Trial Set Results vs. Experimental Data	100
Table X	Final Recommended Cross Sections for TWODB-UM	101

LIST OF SYMBOLS

r - spatial coordinate

E - energy

$\hat{\Omega}$ - solid angle (direction in which neutron travels)

ϕ - neutron flux

Σ_t - macroscopic total cross section

Σ_s - macroscopic scattering cross section

$\chi(E)$ - fission spectrum

ν - average number of neutron births per fission

Σ_f - macroscopic fission cross section

J - neutron current

D - diffusion coefficient

f - reaction rate

Σa - macroscopic absorption cross section

Σ_{fine} - fine group macroscopic cross sections

N_i - number of neutrons in group i

σ - microscopic cross section

s - number of neutrons entering a group due to a source

u_n - lethargy of nth group

RI - resonance integral

$P_\ell(u)$ - legendre polynomials

$W(E)$ - Maxwellian distribution

E_c - thermal cutoff energy

$T(x,x',E)$ - scattering kernel

ACKNOWLEDGEMENTS

The author would like to thank Dr. Roger Rydin for his guidance. Whether the discussion took place in his office or on phone calls from Charlottesville to Europe, or from New York to Charlottesville, he was always generous with his time. Thanks are also due to Mary Fehr, and Dave Freeman for all their comments and suggestions. A special thank you goes to Lisa and Kathy Wasserman. To Lisa, for running all over New York City to help with the final copy at a time when she had plenty of her own work to worry about, and to Kathy for putting up with the always-growing stack of paper which has occupied the corner of her living room for the past year.

DEDICATION

To my grandfather, Ralph Roimisher. This paper is as much a product of his hard work as it is mine.

ABSTRACT

In order to predict control margins for the proposed University of Virginia Reactor (UVAR) Low Enrichment Uranium (LEU) core, effective control-rod cross sections need to be developed and verified against experimental data. Although diffusion theory is sufficient for most of the core analysis, the strongly absorbing control-rods must be treated using transport theory.

Effective two group absorption cross sections were developed based on parameters taken from two transport theory computer codes, THERMOS and GAMTEC. These cross sections were adjusted in the diffusion code, EXTERMINATOR, until cell model transport parameters were matched.

When the effective cross sections were subsequently input into a full core model in the diffusion code TWODB-UM the calculated control-rod worths were predicted within 15% of experimental values for each of the three control-rods.

1. INTRODUCTION

1.1 Background

A number of the nuclear reactors in the United States are used exclusively for research purposes. Presently, most of these reactors are powered by high enriched uranium (HEU) fuel. HEU is considered to be weapons-grade material because it contains at least 90% ^{235}U. As a response to the possible threat of terrorism the government recently ordered all research reactors to convert to fuel powered by low enriched uranium (LEU) which is enriched with no more than 20% ^{235}U [1]. Because each reactor has different physical characteristics, each one requires its own redesign study. The study being performed on the University of Virginia Reactor (UVAR) uses the 2DB-UM [2] computer code to predict neutron multiplication factors during the burnup of both existing and proposed new cores. 2DB-UM is based upon neutron diffusion theory as opposed to the more exact transport theory.

The current UVAR standard fuel elements consist of eighteen HEU fuel plates, while the control-rod elements contain nine HEU fuel plates positioned around a control-rod. The new LEU fuel will be enriched with approximately 20% ^{235}U compared to 93% ^{235}U in the HEU. If no other changes were made, the LEU's multiplication factor would be less than the HEU's because of the decrease in ^{235}U as well as the

increase in absorptions due to the extra ^{238}U. Therefore, in order to consider the LEU as a direct replacement it is necessary to increase the quantity of uranium in each fuel element. The fuel conversion study explored options such as increasing the mass of uranium per plate, increasing the number of plates per fuel element, or some combination of the two.

1.2 The Problem

Before any change in a nuclear reactor core may be implemented, it is first necessary to have the ability to predict the corresponding effects on the neutron flux distribution throughout the core. Although obtaining solutions to the multi-group diffusion equation is adequate for most of a core analysis, the transport equation must be considered in the vicinity of a strong absorber. Therefore, if a core study is to be done utilizing a diffusion theory computer code, it is necessary to develop a relatively simple and inexpensive method of incorporating a transport theory study of the control-rod region.

The main tool used in the UVAR conversion study was the two dimensional diffusion theory computer code 2DB-UM. Most of the necessary cross sections were generated and input to 2DB-UM by the LEOPARD and LINX computer codes, respectively. LEOPARD was not used to compute cross sections for the control-rod regions. This did not present an inconvenience

because the diffusion theory code could not be directly applied to the rod region, anyway. Therefore, the problem boiled down to choosing "effective" cross sections for the rod regions in such a way that they would cause 2DB-UM to yield accurate results in the rod regions.

1.3 The Solution

The first step of the effective cross section development was to obtain an accurate picture of neutron behavior in a control-rod fuel element. Neutron transport theory codes were used for this purpose, because transport theory's validity is not compromised in the vicinity of a strong absorber. Two transport codes, Battelle-Revised-THERMOS (BRT) [3] and GAMTEC [4] were both applied to the control-rod cell. The physical modelling of the control-rod's shape for input to the transport codes proved to be a very significant part of the study. BRT is a one dimensional code which solves the integral transport equation in the thermal energy range. GAMTEC solves the neutron balance equation over the energy range 0-10 Mev by breaking the problem into a thermal and a fast calculation. The thermal calculation utilizes the transport equation while a spatially flat flux approximation is invoked during the fast calculation. BRT's method of solution is considered to be more accurate, because it does not assume that the space and energy dependence of the flux are separable. Therefore the

accurate representation of the control-rod combines thermal parameters chosen from BRT's output with fast parameters taken from GAMTEC's description of the fast neutron behavior.

Next, thermal and fast cross sections generated by BRT and GAMTEC, respectively, were used as input for EXTERMINATOR [5]. EXTERMINATOR is a two-dimensional few-group diffusion theory code. When the actual cross sections were input to an EXTERMINATOR control-rod element cell model, some expected discrepancies were found between the output of the diffusion and transport models. The discrepancies arose because the diffusion approximation was not valid in the vicinity of the control-rod.

The basic plan of attack was to iteratively change the fast and thermal absorption cross sections in this region until the discrepancies became negligible. These new cross sections were referred to as the effective diffusion theory cross sections. It is important to note that the rod region had to be treated as a black box. In other words, we could not exactly mimic the neutron flux throughout the region, but we hoped to create a situation in which most of the more important parameters seen by the rest of the cell were fairly accurately predicted.

Finally, it was possible to use the effective cross sections as input data for 2DB-UM. While the EXTERMINATOR

model was based strictly on one control-rod fuel element, the 2DB-UM model consisted of the full core; sixteen fuel or rod elements plus graphite and water surroundings. 2DB-UM was used to calculate rod worths for each of the four rods. These rod worths were the primary parameters that were checked against experimental data in the verification of the effective cross sections.

1.4 Outline

Following the introduction, Chapter 2 gives a short review of the differences between diffusion and transport theory. This section was included to be sure that the reader fully appreciates why the control-rods warrant special treatment in a diffusion theory study, and consequently, why effective cross sections are needed.

The computer codes are introduced in Chapter 3. Special attention is given to the approximations that each code uses before solving the transport equation. This approach was taken because the computer codes were viewed only as tools that could predict neutron behavior. The approximations that were required dictated when and how each "tool" should be applied.

Chapter 4 consists of the transport theory study of the control-rod element. Different physical models were compared, and the best model was selected. All subsequent transport theory data was taken from this model.

Chapter 5 consists of a description of the diffusion theory cell model and the method used to generate effective cross sections for this model.

Chapter 6 describes how and why the less highly absorbing regulating rod was treated differently than the control-rods.

Finally, the effective cross sections are verified against experimental data in Chapter 7.

2. Diffusion Theory Versus Transport Theory

2.1 The Transport Equation

The steady state neutron transport equation is derived by performing a balance over all possible neutron production and destruction reactions in an arbitrary volume. Productions, at a specific energy, include fission and scattering reactions into this energy and spatial region. Destructions are caused by absorptions, and scattering out of this energy or spatial region. When the cross sections may be considered constant throughout the volume of interest, the result of this balance is

$$\hat{\Omega}\cdot\nabla\phi(r,E,\hat{\Omega})+\Sigma_t(r,E)\phi(r,E,\hat{\Omega}) - \int_{4\pi} d\hat{\Omega}\int_o^\infty dE'\Sigma_s(E'\rightarrow E,\hat{\Omega}'\rightarrow\hat{\Omega})\phi(r,E',\hat{\Omega}')$$
$$+ \frac{\chi(E)}{4\pi}\int_{4\pi} d\hat{\Omega}\int_o^\infty \nu(E')\Sigma_f(E')\phi(r,E',\hat{\Omega}') \qquad (2\text{-}1)$$

The only assumptions made so far are that all fission neutrons are emitted simultaneously and isotropically. In every other respect this is an exact equation for a single energy (energy=E) in a spatially homogenous region. A system of equations, comprised of the transport equation for as many discrete energy groups and spatial regions as desirable, must be solved over the full core to completely determine the steady state neutron behavior.

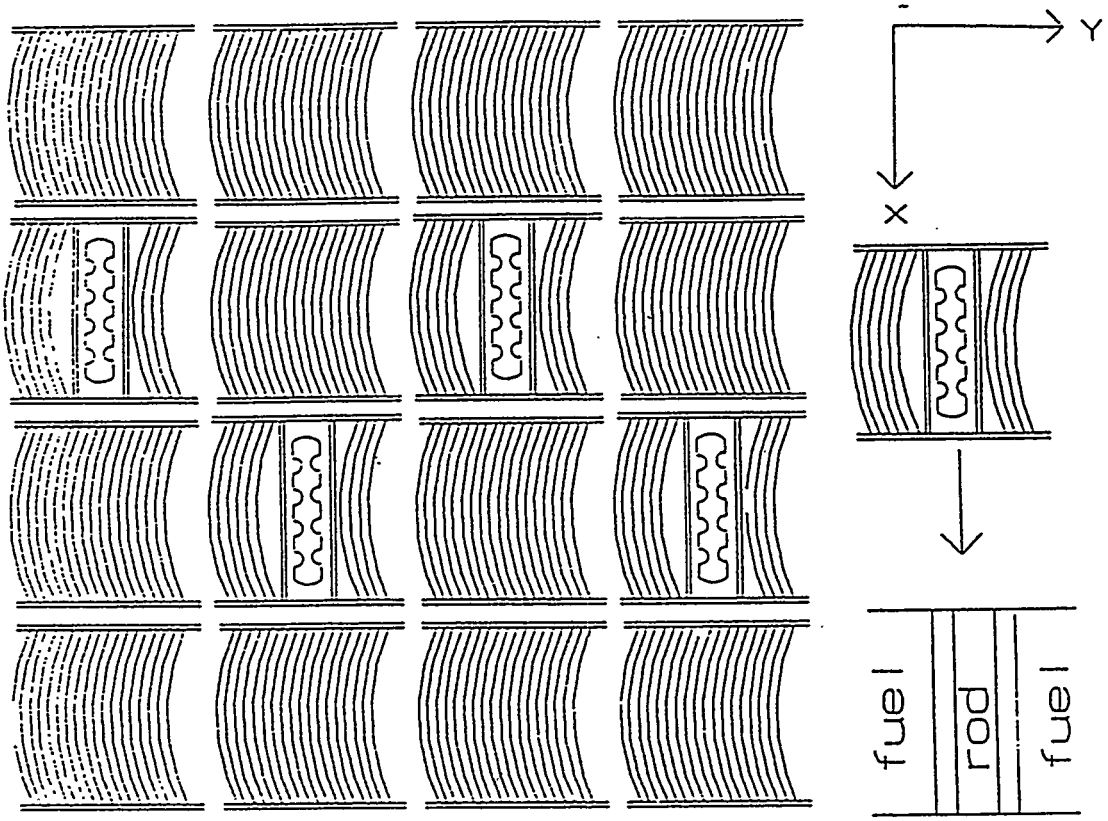
In order to obtain these solutions in a heterogenous cell some approximations are necessary. First, the cell is

spatially sectioned. All the nuclides within each section are homogenized, thereby yielding constant cross sections for each region. Consequently, neutron balances need be written only for a relatively small number of homogenous mixtures. The system of equations may be further simplified by assuming that the system is infinite in one, two or three directions (Figure 2-1). The flux is then assumed constant in these directions thereby decreasing the dimensionality of the problem. Usually, because of the effort necessary to solve the transport equation, the flux is assumed constant in two dimensions when it is solved.

2.2 The Diffusion Equation

Another common approximation is the diffusion approximation, which essentially states that neutrons will travel from regions of high neutron density to regions of lower density. The diffusion approximation is actually the result of the P_1 approximation which states that the directional dependence of the angular flux ($\phi(r,\Omega,E)$) is only linearly anisotropic. When the higher orders of angular dependence are ignored, and Equation (2-1) is integrated over angle, the identities

$$\int_{4\pi}\phi(r,E,\hat{\Omega})d\hat{\Omega} = \phi(r,E)$$



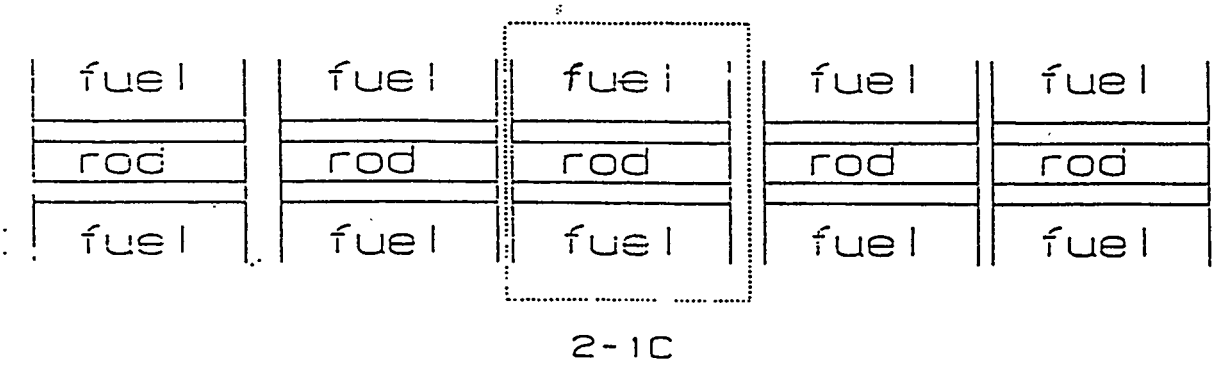


Figure 2-1: Modelling Approximations

Figure 2-1A shows one possibility for an actual core configuration. Figure 2-1B illustrates how one cell might be modelled in one dimension. Note that the model may have inhomogeneities in only one direction. Figure 2-1C portrays a boundary implication of assuming the system is infinite parallel to the x-axis. In effect the calculation is performed on the element within the dotted box as if the element is bordered by identical elements on either side. Compare this to actual bordering materials shown in 2-1A.

and

$$\int_{4\pi}\hat{\Omega}\cdot\nabla\phi(r,E,\hat{\Omega})\,d\hat{\Omega} = \nabla\cdot J(r,E)$$

may be used to write

$$\nabla\cdot J(r,E)+\Sigma_t(r,E)\phi(r,E) = \int_o^\infty dE'\Sigma_s(E'\to E)\phi(r,E') + \chi(E)\int_o^\infty \nu(E')\Sigma_f(E')\phi(r,E')$$

If D(r,E) is taken to be the constant of proportionality, the approximation is written as Fick's law,

$$J(r,E) = -D(r)\nabla\phi(r,E)$$

which leads to the diffusion equation

$$-\nabla\cdot D(r,E)\nabla\phi(r,E) + \Sigma_t(r,E)\phi(r,E) = \int_o^\infty dE'\Sigma_s(E'\to E)\phi(r,E')$$
$$+\chi(E)\int_o^\infty \nu(E')\Sigma_F(E')\phi(r,E')dE'$$

2.3 Validity of the Diffusion Approximation

As mentioned earlier the diffusion approximation is not valid in the vicinity of a strong absorber. To understand this phenomenon, it is informative to know how reactor diffusion theory differs from the diffusion theory of gases. Gaseous diffusion theory is based on the assumption of many scattering collisions between the gas particles. When a gas molecule travels into a highly populated region it has a greater chance of striking another gas particle, and consequently a greater chance of backscattering. The

spatial distribution of particles is flattened because particles tend to travel to less populated regions.

Neutron diffusion theory predicts results which are similar to the gas theory results even though the logic is different. The probability of a neutron-neutron interaction is so small relative to that of a neutron-nucleus collision that the neutron-neutron collision can be neglected in nuclear reactor theory, thus making the equations linear. The reaction rate for a neutron-nucleus reaction is given by

$$f=\Sigma\phi \qquad (2-2)$$

In a homogenous medium the scattering cross section is constant, so Equation (2-2) shows that the scattering frequency is only dependent upon the flux. Therefore, in a region of higher neutron density the scattering frequency (as well as the frequency of any other neutron-nucleus reaction) is greater. As a result neutrons, like gas molecules, tend to travel to regions of lower concentration. Consequently, the neutron's directional dependence is primarily a function of the gradient of the spatial flux. In other words, the angular flux may be assumed to be linearly anisotropic and the diffusion approximation is valid.

The previous paragraph implies that the diffusion approximation should not be valid at the border between any

two materials with different cross sections. If this were true the approximation would not be much help at all. Fortunately, the physical properties of most reactor materials are close enough alike, in reference to the diffusion approximation, that the behavior at the border is dominated by a boundary condition which only demands that the bordering fluxes and currents match at the boundary.

When one of the border materials is a control-rod the behavior is no longer dominated by these boundary conditions. To illustrate this point consider the border between a control-rod and a material which has a scattering cross section exactly equal to that of the control-rod. Even if the flux were spatially flat, the scattering probability would be dependent upon position thereby invalidating the diffusion approximation. Because of the rod's extraordinarily large absorption cross section, the same number of neutrons travelling into the rod create far fewer scattering collisions (due to the increased probability of absorption) than if they were travelling away from the rod.

Table I illustrates this situation. The table shows that even if the scattering cross section is constant, the large deviation in absorption cross section at a control-rod border invalidates any thought of a constant scattering probability. The scattering probability is no longer solely

Table I: A Hypothetical Boundary

	Σ_s	Σ_a	Neutrons entering the region	Neutrons absorbed in the region	Neutrons scattered in the region
Control-rod	10b	190b	500	475	25
Border region	10b	10b	500	250	250

a function of the spatial flux, it is also dependent on the medium's composition. The matching boundary conditions cannot be relied on to compensate for the problem because of the large variations in the spatial flux distribution expected at this point. The angular flux cannot be considered to be only linearly anisotropic, because neutron transport in this vicinity is affected by changes in properties of the medium as well as neutron flux fluctuations.

A related problem occurs even when the diffusion approximation is applied within the control-rod region, away from the boundaries. In the rod, the probability of an absorption reaction dominates over the probability of any other reactions. Therefore, it cannot be assumed that a neutron will undergo the large number of scattering

reactions required in the diffusion theory assumptions. As a result the angular flux cannot be assumed to be a simple function of the spatial gradient. These problems with the diffusion theory make it necessary to consider the transport equation when treating the control-rod.

3. Description of the Computer Codes

Several FORTRAN computer codes are available to solve the transport equation in one dimension. Each code employs a different method of solution and therefore has it's own advantages and disadvantages. A basic understanding of these solution methods will help to maximize the benefits to be derived from the codes. The two transport computer codes chosen for this project were BRT and GAMTEC.

3.1 GAMTEC

GAMTEC solves the multi-group P_1 equations with sixty eight fast energy groups, as well as a continuous thermal-energy treatment. GAMTEC's principal advantage over BRT is that it allows the user to collapse these groups into one thermal and a few fast groups, and treat each group separately. It is beneficial to treat the groups differently because different reactions should be emphasized in each group. In the fast groups upscattering may be ignored while the fission spectrum, downscattering and resonance absorption determine the neutron behavior. In comparison, the thermal motion of the nuclei and chemical binding play significant roles as thermal neutrons approach thermal equilibrium with their surroundings. GAMTEC possesses the capability to treat fast and thermal groups differently because it is actually a combination of two

codes, GAM and TEMPEST. GAM performs the fast calculations while TEMPEST does the thermal calculations.

3.1.A GAM

The most significant point to consider regarding the fast calculation is that it is done in zero dimensions. This means that all the materials in the cell must be combined to form one homogenous mixture. An important implication of this "zero dimensionalization" is that the fast neutron flux is assumed to be spatially flat. Mathematically this is written as

$$\phi(r,E)=C\phi(E) \tag{3-1}$$

where C is a constant. In preparing the fast-group libraries for GAM, a rough estimate of the flux is made by assuming that the energy dependence is of the form 1/E so that

$$\phi(r,E)= C/E \tag{3-2}$$

Now, weighted fine-group constants are calculated from expressions such as

$$\Sigma_{fine} = \frac{N_i\int_{E_n}^{E_{n+1}} \sigma_i(E)\phi(E)dE}{\int_{E_n}^{E_{n+1}}\phi(E)dE} \tag{3-3}$$

where σ_i are tabulated cross sections taken from a more detailed library. In some cases, which will be discussed

shortly, Equation 3-3 is modified to correct for obvious errors caused by the zero-dimensionalization.

These cross sections allow GAM to obtain a more accurate energy-dependent flux by numerically solving the P_1 slowing down equations. The slowing-down equation for a discrete energy has the general form

$$\Sigma_a(E)\phi(E) + \Sigma_s(E)\phi(E) = S(E) + \int\Sigma_s(E'\rightarrow E)\phi(E')dE' \qquad (3\text{-}4)$$

After solving this equation, the code has access to the fluxes and cross sections for 68 energy groups. This data is used to calculate all the output parameters which are desired by the user.

Since the output parameters obtained from the solution to Equation 3-4 were vital to the remainder of the project it was necessary to verify that the assumptions involved in the equation's solution were applicable to the problem of interest. The homogenization of the cell, which was critical to obtaining the solution to the slowing-down equations, implied a flat spatial flux. Obviously, if a physical system proved to have large spatial fluctuations, then GAM's approach could not be applied.

The flat flux approximation was supported by four facts. First, the most obvious cause of large fluctuations was easily eliminated, because there are no strong absorbers of fast neutrons in a thermal reactor. A second

justification may be obtained by noting that the primary source of fast neutrons is fission reactions. If fission events create fast neutrons which travel large distances quickly and isotropically, relative to the cell size, then a spatially flat flux is a fair assumption. Also, in a thermal reactor only a small percentage of the high energy fuel absorptions lead to fission reactions. In other words, a fast group absorption in the fuel is likely to have the same result as any other absorption. Therefore, spreading the fuel evenly throughout the cell should not be detrimental to the calculations. Finally, GAM's primary concern is the slowing down of fast neutrons to thermal energies. The main forces in this process are resonance absorption, and scattering reactions. The fraction of neutrons which slow down is determined by the ratio of absorption to scattering, and the energy loss per collision. These properties are constant for each particular nuclide regardless of the surrounding materials. The variable is the quantity of flux exposed to each nuclide. Given that we are starting with a fairly flat spatial flux, each nuclide sees an equal number of neutrons and it follows that the absorption-to-scattering ratio may be considered not to be a function of position. Therefore, while the homogenization of the cell eased the computation it did a minimum of harm to it's validity.

Even though there are theoretical grounds for homogenizing the cell, GAM still needs to make corrections for obvious errors due to the neglect of spatial effects. For example, the fact that the fuel is actually lumped together leads to a higher fast fission factor than that which would be computed for a homogenized cell. In the homogenized model, neutrons are exposed to the moderator immediately after their births. In reality, neutrons born a few path lengths within a fuel lump may undergo a number of collisions in the fuel before they ever reach the moderator. Because these neutrons have not been slowed down, the probability that their energies are above the fast fission threshold is greater than the probability that would be calculated for a homogenized model.

GAM accounts for these additional fast fissions by modifying the atom densities of U^{238} seen by high energy neutrons, and consequently changing the effective absorption and fission cross sections. To obtain the appropriate correction GAM relates the fuel and cell radii to calculate the probability of a neutron's first and successive collisions occurring in the fuel. This method's major restriction is that the calculation of n-flight collision probabilities is only applied to concentric geometries.

Another modification is necessary to account for the increase in the resonance escape probability due to fuel

lumping. Because the absorption cross sections are so large for the resonance energies most neutrons in these energy ranges are absorbed near the surface of the fuel. This leads to a scarcity of neutrons in the resonance ranges in the center portions of the fuel. Therefore, resonance absorbers located away from the fuel surface absorb fewer neutrons than they would in the homogenized model.

GAM treats resonance absorption and the spatial self-shielding effect by modifying the absorption cross section for any energy group containing a resonance peak [6]. The first step in this process is to split the absorption cross section into resonant and non-resonant components. The smoothly varying non-resonant cross section is determined by Equation (3-3) as described earlier. The resonant component requires a different approach, because the resonance invalidates the assumption that the flux is of the form 1/E by significantly perturbing the flux. In order to treat the perturbation, spatial self shielding must be considered. Therefore Σ_a^{res} is determined by

$$\Sigma_a^{res} = \frac{N}{\Delta u_n} \sum_{i-n} (RI)_i \ .$$

where $(RI)_i$ is the resonance integral of the i^{th} group and u_n is the lethargy width of the group. The resonance integral is a measure of absorptions within a given

resonance peak based upon the fuel's average chord length and Doppler broadening. GAM uses tables developed by Adler and Nordheim to obtain resonance integrals based upon these parameters.

GAM substitutes the modified cross sections into the fine-group slowing down equations and solves them using the method which was previously outlined. In addition to determining broad-group cross sections, the solution yields information which will be valuable to TEMPEST during the thermal calculation. The most important bit of information obtained from GAM will be the fraction of fast neutrons which survive to reach the thermal group.

3.1.B TEMPEST

There are significant differences between the methods applied by GAM and TEMPEST to determine fluxes and effective cross sections. The foremost difference being that while GAM solves the energy-dependent P_1 slowing down equations, TEMPEST must first solve the more complicated one-speed P_3 equations. The P_3 equations are basically a set of one-dimensional transport equations which incorporate the assumption that the angular flux may be written as the first four terms of

$$\varphi(r,\mu,E) = \sum_{\ell=0}^{\infty} \phi_\ell(r,E)P_\ell(\mu)$$

where $P_l(\mu)$ are the Legendre polynomials. The presence of strong thermal absorbers combined with the vast differences between thermal neutron behavior in the fuel and moderator prevent TEMPEST from disregarding the spatial dependence of the flux. Therefore, TEMPEST must seek a solution which is dependent on both energy and position.

To simplify the problem TEMPEST assumes that the spatial and energy dependencies of the solution are separable. Mathematically,

$$\phi(r,E) = f(r)g(E) \qquad (3\text{-}5)$$

which leads to the creation of two separate differential equations. Solving the equation in this manner implies that the spatial solution shape will have absolutely no effect on the energy-dependent solution. This is a questionable statement with regard to the thermal group. Consider the spatial self-shielding effect discussed earlier which would lead to a dip in the flux of any highly absorbed energy in the center of that absorber. In order to account for self-shielding it is necessary to consider spatial and energy effects simultaneously. In situations where self-shielding is not a major concern the space-energy separability assumption may be applied with greater confidence.

TEMPEST's next simplification is to treat the problem in only one spatial dimension. As GAM's zero-

dimensionalization implied a homogenous flux throughout the core, TEMPEST's one-dimensionalization implies a flat flux in two dimensions. In order to be consistent with GAM, TEMPEST must solve the transport equation in cylindrical geometry. Generally, the core composition changes most dramatically in the radial direction so TEMPEST chooses to perform a radial calculation while assuming flat fluxes in the θ and z planes. By treating the problem in only one dimension TEMPEST distinguishes between the fuel and moderator regions while still keeping the difficulty of the problem reasonable.

To begin, TEMPEST assumes that all thermal neutrons are in thermal equilibrium with their surroundings. Each concentric region is assigned a temperature by the user, and the initial flux is a Maxwellian distribution, W(E), based upon these temperatures. Thermal cross sections for each spatial region are determined by combining the flux and material composition using the expression

$$\Sigma = \frac{\int_o^{E_c} dE\ \Sigma^{region}(E)W(E)}{\int_o^{E_c} dE\ W(E)}$$

A one speed P_3 approximation is then used to solve the space-dependent portion of Equation 3-5 analytically for f(r). The number of separate regions, and mesh points per region at which results are to be printed are selected by

the user. The important results from this portion of the calculation are the relative fluxes of each region. The ratios of the average fluxes of each region are known as the disadvantage factors.

The disadvantage factors enable data obtained from the space-dependent P_3 solution to be incorporated into the energy-dependent equation. The disadvantage factors are used to weigh the spatial atom densities according to the spatial flux before the volumetric homogenization. The modified atom densities are used as input to the energy-dependent equation.

The method used to solve the energy-dependent portion of the equation is similar to the method used by GAM, but the equation to be solved is the Wigner-Wilkins equation. The Wigner-Wilkins equation is more complicated than the slowing-down equation because it must account for things like the motion of the nucleus, and upscattering. Macroscopic cross sections, based on the P_3 spatial homogenization, are substituted into the Wigner-Wilkins equation. An analytical solution yields the energy-dependent flux g(E). The final flux, from which all output data is based, is obtained by combining g(E) with f(r) as in Equation 3-5.

3.2 BRT

An alternate, and more accurate treatment of the thermal group is employed by the BRT code. BRT's method allows Equation 2-1 to be solved after making only two notable approximations. By considering the problem to be symmetric about one dimension, and assuming isotropic scattering, Equation 2-1 may be simplified to

$$\hat{\Omega} \cdot \frac{d\phi}{dx} + \Sigma_t(x,E)\phi(x,E,\Omega) = \frac{1}{4\pi}\int_o^{E_c} dE' \int d\Omega' \Sigma_s(x,E'\rightarrow E)u(x,E,\hat{\Omega}) + \frac{S(x,E)}{4\pi} \quad (3\text{-}6)$$

where E_c is the cutoff of the thermal energy group. Because all fission births occur in the fast group, the source term for any thermal group is

$$S(x,E) = \int_{E_c}^{\infty} dE' \Sigma_s(r,E'\rightarrow E)\phi(r,E') \quad (3\text{-}7)$$

Equation 3-7 is substituted into Equation 3-6 and the resulting equation is integrated over space and angle to yield

$$\phi(x,E) = \int dx\ T(x,x',E)\left[\int_o^{E_c} dE' \Sigma_s(x',E'\rightarrow E)\phi(x,E') + S(x,E)\right] \quad (3\text{-}8)$$

where $T(x,x',E)$ is a scattering kernel. The scattering kernel represents the uncollided flux at point x of energy E due to a source of the same energy at x'. BRT solves Equation 3-8 numerically using up to 30 space and 30 energy points while employing either slab or cylindrical geometry.

3.3 Comparison of GAMTEC and BRT

Theoretically, more confidence is placed in BRT relative to TEMPEST because it performs it's calculation without the questionable assumption of space-energy separability. Computationally, BRT utilizes 30 fine energy groups within the range of 0-0.683 electron volts while the same range is covered analytically in GAMTEC. BRT's method of solution also has greater flexibility which allows the problem to be solved in different geometries.

BRT's primary disadvantage is one of cost. The iterative multigroup calculation consumes larger amounts of computer time and money. Another drawback is that BRT does not contain any type of internal calculation for the fast group.

3.4 EXTERMINATOR and 2DB-UM

The major assumption invoked by both EXTERMINATOR and 2DB-UM is the diffusion approximation. This is such a great simplification that it makes it feasible to perform the calculation in two dimensions. This allows the diffusion code computer models to have much greater spatial detail than the transport models. Figure 2-1 illustrates the advantages of using a code which has the capability to treat a two-dimensional model. A one-dimensional model would not even be able to differentiate between a control-rod element and a fuel element, because this would require inhomoge-

neities in two directions. Therefore, whenever the applicability between a diffusion and a transport treatment is similar, the diffusion treatment is usually used.

EXTERMINATOR solves the steady-state multi-group diffusion equation. A big difference between EXTERMINATOR and the transport codes is that EXTERMINATOR demands that all cross sections be input manually. EXTERMINATOR does not treat the thermal and fast groups differently, as GAMTEC does, because it expects that the differences are accounted for in the selection of cross sections. This approach gives the user the flexibility to choose the number and range of the energy groups as he likes. Once the size and space points per region are chosen, the code may substitute the cross sections into the diffusion equation and solve for the flux, multiplication factor, etc. numerically.

2DB-UM has an added advantage in that it solves the time-dependent multi-group diffusion equation. This gives 2DB-UM the ability to calculate the burnup of the fuel, and subsequently, fluxes and multiplication factors at different times throughout the core's life. Cross sections are calculated by the LEOPARD computer code, and input to 2DB-UM by a code called LINX. LEOPARD could not be used to calculate control-rod cross sections, because it demanded that the fuel be in the center of any model.

EXTERMINATOR was used as a link between the transport codes and 2DB-UM for a few reasons. One reason was that at the time it seemed to be an easier code to use than 2DB-UM. The second, and the real deciding factor, was that EXTERMINATOR was up and running on our computer system while kinks in 2DB-UM were still being worked out. Finally, EXTERMINATOR has special numerical features that allow it to run cell problems with symmetry conditions on all sides, whereas some codes do not converge well under these conditions.

4. The Transport Computer Models

4.1 The Problem

The transport codes were used to obtain an accurate description of neutron behavior in the control-rod fuel element. The key to achieving this goal was an appropriate conversion of the actual three-dimensional cell into a one-dimensional model to which the transport codes could be applied. An accurate conversion was essential, because the model was actually the problem statement. Even though the transport codes were known to be applicable to the rod regions, their outputs were worthless unless they were asked to solve the proper problem.

The conversion of the cell into a one-dimensional model presented a problem, because it required that some cell characteristics be input incorrectly. For example, it was impossible to simultaneously use the rod's actual length, density, and exposed surface area. Consequently, a choice had to be made between which one (or two) of these parameters would have the least effect on the calculation if it were to be "fudged". The parameter which proved to have the greatest effect on the calculation, and therefore would be input accurately, will be referred to as the "primary parameter".

The second half of the problem was to form a cell representation based on the output of the transport codes.

Two parameters had to be chosen from the codes' output which told as much information about the cell's behavior as was possible (these will be referred to as the "output parameters"). Only two parameters could be chosen because effective cross sections were to be developed for two groups. Each cross section was to be developed by forcing the diffusion model to match one of the chosen "output parameters" from the transport model. Therefore, the use of these cross sections insured that, at the very least, the control-rod region of the 2DB-UM model would behave as the transport codes predicted with respect to these two parameters.

4.2 The Solution

The plan of attack for obtaining an HEU control-rod cell model was to construct a few different models and choose the best one. Simple logic suggested why one model might highlight the actual cell's more important characteristics better than the other models. A comparison of the codes' treatment of different models actually confirmed this logic. Of course, the final check involved a comparison to experimental data. The effective cross sections for each case were used to calculate control-rod worths which were compared to measured rod worths. Since the final cell representation combined output from BRT and GAMTEC, each trial case actually consisted of a group of

three models. For each case, a slab BRT model was constructed first. Next, cylindrical BRT and GAMTEC models were constructed consistent with the logic used in developing the BRT slab model. For example, if the mole numbers in each region had been preserved throughout the slab model construction, then they would also be preserved throughout the construction of the remaining models for that trial case.

Next, a few values from the transport code outputs were chosen as reasonable possibilities for being the "output parameters", the parameters which contained the most information about the cell's behavior. Two sets of effective cross sections were generated for each trial case by forcing the EXTERMINATOR model to match the output parameters. Each set of effective cross sections was based on a different set of possible "output parameters". Knowledge of each case's effective cross sections made it possible for 2DB-UM to calculate control-rod worths for each trial set of models. The control-rod worths were compared to experimental data to help choose the best representation of the cell. The logic that proved to lead to the best representation of the HEU cell could then be confidently applied in the development the LEU cell models.

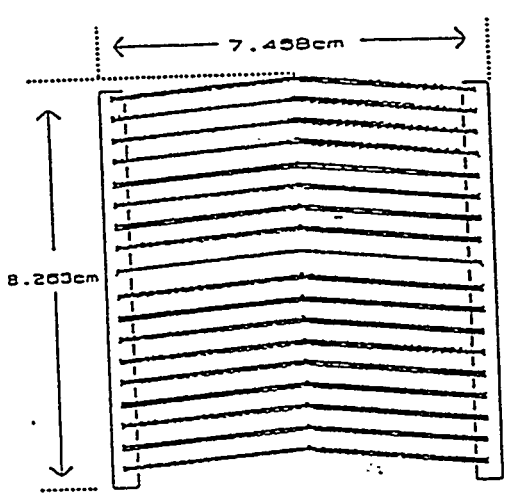
4.3 The Actual Control-Rod Cell

An actual HEU control-rod fuel element is shown in Figure 4-1B. It consists of nine curved HEU fuel plates, two aluminum guide plates, two outer aluminum side plates, a grooved control-rod, and the water between all the components. A single fuel plate is shown in Figure 4-1D. An alloy of U-Al comprises the fuel. The uranium is 93.7% ^{235}U and 6.3% ^{238}U by mole number. The alloy is enclosed in an aluminum clad. The aluminum clad on the two outer plates is slightly thicker than on the others.

The control-rod's size and shape can be seen clearly in Figure 4-2. The rod's composition is a mixture of 1.5% boron and 98.5% stainless steel (ss304) by weight. It is important to make a note of the rod's shape. This shape, which significantly increases the rod's surface area, would prove to be the major stumbling point in modeling the rod. The entire rod was enclosed in a thin layer (0.0254 cm) of Al.

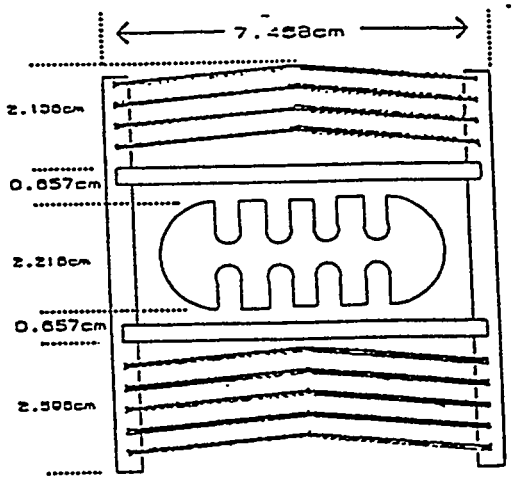
4.4 Preliminary Calculations

The first step in developing the computer models of the cell was to calculate the volumes, and mole numbers of each component of the actual cell which were to be included in the model. Most of the initial data was found in the UVAR Safety Analysis Report [7] while the remainder of the data was taken from the UVAR blueprints [8]. A summary of the results is shown in Table II. Note that although the outer



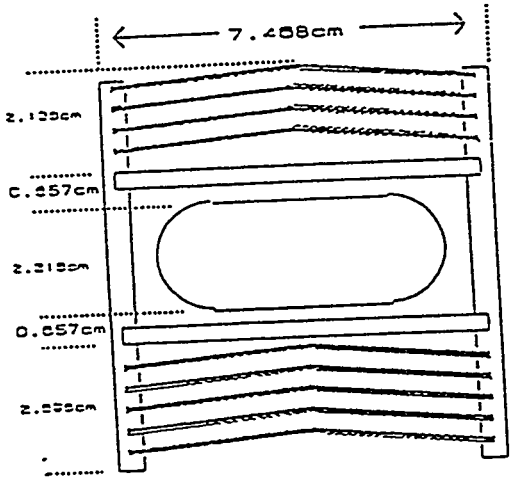
Standard Fuel Element

4-1A



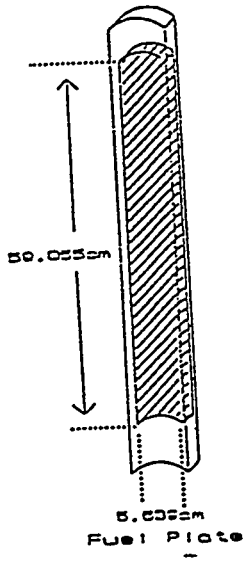
Control Rod Fuel Element

4-1B



Regulating Rod Fuel Element

4-1C

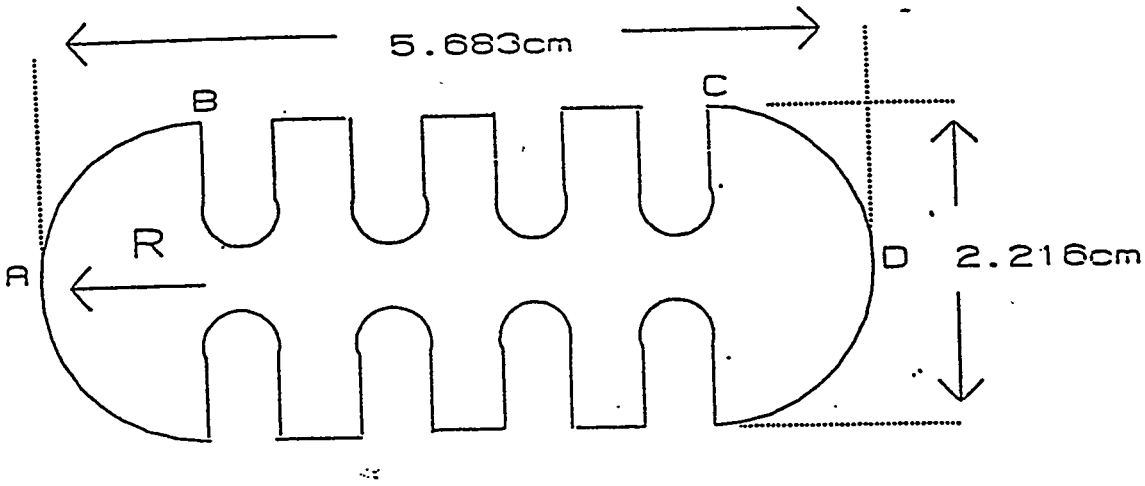


Fuel Plate

4-1D

Figure 4-1: The Fuel Elements

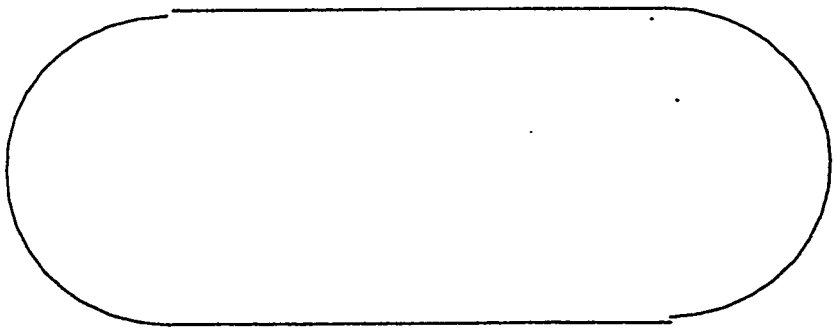
Figures 4-1A, 4-1B, and 4-1C are overhead views of standard, control-rod, and regulating fuel elements, respectively. Fuel plates are represented by the shaded regions. A grooved boron-stainless steel rod is located between two Al guide plates in the control-rod element. Note the different shape of the regulating rod which is composed of 100% stainless-steel. A front view of one fuel plate is shown in Figure 4-1D. The shaded portion represents the U-Al alloy which is enclosed in a coat of Al.



R=1.342cm

Area of one groove = 0.511 cm^2

4-2A



4-2B

Figure 4-2: The Control and Regulating Rods

Figure 4-2A shows the control-rod before the outer layer of aluminum was applied. Note that the grooves result in a decrease in volume and an increase in surface area. Although the regulating-rod (Figure 4-2B) has a greater volume, it has less surface area. The regulating-rod is also a weaker absorber because it does not contain any boron, as the control-rod does.

fuel elements contain more Al clad than the inner plates, the meat portions of the different plates are identical.

Table II: Summary of Initial Calculations

Component	Volume (cm^3)	Composition
One fuel slab (meat)	16.916	1.630 moles Al 0.0463 moles ^{235}U 0.0031 moles ^{238}U
One inner fuel plate	52.865	5.227 moles Al 0.0463 moles ^{235}U 0.0031 moles ^{238}U
One outer fuel plate	68.727	6.815 moles Al 0.0463 moles ^{235}U 0.0031 moles ^{238}U
One guide plate	140.060	14.015 moles Al
The control-rod	460.102	4.584 moles B 3.836 moles Al 58.432 moles steel
The eight grooves	224.500	12.4 moles water
The regulating rod	662.892	96.467 moles steel

4.5 The Models

4.5.1 Modelling Limitations of the Codes

Both BRT and GAMTEC had similar limitations with regard to the models that they would accept. The only notable difference was that BRT would accept slab or cylindrical

models while GAMTEC would accept only cylindrical models. This fact combined with the rectangular shape of the actual cell added support to the theory that the BRT output provided a more accurate description than GAMTEC's.

As mentioned earlier, BRT and GAMTEC's major restriction was that they would only accept inhomogeneities in one dimension. Therefore the first step in building the models was to decide how to divide the cell into regions which would be considered to be, both, homogenous and infinite in two of the three spatial dimensions. Obviously, the objective was to split the cell in such way that the code would best be able to predict the fluctuations in the neutron flux.

Because the codes were only capable of handling inhomogeneities in one dimension, the volumes above and below the fuel alloy were excluded (see Figure 4-1D). This choice allowed the codes to focus on predicting the neutron population in the fuel without diluting the region with the Al and H_2O volumes above and below the fuel (relative to the z-axis). The basis for this decision was that in order to predict changes in the reactor behavior, knowledge of the neutron flux in the fuel portion of the core was deemed more important than knowledge of the flux in the clad or the water above and below the fuel. Therefore, it was better to

ignore the extra region altogether rather than dilute the information which was considered vital.

Another restriction of the transport codes was that they both placed an upper limit on the number of spatial homogenous regions that they would accept. BRT could handle eight different regions while GAMTEC had the capability to accept up to ten regions. Because there are nine fuel plates as well as the control-rod in one cell, BRT clearly did not have the capability to calculate every dip and rise in the flux. Therefore, the cell had to be divided with the objective of predicting the large fluctuations while ignoring the small perturbations in the spatial flux as illustrated in Figure 4-3. This premise led to BRT models in which all the fuel plates on one side of the rod were homogenized into one fuel region. This fuel region's homogenous mixture also included water, and side plate materials. The remainder of the BRT models consisted of two guide-plate regions, a control-rod region, and another fuel region as shown in Figure 4-4.

Before GAMTEC could be applied, it was necessary to convert the slab model into an equivalent cylindrical model. As Figure 4-5 shows, the conversion was achieved by combining the slab model's two fuel, and two guide-plate regions into one perimeter fuel region, and a concentric guide-plate region, respectively. Therefore, the cylindrical

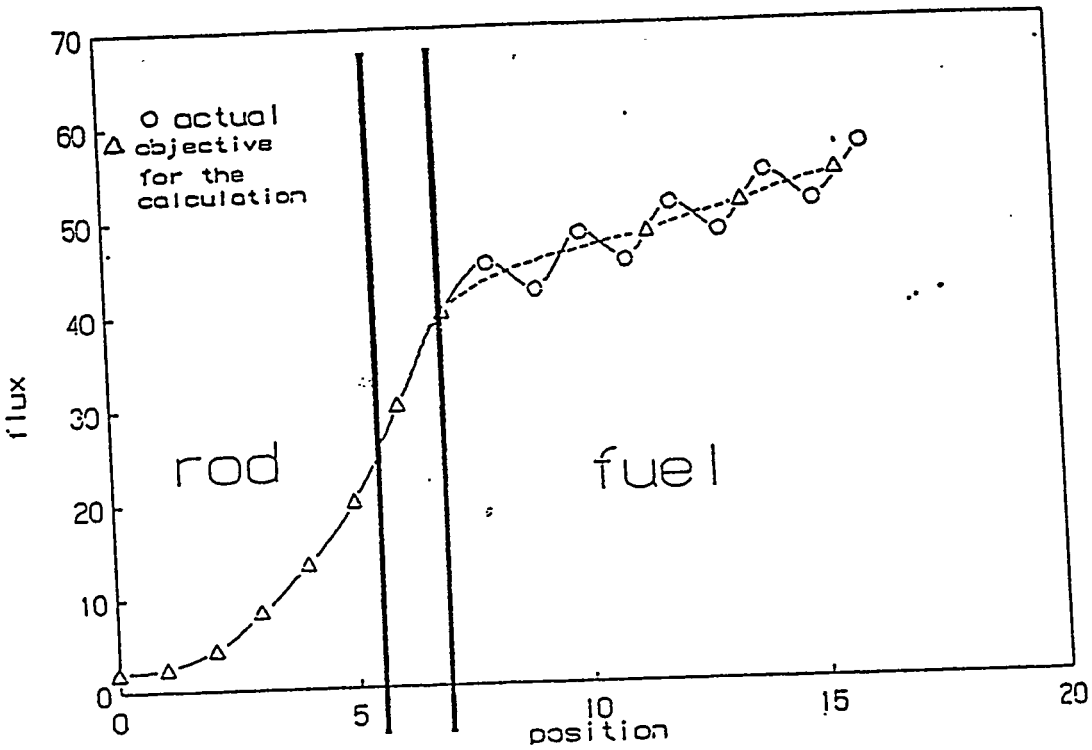


Figure 4-3: Computer Code Limitations

Theoretically, it is known that the actual thermal flux will fluctuate in the fuel region corresponding to the alternating regions of fuel and water (Figure 4-1). It was impossible to simulate each peak because BRT can only handle up to eight regions. A workable objective was to try to simulate an average flux through this region.

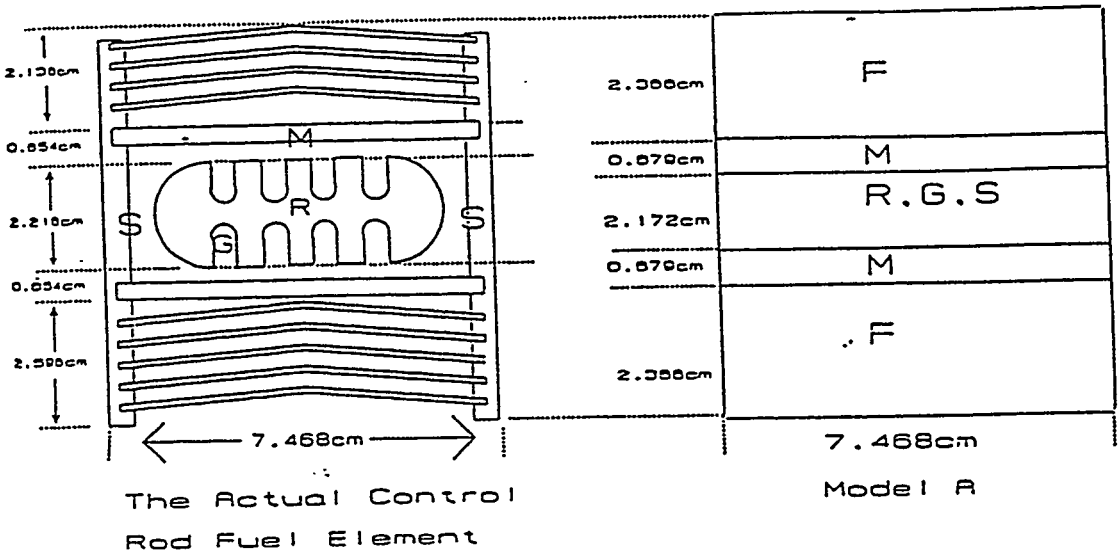


Figure 4-4: Slab Model A vs. the Actual Cell

Figure 4-4: In this and the figures which follow the following names will be used to refer to the given sets of materials in the actual control-rod element in order to simplify the descriptions of the different models.

control rod- The Boron-ss-Al mixture which makes up the rod. Shown as component R in the figure of the actual cell.

groove water- The volume of water which fills the rod grooves. One of the eight grooves is shown as component G in the figure of the actual cell.

side water- The remaining water and Al which occupy the same length as the rod. This region is marked S in the figure, and it's boundaries are the two dotted lines above and below the S.

guide mixture- A mixture composed of the water above and below the rod, the guide plates, as well as the Al side plates which border the region. One of the two guide mixture regions is marked M, and again is outlined by a dotted line below and the top of the guide plate above.

fuel mixture- A mixture made up of all the materials above and below the top and bottom guide plates, respectively. This mixture includes the fuel, water, and side plates.

There are two important points to note regarding model A. First, the length of the rod region is equal to the length of the actual rod before calorization. The second point is that the side and groove water are included in the rod region. These facts are consequences of choosing the length as the "primary parameter".

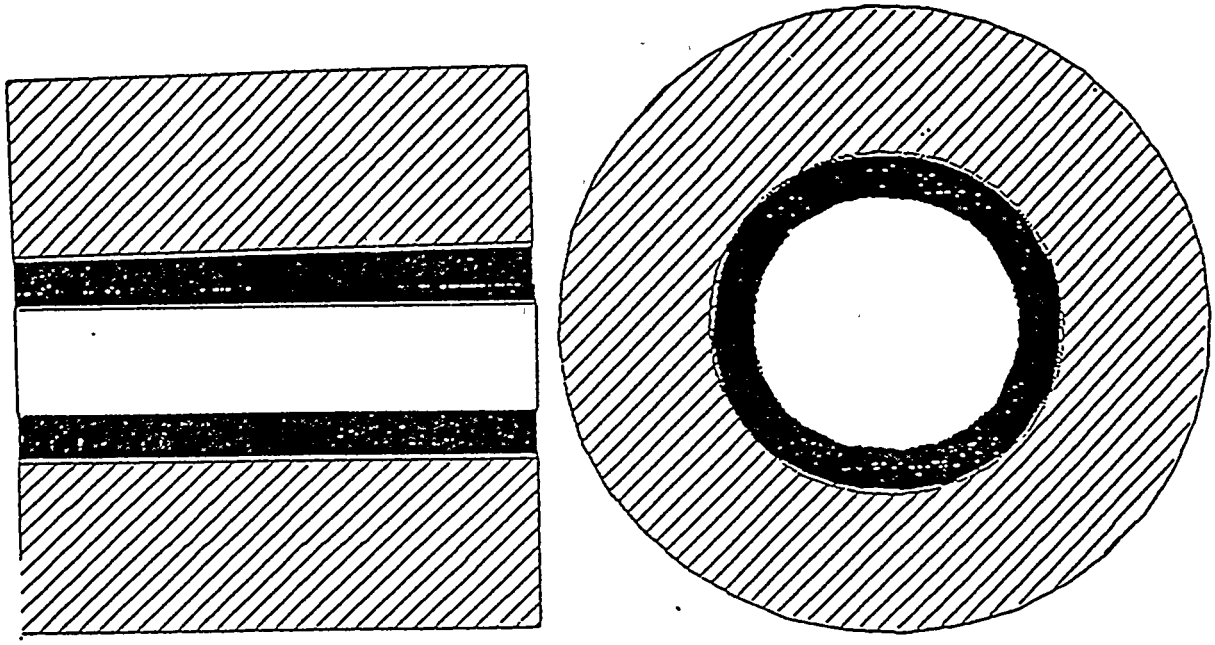


Figure 4-5: Conversion of a Slab Model into a Cylindrical Model

The slab models were converted to cylindrical models as illustrated above. The materials in each slab region were inserted into the corresponding cylindrical region which can be identified by the shading.

model consisted of three regions instead of the slab model's five. The control-rod region was considered to be the center of the cell. The rod region was surrounded by the guide-plate region, and then the fuel region.

4.5.2 Trial Case Constants

Before discussing how the trial cases differ from each other, it is important to mention some of the parameters which were held constant for the different cases. The most significant input data which fell into this category were the boundary conditions. Reflecting boundary conditions were used in all trial cases. Because BRT and GAMTEC are one-dimensional codes they automatically assumed that the cell was bordered by identical control-rod cells in their two homogenous directions (Figure 2-1). Of course, this is irrelevant in the cylindrical model's theta direction. Reflecting boundary conditions implied that the model cell was also bordered by identical cells in the direction in which inhomogeneities were allowed.

Reflecting boundary conditions were chosen because in most cases the actual cell was bordered by fuel cells in the inhomogeneous direction (Figure 5-1). Even though one would expect the average fuel-cell neutron flux to be greater than that of a control-rod element, reflecting boundary conditions were valid. They were valid because the control elements border region contained at least four fuel plates.

Therefore, reflecting boundary conditions correctly implied that the cell was bordered by fuel plates.

Another decision which was based on the presence of bordering fuel plates pertained to the composition of the fuel regions. The actual element contained one region with four fuel plates, and a second region with five plates. The second region was larger so that there was an equal volume of water between every pair of plates. Instead of creating unsymmetric models, all the models were constructed with the contents of four and one-half fuel plates in each of two equally sized regions.

The basis for constructing the models in this manner can be seen from Figure 2-1. The figure shows that in any configuration, each rodded element will be bordered by at least one fuel element along it's y-axis. It is well known that each control-rod element is influenced by the materials which border it. In a case where there are fuel elements both above and below the control-rod element, the control-rod would see an equal number of fuel plates per unit length in either direction. Therefore, the placement of four and one-half plates on either side of the rod should lead to more realistic predictions.

GAMTEC required four additional input parameters for which the same values were used in each trial case. A geometric buckling was required to allow GAMTEC to estimate

the flux shape in the z direction. The buckling was calculated by

$$B^2 = (\pi/H)^2 = 0.00283$$

The larger distances travelled by fast, in comparison to thermal, neutrons suggests that the geometric buckling is more important to the fast calculation. Without a correction for buckling the flux on the upper edge of the cell is assumed to be equal to the flux in the center. This was acceptable for the thermal calculation because most of the collisions were expected to occur in the center of the cell (with respect to the z-axis). The high collision rate was due to the combination of the high flux in the x-y plane of the fuel, which was located in the center, with the average path length of

$$\lambda = 1/\Sigma_t \approx 0.0026 \text{cm}.$$

These facts support the assumption that thermal neutrons located in the fuel had a low probability of reaching the edge of the cell before undergoing a collision.

The effectiveness of the moderator was included by a logarithmic energy-decrement factor. This factor gave the code information pertaining to the fraction of energy lost per collision with a moderator molecule. The energy-decrement factor for water is 0.92.

The effect of neutrons originating in other fuel cells that were scattered into the cell of interest were taken into account by using the Dancoff shielding factor. The value was taken from a tabulated chart which related the radius of the cell, the distance between neighboring cells, and the moderator scattering cross section [9]. The shielding factor was found to be 0.0001. GAMTEC also asks for the circumference of the outermost region of the cell so that it may calculate the fast fission effect. The circumference was 27.85 cm.

4.5.3 Trial Case A - Slab Model

The slab model was constructed first because it most resembled the actual cell. Therefore, it required fewer approximations, and consequently, there were fewer chances to create errors. The five slab regions were constructed slightly differently for each trial case. The slab model used in trial A was the result of a first impulse to make the appearance of the model resemble the actual cell as closely as possible. The relative length, and molecular composition of each region were chosen as the input parameters which would have the greatest effect on the cell behavior. Therefore, these two parameters were taken exactly from the actual cell while other parameters, such as surface area of components, were given values which were

dictated by the conservation of region length and composition.

While the length of the cell, and of each region, were included in the one-dimensional slab model, the cell height and width were indirectly implied. Both GAMTEC and THERMOS require the molecular composition to be input in units of atoms/barn·cm, a three-dimensional quantity. Therefore, before computing the molecular composition it was necessary to define the other two spatial dimensions of the actual cell which were to be included in the one-dimensional model. The actual cell height was taken to be 59.055cm while the width was taken as 7.468cm. The height corresponded to the height of the fuel portion of the fuel plate (Figure 4-1D) while the width corresponded to the width of the actual cell (Figure 4-1B).

Figure 4-4 shows slab model A and the actual cell side by side. The actual cell's components were grouped according to the dotted lines in the figure of the actual cell. Next, the sizes of the corresponding model regions were chosen based on the length of the regions shown in the [illegible]. The [illegible] were [illegible] by homogenizing each group of [illegible] and the [illegible] volume.

The length of the model's two equivalent fuel regions (regions I, and V) was arrived at by averaging the actual

cell's unequal fuel regions. The rod region's (region III) length was taken to be equivalent to the length of the boron-ss mixture in the actual cell. The remaining length of the actual cell was then split between the two equivalent guide-plate regions (regions II and IV) which separated the rod from the fuel regions. Note that this implies that although the rod's outside layer of Al was homogenized into the rod region, the rod region's volume was chosen as if this layer was not part of the rod. Instead this volume was incorporated into the more weakly absorbing guide-plate region.

It was now possible to calculate mole number densities for every nuclide (the chemical elements will be referred to as nuclides to avoid confusion with the fuel elements) present in each model region. After mole numbers were obtained for each group of components the number density was found by

number density= molecules of nuclide in region/region volume

As mentioned earlier the two actual fuel regions were combined for this calculation and the resulting mole number density was used for both model regions. Therefore, each model fuel region contained a homogenous mixture composed of 4½ fuel plates, 2 aluminum side plates each 2.235cm in length, and water. Each guide-plate region contained the

molecular content of one guide-plate, two Al side plates each 0.678cm long, and water. The molecular content of the Al layer which enclosed the rod was included with the boron-ss mixture, two Al side plates each 2.22cm long, and water in the rod region. Each region's water volume was determined by computing the total volume of all components, and then taking the remaining volume as water.

4.5.4 Trial Case B- Slab Model

The construction of model B was based on two premises. The first premise was that the volume of the control-rod relative to rest of the cell was the "primary parameter". The second assumption was actually a modification to the first. It stated that the eight grooves (see Figure 4-2) actually increased the rod's absorbing strength.

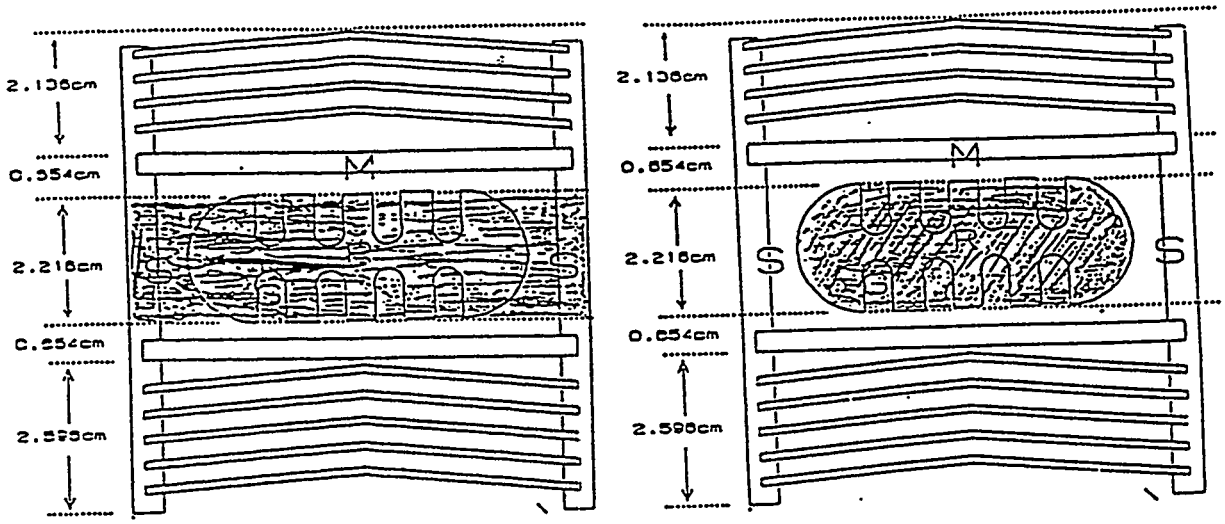
The presence of the grooves changed two characteristics of the rod. They significantly increased the rod's surface area, and simultaneously decreased the rod's total volume. The theoretical implication of the second premise was that the consequences of the additional surface area outweighed those of the volume loss. Due to the rod's high absorption cross section most neutrons were absorbed in the boundary layer of the rod. Therefore, a change in surface area would be expected to have a much greater effect than a change in the interior volume. In regard to the model, this implies

that it would have been a mistake to shrink the rod volume in response to the presence of the grooves.

This line of reasoning led to the model portrayed in Figure 4-6. The control-rod region (slab region III) volume was taken to be equal to the rod volume prior to the grooves being cut into it (see Figures 4-2 and 4-6). Because of the desire to keep the model width identical to the width of the actual cell, the length of the region was adjusted to 1.551cm to obtain the desired volume. The material composition included the boron-ss mixture, the enclosing Al layer, and water. The quantity of water was chosen to exactly fill the difference in the volumes of the region and the rod (including the Al layer). From here on this volume will be referred to as the groove volume.

The water and side plates which had been included in slab model A's region III, but had been excluded in model B's, were divided equally between model B's regions II and IV. Thus, model B's guide-plate regions contained the same materials as model A's guide-plate regions, as well as the additional water and Al. The length of these regions were adjusted to 0.990cm to account for the additional volume. Slab model B's fuel regions were identical to those of model A.

A comparison of the first two models shows that the primary differences were the size of the rod region, and the



The shaded portions of the two figures shown above represent the volumes included in the rod regions of models A and B, respectively.

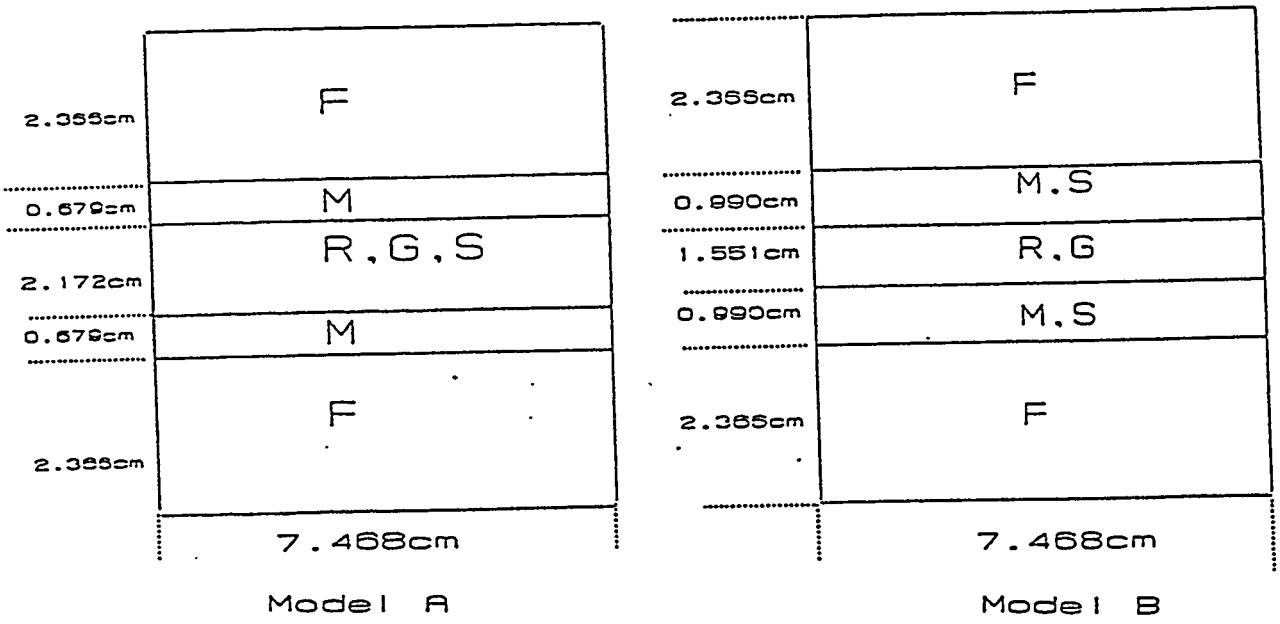


Figure 4-6: Slab Model A vs. Slab Model B

This figure illustrates the differences between models A and B. The length of model B's rod region has been shortened so that it's volume is equal to that of the actual rod plus the groove water (the shaded portion in the figure above model B). The rod region's homogenous mixture is composed of the rod and the groove water. The side water has been included in the mixture of regions II and IV, which have had their lengths increased to preserve the distance between the guide plates.

density of the rod materials. While model A spread the rod composition of 6.730 moles of boron and 91.707 moles of SS304 over a volume of 957.718cm^3, model B spread the same number of moles over a volume of 684.152cm^3. A neutron travelling through the models lengthwise would encounter 2.172cm of control-rod material in model A, and 1.551cm in model B.

4.5.5 Trial Case C- Slab Model

In contrast to model B, the construction of model C (Figure 4-7) stuck strictly to the premise that the volume of the rod region relative to that of the entire cell was the "primary parameter" in the model construction. According to model C's premise, both models A and B incorrectly increased the rod's absorbing power by spreading the boron-ss mixture over larger volumes than the actual rod had. Although this statement sounds reasonable by itself, recall from section 4.5.4 that it implies that the rod's increased surface area was neglected in model C.

The implied volume of the rod region was made to equal the actual rod volume by adjusting the region's length to 1.043cm. The implied width and height were held at 7.468cm and 59.055cm, respectively. The composition of this region consisted solely of the aluminum, boron and ss which comprised the control-rod.

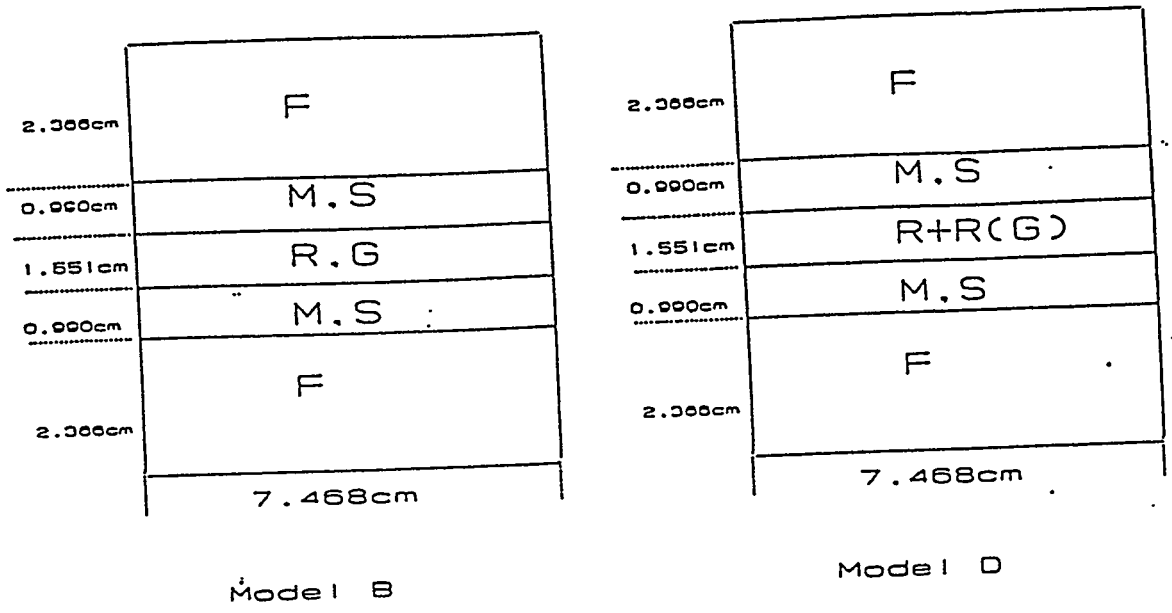


Figure 4-8: Slab Model B vs. Slab Model D

Models B and D are structurally equivalent. The difference between the models is that model D attempts to account for the grooves by replacing the groove water with an equivalent volume of boron-ss.

As a result of decreasing region III's volume from the previous models, the volumes of regions II and IV were increased. The length of regions II and IV was increased to 1.244cm which implied a combined volume of 548.632cm^3. This volume corresponded exactly to the volume of the actual cell between the two guide-plates' outer edges after subtracting out the control-rod's volume. It followed that the molecular composition for these regions was a mixture of all the materials between outer edges of the guide-plates excluding the control-rod.

4.5.6 Trial Case D- Slab Model

Slab model D (Figure 4-8) was based on the same two premises as model B with respect to the actual cell. It differed from model D in that it proposed to portray these premises differently in the computer model. Like model B, model D assumed that in the actual cell the rod's absorbing power varied directly with the rod's volume, and was increased by the presence of grooves. Whereas model B depicted the situation by increasing the rod region's volume from the actual cell by including the groove water in the rod region, model D replaced the groove water with an equivalent volume of control-rod material. The result was a control-rod region composed solely of the boron-ss mixture.

Model D helped to answer the question of whether the control-rod could be homogenized with water without

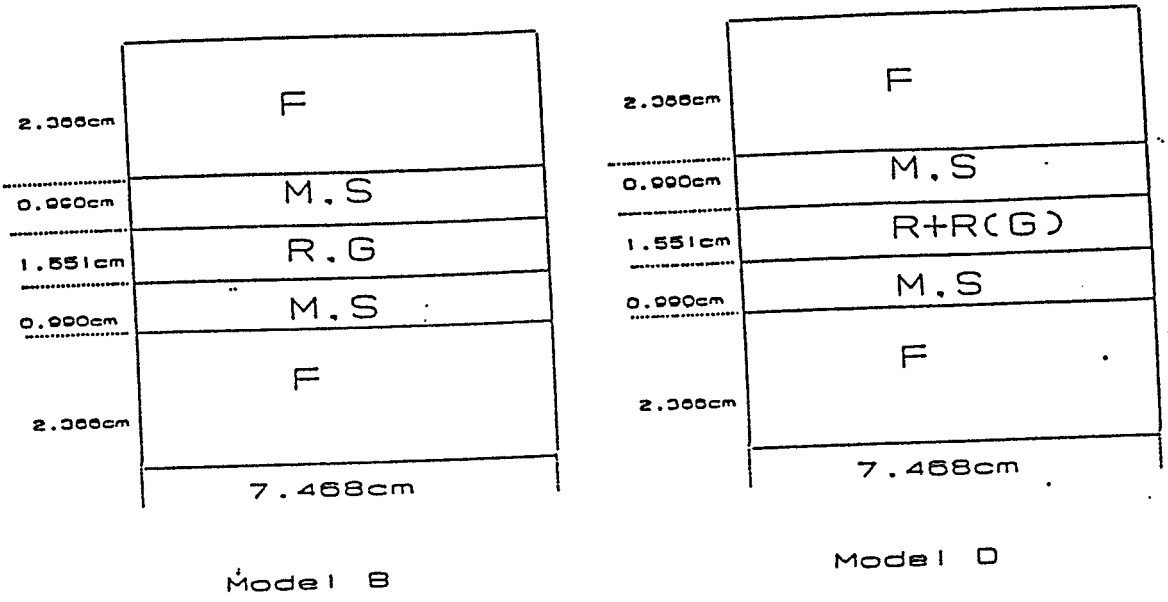


Figure 4-8: Slab Model B vs. Slab Model D

Models B and D are structurally equivalent. The difference between the models is that model D attempts to account for the grooves by replacing the groove water with an equivalent volume of boron-ss.

influencing it's properties. The logic which led to model D said that since the rod was a solid block of boron-ss, it should not be portrayed as a mixture of boron-ss and water. The fuel regions were not changed even though this line of thought seemed to demand it. Recall from Figure 4-1 that the actual fuel regions contain thin fuel plates separated by water. Therefore, homogenizing the fuel and water was deemed allowable while the mixing of the rod and water was not.

Regions I, II, IV, and V of model D were identical to those of model B. The spatial dimensions of model D's rod region were also identical to those of model B. The only difference between the two models occurred in the molecular make up of the rod region. Whereas region III of model B contained 4.584 moles of boron, 58.432 moles of ss and 6.200 moles of water, the same region of model D contained 7.024 moles of boron and 89.472 moles of ss. Therefore, a rod region was created with the volume, and molecular composition that the rod had before having any grooves cut into it.

4.5.7 Trial Case E- Slab Model

Slab model D attempted to account for the additional absorbing power caused by the grooves by filling in the grooves with boron-ss. Effectively, this resulted in the rod being portrayed as if the grooves had never been cut.

Therefore, model D did not satisfactorily account for the grooves. At best, it prevented the absorbing power from being decreased because of the grooves. In order to increase the absorbing power the three remaining models used the surface areas of the rod as their "primary parameter".

Up to this point the rod surface area had not been tried as the "primary parameter" because it required that the length and width of the transport model differ from that of the 2DB-UM model. At first the thought of altering the model size seemed to contradict the purpose of the project. This viewpoint changed when it was realized that the transport model could be altered without changing the diffusion model. The purpose of the transport codes was to obtain an accurate picture of the cell's behavior. The only values from the "transport portion" which were important to the remainder of the project were the two "output parameters" chosen to represent the cell. Therefore, the size of the transport model was irrelevant. Any sized model was acceptable as long as it led to the most accurate prediction of the "output parameters".

At this point, slab regions I, II, IV and V of the first four models were considered to be satisfactory, but there was still a desire to improve region III. Consequently, the objective of slab model E was to create a rod region with the perimeter of the actual rod without

changing the fuel, nor the guide-plate regions from models A-D. To accomplish this objective the implied model width had to be held at 7.468cm while the perimeter of the rod region was adjusted to 25.554cm (the perimeter of the actual rod excluding the aluminum coating). The only way to obtain a model with these characteristics was to increase the length of the rod region to 5.309cm (see Figure 4-9). The resulting rod region had a "fudged" volume of 2340.55cm^3 which was filled with 2340.55cm^3 of the boron-ss mixture.

4.5.8 Model F- Slab Model

In slab model F, the restriction which demanded that regions I, II, IV and V be preserved was abandoned. Model F explored the suggestion that more could be gained by improving region III than would be lost by slight changes in the other regions. This proposition was actually a direct consequence of choosing the rod surface area as the most important parameter in the model.

Although model E did preserve the surface area of the rod, a quick glance at Figure 4-9 shows how model E missed the point. The surface area was chosen as a significant characteristic because a greater surface area allowed more water to be in contact with the rod, and consequently the rod became a more effective absorber. The diagram shows that model increased region III's perimeter by stretching it's

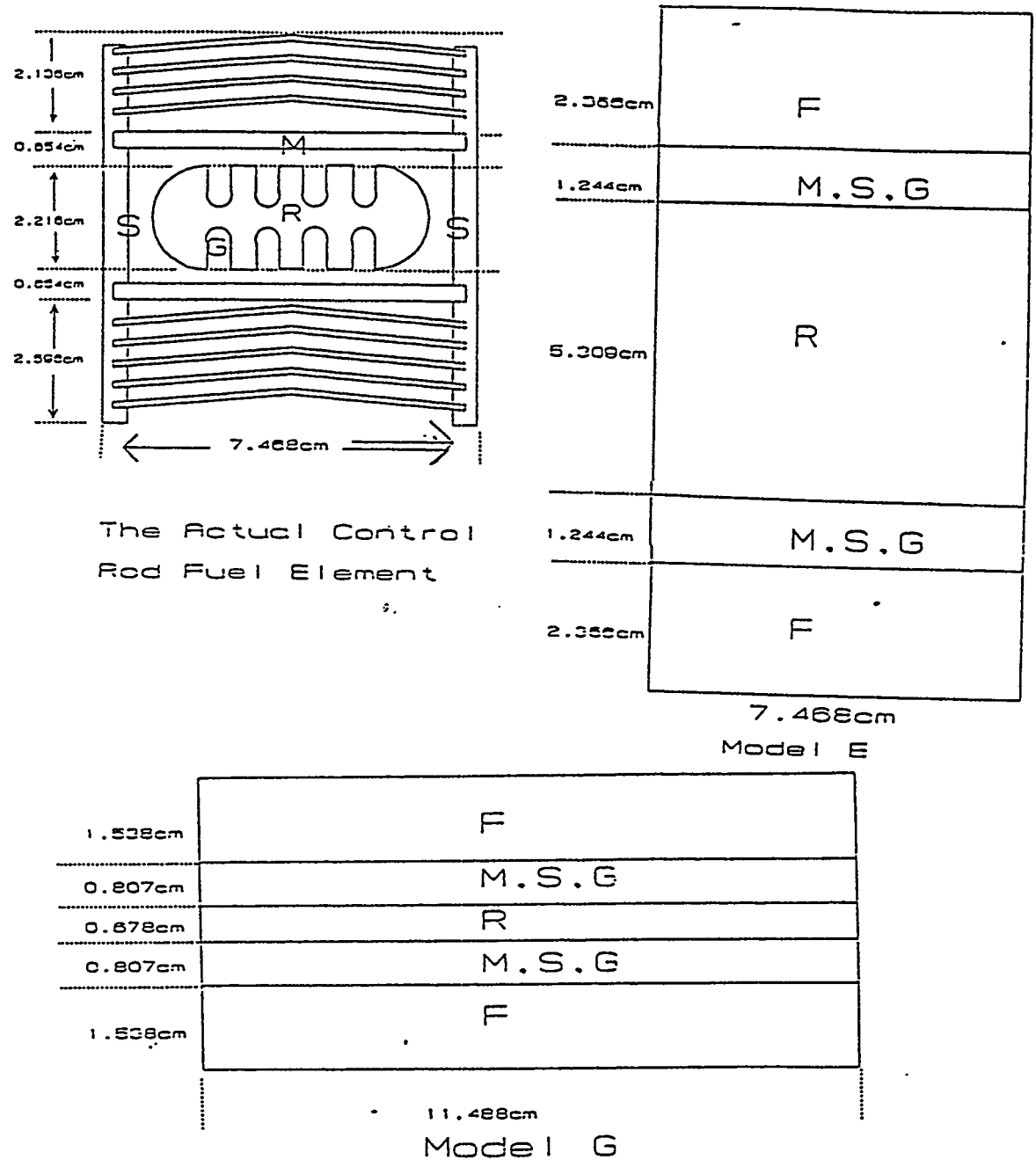


Figure 4-9: Slab Models E and G

Models E and G both attempt to simulate the control-rod's grooves by creating rod regions which preserve the actual rod's perimeter. Note that model G is more effective, because it actually increases the area in contact with regions II and IV.

length. It did not increase the area of region III which was in contact with the other regions.

In contrast to model E, when model F increased region III's perimeter the area in contact with regions II and IV was increased. This capability was a consequence of allowing model F to vary it's width from the other models. The model width was chosen to coincide with the "effective" width of the rod. The "effective" rod width can best be described by looking at Figure 4-2. In this case the effective width was taken as the distance travelled if the rod boundary was traced from point B to C. This distance was 9.370cm. Next, the region length was chosen to be 0.8315cm which caused the area of the rod region equal to that of the actual boron-ss mixture. Because the cell width had been changed, the lengths of regions I, II, IV and V were also changed so that they would cover the same area that they had in model C. Therefore, the number densities for the cell were identical to those of model C.

4.5.9 Model G -Slab Model

The logic behind model G (Figure 4-9) was identical to the logic behind model F. The only difference was in the selection of the "effective width". Figure 4-1 shows that instead of tracing the distance from B to C, model G used the distance from A to D. Again, the region length was chosen so that the region area would match the actual area.

Therefore, the surface area of region III which was exposed to regions II and IV exactly matched the exposed surface area of the actual rod. In this case the "effective" width was 11.488cm, and the region length was 0.678cm. Following the same logic as was used in model F the length of the fuel and guide-plate regions were 1.538cm and 0.807cm, respectively.

4.5.10 The Cylindrical Models

In order to apply GAMTEC, the slab models were converted into equivalent cylindrical models. As Figure 4-5 shows, the cylindrical models consisted of three regions instead of five, as in the the slab models. The control-rod region was considered to be the center of the cell. The rod region was surrounded by a guide-plate region, and then a fuel region. In each case, the molecular contents of slab regions II and IV were combined to form the guide-plate region while slab regions I and V comprised the fuel region.

The size of a region in a cylindrical model was dictated by the choice of radius. In models A-D the region radii were chosen so that the area of each region would equal the implied area of the corresponding region in the slab model. Therefore, the region radii were dictated by

$$\pi r^2_2 - \pi r^2_1 = (7.468\text{cm}) \cdot L$$

where r_2 and r_1 were the inner and outer radii, respectively, of the region, 7.468cm was the implied width of the slab model, and L was the combined length of the slab regions that were being converted. The resulting regions had radii of 1.9205cm, 2.897cm, and 4.432cm for cylindrical regions I, II, and III respectively.

Only one cylindrical model was developed which attempted to conserve surface area. The primary reason for developing only one model was that the cylindrical model was being developed in order to perform calculations for the fast group. Since the rod's absorbing power was much weaker with respect to the fast group, the reasoning which suggested that the grooves would cause many more thermal absorptions (see section 4.5.4A) did not apply to the fast group.

A secondary reason for constructing only one model was practicality. The radius of the center region was chosen so that the rod region had the desired perimeter. This fact meant that the region volume was automatically chosen. It could not be adjusted as it had been in the slab model by varying the region length. This was a problem because the preservation of the actual surface area led to rod regions with volumes three to four times the actual volume. At the same time, the large radius of the center region forced the fuel region to be very thin relative to the rod region.

The one model which was developed most resembled slab model F. The rod region perimeter was taken to be twice the effective length which was used in slab model F. The resulting radius and volume were 2.983cm and 1650.388cm^3, respectively. The actual rod mole numbers were spread over this volume. The radii of the guide-plate and fuel regions were selected to be 3.849cm and 5.105cm so that their volumes would be the same as in model C. Therefore the number densities from cylindrical model C could be used here.

The significant point here was that in each case, a cylindrical cell was constructed in which the "primary parameter" was preserved from the corresponding slab model. In models A-D, each cylindrical region had an implied volume, and contained a molecular content exactly the same as it's corresponding slab region. Cylindrical model F corresponded to slab models E-G because it preserved rod surface area.

4.6 The Output Parameters

4.6.1 The Thermal Group

After applying BRT and GAMTEC to each model, the next problem was to choose the two values from the codes' output which would give the most information about the cell. One value was taken from BRT to describe the thermal group

behavior while the other parameter was chosen from GAMTEC to describe the fast group behavior.

Early in the project, the fraction of thermal absorptions in the fuel region relative to the entire cell was chosen as the thermal parameter. Throughout the remainder of the project no other parameter was suggested which could challenge the absorption fraction in the fuel as the one thermal parameter which told the most about cell behavior. Very simply, the most important information pertaining to a thermal neutron was knowing whether or not it caused a fission reaction. Combined with knowledge of the cross sections in the fuel, the fraction of absorptions in the fuel told what fraction of neutrons would cause fissions.

An argument could have been made for attempting to match the shape of the thermal flux instead of the fuel absorption fraction. Although the flux shape was considered, it was never used. The main reason that the flux shape was of interest was to gain insight to the fraction of neutrons being absorbed in the different regions. Since the codes gave direct access to these fractions, knowledge of the flux was of secondary importance.

4.6.2 The Fast Group

At first, the cell multiplication factor was taken from GAMTEC to be the fast group "output parameter". The

multiplication factor was chosen to take advantage of the fact that GAMTEC could perform a calculation which included both groups. What was overlooked was that in the process used to develop effective cross sections this choice actually nullified the BRT calculation. This was definitely not desired because the BRT calculation was considered the more accurate of the two.

The second suggestion for a fast "output parameter" was the fraction of fast neutrons which survived to reach the thermal group without being absorbed. Like thermal neutrons, the most vital knowledge regarding a fast neutron is whether or not it causes a fission in the future. By combining knowledge of the fraction of fast neutrons which reach the thermal group with the fraction of thermal neutrons which cause a fission, an adequate picture of cell behavior would be obtained. The advantage of this parameter over the multiplication factor was that it had no effect on the more accurate thermal calculations.

4.7 Transport Code Output

4.7.1 Slab vs. Cylindrical Models

Section 4.5 described the different approaches taken to model a control-rod element in one dimension. As some of the

explanations of 4.5 hinted, the later models were inspired by drawing conclusions based on the output of the earlier models. In some cases, comparisons between the output of different trial cases yielded definite answers as to whether or not the selected model should have certain characteristics. Section 4.7 will concentrate on how these comparisons led to the creation of model G, and why that model was expected to yield the best representation of the control-rod element.

One question which had to be answered before proceeding was how well did the data generated by the BRT slab, BRT cylindrical, and GAMTEC cylindrical models agree. Earlier discussions (sections 3.3 and 4.5.3) explained why it was assumed that the BRT slab model would lead to the best results with respect to the thermal group. Recall that because of this assumption, the objective in developing a cylindrical model was to make it behave like the equivalent slab model. Therefore, the cylindrical models were judged by comparing their output to that of the BRT slab models.

All the relevant information has been compiled in Table III. The fraction of all thermal neutrons absorbed in the fuel, $(\nu\Sigma_f/\Sigma_a)_{cell}$ (all cross sections referred to in this chart are thermal cross sections), and $\Sigma_{rod}A_{rod}$ were chosen as three parameters which summarized the predictions of cell

behavior made by each model. Two comparisons were made from the chart.

Table III: Transport Output Parameters

	Fraction absorbed in the fuel region			$\nu\Sigma_f/\Sigma_a$			$\Sigma_{rod}A_{rod}$		
	BRT Slab	BRT Cyl	GAM Cyl	BRT Slab	BRT Cyl	GAM Cyl	BRT Slab	BRT Cyl	GAM Cyl
Model A	0.421	0.391	0.380	0.697	0.648	0.624	17.46	17.79	31.51
Model B	0.455	0.455	0.537	0.755	0.754	0.723	17.72	18.06	31.43
Model C	0.502	0.546	0.580	0.833	0.906	0.962	19.11	19.90	31.38
Model D	0.492	0.487	0.533	0.815	0.807	0.881	27.27	28.36	48.05

The first comparison looked at the results of performing the same calculation on two different models. The application of two different codes to the same model was the source of the second comparison.

Applying BRT to both the slab and cylindrical models allowed a judgement to be made on whether equivalent models had been constructed in the two different geometries. Table III shows that in each trial case, every value calculated from the BRT cylindrical output was within 10% of the same value generated by the slab model. That is to say when the same calculation was conducted on two different models the

results were similar. This fact verified that the method used to transform the slab model into a cylindrical model did indeed create an "equivalent" model.

The next step was to apply both BRT and GAMTEC to the same cylindrical model. The table shows that in every case the application of BRT to the cylindrical model came significantly closer to reproducing the BRT slab output than when GAMTEC was applied to the same model. This fact confirmed our earlier suspicion that the differences in the solution methods of the codes could not be ignored. If the differences had been negligible then BRT would not have been necessary, because it had already been decided that the cylindrical model was "equivalent" to the slab model.

It is interesting to note that when the rod element was treated in it's entirety, GAMTEC's results were all in the same ballpark as BRT's, but when the individual regions were examined the differences became quite large. The table shows that for the two parameters which pertain to the entire cell, (that is the fraction of neutrons absorbed in the fuel and $v\Sigma_f/\Sigma_a$), the GAMTEC values were always within 18% of the BRT slab values. In contrast, GAMTEC values for $\Sigma_{rod}A_{rod}$, which only pertained to the rod region, differed from the BRT values by as much as 76%.

Some insight into how BRT's and GAMTEC's region values could differ by so much while the cell values came fairly

close can be found in Figure 4-10. This figure shows the different flux shapes predicted by BRT and GAMTEC when they were applied to cylindrical model D. The figure shows that while GAMTEC predicted a lower thermal flux in the rod region, it predicted a higher flux in the fuel region. Therefore, parameters which pertained to individual regions reflected these differences in flux, and parameters which pertain to the whole cell reflect the fact that these differences declined when the flux was averaged over the entire cell.

The differences in region fluxes can easily be explained by recalling the primary difference between BRT's and GAMTEC's solution methods. Chapter three explained that the major difference with regard to the thermal group was that TEMPEST failed to separate the spatial and energy dependences of the flux. This fact led to a neglect of self-shielding effects, thereby making both the rod and fuel regions into stronger absorbers than they actually were. In the rod region this is portrayed by a lower flux while in the fuel region the additional absorptions lead to more fission reactions and therefore a higher flux. To reiterate, this illustrates that GAMTEC's assumption of space-energy separability does lead to unnecessary errors, and supports the decision to select the thermal "output parameter" from the BRT output.

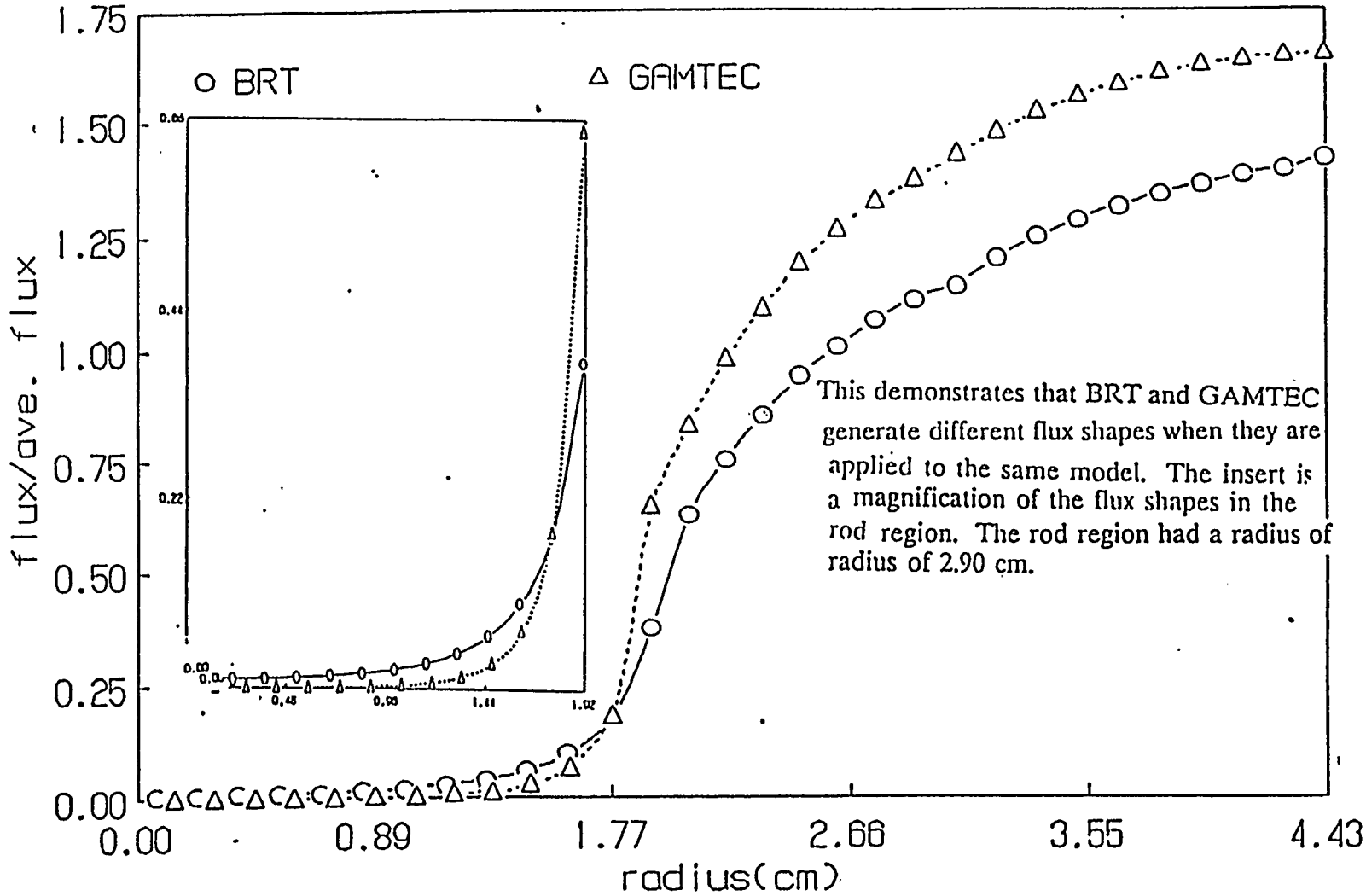


Figure 4-10: Comparison of the Fluxes Generated by Cylindrical Model D

The fact that BRT's thermal calculation was more accurate than GAMTEC's was also the reason that GAMTEC's multiplication factor was rejected as a potential fast group "output parameter". The multiplication factor was originally chosen to take advantage of the fact that GAMTEC treated both the fast and thermal groups. A little more thought shows why this fact was actually the major flaw in using the multiplication factor.

In order to calculate a cell multiplication factor, GAMTEC needed to make use of parameters calculated by both TEMPEST and GAM. Therefore, any attempt to force the diffusion model to match GAMTEC's multiplication factor not only implied an acceptance of the TEMPEST calculation, but could also force the diffusion model's thermal output to move away from the more accurate BRT thermal "output parameter".

This problem was easily solved by choosing a fast-group parameter which was calculated by GAM and would only affect the diffusion model's fast group. GAMTEC calculated a resonance escape probability which was defined as the fraction of fast neutrons born which survived to reach the thermal group. The use of this value as the fast group "output parameter" took advantage of GAMTEC's fast-group calculation while neglecting it's thermal calculation, for which a better code was available.

4.7.2 The Composition of the Rod Region

One significant question regarding the model configuration was whether or not water should be included in the rod region. An examination of the output parameters from models B and D provided the answer. Recall that these two models were identical except that model D replaced the groove water in the rod region with an equivalent volume of boron-ss. Therefore, any differences between the models' output parameters could be attributed to the inclusion of water in the rod region.

An obvious expectation was that the excess of absorbing material would cause model D's rod region to absorb a higher fraction of the total neutrons than the same region in model B. Table IV shows that the codes predicted a result which was just the opposite of that expectation. The table is a summary of data generated by BRT and GAMTEC which was considered relevant to choosing a proper rod-region composition. The first two lines consist of output from BRT's thermal calculation. They show that BRT predicted that model B's mixture of rod and water would be a stronger thermal absorber than model D's solid rod even though the solid rod contained more boron in an equal volume. In contrast, the Table shows that GAMTEC predicted that model B's rod would allow a greater number of fast neutron to slow down to the thermal energy range before being absorbed. Therefore, the

inclusion of water in the rod region seemed to multiply the thermal absorbing power of the rod, while having little or no effect on the fast group calculation.

One hypothesis, which explains why the addition of water would increase the rod's thermal absorbing power more than the addition of boron, was formed. The hypothesis was that the primary effect of adding water to the rod region was that probability of scattering increased. The increase in the number of scattering reactions caused two things to happen. Each scattering reaction slowed the neutron down to energies where boron's absorption cross section was higher, and each reaction allowed a neutron to penetrate further into the rod where the absorption probability was higher due to the lower flux. Remember that because BRT did not assume space-energy separability it accounted for the fact that not many neutrons survived to reach the center of the rod.

This hypothesis was supported by examining some of the macroscopic cross sections for the rod region calculated by BRT. Table IV shows that even though BRT predicted that model B's rod region would be a stronger absorber than model D's, it also calculated a smaller absorption cross section. If the addition of water to the rod region was not increasing the absorption cross section, the only way it could increase the absorbing power was to make more neutrons available to be absorbed. A look at the scattering cross

sections shows that the addition of water led to an increase by a factor of about 1.5. Although these facts do not prove the hypothesis, they do make a very good case to support it.

Table IV: Model B vs. Model D

	Slab Model B	Slab Model D	Cylindrical Model B	Cylindrical Model D
BRT thermal fuel absorption fraction	0.4552	0.4915	0.4547	0.4867
BRT thermal $\nu\Sigma_f/\Sigma_a$	0.7549	0.8151	0.7540	0.8071
BRT thermal $\Sigma_{a\ rod}$	1.53	2.35	1.56	2.45
BRT $\Sigma_{s\ rod}$	1.31	0.889	1.32	0.889
GAMTEC thermal absorption fraction	----	----	0.7232	0.8812
GAMTEC thermal $\nu\Sigma_f/\Sigma_a$	----	----	0.5369	0.5326
GAMTEC resonance escape probability	----	----	0.7464	0.6448
GAMTEC mult. factor	-----	----	0.5838	0.6104

The reason that the rod's absorbing power with respect to the fast group is not increased by the presence of water can be found by returning to the methods employed by each code to solve the transport equation. The fast group behavior is easily explained by recalling that GAM solves the equation in zero-dimensions. Therefore, the additional water was not added to the rod region but it was added to the homogenized cell. In this case the rod has already been homogenized with water, so adding more water to the cell will only have a small effect on the rod. On the other hand, the addition of more boron has a greater effect because it is exposed to all the neutrons throughout the cell.

This discussion was relevant because it allows an intelligent decision to be made about the rod region's composition. Since the actual rod was indeed a solid mass with no water mixed into it, it was clear that the actual rod did not experience any additional absorbing strength due to the effects described. Therefore, it was clear that the final model should not have any water homogenized into the rod region.

4.7.3 Modelling the Grooves

Some of the problems related to modelling the grooves were mentioned in section 4.5. It was a fact that the grooves increased the rod's absorbing power by increasing it's surface area. Basically, the problem was to create a

logical algorithm for increasing the absorbing power of the computer model's rod region by the same amount as the grooves increased the actual rod's absorbing power. An easier solution might have been to just keep adding boron to the region until the computer output matched the experimental results. The problem with this solution was that it did not create any guidelines which could be followed when developing the LEU computer models.

As discussed earlier the first attempt at a solution, model D, was disqualified on theoretical reasons. The basis of model D was to increase the absorbing power by filling in the groove volume with the boron-ss mixture. The result was that the rod was portrayed as it was prior to having the grooves cut into it. Now, if it was known that the grooves were inserted in order to increase the rod's absorption strength, then this portrayal would necessarily lead to a rod region with less absorbing power than the actual rod's. Therefore, a good check on any solution would be to make sure that it's rod region absorbed a higher fraction of neutrons than model D's region did.

A better line of reasoning noted that the grooves increased absorbing power by increasing surface area. Therefore, if any logical system was to be developed, it should be based on matching the surface area. Two approaches were taken. In model E the length of the rod region was changed

while in model G the width of the region was changed in order to create a region with the actual surface area. As mentioned earlier, a consequence of changing the region's width was that the width of all the other regions had to be changed accordingly.

BRT predicted that the rod regions of both models E and G would absorb a higher fraction of the thermal neutrons than the same region in model D. Since both models fulfilled this requirement, it could not be used as the sole criterion in deciding which model was a better representation. Table V shows that the approach taken in model G was much more effective at increasing the rod's absorbing power, but this did not necessarily prove that it was a more accurate picture of the actual cell.

Table V: Model D vs. Model G

	Slab model D	Slab model E	Slab model G
Fraction of thermal neutrons absorbed in the rod region	0.5085	0.5196	0.6180
Volume fraction of the cell in the rod region	0.4273	0.6223	0.4270
thermal absorption fraction / rod volume fraction	1.190	0.8349	1.447

A review of sections 4.5.8 and 4.5.9 shows that the main assumption made while developing model G claimed that model D did not really conserve surface area. If this assumption was substantiated by the output data, then the choice of a better representation would be clear. Recall that the phenomena which the models were attempting to simulate was that the rod was made into a stronger absorber by cutting grooves into it. Therefore, when the final model's rod region was compared to that of model D, it should reflect both an increase in the absorption fraction, and a decrease in volume.

The ratio of the fraction of all thermal absorptions which occurred in the rod to the fraction of the cell's volume made up by the rod region was calculated in Table V. As the table shows, BRT predicted that only model G would produce a relative increase in absorptions per unit area from model D. This fact proved that although model E did increase the rod's absorption fraction, this increase was not caused by an increase in surface area. On the other hand, model G seemed to fulfill all of the requirements expected of a model which was simulating an increase in rod surface area.

4.7.4 The Fast Group

Knowledge of GAM's solution method made the fast group analysis quite simple. Almost all of the points considered

in the thermal analysis were ignored because GAM performed it's calculation in zero-dimensions. For example, the question of control-rod region composition or surface area were irrelevant in a zero-dimension calculation. The only factors which could be controlled were the density and composition of the homogenous mixture.

Cylindrical models A, B, and C were all equivalent with respect to the fast group. The same mixture was obtained whether model A, B, or C was homogenized. There was not much of a case to be made against this mixture because it was the mixture which would have resulted had the actual cell been smeared into a homogenous cell.

Model C was used because the output suggested that the thermal calculation did have an impact on the fast calculation. Recall that model C was the only model of the three which fulfilled the requirement that no water be included in the rod region. Table VI illustrates the extent of this impact.

4.7.5 The Final Transport Representation

Sections 4.7.1-4.7.4 provided the reasoning which led to the "final transport representation". Basically, this final representation consisted of the two parameters which were expected to predict the cell's behavior most completely and accurately. According to the last few sections, these two parameters were the fraction of all thermal absorptions

which took place in the rod region predicted by model G, and model C's prediction of the fraction of fast neutrons which reach the thermal group. The final representation was that 0.382 of all thermal neutrons were absorbed in the fuel, and that 0.765 of all fast neutrons survived to reach the thermal group.

The diffusion model was also forced to match a few other combinations of output parameters, because this final representation was only an educated guess at how the cell behaved. Therefore, the results obtained from the other combinations could also be compared to the experimental data. If the logic used to form the final representation was good, then the control-rod worths calculated for the diffusion model based on it should come closer to the experimental data than the control-rod worths based on the other diffusion models.

Table VI: Comparison of the Cylindrical Models

	Cylindrical model A	Cylindrical model B	Cylindrical model C
Resonance escape probability	0.746	0.746	0.765
Multiplication factor	0.510	0.584	0.777
thermal absorption fraction in the fuel	0.380	0.537	0.580

5. The Diffusion and Effective Diffusion Models

5.1 The 2DB-UM Model

Whereas the transport codes were used to accurately predict the actual cell's behavior, the diffusion codes were used to predict how different control-rod element models would be treated during the core analysis. The core analysis applied the time-dependent diffusion code 2DB-UM to calculate multiplication factors and fuel depletion. Our objective was to develop effective absorption cross sections which would force 2DB-UM to treat the control-rod cell as transport theory predicted it should. This was accomplished by using the steady-state diffusion code EXTERMINATOR to simulate 2DB-UM's treatment of a control-rod element. The rod's absorption cross sections were varied in the EXTERMINATOR model until EXTERMINATOR produced the output parameters which had been predicted by the transport codes. These cross sections then became part of the 2DB-UM model with the hope that they would cause 2DB-UM to yield proper results.

If this reasoning was to hold up, it was absolutely imperative that the 2DB-UM and EXTERMINATOR control-rod models be identical. Not only did the models need to have the same size regions, but the regions needed to have mesh spacings which were as near alike as was possible. After all, the algorithm was based on the assumption that both

EXTERMINATOR and 2DB-UM applied the same theory to the same model, and therefore should produce identical results. EXTERMINATOR was used, because it was very easy to calculate the output parameters from it's output.

The 2DB-UM model (Figure 5-1) was developed by Mary Fehr [10] as part of her core analysis. The control-rod element is portrayed in Figure 5-2 as nine regions arranged in a 3 X 3 matrix. A fuel region, rod, and then another fuel region made up the middle column. On either side of these regions were placed thinner regions consisting of an aluminum and water mixture. The region sizes and mesh-space configuration are shown in the figure. The fuel elements in the 2DB-UM model were set up in an identical manner except that the rod region was replaced with a third fuel region.

The compositions of 2DB-UM's regions were described by their macroscopic cross sections, in contrast to the transport codes where the region composition was described by their nuclide densities. 2DB-UM obtained the cross sections from the LEOPARD and LINX codes. Nuclide densities were input to the LEOPARD-LINX combination which calculated cross sections for each region and fed them to 2DB-UM. Since LEOPARD and LINX demanded that fuel be located in the center of their model, they could not be applied to the control-rod element. This fact created the opportunity to manually input "effective cross sections" in this region.

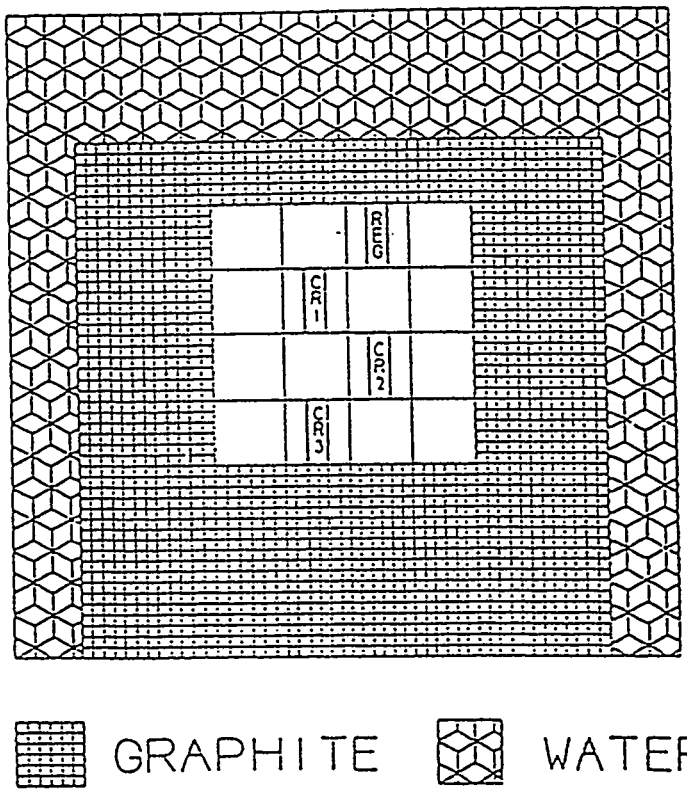


Figure 5-1 [10]: Complete TWODB-UM Model

The TWODB-UM core model includes the graphite and water which are located around the core to act as a reflector. The core is comprised of 16 elements in a 4 x 4 array. The core is surrounded on all sides by the equivalent of three cells of reflector material. The location of the three control-rods, and the regulating-rod can also be seen in the figure.

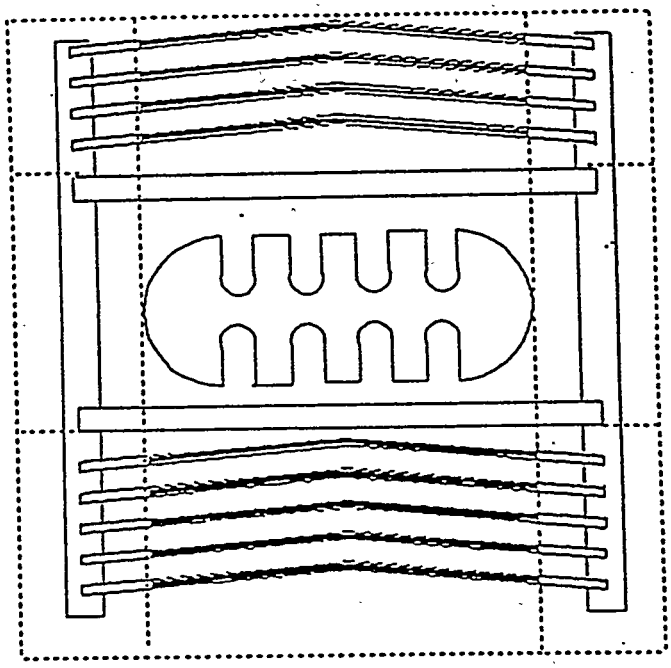


Figure 5-2: TWODB-UM Control-Rod Cell Model

The dotted lines show how the control-rod cell was split into nine homogenous regions in the TWODB-UM model. Our objective was to create effective cross sections for the center region.

5.2 The EXTERMINATOR Cell Model

The purpose of using EXTERMINATOR was to simulate the 2DB-UM calculation on the rodded element. This implied that the ideal EXTERMINATOR model would have been identical to the 2DB-UM model. Therefore, the size, as well as the region and mesh configurations of the EXTERMINATOR model were identical to those used in the 2DB-UM model's control-rod element representation.

The only differences between the two models were their macroscopic cross sections. The LINX-LEOPARD combination calculated cross sections for all 2DB-UM's regions except the rod region. Although we planned to "fudge" the absorption cross section for this region, we still needed a method to calculate the transport and scattering cross sections. Therefore, the EXTERMINATOR cross sections could not all be taken from the 2DB-UM model, as all the other model characteristics had been.

EXTERMINATOR gave the user the option of either inputting macroscopic cross sections, or inputting the combination of nuclide densities and microscopic cross sections. EXTERMINATOR's initial run utilized the second option to generate the needed macroscopic cross sections. In this case, EXTERMINATOR was applied to a model in which the structure and nuclide densities were identical to those of the control-rod element in the 2DB-UM model. The fast group

microscopic cross sections were taken from the output of the GAMTEC model C run while thermal microscopic cross sections were taken from THERMOS' slab model G output. To summarize, the purpose of EXTERMINATOR's first run was to obtain macroscopic cross sections generated by a diffusion theory code which was applied to a model strongly resembling the rodded element in the 2DB-UM model. Therefore, these cross sections would be used in future runs to approximate the cross sections that the LINX-LEOPARD combination would have generated had it been applied to the rod region.

The next, as well as all of the remaining, EXTERMINATOR runs used the macroscopic cross section input option. The purpose of the second run was to obtain an idea of how 2DB-UM would have treated the rodded element had the diffusion theory cross sections been used without any modifications. Therefore, the macroscopic cross sections generated in the first run were used as input to each of the nine regions. As expected, the output of the first two runs were identical. Employing the macroscopic cross section input option was advantageous because it allowed us to study the effects of varying one macroscopic cross section. Once we found a value which caused the EXTERMINATOR model to behave as the transport representation predicted, it was very simple to insert this value for the macroscopic cross section in the 2DB-UM model. In contrast, no simple mechanism existed for

changing the nuclide density or microscopic cross sections in the rod region of the 2DB-UM model.

5.3 The Effective Cross Sections

As mentioned in the introduction, the crux of our problem was that the output of these preliminary EXTERMINATOR runs differed from the output produced by the transport codes. For our purposes, the most important difference was that when the output parameters were calculated based on the EXTERMINATOR data, they were not equal to those chosen to constitute the transport representation. EXTERMINATOR predicted that 0.355 of all thermal absorptions occurred in fuel regions and that 0.725 of all fast neutrons survived to reach thermal energy levels while the transport representation predicted 0.382 and 0.765, respectively.

The algorithm's next step was to determine a set of fast and thermal cross sections for the rod region which would cause the EXTERMINATOR code to yield output parameters equivalent to those in the transport representation. The EXTERMINATOR code was run repeatedly, with slight adjustments made to the model before each run. The fast and thermal macroscopic cross sections were varied while all the other model characteristics were held constant with respect to the preliminary EXTERMINATOR model. The absorption cross sections were so much larger than any of the other rod cross sections that it was safe to assume that they were the two

parameters which dictated neutron behavior in the rod region. Consequently, the variation of absorption cross sections seemed to provide the largest range and greatest flexibility with regard to possible output parameters than variations in any other set of input parameters.

The iterative process was very simple. The first step was to compare the transport representation's fast group output parameters with those of the preliminary EXTERMINATOR model. This comparison allowed an educated guess to be made at the fast group absorption cross section value which would cause EXTERMINATOR to generate a fast group output parameter equivalent to that of the transport representation. The original cross section was then replaced with the new estimate in the EXTERMINATOR input deck and the code was applied again. This process was repeated until an acceptable cross section was found.

Next, the same procedure which had been applied to the fast group was applied to the thermal group. At this point, we had to return to the fast group to make sure that the change in the thermal cross section had not had a large effect on the fast group. This step was vital because the effective cross sections were to be input to 2DB-UM as a set, and therefore we had to be sure that the set performed the desired function. If the thermal group changes did have a significant effect on the fast output parameter, both

cross sections were adjusted again using the same process. The only difference from the first adjustment was that the second one began with the cross sections obtained in first adjustment. This led to much smaller adjustments to the cross sections than in the previous iteration, and consequently the changes in the thermal cross section had less of an effect on the fast group. The process was repeated until the changes in the thermal cross section led to inconsequential changes in the fast group output parameter. The resulting cross sections were the effective cross sections.

Chapter Four contained the explanations for assuming that the fraction of neutrons which reached the thermal group was the best choice to be the fast group output parameter, and that slab model G was the best one-dimensional model. Since these assumptions certainly had not been proven beyond a shadow of a doubt, the iterative process was applied to a few different sets of models and output parameters. If the effective cross sections generated from the combination of slab model G and the fraction of fast neutrons reaching the thermal group had the best agreement with the experimental data then this would be another bit of evidence for assuming that this combination should be used in the LEU modeling.

Details of the development of effective cross sections for different sets of models and output parameters are given in Appendix A. A summary of the results is shown in Table VII.

5.4 Effects of the Diffusion Approximation

Although it was not critical to obtaining the proper "effective" cross sections, it was interesting to look at the direct effects of improperly applying the diffusion approximation to a strong absorbing region. Recall that the preliminary EXTERMINATOR run predicted that a smaller fraction of all thermal absorptions took place in the fuel region than the transport representation had predicted. This data seemed to imply that diffusion theory over-estimated the absorber's power. Although this statement may be true, at this point it would have been incorrect to attribute the over-estimation solely to the diffusion approximation. Instead, it had to be taken into account that the two theories had been applied to significantly different models. For example, the BRT model had thirty mesh points in the x-direction while the EXTERMINATOR model had only nine mesh points in the same direction.

The simple solution to this problem was to apply both theories to the same model. Since it was impossible to apply BRT to a two-dimensional model, EXTERMINATOR was applied to the one-dimensional slab BRT model G. The comparison of the

Table VII: Effective Cross Sections for Different Transport Models

Cross Section Set	Thermal Output Parameter	Fast Output Parameter	Rod Σ_{a2}	Rod Σ_{a1}
Set I	Fuel absorption fraction BRT slab model A	Resonance escape prob. GAMTEC model A	1.33×10^{-1}	1.77×10^{-2}
Set II	Fuel absorption fraction BRT slab model A	Multiplication factor GAMTEC model A	1.34×10^{-1}	2.64×10^{-2}
Set III	Fuel absorption fraction BRT slab model B	Resonance escape prob. GAMTEC model B	1.11×10^{-1}	1.78×10^{-2}
Set IV	Fuel absorption fraction BRT slab model B	Multiplication factor GAMTEC model B	1.11×10^{-1}	2.09×10^{-2}
Set V	Fuel absorption fraction BRT slab model C	Resonance escape prob. GAMTEC model C	8.90×10^{-2}	1.58×10^{-2}
Set VI	Fuel absorption fraction BRT slab model C	Multiplication factor GAMTEC model C	8.88×10^{-2}	5.84×10^{-3}
Set VII	Fuel absorption fraction BRT slab model G	Resonance escape prob. GAMTEC model D	1.01×10^{-1}	2.64×10^{-2}
Set VIII	Fuel absorption fraction BRT slab model G	Multiplication factor GAMTEC model D	1.01×10^{-1}	2.03×10^{-2}
Set IX	Fuel absorption fraction BRT slab model D	Resonance escape prob. GAMTEC model C	1.71×10^{-1}	1.78×10^{-2}

thermal flux shapes predicted by the two theories, displayed in Figure 5-3, shows that the two codes predicted similar shapes. BRT did predict that 0.382 of all thermal absorptions took place in the fuel compared to EXTERMINATOR's prediction of 0.355. Basically, there were no vast differences between the two codes' output with respect to this model.

Two possible conclusions can be reached based on this information. One possibility is that invoking the diffusion approximation really does not have a negative effect. The second possibility is that the fine mesh spacing combined with the rod region's shortened width help to nullify the negative effects of the approximation. My first reaction was that some insight into these two possibilities could gained by comparing the small differences in the flux shapes to the expectations of the effects of the approximation. The only problem with this approach was that just about any flux shape could be explained by emphasizing different effects of the diffusion approximation.

The only notable differences were that the transport code predicted a slightly higher relative flux in the guide plate region while the diffusion code predicted a slightly higher flux in the fuel region. In order to decide if these differences were due to the approximation, we should review the expected errors which would be caused by incorrectly

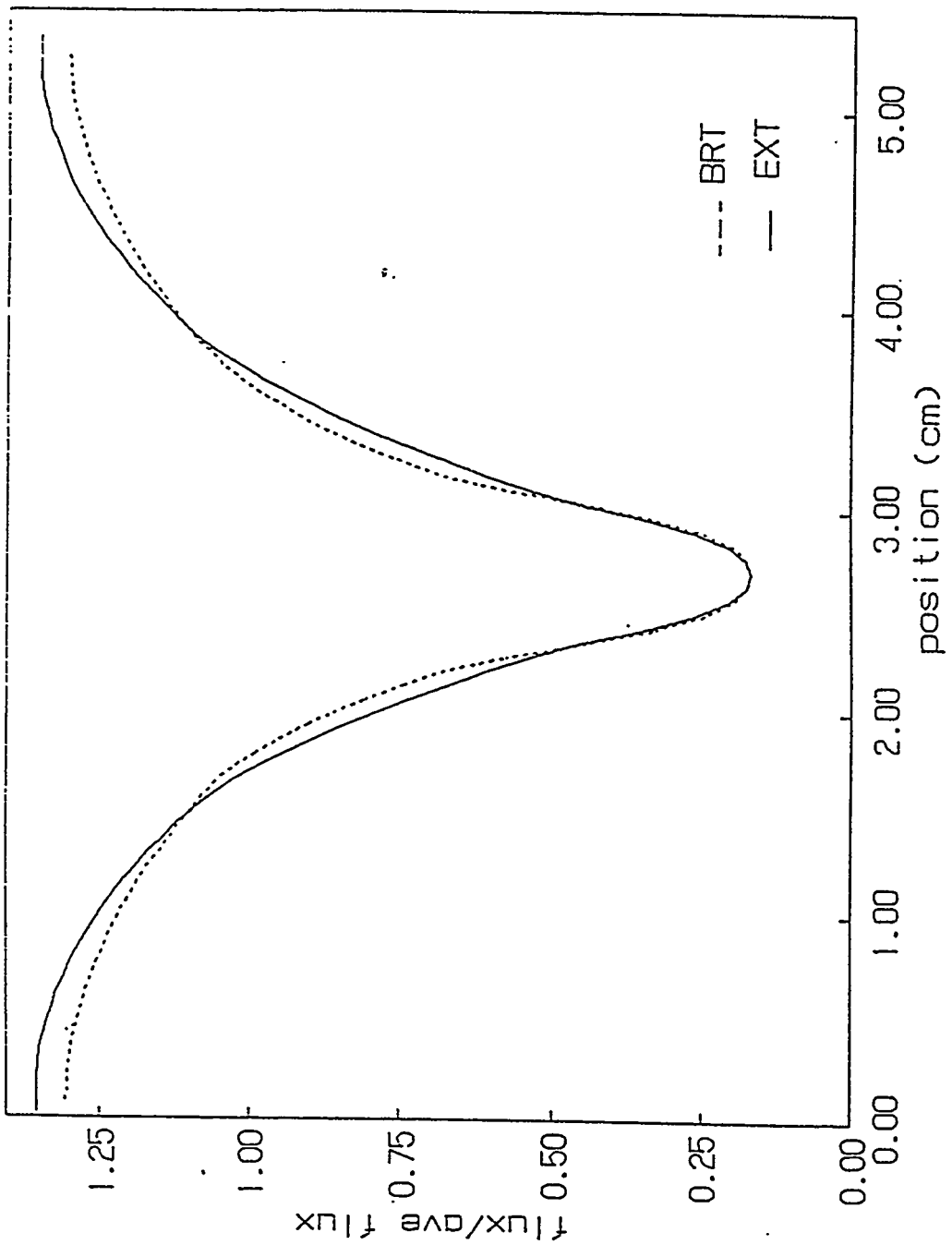


Figure 5-3: BRT vs. EXTERMINATOR

This graph illustrates the thermal flux shapes predicted by BRT and EXTERMINATOR when they are both applied to the same model. The one-dimensional model used had thirty mesh spaces.

invoking it. Recall that the major problem with applying the approximation to the rod region was that the approximation assumed that the probability of a scattering reaction occurring was fairly constant. In fact, the scattering probability severely dropped at the border of the rod region. Therefore, we expected that the diffusion code would over-estimate the number of neutrons leaving the rod region. On the other hand, the diffusion approximation assumed that the number of neutrons travelling in any direction was directly related to the flux gradient. Therefore, in a region with a very large gradient we would expect that the diffusion code would over-estimate the number of neutrons travelling towards the region of lower neutron population. At the rod border these two effects work in opposite directions. For different models, or mesh-space configurations one effect may outweigh the other. Therefore, any judgement on the effects of the approximation in regard to these models would require more effort than it's worth to this project.

In either case, the necessity of developing effective cross sections can be seen in Figure 5-4 where the flux shape predicted by the application of EXTERMINATOR to the 2DB-UM model has been included in the graph. Recall that this was the data which would have been included in the core analysis in the absence of the effective cross sections.

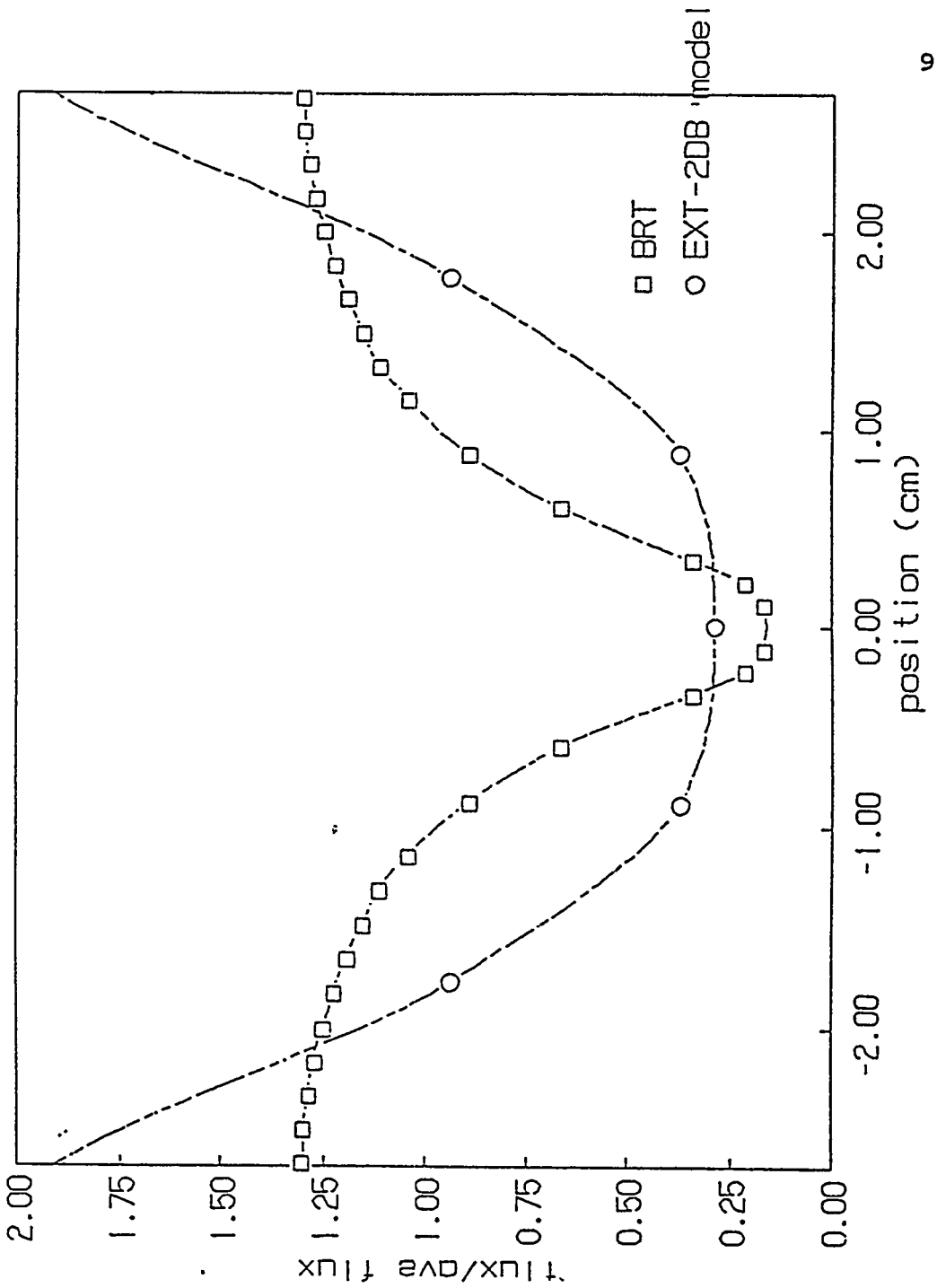


Figure 5-4: BRT Predictions vs. TWODB-UM Predictions

This graph illustrates the different flux shapes predicted by BRT and TWODB-UM. Recall that the BRT output has been accepted as the most accurate predictions available. The TWODB-UM calculation is simulated by applying EXTERMINATOR to the TWODB-UM model. This calculation yields the data which would have been used in the core study if no corrections were made to the control-rod region.

This graph also clearly shows that there was no hope of simulating the flux shape of the transport code because of a shortage of mesh points available in the 2DB-UM model. This fact was the reason that the flux shapes were totally ignored while the effective cross sections were used to forced the 2DB-UM code to match the output parameters of the transport representation.

6. The Regulating-Rod

The last order of business before control-rod worths were calculated was to develop effective cross sections for the regulating-rod. Following the same procedure which had been applied to the control-rods, the LEOPARD and LINX codes were not used to calculate macroscopic cross sections for the regulating-rods. Therefore, effective cross sections were necessary so that they could be manually input to the 2DB-UM code.

Two characteristics differentiated the regulating-rod from the control-rods. The principal difference was that the regulating-rod was composed of one hundred per cent stainless steel. A quick glance at the control-rod's microscopic cross sections shows that it was the presence of boron which made the rod such a strong absorber. The second difference was that the regulating-rod did not have any grooves cut into it (Figure 4-2). The combination of decreased surface area and lack of boron severely reduced the regulating-rod's absorbing power relative to that of a control-rod. Therefore, the logic used to develop the transport models of the control-rods was not applicable to the regulating-rod.

Actually, the development of a regulating-rod model was much simpler than the development of the control-rod model. Recall that the control-rod's high absorption cross section

led us to believe that most neutron absorptions would take place within a small area along the rod's border. Therefore it was imperative to construct a model which accounted for the grooves by conserving surface area. In the absence of the grooves and high absorption cross section it was assumed that the rod's volume and nuclide densities became the factors which dictated the cell behavior. Therefore, the model of the regulating-rod fuel cell conserved these parameters.

After the model was constructed, the procedure was exactly analogous to that outlined for the control-rod. The macroscopic absorption cross sections were varied in the EXTERMINATOR model until the output parameters matched those predicted by the transport models. The set of cross sections which forced the diffusion code to match the transport codes' output was deemed to be the effective cross sections.

7. Results

7.1 The Experimental Data

The only remaining task was to check how well the effective cross sections had served their purpose. This task included the comparison of the 2DB-UM output with the experimental data, and the verification of the chosen transport representation as the most accurate.

Experimentally measured control-rod worths were available for the HEU core. These worths were taken from Farrar, J.P. (1975) and are shown in Table VIII. The experimental error was estimated to be at least ten percent. It should be noted that these worths were determined from rod calibrations. In other words, the worth of one rod was measured while the others were partially inserted into the core. The presence of three other rods was expected to slightly affect the rod worth being measured.

Table VIII: Experimental Rod Worths

Rod #	Measured Worth
1	$4.75
2	$5.00
3	$3.06
Regulating	$0.57
All in	$13.38

Table VIII shows that each of the control-rods had different worths even though they were physically identical. This fact makes it very clear that the rod worths were very dependent upon the rod's position. That is to say, the higher fluxes and importances in the center of the core led to higher worths for the rods placed in the center as opposed to along the core border.

This is an important point because the flux was included in the effective cross section development. Therefore, the differences in the fluxes would result in slightly different actual weighted cross sections for each rod. We cannot hope to duplicate these differences because the effective cross sections were developed for each rod as if each rod element was surrounded by other control-rod elements (recall the reflecting boundary conditions). An argument was made that the neighboring control-rod element would do an acceptable job of simulating other fuel cells. Therefore, we might expect the simulated rod worths of rods 1 and 2 to come a little closer to the experimental worths than the regulating-rod or rod 3 which both are located on the core border.

7.2 Calculated Control-Rod Worths

In Chapter Five, nine different sets of possible effective cross sections were developed. Each set was based on a different combination of transport model and output

parameters. A theoretical argument was made that set IX would lead to the most accurate control-rod worths. The best way to check the validity of that argument was to insert each set of cross sections into the 2DB-UM model, and to see which set yielded control-rod worths which agreed with the experimental data. The results of the nine 2DB-UM runs are given in Table IX, where the calculated worths were converted to $ using β_{eff}=0.0074.

Sets II, VII, IX all produce calculated rod worths within the ten per cent estimated error of the measured worths. The major difference between the sets is that set IX predicts a higher thermal and lower fast cross section than the others. The flaws in the development of sets II and VII have already been discussed in detail. Set II was based on model A which incorrectly included water in the rod region, and set VII was based on model D which simulated the rod without grooves. Therefore, we have to assume that the accuracy of these sets' predictions is due more to luck than a carefully thought out procedure. It follows that we cannot hope to achieve the same accuracy when the same procedure is applied to the HEU core.

The method which led to set IX was chosen as the method to be applied to the LEU core, because the HEU rod worths were all within 10% of the measured values and there were not any obvious flaws in the method's logic. Therefore,

Table IX: Trial Set Results vs. Experimental Data

Effective cross section set #	Rod #	Calculated Worth	Measured Worth	Per cent Error
I	1	$4.74	$4.75	0.3
	2	$4.93	$5.00	1.4
	3	$2.82	$3.06	7.8
II	1	$5.38	$4.75	13.3
	2	$5.53	$5.00	10.6
	3	$3.15	$3.06	2.9
III	1	$4.51	$4.75	5.1
	2	$4.64	$5.00	7.2
	3	$2.65	$3.06	13.4
IV	1	$4.72	$4.75	0.6
	2	$4.86	$5.00	2.8
	3	$2.78	$3.06	9.2
V	1	$4.00	$4.75	15.8
	2	$4.11	$5.00	17.8
	3	$2.36	$3.06	29.7
VI	1	$3.23	$4.75	32
	2	$3.32	$5.00	34
	3	$1.90	$3.06	38
VII	1	$4.75	$4.75	0.0
	2	$4.89	$5.00	2.2
	3	$2.76	$3.06	9.8
VIII	1	$4.32	$4.75	9.1
	2	$4.44	$5.00	11.2
	3	$2.52	$3.06	17.6
IX	1	$5.14	$4.75	8.2
	2	$5.29	$5.00	5.8
	3	$3.15	$3.06	2.9
	Reg Rod	$0.57	$0.75	31.0

slab model G and cylindrical model C will be the models used to perform all calculations needed for the LEU core study. The final recommended set of 2-group constants for the control-rod regions are given in Table X.

Table X: Final Recommended Cross Sections for 2DB-UM

Group	Σ_a	Σ_{tr}	Σ_{snn}	Σ_{s12}
Control-Thermal	1.71 E-1	2.06 E-0	1.56 E-0	-------
Control-Fast	1.78 E-2	2.70 E-1	5.73 E-1	2.29 E-2
Regulating-Thermal	3.68 E-2	1.24 E-0	1.37 E-0	-------
Regulating-Fast	2.24 E-3	2.81 E-1	5.46 E-1	1.60 E-2

7.3 Conclusions

The most important statement that can be at this point is that the method worked. The effective cross sections make it possible to apply 2DB-UM to the entire core. The same method can now be applied to an LEU control-rod element. The cross sections generated will make it possible to apply 2DB-UM to different cores (by changing fuel plates per element, number of elements, etc.). 2DB-UM's predictions will be used to choose the most practical core.

An important point to keep in mind is that The EXTERMINATOR and 2DB-UM control-rod models should be

identical. Very simply, in order for the effective cross sections to produce the proper results, they must be used in the manner that they were developed.

7.4 Recommendations

The effective cross section development could be checked further by applying it to different stage in the depletion of both LEU and HEU cores. It might also be checked against other methods, such as Argonne National Laboratory's Monte Carlo Method. It would also be interesting to attempt to apply the algorithm to other reactors. The only drawback to this suggestion is that it would require that the other reactor have control-rods shaped similarly to the UVAR's rods.

REFERENCES

[1] "Limitations on the Use of Highly Enriched Uranium in Domestic Non-power Reactors," 10 CFR 50.64, Jan. 1 1987 Ed.

[2] "2DB-UM (APOLLO VERSION)," (input manual for 2DB-UM, Version #10, July86), Sept. 1986.

[3] Bennett, C.L., Purcell, W.L., "BRT-I: Batelle-Revised-THERMOS," BNWL-1434, Batelle Memorial Institute, Pacific Northwest Laboratories, June 1970.

[4] Carter, L.L, Richey, C.R., Hughey, C.E., "GAMTEC II: A Code for Generating Consistent Multigroup Constants Utilized in Diffusion and Transport Theory Calculations," BNWL-35, Pacific Northwest Laboratory, March 1965.

[5] Fowler, T.B., Tobias, M.L., Vondy, D.R., "EXTERMINATOR2: A FORTRAN IV Code for Solving Multigroup Neutron Diffusion Equations In Two Dimensions," ORNL-4078, Oak Ridge National Laboratory, 1961.

[6] Dresner, L. "Resonance Absorption in Nuclear Reactors, Pergamon Press, 1960.

[7] "University Of Virginia Reactor Safety Analysis Report,"

[8] "Fuel Element - Control Rod," Blueprint # NE-34, Nuclear Science Center; A&M College of Texas, Department of Nuclear Engineering, Sept. 6, 1960.

[9] Rydin, R., "Nuclear Reactor Theory and Design," University Publications, 1977.

[10] Fehr, M., "Design Optimization of a Low Enrichment University of Virginia Nuclear Reactor," University of Virginia, Jan. 1989.

APPENDIX IV

HEU TO LEU FUEL CONVERSION REPORT

SAFETY ANALYSIS REPORT

FOR THE

LOW-ENRICHED URANIUM FUELED

UNIVERSITY OF VIRGINIA REACTOR

("LEU-SAR")

JANUARY, 1991

SAFETY ANALYSIS REPORT

FOR THE

LOW-ENRICHED URANIUM FUELED

UNIVERSITY OF VIRGINIA REACTOR

("LEU-SAR")

Contributors, past and present:

J.R. Ball	T.G. Foster	J.S. Brenizer	M. Fehr
M.G. Bickel	W.R. Johnson	R.U. Mulder	S. Wasserman
J.A. Dahlheimer	J.L. Kelly	R.A. Rydin	P. Benneche
R.D. Derry	A.B. Reynolds	D.W. Freeman	
J.P. Farrar	J.H. Rust	B. Hosticka	

This report is issued in support of a license amendment to License R-66 for the conversion of the University of Virginia's 2 MW reactor (UVAR) from high enriched uranium (HEU) to low enriched uranium (LEU) fuel. The report supersedes the original SAR for HEU cores and all its revisions and amendments as well as the so-called "UVAR Design and Analysis Handbook", which was the heretofore updated SAR. The present SAR may be referred to as the "LEU-SAR" to distinguish it from the previous SAR.

Table of Contents

		Page
1.0	Introduction	1-1
	1.1 Summary of Previous Documentation	1-2
2.0	General Description of Facility	2-1
	2.1 Reactor Site	2-7
	2.2 Reactor Building	2-7
	2.3 New Construction	2-7
	2.4 Wind Direction and Velocity	2-13
	2.5 Hydrology	2-13
	2.6 Seismology	2-15
3.0	Reactor Components and Control	3-1
	3.1 Reactor Assembly	3-1
	3.2 Fuel Elements	3-4
	3.3 Fuel Plates	3-9
	3.4 Control Rods and Drives	3-9
	3.5 Reactor Reflectors	3-12
	3.6 Core Loadings	3-12
	3.7 Fuel Storage Facilities	3-14
	3.8 Reactor Data	3-16
	3.9 Reactor Kinetics	3-20
	3.10 Fission Product Inventory	3-21
	3.11 Nuclear Instrumentation	3-21
	3.11.1 General Description	3-21
	3.11.2 Source Range Circuit	3-24
	3.11.3 Intermediate Range Circuit	3-26
	3.11.4 Power Range Drawer	3-29
	3.11.5 Scram Logic Drawer	3-31
	3.12 Scrams, Interlocks and Alarms	3-38
	3.12.1 Scrams	3-38
	3.12.2 Interlocks	3-39
	3.12.3 Alarms	3-39
	3.13 Automatic Control for Maintaining Constant Power	3-40
4.0	Reactor Systems	4-1
	4.1 Pool	4-1
	4.2 Filling and Draining the Pool	4-1
	4.3 Primary Cooling System	4-3
	4.4 Measurement of Temperature Differential	4-6
	4.5 Secondary Cooling System	4-6
	4.6 Design Specifications	4-7
	4.7 Water Purification	4-7
	4.8 Liquid Waste Disposal System	4-7
	4.9 Building Ventilation System and Airborne Effluents	4-12
	4.10 Core Spray System	4-26

Table of Contents (cont.)

		Page
5.0	Experiment Facilities	5-1
	5.1 Beamports	5-1
	5.2 Large Access Facilities	5-6
	5.3 Rabbit Facility	5-7
	5.4 Fueled Experiments	5-9
6.0	Rabbit Hazards	6-1
	6.1 Confinement	6-1
	6.2 Shielding	6-6
	6.3 Hazards During Normal Operations	6-13
7.0	Health Physics	7-1
	7.1 General Information	7-1
	7.2 Education in Health Physics	7-1
	7.3 Personnel Monitoring and Protection	7-2
	7.4 Permanent Monitoring and Surveys	7-2
	7.5 Prohibitions and Sanctions	7-3
	7.6 Waste Disposal	7-4
	7.7 Shipping and Transport	7-4
8.0	Administration	8-1
	8.1 General Organization	8-1
	8.2 Radiation Safety Committee	8-1
	8.3 Reactor Safety Committee	8-1
	8.4 Procedures	8-3
9.0	Safety Analysis	9-1
	9.0 Safety Analysis	9-1
	9.1 Thermal Hydraulic Analysis of the UVAR	9-1
	9.2 Forced Convection Heat Transfer	9-4
	9.3 Prediction of Incipient Boiling	9-5
	9.4 Burnout Heat Flux	9-6
	9.5 Flow Instability	9-12
	9.6 Burnout Ratio	9-18
	9.7 Nomenclature Used in Thermal Hydraulic Analysis	9-19
	9.8 Hot Channel and Minimum Core Loading	9-21
	9.9 Allowance for Error in the Burnout Determination	9-24
	9.10 Safety Limit	9-24
	9.11 Limiting Safety System Settings and Measurement Errors	9-31
	a) Coolant Inlet Temperature	9-31
	b) Flow Rate	9-31
	c) Reactor Power	9-32
	9.12 Short Period Transient	9-32
	9.13 Loss of Flow Transient and Natural Convection	9-35
	9.14 HEU Analysis for Loss of Flow Transient	9-36
	9.15 HEU Analysis for Natural Convection	9-50
	9.16 Maximum LEU-22 Fuel Temperatures Following LOCA	9-51
	a) Introduction	9-51
	b) Calculation of Peak Fuel Temperature Following LOCA	9-54

Table of Contents (cont.)

		Page
9.17	Emergency Core Spray System Analysis	9-61
9.18	Time to Uncover Core Following a LOCA	9-65
	a) Flow Rate Without Frictional Losses	9-66
	b) Flow Rate With Frictional Losses	9-69
	c) Time to Uncover Core With Double-Ended Pipe Break	9-71
	d) Time to Uncover Core With Crack in Pool Wall	9-72
	References for Chapter 9	9-73

List of Figures

Figure		Page
2-1	Aerial View of Reactor Site and Immediate Vicinity (1967)	2-2
2-2	Aerial View of Reactor Site and Immediate Vicinity (1964)	2-3
2-3	Contour Map of UVAR Site with Exclusion Fence	2-5
2-4	Map of Charlottesville and Vicinity	2-6
2-5	U.Va. Research and Training Reactor Facility	2-8
2-6	First Floor Plan of UVAR Section of Building	2-9
2-7	Mezzanine Level of UVAR Section of Building	2-10
2-8	Ground Floor Plan of UVAR Section of Building	2-11
3-1	Cross-Section View of Reactor Pool and Reactor Room	3-2
3-2	8 x 8 UVAR Gridplate	3-3
3-3	Top View of UVAR Standard and Partial LEU Fuel Element	3-5
3-4	Side View of UVAR Standard and Partial LEU Fuel Element	3-6
3-5	Top View of UVAR Control Rod LEU Element	3-7
3-6	Side View of UVAR Control Rod LEU Element	3-8
3-7	Nuclear Instrumentation System	3-22
3-8	Source Range Drawer	3-25
3-9	Intermediate Range Drawer	3-28
3-10	Power Range Drawer	3-30
3-11	Scram Logic Drawer	3-32
3-12	High Power Trip	3-36
4-1	Cooling System Flow Diagram	4-4
4-2	Exhaust System to Stack	4-13
4-3	Spray Header Mock-up	4-28
4-4	Core Spray System Elevation View	4-29
4-5	Core Spray System Plan View	4-30
5-1	Beam Hole Detail	5-2
5-1a	Top View of North Beamport Shielding and Access Control Walls	5-3
5-1b	North Beamport Drain Fill System	5-4
5-2	Large Access Facility	5-5
5-3	UVAR Optimum Configuration	5-8
6-1	Personnel Door	6-2
6-2	Exit Manhole	6-3
6-3	Pressure-Tight Air Duct	6-5
6-4	UVAR Confinement Room Count Rate Data	6-7
6-5	Thermal Neutron Fluxes	6-8
6-6	Fast-Neutron Dose Rates	6-9
6-7	Gamma Ray Dose Rates	6-10
6-8	Dose Rates Near Surface of Pool	6-12
8-1	Organizational Structure of U.Va. Reactor Facility	8-2

List of Figures (cont.)

Figure		Page
9-1	Heat Flux Distributions	9-3
9-2	Calc. vs. Exp.; Incipient Boiling in the ORR	9-7
9-3	Calculated and Experimental Burnout Heat Fluxes	9-11
9-4	Core Loading Configuration (showing peak flux location)	9-22
9-5	Vertical Flux Traverse	9-23
9-6	LEU Core Power versus System (Core) Flow	9-30
9-6a	HEU Core Power versus System (Core) Flow	9-37
9-7	Flow and Power Coastdown (Header Up)	9-38
9-8	Flow Header Jammed in Cocked Position	9-42
9-9	Flow Reversal After LOF Transient from 3.45 MW	9-43
9-10	Comparison Between OWR and UVAR Corrilations	9-53
9-11	Maximum Fuel Temperature After LOCA, LEU-22, 4x4	9-60
9-12	Power of Hottest Element & ECSS Cooling After Shutdown	9-64
9-13	Primary Piping	9-67
9-14	Geometry For Calculating V2	9-68

List of Tables

Table		Page
2.1	Hourly Wind Speeds	2-14
2.2	Hourly Wind Direction	2-14
3.1	LEU-22 Reactor Data	
	I. Typical 4x4 and 4x5 Core Parameters	3-17
	II. Fuel Element Parameters	3-17
	III. Fuel Plate Parameters	3-18
	IV. Side Plate Parameters	3-18
	V. Guide Plate Parameters	3-18
	VI. Control Rod Parameters	3-18
	1. Safety (Shim) Rods	3-18
	2. Regulating Rods	3-19
	VII. Feedback Coefficients	3-19
	VIII. Kinetic Parameters	3-19
3.2	Prompt Neutron Lifetimes for LEU and HEU Fueled UVAR Cores	
4.1	Heat Exchanger Specifications	4-8
4.2	Cooling Tower Specifications	4-9
4.3	Secondary Pump Specifications	4-10
4.4	Primary Pump Specifications	4-11
4.5	Ar-41 Releases	4-18
4.6	Radioactive Gases	4-24
4.7	Iodine Concentrations	4-25
5.4.1	Exclusion Radius Fractional Exposures	5-14
5.4.2a	Reactor Room-5 min. exposure	5-15
5.4.2b	Experimental-5 min. exposure	5-16
9.1	LEU-22 Data And Parameters	9-27
9.2	CR Time to Drop from Predetermined Position	9-33
9.3	Maximum Peak Fuel Temperature Following LOCA	9-59
9.4	Characteristics of Core Spray System	9-63
9.3	Time to Uncover Core for Various Leakage Mechanisms	9-65

1.0 Introduction

The University of Virginia Reactor (UVAR) first went into operation in 1960 at a maximum licensed power level of one megawatt under facility license No. R-66. The reactor core consisted of MTR plate type high enriched uranium (HEU) fuel elements. In 1971 the authorized power limit of the UVAR was increased to two megawatts. The operating license for the UVAR was extended for 20 years in September of 1982.

In 1989, high-enriched to low-enriched uranium fuel (LEU) conversion studies were concluded by the University of Virginia reactor staff. The NRC mandated conversion resulted in adoption of a higher fuel loading, with the number of plates per standard element increasing from 18 to 22, to maintain the operating characteristics of the reactor. The present safety analysis report is an updated version of the original HEU Safety Analysis Report, and for differentiation is called the Low Enriched Uranium (LEU) Safety Analysis Report (SAR). This report was reviewed and approved by the Reactor Safety Committee at the end of the summer of 1989.

The UVAR is operated by the Department of Nuclear Engineering and Engineering Physics, which is part of the School of Engineering and Applied Science of the University of Virginia. The reactor is primarily utilized as a research and training facility of nuclear engineering students and for the generation of radioisotopes, neutron activation analysis, neutron radiography, radiation damage

studies and other research. The reactor and experimental facilities are made available to the entire university as well as to outside agencies under suitable contract arrangements. The facility is also made available to students from other colleges and universities in the state under a reactor sharing program sponsored by the Department of Energy.

1.1 Summary of Previous Documentation

Documentation relevant to the UVAR and Facility License No. R-66 is summarized chronologically below. Most of these documents are on file under Docket No. 50-62, License No. R-66 in the Division of Reactor Licensing, Nuclear Regulatory Commission.

1) March 14, 1957, application to AEC for Class 104 license and construction permit by Colgate W. Darden, Jr., President, University of Virginia, and Lawrence R. Quarles, Dean, School of Engineering.

2) March 14, 1957, enclosed with the above application was UVAR-3, "A Hazards Summary of the Proposed Research and Training Reactor," by Lawrence R. Quarles and Walter P. Walker.

3) June 7, 1957, Amendment to Hazards Summary submitted by Quarles and Walker.

4) Fall of 1957, Construction Permit No. CPPR-15 issued, signed by H.L. Price.

5) September 23, 1958, Application to AEC to convert Construction Permit CPPR-15 to a class 104 license, signed by Darden and Quarles.

6) September 23, 1958, enclosed with the above application was UVAR-8, "The University of Virginia Reactor, Description and Operation," by J.L. Meem.

7) May 25, 1959, Amendment No. 1 to UVAR-8 submitted by Meem and Quarles.

8) December 4, 1959, Amendment No. 2 to UVAR-8 submitted by Meem and Quarles.

9) February 5, 1960, Amendment No. 3 to UVAR-8 by Meem and Quarles.

10) June 24, 1960, Facility License No. R-66 issued and signed by R.L. Kirk.

11) January 27, 1961, Amendment requested to License R-66 for the use of boron stainless steel control rods signed by Meem and Quarles.

12) April 13, 1961, Amendment requested to License R-66 to permit irradiation of rare earths and uranium isotopes, signed by Meem and Quarles.

13) May 17, 1961, Submission of supplementary information on the use of boron stainless steel control rods, signed by Meem and Quarles.

14) September 1, 1961, Amendment No. 1 to Facility License R-66 granted, authorizing the use of boron stainless steel control rods and authorizing the irradiation of rare earths and uranium isotopes, signed by Edson G. Case.

15) November 21, 1961, Amendment requested to License R-66 to utilize a concentration reduction factor of 500 for argon and noble gases, signed by Quarles and Meem.

16) February 22, 1962, (UVAR-14), Amendment requested to License R-66 for the conduct of a broad irradiation program, signed by Meem and Quarles.

17) April 26, 1962, Amendment No. 2 to Facility License R-66 granted, authorizing the use of a concentration factor of 500 for argon and noble gases, signed by Robert H. Byran.

18) August 23, 1962, Amendment No. 3 to Facility License R-66 granted, authorizing the conduct of a broad irradiation program, signed by Robert H. Bryan.

19) December 17, 1962, Amendment requested to License R-66 to reduce the frequency of inspection of the control rods, signed by Meem and Kuhlthau.

20) January 15, 1963, Amendment requested to License R-66, for the use of 250 grams of U-235 in a fission plate, signed by J.L. Meem.

21) February 18, 1963, Supplementary information provided for January 15, amendment for use of a fission plate, signed by J.L. Meem.

22) March 19, 1963, Amendment No. 4 to License R-66 granted to reduce the frequency of inspection of the control rods, signed by Robert H. Bryan.

23) March 19, 1963, Amendment No. 5 of Facility License R-66 granted, authorizing use of 275 grams of U-235 in a fission plate, signed by Robert H. Bryan.

24) February 27, 1964, Amendment requested to License R-66 for the use of 135 grams of U-235 in a second fission plate, signed by Williamson and Meem.

25) May 18, 1964, Amendment No. 6 to License R-66 granted authorizing the use of 135 grams of U-235 in a second fission plate, signed by Roger S. Boyd.

26) Submitted August 22, 1967, UVAR-17, Safety Analysis in support of amendment of License R-66 for two megawatt operation.

27) November 18, 1968, Change No. 1 to License R-66 granted authorizing round grooves vs. square grooves in the safety shim rods.

28) January 29, 1969, Change No. 2 to License R-66 granted authorizing the replacement of the weather recording instruments with a wind vane and an anemometer, signed by Donald J. Skovholt.

29) June 4, 1969, Amendment No. 7 to License R-66 which authorized the increase of U-235 inventory limit from 6.9 kilograms to 12.0 kilograms and increase in allocation of special nuclear material from 6.9 kilograms to 12.0 kilograms U-235, signed by Donald J. Skovholt.

30) August 4, 1971, Amendment No. 8 to License R-66 to allow storage of 70,000 curies of Cobalt-60 in reactor pool, signed by Donald J. Skovholt.

31) November 4, 1971, Amendment No. 9 to License R-66 to allow operation at 2 MW and incorporate Technical Specifications into the license and to receive, possess, and use up to 7.9 kilograms of contained uranium-235 for use in connection with the operation of the reactor and receive, possess, and store up to 6.1 kilograms of contained uranium-235 not for use in connection with operation of the reactor, signed by Donald J. Skovholt.

32) February 6, 1975, Amendment No. 10 to License R-66 to receive, possess and use up to 14.0 kilograms of contained uranium-235 and 16 grams of plutonium in a Pu-Be source for use in connection with operation of the reactor. Also change No. 1 to the Technical Specification 5.1 describing the fuel elements used in the reactor, signed by Karl R. Goller.

33) May 17, 1976, Amendment No. 11 to License R-66, Change in Technical Specification 3.7 to clarify the use of fueled experiments in the reactor facility, signed by George Lear.

34) December 19, 1978, Amendment No. 12 to License R-66 to change the requirement of visual inspection of control rods as stated in Technical Specification 4.1.C, signed by Morton B. Fairtile for Robert W. Reid.

35) December 22, 1978, Amendment No. 13 to License R-66 to allow the receipt, possession, and use of 1.0 grams of Neptunium-237 in connection with the operation of the reactor. Also a change in Technical Specification 3.5 regarding the exit manhole hatch cover, signed by Morton B. Fairtile for Robert W. Reid.

36) August 25, 1981, Amendment No. 14 to License R-66 adding the Physical Security Plan to the License, signed by James R. Miller.

37) September 30, 1982, Amendment No. 15 to License R-66 renewing the operating license for 20 years, signed by Cecil O. Thomas.

38) February 25, 1986, Final Rule on Conversion to LEU fuel given in 10CFR50.64, effective March 27, 1986.

39) April 25, 1988, Amendment No.16 to License R-66 to clarify the possession, storage and use in the UVAR pool of up to 70,000 Curies of Cobalt-60 in the form of doubly encapsuled rod sources, signed by Lester S. Rubenstein.

40) December 16, 1988, Amendment No. 17 to License R-66 to change the Technical Specifications for minimum shutdown margin so that it is provided by shim rods only instead of control rods, signed by Charles L. Miller.

41) July 20, 1989, Amendment No. 18 to License R-66 to change the Technical Specifications changing the organizational structure to allow the Health Physicist to report to the Department of Nuclear Engineering.

2.0 GENERAL DESCRIPTION OF THE FACILITY

2.1 Reactor Site

The UVA reactor (UVAR) is located approximately 2000 feet west of the of Charlottesville, in Albemarle County, Virginia, [latitude 38° 2'30" N, longitude 78°, 31' W] and at an elevation of 700 feet. The Reactor Facility housing the reactor is next to an abandoned reservoir (pond), 200 feet up the ridge that runs between Mt. Jefferson and Lewis Mountain. The pond has a watershed area of 10^5 square feet. The reactor building is approximately 50 feet above the water level of the pond.

North, east, and south of the site, no closer than 2000 feet, are city residential districts, and 3/4 mile west over the ridge are suburban developments. The downtown business district of Charlottesville is two miles away.

Figures 2-1 (1967) and 2-2 (1964) are aerial photographs of the reactor site. Additional construction near the Reactor Facility occurred between 1964 to 1967, as seen in Fig. 2-1, taken in March 1967. Comparison should be made with Fig. 2-2 taken in 1964, on which newer construction is marked with an asterisk (*). The nearby buildings are: Radio Astronomy Laboratory (RAL*), a group of dormitories (Dorm#), and the 5.5 MeV Van de Graaf (VdG#). The Buildings and Grounds divisions complex (B-G) (now called Physical Plant), the City Water Filtration Plant (Filt), the Observatory (Obs), and the buildings of the former Research Laboratory for Engineering Sciences (RLES), now Aerospace Research Laboratory (ARL), were all in existence prior to construction of the reactor. An addition to the reactor building was completed in 1970.



FIGURE 2-1. AERIAL VIEW OF REACTOR SITE AND IMMEDIATE VICINITY (1967)

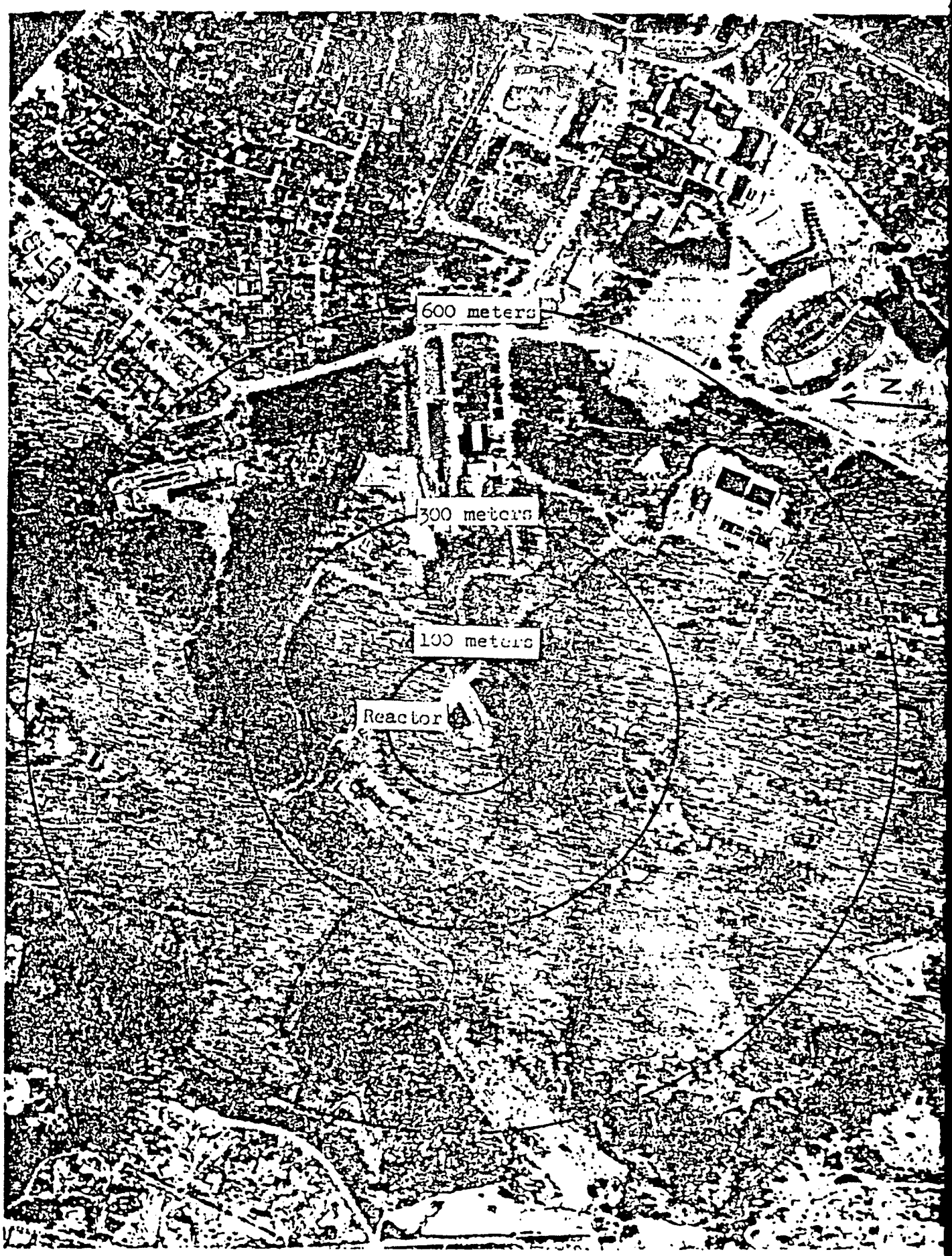


FIGURE 2-2. AERIAL VIEW OF REACTOR SITE AND IMMEDIATE VICINITY (1964)

The Van de Graaf building is approximately 125 meters to the southeast of the reactor facility and the Radio Astronomy Laboratory is about 250 meters to the northeast of the reactor. These buildings are occupied by technical people able to understand and respond to a reactor emergency. Farther away to the east, the student dormitories are at a nearest distance of about 325 meters. A copy of the Reactor Emergency Actions List is posted at the nearby Office of Environmental Health and Safety (EH&S). The University police force is prepared to evacuate any of these areas if necessary.

By virtue of its position in the draw, the reactor has a natural terrain shield for approximately 270 degrees of its circumference, with the elevation of the heavily wooded slopes ranging from 215 meters at the lowest points to 265 meters at the point of highest elevation. Therefore, the UVAR is exposed for only a 90 degree sector from the northeast clockwise to the southeast, as shown in Fig. 2-3. In the easterly direction, the elevation drops rapidly, so that approximately 1200 meters from the reactor, the elevation if 150 meters.

As shown in Fig. 2-4, residential areas are found to the north, east and south, with major business districts to the northeast and east at approximately 2500 meters and 3500 meters respectively. The population of the city of Charlottesville is estimated at about 50,000.

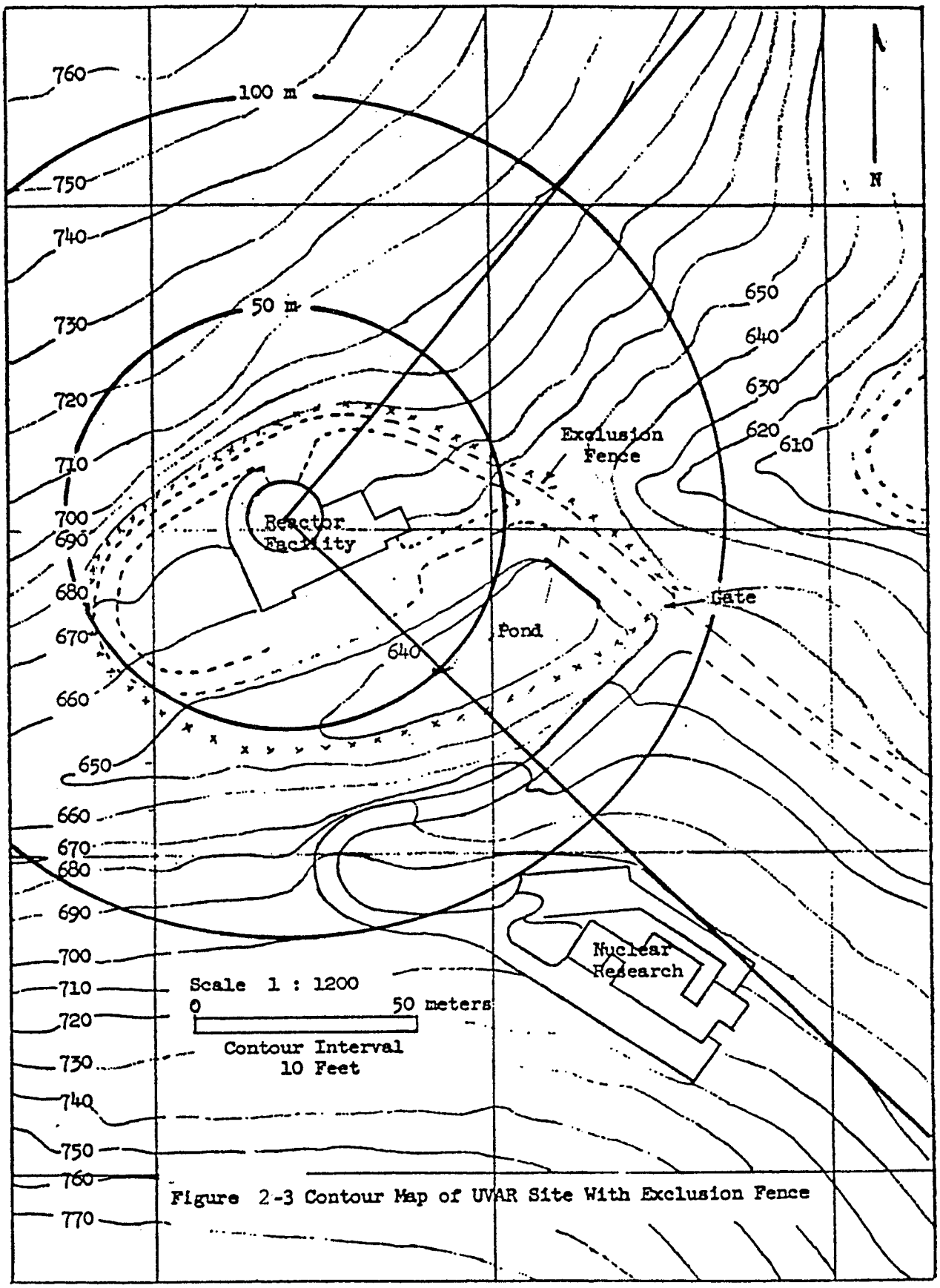


Figure 2-3 Contour Map of UVAR Site With Exclusion Fence

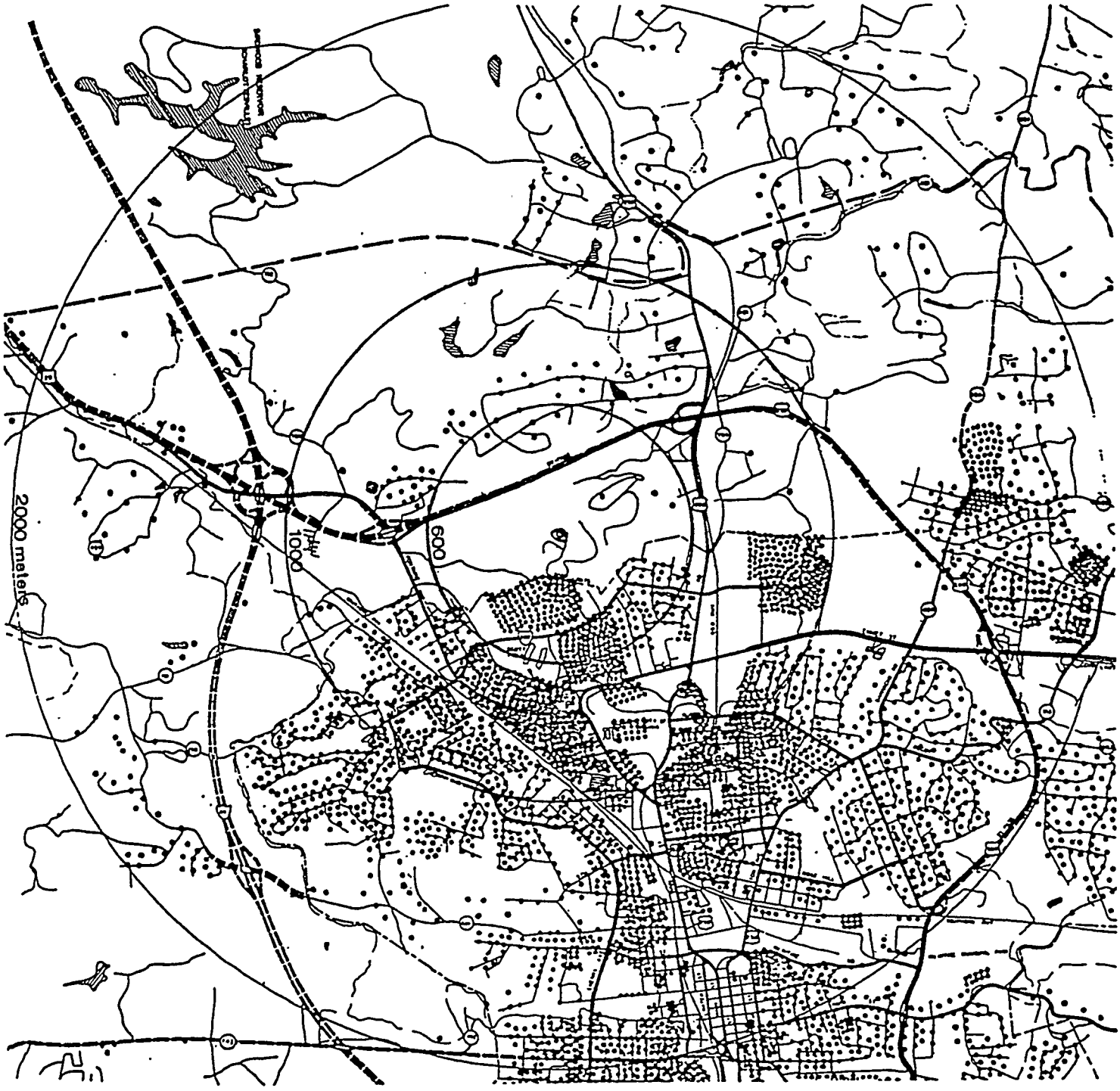


FIGURE 2-4 POPULATION DENSITY DISTRIBUTION (1968)
(Each Dot = 10 Persons)

The Reactor Facility has an exclusion fence as shown in Fig. 2-3. This fence is approximately 70 meters from the reactor building in the terrain "unshielded" direction. Within a 600 meter radius of the UVAR there are very few buildings and all of these, with the exception of approximately a dozen privately owned homes just inside this radius, are operated either by the University, City of Charlottesville or State of Virginia.

2.2 Reactor Building

The Reactor Facility building, shown in Fig. 2-5, consists of the main reactor room, radiation laboratory, supporting laboratories, hot cell and office space. Figures 2-6, 2-7, and 2-8 show floor plans for the three levels. The construction is of conventional masonry, with the exception of the main reactor room. This portion of the building is cylindrical in shape to increase its ability to withstand internal pressure. The walls are of reinforced masonry, plastered on the inside for gas tightness, while the roof is a concrete slab. This portion of the structure is windowless and the doors are gasketed. The reactor bay ventilation is described in Section 4.9.

2.3 New Construction

Construction of an addition to the Reactor Facility was completed in 1970. The new addition provides more office space, classroom, machine shop, electronics shop, low background counting room, health physics and student laboratories.

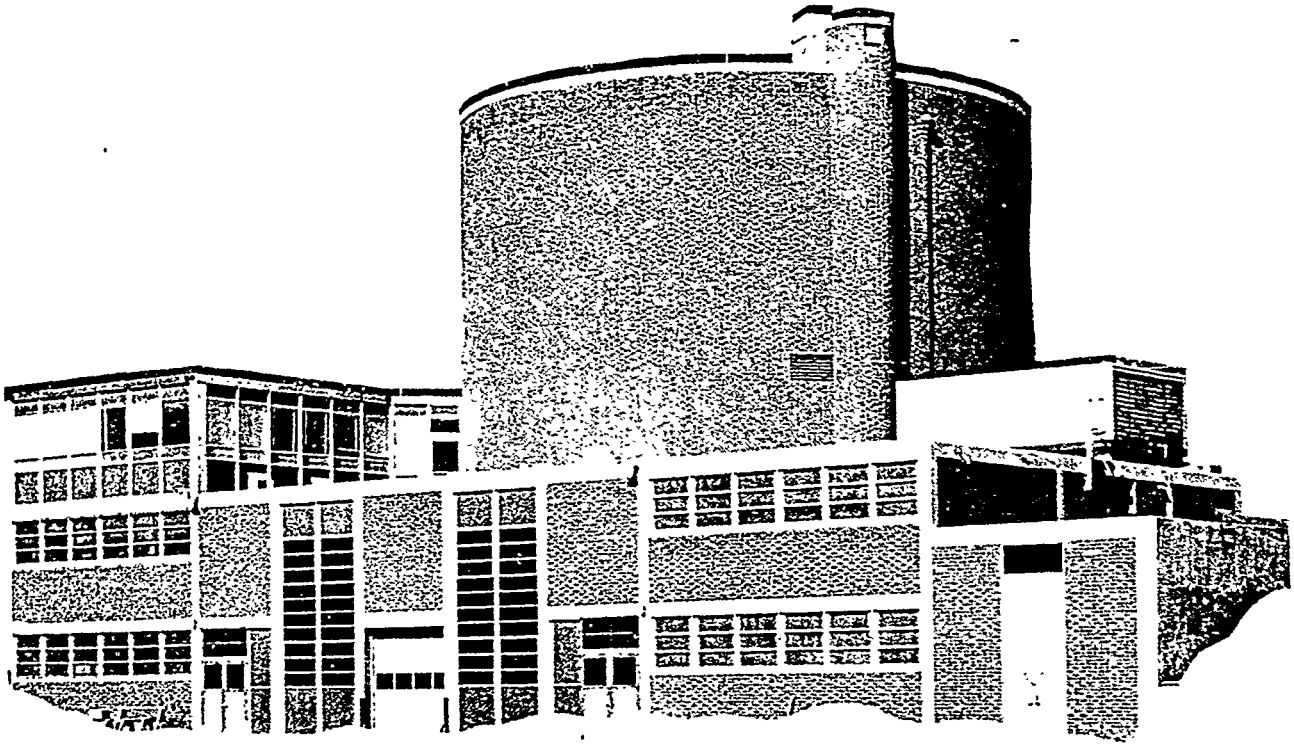


Figure 2-5 University of Virginia Research and Training Reactor Facility.

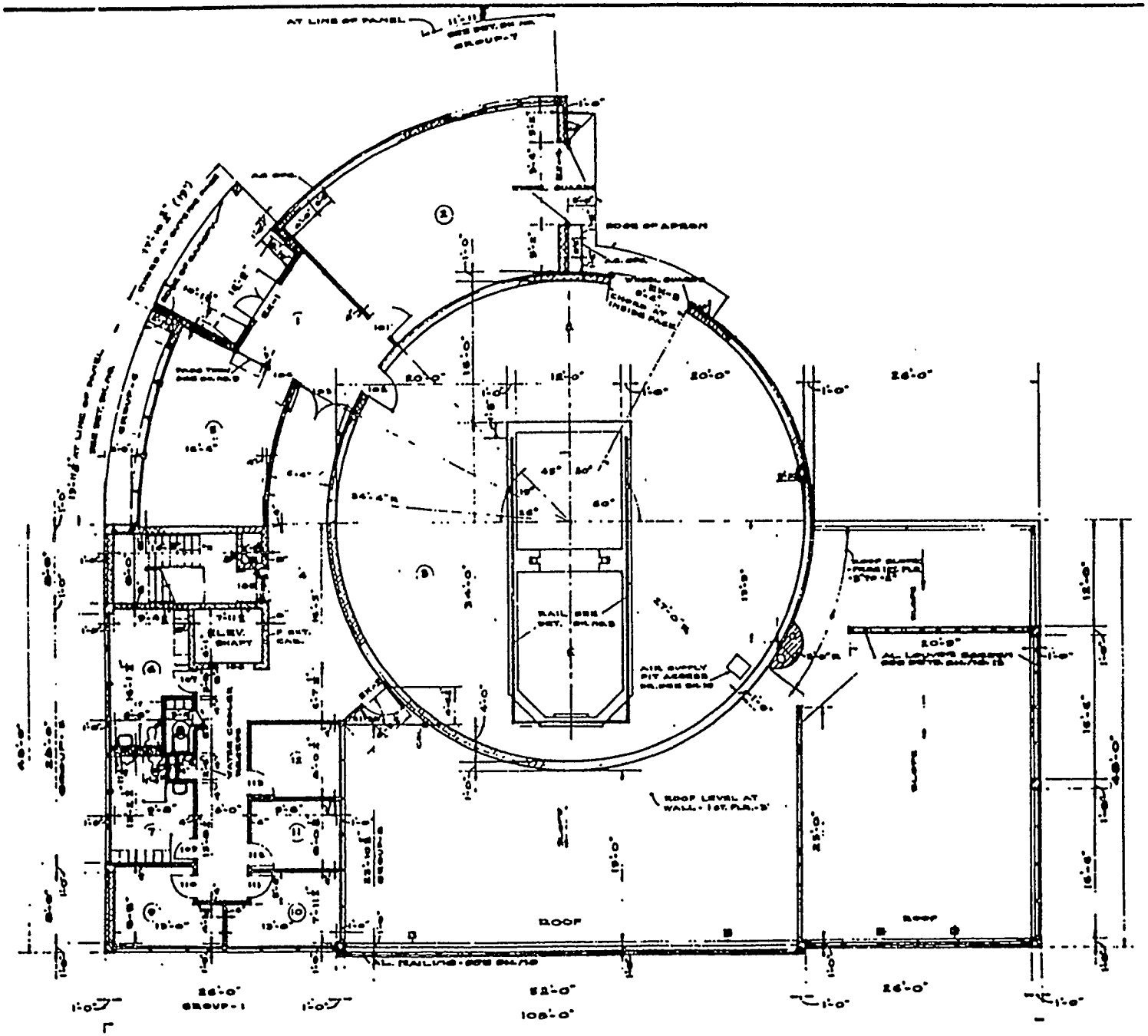


FIG. 2-6 FIRST FLOOR PLAN

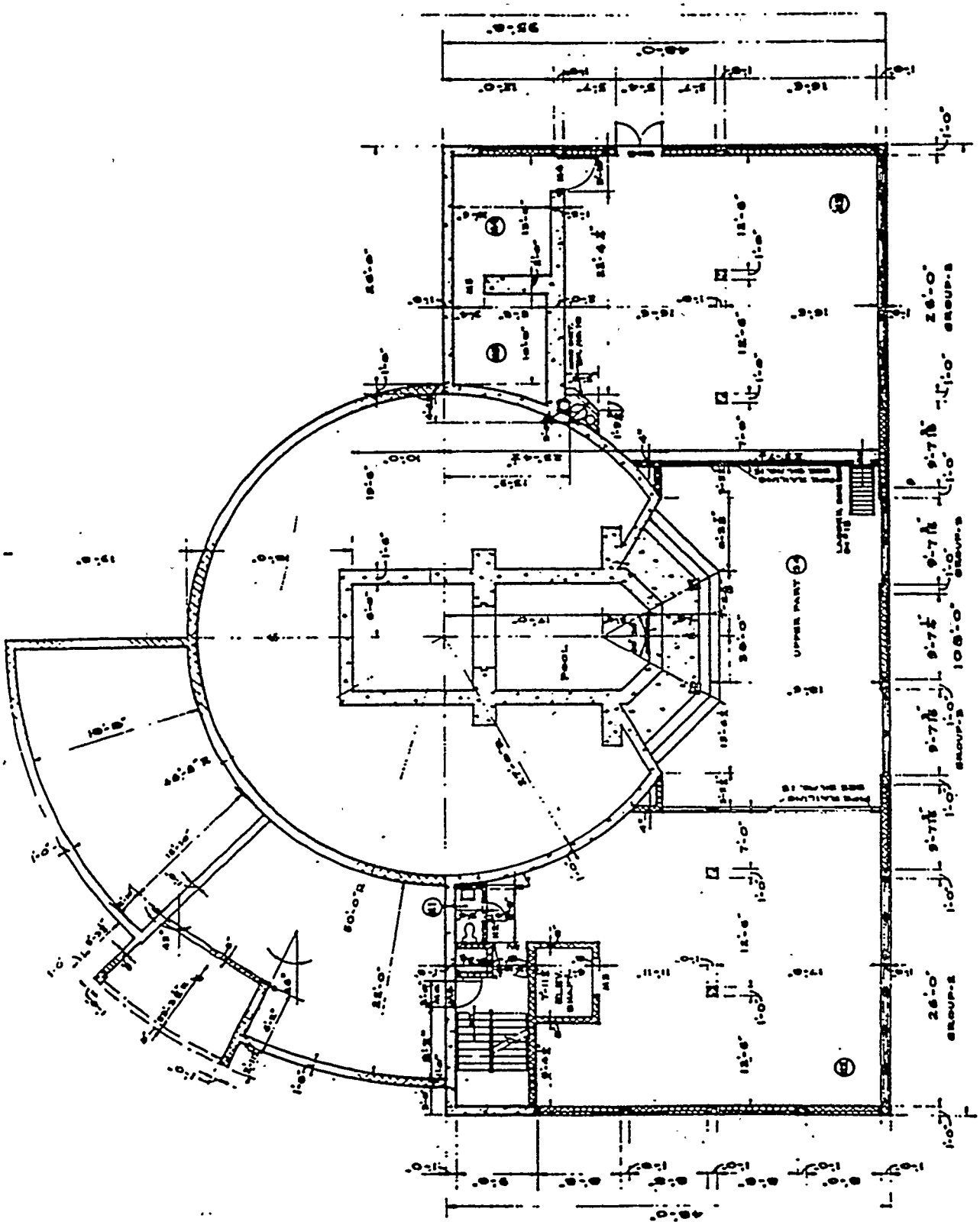


FIG. 2-7 MEZZANINE LEVEL

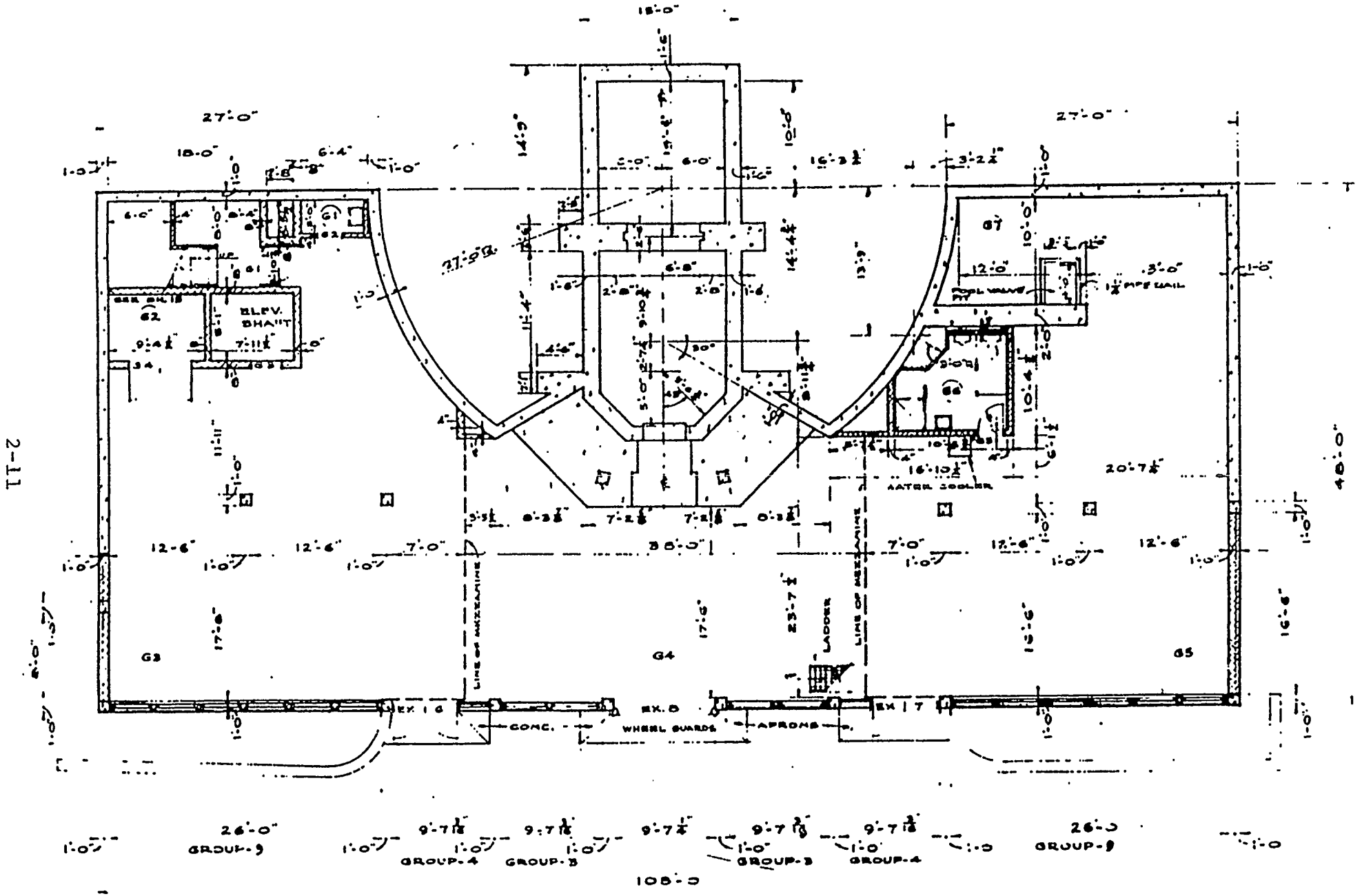
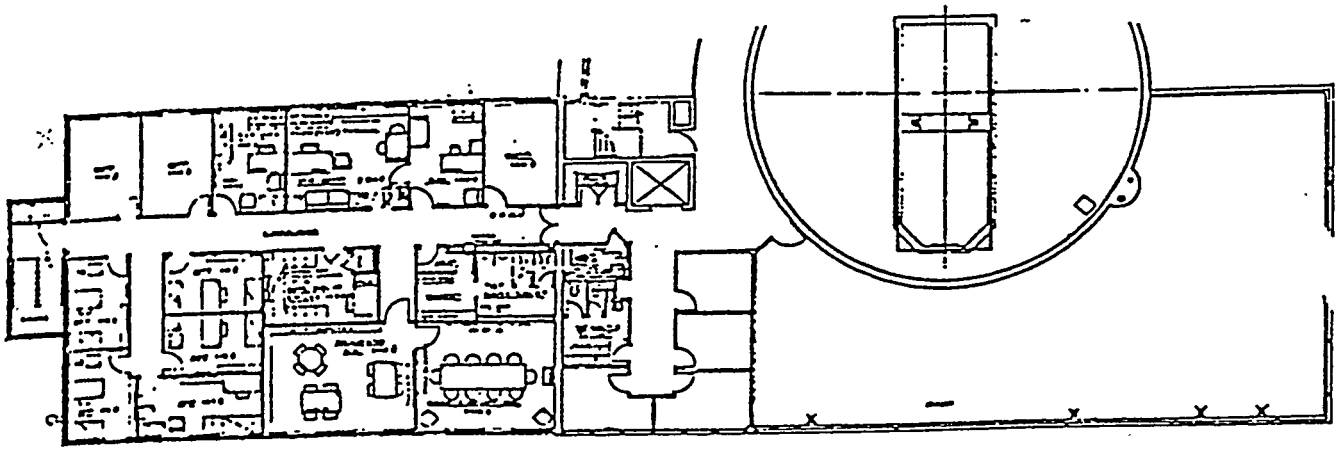
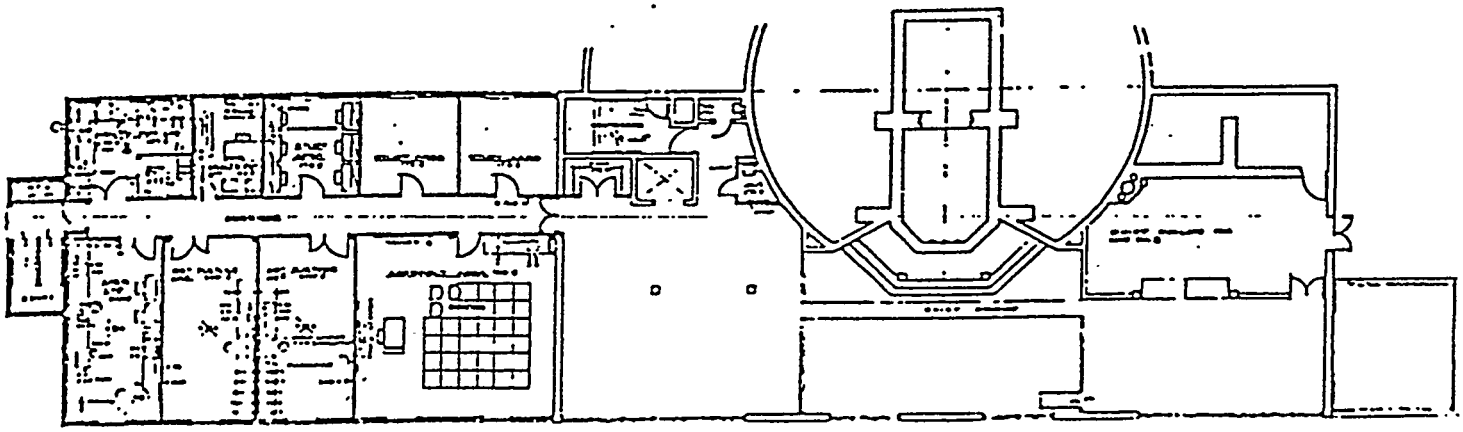


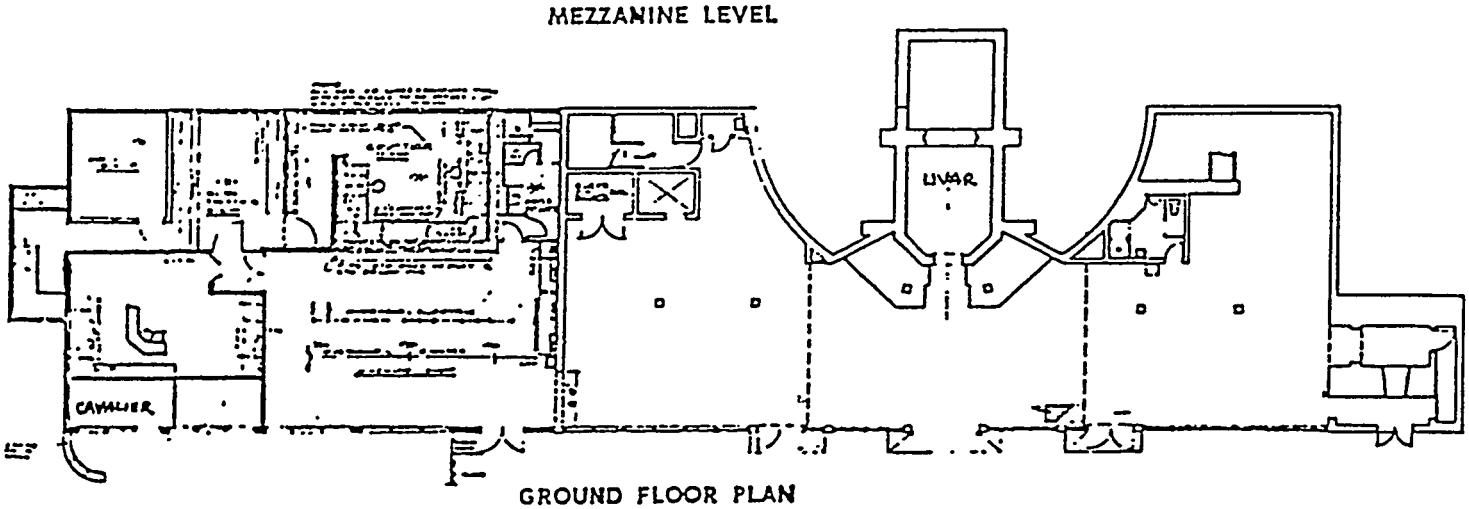
FIG. 2-8 GROUND FLOOR



FIRST FLOOR PLAN



MEZZANINE LEVEL



GROUND FLOOR PLAN

FIGURE 2-9 PLANS OF THE NUCLEAR REACTOR FACILITY

2.4 Wind Direction and Velocity

During the first few years of University of Virginia Reactor operation, records of wind velocity and direction at the reactor site were maintained. Tables 2.1 and 2.2 represent the equivalent of one year's data, from 21 June 1961 to 21 June 1962. For that year, winds from the Northeast to Northwest quadrant are dominant with a strong contribution from the West. The summer season has a high percentage of calms with principal winds from the Southeast to the Southwest quadrants. Therefore, gaseous effluent discharged or fission products released into the atmosphere would, with greatest probability, be transported in the direction of highest population density, except in the summer season where the reverse would be true.

2.5 Hydrology

As mentioned elsewhere (Sections 2.1 and 4.8) of this report, liquid effluents from the reactor building may discharged, upon dilution with water from the adjacent pond to concentrations below MPC, to Meadowbrook Creek which flows into the Rivanna River. Releases are made in accordance with the restrictions set forth in 10 CFR Part 20.

Due to its location on the side of a draw between Mt. Jefferson and Lewis Mountain, the reactor is not subject to flood conditions.

TABLE 2.1

RELATIVE FREQUENCY OF HOURLY WIND SPEEDS
IN PER CENT BY SEASON

Wind Speed Type	mph	Summer	Fall	Winter	Spring	Year
Calm	0-1	43.5	9.0	3.5	20.7	18.7
Light	1-3	15.3	2.0	1.4	8.1	6.4
Gentle	4-10	28.0	10.7	14.3	31.7	20.0
Moderate	11-21	11.6	33.3	61.8	37.9	36.3
Strong	21-up	1.6	45.0	19.0	1.6	18.6
Total		100.0	100.0	100.0	100.0	100.0
Avg. Speed (mph)		4.26	15.0	13.1	7.71	10.36*

*The average wind speed of 10.36 mph is equivalent to 4.63 m/sec.

TABLE 2.2

RELATIVE FREQUENCY OF HOURLY WIND DIRECTIONS
IN PER CENT BY SEASON

Direction	Summer	Fall	Winter	Spring	Year
North	5.6	27.4	30.3	8.4	16.9
Northeast	7.4	10.2	28.3	24.5	16.8
East	5.7	0.0	2.6	0.0	2.6
Southeast	7.8	12.4	8.0	2.6	8.1
South	10.6	3.8	3.0	10.2	7.8
Southwest	8.5	10.3	4.6	5.0	7.7
West	3.8	15.9	12.5	9.2	10.0
Northwest	7.1	10.9	7.5	10.4	11.4
Calms	43.5	9.1	3.5	20.7	18.7
Total	100.0	100.0	100.0	100.0	100.0

2.6 Seismology

The Central Appalachian region is characterized by a moderate amount of low level earthquake activity. Because of the low seismic energy release, this region has received very little attention from earthquake seismologists. A study by Dr. G.A. Bollinger of Virginia Polytechnic Institute covering the period of 1758 through 1968, indicates a history of 9 earth tremors in the city of Charlottesville and Albemarle County during that period.

The tremors felt in this area and their intensity on the modified Mercalli Scale, when of sufficient magnitude for assignment, are listed below:

Date	Intensity at Epicenter
August 27, 1933	VI
April 29, 1852	VI
September 1, 1886	V-VI
December 26, 1929	VI
April, 1936	Not Available
February 2, 1937	III-IV
May 24, 1946	Not Available
March 26, 1948	Not Available
September 10, 1952	IV
May 31, 1966	Not Available
November 19, 1969	Not Determined

Considering the low level of earthquake activity and intensity in this area and the reinforced construction of the pool, earthquake activity is not considered to present a danger to the facility.

3.0 REACTOR COMPONENTS AND CONTROL

3.1 Reactor Assembly

The reactor assembly is comprised of fuel elements, control rod fuel elements, control rods and graphite reflector elements; all of which sit in the reactor gridplate near the bottom of the reactor pool. The reactor gridplate is supported by an aluminum framework from a movable bridge. The bridge can be rolled back and forth across the pool in the north-south direction and is designed such that the minimum distance between the core and the pool wall is about 4 feet. This distance is sufficient to prevent significant activation of the concrete walls. The bottom of the core is about 4.5 feet above the pool floor and the top of the active core is about 20 feet below the pool surface (see Figure 3-1). The heat capacity of the pool is sufficient for steady-state operation at 200 kW with natural convection cooling; but for higher power operation, a forced convection system is required. The forced convection cooling system, described in Section 4.3, uses downflow in order to minimize nitrogen-16 activity in the reactor room.

The reactor gridplate, shown in Figure 3-2, is made of aluminum and contains an eight by eight array of holes used for positioning reactor components. Each positioning hole is approximately 2 1/2 inch in diameter. The center-to-center spacings are 3.2 inch in the East-West direction, and 3.0 inch in the North-South direction. Small holes (not shown in Figure 3-2) are interspaced between the positioning holes to provide cooling flow between reactor components.

Reactor components include: 1) fuel elements, 2) graphite elements, 3) gridplate plugs and 4) in-core experiments.

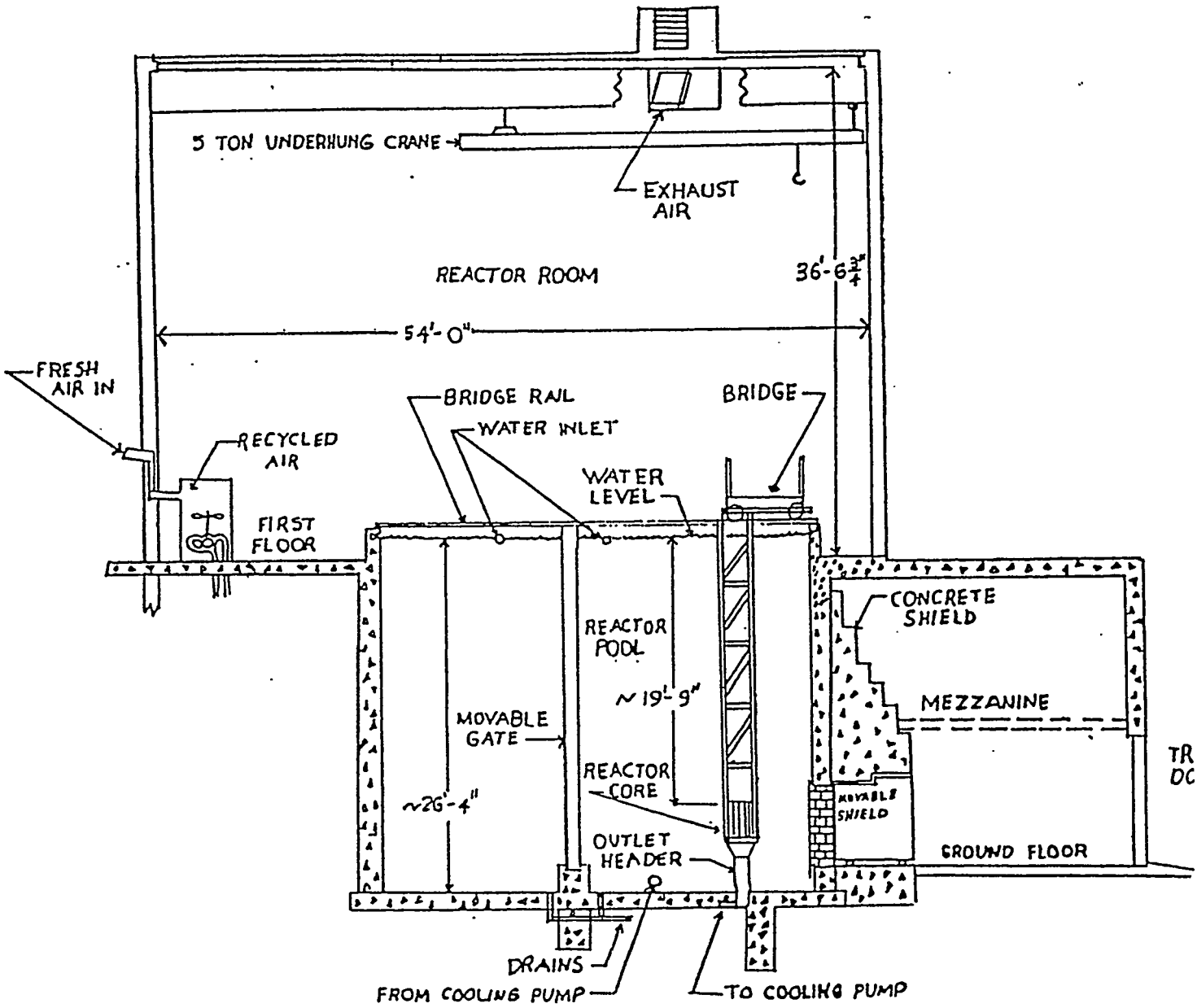


Figure 3-1. Cross-Section View of Reactor Pool and Reactor Room

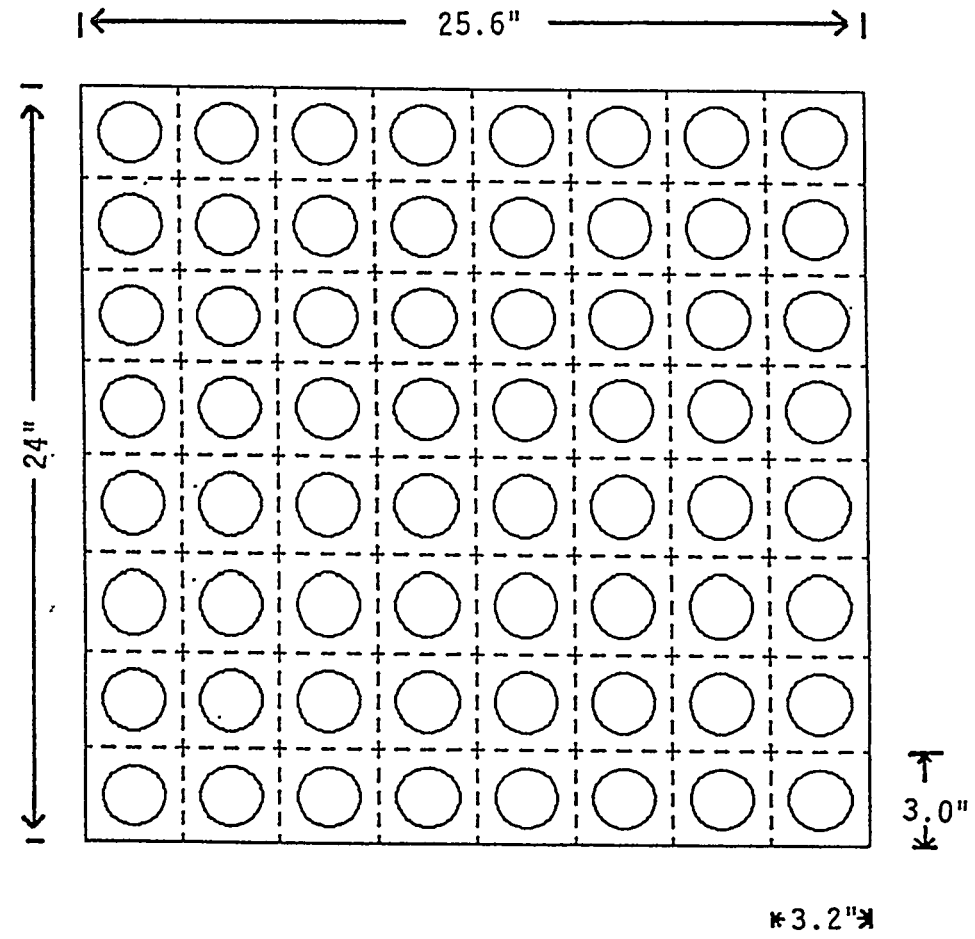


Figure 3-2. UVAR Gridplate

3.2 Fuel Elements

Three types of fuel elements are used in the UVAR: 1) standard fuel elements, 2) partial fuel elements and 3) control rod fuel elements. Each type of fuel element uses generic fuel plates (described in Section 3.3) and has similar outer cross sectional dimensions of about 3 inch by 3 inch. The standard and partial elements are about 34 inches in height and the control rod element is about 38 inches in height. The bottom of each element consists of a cylindrical tapered nozzle which fits snugly into the gridplate positioning holes.

The standard low-enriched uranium fuel element, shown in Figures 3-3 and 3-4, contains 22 fuel plates. The initial loading of a standard fuel element is 275 grams of uranium-235. The water gap between fuel plates is 0.092 inch. The metal to water ratio of the active standard fuel element is 0.76.

Partial fuel elements have the same dimensions as standard fuel elements but contain only half the amount of fuel. Partial elements are loaded into the core when relatively small changes in reactivity are desired. The partial element has 22 plates, of which 11 are fuel plates and 11 are aluminum "dummy" plates, with fuel and dummy plates alternating. Dummy plates have the same outer dimensions as fuel plates. The partial fuel element initially contains 138 grams of uranium-235.

Control rod elements, shown in Figures 3-5 and 3-6, have dimensions similar to standard fuel elements and use the same water gap between fuel plates. The control rod element contains 11 fuel plates (138 grams of uranium-235) and has an open center (referred to as the water hole) where the control rod travels. Two guide plates on either side of the water

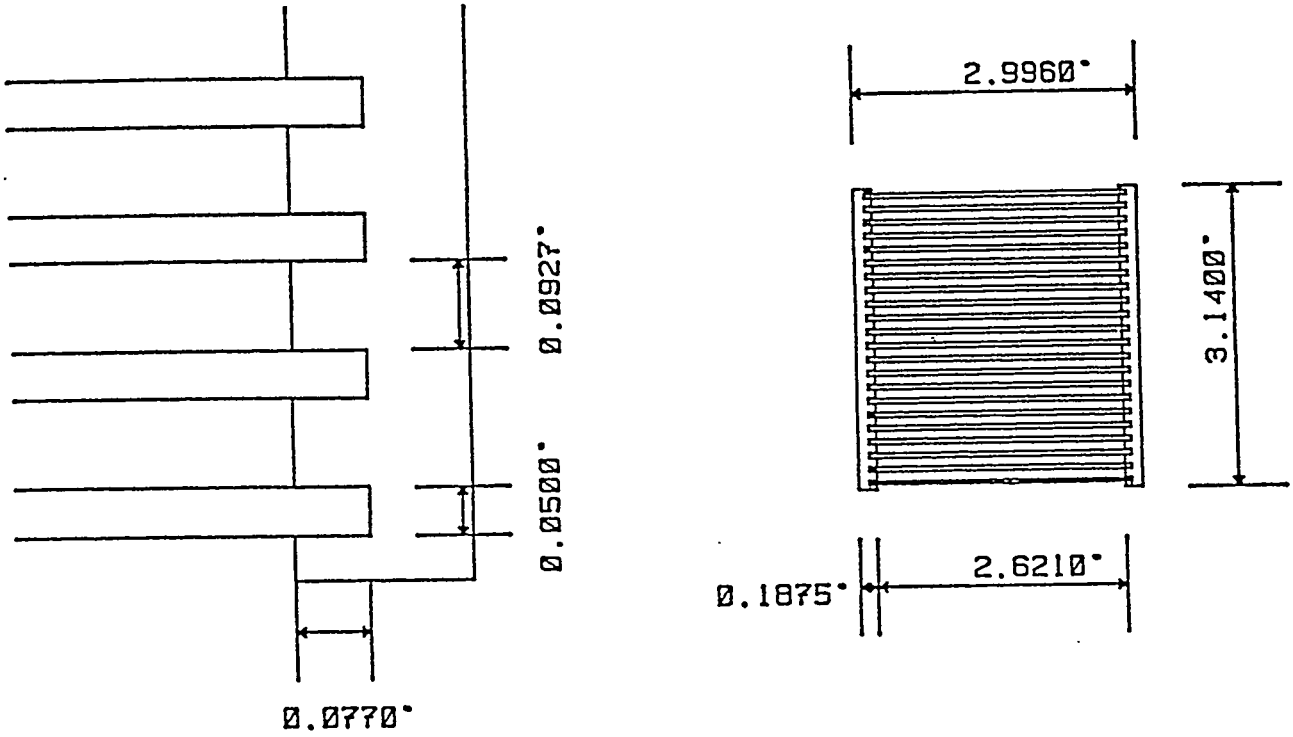
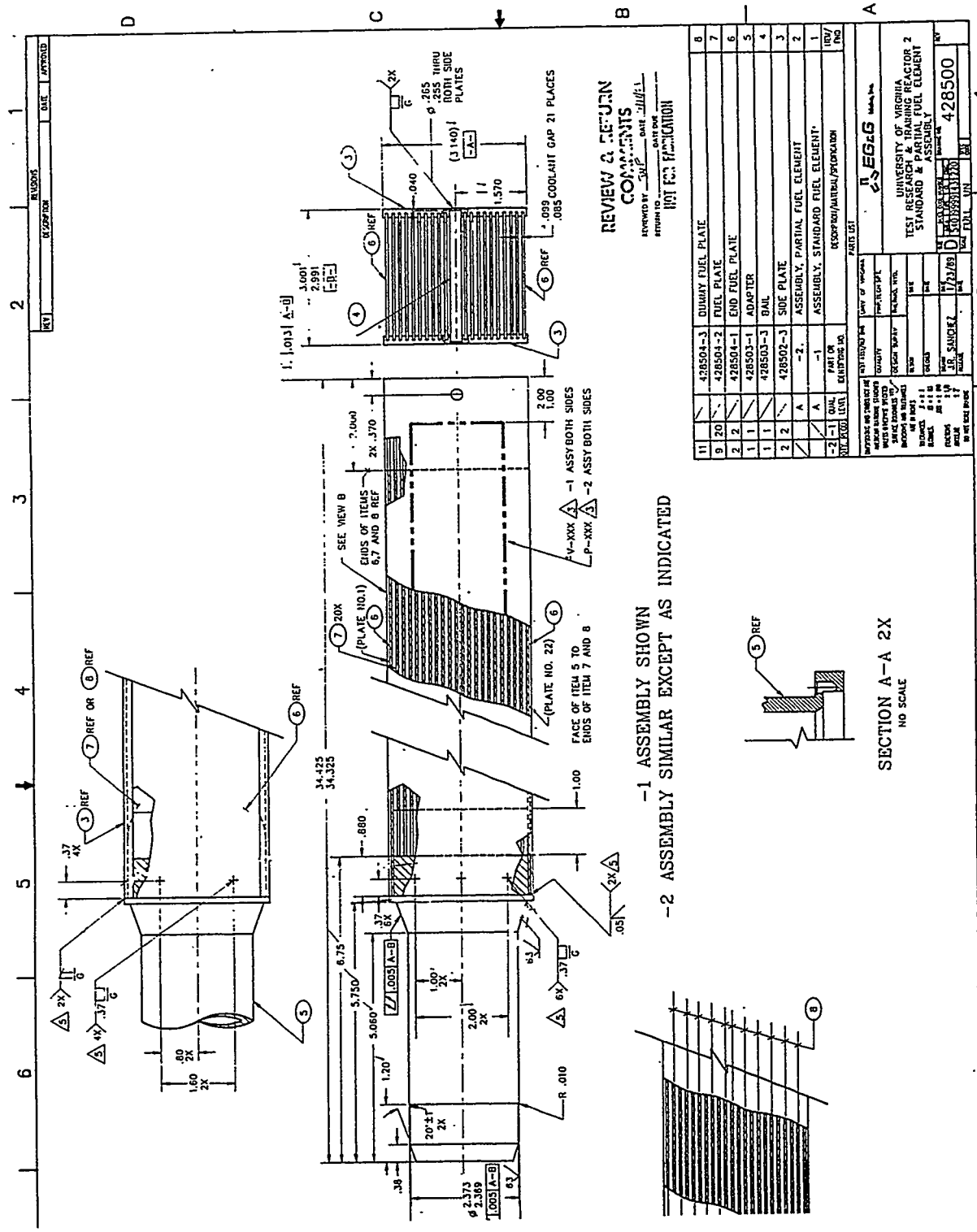


Figure 3-3. Top View Of Standard and Partial LEU Fuel Element

Figure 3-4. Side View Of Standard and Partial LEU Fuel Element



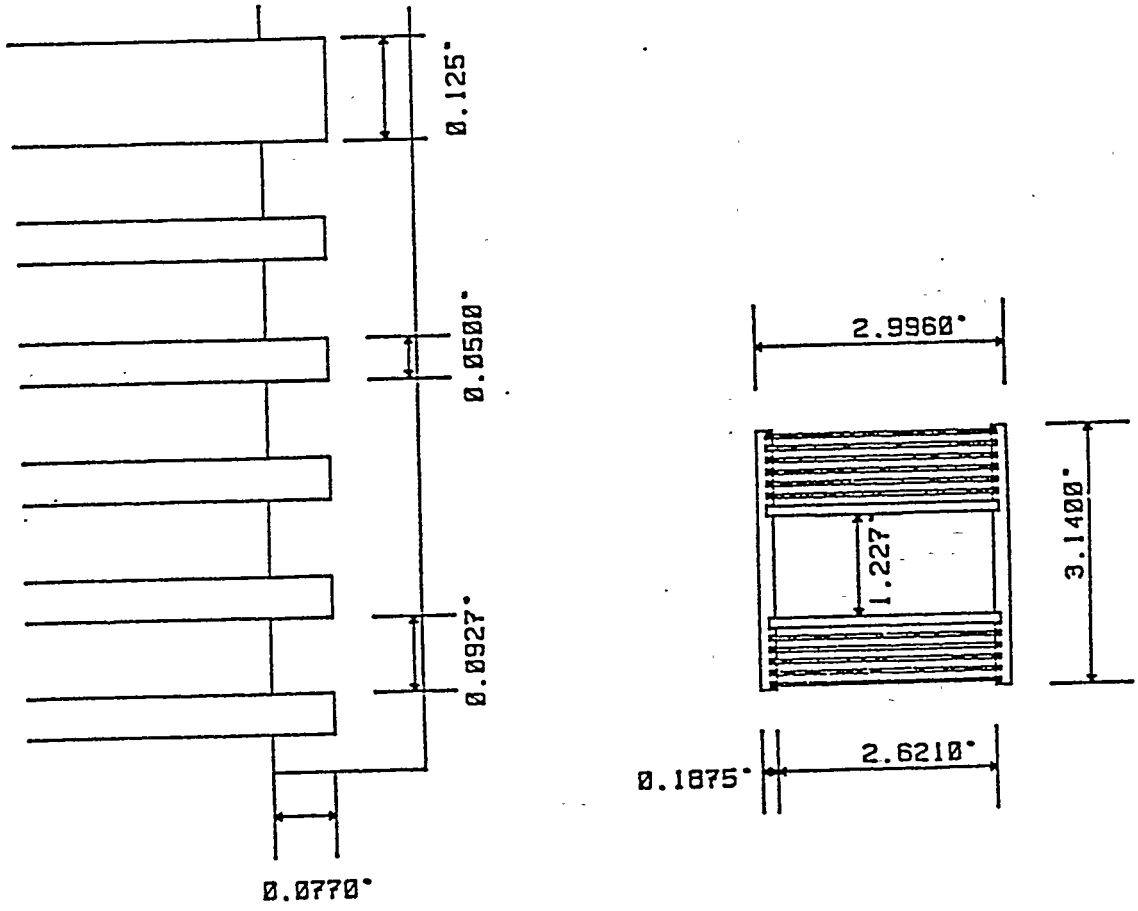
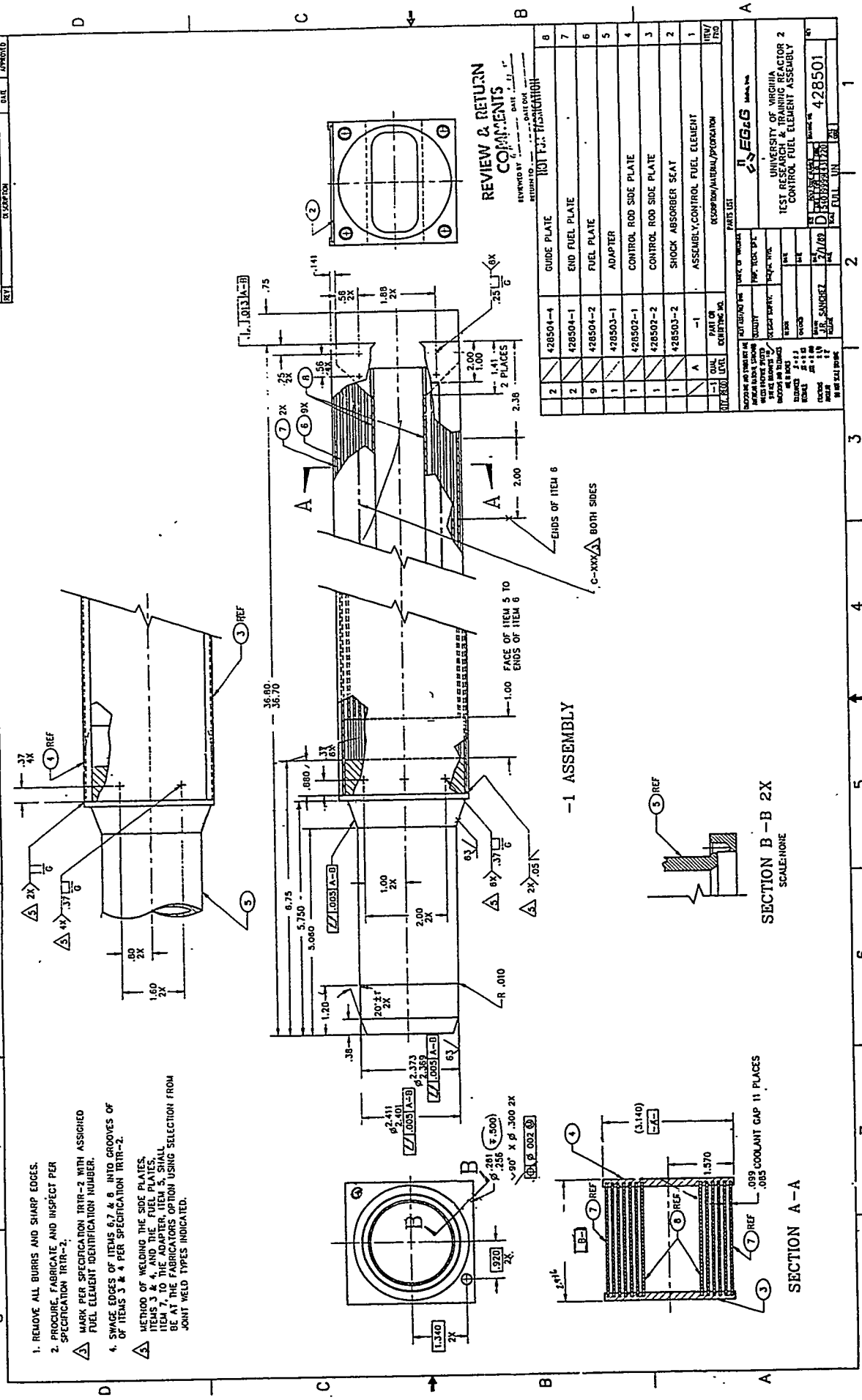


Figure 3-5. Top View Of Control Rod LEU Element

Figure 3-6. Side View Of Control Rod LEU Element



hole assure that the control rod will not contact or damage the fuel plates. The metal-to-water ratio of the control rod element is 0.52.

Detailed dimensions of UVAR LEU fuel elements are available in References [1] through [4].

3.3 Fuel Plates

The fuel plates are flat and each initially contains 12.5 grams of uranium-235. The plates contain low-enriched uranium (LEU) fuel meat clad in aluminum. The fuel plate is 0.05 inch thick, 2.80 inch wide, and 24.6 inch long. Detailed fuel plate dimensions are provided in Reference [5].

The fuel meat is composed of uranium-silicide (U_3Si_2) dispersed in an aluminum matrix. The uranium is 19.75 percent enriched in uranium-235. The fuel meat is 0.02 inch thick, 2.40 inch wide, and 23.3 inch long.

The aluminum clad is 0.015 inch thick and surrounds the fuel meat.

3.4 Control Rods and Drives

The reactor has four control rods. Three of these, designated as Shim rods (or Safety rods) are designed for gross control and safety. Shim rods are magnetically coupled to their drive mechanisms and drop into the core by gravity on a scram signal. The fourth rod is a regulating rod which is fixed to its drive mechanism and is therefore non-scramable. The regulating rod is primarily used to compensate for small changes in reactivity associated with normal operations. LEU cores use the same control rods and drive mechanisms used previously in the HEU

cores. Detailed control rod and drive specifications are presented in References [6] through [8].

The reactivity worth of the shim rods in HEU cores have typically varied between about $3 and $5, depending on factors such as core/reflector configuration, rod position in the core, core burn-up, etc. Analyses presented in Reference [9] show that the shim rod worths for the LEU core are not significantly different from shim rod worths in HEU core. Therefore, the shim rods should provide adequate control for safe operation.

The reactivity worth of the regulating rod in HEU cores has typically varied between $0.4 and $0.8. The analysis provided in Reference [9] shows that the reactivity worth of the regulating rod in the LEU cores is similar to its worth in HEU cores. Therefore, the regulating rod is expected to adequately perform its function of compensating for small reactivity changes in LEU cores.

All of the rods are of the bayonet type, fitting into the control rod fuel element water hole. The control rod, rod drive, and extension assembly is bolted to the top of the control rod fuel element, thus creating a single rod unit. A rod unit may be located in any core position by locating the control element nozzle into the desired gridplate position.

The absorbing section of the shim rods is boron-stainless steel, clad in aluminum. The stainless steel is alloyed with about 1.5% boron by volume. Each absorbing section is 24-13/16-inches long and has an oval cross section of 2-1/4 x 7/8-inches with semi-circular ends. Four

groves are cut in each side of an absorbing section to increase the surface area.

The shim rods are suspended magnetically from the drive mechanism. The drive is provided by a 115 volt, 60 cycle, split phase synchronous motor. The motor, lead screw-drive, and position indicating equipment are contained in a cylindrical tube extending from the top of the core to above the water level where it is supported from the bridge. A scram signal will de-energize the magnet holding the absorber section, allowing it to drop freely until it is hydraulically damped and stopped, fully in the core. The supporting magnet must be driven down to contact the bottom absorber section before the control rod can be raised after a scram. The shim rods are driven at about 3.7 inches per minute in both directions.

The regulating rod has the same overall dimensions as the safety rod, except there are no grooves in the regulating rod. The regulating rod is made of stainless steel and is clad in aluminum. The regulating rod is permanently fixed to its drive mechanism and does not drop on a scram signal. It is driven by a 115 volt, 60 cycle two phase control motor which, along with the lead screw and position indicating equipment, is contained in a cylindrical tube similar to that employed for the safety shim rods. The regulating rod is connected to the automatic control system of the reactor described in Section 3.12. The regulating rod travels at a speed of approximately 24 in/min in both directions.

Each shim rod is removed from the reactor and visually inspected on an annual basis. The inspection includes checking for cracks and swelling.

Rod drop times are measured semi-annually and whenever a safety rod is maintained or repositioned in the core. The maximum allowable time from scram initiation to full insertion is less than one second.

3.5 Reactor Reflectors

The primary reflectors used in the UVAR are graphite elements and pool water. Experiments located near the core may also behave as reflectors.

Graphite elements have the same approximate outer dimensions as the fuel elements and consist of a solid graphite core surrounded by aluminum. Graphite elements are significantly better reflectors than pool water.

Gridplugs are used to prevent water flow through empty gridplate locations. A gridplug is a short metal cylinder, approximately 3 inches in diameter, mounted on a tapered nozzle. When inserted in the gridplate, the plug extends no more than a few inches above the gridplate effectively providing pool water reflector at that gridplate location.

Other types of reflectors include items such as experiments or experimental facilities, located in close proximity to the core.

3.6 Core Loadings

A wide variety of critical loadings are possible with the UVAR reactor. Core loadings are limited by Technical Specification restrictions on shutdown margin ($0.55) and excess reactivity ($7.00). The minimum critical loading is a graphite reflected four-by-four array of elements, including 12 standard fuel elements and 4 control rod elements. This loading has a mass of 3850 grams of uranium-235.

Excess reactivity and shutdown margin are functions of items such as the amount of fuel in the core, fuel and reflector configuration, control rod locations, fuel burn-up, etc. The core configuration of the UVAR is frequently changed to enhance characteristics of experimental facilities, perform new experiments, or compensate for fuel burn-up. Shutdown margin and excess reactivity are experimentally determined after each core configuration change. Additionally, shutdown-margin and excess reactivity are periodically reevaluated to account reactivity changes associated with fuel burn-up.

Initial loading of a new core is performed carefully. Sub-critical multiplication data is collected with the addition of each fuel element. Analysis of this data allows a fairly accurate prediction of when initial criticality will be achieved. Final fuel additions are made in half-element increments until a desired core is achieved. Operation of the new core is limited to 1 kilowatt for the purpose of obtaining experimental data to calibrate the control rods. The shutdown margin and excess reactivity are determined from the rod calibration data and a determination of acceptability of these parameters must be made prior to operating the new core in excess of 1 kilowatt.

Analyses presented in Reference [9] show that the reactivity of unburned LEU and HEU fueled cores are similar. The loading of LEU cores is expected to result in core reactivity parameters similar to those verified through past experience with the HEU cores.

It should be noted that LEU 22 plate/element fuel is expected to have a somewhat longer core life than 18 plate/element HEU fuel. This

should result in fewer core modifications to accomodate fuel burn-up, which is beneficial with regards to experiments and fuel costs.

3.7 Fuel Storage Facilities

UVAR Technical Specifications require all fuel elements not in the reactor core to be stored in a geometric array such that the k-effective is less than 0.9. Existing fuel storage facilities at the UVAR Reactor Facility have been evaluated for compliance with the Technical Specification reactivity requirement, with regard to LEU 22 plate/element fuel.

The current fuel storage facilities are described below:

1) **Fuel Storage Room** - The Fuel Storage Room is located in the CAVALIER Room and consists of an aluminum rack with a rectangular array of square holes in which fuel elements may be stored. The center-to-center distance of the holes is 12 inches in both directions. The Fuel Storage Room is dry and is located above ground. The Fuel Storage Room is primarily used for the storage of unburned fuel elements. Elements in the Fuel Storage Room are secured with chains bolted across the rack openings.

2) **Auxiliary Fuel Storage Rack** - The Auxiliary Fuel Storage Rack (AFSR) is normally stored at the pool bottom. The AFSR contains two linear arrays of fuel storage positions. The two linear arrays are separated by a distance of two feet. Each linear array consist of twelve fuel storage locations, separated by a center-to-center distance of 6 inches. Elements

in the AFSR are mechanically held in place by the rack lids which may be bolted shut.

3) Four Element Racks"Lunar Landers" - There are currently 3 Lunar Landers. Lunar Landers loaded with burned fuel are stored at the pool bottom. The Lunar Landers each hold up to 4 elements in a square configuration with the elements being located at the corners of the square. The center-to-center distance between elements in the x-y direction varies from 7 to 8 inches. Elements are secured by bolting an aluminum top onto the lander.

4) Wall Rack - The Wall Rack is used for temporary underwater storage of fuel elements. It consists of a linear array of 12 fuel storage locations. Each fuel storage location is separated by a center-to-center distance of 3.5 inches.

An analysis applicable to the Fuel Storage Room, Auxiliary Fuel Storage Rack, and Lunar Landers has been performed using two dimensional diffusion theory computer modeling. A unit LEU fuel cell surrounded by water was modeled in x-y geometry. Flat flux boundary conditions were used to simulate an infinite array. The k-effective of a water moderated infinite array of fuel was determined to be 0.8 for a center-to-center distance of 5.5 inches. This analysis is conservative in that 1) it neglects leakage from the boundaries of a storage facility and 2) the value of k-effective = 0.8 associated with the 5.5 inch spacing is significantly lower than the required value of 0.9. Based on this information, LEU-22 fuel storage facilities with an x-y storage array with center-to-center spacings in excess of 5.5 inches meet the Technical Specification reactivity requirement.

An analysis applicable to the Wall Rack (and to the Auxiliary Fuel Storage Rack) was performed for an infinite linear array of water moderated (and reflected) LEU fuel elements positioned side-by-side, (i.e. no separation between elements). The k-effective for this array is 0.74, which also meets the Technical Specification criteria.

In summary, modeling results show that all of the existing fuel storage facilities meet the Technical Specification reactivity criteria when loaded with LEU-22 plate/element fuel.

3.8 Reactor Data

For ease in reference, pertinent data for the UVAR reactor are presented in Table 3.1. Information detailing the UVAR LEU-22 fuel elements, fuel plates, and fuel meat is provided in Reference [10].

Table 3.1 Reactor Data for LEU Cores

I. Typical 4-by-4 and 4-by-5 Core Parameters

Parameter	4-by-4 Core Configuration	4-by-5 Core Configuration
1. Core Dimensions		
a) Active height	23.3 inch	23.3 inch
b) Width	12.6 inch	12.6 inch
c) Length	12.0 inch	15.0 inch
d) Volume	3,520 $inch^3$	4,400 $inch^3$
2. Number of Elements		
a) Standard	12	16
b) Control	4	4
3. Mass U-235	3.85 kg	4.95 kg
4. Metal-to-Water Ratio (by volume)	0.70	0.74

II. Fuel Element Parameters

Parameter	Value
1. Outer Dimensions	
a) Height	34.4 inch
b) Width	3.14
c) Length	3.00
2. Water Gap	0.092 inch
3. Standard Element	
- Number of Fuel Plates	22
- Number of Side Plates	2
- U-235 Content/Fuel Plate	12.5 gram
- Metal-to-Water Ratio (by volume)	0.76
4. Control Element	
- Number of Fuel Plates	11
- Number of Side Plates	2
- Number of Guide Plates	2
- U-235 Content/Fuel Plate	12.5 gram
- Metal-to-Water Ratio	0.52
5. Partial Element	
- Number of Fuel Plates	11
- Number of Side Plates	2
- Number of "Dummy" Plates	11
- U-235 Content/Fuel Plate	12.5 gram
- Metal-to-Water Ratio	0.76

III. Fuel Plate Parameters

1. Overall Dimensions	
a) Length	24.6 inch
b) Width	2.80 inch
c) Thickness	0.050 inch
2. Fuel Meat	
a) Type	U_3Si_2 in Al matrix
b) Uranium Enrichment	19.8% U-235
c) U-235 Content	12.5 gram
d) Length	23.3 inch
e) Width	2.40 inch
f) Thickness	0.020 inch
3. Clad Thickness	0.015 inch

IV. Side Plate Parameters

Length	
a) Standard	28.5 inch
b) Control	30.9 inch
Width	3.14 inch
Thickness	0.188 inch
Composition	Aluminum

V. Guide Plate Parameters

Length	27.6 inch
Width	2.80 inch
Thickness	0.125 inch
Composition	Aluminum

VI. Control Rod Parameters

1. Safety (Shim) Rods

Absorber Material	Boron-Stainless Steel 1.5% Boron
Clad	Aluminum
a) Dimensions, Overall	
Width (Approx.)	1 inch
Depth (Approx.)	2.38 inch
Length (Approx.)	27.5 inch
Travel (Approx.)	24 inch
Weight (Dropping Section)	5.5 inch
b) Drive - Electric motor, 115 V 60 cycle, split phase. 3600 rpm at 60 cps. From top by lead screw.	
c) Drive Speed	3.74 in/min
d) Release - Magnetic; after release, mechanism must be driven down to re-engage absorber	
e) Typical reactivity, fully inserted	$ 3 to $ 5
f) Typical reactivity per inch	$ 0.1 to $ 0.3
g) Typical rate reactivity increase in up travel (per second)	$ 0.01 to $ 0.02
h) Excess reactivity controllable with all rods, typically	$ 9 to $15

2. Regulating Rod

a)	Absorber Material	Stainless Steel
b)	Dimensions	Same as Shim Safety (No grooves)
c)	Travel	24 in.
d)	Release	None - does not drop on scram
e)	Typical Reactivity Fully inserted	$ 0.3 to $ 1.0
f)	Typical Reactivity per in.	$ 0.01 to $ 0.04
g)	Typical rate of Reactivity increase in up travel (per second)	$ 0.004 to $ 0.02

VII. Feedback Coefficients (Reference [9])

1.	Doppler Coeff ($/°C)	$- 1.5 \times 10^{-3}$
2.	Void Coeff ($/% void)	
	a) Uniform void (1 to 10% void)	- 0.3
	b) Local void (1 to 14% void)	- 0.8
3.	Moderator Coeff ($/°C)	- 0.02

VIII. Kinetics Parameters (Reference [9])

1.	Prompt Neutron Lifetime	53 to 67 microsecs
2.	Effective Delayed Neutron Fractions	0.0074

3.9 Reactor Kinetics

An analysis determining important kinetics parameters (i.e. prompt neutron lifetimes and delayed neutron fractions) for the LEU fueled UVAR core is presented in Reference [9]. This analysis provided a comparison of kinetics parameters associated with LEU and HEU fueled UVAR cores. Results of that analysis are discussed below.

Prompt neutron lifetimes determined for both LEU and HEU fueled UVAR cores are presented in Table 3.2. Both graphite and water reflected cores were evaluated.

Table 3.2. Prompt Neutron Lifetimes For LEU and HEU Fueled UVAR Cores (Reference [9])

Core Description	Prompt Neutron Lifetime (μsecs) LEU	HEU-18
1. Graphite Reflector	67	79
2. Water Reflector	53	64

Information presented in Table 3.2 shows that the prompt neutron lifetime of the LEU core is about 15 % lower than that of the HEU core. This is as expected because of the significantly higher uranium-238 loading associated with the LEU fuel. Because the prompt effect is relatively small in the normal operations of the UVAR reactor, this difference is not expected to produce a noticeable change in the UVAR response to reactivity changes.

The effective delayed neutron fractions determined for both the LEU and HEU fueled cores were found to be essentially the same, at a value of about 0.0074.

Based on the information provided above, UVAR LEU cores one expected to behave essentially the same as past HEU cores, with regard to reactor kinetics.

3.10 Fission Product Inventory

Reference [11] states that the total inventory of fission products for LEU cores will not be significantly different from that associated with HEU cores. Additionally, because there are 22 plates in each LEU element as opposed to 18 plates in the HEU elements, the inventory per plate will be less in the LEU cores for the same operating histories.

3.11 Nuclear Instrumentation

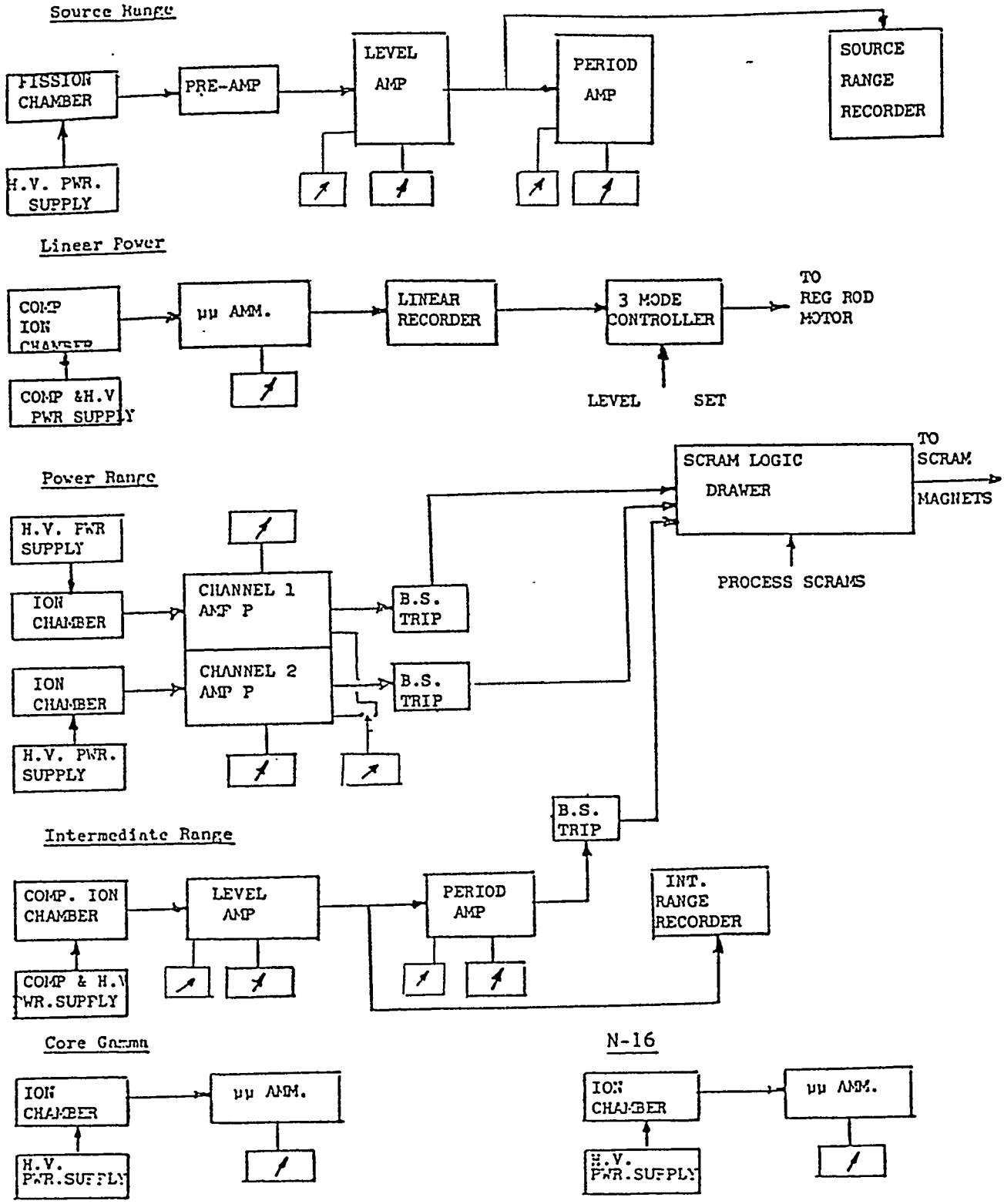
3.11.1 General Description

The UVAR nuclear instrumentation consists of those components necessary to monitor and display the operating parameters over all ranges of operation, from start-up to full power, and to automatically terminate operation before any limiting safety system setting is reached. The overall system is shown in Figure 3-7.

The Source Range contains the circuitry necessary to monitor reactor power level and period from shutdown through six decades of power level increase. The circuit utilizes a fission chamber as a neutron detecting device. The fission chamber is movable by use of a switch on the console. It is moved out of the core after start-up in order to minimize the burn-up of U-235 and buildup of fission products in the chamber while operating at high power levels. Both power level and period measurement are displayed on reactor console meters and the power level is repeated on a chart. The Source Range instrumentation also prevents rod withdrawal unless minimum source counts are present.

NUCLEAR INSTRUMENTATION SYSTEM

FIGURE 3-7



The Intermediate Range instrumentation receives its input from a compensated ion chamber and provides indication of power level and period over seven decades. Both power level and period measurement are displayed on the reactor console and power level indication is repeated on a chart. This instrument provides protection against a too rapid period by scramming the reactor if the period is less than 3 seconds. The scram is accompanied by an audible alarm.

The Power Range instrumentation contains two completely independent power range channels, each of which indicate reactor power over a range of 0 to 150 percent. Each channel is supplied with an input signal from an independent uncompensated ion chamber. The output from these channels are displayed by separate meters on the reactor console. Each of these channels provides independent scram protection from high reactor power. There is a range switch to select full power indication of 2MW when in forced cooling or 200 kW when in natural convection.

Indication of reactor power is also provided by a linear power instrument over 9 decades of reactor power through a range selector switch. This instrument receives its input from a compensated ion chamber and its output is displayed by a meter and a chart on the reactor console. The linear power channel recorder indication also serves as the sensing element for the automatic control system (see Section 3.12) which operates the regulating rod to maintain a set power level.

In addition to the above instrumentation, the following indications are provided for comparative observations of reactor power.

An ionization chamber, located on the ground floor in the heat exchanger room (adjacent to the primary piping), is used to detect gamma

radiation from the decay of nitrogen-16. The signal from this detector is a function of reactor power and is displayed on a meter and a chart at the reactor console.

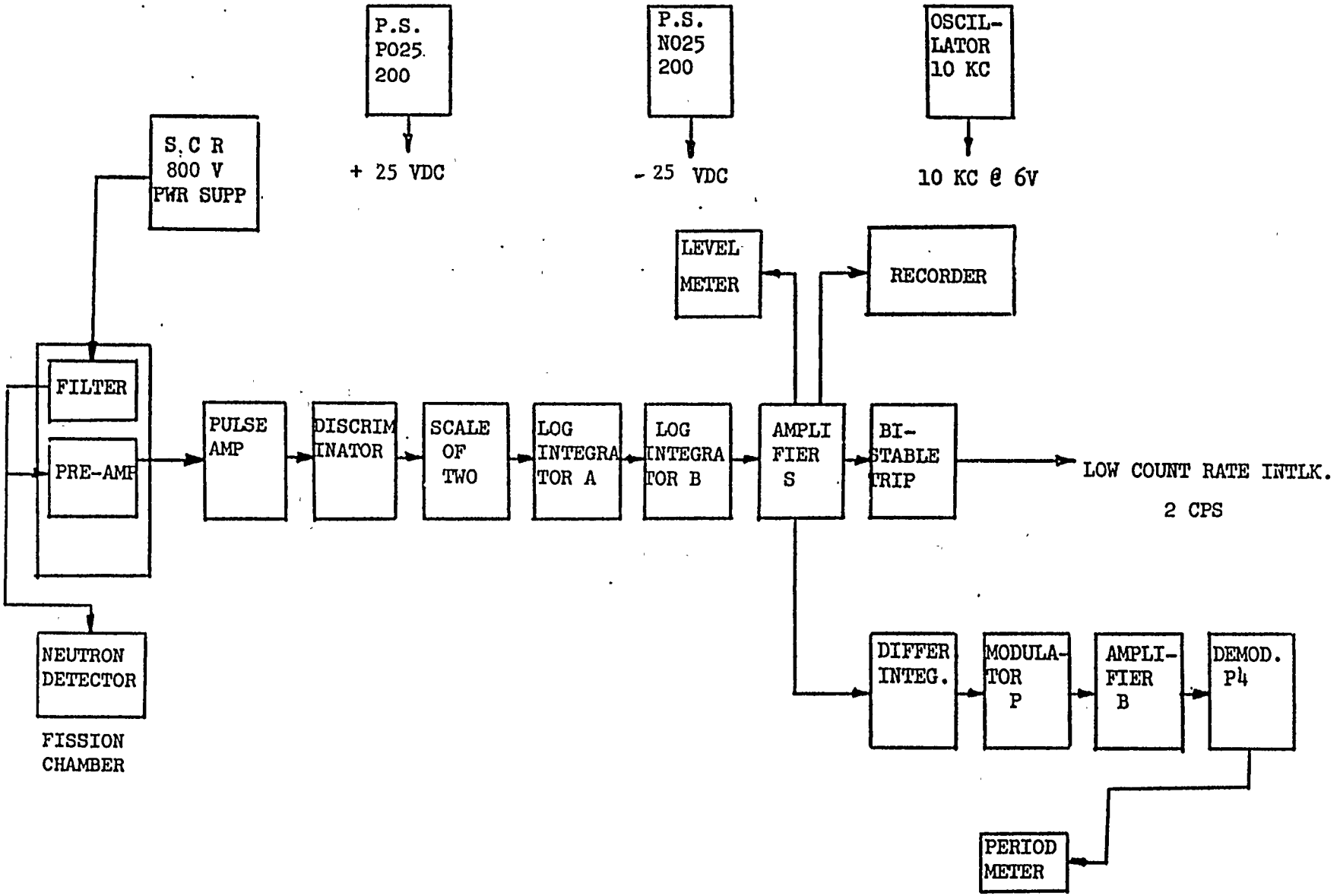
An ionization chamber, referred to as the core gamma monitor, is suspended at a fixed position typically about 7.0 feet above the reactor core. The signal from this detector is displayed on a picoammeter on the secondary console and is a measure of core gamma flux. The core gamma monitor is provided for comparative observation of power and has a floating point alarm that sounds on the common alarm panel.

3.11.2 Source Range Circuit

The Source Range Circuit (see Figure 3-8) contains circuitry required to monitor reactor power level and period from shutdown through six decades of power level increase. The circuit utilizes a fission chamber to detect neutrons.

A combination high voltage filter and pre-amp, mounted on the detector support pole, provides final high voltage filtering and a two stage pre-amplifier in one module. On entering the drawer, the input signal passes through a pulse amplifier, a discriminator, and a scale of two counter. The discriminator has a fixed discrimination level of 2.2 volts. Actual discrimination can be changed by varying the gain of the preamplifier or the pulse amplifier that precedes the discriminator. The scale of two counter divides the input frequency by two so the output is a square wave whose frequency is one-half of the input signal frequency. Log integrators A and B provide a DC voltage proportional to the log of the input frequency.

FIGURE 3-8 SOURCE RANGE DRAWER



Amplifier S is a DC Amplifier whose output provides source range log level indication, level bistable trip logic, input to the source range period second, and remote recorder output.

The period section of the Source Range Drawer consists of a differentiator integrator (D-I) which converts the level input from Amplifier S to signal proportional to the rate of change of reactor power level. Modulator P combines the DC input from the D-I with a 10 KC input from the Oscillator module. The resultant, a 10 KC signal proportional in amplitude to the DC input signal, is applied to amplifier B.

Amplifier B is an AC amplifier which amplifies the signal from Figure 3-8. Source Range Drawer Moderator P and feeds it to demodulator P4 where the AC signal is converted back to a DC signal proportional to the exponential rate of change of reactor power. The Demodulator P4 feeds a front panel period meter.

The bistable module installed in the Source Range Drawer is a solid state multivibrator circuit which prevents rod withdrawal in the absence of a sufficient count rate. The output is a logic signal of 0 volts (tripped) if the count rate is less than 2 counts per second, or 10 volts (untripped) if the count rate is greater than 2 counts per second. The Source Range Drawer contains a test module that performs alignment and operational checks of both the level and period sections without the use of additional test equipment.

3.11.3 Intermediate Range Circuit

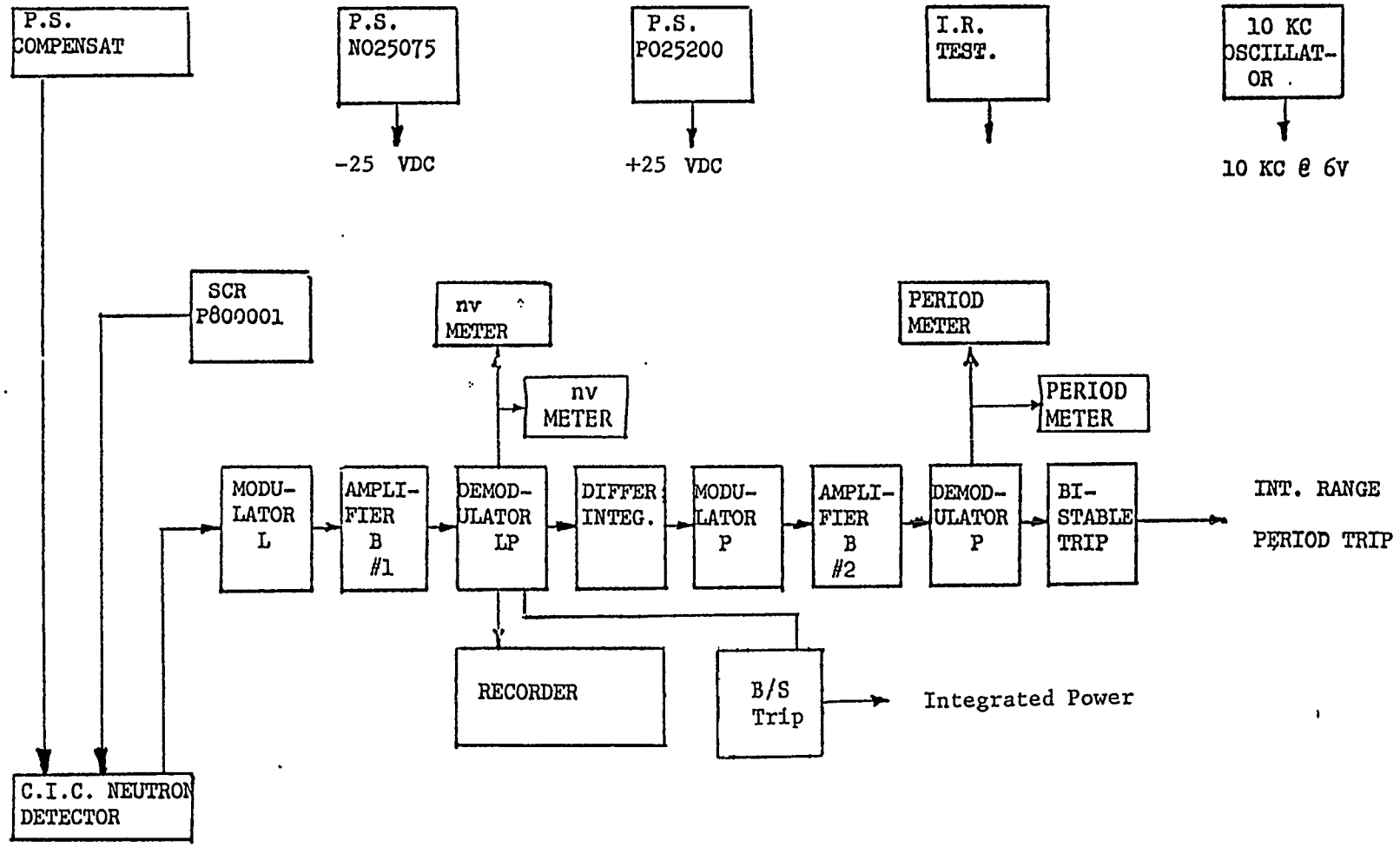
The Intermediate Range circuit (see Figure 3-9) receives its input from a compensated ion chamber (CIC) and provides log level indication

over several decades, period indication and scram and control logic outputs.

The power supply provides 200-800 volts DC high voltage to the CIC with regulation as close at ± 0.1%. A variable DC power supply provides variable compensating voltage to the CIC.

The DC current proportional to neutron level from the CIC is fed first to Modulator L where it is dropped across a string of forward biased diodes to a voltage proportional to the Log of the current and is combined with a 10 KC sine wave. The resultant is a 10 KC signal proportional in amplitude to the Log of the DC input current. The Demodulator, as the name implies, converts the AC output from Amplifier B back to a DC signal which is proportional to the Logarithm of reactor

FIGURE 3-9 INTERMEDIATE RANGE DWR.



flux level. The log level output of the demodulator feeds five devices:

1) Local log level meter

2) Remote log level meter

3) Remote recorder

4) Differentiator-Integrator for the period circuit

5) A bistable that activates the power integrator

The Differentiator-Integrator accepts an input from the Demodulator and converts it to a signal proportional to the exponential rate of change of the neutron flux. Modulation of this DC period takes place in Modulator LP where the signal is combined with a 10 KC sine wave and the output feed to Amplifier B No. 2 for amplification. Demodulator P receives an amplified AC signal from Amplifier B No. 2 and converts it to a DC signal which is proportional to the exponential rate of change of neutron flux (period). The outputs of the Demodulator P are:

1. A front panel period meter

2. A remote period meter

3. A bistable period trip set at a less than 3 seconds

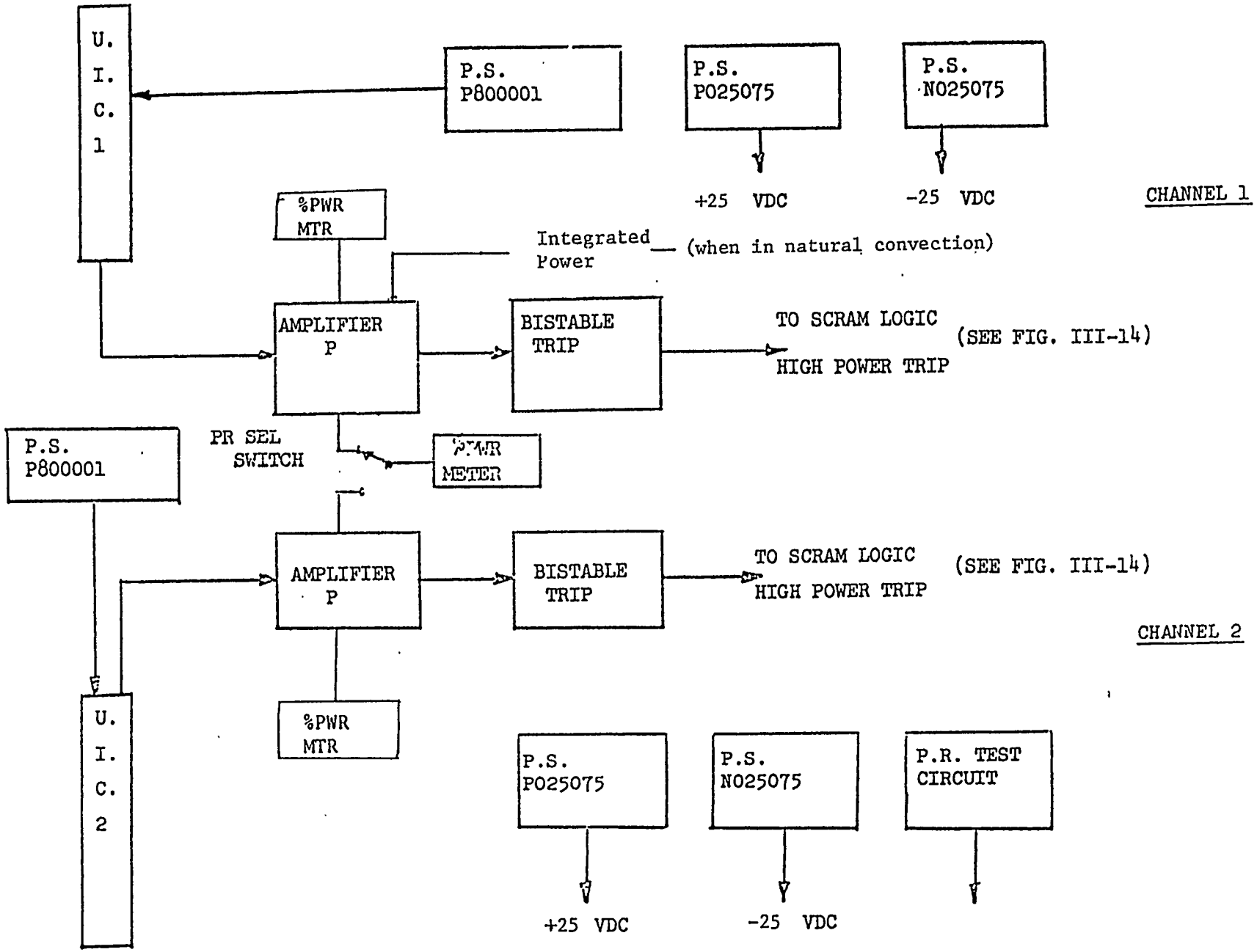
The bistable modules of the intermediate range circuit are identical to those in the source range circuit

The Intermediate Range drawer contains a test module that performs alignment and operational checks of both the level and period sections without the use of additional test equipment.

3.11.4 Power Range Drawer

The Power Range drawer (see Fig. 3-10) contains two completely independent power range channels which will indicate reactor power over the range of 0 to 150 percent. Each power range channel has its own detector power supply, and its own ± 25 volt power supply. The

FIGURE 3-10 POWER RANGE DRAWER



the power range drawer. Each power range channel is supplied an input from an uncompensated ionization chamber (UIC). Outputs from each channel include a common local power level meter, separate remote power level meter, and a high power bistable trip logic signal. In addition, Power Range #1 supplies a signal to the power integrator when in natural convection.

A high voltage power supply provides 200-800 volts DC to the detector. The output of the UIC is a DC current proportional to reactor power. The signal is fed to Amplifier P, which is a DC amplifier, where the signal is amplified to a level suitable for use. When in the "200 kW" range the full signal is amplified. When in the "2MW" range only one tenth of the signal is amplified. The outputs of Amplifier P are:

1. Local common percent power meter
2. Separate remote power meter
3. High Power Bistables
4. Power signal to the power integrator when in natural convection

It should be noted that the amplifier is designed so that a short or open circuit, in any of the outputs, will not cause the other outputs to vary more than a fraction of a percent.

The bistable modules of the power range circuits are identical to those described previously for the Source Range Circuit.

The Power Range drawer contains a test module that performs alignment and operational checks of each power range channel without the use of additional test equipment.

3.11.5 Scram Logic Drawer

The Scram Logic drawer (see Figure 3-11) contains the logic circuitry necessary to process the scram function inputs and to shutdown

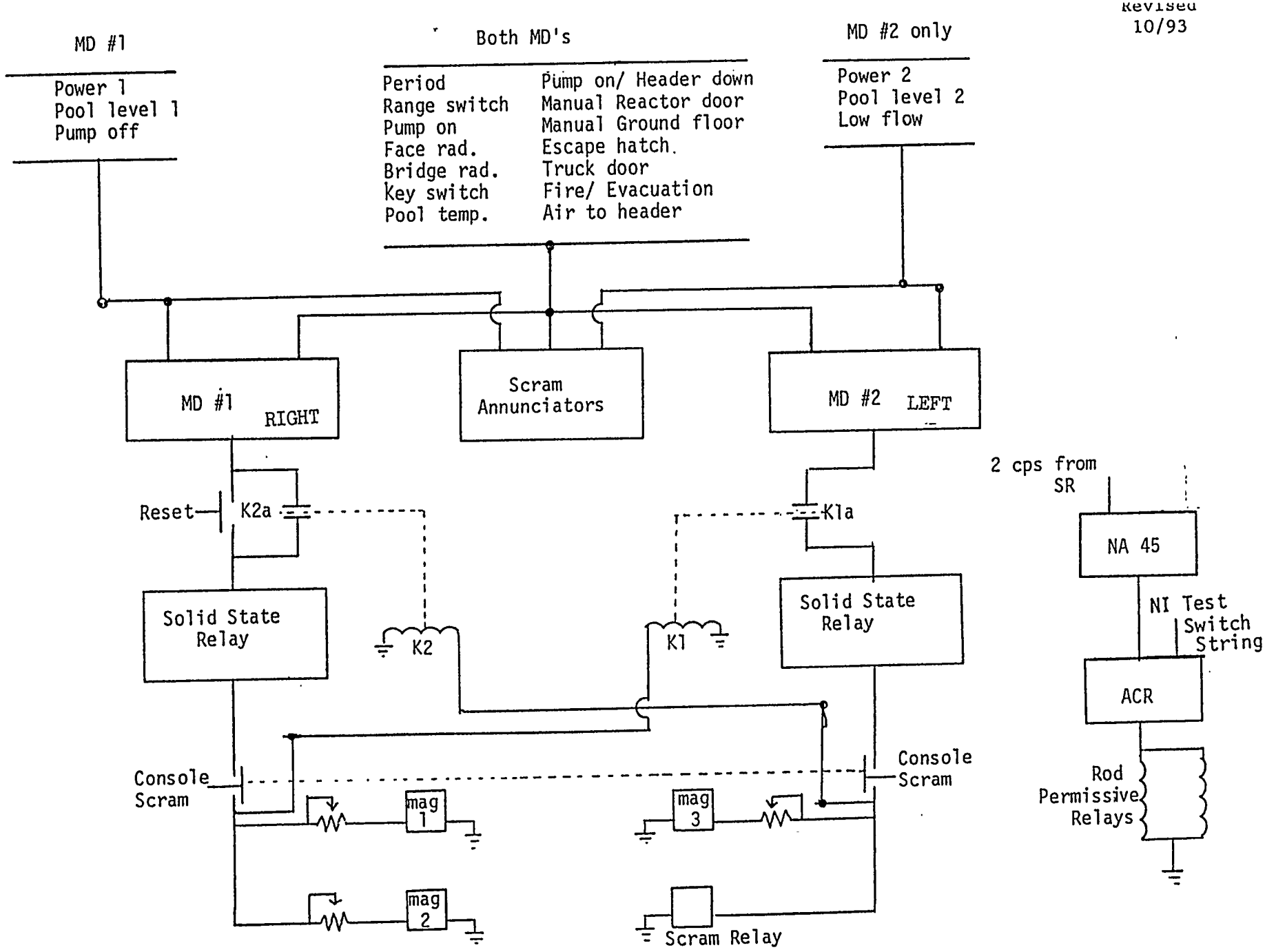


Figure 3-11 Scram Logic Drawer

the reactor automatically should conditions warrant. The drawer also contains the interlock circuitry to prohibit safety rod withdrawal if certain minimum conditions are not met.

To understand the operation of the Scram Logic circuit, it is only necessary to understand the operation of four basic modules. Negative logic is used throughout the system, in that the normal, safe, input signal ±10 volts and the abnormal, unsafe, signal is 0 volts. All available inputs to these modules may or may not be used.

1. Transistor Gate NA-45 consists of five separate, four-input, negative logic AND gates, hence the designation NA-45. For each separate AND gate, all four inputs must fall to zero volts to obtain a 0-volt output signal. Any input at +10 volts will hold the output of that gate at +10 volts. The inputs (up to 20) are logic 0 or +10 volt signals and the outputs (up to 5) are also logic 0 to +10 volt signals. As explained later, the rod withdrawal interlock is derived from two logic inputs to NA-45.
2. The Auxiliary Control Module takes logic inputs in the form of 0 or +10 volt signals and provides a relay output capable of handling 110 VAC and 2 amps. The input stage consists of a four input OR gate where all inputs must be at +10 volts to have the relay energized. The relay is de-energized if any input is at zero volts.
3. There are two Mixer Driver B's. A Mixer Driver B is essentially a 28 input OR gate. Any one of the 28 logic inputs falling to 0 volts is sufficient to cause the output to fall to

0 volts. Only when all inputs are at +10 volts is the output at +10 volts. The input is 28 logic signals, while the outputis one logic signal.

4. There are two Solid State Relay modules. A Solid State Relay Module takes one logic signal (0 to +10 volts) as its input and provides up to 5 amps DC of output current to the scram magnets if a safe input condition exists. The Solid State Relays are subject to one type of failure that could render the model inoperable as a device for cutting off magnet current. This type of malfunction of the entire module would necessitate the simultaneous failure of two components within the module, in the form of a short circuit in two series silicon controlled rectifiers (SCR). Built-in circuitry within the drawer has been provided that will annunciate a short circuit in one SCR as a warning light. If a short circuit occurs subsequently in the other SCR, the solid state relay will continue to provide current to the scram magnets even if a unsafe input is applied. As will be explained in the overall operation of the Scram Drawer, even the existence of the above mentioned conditions will not render the entire system inoperable as a parallel network exists which could de-energize at least one safety rod and thereby shut the reactor down.

The Scram Logic Drawer, as a safety system, can be divided into two sections. Namely, a scram logic process section and an activation section. The process section takes logic signals from the various

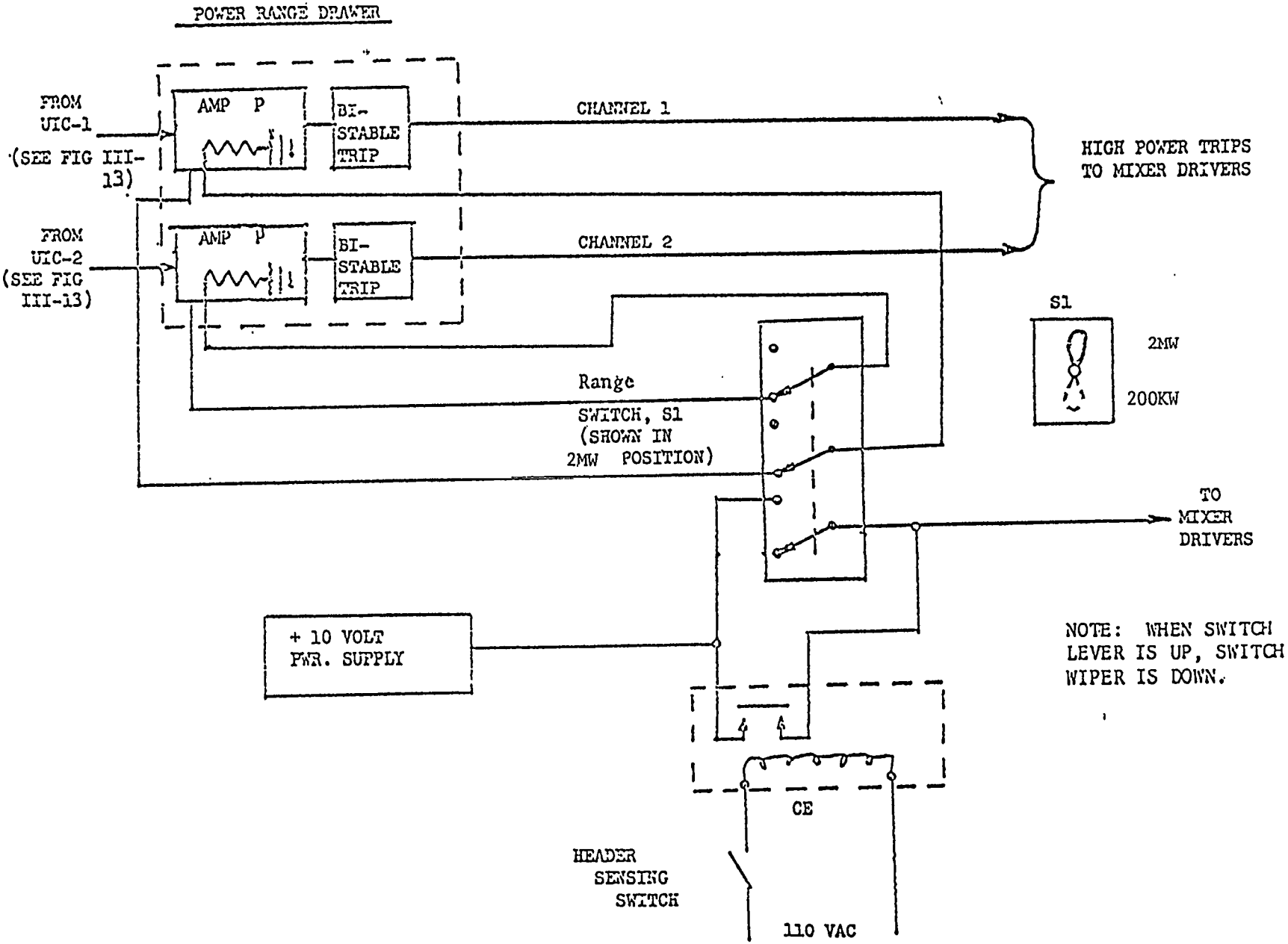
bistables, power supplies and relays; processes these signals with respect to preconditions and emits output signals that exercise either scram control or rod interlock control. The modules included in this section are the NA-45 gate circuits and the Auxiliary Control Relay. The actuation section, consisting of the Mixer-Drivers and the Solid State Relays, take only safe or unsafe logic inputs, and, depending on the nature of the inputs, control current to the safety rod scram magnets.

The rod withdrawal interlock is derived from two logic inputs to NA-45 (1). A +10 volt signal is emitted from the source range level bistable if the source count rate exceeds 2 counts per second. A second +10 volt signal comes from a series circuit that is closed when source range, intermediate range, pool temperature, and power range instruments are not in test. These two signals are fed to one gate. If these inputs are at +10 volts the appropriate output is at +10 volts on an Auxiliary Control Relay (ACR) which energizes its output relay permitting safety rod withdrawal. If either input to the ACR drops to zero, this zero volt input signal will cause the output relay to de-energize, preventing the withdrawal of any shim rod.

The reactor can be operated at 2 megawatts with forced convection cooling or at 200 kilowatts with natural convection cooling. The High Power Trips are initiated from the power range drawer (see Figure 3-10) and provide overpower protection in both the natural convection cooling mode and the forced convection cooling mode of operation as shown in Figure 3-12. A range switch is used to determine the scram point for each mode.

In the natural convection mode (see Figure 3-12), the flow header is down and header position relay CE is de-energized. A safe +10 volt logic

FIGURE 3-12 HIGH POWER TRIP



signal is passed through the range switch only if the switch is in the 200 kW position. Under this condition, the power range channels are sensitive over a range of 0-300 kW for an amplifier output of 0-150% of normal range, i.e., 100% of output from the amplifier corresponds to 200 kW. If the reactor power level reaches 250 kW, the power range channel will indicate a power level of 125% and will send an unsafe (0 volt) Figure 3-12 High Power Trip signal to the mixer drivers scramming the reactor.

When the reactor is operating in the forced convection mode, the flow header is in the UP position. Therefore, relay CE is energized, which allows the range switch to be placed in the 2MW position without losing the 10 volt safe signal. In the 2MW position, the range switch also reduces the output sensitivity of the two power range amplifiers by a factor of ten. Each channel indicates over a range of 0-150%, which corresponds to a maximum reactor power of 3MW. The scram trip point is also increased by a factor of ten by placing the range switch in the 2MW position and will scram the reactor when reactor power reaches 2.5 MW. When operating in the natural convection mode, any attempt to change the position of the range switch to the 2MW position will immediately initiate the scram, through loss of the 10 volt signal through the switch.

Referring again to Figure 3-11, the intermediate range period trip function originates at the period trip bistable, (see Figure 3-9). This logic signal is sent directly to the Mixer Drivers.

The scram actuating portion of the Scram Logic Drawer consists of two independent channels cross connected in such a way as to afford

maximum scram protection against component malfunction. The two Mixer Drivers receive several logic inputs in parallel. If one of these inputs is an unsafe signal (0 volt), the output of both MD's will be at zero volts. The input to each Solid State Relay going to zero causes the outputs to stop conducting, cutting off current flow to the scram magnets. To nullify the effects of a complete failure of one MD, the two scram channels are cross connected through relays R1 and R2. If a failure occurred in one of the MD's, say MDB1, which would prevent it from tripping off when an unsafe input signal is received, MDB2 would be tripped off by the same unsafe input signal, SSR2 would stop conducting, dropping magnet 3 and de-energizing relay R2. The contacts on R2 which feed an input to SSR1 would be opened, causing SSR1 to also stop conducting the dropping magnets 1 and 2.

Both mixer drivers receive separate inputs from redundant channels (i.e. high power, low pool level, and low flow). An unsafe (0 volt) signal from one of these inputs causes the affected mixer driver to give a 0 volt output causing a reactor scram.

The simultaneous failure of both MD's in the safe mode or a failure of four diodes in two separate modules, the SSR's, could result in the scram logic system being rendered as "can't scram."

3.12 Scrams, Interlocks, and Alarms

3.12.1 Scrams

The following scrams are required by the UVAR Technical Specifications:

Scram	Operating Mode Required
1. 2 Safety Channels for high power scram	
a) range switch in high power position	Forced convection
b) range switch in low power position	Natural convection
2. Bridge radiation monitor scram	All modes
3. Pool water high temperature scram	All modes
4. Loss of power to primary pump scram	Forced convection
5. Application of power to the primary pump scram	Natural convection
6. Low primary coolant flow rate scram	Forced convection
7. Manual scram button	All modes
8. Fast reactor period scram	All modes
9. Air pressure to header scram	All modes
10. Low pool level scram	Forced convection

The above listed scrams must be operational as required during reactor operation. Other scrams, not listed, may be added as appropriate to provide for added protection of personnel, experiments and equipment.

3.12.2 Interlocks

The UVAR Technical Specifications requires an interlock on the Source range instrument which prevents shim rod withdrawal unless a minimum of 2 cps are detected.

3.12.3 Alarms

Both audible and visual alarms are used at the reactor console to alert the operator of alarm conditions. A continuous tone audible alarm and a red light visual alarm accompanies a reactor scram signal. This audible alarm may be silenced by either resetting the scram logic drawer

or pressing the "silence" button on the common alarm panel. The visual alarm is cleared only by resetting the scram.

An intermittent tone sounds and a visual indicator is actuated for each of the following conditions:

a) Regulating rod control shifting from automatic to manual

b) High radiation on any area monitor or on either argon monitor

c) High radiation on core gamma monitor

d) High radiation on criticality monitor

e) High radiation on constant air monitor

f) Entry into the demineralizer room

g) Entry into the heat exchanger room

h) High differential temperature across reactor core

i) High demineralizer conductivity

j) Secondary pump de-energized

The audible alarm will automatically reset after about two minutes or may be reset manually by pressing the "silence" button.

Local alarm bells are supplied at the heat exchanger room and demineralizer room when the key switch is on which warns personnel entering the area of a possible high radiation area.

Other audible and visual alarms may be used, as necessary, to provide extra personnel safety or equipment protection.

3.13 Automatic Control For Maintaining Constant Power

A voltage signal proportional to reactor power is developed by a slide wire potentiometer in the linear power recorder. This signal is compared to the voltage developed by the "Power Set" potentiometer on the control console. Any difference in these signals is displayed on a

deviation meter and supplied to the controller as an error signal. The controller converts this small error signal into 60 cycle power either in phase or 180° out of phase with line voltage. This power supplied to the servo motor for the regulating rod will drive the rod in if the linear signal is higher than the power set voltage or out if the linear signal is below the power set voltage.

Several conditions will automatically cause control to shift into the manual mode and sound an alarm to alert the operator that power is no longer being controlled automatically. These are:

1) Any attempt to move the regulating rod with the normal control switch; this insures that manual control is always instantly available to the operator.

2) The regulating rod either at its top limit or bottom limit; this insures that regulating rod has free movement to control reactor power.

3) The error signal, as displayed on the deviation meter, exceeds 7.5% (arbitrary units); this insures control is shifted if the regulating rod is unable to control power for any reason, such as the reg rod being stuck.

4) The linear power recorder is turned off. This ensures the feedback loop is complete.

5) A switch is provided that allows the operator to select either the manual or automatic mode of operation.

References For Chapter 3

1. EG&G Idaho, Inc.,"University of Virginia Test Research And Training Reactor 2, Standard And Partial Fuel Element Assembly", Drawing Number 428500, Revised August, 1989.

2. EG&G Idaho, Inc., "University of Virginia Test Research And Training Reactor 2, Control Fuel Element Assembly", Drawing Number 428501, revised August, 1989.

4. EG&G Idaho, Inc.,"University of Virginia Test Research And Training Reactor 2, Sideplates", Drawing Number 428502, Revised August, 1989.

3. EG&G Idaho, Inc.,"University of Virginia Test Research And Training Reactor 2, Shock Absorber Seat, Adapter, & Bail", Drawing Number 428503, Revised, August 1989.

4. EG&G Idaho, Inc.,"University of Virginia Test Research And Training Reactor 2, Fuel & Guide Plates", Drawing Number 428504, Revised August, 1989.

5. EG&G Idaho, Inc.,"Test Research And Training Reactor LEU Fuel Plate", Drawing Number 422264, Revised August 1989.

6. Diamond Power Speciality Corporation, "Shim Safety Rod Assembly Top Magnet Control", Drawing #EX-7935-0, April 21, 1958.

7. Diamond Power Speciality Corporation, "27 Feet Regulating Rod Assembly", Drawing #EX-7769-0, April 21, 1958.

8. Diamond Power Speciality Corporation, "Element-Shim Safety", Drawing #7006181122, October 26,1960.

9. Freeman, D., Neutronic Analysis For The UVAR Reactor HEU To LEU Conversion Project, Master's Thesis For The Nuclear Engineering and Engineering Physics Department, University Of Virginia, July, 1989.

10. EG&G Idaho, Inc.,"TRTR-2 For University of Virginia Standard, Partial And Control Fuel Element Assemblies For The University Of Virginia Reactor", Revision 1, June, 1989.

11. U.S. Nuclear Regulatory Commission, Safety Evaluation By The Office Of Nuclear Reactor Regulation Supporting Conversion Order To Convert From High Enriched To Low Enriched Uranium Fuel, Facility Operating License NO. R-61, Worchester Polytechnic Institute, Docket No. 50-134, September 12, 1988.

4.0 REACTOR SYSTEMS

4.1 Reactor Pool

The pool in which the reactor operates is 32 feet long, 12 feet wide, 26 feet 4 inches deep, and holds about 75,000 gallons of water. An aluminum gate is provided approximately mid-way of the pool so that either side may be drained independently of the other while the reactor itself is adequately shielded by the water in the undrained side. With the reactor in position at a far end of the pool, the radiation level in the emptied section will be low enough to permit personnel to alter or set up experimental equipment and perform maintenance.

The south end of the pool is above ground level and faces the main radiation laboratory experimental area. The shielding provided by the water and the pool wall is augmented by the addition of sufficient concrete to reduce the radiation well below tolerance levels at maximum operating power. The south wall of the pool is penetrated by experimental facilities which will be further explained in Section 6.0.

The level of the water is about 20 feet above the active core when the pool is full. An alarm and scram is actuated by two pool level devices if the pool level drops 19 feet 2 inches above the top of the active core.

Figure 3-1 shows a vertical section of the pool and related building spaces.

4.2 Filling and Draining the Pool

Two systems may be used for filling the UVAR pool; 1) a

dedicated fresh water make-up system, and 2) the main demineralizer system.

The dedicated fresh water make-up system is located in the UVAR room and consists of a small filter and H-OH mixed bed ion exchangers to which city water is supplied. The system discharges deionized water into the UVAR pool through a stand-pipe to preclude the possibility of pool water backflow into the city water system. The system has a flow rate of about 5 gallons per minute.

The pool can also be filled using the main demineralizer system as shown in Figure 4-1. City water enters a catch tank through a hand valve and a float valve. The water entering the pool through the demineralizer system is drawn from this tank. The float valve discharge is higher than the tank overflow, thus precluding the possibility of any backflow of radioactive water into the city water system. The pool can be filled at a rate up to about 20 gallons per minute through a mixed bed demineralizer. With the pool gate in place, either side of the pool may be filled independently.

The pool is drained through two manually operated valves located in a sump pit in the heat exchanger room. These valves are normally locked shut. Either side of the pool may be drained when the gate is in place. The discharge from the drainage system empties into the waste pond and is described in Section 4.8.

4.3 Primary Cooling Systems

With the reactor in position at the south end of the pool, an air operated header may be raised into place. This header is actuated by the emission of compressed air at about 50 psi into a header skirt which floats the header up to the reactor grid plate. Once positioned the header is held in place by a differential pressure of 0.30 psi created by the downward flow in excess of 1000 gallons per minute through the reactor to the primary piping system. After the pump has started and sufficient flow is established to hold the header in place, the air pressure is vented to allow the header to drop automatically for natural convection cooling in case of pump failure. Such pump failure initiates a scram as does the existence of 2 psi air pressure in the header. This precludes the possibility of raising the header while the reactor is operating in the natural convection mode with the pump secured. The reactor is in a scram condition if the pump is operating with the header down.

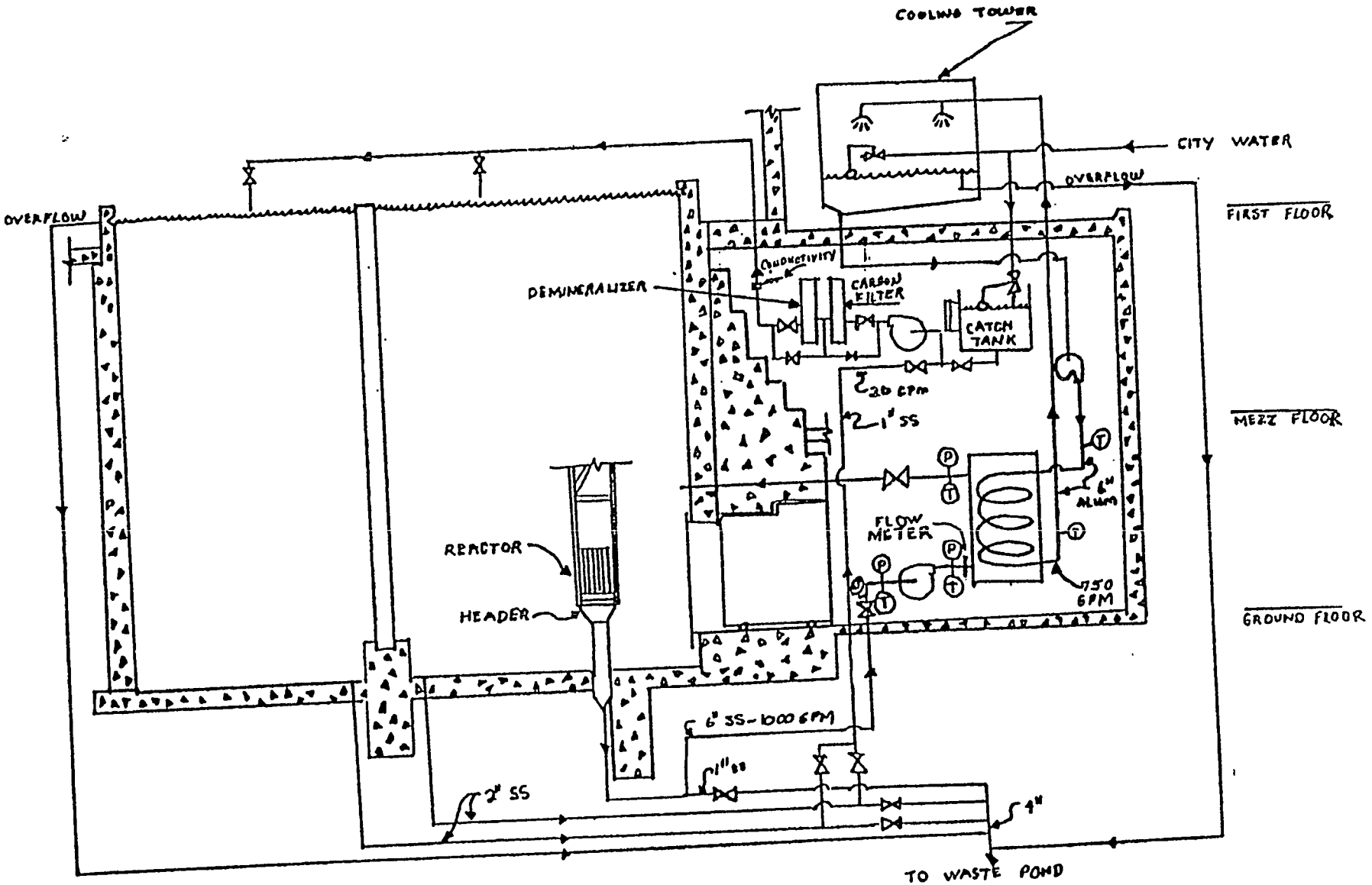


Figure 4.1 Cooling System Flow Diameter

The water flows from the header through a six inch line to a strainer and the primary pump. The primary pump is of the centrifugal type with a stainless steel casing, impeller, and shaft. A self-adjusting mechanical seal is used to seal the shaft. The pump is driven by a 30 horsepower 1700 RPM induction motor and is rated at ~ 1100 gallons per minute flow against a 50 foot head of water. The actual flow rate is ~1055 gal/min. The flow rate is measured by the differential pressure across an orifice in the primary piping and displayed on the secondary console.

The water proceeds through the six inch line, through an orifice, used to measure the flow rate, into the shell side of an aluminum tube and shell heat exchanger. The primary water makes one pass through the heat exchanger and is returned to the pool. The water enters the pool through a flow diverter which directs it toward the wall at the greatest distance from the reactor, thus gaining the greatest mixing and minimizing nitrogen-16 gamma activity at the pool surface.

Water temperature and pressure are measured on the inlet and outlet sides of the heat exchanger. The temperatures are displayed on the secondary console in the reactor room. A separate continuous monitor is located above the core which will initiate a scram if the pool water temperature exceeds 105°F.

4.4 Measurement of Temperature Differential

A system has been installed to continuously monitor the temperature rise across the core, delta-T, when the reactor is operated with forced convection cooling. The Delta-T value measured directly by this system, and the primary flow rate can be used to determine the reactor thermal power level. The sensing elements used in the system are platinum resistance temperature detectors (RTD). The RTD that senses core inlet temperature is located in the reactor pool about three feet above and to the side of the core. Core outlet temperature is sensed by an RTD in the primary coolant line just upstream of the primary coolant pump. Each temperature is measured independently by a single commercial instrument which also determines the analog difference between the two measured temperatures. The differential temperature outlet of the commercial meter is displayed at the reactor console on a digital meter. Three alarms are provided as part of this system. There are both an analog alarm and a fixed digital alarm that are always set at just above the normal Delta-T corresponding to 2 MW. The other is a digital alarm adjustable by the operator for those times that the reactor is operated at less than 2 MW.

The range of the instrument is 0-20 °F, while the normal Delta-T across the reactor core at two megawatts is about 13 °F. At the option of the operator the displayed value can be momentarily scaled to read directly in megawatts assuming the nominal primary flow rate.

An Integrator is attached to the Delta-T system to keep track of integrated power in megawatt-hours. The single parameter integrator assumes a nominal primary coolant flow rate. When the reactor is operated in natural convection, the input signal for the integrator is derived from the reading on Power Range #1.

A separate system using thermistors is also available to measure the coolant inlet and outlet temperatures individually. They are read periodically and subtracted manually to obtain the temperature rise across the core as a cross check on the Delta-T monitor.

4.5 Secondary Cooling System

Water on the secondary side of the heat exchanger is pumped at about 1200 gallons per minute from the basin of a conventional cooling tower rated at a cooling capacity of 2 MW with a 95 °F entering water temperature and 73 °F wet bulb atmospheric temperature. The system utilizes a conventional centrifugal pump driven by an induction motor. Water for evaporative cooling in the cooling tower comes directly from the city water supply and overflows to the waste pond. Water temperature is measured on the inlet and outlet of the heat exchanger and is displayed on the secondary console in the reactor room.

4.6 Design Specifications

The design specifications for the Heat Exchanger, Cooling Tower, Secondary Pump and Primary Pump are given in Tables 4.1 through 4.4.

4.7 Water Purification

The pool water purity is maintained by circulating it at a rate of 20 gallons per minute through a carbon filter and a mixed bed ion exchange demineralizer. The water is normally maintained at a pH of 6.0 to 7.0 with a conductivity of less than 5 micromhos.

4.8 Liquid Waste Disposal System

The reactor facility can collect radioactive liquid waste in two underground retention tanks of 5000 gallons each located outside of the Reactor Facility building, but within the site area. The waste is recirculated and filtered, as well as given decay time before it is either discharged into the pond or discharged along with the pond as normal procedure. Other storage tanks within the Reactor Facility may also be used to temporarily store liquid waste. The option for sanitary sewer release has not been exercised but is not precluded. All radioactive releases are made in conformance with applicable regulations. Two additional tanks of 250 gallons receive all waste from the Hot Cell. These tanks were installed as underground retention tanks in the

TABLE 4.1 Heat Exchanger Specifications

Heat Transferred -- 6.83×10^6 Btu/h

Materials -- Aluminum. All materials must be compatible with aluminum. For this reason no copper containing alloys can be used.

Maximum Length -- 18 feet

	Shell Side	Tube Side
Fluid Circulated	High purity water	Cooling tower water
Liquid Flow	1100 gallons/minute	1200 gallons/minute
T inlet	110.2°F	82°F
T outlet	95°F	93.4°F
Pressure Drop Allowed	8 psi	8 psi
Design Pressure	50 psi	50 psi
Test Pressure	75 psi	75 psi
Design Temperature	150°F	150°F
Inlet and Outlet Pipe	8 inch	8 inch

To be fabricated in accordance with ASME Code, Section VIII, Division 1. Shall be inspected, certified, and stamped with the Code U - Symbol.

TABLE 4.2 Cooling Tower Specifications

Water Flow Rate	1200 gallons/minute
Heat Transferred	6.83×10^6 Btu/h
Wet Bulb Temperature	$73^\circ F$
Water On	$93.4^\circ F$
Water Off	$82^\circ F$

Fill and construction materials -- Redwood

All materials must be compatible with aluminum. For this reason no copper-containing alloys can be used.

TABLE 4.3 Secondary Pump Specification

Centrifugal end suction pump

To pump 85°F chromated water from cooling tower

Flow Rate: 1200 gallons/minute

Dynamic Head: 70 feet

All wettable parts to be stainless steel

To include Teflon packing

Flooded suction

Mounted on base plate with coupling

Motor: 1750 rpm, 3-phase, 60-cycle, 220-volts

Open drip proof enclosure

TABLE 4.4 Primary Pump Specification

Centrifugal end suction pump

To pump 70° - 100°F Demineralizer water from pool through heat exchanger

Flow Rate: ~1100 gallons/minute

Dynamic Head: 50 feet

All wettable parts to be stainless steel\

Size of Impeller: 10 Inches

Mounted on Base Plate with Coupling

Motor: 30 H.P., 3 phase, 60-cycle, 220 volts

event of waste discharge from the hot cell. These tanks empty into the pond.

The water released from the pond is sampled prior to, at the beginning, during and at the end of each release. The results of these sample analyses are maintained by the reactor health physicist. No waste is released off-site with an active concentration in excess of $1x10^{-7}$ microcuries per milliliter, annual average. This limit is based on 10 CFR Part 20 limits for facilities producing waste where no iodine 129 or radium are present.

4.9 Building Ventilation System and Airborne Effluents

The reactor building ventilation system consists of the following major items.

1. An axial vane exhaust fan on the reactor room roof, the primary function of which is to provide circulation for the reactor room.

2. A short, duct-work stack on the reactor room roof.

3. A centrifugal blower on the mezzanine which exhausts the ground floor experimental facilities, hot cell, and fume hoods, through duct-work, to the suction of the roof top fan.

A schematic diagram of the system is shown in Figure 4-2 showing the fan, blower, nominal flow rates, and the general layout of the various connecting duct work. Ducts leading from the reactor experimental facilities (beamports, large access and thermal column access), the hot cell, and fume hoods are all provided with in-line filters and either have, or have provision for, in-line radiation monitoring.

As a result of normal reactor operations, and in the event of certain types of experimental failures that may be expected to occur,

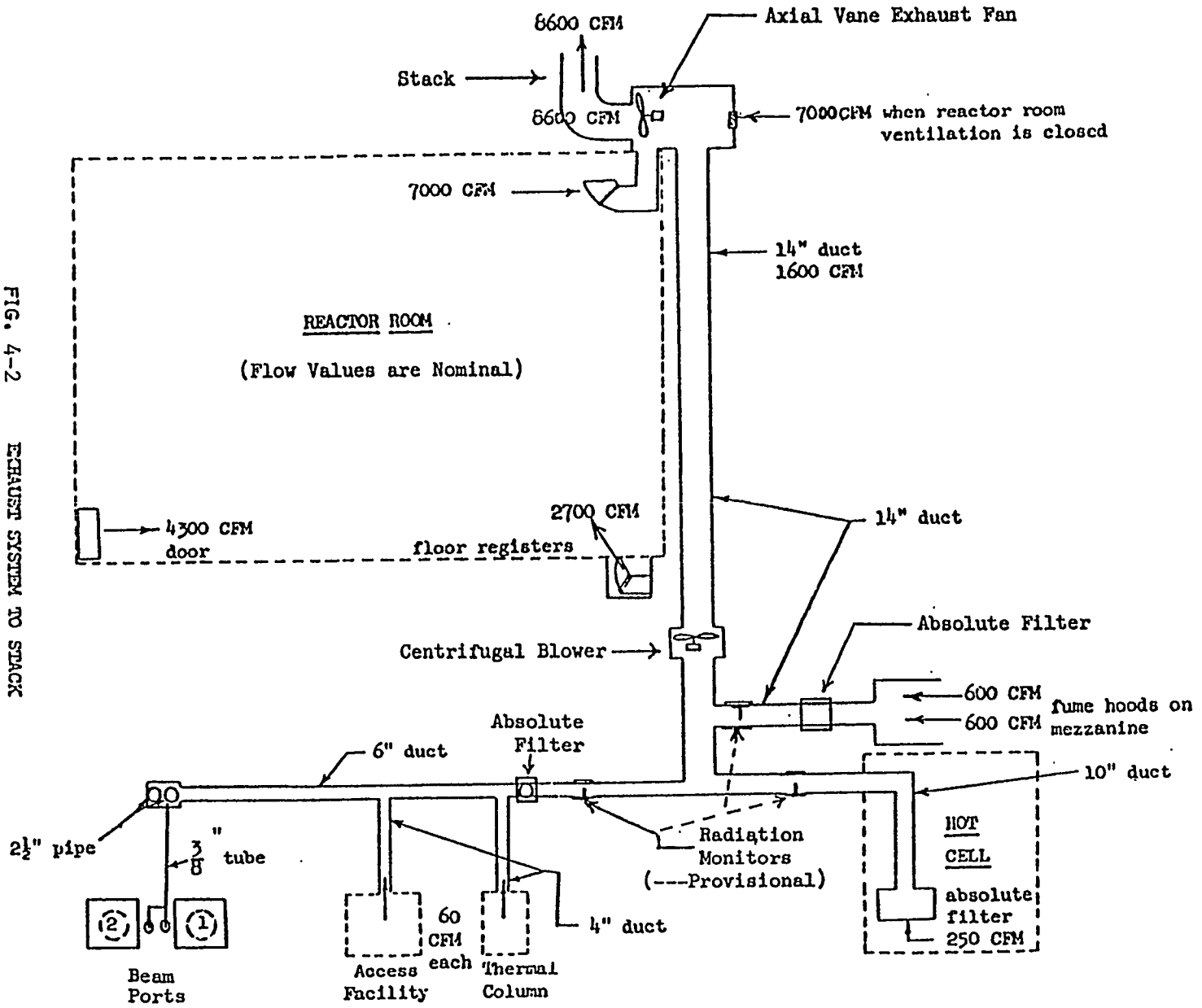


FIG. 4-2 EXHAUST SYSTEM TO STACK

there may be some release of gaseous, or airborne particulate, radioactive material from the facility. In general, such effluents would be released from the stack. The purpose of this section is to identify normally occurring and potential sources of such effluents, and to evaluate the consequences of both.

4.9.1 Sources

The gaseous radioactive isotope produced during normal operations which is of potential concern is Argon-41, produced by thermal neutron capture in the stable Ar-40 isotope present in air to about 1.3% weight. A small amount of Ar-41 is produced and released, as a result of air dissolved in the reactor pool water, being irradiated in passing through the reactor, and then coming out of solution into the reactor room atmosphere. This isotope is subsequently released as the reactor room is normally ventilated. While Ar-41 is continuously produced while the reactor is operating, its release is somewhat variable and to a large extent uncontrollable. However, the Ar-41 releases from the UVAR are small and of negligible consequence, as shown below.

Ar-41 may also be produced if air is irradiated in the various facilities on the ground floor experimental area. This source can be controlled by limiting the volume of air exposed and is thus very small. Brief releases of Ar-41 would be a normal consequence of reflooding a beamport, in which air had been irradiated. However, when in operation the beamports are usually filled with a low activatable gas, such as helium or carbon dioxide.

Accidental gaseous releases may occur as a result of experiment failure, either in an experimental neutron irradiation facility, in a

fume hood or hot cell. A severe case of such a failure, the complete melting of a 1-watt U-235 fueled experiment, is analyzed in Section 5.4 of this document.

4.9.2 Consequences of Gaseous Effluent Release - General

Figure 2-1 is an aerial photograph which indicates the position of buildings nearest to the reactor, including those constructed since the photograph shown in Figure 2-2 was taken. There follows an analysis of the atmospheric dilution of the reactor stack effluent at 2 points on the site boundary (fence) and at the seven buildings nearest to the reactor, identified in Figure 2-1. This analysis is performed on a yearly average or long-term basis and is thus pertinent to the calculation of the consequence of materials continuously released during operations.

The following assumptions are made in the calculations:

1. Wind frequency and velocity data taken at the site, Table II-1 and II-2, are representative of average conditions.

2. Pasquill-D type of dispersion conditions exist on the average over a year's time, with a wind speed of 2/3 of the annual average measured (Reference 1 at end of this Chapter).

3. No elevation differences are accounted for (i.e., "0" stack height).

4. Effluent materials are uniformly distributed over each 45° sector (Reference 2 at end of this Chapter).

5. No credit is taken for the rise or mixing of materials leaving the stack, although the stack effluent velocity is ~ 15 ft/sec.

The dispersion equation recommended in Reference 2 for releases is:

$$\frac{X(x_i)}{Q} = \left(\frac{2}{\pi}\right)^{1/2} \frac{f_i}{\sigma_z(x_i)\bar{\mu}(2\pi x_i/N)}$$

where

$X(x_i)$ = the concentration of material at x_i, Ci/M^3

Q = the average release rate of materials at the stack, Ci/sec.

f_i = the fraction of time during a year that the wind blows into compass section i.

x_i = distance to site, in sector i, M.

$\sigma_z(x_i)$ = standard deviation of plume in vertical direction at distance x_i, for Type-D conditions M.

$\bar{\mu}$ = average wind velocity, M/sec ($\bar{\mu}$ = 4.63x2/3 = M/sec)

N = number of compass sectors for which there is data (N=8)

The results of the application of this equation to the 9 sites are presented in Table 4.5. Column 8 shows the percent of the 10 CFR Part 20 limit of Ar-41 that would result from a continuous release of 10^{-5} Ci/sec. (10 μ Ci/sec).

For long term releases, dilution factors, X/Q, of about 2.5×10^{-4} exist even very close to the release point, resulting in an average Ar-41 concentration of about 6.5% of the Part 20 limit for Unrestricted Areas assuming a 10 μ Ci/sec release rate. This rate will be shown to be higher by at least a factor of 20, than that which may be expected for this isotope.

For accidental releases and other short term releases, Pasquill-F type conditions, a 1 meter/sec wind speed, and 0 stack height will be

conservatively assumed as described in TID-14844. A dilution factor at 70 meters of 0.039 for these conditions will be used to determine downwind isotopic concentrations. the consequence of noble gas release under stable meteorological (Type F) conditions will be evaluated by determining whole body dose from the cloud, as an undiluted line source.

4.9.3 Specific Cases

In this section, several specific cases of gaseous release will be considered and the consequences thereof evaluated.

4.9.3.1 Argon-41 from Reactor Room, Long Term

The production and release to the reactor room of Ar-41 was discussed in Section 4.9.1. The specific activity of this isotope in the reactor room has been monitored for several years. With the reactor room ventilated, the concentration normally does not exceed 1/30 of the MPC for Ar-41 in Restricted Areas (2×10^{-6} μ Ci/cm^3. The normal exhaust rate for this room is 7,000 CFM (3.3×10^6 cm^3/sec). If one assumes that an Ar-41 concentration of 6.7×10^{-8} μCi/cm^3 exists continuously in the reactor room, the resulting effluent source is:

$$(3.3 \times 10^6 \text{ cm}^3/\text{sec})(6.7 \times 10^{-8} \mu\text{Ci/cm}^3) = 2.2 \times 10^{-1} \mu\text{Ci/sec}$$

or about a factor of 45 lower than that assumed for the calculations of Column 8, Table 4.5.

Even considering the factor of 2 increase for 2 MW operation, the release associated with Ar-41 production in the reactor pool appears to be of insignificant consequence.

4.9.3.2 Reactor Room Ar-41, Persistent, Stable Conditions

The most extreme case for this type of release would be that of a long persistence of Type F dispersion conditions. As is standard

TABLE 4.5

PERCENT OF 10 CFR PART 20 LIMIT OF A-41 RESULTING FROM CONTINUOUS RELEASE OF 10^{-5} Ci/SEC

Site No.	Site Identification	Distance (x_i) Meters	$\sigma_z(x_i)$ Pasquill-D (Ref. 3)	Bearing from Reactor	f_i	$\frac{X}{Q} \times 10^4$	% of MPC for A-41 with $Q=10^{-5}$ Ci/sec
1	North Fence[a]	50	2.6	N	0.10[a]	2.6	6.5
2	South Fence[a]	70	3.4	S	0.17[a]	2.5	6.3
3	Van de Graaf Bldg.	115	5.1	SE	0.12	0.72	1.8
4	RLES Laboratory	160	6.5	NW	0.09	0.30	0.75
5	Radioastronomy Lab.	265	11.0	NE	0.08	0.095	0.24
6	Observatory	300	13.0	SSW	0.17	0.15	0.40
7	Building & Grounds	300	13.0	E	0.10	0.089	0.23
8	Dormitory	375	15.0	ESE	0.12	0.072	0.18
9	Filter Plant	430	17.0	SE	0.12	0.058	0.15

a) The North and South Fence sites represent average distances to the facility fence in these two directions, and the corresponding wind frequencies are averaged over all northerly and southerly directions. The University of Virginia also owns the land out to at least 300 meters in all directions from the reactor, and controls its use. Other than the sites listed above, there are no areas normally occupied within the 300 meter distance.

practice for noble gas exposure (Reference 3 at end of this Chapter), this situation has been analyzed on the basis of the direct, whole-body gamma-ray dose to an individual standing at the center of the narrow plume that would result. For these calculations, the plume is considered to be an infinitely long, line source passing the receptor at a distance of 6-inches. Since no dispersion in the atmosphere is accounted for, this model is independent of source-to-receptor distance. Assuming that the Ar-41 release rate at 2 MW is twice that calculated in 4.9.3.1 for 1 MW, the whole-body dose rate in the plume is about 0.006 mR/hr. For 24-hour persistence of this condition, the total calculated dose would be 0.15 mR.

4.9.3.3 Exhaust from Reactor Room after Ar-41 Buildup

If the reactor room exhaust is stopped temporarily, the Ar-41 concentration within the reactor room could eventually build up to Restricted Area Limits (2×10^{-6} μ Ci/cm^3). If the room is then exhausted, a short-term source of 6.7 μ Ci/sec exists, but will quickly die away as the reactor room inventory is depleted (exhaust half-period of about 10 min.) The calculated dose rate in the stable plume under these conditions is only 0.1 mR/hr, and the total dose to someone in the plume of 0.02 mR.

4.9.3.4 Exhaust from Beamport

The standard UVAR beamports have a section near the core which is filled with water when the port is not in use, and is drained prior to use. During port operations this section may be filled with air (although He or CO_2 is preferred), under neutron irradiation. If the port is refilled with water after operation, the Ar-41 produced when air

is used is exhausted into the experimental area exhaust system, and hence to the stack and atmosphere. A pump unassisted beamport drain takes several hours, and the refill (and thus the Ar-41 exhaust portion) 20-30 minutes.

Flooding a beamport immediately after a long period of operation at full power with air in the beamport results in the most severe Ar-41 dose that can be reasonably postulated. This situation is evaluated using stable meterological conditions and the line source approximation. Constants and assumptions used in the calculation are listed below.

1. Activation cross section of Ar-41 in normal air

   $\Sigma_a = 1.59 \times 10^{-7}$ cm^{-1}

2. Volume of 8-inch beamport, for 4.7 foot length,

   $V = 4.7 \times 10^{4}$ cm^{3}

3. Thermal neutron flux, $\phi = 2 \times 10^{12}$ n/cm^{2}-sec

4. Flooding time 1000 sec (16.7 min)

5. Saturation Ar-41 inventory, 0.4 Ci (product of $\Sigma_a \phi V / 3.7 \times 10^{10}$)

Using the line source approximation, the calculated dose rate in the plume during the 1000 seconds of discharge is 5.8 mR/hr. The calculated total dose to an individual in the plume as a result of the Ar-41 discharge is 1.6 mR.

During the spring of 1983 the North Neutron Beamport was modified into a closed loop system to eliminate the buildup of Ar-41 activity. The system incorporates demineralized water and a helium cover gas and a reversible peristaltic pump. When the front tube (pool side) is drained it is replaced with Helium gas, thereby eliminating Ar-41 activity

production in the tube. This beamport is being used extensively for neutron radiography experiments. The drain-fill operating mechanism is remotely located to reduce personnel exposure while the reactor is at power.

4.9.3.5 Experimental Failures

In Section 5.4 the offsite consequences of gaseous release as a result of an experimental failure are evaluated for the case of a fission gas release from a U-235 plate operated at 1 watt for a long time. Such an incident represents an upper bound on the type of major experimental failures which may be postulated, in view of the past and currently projected experimental programs.

4.9.4 Effluent Monitoring

Each of the ducts leading from the experimental facilities may be fitted with an internal G-M tube radiation monitor. Such a monitor has been used on the duct leading from the beamports and access facilities for many years. (See Figure 4.2).

A thin-walled G-M tube inside a duct has a count rate signal proportional to the specific beta activity of radioactive materials in the duct. In addition, the count-rate depends on the beta energies, the diameter and length of the duct. The exact relationships defining these dependencies are complicated but in general the count rate, for a given specific activity in the duct, will vary directly as the duct volume, and will be rather insensitive to beta energy unless the average beta particle range is less than the wall thickness of the G-M tube.

The best means for calibrating such a monitor for a particular isotope is by filling the duct with the beta emitting material in known

concentration and measuring the count rate. This has been done with Ar-41 in a section of duct similar to that in which the monitor is located in the exhaust line for the beamport and access facilities. The calibration of this monitor, thus obtained, was about 200 cpm, for an Ar-41 concentration of 10^{-6} μ Ci/cm^3 in the duct. Once a monitor has been calibrated, it can be checked for proper operation by noting the G-M tube's response to a gamma-ray source located outside of the duct.

4.9.4.1 Monitoring Performance for Ar-41

The function of the exhaust duct radiation monitor is to notify the reactor operator of abnormal levels of airborne radioactive effluent in the duct. The monitor in the beamport and access facility exhaust duct is normally set to alarm in the reactor room for a count-rate in excess of 800 cpm. For a normal background of 100 cpm, this count-rate would indicate an Ar-41 concentration in the duct of

$$(700/200)\times10^{-6} = 3.5 \times 10^{-6}\ \mu\text{Ci/cm}^3.$$

The nominal flow in this duct is 150 cfm, or 7.1×10^4 cm^3/sec. Thus a monitor alarm corresponds to an Ar-41 release at the stack of about 0.25 μ Ci/sec. This amount, on the basis of the conservative analysis of Section 4.9.3.2, would lead to a maximum offsite dose rate of 0.004 mR/hr. The expected Ar-41 production rate for any experimental facility can be determined analytically, if the thermal neutron flux and volume of air irradiated are known. One cubic foot of air, exposed to a flux of 10^9 n/cm^2-sec will yield about 0.013 μ Ci/sec of Ar-41.

4.9.4.2 Monitor Performance for Other Isotopes

The G-M tube duct monitors will respond to other radioactive gases or airborne particulates in a manner similar to its response for Ar-41,

as long as their beta particle ranges are well above the wall thickness of the G-M tube. The latter dimension for the current tube is 30 mg/cm^2 (0.0044" Al), equivalent to the range of an electron of ~ 0.16 MeV. Table 4.6 gives beta particle decay for various activation and fission product gases, and the rate at which the latter would be produced in a fueled experiment operating at 1 watt. Inspection of the Table shows that the isotopes of Chlorine and Bromine, and the more intense fission product isotopes I-132, I-134, and Kr-87 have beta energies similar to that of Ar-41, and would thus be expected to produce a similar monitor response. Thus, a fission product gas release of 0.25 μ Ci/sec would be sufficient to cause a monitor alarm. This value amounts to 1% of the fission products being produced by a 1-watt, fueled experiment.

4.9.4.3 Consequence Evaluation, Fission Gas Release

The consequences of a fission gas release that would produce a count rate just below the duct monitor alarm setting have been determined and are presented in Table 4.7 for the iodine isotopes. Two types of release are considered -- long term in which the dispersion factors at the site fence (Table 4.5) are used, and a short term release under stable, Pasquill-F type conditions.

The results of Table 4.7 show that for long term operation at the alarm point, the release of fission product gases produces site boundary concentrations of less than 2% of Part 20 limits for Unrestricted Areas. The short term release at this level, using extremely conservative dispersion conditions yields concentrations which are only 2.5 times these limits. Thus, the duct monitor appears to provide adequate protection in the case of accidental fission product gas releases.

TABLE 4.6

DATA FOR RADIOACTIVE GASES

Isotope	Major Beta Particle: Maximum Beta Energy	Major Beta Particle: Fraction of Emission	Production Rate for a 1 Watt Fueled Experiment μ Ci/sec	MPC, μ Ci/cm^3 Part 20 Appendix B, Table 2
Ar-41	1.2 MeV	0.99		4×10^{-8}
Cl-38	>1.1 MeV	1.0		7×10^{-8}
Br-80	2.0 MeV	0.92		
Br-82	0.44 MeV	1.0		6×10^{-9}
Fission Products				
I-131	0.61	0.90	0.027	1×10^{-10}
I-132	>1.0	0.79	3.2	3×10^{-9}
I-133	1.3	0.93	0.53	4×10^{-10}
I-134	>1.2	1.00	14.90	6×10^{-9}
I-135	>1.0	0.65	1.53	1×10^{-9}
Xe-133	0.34	0.99	0.086	3×10^{-7}
Xe-135	0.93	0.97	1.15	1×10^{-7}
Kr-85m	0.82	0.77	0.049	1×10^{-7}
Kr-87	>1.3	1.00	3.30	2×10^{-8}
Kr-88	0.85	0.23	2.10	2×10^{-8}
		Total *Fission Products*	26.9	

TABLE 4.7

IODINE ISOTOPE CONCENTRATIONS FOR A 0.25 μ Ci/SEC FISSION PRODUCT RELEASE

Isotope	Release Rate μ Ci/sec	Long Term Conc. at Fence μ Ci/cm^3	Long Term Fraction of 10 CFR 20	Short Term Conc. at Fence μ Ci/cm^3	Short Term Fraction of 10 CFR-20
I-131	2.7×10^{-4}	6.8×10^{-14}	0.00068	1.04×10^{-11}	0.01
I-132	3.2×10^{-2}	8×10^{-12}	0.0027	1.2×10^{-9}	0.40
I-133	5.3×10^{-3}	1.3×10^{-12}	0.0033	2.0×10^{-10}	0.50
I-134	1.5×10^{-1}	3.8×10^{-11}	0.0064	5.8×10^{-9}	1.00
I-135	1.5×10^{-2}	3.8×10^{-12}	0.0038	5.8×10^{-10}	0.60
Totals			0.017		2.5

4.10 Core Spray System

The UVAR reactor is equipped with two independent core spray systems. Their function is to provide protection against a postulated core damage in the event of a very sudden and severe loss of coolant accident (LOCA). Each system consists of a pair of spray headers and an emergency water storage tank. The two water storage tanks are mounted on the inner side of two of the pool walls and each holds approximately 200-foot^3 (1500 gallons). Either system is designed to deliver an average spray flow of 10 gpm to the core for at least 1 1/2 hours, considered to be an adequate flowrate and time to prevent core damage. The two core spray systems are illustrated (elevation and plan view) in Figures 4-4 and 4-5.

Recirculating water from the demineralizer continuously flows into each of the emergency water storage tanks. The tank overflows are located about 2-inches above the highest operating level of the pool water. Accordingly, there is a slight head (2") of water on the tanks and a continuous flow of water through the headers into the pool. This assures that the tanks are always full and that stagnant water and resultant corrosion does not occur in the spray headers. The material used in the construction, aluminum, and the flexible stainless steel couplers, serve to enhibit corrosion.

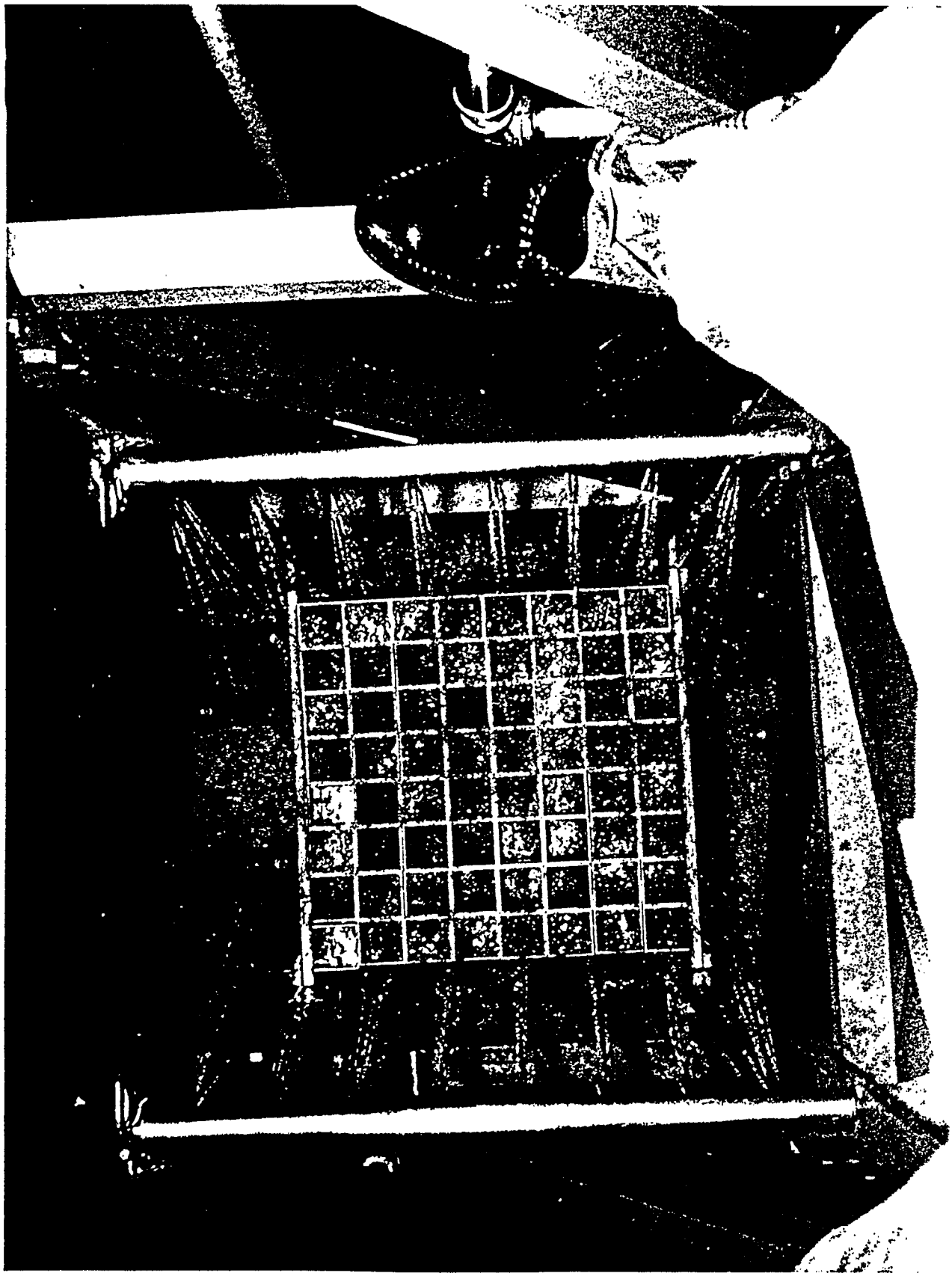
The two sets of spray headers are mounted on either side of the core support structure, approximately 5-feet above the top of the core. A spray header consists of an approximately 1-inch diameter aluminum pipe, 2-feet long, with approximately 80 small holes drilled at a proper angle and spacing to provide a uniform spray over the top of the core. A mockup of one pair of core spray headers is shown in Fig. 4-3. (The flow rate was 10 gpm when this picture was taken.)

Technical Specifications require a core spray flowrate of at least 10 gpm at 30 minutes after LOCA onset. Actually, the calculated spray flowrate is 10.8 gpm after 30 minutes, reaching 10 gpm only after 47 minutes.

When the reactor bridge is returned to the full power position, the piping connecting the storage tank to its pair of spray headers is engaged with a remote coupler. After the coupling is made, a pressure test is conducted using an insert tube screwed into the pipe leading from the bottom of the storage tank, as shown on the right hand tank in Fig. 4-4. Air pressure is applied and a visual observation made to ensure that air bubbles are not leaking from the remote coupling. Air bubbles will emerge from the spray headers at approximately 7 1/2 psig air pressure. At 1/2 psig the coupler will be filled with air but the spray headers will not. The absence of air bubbles from the coupler will be a positive verification that the coupler is securely engaged and is not leaking.

The pressure test insert tube is removed after it has been verified that there is no leak from the coupler. A coupler leakage test is made every time the reactor bridge is moved and returned to the high power position, after the coupler has been re-engaged. A flowrate test, using a small water tank to provide a known head, is repeated at least once each year for each of the two spray systems, to demonstrate that at least 10 gpm are available for emergency core cooling for the first 30 minutes after a loss of coolant accident.

In summary, the emergency core spray system is expected to provide an immediate supply of water to the core in case coolant is suddendly lost. The system has no moving parts that can fail and no automatic electronic or mechanical devices are required to function. SAR Section 9 discusses the loss of coolant accidents.



Top View

FIGURE 4-3 Mockup of Core Spray Headers

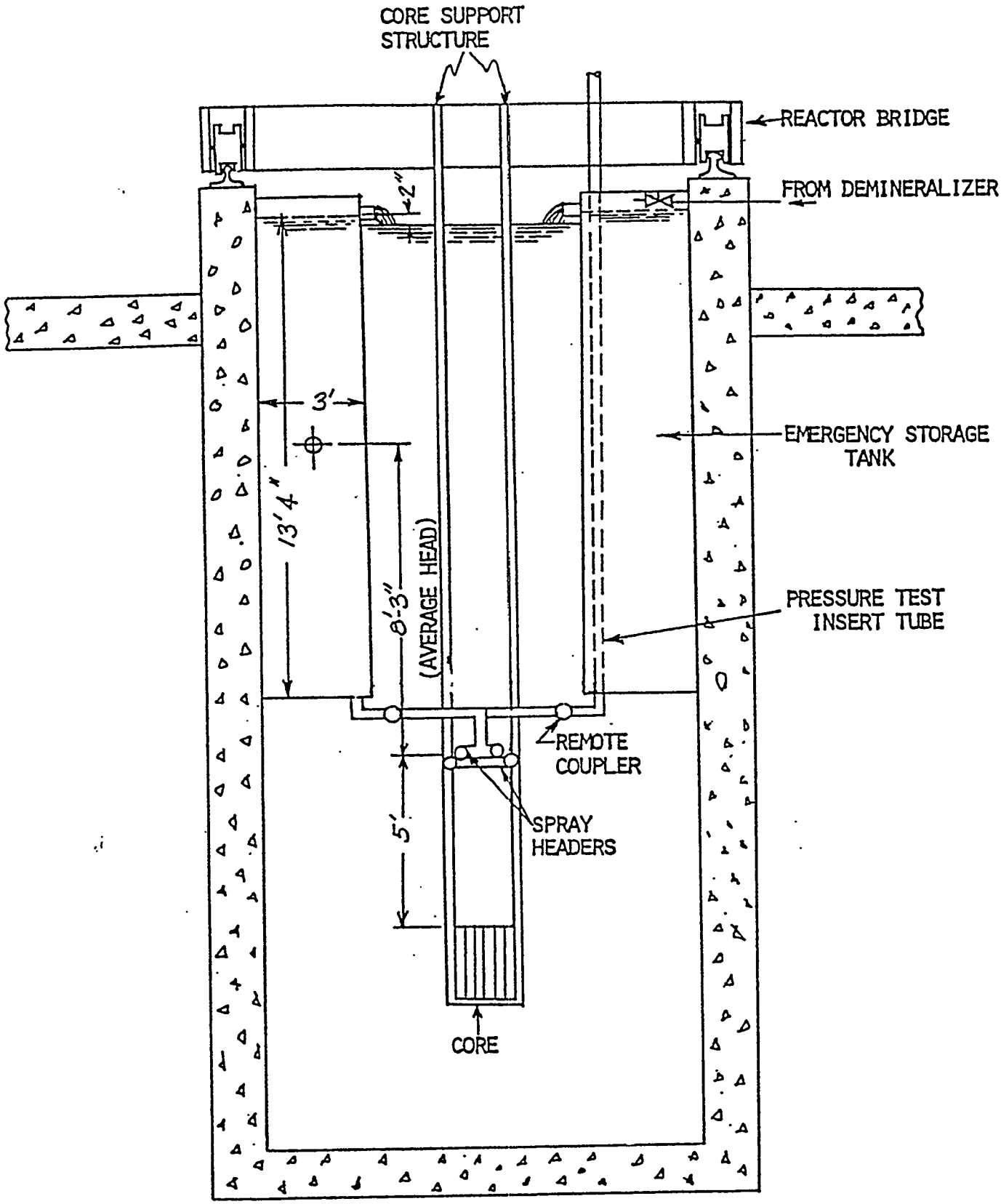


FIGURE 4-4 , CORE SPRAY SYSTEM ELEVATION VIEW

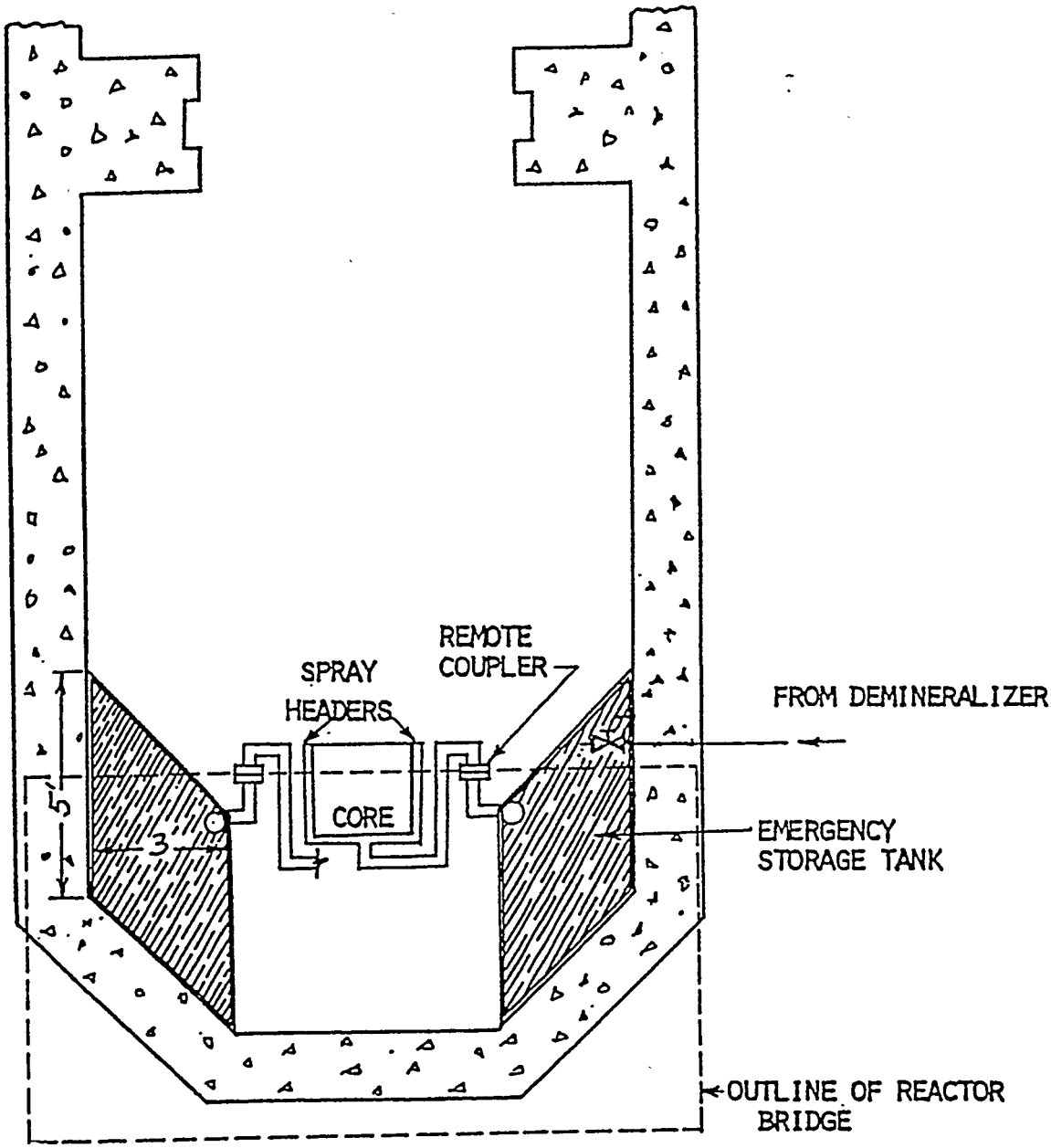


FIGURE 4-5 , CORE SPRAY SYSTEM PLAN VIEW

References for Chapter 4.0

1. "Radiation Dose Evaluation Model for Maximum Credible Accidents," p. 23, Proposed DRL Safety guide -- Private Communication.

2. Slade, David H., Edt. "Meteorology and Atomic Energy, 1968," Section 3-3.5.4, p.113, USAEC, July 1968.

3. Rogers, Lester, and C.C. Gamertsfelder, "U.S. Regulations for the Control of Releases of Radioactivity to the Environment in Effluents from Nuclear Facilities," I.A.E.A. SM-146/8, p. 8, paper presented at I.A.E.A. Symposium on Environmental Aspects of Nuclear Power Stations, U.N. Headquarters, New York City, N.Y., August, 1970.

5.0 Experimental Facilities

5.1 Beamports

Two 8-inch neutron beamports penetrate the concrete shield in the southwest side of the pool. The ports extend through the wall and up to the side of the reactor. The ports on the pool side are normally filled with water when not in use. A blank flange aluminum plate separates the aluminum port extension from the concrete shield penetrations. Beam hole design is shown in Figure 5-1.

The South Beam Port Extension (see Figure 5-1a) is vented to the duct exhaust system. The North Beam Port is used for Neutron Radiography experiments and its extension is a closed system. The system uses demineralized water with a helium cover gas and a reversible peristaltic pump as shown in Figure 5-1b. When the front tube is filled with water, the tank holds an amount of excess water and a large volume of helium gas. When the front tube is drained the tank is almost filled with water causing the front tube to be filled with helium gas. This eliminates the production and release of argon-41 to the atmosphere. The drain/fill pump circuitry requires switch actuation by both the experimenter and the reactor operator.

There is a concrete shielding block wall around the beam ports on the ground floor (see Figure 5-1a). The wall is roofed with steel and wood beams and plywood decking which holds graphite, paraffin and borax shielding. The back wall thickness is three blocks. The beam stop is constructed of cadmium sheets, lead sheets, concrete and paraffin. Access to this structure is limited by a lockable door. Entrance to the inside of the blockhouse is procedurally controlled at all times. When

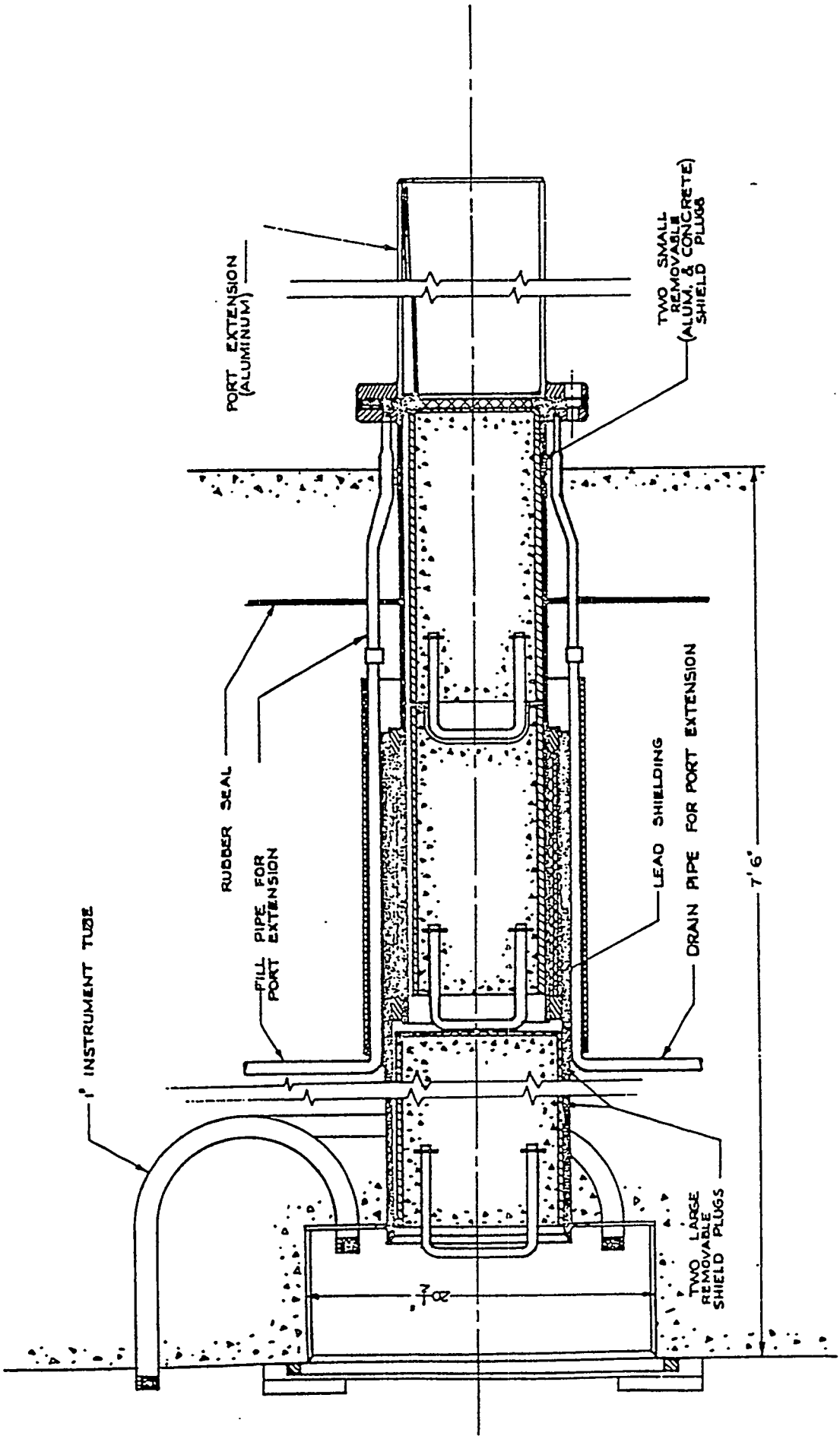


FIG. 5-1 BEAM HOLE DETAIL

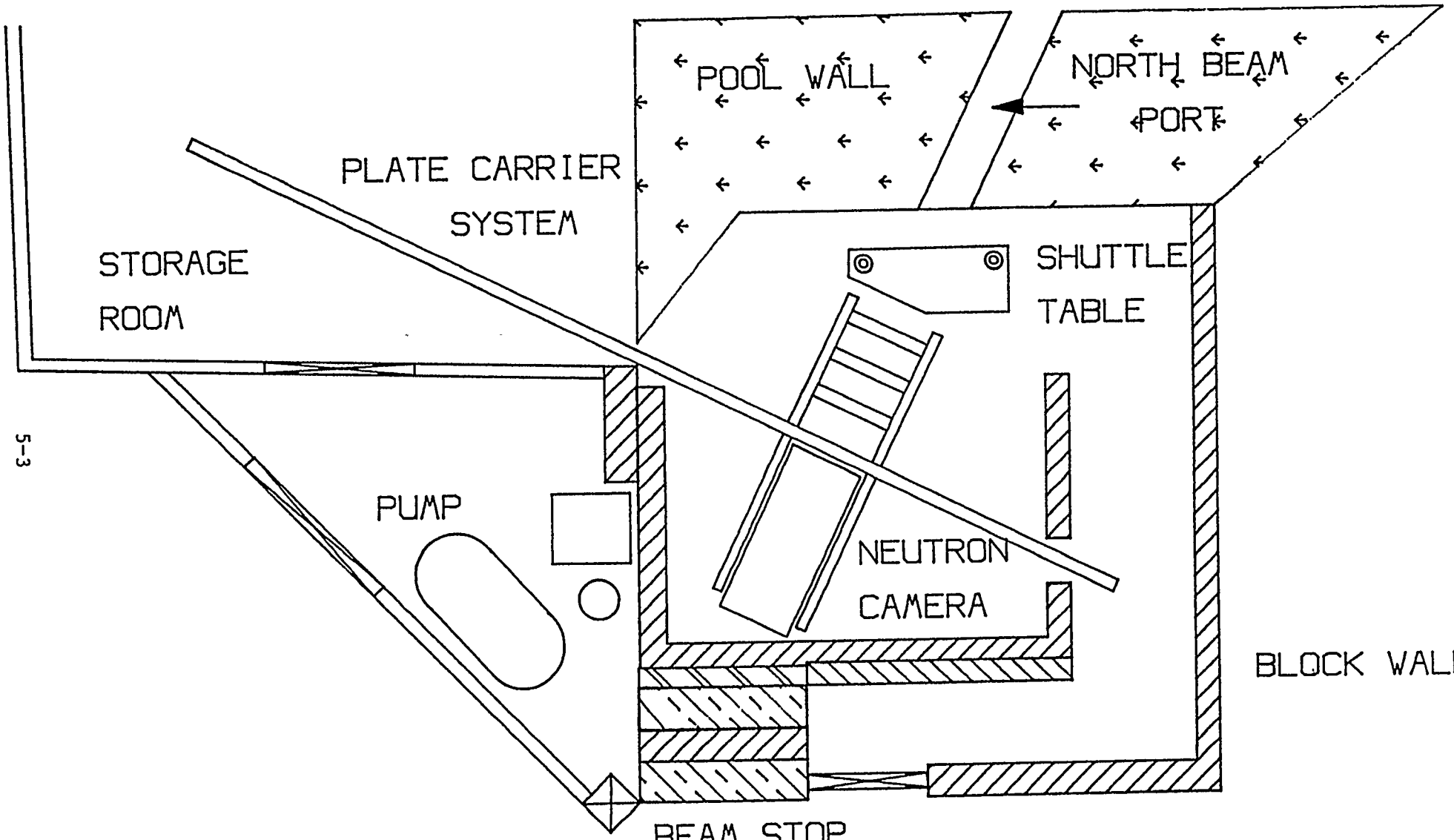


Figure 5-1a Top View of North Beam Port Shielding and Access Control Walls

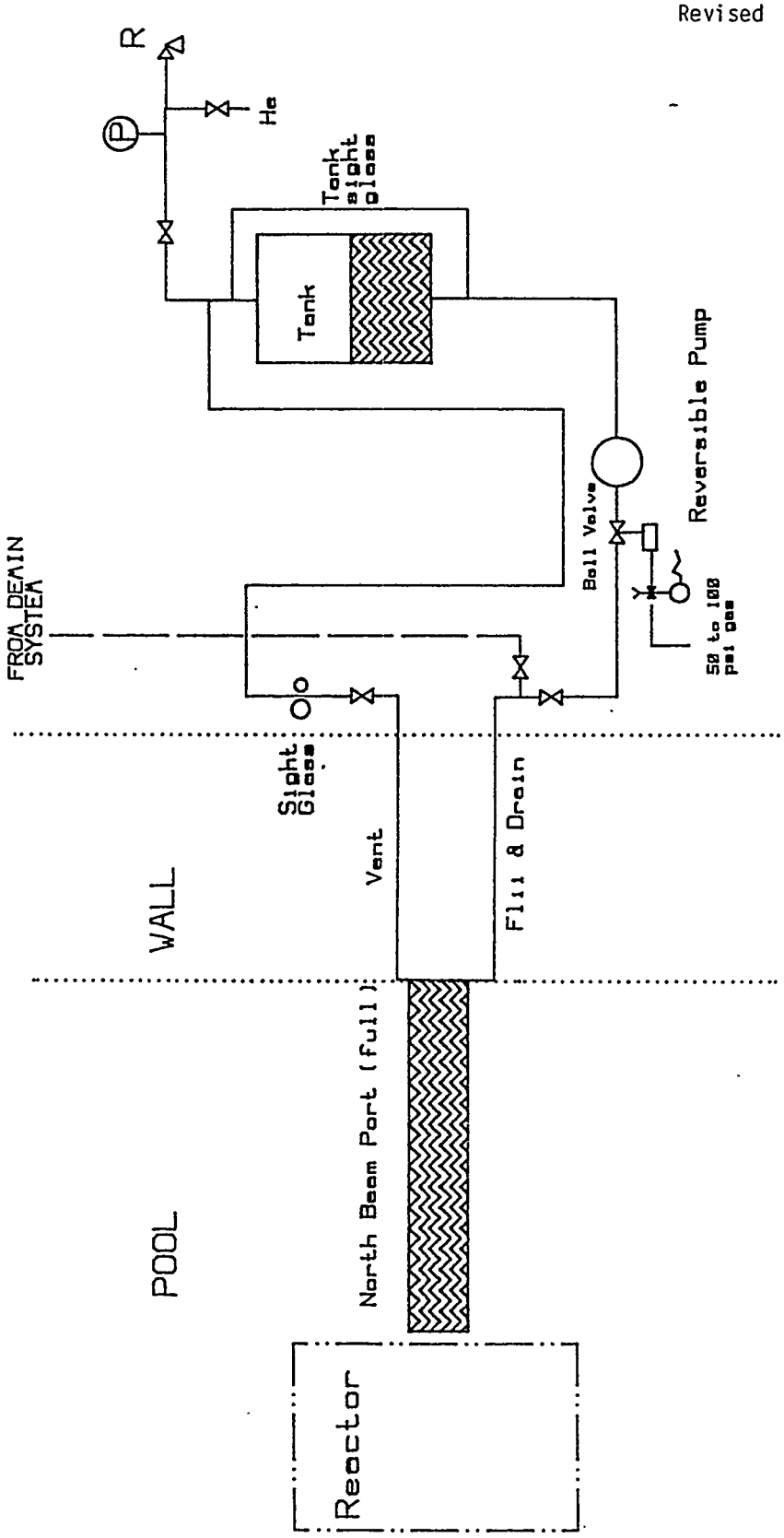


Figure 5-1b North Beam Port Drain/Fill System Schematic

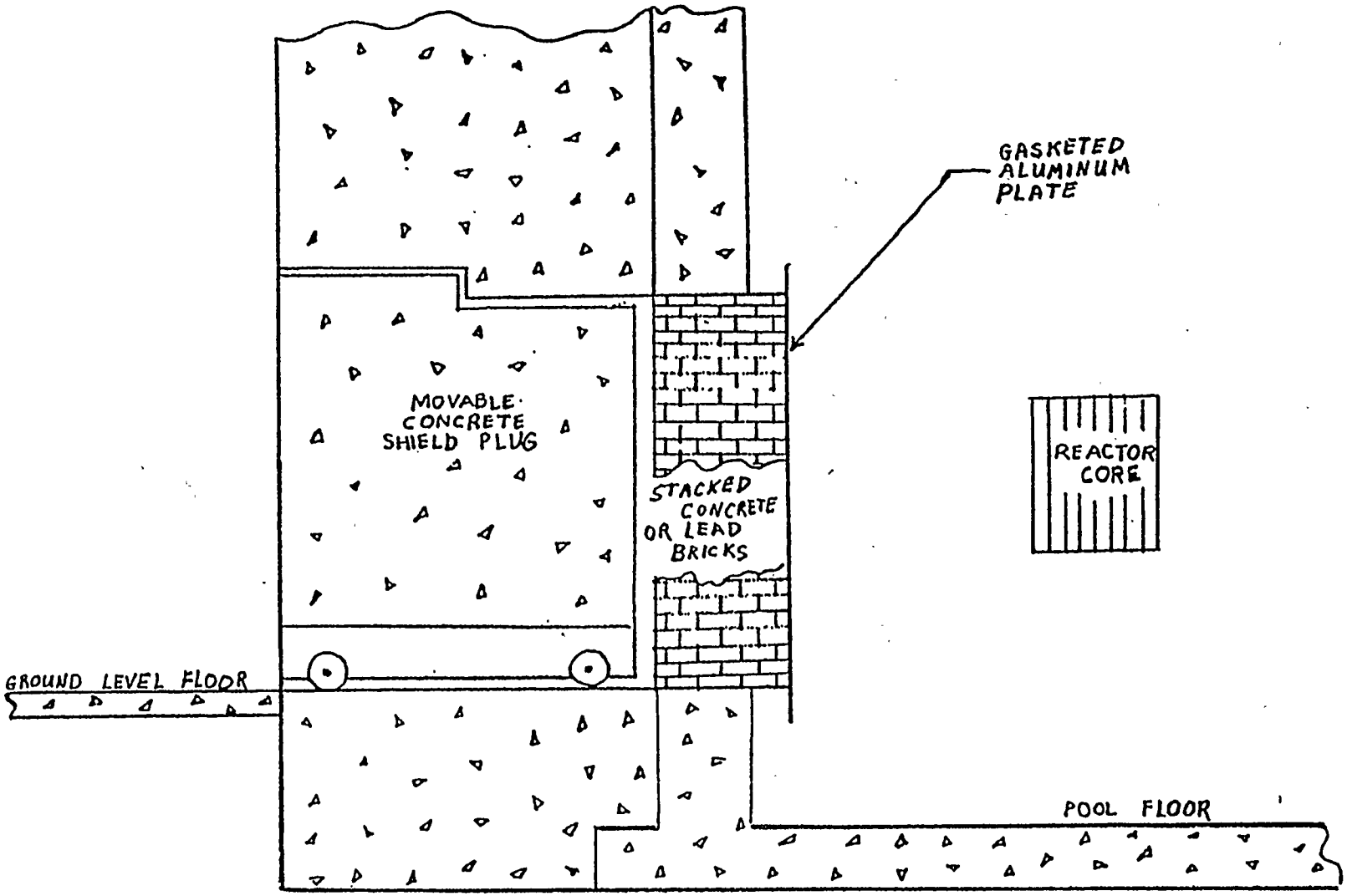


Figure 5-2 LARGE ACCESS FACILITY

the front tube of the beamport is partially or fully drained, several alarm systems are activated. These include:

1. An audible alarm on the opening of the blockhouse door based on signals from either the LED water detector on the vent tube, or the LED water detector on the top sight glass tube, or a BF_3 neutron detector within the beam tube. This is a one of three logic system.
2. An LED sensor on the top sightglass tubes of both neutron beamports which gives a drained/filled indication at the reactor console. The north beamport LED detector enables an alarm and reactor scram upon breaking a light beam actuator placed inside the blockhouse corridor prior to entering the north beamport beam path.
3. A neutron detector located on the reactor side of any movable shielding or experimental apparatus enables a scram and a local alarm associated with the light beam actuator whenever neutrons are detected in the beam. The Radiation Area lights and the door alarm and beam open light are also controlled by this detector. The setpoint of the detector is chosen based upon neutron and gamma ray sensitive portable survey instrument readings in the beam.

5.2 Large Access Facilities

The south wall also accommodates two large access solid concrete facilities measuring 5-feet wide by 6-feet high, rolled in the wall recess on dollies. Each facility is closed off from the pool by a

plate. A large access facility is shown in Figure 5-2. A thermal column may be incorporated in a large access facility. Small diameter beamports are available for use in conjunction with the access facilities.

5.3 Rabbit Facilities

a) Two pneumatic rabbit facilities are located on the reactor grid plate to accommodate thermal and epithermal irradiations, and they are used primarily for activation analysis experiments. The pneumatic transfer system may be connected to either the thermal or epithermal irradiation facility by manually changing the tubing at the top of the reactor bridge. Samples may be loaded in a room next to the counting room on the lower level of the building and pneumatically sent to the top of the reactor pool. The reactor operator then takes control of the sample and can by computer control insert it in the rabbit facility for a preset amount of time. When the sample is removed it can be stopped approximately 5 feet under water and measured for radiation exposure. An administrative limit of 240 mR/hr(Gamma) at one foot is placed on samples transported through this system. If the radiation is less than this the reactor operator can activate the system to transport the sample to the counting room for analysis. This system is very useful for investigating short-lived isotopes.

b) A hydraulic rabbit facility is also located in the reactor grid plate. Samples run in this facility must be loaded and unloaded from the top of the reactor pool. The overall configuration of possible experimental facilities is shown in Figure 5-3. All facilities shown are not necessarily in place at one time.

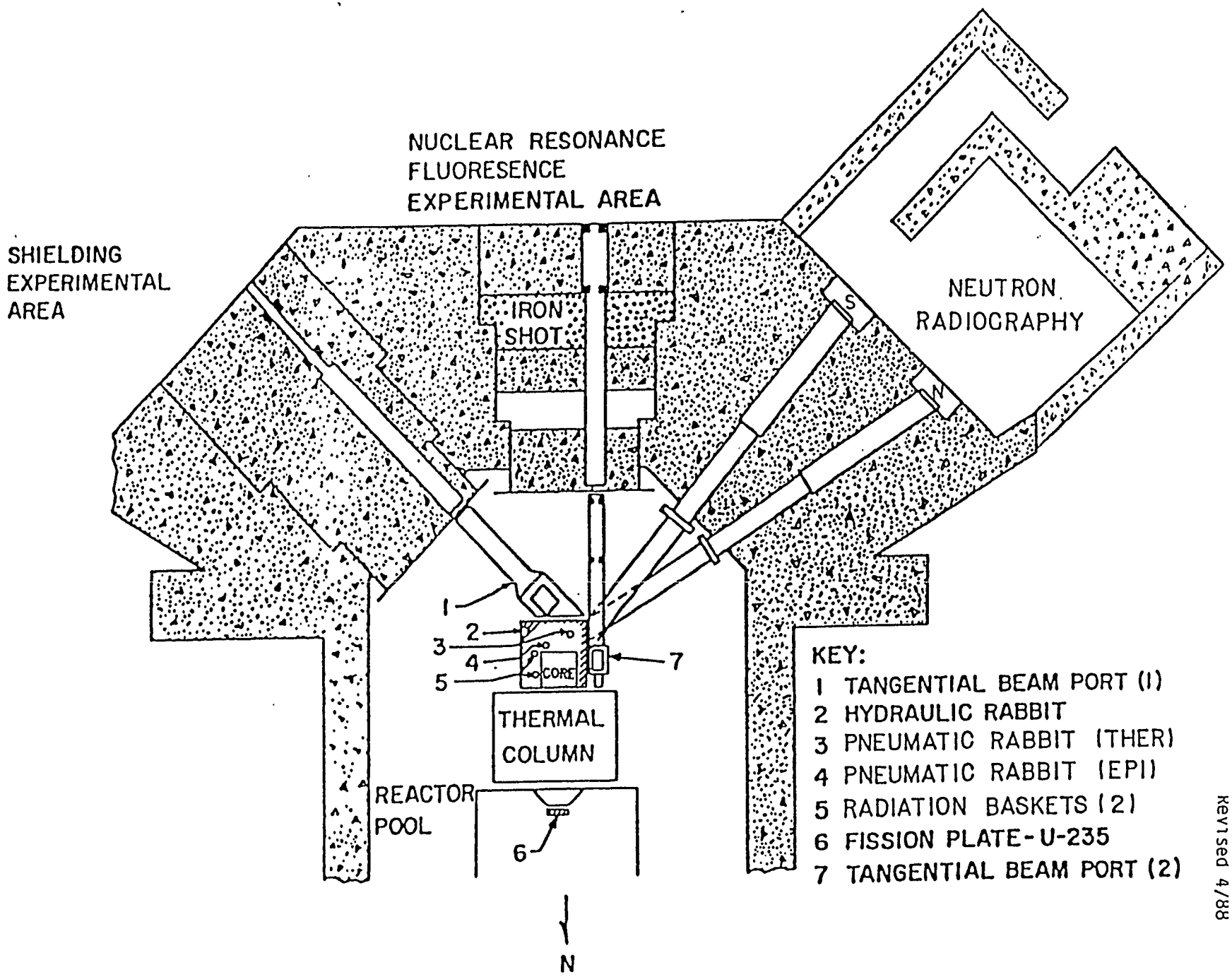


FIGURE 5-3 UNIVERSITY OF VIRGINIA REACTOR OPTIMUM CONFIGURATION
CORE IN FORCED CONVECTION COOLED POSITION.

Revised 4/88

5.4 Fueled Experiments

5.4.1 Introduction

The purpose of this analysis is to assess the hazard associated with the failure of a fueled experiment and subsequent release of its fission product inventory. The Maximum Permissible Concentrations of 10CFR-Part 20, averaged over a 1-year period, will be used as a measure of the consequence of a fission product release. Exposure to an isotope, in the concentration shown in Table II, Appendix B of 10 CFR-20, for a year (3.15×10^7 sec) is considered to be the Part 20 limit. Accident exposures to concentrations of the same isotope, for specific time periods, are evaluated according to the following equation.

$$\text{Fraction Exposure(FE)} = \frac{(\text{Accident Concentration}, \frac{\mu c}{cc} \times (\text{Time of Exposure})(\text{BRR})}{\text{MPC (Table II)}(3.15 \times 10^7 \text{ sec})} \qquad (5.4.1)$$

where BRR = breathing rate ratio, the ratio of the breathing rate assumed during an accident to an average breathing rate.

Only the isotopes of Iodine and Strontium-90 are considered in this analysis. The reason for this is that these are isotopes having relatively high fission yield and very low permissible concentrations. If the concentrations of these isotopes are within permissible levels, the concentration of others will also be tolerable.

5.4.2 Isotope Release

The amount of radioisotope released from a fueled experiment and becoming airborne is assumed to be that specified by TID-14844: 100% Noble Gas; 50% Halogen; 1% Solid Fission Products. These values provide

a very conservative upper limit for fission product release from a fueled experiment over a broad spectrum of accidental conditions (e.g., fission plate clad failure).

Isotopes initially released to the reactor building in general (other than to the reactor room), are assumed to be released subsequently to the atmosphere at a uniform rate, over a 2-hour period. This assumption maximizes the inhalation dose (or isotope concentration) for a 2-hour exposure time, by making the entire isotope inventory available for inhalation. For material released to the reactor room, which is automatically closed upon receipt of a high radiation level signal, the isotopes are assumed to be released at a uniform rate over a period of 20-hours.* The retention properties of the reactor room, a windowless structure designed to provide confinement, have been measured, and the 50%-in-20 hours exfiltration value verified (see Section 6.1).

In case of fueled experiments which are operated in the reactor pool, a reduction of a factor of 10 will be assumed for iodine isotopes released to the atmosphere. This "partition factor" accounts for the

---

*A gamma-ray sensitive chamber at the top of the reactor pool provides automatic closure of the reactor room (and a reactor trip) for radiation levels above the set point, normally 30 mR/hr. In addition there are 2 independent air monitoring instruments in the reactor room which would sense a fission produce release and alarm. The operator would have ample time to close the reactor room to prevent an excessive amount of exfiltration by the building exhaust system--normal rate ~11% per minute. Note that forced exfiltration by the building exhaust would give an elevated, puff-type release, resulting in lower site boundary doses.

solubility of iodine gas in water, and the fact that any fueled experiment operating in the pool, at a significant power level, must be located near the reactor core--under approximately 20 feet of water. In a fission gas release from a fission plate at the UVAR on May 3, 1968, isotopic concentrations of noble gases were measured in the reactor room, amounting to ~0.1% of the total fission plate inventory. Iodine isotope concentrations were too low to be detected. However, by inference from the instrument sensitivity, they were released form the pool in amounts smaller by at least a factor of 10 than the noble gases.

5.4.3 Offsite Exposures

For isotope releases from the facility, the following information is used to determine fractional exposure to an isotope. Accident concentrations are computed using the conservative meteorological model of TID-14844, and a 70 meter exclusion radius. The time of exposure is taken to be 2 hours (7200 sec). An accident breathing rate of 3.47×10^{-4} M^3/sec is assumed, and a yearly average breathing rate of 2.32×10^{-4} M^3/sec (i.e., BRR = 1.56). MPC values used are taken from 10 CFR Part 20, Appendix B, Table II.

5.4.4 In-Facility Exposures

Fractional exposures due to inhalation of isotopes by personnel within the building are computed by assuming mixing of the isotope in question with the air in the space in which the release occurs. For calculational purposes, the exposure times are set at 5 minutes, a period considered long enough a detect a release and evacuate the affected areas. No correction is made for exfiltration from the building during exposure time.

5.4.5 Calculations

5.4.5.1 Offsite Exposures

Fractional exposures (FE_i) for each isotope, and the doses due to each may be calculated. The atmospheric diffusion expression of TID-14844 (Section B) may be used to determine the downwind, site boundary, concentration of any isotope.

Concentration:

$$X_i(d) = \frac{2Q_i}{\pi \bar{\mu} C_y C_z d^2 n} \qquad (5.4.2)$$

where $X_i(d)$ = concentration of isotope "i" at a distance of d, Ci/M^3

Q_i = isotope "i" source, Ci/sec, = inventory/exfiltration time

$\bar{\mu}_i$ = wind speed, 1 meter/sec

C_y = horizontal diffusion coefficient, 0.40 $meters^{n/2}$

C_z = vertical diffusion coefficient, 0.07 $meters^{n/2}$

d = distance downwind, 70 meters for exclusion radius

n = 0.5

$$\frac{X_i\ (70\ M)}{Q_i} = \frac{1}{\pi \cdot 1 \cdot (0.4)(0.07)(590)} = 0.039$$

Fraction exposures are determined using Eq. (5.4.1), in which the accident concentration, $X_i(70)$ found by calculating a value of Q_i for each isotope:

$$Q_i = \frac{\text{(Inventory of Isotope "i") x (Release Fraction)}}{\text{Exfiltration Time (2 or 20 hrs.)}}$$

Table 5.4.1 presents fractional exposures calculated for the iodine isotopes and Strontium-90. The iodine inventories refer to infinite-time experiment operation at 1 watt, and the Strontium-90 concentration to 6 years of continuous operation at 100 watts. The period of isotope release (exfiltration time) and of inhalation exposure are both two hours.

For the case release from the pool to the reactor room, the iodine inventories specified are 100 times greater, corresponding to infinite operation at 100 watts. Here a water-to-air iodine partition of 10 and a 20-hour exfiltration time are assumed. These factors combine to reduce the iodine isotopic release to exactly that of a 1-watt building release (2-hour), and the Fractional Exposures are the same as in Table 5.4.1 for the iodine isotopes. Sr-90 Fractional Exposure for a reactor room release would be lower than for a building release by a factor of 10, due to the increased exfiltration time.

5.4.5.2 Building Exposures

To calculate building exposures, the isotope concentrations are found by dividing the fraction of the isotope inventory released by the volume of the space into which the exposure takes place. Fractional exposure is then calculated in the same manner as for offsite releases. The results of such computations are shown in Tables 5.4.2a and 5.4.2b below, for the reactor room ($2.3 \times 10^3 M^3$) and first floor experimental area ($1.7 \times 10^3 M^3$).

TABLE 5.4.1

EXCLUSION RADIUS FRACTIONAL EXPOSURES

Isotope	Isotope Inventory, Curies	Accident Release, 50% or 1%	2-Hour Release Rate Q_i, Ci/sec	70 Meter Concentration, X_i, Ci/M^3	10 CFR-20 Appendix B, TABLE II MPC_i Values	Fractional Exposures $\frac{(X_i)(7.2\times10^3\text{sec})(\text{BRR}=1.56)}{(MPC_i)(3.15\times10^7\text{sec})}$
I-131	0.0251	0.013	1.93×10^{-6}	7.5×10^{-8}	1×10^{-10}	0.27
I-132	0.0381	0.019	2.64×10^{-6}	1.03×10^{-7}	3×10^{-9}	0.012
I-133	0.0563	0.028	3.9×10^{-6}	1.52×10^{-7}	4×10^{-10}	0.136
I-134	0.0658	0.033	4.6×10^{-6}	1.8×10^{-7}	6×10^{-9}	0.010
I-135	0.0510	0.026	3.6×10^{-6}	1.4×10^{-7}	1×10^{-9}	0.051
Total Iodine	0.2363					0.49
Sr-90	0.75	0.0075	1.04×10^{-6}	4.1×10^{-8}	3×10^{-11}	0.49*

*Sr-90 Fractional Exposure = 0.05 for a reactor room release.

TABLE 5.4.2a

REACTOR ROOM - 5 MIN. EXPOSURE

Isotope	Isotope Inventory, Ci	Accident Release, (0.05 or 0.01) Ci	X_i in Room Ci/M^3	Fractional Exposures $\frac{(X_i)(300\ sec)(BRR)}{MPC(3.15x10^7 sec)}$
I-131	2.51	.13	$5.7x10^{-5}$	8.5
I-132	3.81	.19	$8.3x10^{-5}$	.41
I-133	5.63	.28	$1.2x10^{-4}$	4.4
I-132	6.58	.33	$1.44x10^{-4}$	.36
I-135	5.1	.26	$1.14x10^{-4}$	1.7
Total Iodine				15.4*
Sr-90	.75	.0075	$3.3x10^{-6}$	1.63

*The reactor room is a Restricted Area, thus the MPC values of Table II, Appendix B, 10 CFR-20 do not apply strictly. Since yearly dose limits on such areas are ~10 times greater than for unrestricted areas, the total iodine FE value of column 5 is the order of 1.5 times allowable.

TABLE 5.4.2b

EXPERIMENTAL AREA - 5 MIN. EXPOSURE

Isotope	Isotope Inventory, Ci	Accident Release, (0.5 or 0.01) Ci	X_i in Area Ci/M^3	Fractional Exposures $\frac{(X_i)(300\ sec)(BRR)}{MPC(3.15 \times 10^7 sec)}$
I-131	0.0251	0.013	7.7×10^{-6}	1.15
I-132	0.0381	0.019	1.12×10^{-5}	.05
I-133	0.0563	0.028	1.62×10^{-5}	.60
I-134	0.0658	0.033	1.95×10^{-5}	.05
I-135	0.051	0.026	1.55×10^{-5}	.23
Total Iodine				2.0
Sr-90	0.75	0.0075	4.5×10^{-6}	2.2

5.4.6 Conclusion

The offsite Fractional Exposures for Iodines and Strontium-90 (Table 5.4.1) are within the limits of 10-CFR-20, for very conservative isotope release assumptions (TID-14844). The Fractional Exposures for spaces within the reactor building, considering the same conservative release fractions, and a 5-minute exposure, are only slightly greater than the 10 CFR-20 limits for these isotopes.

It is concluded that fueled experiments can be operated within power limits set by the Technical Specifications without undue hazard to the general public, the reactor staff or visitors. It is noted that the isotope inventories are related to fueled experiment thermal power or fission rates. These values can be ascertained by fission product radiation intensity measurements, or from fission neutron yield measurements (G.I. Coulbourn and T.G. Williamson, NSE, 35, 367 (1969)).

6.0 RADIATION HAZARDS

6.1 Confinement

The reactor room above the pool level is of cylindrical construction 54 feet in diameter and 36 1/2 feet high. It is designed to withstand a differential pressure of 1/2 psi. The walls are of reinforced masonry, plastered on the inside for gas tightness while the roof is a concrete slab. The openings into the room are the truck door, the personnel door, the escape manhole, and the air intake and exhaust ducts.

The truck door is of steel construction and is opened and closed by use of a manually operated chain fall and gear arrangement. It initiates a scram condition to the reactor when moved from the fully closed position, thereby precluding reactor operations when confinement is broken at this point.

The personnel door swings closed against a rubber gasket by gravity. It is held open during operations by a magnet which releases automatically in the event of a high radiation level in the reactor room as detected by the monitor located on the reactor bridge. Should an incident occur and pressure build up in the reactor room, the pressure will seal the door tightly. The personnel door is illustrated in Fig. 6-1.

In the event of an accident which seals the personnel door, the operator would be trapped in the room. A simple underwater escape hatch is provided as an emergency exit. The emergency escape hatch is normally closed and secured with a slide bolt which will allow easy opening from the inside in the event of an emergency. The escape system is shown in Fig. 6-2.

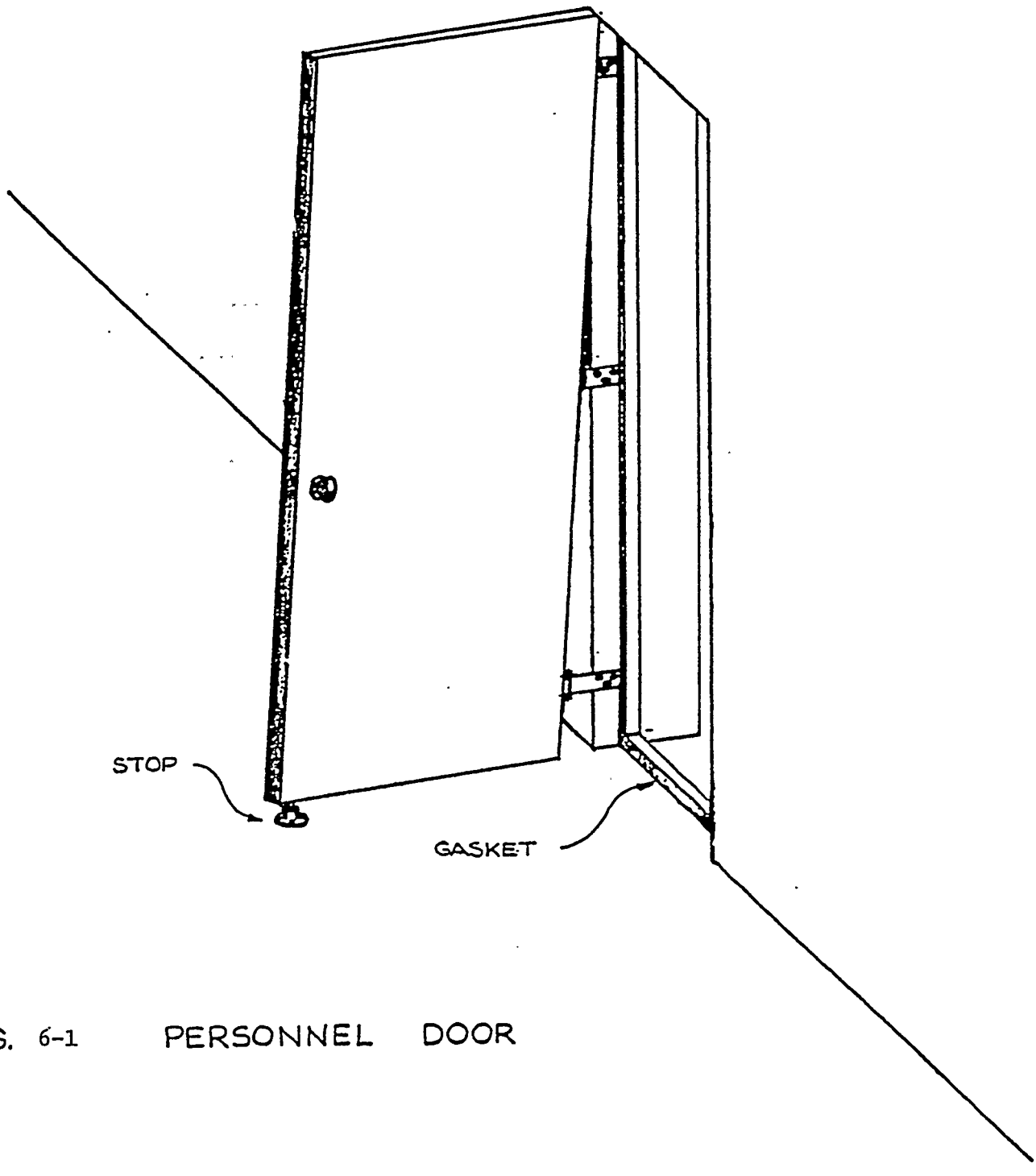


FIG. 6-1 PERSONNEL DOOR

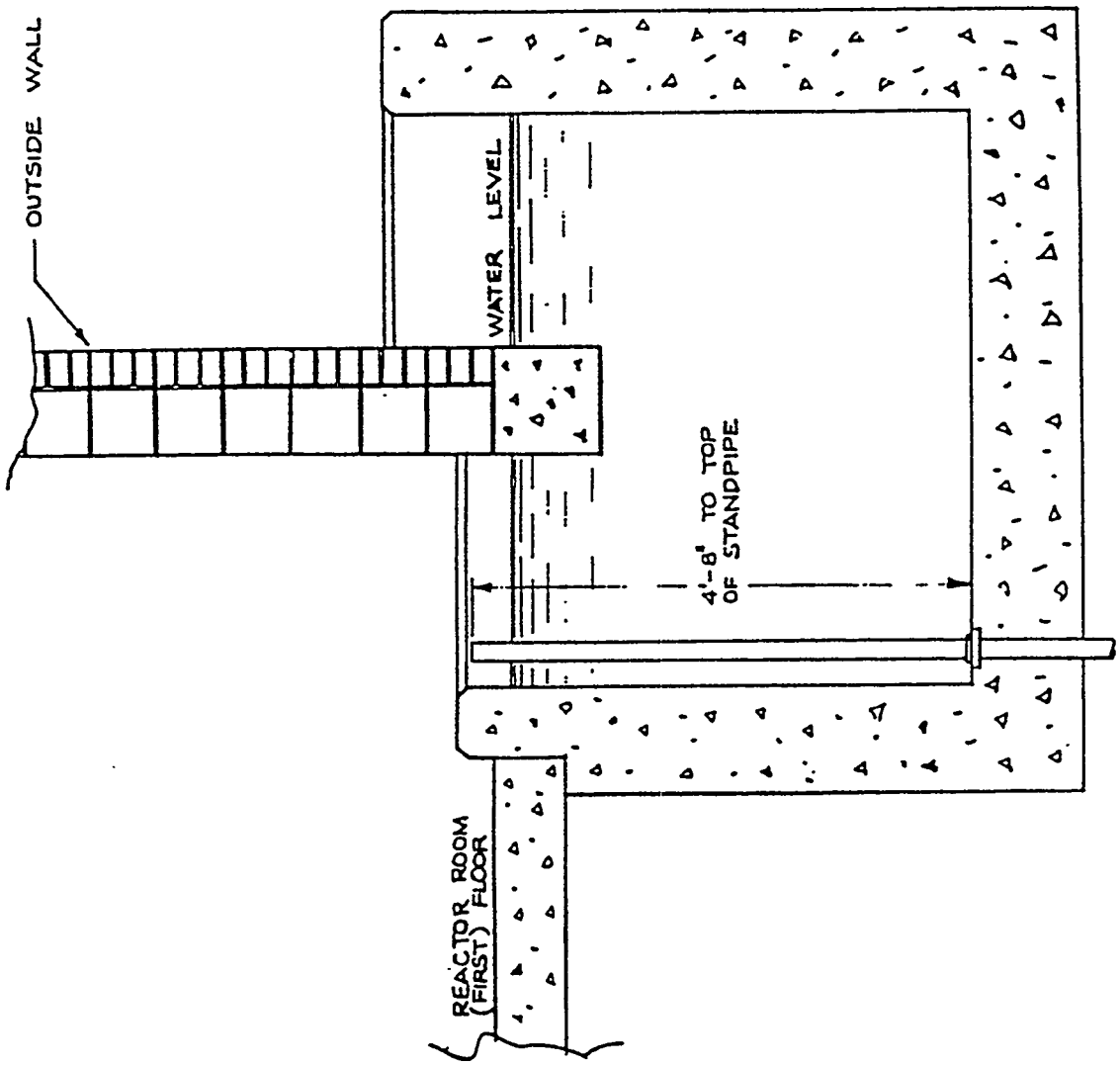


Fig. 6-2 EXIT MANHOLE

The reactor room ventilation exhaust ducts are operated in a manner similar to the personnel door. Each duct has a gasketed, solid, inside door which is opened manually and held open by a magnet. As in the case of the personnel door, these magnets release automatically upon a high radiation level at the reactor bridge. The pressure tight air duct is shown in Fig. 6-3.

Past measurements of the leak rate from the reactor room verified that the exfiltration rate is less than 100% in 20 hours. The leak rate of the reactor room was measured using ^{85}Kr as a tracer. The measurement involves releasing a small amount of the tracer isotope into the containment volume, and subsequently monitoring changes in the relative specific activity of the air in the room. Such changes can be related to the rate of air leakage.

Krypton itself is one of the principal fission product gasses, so its use allows the measurement to be made with an actual isotope of interest. ^{85}Kr has a half-life of 10.7 years, and decays with the emission of a 0.67 MeV beta particle (99+%), and a gamma ray of energy 0.52 MeV (0.7%). The two decay products allow two independent measurements to be made.

To make the measurements, detectors are arranged so that they view the air space within the containment. The beta counting channel need only consist of relatively thin-walled G-M tubes. The range of ^{85}Kr beta particles in air is about two meters, thus the count rate in this channel reflects the local specific activity and is indicative of average specific activity only if there is good air mixing. The gamma-ray counting channel must be able to detect selectively the 0.52

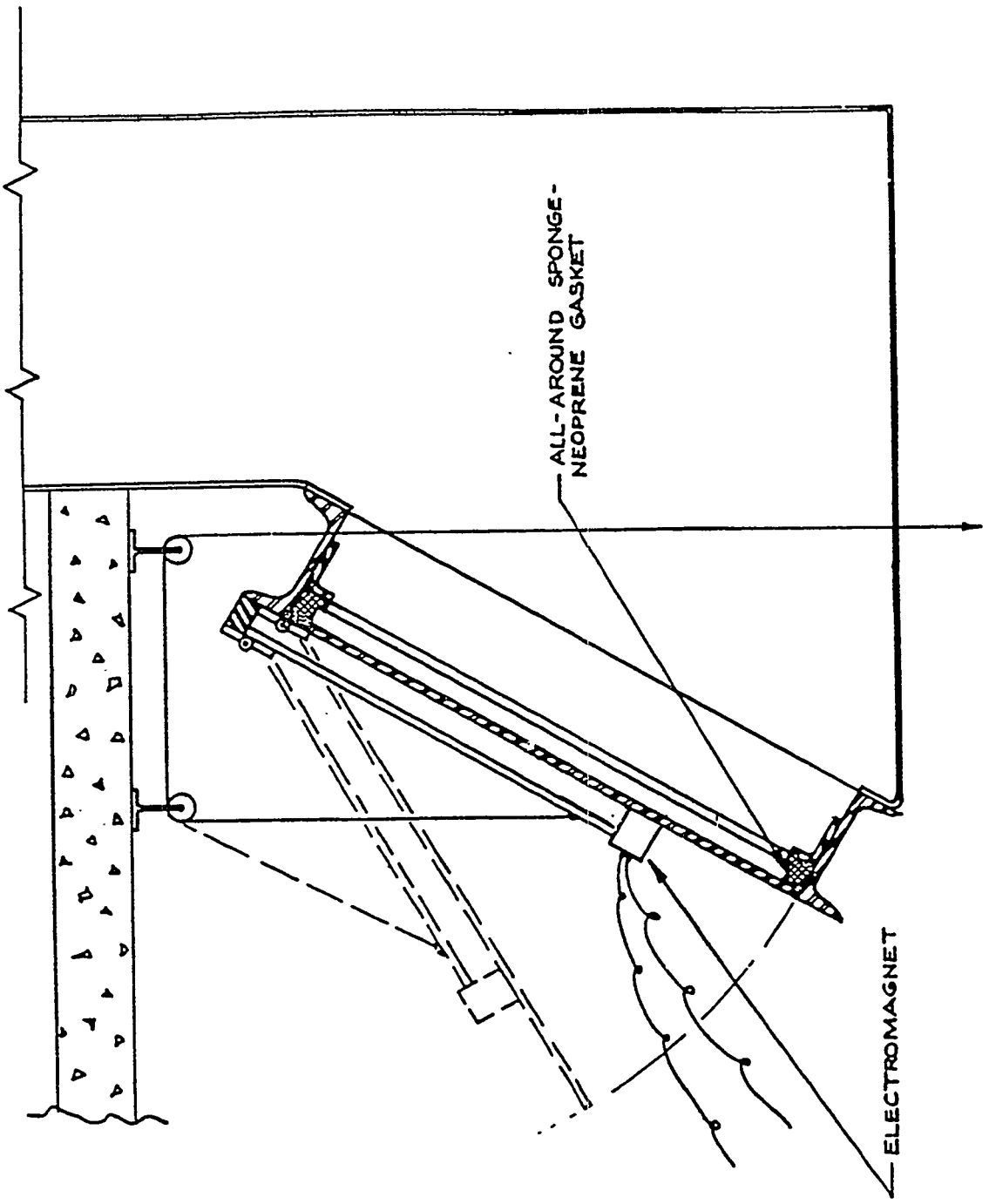


FIG. 6-3 PRESSURE-TIGHT AIR DUCT

MeV photon from ^{85}Kr. The gamma ray count rate provides a direct measurement of the average specific activity, because of the long range of these photons in air (relaxation length about 90 meters).

The release of a concentration of ^{85}Kr of 8×10^{-6} $\mu Ci/cm^3$ provided an initial count rate of 3000 cpm above background from a bank of 3 aluminum-walled G-M tubes, 3-inches long, and 3/4-inch in diameter. The 0.5 MeV photopeak count was 50 cpm, for a 3-inch x 3-inch NaI(Tℓ) crystal.

Figure 6-4 shows the count rate as a function of time for both beta and gamma rays. The leak rate of 26% per 20 hours was well within the Technical Specification 3.7 exfiltration rate of 50% in 20 hours.

6.2 Shielding

The pool is shielded by earth on three sides, but the fourth side consists of a massive concrete shield with thicknesses ranging from a maximum of 90-inches at the bottom, near the core region, to a minimum of 30-inches at the extreme top. This shield is penetrated by two 8-inch beam holes, a large access facility and a thermal column. These penetrations are filled with concrete plugs when not in service. Further descriptions of these facilities are provided in Section 5.0.

A complete survey of the University of Virginia Reactor Shielding was made by the Neutron Physics Division of the Oak Ridge National Laboratory. The results from that survey with the reactor at a power of one megawatt are described in the next paragraphs.

The thermal-neutron dose rates observed over the surface of the shield are plotted in Fig. 6-5, in which the three accessible surfaces have been developed, or "unfolded" to lie flat on the page.

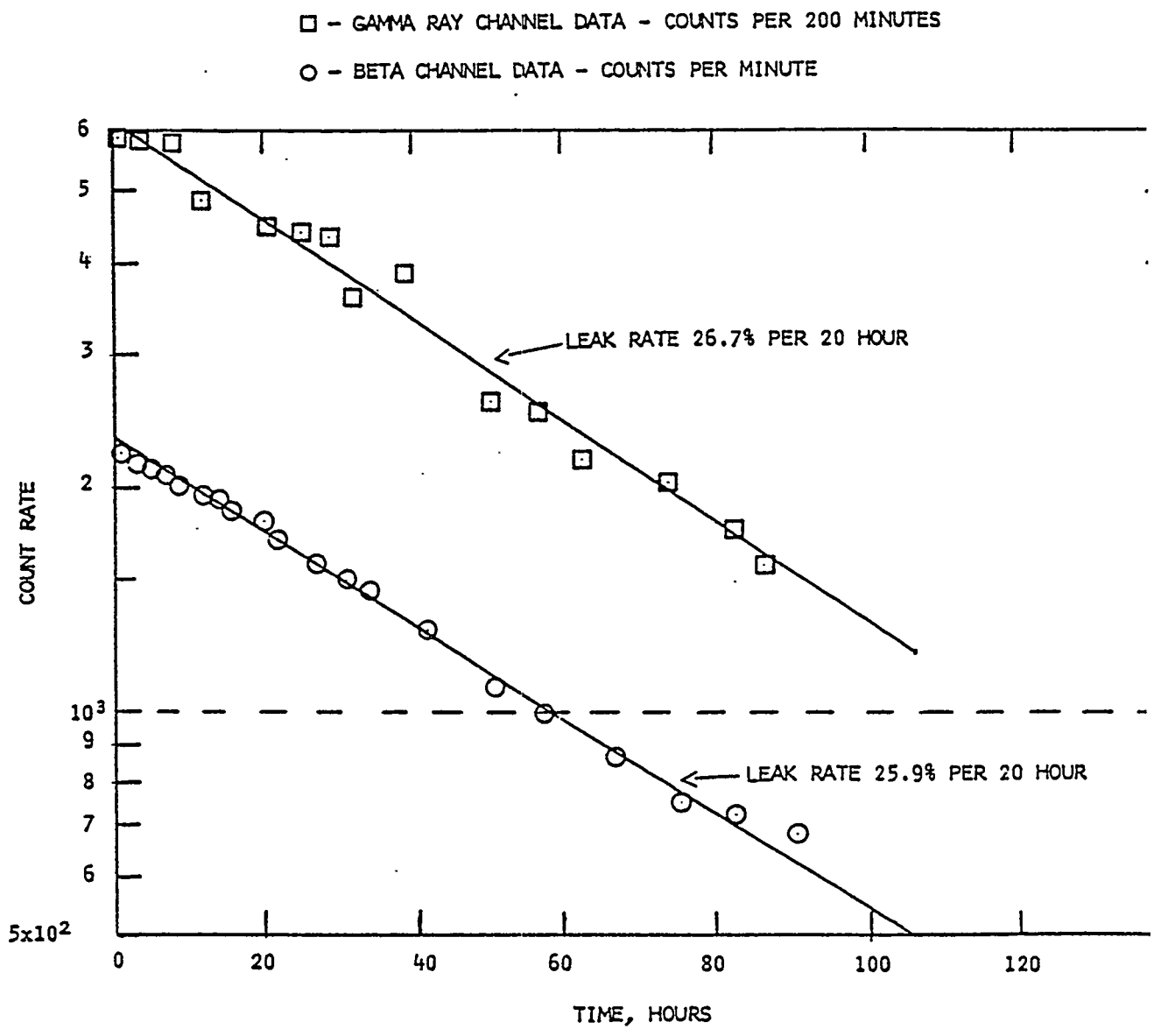


FIGURE 6-4 UVAR CONFINEMENT ROOM COUNT RATE DATA

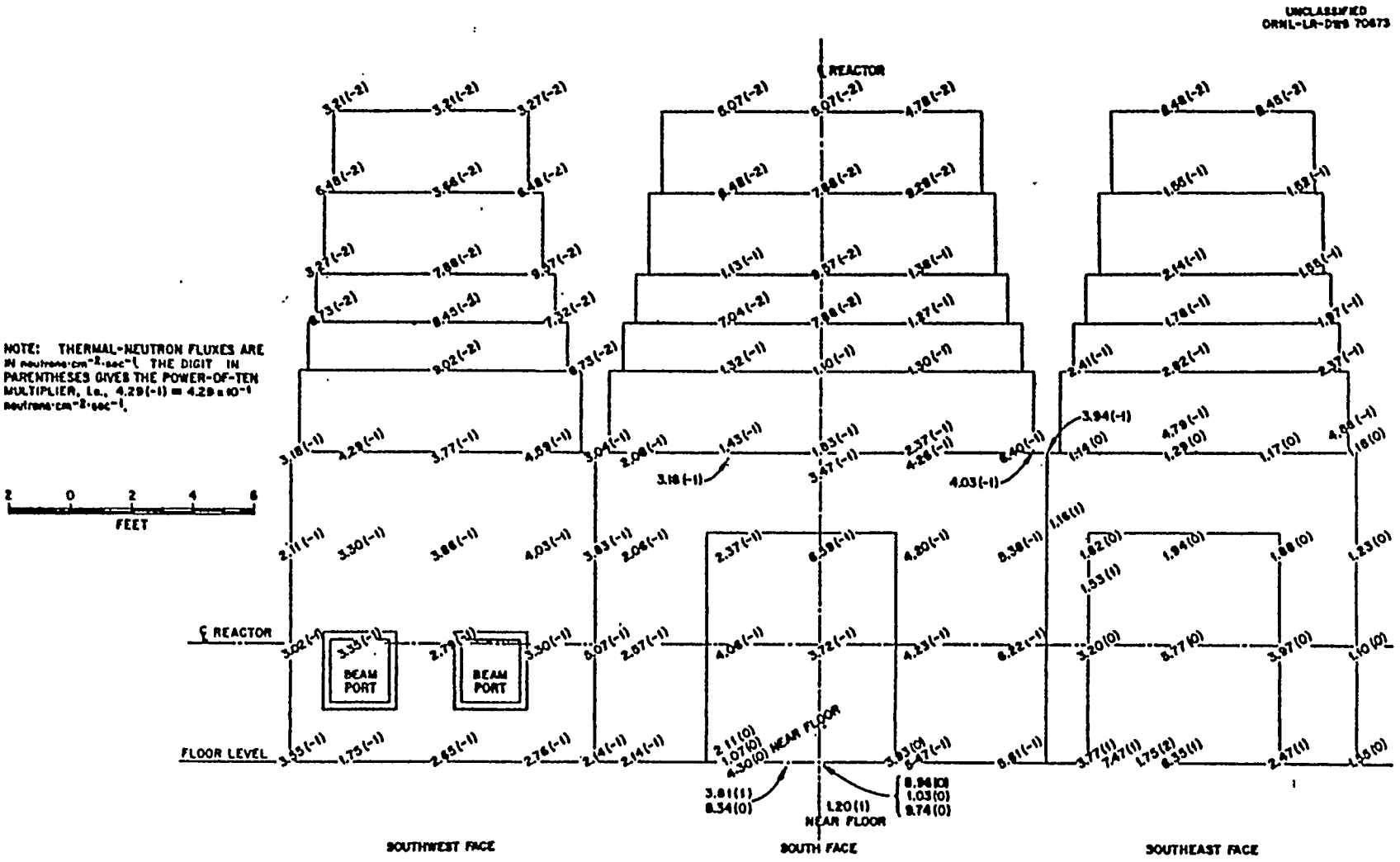


Figure 6-5 Thermal-Neutron Fluxes at the Surface of the University of Virginia Reactor Shield.

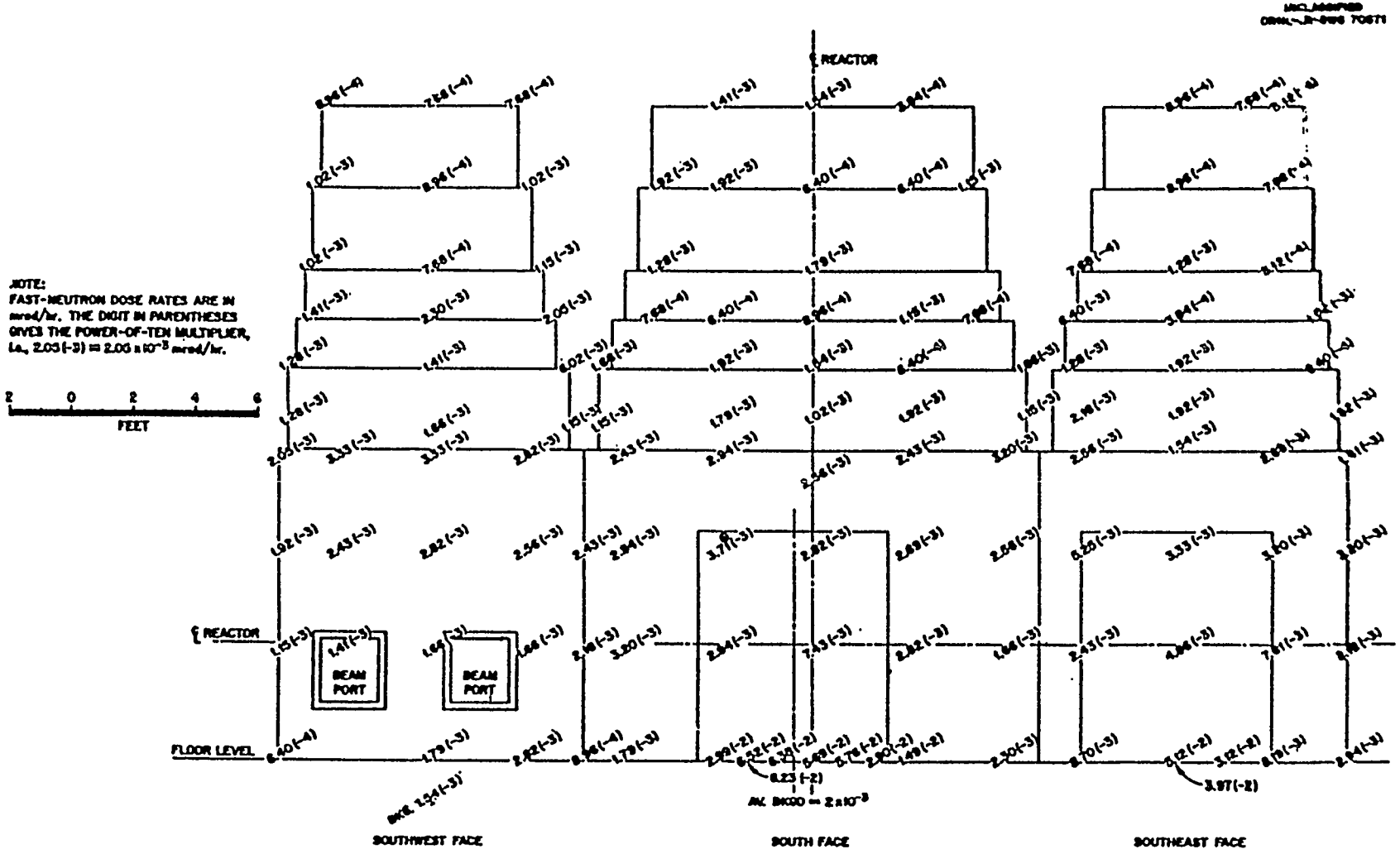


Fig. 6-6 Fast-Neutron Dose Rates at the Surface of the University of Virginia Reactor Shield.

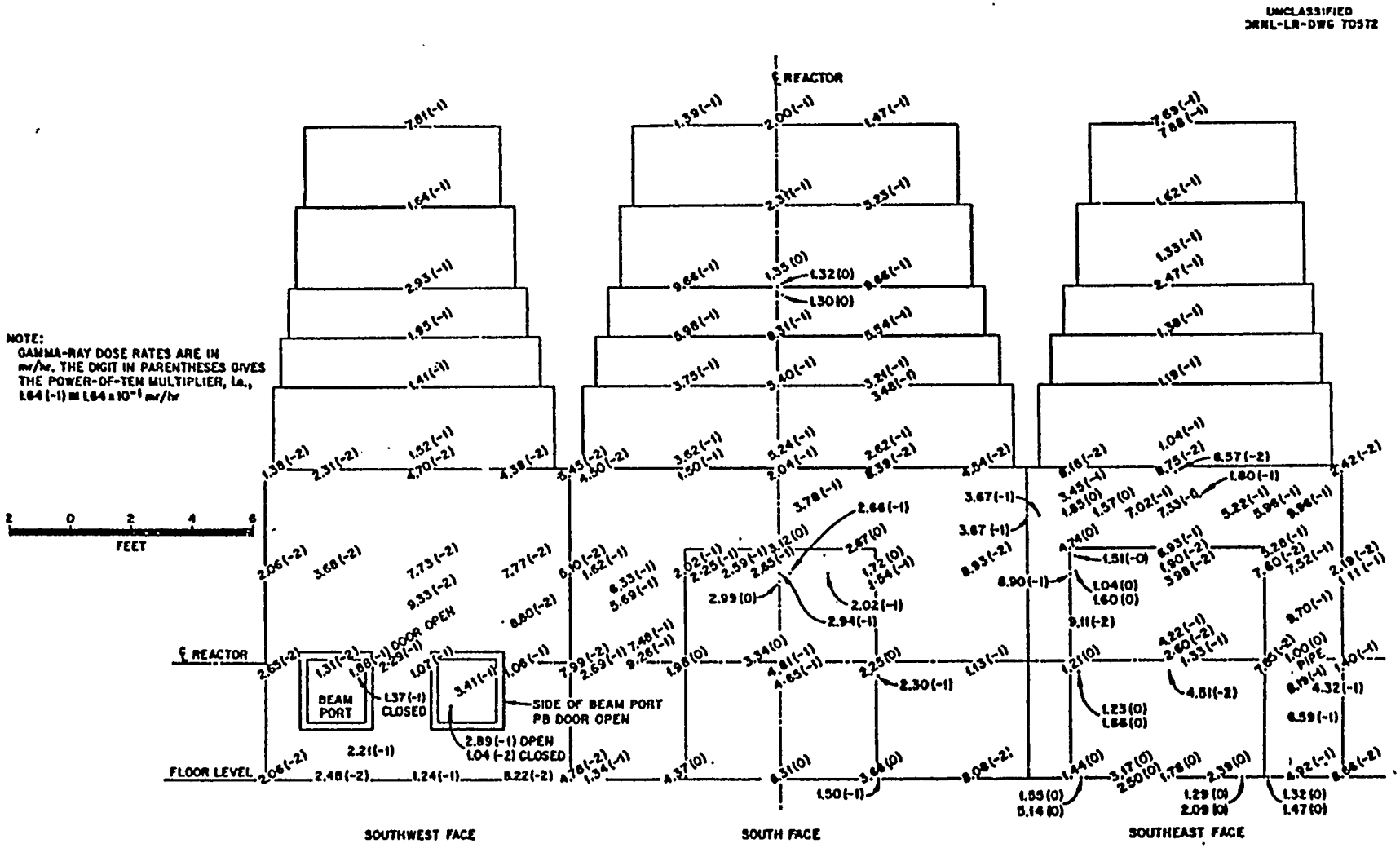


Figure 6-7 Gamma-Ray Dose Rates at the Surface of the University of Virginia Reactor Shield.

Fast-neutron dose rates are plotted in similar fashion in Fig. 6-6, and gamma-ray dose rates in Fig. 6-7.

In connection with the fast-neutron dose rates reported in the present work, some comments are required. The modified long counter with which the fast-neutron data were obtained is strongly directional, responding in terms of correct dose only when the neutrons are incident upon its front face. This factor is inherent in its design. Its response to neutrons impinging upon its sides is considerably higher. Thus, the dose rates measured by the modified long counter must be considered to be an upper limit to the true fast-neutron dose at the point of the measurement. Against a shield face, or in measuring neutron streaming through a crack or hole in a shield, the dose rate measured is probably very close to the true value. As the neutron field surrounding the counter approaches isotropicity, the dose measured is expected to be an overestimate, possibly a considerable overestimate. This latter condition would apply to measurements made in the vicinity of the heat exchanger.

Fluxes and dose rates were in general very low. Streaming around the thermal column and access facility closures was somewhat evident, amounting to a maximum fast-neutron dose rate of 0.0652 mrad/hr, a thermal-neutron flux of 10 to 12 neutrons cm^{-2} sec^{-1}, and gamma-ray dose rates of roughly 6 mr/hr.

Data was also obtained at distances from 4 to 6-inches above the pool water surface. These values are plotted in Fig. 6-8. Gamma-ray dose rates as high as 7 mrad/hr were measured.

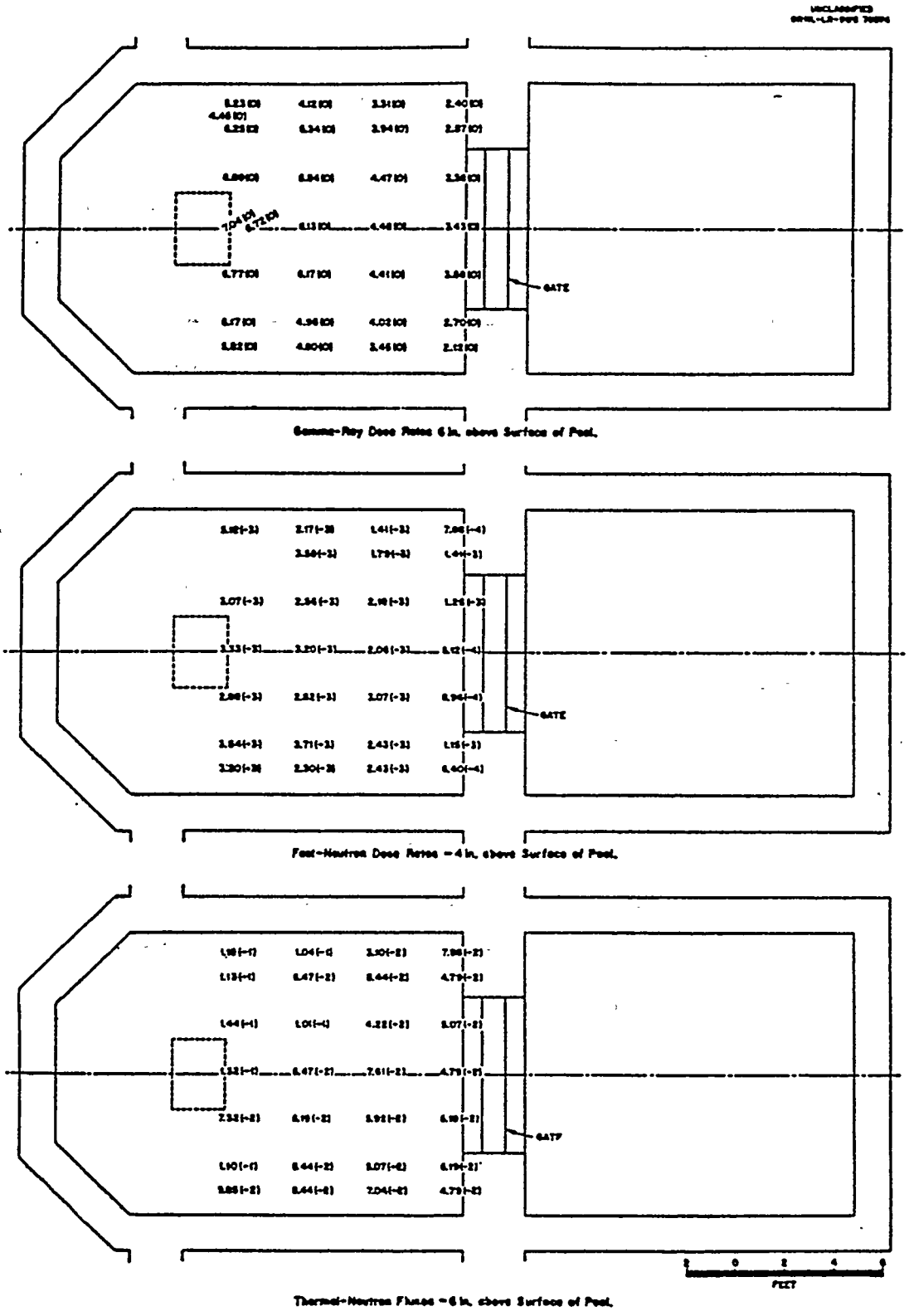


Figure 6-8 Gamma-Ray and Fast-Neutron Dose Rates and Thermal-Neutron Fluxes Near Surface of University of Virginia Reactor Pool.

6.3 Hazards During Normal Operation

Calculation of the concentration of Argon-41 in the beamport extension after prolonged operation at 2 MW predict a discharge to the atmosphere that was approximately a factor of two below the maximum permissible concentration. Comparison of experimental measurements by the ORNL team and calculated values of Argon-41 concentrations demonstrated that the assumptions made in the calculation were conservative by an additional factor of three. These factors, combined with the ease with which the concentration of radioactive Argon-41 can be reduced by delaying release after operation to permit decay, indicate that this hazard presents no problem at a reactor power level of 2 MW.

The measurements of radiation intensity by the ORNL team at 2 MW indicate high gamma-ray dose rates at four locations: (1) at the surface of the pool immediately above the reactor core, (2) around the shield plug of the large access facilities, (3) in the heat exchanger room, (4) in the main demineralizer room and (5) in the source storage room. Current policies limit access to the heat exchanger room during operation and the safeguards are adequate to control this hazard. When the limited amount of time spent at the other three locations is considered, these do not appear to be a serious hazard. However, marking these locations will serve to remind personnel of the existing dose rate at 2 MW.

7.0 HEALTH PHYSICS

7.1 General Information

The Reactor Facility is a research tool of the University and as such, subject to use by all of its schools. It is the responsibility of the operations staff and the Health Physicist to provide and maintain full use of this tool, yet prevent undue risks and hazards to the individual workers, the University and the Community at large.

The Health Physicist is responsible for assuring that those measures and regulations pertaining to the Health Physics aspects of the reactor and its operation are carried out and mantained. The Director of the Reactor Facility is advised by the Health Physicist in all pertinent matters. The close association but independence of the Health Physics and Reactor Facility operations has worked well at other reactor installations, and the University has patterned its organization accordingly.

7.2 Education in Health Physics

It shall be the duty of the Health Physicists, or his designee, to periodically instruct Reactor Facility personnel about the risks and hazards of radiation and the means of lessening this danger to themselves and others. This shall be done as follows:

(A) Each individual with unescorted access to the Reactor Facility will be given an initial indoctrination lecture about Health Physics, followed by a question and answer period, so that the biologic aspects and the genetic aspects of radiation change are understood.

(B) On-the-spot lectures may be given by the Health Physicist, during a particular phase of operations, to emphasize the protection aspects of Health Physics.

(C) Pre-experiment evaluation of hazards associated with a particular experiment will be performed first by the individual proposing a new experiment and then by the Health Physicist.

(D) A radiation log will be prepared for each "permanent" worker at the facility. In this log the monthly dose data will be recorded.

7.3 Personnel Monitoring and Protection

The Health Physicist is charged with the procurement and maintenance of the detection equipment and the dose badges for personnel exposure monitoring.

Badges: These will be used for monthly checking of personnel neutron and/or gammma dose, with the dose evaluations performed by a commercial supplier.

Pocket chambers: Direct reading - will be worn by personnel working in suspected high radiation areas.

Finger badges - will be worn by personnel handling highly radioactive material.

Protective clothing - street clothes are worn by the majority of workers at the facility; however if there is a possibility of personal or area contamination, protective and/or disposable clothing is provided and will be worn.

7.4 Permanent Monitoring and Surveys

Fixed Radiation monitors are mounted in the following areas:

1) On the reactor bridge,

2) Ground floor wall (reactor face area),

3) Outside the hot cell,

4) In the demineralizer room.

The readings of these monitors are displayed individually on the

secondary console in the reactor room. The existence of excessive radiation in any of these areas causes an audible alarm to sound at the console. The initiation of the reactor bridge monitor alarm and the ground floor monitor alarm isolates the containment, as described earlier, and scrams the reactor. In addition, numerous portable instruments are available for surveying all areas in the facility.

Calibration of these instruments on a regular basis will be assured by the Health Physicist. Calibration records will be mantained.

The initial run of a new experiment or the use of radioactive materials will be extensively monitored and a record maintained of the results, if the work is such that the Health Physicist determines a possible radiological hazard to personnel exists.

Facility radiation surveys, air sampling, and contamination smears will be performed in work areas on a regular basis by the Health Physicist or his designee. Such official will be recorded. Informal surveys made by the experimenters of their work areas to confirm typical (safe) radiation levels may be made unofficially and need not be recorded. However, if excessive levels not previously identified are found, the experimenter will notify the Health Physicist, who will then make an official survey.

7.5 Prohibitions and Sanctions

The Reactor Safety Committee and the Reactor Facility Director are responsible for enforcing all applicable Federal, State and University regulations necessary to run the facility. The Health Physicist will report irregularities and recommend necessary steps for

their correction to the Director and the Safety Committee. The Director will determine corrective actions to be taken in such cases. However, the Health Physicist may issue emergency orders if necessary, on his own responsibility.

Safe areas for eating and drinking will be designated by the Health Physicist. Smoking is permitted in private offices and specially designated common areas where unsealed radioactive materials are not used.

The University of Virginia has established a whole body personnel dose limit of 0.5 rem/year which is 10% of the limits in 10CFR, Part 20. If an individual receives a radiation dose in excess of these limits as determined by ionization chambers, dosimetry badges or other methods, the Health Physicist will notify the Facility Director. The Health Physicist will provide information concerning the amount and type of exposure and recommend actions to be taken by the individual to avoid further, similar exposures.

7.6 Waste Disposal

The Health Physicist will check radioactive waste and refuse from the Reacator Facility, monitoring it prior to legal disposal. The public water system will be separate from water drainage systems used to collect and discard radioactive material. The disposal of liquid radioactive wastes is discussed in Section 4.8 of this document. Dry litter and waste will be stored until it has decayed to safe levels or can be shipped to a licensed burial site. Radioactive materials may be released only with the approval of the Health Physicist.

7.7 Shipping and Transport

Radioactive material produced or purchased by the Reactor Facility will generally be used on-site. However, in instances where material must be shipped from the reactor to one of the schools on the University grounds, or to national or international recipients, applicable DOT regulations governing shipments of radioactive material, as outlined in 10 CFR Part 71, will be followed. Radioactive material will not be allowed to leave the reactor site unless the recipient is qualified to receive the materials under NRC or international regulations, as applicable.

8.0 ADMINISTRATION

8.1 General Organization

The reactor is operated under NRC License R-66 granted in 1960. The Reactor Facility organization responsible for assuring safe reactor operations and use of radioactive materials at the University of Virginia is shown in Fig. 8-1. This organization includes two major committees: the University Radiation Safety Committee and the Reactor Safety Committee.

8.2 Radiation Safety Committee

The Radiation Safety Committee is appointed by the President of the University and must approve the possession and use of radioactive materials at the University of Virginia with the exception of those associated with the Reactor Facility. Production, possession and usage of radioactive materials at the reactor comes under the reactor license and is reviewed by the Reactor Safety Committee.

8.3 Reactor Safety Committee

As required by the license, a Reactor Safety Committee is active. As a minimum, the Reactor Safety Committee is composed of at least five members and includes the University's Radiation Safety Officer, the Reactor Director and a professor from a department other than Nuclear Engineering. Senior members of the Reactor staff attend committee meetings in an advisory capacity, but there is only one vote by the Reactor Staff which is cast by the Reactor Director. This is to prevent domination of the Committee by members of the operating organization of the reactor. The Reactor Health Physicist is also welcome to attend Reactor Safety Committee meetings.

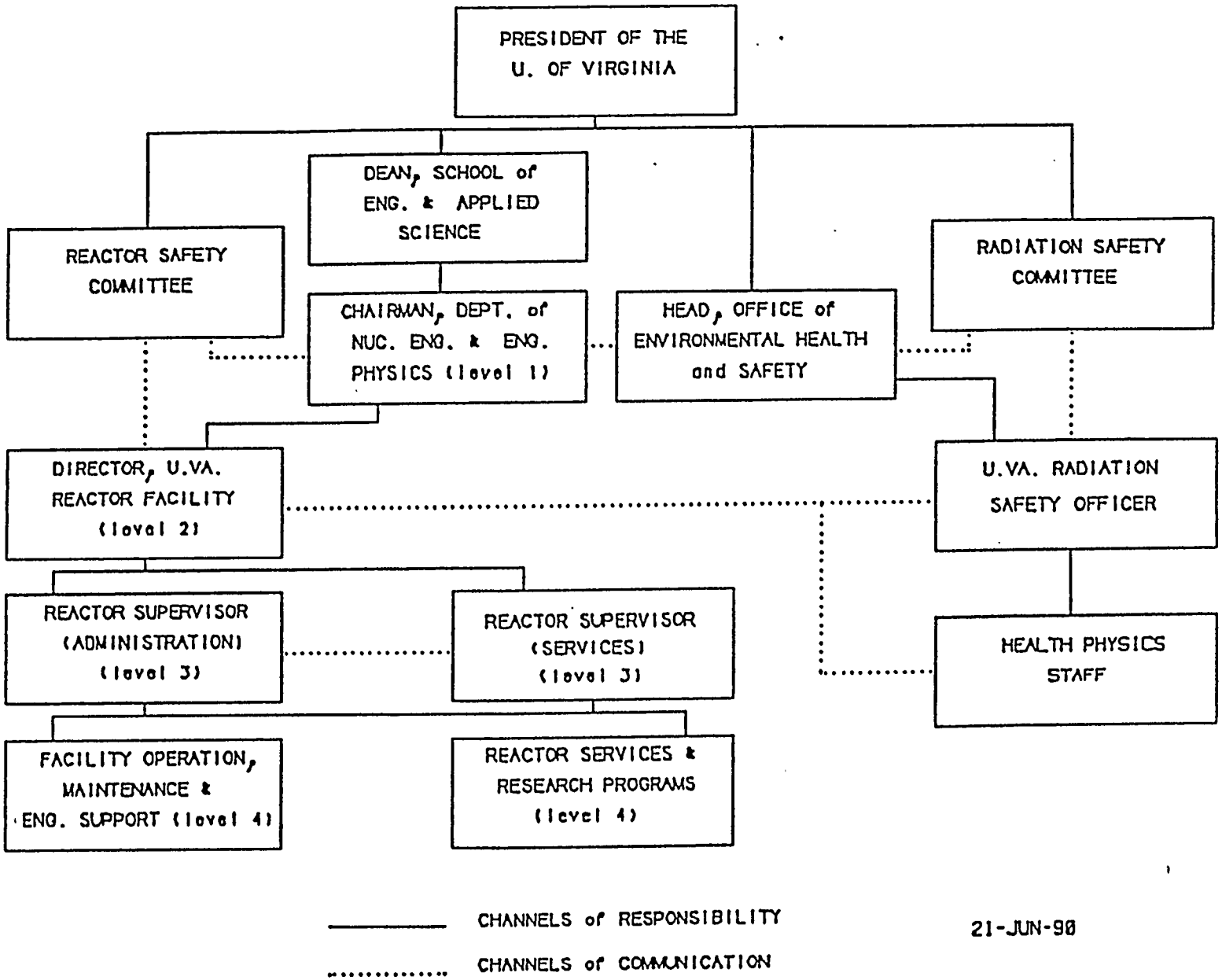


Figure 6.1 Organizational Structure of U.Va. Reactor Facility

The Committee reviews and passes on new experiments that could affect the safety of the reactor. These include critical experiments, as well as experiments in which the reactor is used as a radiation source. Written standard operating procedures (SOP's) and emergency plan and implementing procedures (EPIP's) approved by the Committee are in effect for reactor operations. Experiments involving the reactor are run under written and Reactor Safety Committee approved procedures. While the Reactor Safety Committee approves the procedures to be followed for safe operations and experiments, the detailed routine enforcement of reactor safety is the responsibility of the operating staff. Also, while the Reactor Safety Committee has the authority to require and approve specific procedures to prevent unacceptable exposure of personnel to radiation, the immediate responsibility for compliance with Title 10, Code of Federal Regulations, Part 20, rests with the Reactor Staff and, in particular, with the Health Physicist.

8.4 Procedures

The reactor is operated in accordance with written standard operating procedures (SOP's) approved by the Reactor Safety Committee. These procedures include normal startup, operation and shutdown of the reactor. Emergency plan implementing procedures (EPIP's) exist to implement a Reactor Safety Committee and NRC approved Emergency Plan (EP). General procedures for the handling of radiation experiments are promulgated by the University but these are supplemented by special procedures which apply only to the experiment under consideration.

Procedures dealing with the operation of the reactor and associated experiments must have the approval of the Reactor Safety Committee.

Changes to these procedures require the approval of this committee, however, minor deviations not changing their intent may be made by the Reactor Director, and is permitted by the SOP's. When deviations to SOP's occur, the RSC is informed by memo from the Reactor Director. It is to be recognized that procedures notwithstanding, the safe operation of the reactor is dependent upon the Reactor Staff and their exercise of good judgement.

All personnel, including students who work routinely at the Reactor Facility, wear dosimetry badges. Occasional visitors are issued self-reading pocket dosimeters. For large groups of visitors, two pocket dosimeters are worn by the staff member acting as a guide. This permits tours to be conducted without issuing large number of individual pocket dosimeters.

8.4 Records

The reactor log book and all other records are open for inspection by the Reactor Safety Committee. These records, plus all the records of the activities of the Safety Committee, are also available for review by NRC compliance inspectors. An annual report is submitted to the NRC listing changes made to the facility under 10CFR50.59 and describing minor accidents pertinent to safety. Major incidents are reported to the NRC as required by the Technical Specifications.

9.0. Safety Analysis

The UVAR's MTR type LEU fuel elements contain plates with low enriched uranium fuel clad with aluminum. Standard elements contain 22 flat fuel plates, control rod elements contain 11 fuel plates, and partial elements contain 11 fueled and 11 non-fueled plates in an alternating array. The overall external dimensions of these three element types are essentially the same, so that they may fit anywhere on the 8 by 8 reactor core grid plate. Details of the physical arrangement are contained in Section 3.0.

The limiting conditions of reactor power, coolant water flow rate and inlet pool water temperature are given in the UVAR Technical Specifications. The bases for the Safety Limit and Limiting Safety System Settings and the thermal-hydraulic analysis are presented in this chapter. References used in the analysis are listed at the end of this chapter.

9.1. Thermal Hydraulic Analysis of the UVAR

To establish the safety limit, limiting safety system settings, limiting condition of operation, and normal operating conditions for pool reactors it is necessary to examine factors such as burnout, or an excursive hydraulic instability resulting in subsequent burnout, which may lead to the disruption of fuel plate integrity. In addition, it is necessary to determine by calculation the operating conditions at which the onset of nucleate (incipient) boiling will occur in a coolant channel, so that reactor operating conditions may be set at levels which prevent these phenomena.

An analytical procedure was developed to predict: 1) burnout, 2) hydraulic instability, and 3) incident boiling, in the hot channel of a UVAR LEU 22 plate fuel element. The effects of the following parameters were studied: (1) channel inlet (pool) temperature, (2) heat flux distributions, i.e. uniform, chopped cosine and exit peak, and (3) coolant flow rate.

The Gambill[1] correlation was used for estimating burnup heat fluxes for subcooled boiling. Only downflow was considered for forced cooling in the analysis. An equation proposed by Rohsenow and Bergles[2] was used for predicting the onset of nucleate boiling and a comparison was made with experimental data obtained from the Oak Ridge Research Reactor.[3]

Three vertical power profiles were considered in the analysis: 1) uniform power profile, 2) chopped cosine power profile, and 3) exit peak power profile. The exit peak power profile illustrated in Figure 9-1 was found to be the most limiting and was used throughout this analysis. The exit peak power profile is based upon neutron flux measurements in the hot channel of the UVAR HEU core which is located in a control rod element and is next to the water filled gap left by the withdrawn control rod.

Numerous empirical correlations were used in the thermal-hydraulic analysis of the LEU UVAR. Because of the importance of justifying the use of these correlations, the following sections provide a brief discussion of the correlations and the ways in which they were employed in the calculations. Where possible, comparisons of analytical calculations with experimental data are made.

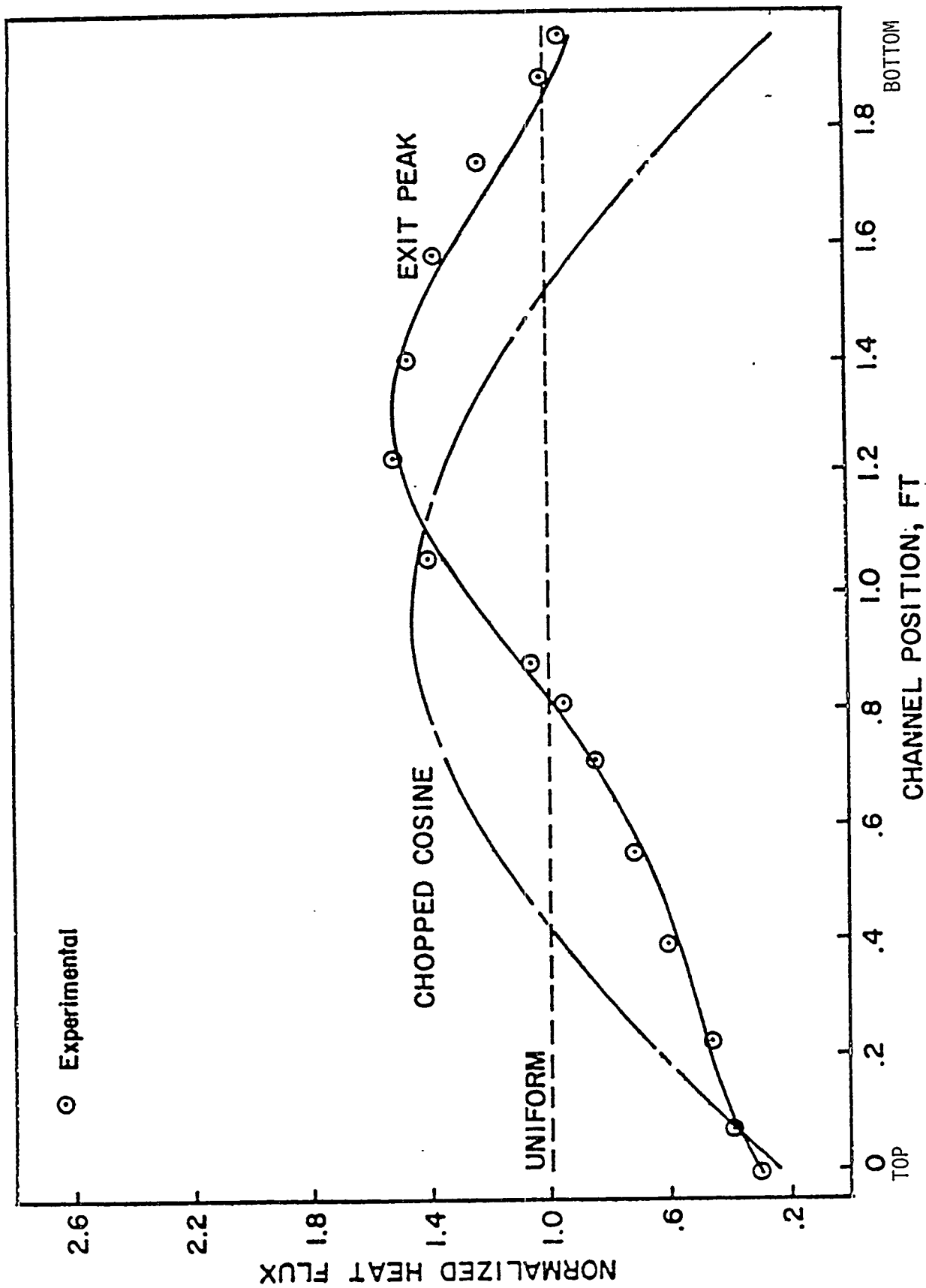


FIG. 9-1 HEAT FLUX DISTRIBUTIONS

9.2. Forced Convection Heat Transfer

In the thermal-hydraulic analysis of the LEU UVAR, the flow velocities are small and the channel length-to-equivalent diameter ratio is 130. As a consequence, part of the analysis involves flows in the transition Reynolds number range and entrance effects exist over a substantial portion of the channel length. The Hausen[4] equation accounts for these factors and was therefore used. The expression for the local heat-transfer coefficient is given by

$$h(z) = 0.116 \left(\frac{k}{D_e}\right) \left[N_{Re}^{2/3} - 125\right] N_{Pr}^{1/3} \left[1 + \frac{1}{3}\left(\frac{D_e}{z}\right)^{2/3}\right] (\mu_b/\mu_w)^{0.14} \quad (9.1)$$

where: $h(z)$ = local heat-transfer coefficient, BTU/hr-ft^2-^{o}F

k = fluid thermal conductivity, Btu/hr-ft-^{o}F

D_e = channel equivalent diameter, ft

N_{Re} = Reynolds number

N_{Pr} = Prandtl number

z = axial location in channel, ft.

μ_b = fluid viscosity at local bulk temperature, lb_m/sec-ft

μ_w = fluid viscosity at local wall temperature, lb_m/sec-ft

Except for μ_w, the fluid physical properties in Eq. (9.1) are evaluated at the local bulk temperature. Since the wall temperature is needed to use Eq. (9.1), an iterative technique is required in its application.

9.3. Prediction of Incipient Boiling

Based upon a semi-empirical approach, Bergles and Rohsenow obtained a correlation for predicting incipient boiling that is dependent only on pressure and wall temperature. Although some of their experimental data indicated that bulk fluid subcooling had an effect upon incipient boiling, this factor was not incorporated in the correlation. For water, over a pressure range from 15 to 2000 psia, the heat flux at incipient boiling is given by[2]

$$q''_{IB} = 15.6\ p^{1.156}\ (T_w - T_{Sat})^{2.30}/p^{0.0234} \qquad (9.2)$$

where q''_{IB} = incipient boiling heat flux, Btu/hr-ft^2

p = pressure, psia

T_w = local wall temperature, ^oF

T_{sat} = fluid saturation temperature, ^oF

For pool reactors with low velocity flows, Eq. (9.2) generally predicts incipient boiling at lower wall superheat temperatures than is actually the case. This is attributed to an absence of very large cavities which would support nucleation at the lower heat fluxes in such a system[2].

The wall temperature must be determined in order to use Eq. (9.2). This quantity is calculated using the heat-transfer coefficient given by Eq. (9.1). The solution q_{IB}'' requires an iterative procedure since h is dependent upon wall temperature, which is related to the local heat flux.

In order to test the validity of the use of Eqs. (9.1) and (9.2) for pool reactor thermal analysis, a comparison was made between calculated incipient boiling and experimental results obtained from the Oak Ridge Research Reactor (ORR). Figure 9-2 shows the results of the comparison, and as seen, a very good agreement exists. For the experimental curve, the anomalous behavior shown by the dashed line has not been explained. However, the Oak Ridge investigators thought that gas bubbles other than steam may have been produced in the core during this part of the experiments.

9.4. Burnout Heat Flux

Numerous correlations have been proposed for the prediction of subcooled and quality burnout. Unfortunately, most of these correlations are not applicable to the UVAR parameter range. Selection of burnout correlations should be made on the basis of burnout data that fall within the pertinent parameter range. Data collected by Gambill were at conditions representative of the UVAR parameter range.

Gambill's correlation for subcooled burnout was used for the UVAR analysis because it is quoted as being applicable for the UVAR parameter range and its predictions are reasonably accurate when applied to the available data that is closest to the UVAR parameter range.

Gambill proposes a superposition approach for treating burnout which is given by[1]

$$q''_c = q''_{PB}(\text{pool boiling}) + q''_{FC}\ (\text{forced convection}) \qquad (9.3)$$

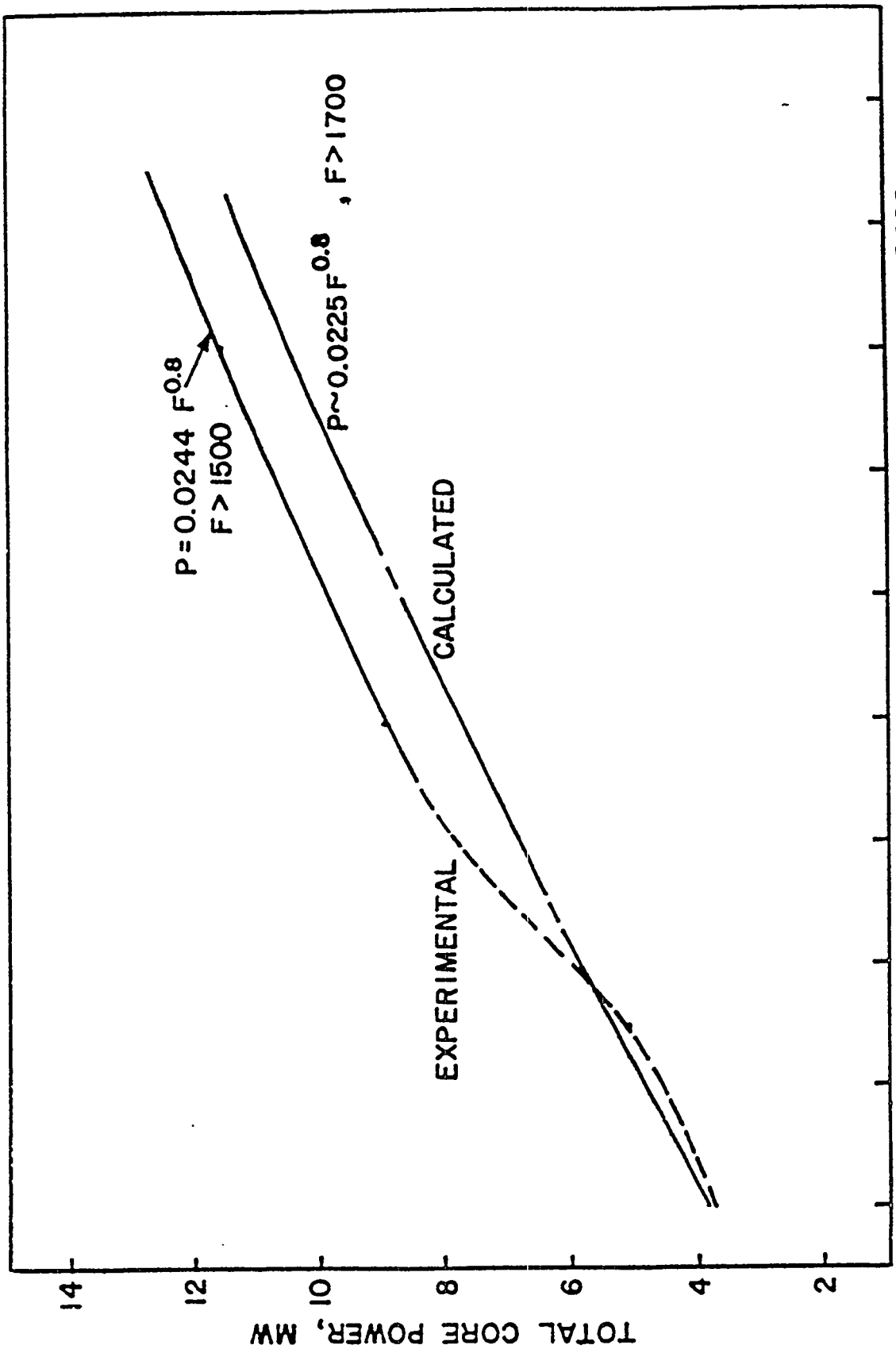


FIG. 9-2 -CALCULATED vs. EXPERIMENTAL INCIPIENT BOILING IN THE ORR

The pool boiling term for conditions representative of pool reactors is[5]

$$q''_{IB} = 0.15\, h_{fg}\sqrt{\rho_g}\left[\sigma g g_c\ (\rho_f - \rho_g)\right]^{1/4} \times \left[1 + \left(\frac{p_f}{p_g}\right)^{3/4} \frac{c_p(T_{Sat} - T_b)}{9.8\, h_{fg}}\right] \tag{9.4}$$

where h_{fg} = latent heat of vaporization, Btu/lb_m

σ = liquid-vapor interface surface tension, lb_f/ft

g = acceleration of gravity, ft/sec^2

$$g_c = 32.2 \frac{lb_m}{lb_f} \frac{ft}{sec^2}$$

ρ_f = saturated liquid density, lb_m/ft^3

ρ_g = saturated vapor density, lb_m/ft^3

c_p = liquid specific heat, btu/lb_m - ^oF

T_{Sat} = saturation temperature, ^oF

T_b = local bulk fluid temperature, ^oF

The forced convection term is

$$q''_{FC} = h(T_{WB} - T_b) \tag{9.5}$$

where h is the Hausen local heat-transfer coefficient given by Eq. (9.1) and T_{WB} is the Bernath critical wall temperature given by[6]

$$T_{WB} = 102.5 \ln p - 97.2 \left(\frac{p}{p + 15}\right) - 0.45u + 32,\ ^oF \tag{9.6}$$

where p is the fluid pressure in psia and u is the mean fluid velocity in ft/sec.

Because radiation exposure to personnel from N-16 activity in the pool water is a concern, the UVAR uses coolant downflow which has an adverse effect upon burnout. Buoyancy effects reduce bubble velocities and as a result burnout heat fluxes are reduced. Gambill has studied the effects of downflow at low velocities and pressures and recommends the following corrections be applied to his burnout correlation.[5]

$$\frac{q_c''(\text{downflow})}{q_c''} = \frac{1}{6.58\ (N_{Gr}/N_{Ka})^{0.39}} \tag{9.7}$$

The ratio of Grashof to Karman numbers if given by

$$N_{Gr}/N_{Ka} = \frac{p_f^2\ g\ \beta(T_b - T_l)D_e}{f_W G^2} \tag{9.8}$$

where β = liquid volumetric coefficient of expansion, $^oF^{-1}$

T_b = local channel bulk temperature, ^oF

T_l = channel inlet temperature, ^oF

f_w = Darcy-Weisbach friction factor

G = mass velocity, lb_m/ft^2

The evaluation of f_W is addressed later in the discussion of flow stability. All fluid properties in Eq. (9.8) are evaluated at the average channel temperature up to the point of consideration. The range of applicability of Eq. (9.8) is for $0.008 \leq (N_{Gr}/N_{Ka}) \leq 1.0$, for $N_{Gr}/N_{Ka} > 1.0$, and it is recommended that the value 1.0 be used for the ratio in Eq. (9.8).[5]

Some of the downflow burnout data collected by Gambill were at conditions representative of the UVAR parameter range. These data were taken in a 0.9 cm diameter tube of 25 and 30 cm lengths. - The pressure was 16.2 psia, the fluid inlet velocities ranged from 0.29 to 7.7 ft/sec and the fluid bulk inlet temperatures ranged from 51°F to 71°F. Figure 9-3 shows Gambill's ratios of calculated burnout heat fluxes (from Eqs. (9.3) through (9.8)) to experimental burnout heat fluxes. As shown, the agreement is quite good with 90 percent of the predictions falling within ± 30 percent of the experimental values. This agreement causes a considerable amount of confidence to be attached to the analytical procedures.

Two further uncertainties exist in using Gambill's burnout correlation for the UVAR burnout analysis. These uncertainties are: (1) the effects of non-uniform heat generation in the UVAR and (2) the validity of applying a burnout correlation based upon circular tube burnout data to rectangular channels. As regards the first uncertainty, experiments by Todreas[7] indicate that for subcooled burnout the effects of non-uniform heat generation are not substantial. A review of the Non-Uniform Heat Generation Experimental Program of the Babcock and Wilcox Company indicates that the total channel power at burnout is essentially independent of heat flux distribution. As concerns the second uncertainty, it appears the effects of geometry are small or advantageous for rectangular channels[8,9], when burnout data with tubes and rectangular channels having the same equivalent diameter are compared. Some researchers have observed up to 40 percent[8,10] increases in burnout heat fluxes for rectangular channels. For the UVAR thermal analysis,

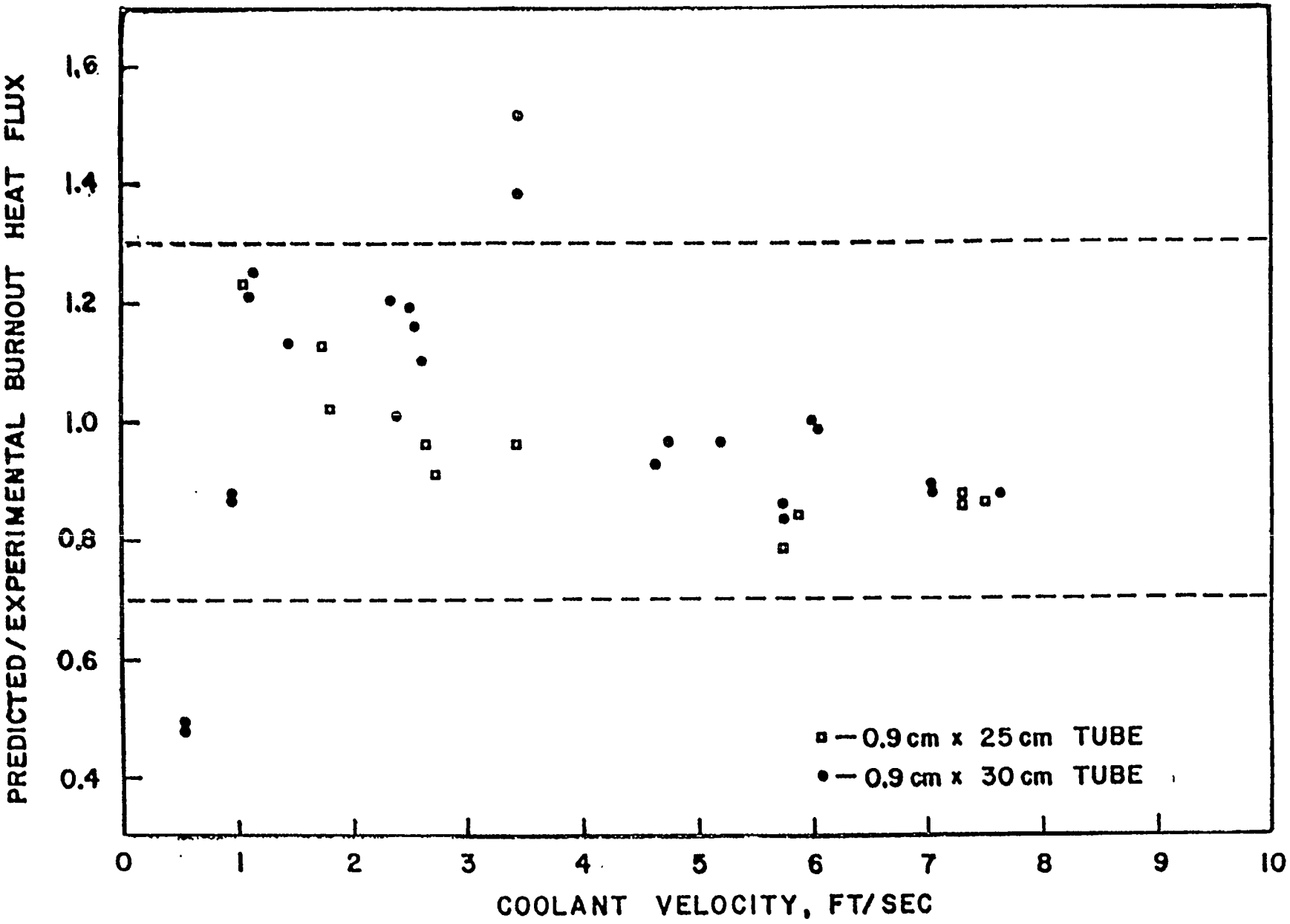


FIG 9-3 -COMPARISON OF CALCULATED WITH EXPERIMENTAL BURNOUT HEAT FLUXES

burnout or a flow instability usually occurs before the water reaches its saturation temperature and burnout is assumed to occur when it reaches its saturation temperature at the channel exit.

9.5. Flow Instability

Due to the effects of increased pressure loss with subcooled nucleate boiling and adverse buoyancy from coolant downflow, an excursive hydraulic instability can occur in pool reactor hot channels. Such an instability occurs with flow in parallel channels when the pressure loss in one or more channels increases with decreasing flow rates. The end result of this effect is a drastic flow reduction or a flow reversal in the unstable channels.

A flow instability is determined by calculating channel pressure losses for successively decreasing flow rates. A minimum on the channel pressure loss-flow rate characteristic curve locates the minimum stable flow rate.

Pressure loss across pool-reactor element coolant-channels is due to the following: (1) inlet and exit losses, (2) channel friction loss, (3) loss due to changes in fluid momentum, and (4) loss due to change in elevation. Since burnout was assumed to occur when the fluid reaches its saturation temperature at the channel exit, only single-phase pressure losses were considered.

Pressure losses were calculated incrementally down the channel in order to account for fluid property changes and transition from regimes of forced-convection heat transfer to subcooled nucleate boiling.

The total pressure loss of the channel inlet was calculated using[11]

$$\Delta p(\text{inlet}) = \frac{K \rho_i u_i^2}{2 g_c} \tag{9.9}$$

where Δp (inlet) = total pressure loss at channel inlet, lb_f/ft^2

K = loss coefficient, dimensionless

ρ_i = fluid density at channel inlet, lb_m/ft^3

u_i = fluid velocity inside channel inlet, ft/sec

The loss coefficient K depends upon the shape of the channel inlet and the ratio of the downstream-to-upstream channel cross section areas, A_2/A_1. For shape-edged entrances K is given by[11]

$$K = 1.5 - 0.4 (A_2/A_1) - (A_2/A_1)^2 \tag{9.10}$$

for

$A_2/A_1 < 0.715$, and

$$K = 1.75 = 0.75 (A_2/A_1) - (A_2/A_1)^2 \tag{9.11}$$

for

$A_2/A_1 \geq 0.715$.

For a sudden expansion in flow area, the pressure rise due to decreased fluid momentum is larger than the pressure loss due to friction. Consequently, there is a pressure rise outside the channel exit. The total pressure change at the channel exit was calculated using[11]:

$$\Delta p \text{ (exit)} = - \frac{\rho_e u_e^2}{g_c} \left[\frac{A_1}{A_2} - \left(\frac{A_1}{A_2}\right)^2 \right] \tag{9.12}$$

where Δp(exit) = total pressure loss at channel exit, lb_f/ft^2

ρ_e = fluid density at channel exit, lb_m/ft^3

u_e = fluid velocity at channel exit, ft/sec

A_1/A_2 = ratio of upstream-to-downstream channel cross section areas at exit.

Friction pressure losses across channel increments were calculated with the following equation[11]

$$\Delta p \text{ (friction)} = f_W \frac{\rho u^2 \Delta L}{2 g_c D_e} \tag{9.13}$$

where f_W = Darcy-Weisbach friction factor

ρ = fluid density, lb_m/ft^3

u = mean fluid velocity, ft/sec

ΔL = axial length of channel increment, ft

D_e = channel equivalent diameter, ft

Experiments have shown that, for isothermal flow, rectangular channel friction factors are close to the Moody curve for smooth tubes.[12] The isothermal friction factors on the Moody curve are well approximated by the von Karman equation[13]

$$f_{W_{ISO}} = \left[\frac{1}{2 \log \left(N_{Re_{ISO}} f_W^{1/2}\right) - 0.8} \right]^2 \tag{9.14}$$

Friction factors are reduced with heating because of the decreased fluid viscosity near the wall. Therefore, to account for the decreased friction factors with heating[14], the isothermal friction factors are multiplied by $(\mu_W/\mu_b)^{0.14}$, or

$$f_W = f_{W_{ISO}} (\mu_W/\mu_b)^{0.14} \tag{9.15}$$

Equation (9.14) is only applicable for fully developed turbulent flow, which implies its range of applicability is for entrance L/D_e ratios greater than 50. Since the L/D_e ratio for the UVAR is 130, the flow is developing over a large portion of the channel length. The friction factors in developing flows are larger than those predicted by Eq. (9.14). Since friction pressure losses add to the stability of parallel channel systems, the use of Eq. (9.14) over the non-boiling channel length is a conservative approach in a stability analysis.

With the occurrence of subcooled nucleate boiling in channels, friction pressure losses increase. A correlation proposed by Reynolds[15] was used to calculate subcooled nucleate boiling pressure loss in the UVAR hydraulic analysis. The correlation is given by

$$\frac{(dp/dL)_{NB}}{(dp/dL)_{ISO}} = \cosh \left[(4.6 \times 10^{-6}\, q'' + 1.2) \left(\frac{T_b - T_{b_{IB}}}{T_{Sat} - T_{b_{IB}}} \right) \right] \tag{9.16}$$

where $(dp/dL)_{NB}$ = local friction pressure gradient with subcooled nucleate boiling, lb_f/ft^3

$(dp/dL)_{ISO}$ = isothermal pressure gradient, lb_f/ft^3

q'' = wall heat flux, $Btu/hr\text{-}ft^2$

$T_{b_{IB}}$ = fluid bulk temperature at incipient boiling, °F

T_b = local bulk temperature, °F

T_{Sat} = fluid saturation temperature, °F

The isothermal pressure gradient is calculated using Eqs. (9.13) and (9.14) with all fluid properties evaluated at the average channel temperature.

The approach used in the analysis was to let q" be the average heat flux in the channel from the position of incipient boiling to the position under consideration. However, because of the low heat fluxes involved with pool reactors, the contribution of the term 4.6×10^{-6} q" in Eq. (9.16) is small compared to 1.2. Consequently, the approach used in evaluating q" is not too important. It should be noted that at conditions in which flow instabilities occur in pool reactors, the heat fluxes are smaller than the heat fluxes used in developing Eq. (9.16).

In heated channels, the fluid undergoes a slight density decrease which in turn causes an acceleration. The increased fluid momentum produces a pressure loss which is quite small compared to the other losses in the channel. However, this loss was incorporated in the hydraulic analysis and the pressure loss across a channel increment is given by

$$\Delta p \text{ (momentum)} = \frac{\rho u^2 \alpha \beta \Delta T}{2 g_c} \qquad (9.17)$$

where α = correlation factor to account for non-uniform velocity in the channel

β = fluid volumetric coefficient of expansion,

ΔT = temperature rise across the channel increment, ^{o}F

Since the flow is turbulent "α" is close to 1.0, which is the value used in the analysis.

With downflow the elevation pressure loss is given by

$$\Delta p \text{ (elevation)} = - \frac{g}{g_c} \int_{\text{Inlet}}^{\text{Exit}} \rho dz \qquad (9.18)$$

where g is the acceleration of gravity. For single-phase flow in a channel increment, Eq. (9.18) is well-approximated by

$$\Delta p \text{ (elevation)} = - \frac{g}{g_c} \rho_1 \Delta L(1-\beta \Delta T_z) \qquad (9.19)$$

where ρ_1 = liquid density at inlet to channel increment, lb_m/ft

ΔL = length of channel increment, ft

β = liquid volumetric coefficient of expansion, $^{o}F^{-1}$

ΔT = temperature rise of fluid in channel increment, ^{o}F

The adverse buoyancy effect due to a decreasing fluid density downstream in a heated channel is the major contribution to flow instabilities in single-phase downflow.

9.6. Burnout Ratio

Because of non-uniform heat generation in the channel, it is possible to calculate two types of burnout ratios defined by the following equations:

$$\text{Local Burnout Ratio} = \frac{q''_c \text{ (predicted)}}{q''\text{(local)}} \tag{9.20}$$

$$\text{Average Burnout Ratio} = \frac{q''_c \text{ (predicted)}}{q'' \text{ (average up to position considered)}} \tag{9.21}$$

In the UVAR safety analysis both burnout ratios were calculated along the channel length. The smaller of these ratios was used in determining the burnout limit.

Equation (9.20) implies that local conditions determine burnout. However, experimental data comparing uniform and non-uniform heat generation burnout indicates that burnout depends on upstream heat flux conditions[16,17,18]. The results of experiments performed by Babcock and Wilcox for uniform, chopped-cosine, inlet peak, and exit peak heat flux distributions, indicate that the total channel power at burnout or the average channel burnout heat flux is essentially independent of axial heat flux distribution[17,18]. Since burnout correlations are developed from uniform heating burnout data, it appears that the non-uniform heat flux burnout data indicates that the use of Eq. (9.21) for calculating burnout ratios is probably a better criterion for determining the burnout safety margin. Equation (9.21) usually predicts smaller burnout ratios than Eq. (9.20) for positions far downstream from the peak heat flux in a

channel. The results of calculations on the UVAR showed that Eq. (9.21) was the limiting criteria for determining the UVAR safety limit.

For relatively high power levels and flow rates, the burnout ratio is the limiting criteria for establishing the safety limit. At lower power levels and flow rates, an excursive flow instability is the limiting criteria. The flow instability in the UVAR hot channel is predominately caused by the adverse buoyancy effect due to downflow.

9.7. Nomenclature Used in Thermal Hydraulic Analysis

A_2/A_1	Ratio of downstream-to-upstream channel cross section areas at channel inlet
c_p	Specific heat, $Btu/lb_m - {}^oF$
D_e	Equivalent diameter, ft
f_W	Darcy-Weisbach friction factor
$F_{W_{ISO}}$	Isothermal Darcy-Weisbach friction factor
g	Local acceleration, ft/sec^2
g_c	Conversion factor, $32.18 \frac{lb_m}{lb_f} \frac{ft}{sec^2}$
G	Mass velocity, lb_m/ft^2 -sec
h	Heat-transfer coefficient, $Btu/hr\text{-}ft^2\text{-}{}^oF$
h_f	Saturated liquid enthalpy, Btu/lb_m
h_g	Saturated vapor enthalpy, Btu/lb_m
h_{fg}	Heat of vaporization, Btu/lb_m
k	Thermal conductivity, $Btu/hr\text{-}ft\text{-}{}^oF$
K	Inlet pressure loss coefficient
L	Channel length, ft

ΔL	Incremental channel length, ft
N_{Gr}	Grashof number, dimensionless
N_{Ka}	Von Karman number, dimensionless
N_{Pr}	Prandlt number, dimensionless
N_{Re}	Reynolds number, dimensionless
p	Pressure, Psia
q''	Local wall heat flux, Btu/hr-ft^2
q''_c	Burnout heat flux, Btu/hr-ft^2
q''_{FC}	Forced convection heat flux, Btu/hr-ft^2
q''_{IB}	Incipient boiling heat flux, Btu/hr-ft^2
q''_{PB}	Pool boiling burnout heat flux, Btu/hr-ft^2
$(dp/dL)_{ISO}$	Isothermal pressure gradient, lb_f/ft^3
$(dp/dL)_{NB}$	Subcooled nucleate boiling pressure gradient, lb_f/ft^3
T_b	Local bulk temperature, ^oF
T_1	Channel inlet temperature, ^oF
T_w	Local wall temperature, ^oF
ΔT	Fluid temperature rise in a channel increment, ^oF
T_{Sat}	Fluid saturation temperature, ^oF
T_{WB}	Bernath's wall temperature at burnout, ^oF
$T_{b_{IB}}$	Fluid bulk temperature at incipient boiling, ^oF
u	Mean coolant velocity, ft/sec
u_1	Coolant velocity outside channel exit, ft/sec
z	Axial position in channel, ft
α	Correction factor for non-uniform flow in a channel
β	Fluid volumetric coefficient of expansion, $^oF^{-1}$

ρ	Local fluid density, lb_m/ft^3
ρ_f	Saturated liquid density, lb_m/ft^3
ρ_g	Saturated vapor density, lb_m/ft^3
ρ_l	Fluid density at inlet to channel increment, lb_m/ft^3
σ	Liquid-vapor interface surface tension, lb_f/ft
μ_b	Local fluid viscosity at bulk temperature, $lb_m/ft\text{-}sec$
μ_W	Local fluid viscosity at wall temperature, $lb_m/ft\text{-}sec$

9.8. Hot Channel and Minimum Core Loading

The hot channel is related to the nominal channel by the radial peaking factor. The hot channel considered in this analysis was calculated for a 4 x 4 core which is the minimum core loading. Larger cores were analyzed; however, their lower power densities and lower non-elemental flows more than compensate for their higher radial peaking factors, resulting in less limiting conditions.

The radial peaking factor for a 4x4 core was determined to be 1.66 using a two-dimensional diffusion theory computer model of the LEU 22 plate-per-element UVAR core[27]. This radial peak was found to be in the channel adjacent to a control rod water hole as shown in Figure 9-4. Sternberg[19] performed a complete map of a UVAR 4x4 HEU 12 plate-per-element core. The location of the measured radial peak flux in Sternberg's core corresponds to the location of the computer calculated peak flux in the 4x4 LEU 22 plate-per-element core.

Sternberg's work provided an exit peak axial distribution which was fitted to a polynomial for the analysis of the 22 plate/element core. Figure 9-5 shows Sternberg's axial flux map in the hot channel. For

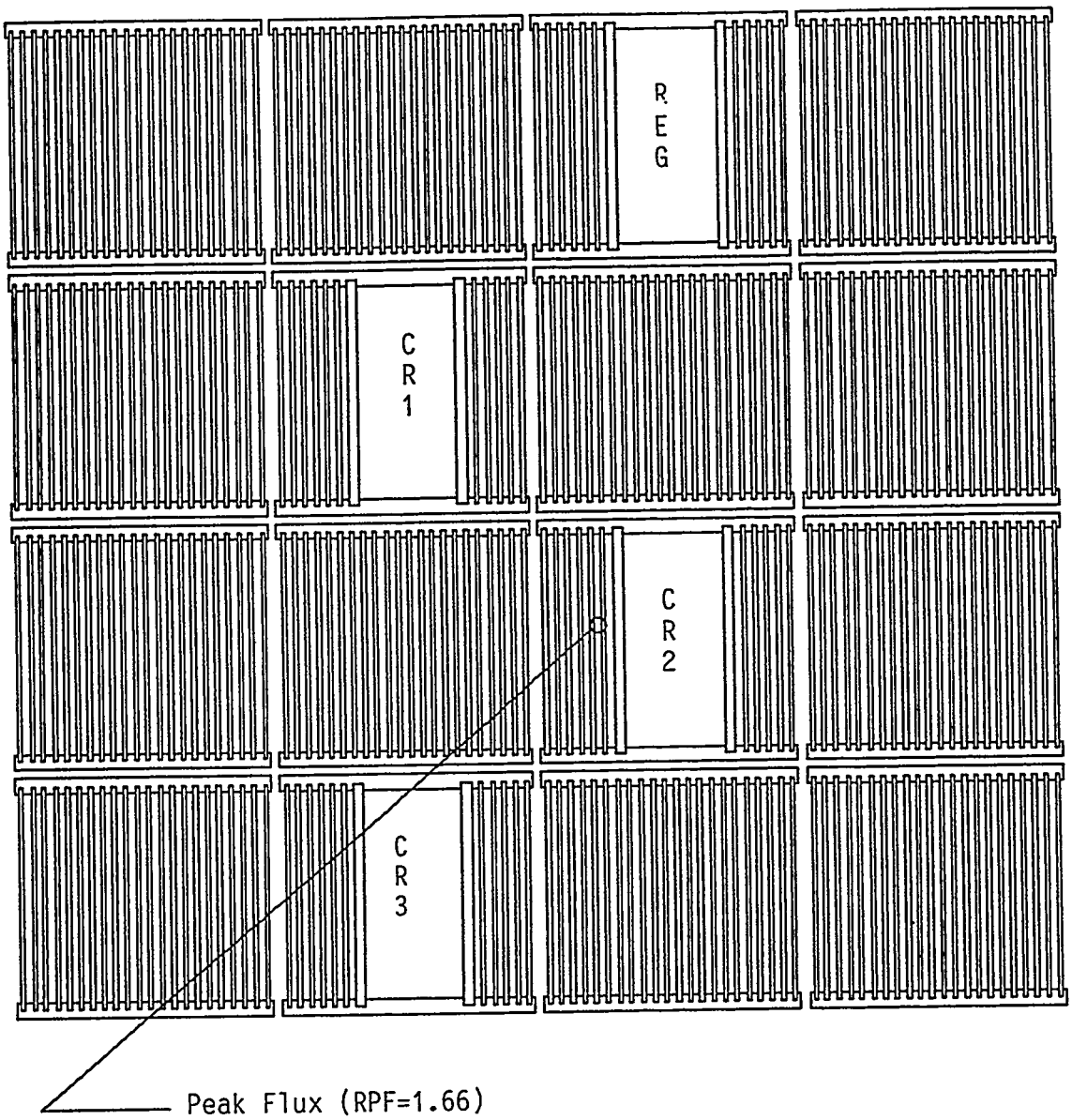
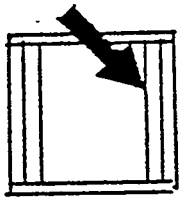


FIGURE 9-4 Core Loading Showing Peak Flux Location



FOIL LOCATION IN FUEL ELEMENT AC5

AN5	AN18	AC4	AN2
AN17	AC6	AN10	AN14
AN9	AN6	AC5	AN13
AN1	AC1	AN20	AN 8

ELEMENT LOCATION IN THE CORE

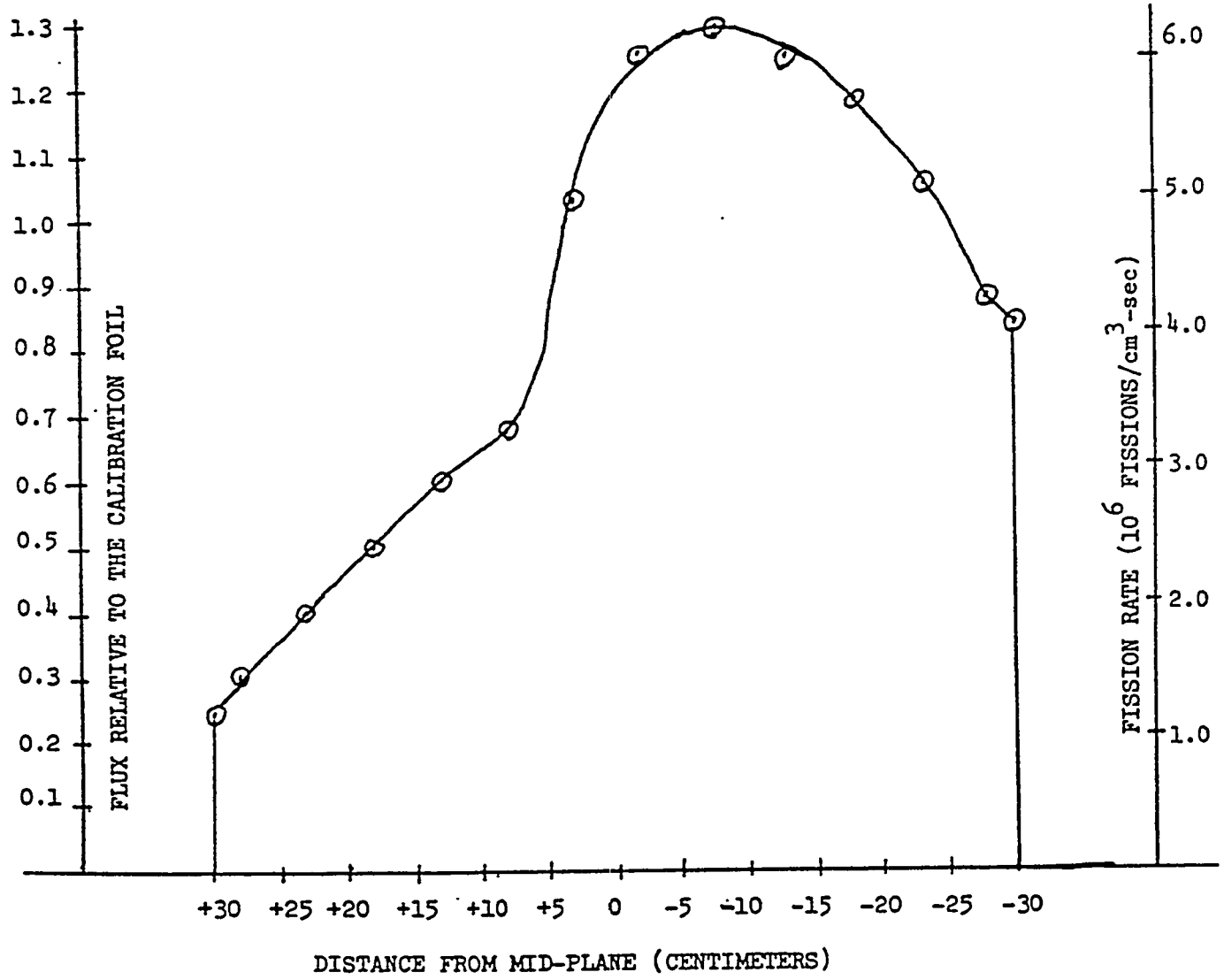


FIGURE 9-5 VERTICAL FLUX TRAVERSE IN POSITION OF AC-5

these measurements, the rods in channel rod elements AC-1 and AC-4 were completely withdrawn and the tips of the rods in control rod elements AC-5 and AC-6 were at about six centimeters above the midplane. This results in the most severe axial flux peaking possible in the reactor. The curve in Figure 9-5 is the basis for the Exit Peak Heat Flux distribution used in this analysis.

9.9. Allowance for Error in the Burnout Determination

In Figure 9-3, a comparison is given of the ratio of calculated to experimental heat fluxes. With the assumption that the points in this figure form a normal distribution (Gaussian error curve), an analysis was performed to find the standard deviation, σ, from the expression

$$\sigma^2 = \frac{1}{n-1} \sum_{1}^{n} (X_1 - \bar{X})^2 \qquad (9.27)$$

where n is the number of points, and $\bar{X}$ is the mean value of all points. A value of $\sigma = 0.21$ was obtained. For 2.32 standard deviations above and below the mean, the probability of occurrence of ratios outside this range is 2%. Half of these occurrences will be above and half will be below this range. Accordingly, for 2.32 σ or a burnout ratio (BOR) of 1.49, there is a 99% confidence factor that burnout will not occur based on Gambill's experimental data.

9.10. Safety Limit

A steady state heat transfer code for downflow in rectangular channels, THERHYD, that incorporates the correlations discussed in the preceding sections, was developed by Dahlheimer[25].

The limiting core power to system flow derived from THERHYD channel power and channel flow define the burnout limit curve for the UVAR with forced convection cooling. The UVAR Safety Limit is set so that the fuel and cladding do not melt. If power and flow conditions that can be reached during various transients are always below the burnout limit curve (lower power for a given flow) the safety limit will not be exceeded. Thus the safety limit is actually based upon the burnout criteria since if burnout (either departure from nucleate boiling or dryout) does not occur, the fuel and cladding will not melt. The Limiting Safety System Settings (LSSS) for power and flow are chosen (see section 9.11) so that the reactor will always operate below the burnout limit curve during any analyzed transient. The LSSS's also take into account uncertainties in measuring the core power, system flow, and pool temperature.

THERHYD was run using the channel and plate dimensions for the 22 plate/element LEU fuel to find the limiting channel flow for a range of channel powers. The exit peak axial flux distribution measured by Sternberg[3] and fitted to a fifth order polynomial by Dahlheimer[25] was used for all analysis. Additional THERHYD runs were performed to obtain differential pressure information for a wide range of powers and flows.

The primary output from THERHYD is the channel flow for various channel powers at a specified limiting condition. The limiting condition used throughout the calculations was a Burnout Ratio (BOR) of 1.49 which section 9.9 demonstrates allows for errors in the correlations used in THERHYD.

Radial peaking factors from 2DB-UM[26] computer models of various

proposed LEU cores were used to convert individual channel power calculated by THERHYD to full core power. Reference fuel element flow parameters experimentally determined by Brunot[4] along with calculated differential pressures from THERHYD were used to convert the individual channel flow calculated by THERHYD to system flow.

The effect of tolerances in fuel loading, fuel width, flow distribution within a fuel element and channel size (Summarized in Table 9-1) were all individually converted to a corresponding increase in channel flow needed to account for each effect. The total increase in flow for these four effects was determined by taking the root of the sum of the squares of the individual effects. The resulting core power vs. system flow is the burnout limit curve for the particular core. In the calculations, the bulk pool water temperature limit of 111° F is used as the inlet temperature and the depth of water to the center of the core is 20.36 feet.

Brunot measured the single element flow in a 4x4 core using 12 plate HEU elements to be 48 GPM when the system flow was 940 GPM. The dynamic differential pressure across the core for this flow condition was calculated using THERHYD to be 0.0776 psi. These conditions are used as a reference point to calculate non-element flow in other core configurations. Non-element flow is any flow that does not go through the fuel portion of the elements. Examples of non-elemental flow are the flow through the 49, 3/4-inch holes in the grid plate used to cool the reflector and channels between elements, and the flow through the rod channels.

TABLE 9-1.

Leu-22 Data and Parameters

Core size	4x4	4x5
Number of Plates	308	396
Number of Channels	294	378
Radial Peaking Factor	1.66	1.71

Axial Power Distribution: Exit Peak as defined by 5th order polynomial in Dahlheimer.

Inlet Temperature: 111° F

Pool Depth to Core Center: 20.36 Ft.

Flow Distribution Factor: 16.5 %

Reference Non-Element Flow Parameters:

- Core: 4x4 12 Plate HEU
- System Flow: 940 GPM
- Element Flow: 48 GPM
- Dynamic D.P.: 0.0776 psi

Element Dimensions:

		Tolerances
Channel Gap	0.0927"	(+/- 0.007")
Channel Width	2.621"	(+/- 0.013")
Fuel Width	2.395"	(+/- 0.075")
Plate Thickness	0.05"	
Plate Loading U-235	12.5 g	(+/- 0.35 g)

THERHYD was run for the nominal channel dimensions as well as for the minimum channel dimensions (both gap and width) to calculate the minimum channel flow with high resolution (0.01 GPM) for a BOR of 1.49. Additional runs were performed with the BOR limit set at 1.00 to obtain differential pressure data for a wide range of flow rates at both nominal and minimum dimensions.

In the computer runs, the resulting channel power for the nominal channel dimensions, with BOR 1.49, were converted to core power using the appropriate radial peaking factor (RPF) and number of plates in the core, according to the relationship:

$$\text{Core Power} = (\text{Channel Power} * \#\text{ of Plates})/\text{ RPF} \qquad (9.28)$$

For each limiting channel flow rate from the above runs, the corresponding dynamic differential pressure (DP) across the core was calculated and the channel flow was converted to system flow, using:

$$\text{Sys Flow} = \text{Chan Flow} * \#\text{ of Channels} + \text{Non-Element Flow} \qquad (9.29)$$

where Non-Element Flow is given by

$$(940\text{ GPM/sys} - 48\text{ GPM/elem} * 14\text{ elem/sys}) * \text{SQRT}(DP/DP_{ref}) \qquad (9.30)$$

where DPref is the dynamic differential pressure calculated for the conditions at which 48 GPM per element at 940 GPM system flow was measured and DP is the dynamic differential pressure for the core

conditions under study. Dynamic differential pressure is the total differential pressure across the core (or channel) minus the difference in hydrostatic head between the inlet and outlet of the core.

Use of equation (9.30) assumes that the non-elemental flow area does not vary from core to core. The 49 small holes are never plugged and the number of rod channels remains fixed at four.

The resulting function of Core Power versus System Flow is the nominal burnout limit without considering any tolerances. The slope of the nominal burnout limit curve was calculated to convert the tolerances on fuel width, fuel loading and power to tolerances on flow. Separate THERHYD runs were performed to determine the limiting flow with a BOR of 1.49 in a channel with the minimum gap and width. The total differential pressure (dynamic and static) required to maintain safe flow in the smallest channel must be applied across the entire core. Therefore, the flow rate in a nominally sized channel at each power level was calculated using the differential pressure required for safe flow in the smallest channel. This results in a significant increase in nominal channel flow. Each increase in flow to account for the tolerances was normalized to the nominal channel flow and added to the nominal channel flow in quadrature.

The dynamic differential pressure for the adjusted channel flow was calculated and again using equations (9.29) and (9.30), the system flow for each core power was calculated. The resulting power to flow curve is the burnout limit for a particular core configuration and set of dimensional tolerances.

The burnout curve in Figure 9-6 is based upon the minimum core

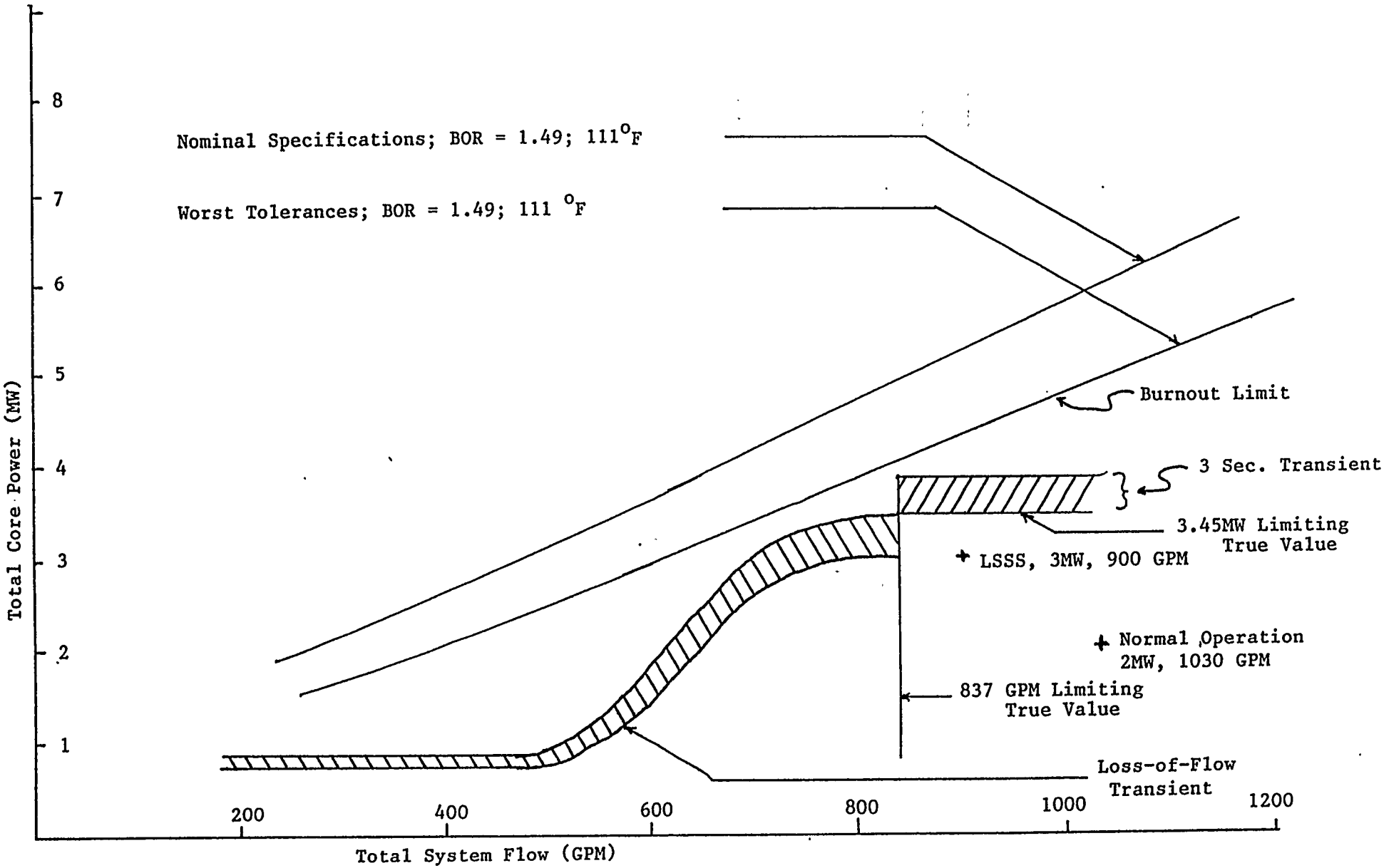


FIGURE 9-6 LEU Core Power vs System Flow, 4x4, RPF=1.66

loading of 14 normal elements and 4 control rod elements in a 4x4 array. Larger cores were analyzed; however, their lower power densities and lower non-elemental flows more than compensate for their higher radial peaking factors, resulting in less limiting conditions.

9.11. Limiting Safety System Settings and Measurement Errors

a) Coolant Inlet Temperature

The Limiting Safety System Setting (LSSS) on coolant inlet temperature (pool temperature) is 108°F. Normal operation is at 105°F or less. The manufacturer's specified probable error on the measuring instrument is ± 0.75°F. The standard deviation would then be ± 1.125°F and using 2.32 standard deviations for a 99% confidence factor, the temperature can be determined within 2.6°F. For an LSSS of 108°F, the limiting true value on the coolant inlet temperature is therefore less than 111°F. All calculations for the curves in Figure 9-6 are based on an inlet temperature of 111°F.

b) Flow Rate

The primary coolant flow is detected by measuring the differential pressure across an orifice in the primary piping. The manufacturer's specified probable error is ± 2% or a standard deviation of ±3%. For a 99% confidence factor that the flow rate will be no less than a specified amount we take 2.32 standard deviations, or 7%. The limiting safety system setting on flow rate is set at 900 gpm. Hence, the true value should then be no less than 0.93 x 900 = 837 gpm. This is the limiting true value on flow rate shown in Figure 9-6.

c) Reactor Power

The reactor power is determined from the product of flow rate x ΔT, where ΔT is the differential temperature across the core. The probable error with the ΔT measurement could be as much as $\pm 0.4^{\circ}F$. At a power of two megawatts the ΔT is about $13^{\circ}F$, for a probable error of $\pm 3.2\%$. The safety level scram point is set by adjusting the neutron chambers to read the same power level as the thermal power. Here, the limiting accuracy is the readability of the indicator which can be read with a probable error of $\pm 2\%$.

There are then three independent probable errors in determining the power level setting:

a) Flow rate $\pm 2\%$

b) ΔT $\pm 3.2\%$

c) Chamber Setting $\pm 2\%$

The combined probable error is obtained from the square root of the sum of the squares and corresponds to $\pm$ 4.27%, with a standard deviation of $\pm 6.4\%$. For a 99% confidence factor, 2.32 σ is 14.8%. Therefore, with a measured value of 3 MW for the LSSS on reactor power, the true value should be no greater than 3 x 1.148 or 3.45 MW. This is the limiting true value on reactor power shown in Figure 9-6.

9.12. Short Period Transient

A limiting condition for operation is that the magnet release time be less than 50 milliseconds. The minimum setting on the period scram is 3 seconds. From the rod calibration curves, the three rods must drop about 3 1/2-inches from the fully

withdrawn position of 26-inches above the bottom of the core to overcome this period. This is the least reactive position of the rods, and normally the rods are operated at a level well below this. However, to allow for variations in core loading, it is assumed that the rods must drop 5-inches from the fully withdrawn position of 26-inches, to overcome a 3-second period. This is a very conservative assumption.

A rod drop time cannot be measured unless the drop terminates on the seating switch at the fully inserted position. Accordingly, drop times were measured from 3, 4, 5, and 6-inches above the fully inserted position as well as from the fully withdrawn position (26-inches). The results obtained are presented in Table 9-2.

TABLE 9-2

TIME TO DROP FROM A PREDETERMINED POSITION

(All times in milliseconds)

	Initial Position				
	3"	4"	5"	6"	26"
Rod 1	160.0	185.0	205.0	225.0	481.2
Rod 2	170.0	195.0	210.0	227.5	506.0
Rod 3	162.5	182.5	203.0	230.0	482.5
Average	164.2	187.5	206.2	227.5	489.9
True Gravity	124.6	143.9	160.9	176.2	366.8

The times for True Gravity (last line) are calculated from:

$$S = \frac{1}{2} gt^2 \qquad (9.31)$$

The actual time for the rod to drop is greater than the True Gravity time because of the friction of the water as the rod drops through it. Of more significance is the slowing up of the rod as it enters the dash pot during the last few inches before it is seated at the bottom of its travel.

The action of the dash pot in slowing the drop time is illustrated by the times to drop from 26 inches (last column). The measured values of the drop times from 3 inches, 4 inches, 5 inches, and 6 inches include some delay from the dash pot action. The drop time for any one of these distances from the fully withdrawn position would be less. For example, a 5-inch drop from 26 inches to 21 inches should be less than 206 milliseconds. On the other hand it would be greater than the true gravity time of 161 milliseconds as there is some frictional resistance from the water as soon as the rod starts to move.

For conservatism, it is assumed that the time for the rods to drop 5 inches from the fully withdrawn position is 3/7 of the time to drop the full travel of 26 inches. Accordingly, for a measured free drop time of 490 milliseconds for full travel, the time to drop 5 inches will be no greater than 210 milliseconds. A maximum free drop time for the full travel is established at 700 milliseconds in the Technical Specifications. Therefore, the time to drop 5 inches will never be greater than 300 milliseconds. Adding the 50 millisecond release time to the 5-inch drop time, the time from the initiation of a scram until the rods are inserted 5 inches will never be greater than 350 milliseconds.

It is not easy for the reactor to go on a short period at high power due to the negative temperature coefficient, which has been determined to

be about $-1x10^4$ $\Delta k/k-^oF$[27]. Neglecting the temperature coefficient, and assuming the reactor is on a period just greater than 3 seconds, and goes through the maximum true value of the LSSS at 3.45 megawatts, the power will rise to a value no greater than

$$P = 3.45 \exp [0.350/3] = 3.88 \text{ MW}. \quad (9.32)$$

The range between 3.45 MW and 3.88 MW is the allowance for a 3 second period transient in Figure 9-6. Thus, 3.88 MW is the maximum power for any transient because transients shorter than 3 seconds will scram the reactor at a lower power on period while longer transients will scram the reactor on high power with less power overshoot.

9.13. Loss-of-Flow Transient and Natural Convection

A loss-of-flow transient is illustrated by the shaded area extending to the left of the LSSS in Figure 9-6. It is assumed for this transient that the reactor is operating at the LSSS of 3.0 MW and 900 gpm, with the flow header jammed in the UP position, and there is a power failure to the pump which then results in a reactor scram signal.

The following sections 9.14 and 9.15 are the original analysis[24] for loss of flow and natural convection. NATCON[28] runs for 22 plate, 18 plate, and 12 plate fuel elements show that the margin of safety increases with the increase in heat transfer area and lower power densities associated with the increase in the number of fuel plates in the 22 plate LEU core over the 12 plate HEU core used in sections 9.14 and 9.15.

To determine the coolant flow coastdown curve, measurements were made for the HEU SAR of the decrease in flow rate versus time, starting with a flow rate of 800 gpm and followed by pump cut-off. For the LEU SAR, the flow rate coastdown was remeasured with the larger primary pump installed in 1981 and referenced to 900 gpm. The results are shown in Figure 9-7. The flow coastdown curve is expressed by the following equation.

$$\text{Flow (gpm)} = 900 - 440 \times t(\text{sec}) \qquad (9.33)$$

The higher initial flow rate and the slower coastdown with the currently installed pump provides a greater margin of safety than the coastdown used in the following analysis.

9.14. HEU Analysis for Loss-of-Flow Transient

A loss of flow transient is illustrated by the shaded area extending to the left of the LSSS in Figure 9-6A. It is assumed that the [HEU] reactor is operating at the [previous HEU] LSSS of 3.0 MW and 800 gpm with the flow header jammed in the UP position. There is a power failure to the pump and the loss of power to the pump then initiates a scram signal to the reactor.

Measurements were made of the decrease in flow rate versus time starting with a flow rate of 800 gpm, and then cutting off the pump. The measurements were made using the output signal from the differential pressure cell across the orifice plate, after calibrating this output signal versus various flow rates through the primary system with the flow header in the UP position. The results are shown in Figure 9-7 and the flow coast down curve is expressed in the following equation:

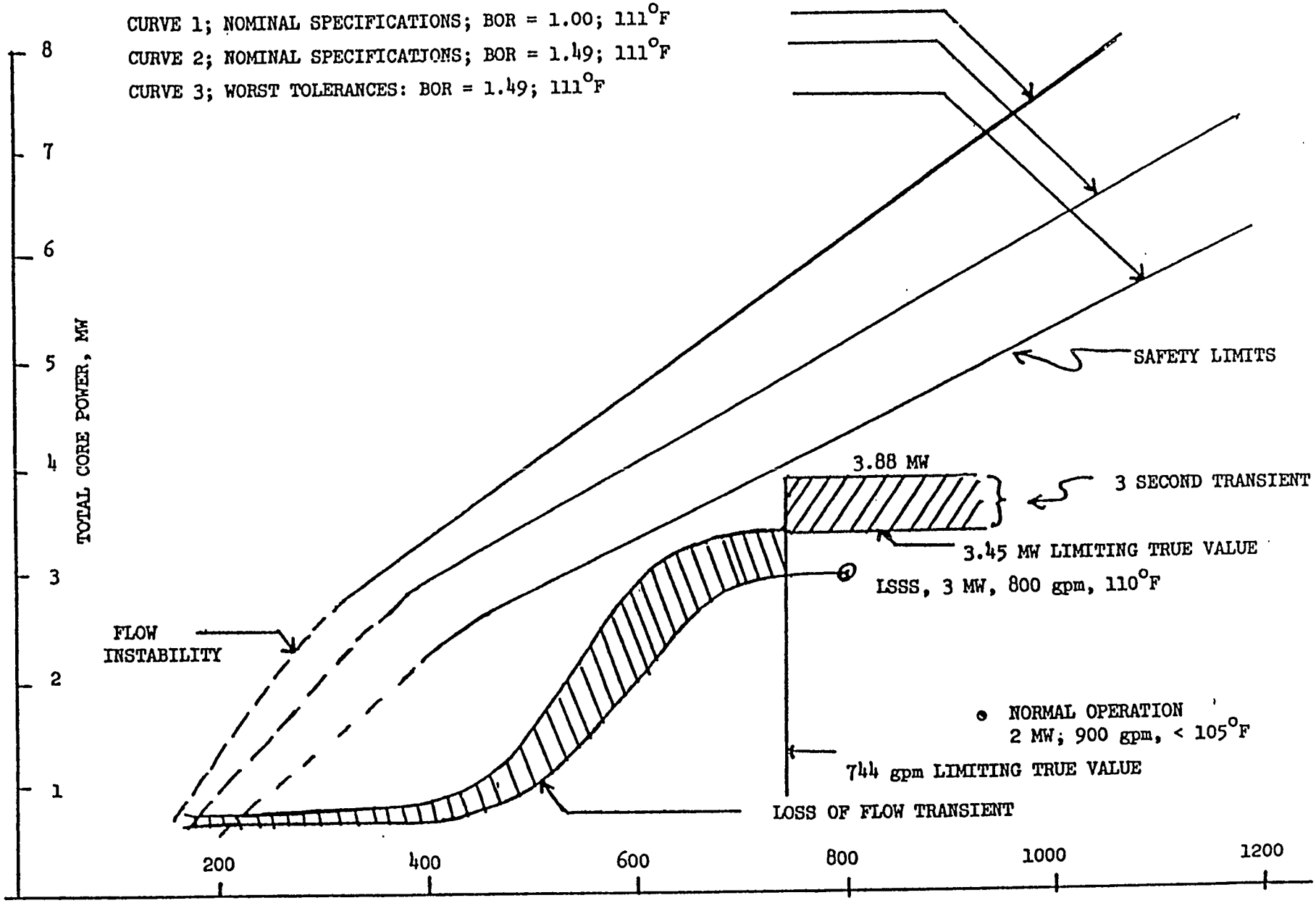


FIGURE 9-6a HEU Core Power vs System Flow, 4x4, RPF=1.37

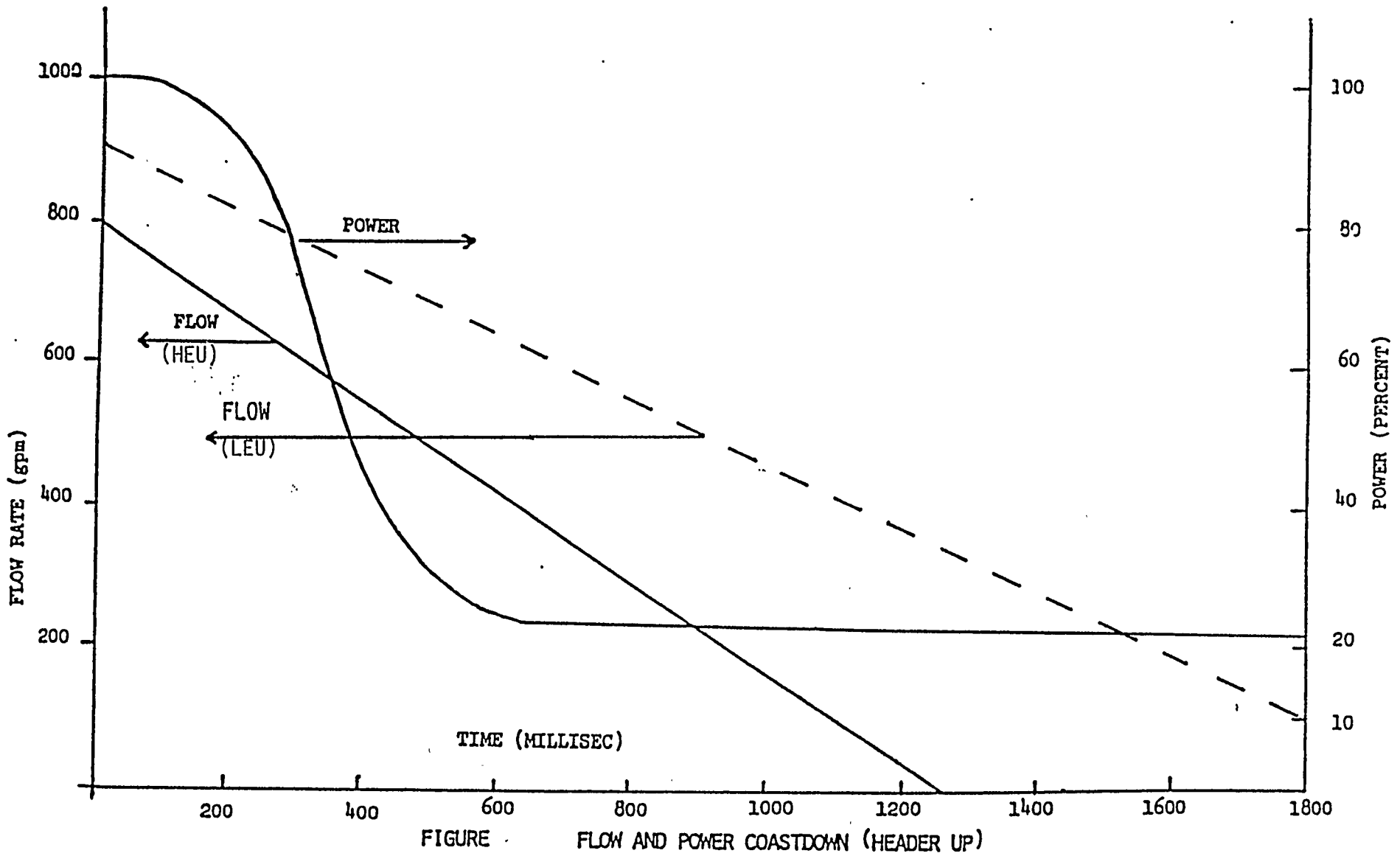


FIGURE FLOW AND POWER COASTDOWN (HEADER UP)

$$\text{Flow (gpm)} = 800 - 636 \times t(\text{sec}) \qquad (9.34)$$

The power coast down curve was calculated by solving the kinetic equations with six groups of delayed neutrons on a digital computer using 0.01 second time increments for the first two seconds and 0.1 second time increments thereafter to 100 seconds. It was assumed that the rods did not move for 50 milliseconds until after initiation of the scram and that they moved with constant acceleration until they had traveled the full length of 26-inches in 700 milliseconds. These assumptions are most conservative but are consistent with the limitations on rod drop times given in the Technical Specifications.

The complete reactivity insertion was assumed to be only 3%Δk/k and the rods were assumed to drop from the fully withdrawn position (also very conservative assumptions). By comparing with rod calibration curves determined experimentally in the reactor, a curve of negative reactivity insertion versus time was plotted, and this data was input to the computer.

It was assumed that 6% of the power at the instant of scram was from the decay of fission products and this was held constant in time thereafter. The power coast down curve is plotted along with the flow coast down curve in Figure 9-7. Because of the same amount of negative reactivity inserted, the power does not approach the 6% in fission products until about 100 seconds. At the instant the flow rate reaches zero (1.258 seconds), the power is still at 21.7% full power. By picking

off powers and flows at equivalent times the curve of power versus flow extending to the left from the LSSS in Figure 9-6A was determined. This is the expected result of a loss-of-flow transient. However, since the true values of power and flow at the LSSS could be 744 gpm and 3.45 megawatts, the procedure was repeated starting from this point in Figure 9-6A. The shaded area between the two curves represents the range of uncertainty for a transient resulting from a loss of flow after steady state operation at the LSSS. Not included in the figure are the results as the flow rate decreases to zero and then reverses due to buoyancy effects. At a downflow rate of 225 gpm and a power of 790 kW, the loss of flow transient curve intersects Curve 3 in Figure 9-6A. The significance of the point of intersection is that if the reactor were operating in the steady state at this power, and this flow rate, a flow instability would occur in the hot channel. (See Section 9.5).

However, the reactor is not in the steady state and the flow rate is changing rapidly. Also, it is impossible for the flow header to jam in the fully UP position. The header is raised by flotation with air as described in Section 4.3. After the header is raised, the pump is started and the header is held up by the pressure drop of the flow through the core. The air pressure which raised the header is vented and the reactor cannot be started until this pressure has dropped below 2 psi. If there is a loss of coolant flow, gravity will cause the header to drop. However, it is possible for the header to jam in a cocked position. The worst possible position in which the header could jam is shown in Figure 9-8. In this case, the header would be wedged with a minimum gap of 0.956-inches between the header and grid plate on one

side.

A transient analysis was made for a loss of flow incident from 3.45 megawatts reactor power with power and flow coast down as shown in Figure 9-7 [HEU]. The header is assumed jammed in the position shown in Figure 9-8 and the transient response of the average flow, average fuel temperature, and average coolant temperature are shown in Figure 9-9. As will be shown, a safety limit can be established, using the maximum fuel plate temperature as a criterion.

The response was calculated with a computer code which treated transient heat transfer at the average power location. Heat transfer coefficients were calculated as a function of flow rate, starting in the turbulent flow regime at rated flow and switching to a laminar flow correlation for Re < 2300. Upflow resulted from buoyancy, which was set equal to the combined effect of (1) the inertia of the water in the core flow channel and the header below the core, and (2) the friction loss through the gap between the wedged header and the grid plate and friction loss in the core-coolant channel.

The pressure drop through the 0.956-inch gap relative to the pressure drop through the core after flow reversal was calculated in order to solve the transient flow equations, as follows:

$$\Delta P = f \frac{h}{D_e} \frac{\rho \bar{V}^2}{2g_c} + 1.5 \frac{\rho V_{gap}}{2g_c} \qquad (9.35)$$

where: first term = friction pressure drop through core

$\bar{V}$ = average velocity in core

second term = pressure drop through gap

V_{gap} = velocity through gap

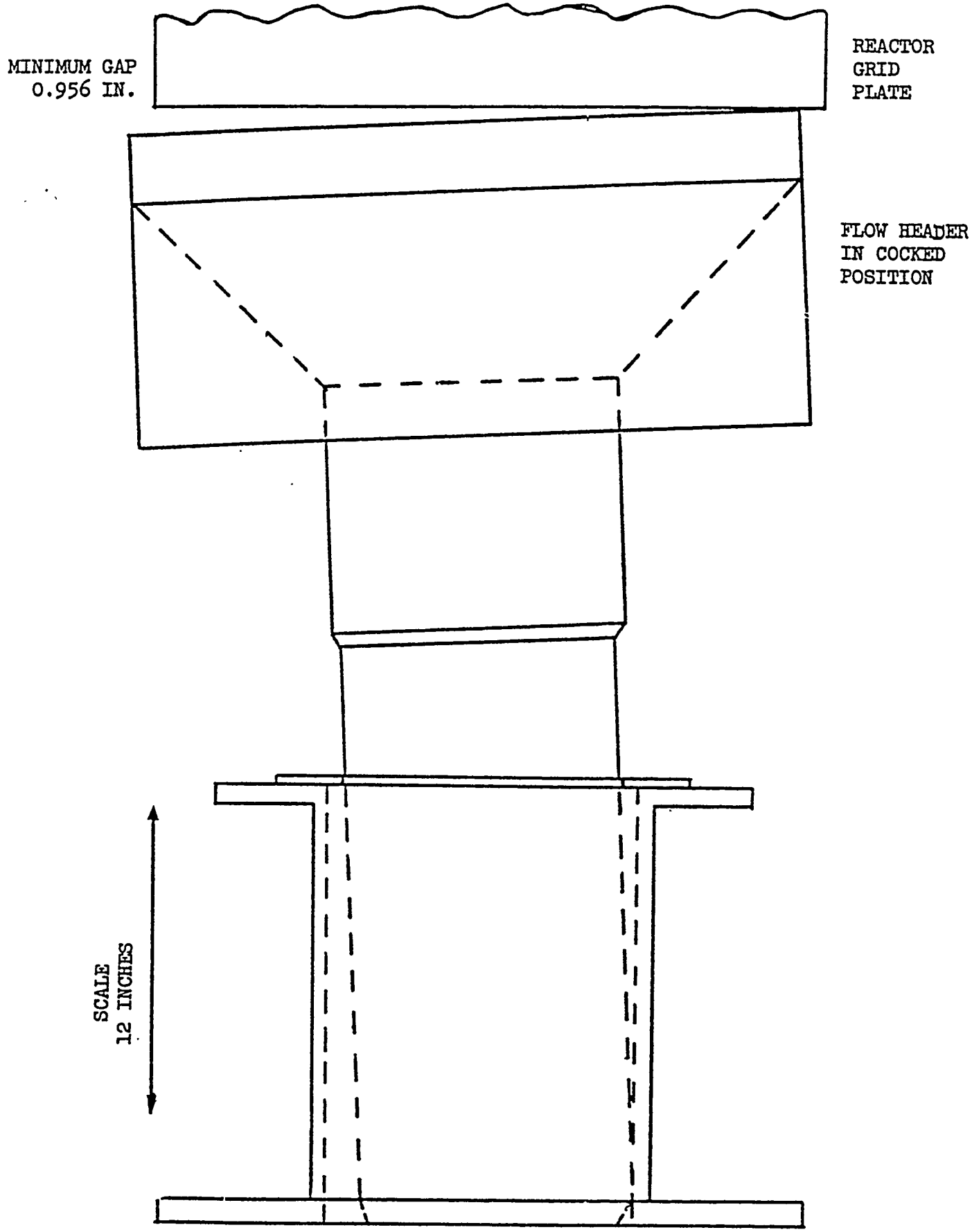


FIG. 9-8 FLOW HEADER JAMMED IN COCKED POSITION

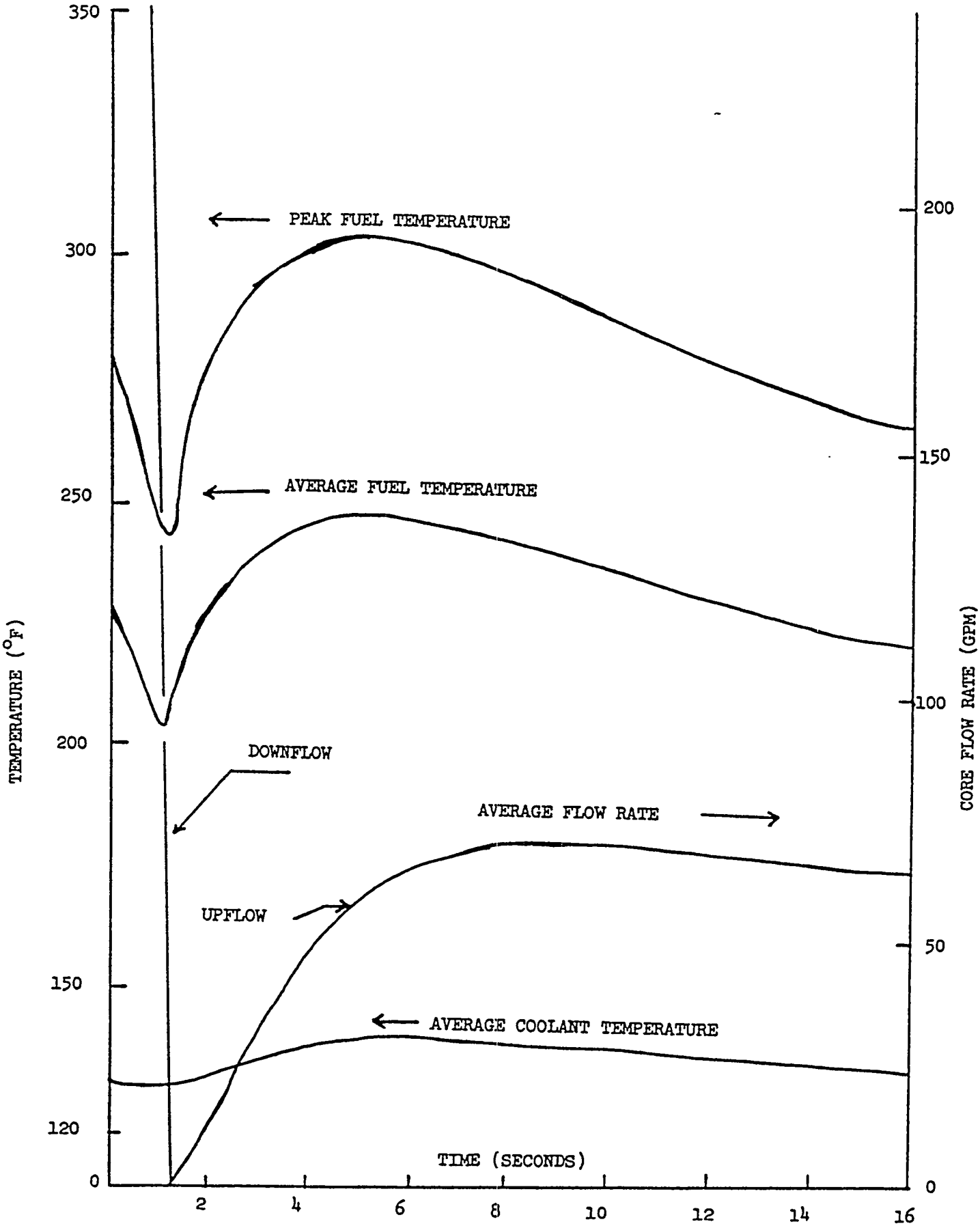


FIGURE 9-9 FLOW REVERSAL AFTER LOSS OF FLOW TRANSIENT FROM 3.45 MW

From continuity, it was found that, for the gap width of 0.956-inches, $V_{gap} = 1.86\ \bar{V}$. The transient heat transfer code has the standard point reactor kinetics and heat transfer equations. The only unusual feature is the momentum equation which controls the coolant flow rate. The time dependent momentum equation was:

$$(\rho-\rho_o)\ h\frac{g}{g_c} = f\ \frac{h}{D_e}\ \frac{\rho_o V^2}{2g_c} + 1.5\ \frac{\rho_o V^2_{gap}}{2g_c} + \frac{\rho_o h}{g_c}\ \frac{d\bar{V}}{dt} + \frac{\rho_o L}{g_c}\ \frac{dV_{gap}}{dt} \quad (9.36)$$

where: $\bar{\rho}$ = average density in heated channel in core

ρ_o = density of water at pool temperature

h = core height

L = equivalent length of flow path between the gap above the funnel and the core.

The flow velocity in the peak channel can be related to the flow velocity in the average channel by setting the pressure drop across both channels equal. For laminar flow and steady state, this results in a value of velocity in the peak channel 1.17 times the velocity in the average channel together with a temperature rise across the core, ΔT, of 1.17 times the ΔT for the average channel. These values assume a radial peaking factor of 1.37. The basis for the factor of 1.17 is as follows: The pressure drop, ΔP, across the hot channel and the average channel are equal, or Buoyancy ΔP = Friction ΔP in both hot channel and average channel.

Define x such that:

Buoyancy ΔP in hot channel = x times greater than Buoyancy ΔP in average channel (9.37)

Since buoyancy ΔP = Friction ΔP at steady state, then Friction ΔP in hot channel = x times friction ΔP in average channel - (9.38)

$$\text{Friction } \Delta P = f \frac{L}{D_e} \frac{\rho V^2}{2g_c} \tag{9.39}$$

$$\text{In Laminar flow, } f = \frac{64}{R_e} = \frac{64}{\rho V D_e/\mu} \tag{9.40}$$

$$\therefore \text{Friction } \Delta P = \frac{64\ L\mu}{VD_e^2} \frac{V^2}{2g_c} = cV \tag{9.41}$$

where: c = constant, independent of channel.

Since Friction ΔP in hot channel = x times friction ΔP in average channel and since Friction ΔP = cV

$$\text{Then } V(\text{hot channel}) = x \cdot V(\text{average channel}) \tag{9.42}$$

Return to buoyancy ΔP to obtain a relation between ΔT (hot channel) and ΔT (average channel).

$$\text{Buoyancy } \Delta P = (\rho_o - \bar{\rho}) L \frac{g}{g_c} \tag{9.43}$$

where: ρ_o = density at inlet temperature (111°F)

ρ = average density in channel

From Eq. (9.37)

$$(\rho_o - \bar{\rho})_{\text{hot channel}} L \frac{g}{g_c} = x.(\rho_o - \rho)_{\text{avg. channel}} L \frac{g}{g_c} \tag{9.44}$$

Since the change with density is about linearly proportional to a change in temperature over a limited temperature range, $\rho_o - \bar{\rho}$ can be written as follows for the hot channel:

$$(\rho_o - \bar{\rho})_{hot} = a(\bar{T} - T_o)_{hot} = 2a(T_{exit} - T_o)_{hot} = 2a\,\Delta T_{hot} \qquad (9.45)$$

Similarly, for the average channel, using the same a,

$$(\rho_o - \bar{\rho})_{avg} = a(\bar{T} - T_o)_{avg} = 2a\,\Delta T_{avg} \qquad (9.46)$$

Substituting Eqs. (9.45) and (9.46) into (9.44) gives:

$$\Delta T_{hot} = x.\Delta T_{avg} \qquad (9.47)$$

We now have two relations, relating V_{hot} to V_{avg} Eq. (9.42) and ΔT_{hot} to ΔT_{avg} Eq. (9.47).

The energy equation allows us to evaluate x as follows:

The Energy Equation is:

$$(\dot{m}\, c_p\, \Delta T)_{avg.\ channel} = \bar{Q}(\text{Btu/h, heat production rate in average channel}) \qquad (9.48)$$

$$(\dot{m}\, c_p\, \Delta T)_{hot\ channel} = 1.37\,\bar{Q}\ (\text{where } 1.37 = \text{Radial peaking factor}) \qquad (9.49)$$

But $m = \rho VA$, where ρ and A are essentially the same for both the hot and average channels.

Hence, Eq. (9.48) can be rewritten as

$$\rho A c_p\, V_{avg}\, \Delta T_{avg} = \bar{Q} \qquad (9.50)$$

Substituting Eqs. (9.37) and (9.47) and V_{hot} and ΔT_{hot} into Eq. (9.49) gives:

$$Ac_p(xV_{avg})(x\Delta T_{avg}) = 1.37\ Q \tag{9.51}$$

Dividing Eq. (9.51) by Eq. (9.50) gives

$$x^2 = 1.37 \qquad \text{or} \qquad x = 1.17 \tag{9.52}$$

Hence, from EQ. (9.42) and Eq. (9.47),

$$V(\text{hot channel}) = 1.17\ V\ (\text{average channel}) \text{ and}$$

$$\Delta T(\text{hot channel}) = 1.17\ \Delta T(\text{average channel}) \tag{9.53}$$

The safety limit [HEU] during a loss-of-flow transient is established such that the maximum fuel temperature shall not exceed 350°F. The average fuel temperature does not exceed 247°F in Figure 9-9 as calculated by the transient heat transfer computer code. This occurred at 5.2 seconds where the average coolant temperature was calculated to be 140°F.

To compare with the steady state heat transfer code it was assumed that the reactor was in steady state at the conditions existing at 5.2 seconds. The steady state code gave an average fuel temperature of 214°F and an average coolant temperature of 143°F. The coolant temperatures are in good agreement, but as to be expected, the fuel temperature is considerably higher in the transient than in the steady state.

The transient code will not give the peak fuel temperature in the hot channel, but a conservative approach is to calculate this temperature for the steady state and ratio up accordingly. From the steady state

code, the peak fuel temperature in the hot channel was 252°F. This occurred near the mid point, axially along the channel where the coolant temperature was 147°F.

The heat transfer coefficients do not vary greatly, so for a given rate of coolant flow in a channel, the channel power, P, is closely proportional to the temperature difference, T, between the fuel plate and the bulk coolant. Accordingly

$$\frac{P(\text{hot channel in transient})}{P(\text{average channel in transient})} = \frac{P(\text{hot channel in steady state})}{P(\text{average channel in steady state})} \tag{9.54}$$

and to a very good approximation

$$\frac{\Delta T(\text{hot channel in transient})}{\Delta T(\text{average channel in transient})} = \frac{\Delta T(\text{hot channel in steady state})}{\Delta T(\text{average channel in steady state})} \tag{9.55}$$

or abbreviating

$$\frac{\Delta T(hc,tr)}{\Delta T(ac,tr)} = \frac{\Delta T(hc,ss)}{\Delta T(ac,ss)} \cdot \tag{9.56}$$

Using the data from the steady state code at 5.2 seconds given above

$$\frac{\Delta T\ (hc,ss)}{\Delta T\ (ac,ss)} = \frac{(252-147)}{(214-143)} = 1.48 \tag{9.57}$$

We assume this ratio is constant at time other than 5.2 seconds. At times far from 5.2 seconds the assumption is poor, but at times near 5.2 seconds where the peak temperatures are encountered, the assumption is quite valid. Accordingly,

$$\Delta T(hc,tr) = 1.48\Delta T(ac,tr). \tag{9.58}$$

$\Delta T(ac,tr)$ can be obtained at any time by subtracting the average coolant temperature from the average fuel temperature shown in Figure 9-9. At 5.2 seconds

$$\Delta T(ac,tr) = 247 - 140 = 107^{o}F \quad (9.59)$$

and therefore, (still at 5.2 seconds)

$$\Delta T(hc,tr) = 1.48 \times 107^{o}F = 158^{o}F \quad (9.60)$$

As mentioned before in laminar flow, to obtain equal pressure drops across both channels, the hot channel must have a flow rate 1.17 times the flow rate in the average channel. The temperature rise of the coolant along the hot channel must also be 1.17 times the temperature rise of the coolant along the average channel. (These two factors of 1.17 combine to give the radial peaking power factor of 1.37 [HEU]).

From Figure 9-9, at 5.2 seconds the average coolant temperature is $140^{o}F$, and subtracting the $111^{o}F$ entrance temperature, gives a temperature rise of $29^{o}F$ to the mid point of the average channel. For the hot channel the temperature rise is $1.17 \times 29^{o}F = 34^{o}F$ giving a temperature at the mid point along the hot channel of $145^{o}F$.

Therefore, the peak flux fuel temperature in the hot channel in the transient is

$$T(pf,hc,tr) = 145^{o}F + 158^{o}F = 303^{o}F$$

This is at 5.2 seconds after the start of the loss-of-flow transient. In general, it is assumed that at any time during the transient, the peak fuel temperature in the transient is

$$T(pf,hc,tr) = 111^{o}F + 1.17\ T(aw,ac,tr) - 111^{o}F) + 1.48\ \Delta T(ac,tr) \quad (9.61)$$

where T(aw,ac,tr) is the average water temperature in the average channel

in the transient and 111°F is the coolant entrance temperature (pool temperature). T(pf,hc,tr) is the peak fuel temperature shown in Figure 9-9. The maximum is 303°F and is well below the [HEU] safety limit of 350°F. This method of analysis predicts a peak fuel temperature of 279°F at the start of the transient (time zero). The more accurate steady state code gave a peak fuel temperature of 252°F in the hot channel prior to the transient, indicating the conservatism of the method.

9.15. HEU Analysis for Natural Convection

[This section, as is the previous section, is the analysis performed for the HEU SAR. Refer to section 9.13 for justification for the validity of including this analysis for LEU]

According to Figures 9-6A and 9-7 and also Figure 2.1 in Technical Specification 2.1 [HEU Technical Specification Ref 29] a loss of flow transient from 3.45 megawatts will result in a flow coast-down followed by natural convection cooling at a reactor power of 750 KW. This power is due to fission product decay and dies off gradually with time. To be consistent with the Loss of Flow Transient Analysis (Section 9.14), 750 KW was chosen as the maximum power for the Safety Limit[29] in the natural convection mode of operation.

The transient heat transfer code (see Section 9.14) was used to determine the equilibrium flow rate established at 750 KW of power with natural convection flow. A flow rate of 129 GPM through 168 channels was established in about 25 seconds and remained steady in time thereafter. With 168 channels (Sec 9.4 of Ref. 24) the average power per channel is

750/168 = 4.46 KW. Multiplying by the radial peaking factor of 1.37 gives 6.12 KW as the power in the hot channel.

The flow rate in the average channel is 129/168 = 0.768 GPM. The velocity in the peak channel is 1.17 times the velocity of the average channel (see Section 9.14). Therefore, the flow rate in the hot channel is 0.768 x 1.17 = 0.90 GPM. Using the power of 6.12 KW and a flow rate of 0.90 GPM in the hot channel as input to the steady state thermal hydraulics code with natural convection upflow, the maximum fuel plate temperature was found to be 259°F with an inlet coolant temperature of 111°F. 750 KW and 111°F were conservatively chosen as the [HEU] Safety Limits in the Natural Convection Mode of Operation, Specification 2.1.2 [HEU Technical Specifications Ref. 29]. A maximum fuel plate temperature of 259°F is well below the temperature at which fuel clad damage could occur.

9.16. Maximum LEU 22 Plate Fuel Temperatures Following LOCA

9.16.A. Introduction

The maximum fuel temperature reached after loss of coolant from the limiting UVAR LEU 22-plate core was calculated using semi-empirical relationships similar to those developed for the safety analysis of the Omega West Reactor (OWR) at Los Alamos[22], which is an MTR-plate-type pool reactor. The fuel clad melting temperature for the UVAR is the melting point of aluminum alloy 6061 at 1080°F, but structural integrity may be lost if the fuel is held above the softening temperature of for a sustained period of time. For the purposes of these analysis, a softening temperature of 840°F[33] was chosen as the limiting criteria for the analysis of a LOCA.

For several potential coolant loss mechanisms, the time required to uncover the core was calculated because it is an important parameter in calculating the maximum fuel temperature following a LOCA. However, the UVAR relies upon the Emergency Core Spray System (ECSS) (analyzed in Section 9.17) to cool the reactor following any LOCA that takes less than 90 minutes to uncover the core after the reactor scrams due to low pool level. Therefore, the minimum time after a shutdown to shift from water cooling to air cooling is taken to be 90 minutes.

The fission fragment heat source used in the analysis was the "Simplified Method for Determining Decay Heat Power and Uncertainty" given in Section 3.6 of ANSI/ANS Standard 5.1[31]. This decay heat power can be 1.5 times as high as the power predicted by the Way-Wigner relation during the limiting LOCA transient. A modification to the heat transfer correlation developed by OWR was made such that, when used with the ANSI/ANS 5.1 heat source, it safely enveloped the temperatures calculated with the original OWR heat transfer correlation and the Way-Wigner heat source. For the benchmark transient based upon uncovering the OWR core 30 minutes following shutdown, the modified heat transfer correlation with the ANSI/ANS 5.1 heat source gave a peak temperature 140°F higher than the original OWR calculations and was higher throughout the transient. Figure 9-10 compares the benchmark OWR transient when calculated using the UVAR correlation and the ANSI/ANS 5.1 heat source with the same transient calculated with the OWR correlation using the Way-Wigner heat source. This comparison, along with similar comparisons in reference 22 between the OWR correlation and experimental data,

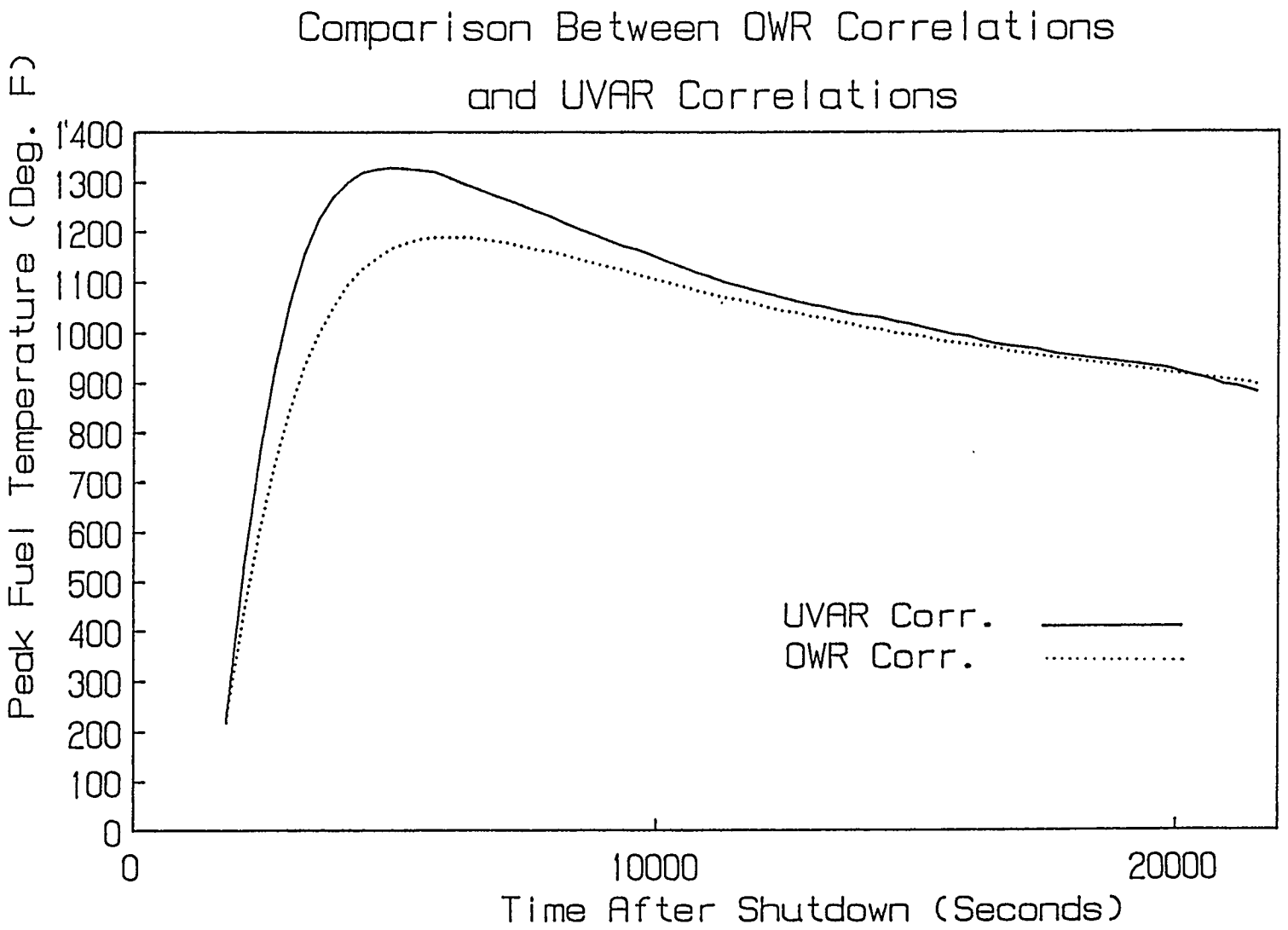


Figure 9-10 Comparison Between OWR Transient using UVAR Correlelations ans OWR Correlations

indicates that the new correlation together with the ANSI/ANS 5.1 heat source will overestimate the maximum temperature reached following a LOCA.

9.16.B Calculation of Peak Fuel Temperature Following a LOCA

After loss of water cooling, the reactor is cooled predominantly by ambient air flowing through the core by natural convection. Since heat conduction to the grid plate and to the upper part of the fuel element occurs together with natural convection and some radiation, the calculation of maximum fuel temperature from first principles is too complex to be reliable. Hence, experimental data from LITR was used by OWR[22] in their safety analysis to develop a heat transfer correlation that, together with the Way-Wigner decay heat relation, safely enveloped the maximum axial temperatures measured in the LITR experiments.

In the LITR experiments, an element was actually removed from an operating core and the maximum fuel temperature along the axial profile was measured as a function of time while the element was cooled by air convection. As described in Reference 22, the LITR experimental data was safely enveloped by the following transient equation which is solved for the difference, θ, between the peak fuel-plate temperature, T_F, and the ambient air temperature, T_a.

$$mc_p \frac{d\theta}{dt} = Q(t) - hA\theta \qquad (9.61)$$

where

$\theta = T_F - T_a$ (^oF)

$Q(t)$ = time dependent heat source (MW)

hA = product of the natural convection heat transfer correlation and the effective heat transfer area of one fuel element (MW/^{o}F)

mc_p = heat capacity of a fuel element, with m being the mass and c_p being the specific heat of the associated fuel element material.

Mc_p for the UVAR 22-plate fuel element was calculated by determining the mass of aluminum and U_3Si_2 in the standard element from the fuel plate specification and the preliminary construction drawings for the elements and applying formulas determined by Argonne National Laboratories[30] for the c_p of these materials as a function of temperature.

$$c_p \text{ Al} = .892 + .00046T \text{ (J-g}^{-1}\text{-K}^{-1}\text{)} \tag{9.62}$$

Mass Al = 5195 g per element

$$c_p \text{ } U_3Si_2 = .199 + .00010T \text{ (J-g}^{-1}\text{-K}^{-1}\text{)} \tag{9.63}$$

Mass of U_3Si_2 = 1505 g per element

Therefore, the total mc_p for a standard element is

$$mc_p \text{ Element} = 4933 + 2.54T \text{ (J-K}^{-1}\text{)} \tag{9.64}$$

For the heat source, Q(t), the method given in Section 3.6 of ANSI/ANS Standard 5.1 for heat production from fission products after shutdown was used. The one sigma uncertainty associated with the decay heat power was included as a positive bias.

$$P_d(t,T) = P'_d(t,T) * G(t) + \Delta P_d \quad (9.65)$$

and

$$P'_d(t,T) = 1.02 \frac{Pmax}{Q}[F(t,\infty) - F(t + T,\infty)] \quad (9.66)$$

where:

P_d = decay power

G(t) = a correction factor for the activation of fission fragments given in Table 10 of ANSI/ANS 5.1

ΔP_d = one-sigma error associated with P_d (see ANSI 5.1)

Q = 200 Mev/fission (conversion factor)

Pmax = the operating power of the hottest fuel element

$F(t,\infty)$ = the fission fragment heat source for thermal fission of U-235 given in Table 4 of ANSI/ANS 5.1

t = time since shutdown from operating at Pmax

T = the time operated at Pmax

Non-linear interpolation between time steps given in the ANSI/ANS 5.1 tables for Eq. (9.65) was done using the time dependency in the Way-Wigner expression for decay heat generation.

The value used for T was 120 hours, or 5 days. The value used for Pmax was 0.209 MW, which is the power of the highest power element in a 4x4 LEU core, at 2 MW total core power, as determined from 2DB-UM[26] flux maps. Larger cores were evaluated and found to be less limiting than the 4x4 element core.

The heat transfer parameter hA was found at OWR by fitting coefficients in the form

$$hA=C(a\theta^n + b) \quad (9.67)$$

to get an expression for hA which was then used in Eq. (9.61) to fit the data from the LITR experiments using the Way-Wigner decay heat source and the appropriate mc_p. The coefficient C includes the heat transfer area

of the fuel plates. The expression for hA used for the present analysis was found by searching for a new constant C in Eq. (9.67) (retaining the other constants found by OWR) that when used in Eq. (9.61) with the ANSI/ANS 5.1 heat source and the case specific input data from OWR, safely enveloped the transients calculated with the original OWR correlations in their safety report. The new expression for hA which incorporates the higher h per plate and includes the number of plates per element as a variable is:

$$hA = 9\times10^{-8}(PN)(6.4\times10^{-3}\ \theta^{0.72} + 0.5)\ \frac{MW}{F^{o}} \qquad (9.68)$$

where PN is the number of fuel plates in the standard element.

Substituting Eqs. (9.64), (9.66), and (9.68) into Eq. (9.61) gives a transient expression which was solved for θ, with the initial conditions of $\theta = 112^{o}F$ at the time at which air cooling starts. The peak fuel temperature, T_f, was obtained from $\theta = T_f - T_a$ assuming that the ambient air temperature, T_a, was $100^{o}F$, or

$$T_f(peak) = \theta + 100.$$

The peak fuel-plate temperatures versus time after shutdown, with time to shift to air cooling in the core as a parameter, are plotted in Figure 9-11. Transients assuming no ECSS and a shift to air cooling 0.3 hours and 1 hour following shutdown are plotted as dotted lines whereas the transient for the minimum specified time to shift to air cooling with ECSS (1.5 hours for flow dropping below 7.5 gpm, see Table 9.4) and a later transient (2 hours) are plotted as solid lines. The maximum fuel temperatures corresponding to these transients are listed in Table 9-3. For the limiting case where the ECSS is used to provide cooling for 90 minutes following a reactor scram due to low pool level, the maximum

temperature reached during the transient is 775°F. This is well below the aluminum cladding softening temperature of 840°_{F} assumed for this analysis.

TABLE 9-3

MAXIMUM FUEL TEMPERATURES

(Operation Time = 120 h at 2 MW)

Time to Shift to Air Cooling (min.)	Maximum Temperature (^{o}F) w/o ECCS	w/ ECCS
20	975	775
60	835	775
90		775
120		730

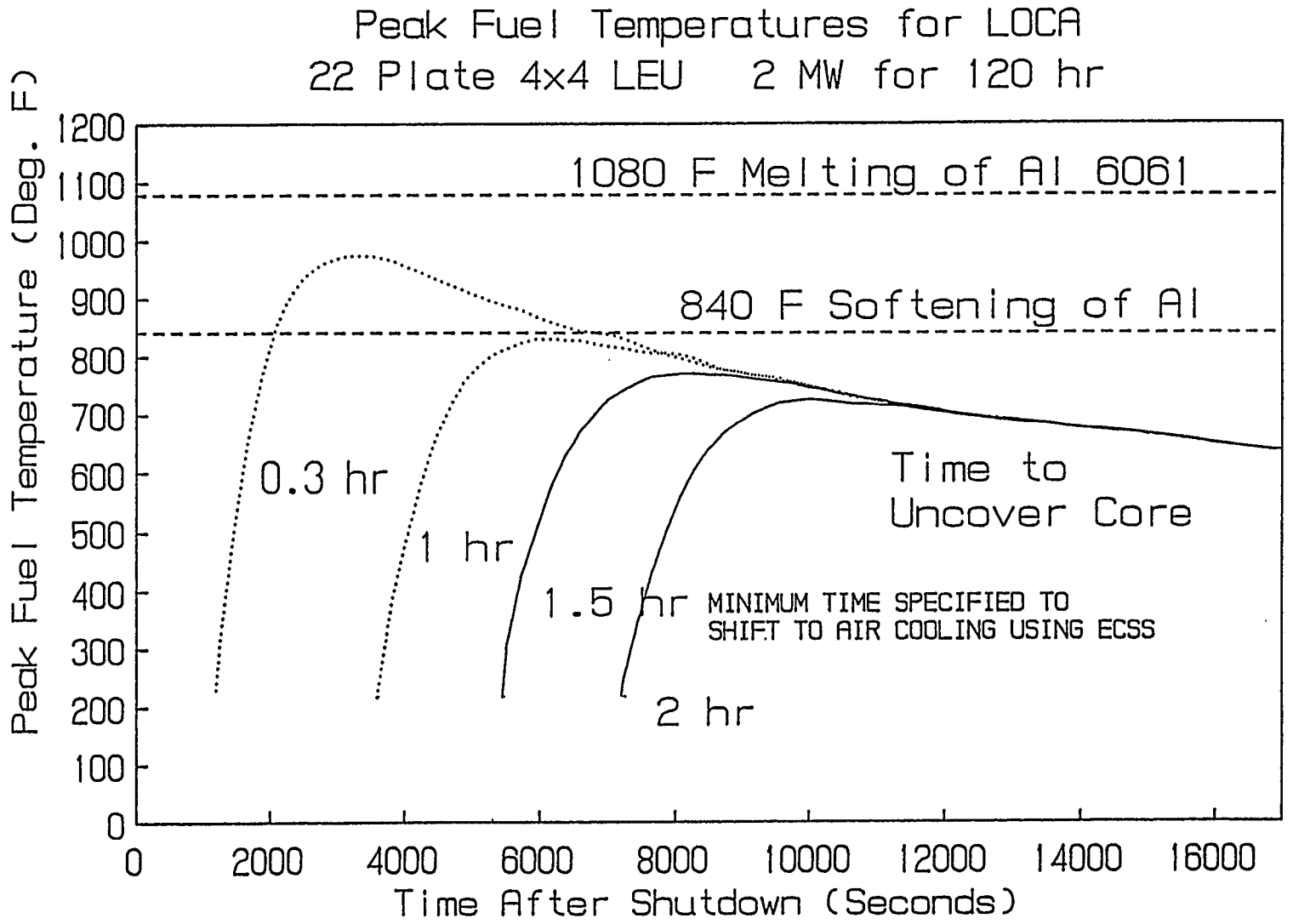


Figure 9-11 Peak Fuel Temperatures for Various LOCA Transients

9.17 Emergency Core Spray System Analysis

The emergency core spray system is described in Section 4.10. Using the decay heat source in ANSI/ANS 5.1 as described in section 9.17, the decay heat power in the hottest element 0.3 hours after shutdown (minimum credible time to uncover the core) is 3.5 kw. Assuming the cooling water is initially at 100°F, a water flow of 0.184 pounds per minute or 0.0221 gal/min is required to remove the decay heat from the hottest element (assuming complete evaporation of the water). A coolant flow of 10 gallons per minute over the entire grid plate will provide an average flow of 0.156 gallons per minute to each of the 64 fuel element positions. Using a flow maldistribution factor of $1/2^{32}$, the minimum flow to any fuel element position is 0.078 GPM. This flow is capable of removing 12.3 kw per fuel element. Thus, the rated flow of 10 gallons per minute to the core area is greater than the flow rate required to remove the decay heat of the hottest element after 0.3 hours by a factor of about 3.5. From 30 minutes to 90 minutes, the rated flow of the ECSS is 7.5 GPM which can remove 9.2 kw per fuel element. During this time the decay heat in the hottest element falls from 3.4 kw to 1.9 kw providing a minimum safety factor of 2.8 for the time the ECSS is relied upon to cool the reactor core.

At five second after shutdown, the decay heat power is 11 kw. This value is well below the 12.3 heat removal capability of the spray system. Even in the incredible situation where all water is lost from the pool in a matter of seconds, the spray system should be able to cool the reactor and prevent core damage. No operator action, automatic electronic, or automatic mechanical mechanism is required for the ECSS to function.

As the water level drops below the level of the spray headers, the

spray system begins to spray water on the core. Using the mockup of the core spray system shown in Fig. 4-3, tests were run of the flow rate versus head of water above the spray headers. Theoretically, if W is the flow rate (gpm) and Z is the head of water above the spray headers, then

$$W = KZ^{0.5} \tag{9.69}$$

Using the spray headers in the mockup it was found experimentally that

$$W(\text{gal/min}) = 0.48\ Z^{0.45} \tag{9.70}$$

where Z is in feet. From this relationship the characteristics of the spray system can be predicted as shown in Table 9-4.

LEU Technical Specifications for the spray system are based on this table, and require that each of the two systems shall be capable of delivering at least 10 gal/min for the first 30 minutes and at least 7.5 gal/min for the next 60 minutes after a LOCA onset. Ideally, this flow would be distributed equally to each of the 64 fuel element positions, but in actuallity this is not practical. It is practical to have (1/2 x 1/64) or 1/128 of the total flow delivered to each element. At the initial installation, measurements[32] were made to verify that each of the two spray systems is capable of delivering 10/128 or 0.078 gpm to each of the 64 fuel element positions at the end of 30 minutes of flow.

Figure 9-12 gives the decay power of the hottest element as a function of time for the first 2 hours after shutdown, the specified heat removal capacity of one ECSS sub system, and the actual heat removal capacity of each ECSS sub system based upon actual flow testing of the ECSS.

TABLE 9-4

CHARACTERISTICS OF SPRAY SYSTEM
(EACH TANK)

Time (min)	Head of Water (feet)	Flow Rate (gal/min)	Volume of Water Used (gal)
0	14.92	12.1	0 (Tank full)
7.8	14	11.8	103
16.6	13	11.4	215
25.7	12	11.0	328
35.2	11	10.6	440
45.1	10	10.1	552
55.6	9	9.7	664
66.7	8	9.2	776
78.4	7	8.6	889
91.0*	6	8.1	1000
105	5	7.4	1113
120	4	6.7	1225
137	3	5.9	1337
158	2	4.9	1450
168	1.58	4.4	1497(Tank empty)

* Flow beyond 90 minutes may be less than the specified 7.5 gal/min and therefore credit is not taken for this flow in the calculations.

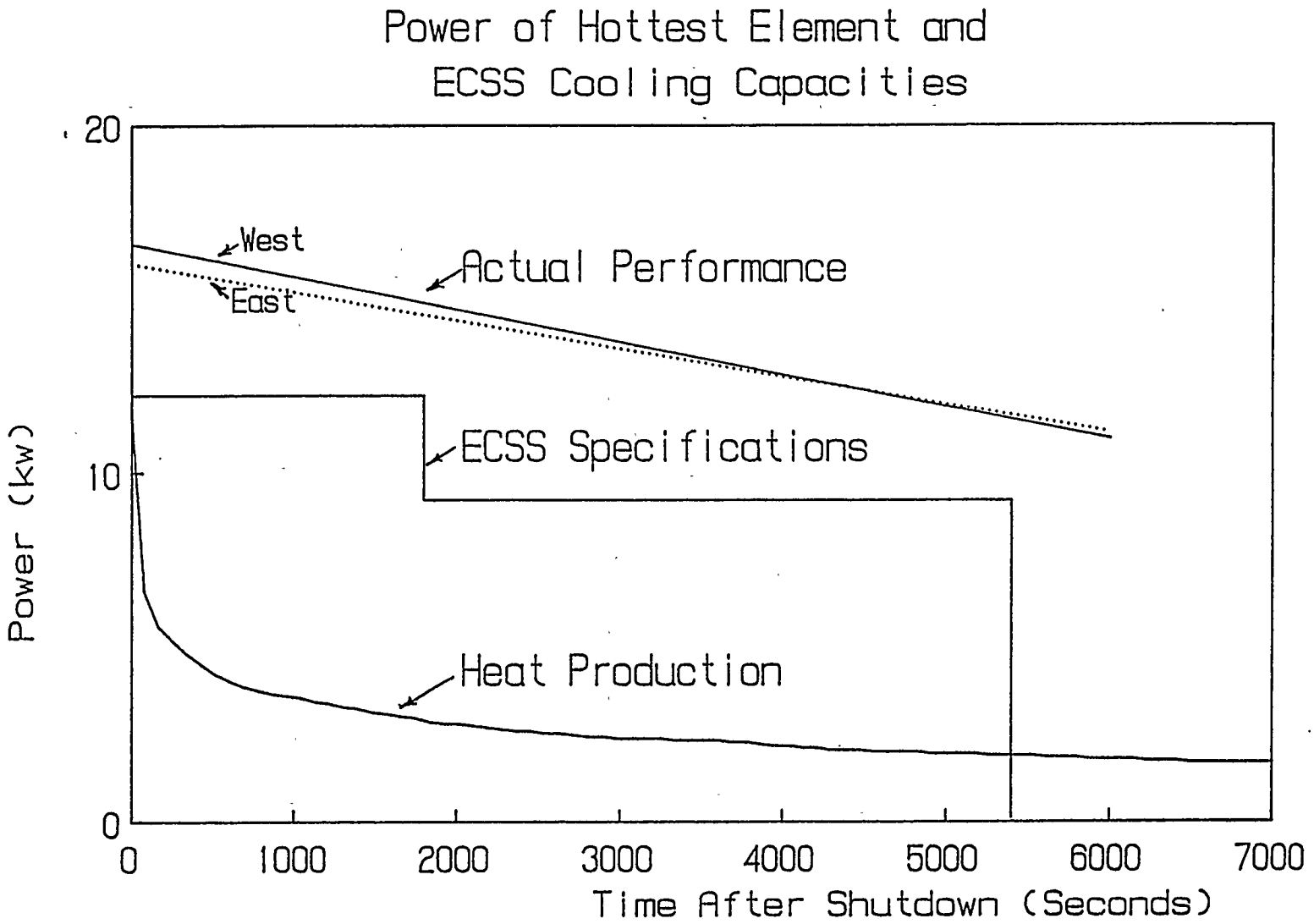


Figure 9-12 Power of the Hottest Element and ECSS Cooling Capacities

9.18. Time to Uncover the Core Following A LOCA

Table 9-5 shows the time it takes to uncover the core for the various mechanisms of pool leakage calculated in Section 9.18.

Table 9-5

Time to Uncover Core

For Various Leakage Mechanisms

Leakage Path	Time to Uncover Core
1) Double ended break at lowest point in 6-inch primary piping	19 minutes
2) Rupture of 8-inch beam port and flange	22 minutes
3) Double ended break in the 6-inch primary pipe at the level of the floor in the heat exchanger room	23 minutes
4) Quarter-inch, vertical crack extending the entire depth of pool, assuming no frictional losses	36 minutes

It is postulated that a guillotine pipe break in the six-inch diameter pipe between the reactor and the heat exchanger is the most rapid way for the UVAR core to uncover. Without subsequent closure of the isolation valves, such a double-ended pipe break would allow flow from both ends of the pipe. The geometry of the system is shown in Fig. 9-13.

Calculations were made assuming that a pipe break would occur at heat exchanger room floor level and at the lowest pipe level. It is noted that this pipe is surrounded by either concrete or earth wherever

it is below the floor level. Since a guillotine pipe break is not likely to occur at this location and water could not freely flow away if it did, the calculations are considered to be conservative. Because the break is assumed to occur close to the pool, there would be little frictional resistance to flow through one end of the break. However, flow through the other end of the break must first travel through the pipe and the heat exchanger, and consequently the resistance would significantly decrease this flow rate. This was taken into account in the calculation of the time to uncover the core.

9.18.A. Flow Rate without Frictional Loss

The flow velocity V_2 through the pipe end for which no frictional loss was assumed was calculated using Bernoulli's equation. With positions 1 and 2 defined on Fig. 9-13, Bernoulli's equation for flow between 1 and 2 is:

$$\frac{V_1^2}{2g_c} + \frac{p_1}{\rho} + z_1 \frac{g}{g_c} = \frac{V_2^2}{2g_c} + \frac{p_2}{\rho} + z_2 \frac{g}{gc} \qquad (9.71)$$

From Fig. 9-14,

$V_1 = 0$ (i.e., V_1 is velocity before the water enters the pipe)

$z_1 = z_2$

$p_1 = p_o + \rho z \frac{g}{g_c}$ (where z is the water level above the pipe break)

$p_2 = p_o = 1$ atm

Hence, for the present case, Bernoulli's equation reduces to

$$\frac{V_2^2}{2g_c} = \frac{p_o + \rho z \frac{g}{g_c} - p_2}{\rho}$$

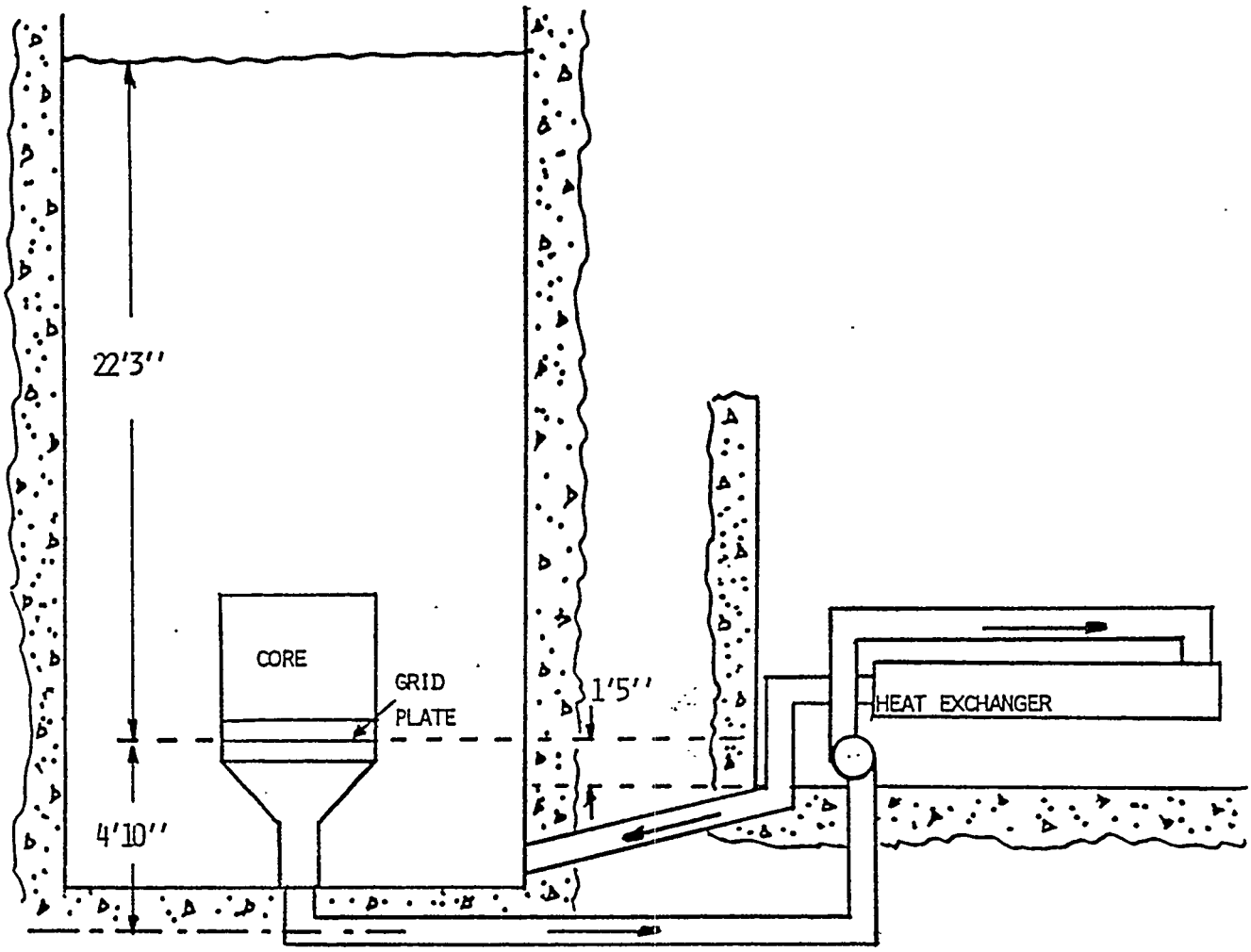


FIGURE 9-13 PRIMARY PIPING

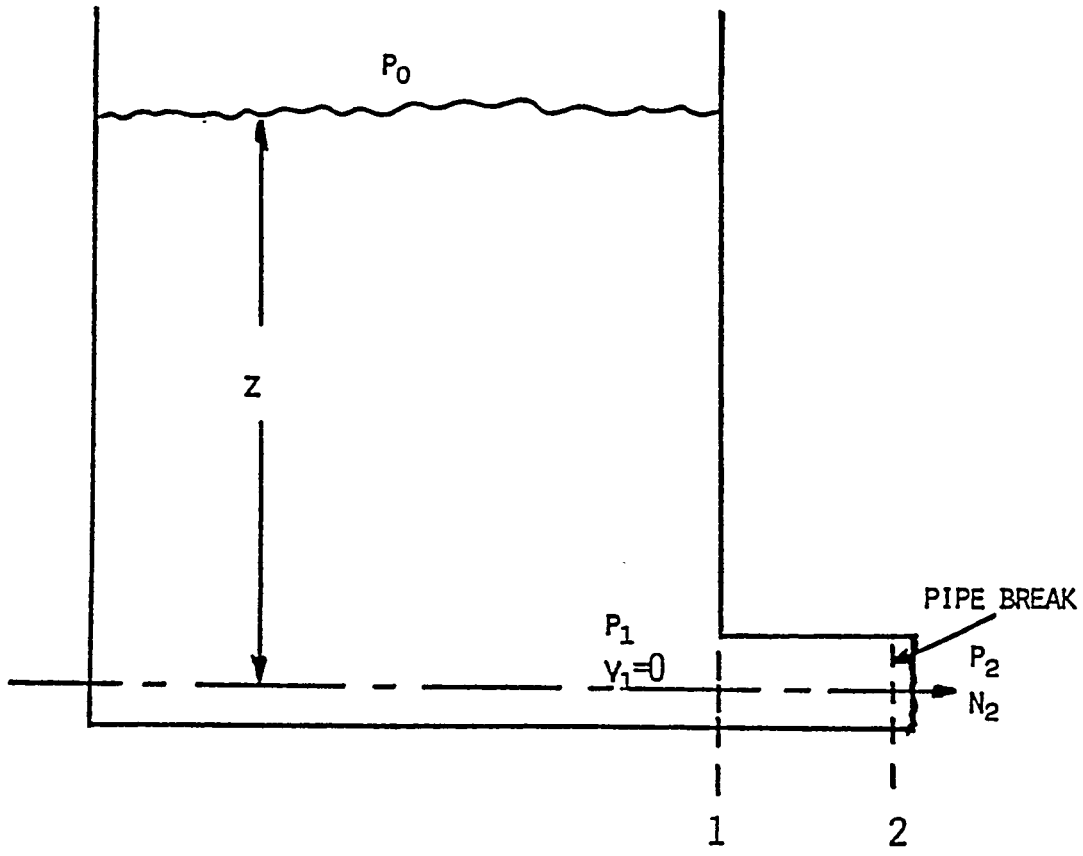


FIGURE 9-14 GEOMETRY FOR CALCULATING V_2

or

$$V_2 = \sqrt{2gz} \tag{9.72}$$

9.18.B Flow Rate with Frictional Loss

The effect of the frictional loss in the pipe and the heat exchanger is to add an energy loss term to the Bernoulli equation, as follows:

$$\frac{V_1^2}{2g_c} + \frac{p_1}{\rho} + z_1 \frac{g}{g_c} = \frac{V_{2,f}^2}{2g_c} + \frac{p_2}{\rho} + z_2 \frac{g}{g_c} + H_\ell \tag{9.73}$$

where $H_\ell = \frac{\Delta p_f}{\rho}$ (and where Δp_f is the frictional pressure drop)

The subscript f is added to V_2 to denote the velocity at position 2 with friction loss taken into account.

Equation (9.73) reduces to:

$$\frac{V_{2,f}^2}{2g_c} + \frac{\Delta p_f}{\rho} = z \frac{g}{g_c} \tag{9.74}$$

In order to solve for $V_{2,f}$, it is necessary to express Δp_f in terms of $V_{2,f}$. This can be done by recognizing that the form of the frictional pressure drop is

$$\Delta p_f = f \frac{L}{D} \frac{\rho V^2}{2g_c}$$

By neglecting the dependence of the friction factor "f" on velocity, this expression for Δp_f has the form,

$$\Delta p_f = aV^2 \tag{9.75}$$

where "a" is a constant. Neglecting the dependence of "f" on the velocity is sufficiently accurate for the present calculation, as can be

shown as follows. The velocity through the 6-inch pipe during normal operation is 11.4 ft/sec, and the associated friction factor is 0.0144. The maximum velocity in the pipe at the beginning of a pipe break, with no resistance to flow, is 41 ft/sec, and the friction factor for this velocity in a 6-inch pipe is 0.0136. The velocity remains between 11.4 and 41 ft/sec until the water level in the pool is 2.0 ft above the pipe break.

The constant "a" in Eq. (9.75) can be evaluated from a knowledge of the pressure drop and velocities for the piping and heat exchanger during rated flow conditions, as follows:

Mass flow rate during normal operation = 500,000 lbm/h (900 gal/min)

V (through 6" dia. pipe) = 4.1×10^4 ft/h

Δp_f (Heat Exchanger) = 9.5 psi = 1370 lbf/ft^2 (during normal operation, as experimentally measured)

Length of pipe in external line, exclusive of heat exchanger $\simeq$ 70 ft.

Re (in 6" pipe) = 7.7×10^5

f = 0.014

Δp_f (pipe) = 1.7 psi = 250 lbf/ft^2

Δp_f (pipe) + Δp_f(heat exchanger) = 11.2 psi = 1620 lbf/ft^2

$g_c = 4.17 \times 10^8 \ \frac{\text{lbm ft}}{\text{lbf hr}^2}$

Using the form for Δp from Eq. (9.75), together with continuity, one can express the sum of the pipe and the heat exchanger pressure loss as a function of the velocity in the pipe as:

$$\Delta p_f = \Delta p_{pipe} + \Delta p_{heat\ exchanger} = aV^2_{pipe}$$

or

$$a = \frac{1620 \text{ lbf/ft}^2}{(4.1 \times 10^4 \frac{\text{ft}}{\text{hr}})^2} \tag{9.76}$$

Substituting Eqs. (9.75) and (9.76) into (9.74) gives the following result for $V_{2,f}$:

$$V_{2,f} = \sqrt{\frac{g\ z}{\frac{1}{2} + 6.5}} = 0.378\ \sqrt{gz} \tag{9.77}$$

This value compares to $V_2 = \sqrt{2gz} = 1.41\sqrt{gz}$ [Eq. (9.72)] where V_2 is the velocity without friction loss, or

$$V_{2,f} = 0.27\ V_2 \tag{9.78}$$

9.18.C. Time to Uncover Core with Double-Ended Pipe Break

To calculate the time to uncover the core with a guillotine pipe break, we equate the following two expressions for the rate at which water is flowing out of the pool:

(1) Flow rate out of the broken pipe

$$= \rho S V_2 + \rho S V_{2,f}$$

$$= 1.27\ \rho S V_2 \quad \text{[from Eq. (9.78)]} \tag{9.79}$$

where S = pipe cross sectional area

(2) Since $-\frac{dz}{dt}$ = the rate of change of water level in the pool, the flow out of the pool is also

$$= -\rho A \frac{dz}{dt} \tag{9.80}$$

where A is the surface area of the pool.

Equating Eq. (9.79) and (9.80) for flow rate gives

$$\frac{dz}{dt} = \frac{-1.27S}{A} V_2$$

Substituting Eq. (9.72) for V_2 gives

$$\frac{dz}{dt} = \frac{-1.27S}{A} \sqrt{2gz}$$

Finally, the time, τ, for the water level to change from $(z_0 + z_1)$ to z_1 (i.e. the time to uncover the core), is

$$\tau = \int_{z_o+z_1}^{z_1} - \frac{A}{1.27S} \frac{dz}{\sqrt{2gz}} \qquad (9.81)$$

$$= \frac{2A}{\sqrt{2g}\ S} \left(\sqrt{z_o + z_1} - \sqrt{z_1}\right)$$

Values used in the calculations reported in Section 9.18 are:

$g = 32.17\ ft/sec^2$

$A = 32\ ft \times 12\ ft$

$S = \frac{\pi}{4} (\frac{1}{2}\ ft)^2$

$z_0 = 22.25\ ft$

For pipe break at floor level of heat exchanger room, $z_1 = 1.92$ ft.

For pipe break at lowest point in pipe, $z_1 = 4.83$ ft. (See Fig. 9-14).

9.18.D Time to Uncover Core with Crack in Pool Wall

For a crack in the pool wall of width δ running the full height of the wall, the time necessary to uncover the core, assuming Bernoulli's equation with no frictional resistance, is

$$\tau = \frac{3A}{\delta\sqrt{2g}} \left(\frac{1}{\sqrt{z_1}} - \frac{1}{\sqrt{z_o + z_1}}\right) \qquad (9.81)$$

where z_1 = distance between bottom of the pool and the bottom of the grid plate and z_o = same as in Fig. 9-13.

REFERENCES FOR CHAPTER 9

1. Gambill, W.R., "Generalized Prediction of Burnout Heat Flux for Flowing, Subcooled, Wetting Liquids," Chemical Engineering Progress Symposium Series, Vol. 59, Houston, 1962.

2. Bergles, A. and Rohsenow, W., "The Determination of Forced-Convection Surface Boiling Heat Transfer," ASME Paper 63-HT-22 (1963).

3. Cox, J., "ORR Operations for Period April 1958 to April 1959," CR-59-39, Oak Ridge National Laboratory (April 1959).

4. Eckert, E.R.G. and Drake, R.M., "Heat and Mass Transfer." McGraw-Hill, New York, 1959.

5. Private Communication from Wallace R. Gambill, ORNL.

6. Bernath, L., "Theory of Local Boiling Burnout and its Application to Existing Data," Ch.E. Progress Symposium Series, Storrs, 1960.

7. Todeas, N., "Effect of Non-Uniform Axial Heat Flux Distribution on the Critical Heat Flux," Ph.D.. Dissertation, M.I.T., Sept. 1965.

8. DeBortoli, R.A., "Forced-Convection Heat Transfer Burnout Studies for Water in Rectangular Channels and Round Tubes at Pressures Above 500 psia," WAPD-188, Oct. 1958.

9. Gambrill, W.R., "Forced Convection Burnout," Nuclear Safety, Vol. 5, No. 2, Winter 1963-64.

10. Tong, L.S., "DNB Studies in an Open Lattice Core," WCAP-3736, Aug. 1964.

11. Perry, J.H. (ed), "Chemical Engineer's Handbook," McGraw-Hill, New York, 1950.

12. Esselman, W.H., et al, "Thermal and Hydraulic Experiments for Pressurized Water Reactors," Proceedings of the 2nd United Nations International Conference on the Peaceful Uses of Atomic Energy, Vol. 7 pg. 758, United Nations, Geneva, 1958.

13. Von Karman, T., NACA Technical Memo No. 611, 1931.

14. Gambill, W.R. and Bundy, R., "HFIR Studies of Turbulent Water Flow in Thin Rectangular Channels," ORNL-3079, June 1961.

15. Reynolds, J., "Local Boiling Pressure Drops," ANL-5178, March, 1954.

16. Barnett, P.G., "The Prediction of Burnout in Non-Uniformly Heated Rod Clusters from Burnout Data for Uniformly Heated Round Tubes," AEEW-R-362, November 1964.

17. "Non-Uniform Heat Generation Experimental Program," Quarterly Progress Report No. 5, July-September 1964, BAW-3238-5, Sept. 1964.

18. "Non-Uniform Heat Generation Experimental Program," Quarterly Progress Report No. 6, October-December 1964, BAW-3238-6, December 1964.

19. Sternberg, H.I., "Thermal Power Calibration and Correlation of UVAR by Foil Irradiation and Heat Balance," Master's Thesis, University of Virginia, June 1964.

20. Brunot, W.K., "An Analysis of Fuel Element Surface Temperature and Coolant Flow Rate in UVAR," Master's Thesis, University of Virginia, November, 1961.

21. Custer, G.A., "The Experimental Determination of the Thermal Neutron Flux in the University of Virginia Reactor Using an Aluminum Hydraulic Rabbit, Master's Thesis, University of Virginia, August 1960.

22. "1969 Status Report on the Omega West Reactor, with Revised Safety Analysis," Los Alamos Scientific Laboratory, LA-4192, July 1969.

23. DiNunno, J.J., et al. "Calculation of the Distance Factors for Power and Test Reactor Sites," TID-14844, 1962.

24. "University of Virginia Reactor Safety Analysis Report," University of Virginia, UVAR-18, Revised January 1979.

25. Dahlheimer, J.A., "Thermal-Hydraulic Safety Analysis of Pool Reactors", Master's Thesis, University of Virginia, 1967.

26. University of Michigan, "2DB-UM Appollo Version", Version #10, September 1986.

27. Freeman, D.L., "Neutronic Analysis for the UVAR HEU to LEU Conversion Project", Master's Thesis, University of Virginia, January 1990.

28. Smith R.S. and Woodruff W.L., "A Computer Code, NATCON, for the Analyses of Steady-State Thermal-Hydraulics and Safety Margins in Plate-Type Research Reactors Cooled by Natural Convection", ALN/RERTR/TM-12, December 1988.

29. "Technical Specifications for the University of Virginia", September 1982, Amended April 1988, and December 1988.

30. Telecopy from Argonne National Laboratory, "Properties of Fuel Meat Materials", August 19, 1988.

31. "Decay Heat Power in Light Water Reactors" American National Standard ANSI/ANS-5.1-1979, Reaffirmed July 1985, American Nuclear Society, La Grange 1979.

32. Meem, J. L., "Emergency Core Spray System Installation And Testing", Report to University of Virginia Reactor Safety Committee, September, 1971.

33. Nagler, A., Gilat, J., Hirshfeld, H., "Evaluation of LOCA in a Swimming-Pool Type Reactor Using the 3D-AIRLOCA Code," paper presented at the XII International Meeting on Reduced Enrichment for Research and Test Reactors, Berlin, Federal Republic of Germany, 10-13 September 1989.

APPENDIX V

HEU TO LEU FUEL CONVERSION REPORT

Procedures for Loading UVAR Fuel Assemblies into the BMI-1 Shipping Cask for Transfer to Savannah River

Approved, as Amended,

by the UVA Reactor Safety Committe

May 6, 1993

Revised:

7-19-93
7-22-93
7-27-93
5-29-94
6-10-94

CONTENTS

List of Figures ii

List of Tables iii

List of Appendices iv

I. INTRODUCTION 1
A. Certificate of Compliance (COC) (No. 5957, Rev. 21) . . 4
B. Personnel Assignments 6
C. Radiation and Contamination Monitoring 6
D. Notification 6
E. Auxiliary Water Tank and Bridge Preparation 7
F. Fork Lift Truck 7
G. 5-Ton UVAR Room Polar Crane 7
H. Auxiliary Crane 8
I. UVAR Single Fuel Assembly Transfer Cask 9
J. Criticality Control 10
K. Emergency Planning 10
L. Documentation 10

II. OPERATIONAL CHECKLISTS 11
A. Pre-Shipment Documentation and Notification Checklist 11
B. Minimum Tools and Equipment Needed for Fuel Shipment 14
C. Preparation for Fuel Transfer Operations Checklist 16
D. Receiving and Preparation of Cask for Loading 18
E. Placement of Truck with Cask 18
F. Initial Equipment Inventory and Radiation and Contamination Surveys 19

III. BMI-1 CASK OPERATING PROCEDURES 24
A. Internal Cask Pressure and Liquid Test 24
B. Opening the Cask 28
C. Loading the Cask 31
D. Securing the Cask 42
E. Pre-Shipment Cask Pressure Leak Test 44
F. Preparation of Cask for Shipping 48

IV. CANCELLATION OF SHIPMENT 56

V. SAFEGUARDS 56

VI. PROCEDURAL REVIEWS 58

List of Figures

Figure 1. UVAR fuel shipment equipment arrangement 2

Figure 2 BMI-1 Shipping Cask perspective 3

Figure 3. UVAR Facility single assembly transfer cask 9

Figure 4. BMI-1 Cask Loading Diagram 38

List of Tables

Table I. Individual and Combined Weights to be Lifted by Auxiliary Crane. 8

Table II. Personnel Exposure Record 40

Table A.1 UVAR Fuel Assemblies to be Sent to Savannah River in Shipment No. 1 . . . . . A.2

Table A.2 UVAR Fuel Assembly Exposure Rates in Shipment No. 1 . . . . . A.2

Table A.3 UVAR Fuel Assemblies to be Shipped to Savannah River in the Second Series of Shipments A.3

List of Appendices

UVAR HEU Fuel Assembly Inventory A.1

Personnel Assignments B.1

Assembly and Test of a Pressure, Leak, and Liquid Test Manifold C.1

Verification of Neutron Absorber Plates in the Texas A&M Basket D.1

BMI-1 Certificate of Compliance E.1

DOT / 49 CFR Quality Assurance Checklist F.1

Distribution List G.1

Notification Addresses, Phone and FAX Numbers H.1

PROCEDURES FOR TRANSFERRING UVAR FUEL ELEMENTS TO BMI-1 SHIPPING CASK

I. INTRODUCTION: UVAR fuel assemblies will be prepared for shipment to Savannah River in Aiken, SC, for reprocessing. There are a total of 44 HEU fuel assemblies that will be transported in 2 series for a total of 4 shipments over a period of time spanning UVAR conversion to LEU fuel. A full list of fuel assemblies to be shipped is included in Appendix A to these procedures; a list of and particular instructions pertaining to the first 12 assemblies to be shipped are included in these procedures. Exact timing and itineraries of the shipments will depend on shipping cask availability, route approval by the NRC, Savannah River's receiving schedule, etc.. In accordance with 10 CFR 73.21, shipment schedules and itineraries are among several categories of information that must be safeguarded. Therefore, such information shall only be available on a need-to-know basis. It shall not be discussed in public places, nor shall it be released to the press until at least ten days after the last of a series of shipments. The Reactor Facility has received authorization to transport Hazardous Radioactive Materials from the Department of Emergency Services for the State of Virginia. This authorization expires September 30, 1994.

BMI-1 cask operating procedures have been developed in accordance with Operating Procedures (BMI-1 SARP Section 7, Rev. A 3-28-80), BMI-1 FUEL CASK INSPECTIONS & PREVENTIVE MAINTENANCE SP-14 (a Cintichem, Inc. Research Reactor document), the philosophy of ALARA, and attention to ordinary industrial safety and efficiency. Loading of fuel assemblies into the shipping cask will be done under water in the UVAR auxiliary tank, following their removal from the UVAR pool in a single assembly transfer cask. As shown in Figure 1, a crane will be positioned outside of the reactor building for cask handling. Shipment will be made under the following applicable regulations, which have been reviewed: NRC (10 CFR Part 71, including but not limited to Subparts A, G, and H of this Part, and DOT Regulations referenced in 10 CFR 71.5: DOT (49 CFR Parts 170-189)); and NRC (10 CFR Part 20). Spent fuel shipment is not addressed by UVAR Technical Specifications or Standard Operating Procedures. Consequently, these procedures and accompanying appendices, henceforth referred to as "these procedures," have been written to assure safety and regulatory compliance during all activities associated with spent fuel shipments. Use of the word

"personnel" in these procedures, unless otherwise noted, shall be understood to mean all personnel actively involved in fuel transfer operations.

Figure 2 provides a perspective view of the BMI-1 cask and includes data on the more important component masses, which are augmented in Table I, in Section I.H.

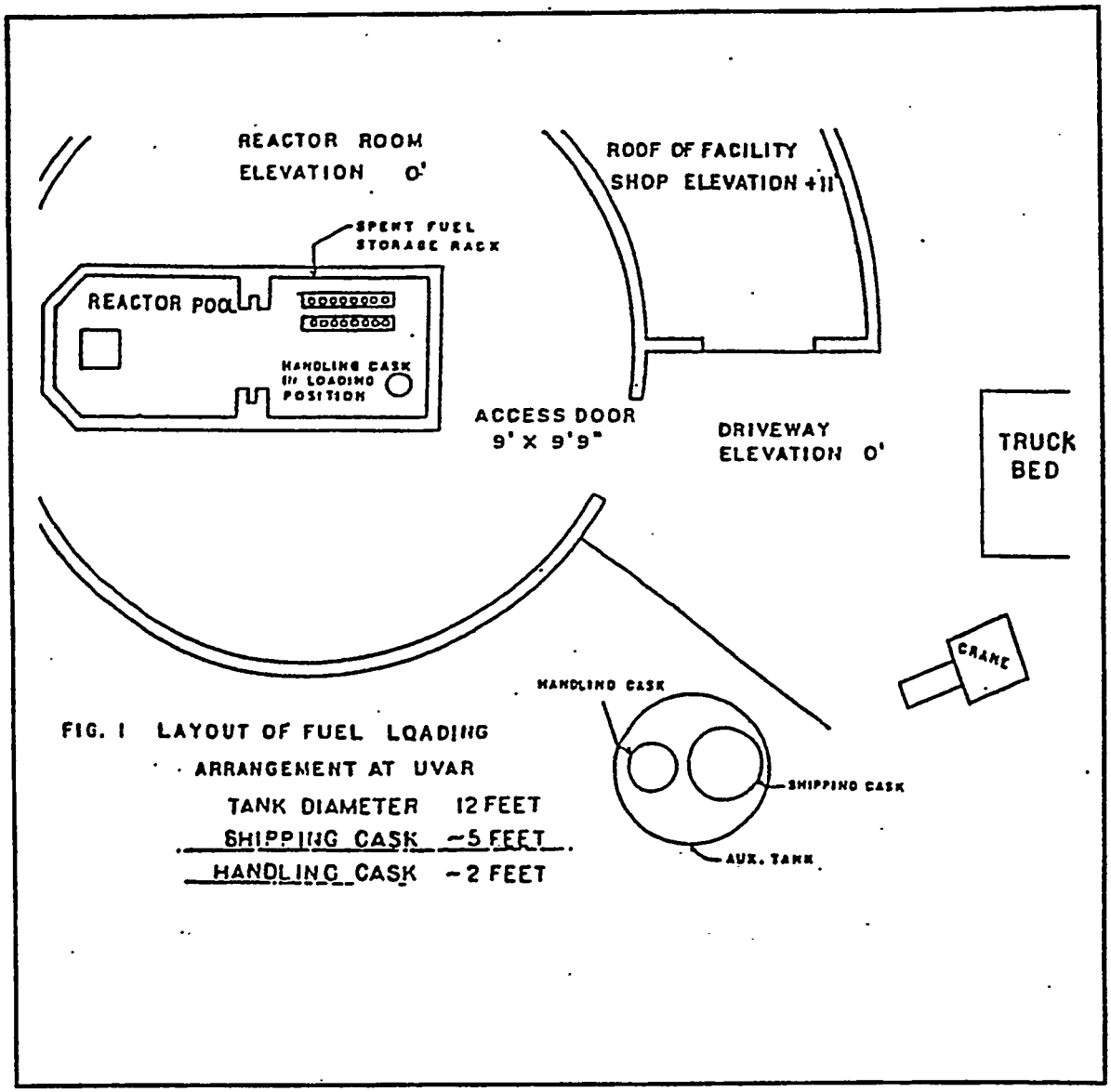


Figure 1. UVAR fuel shipment equipment arrangement

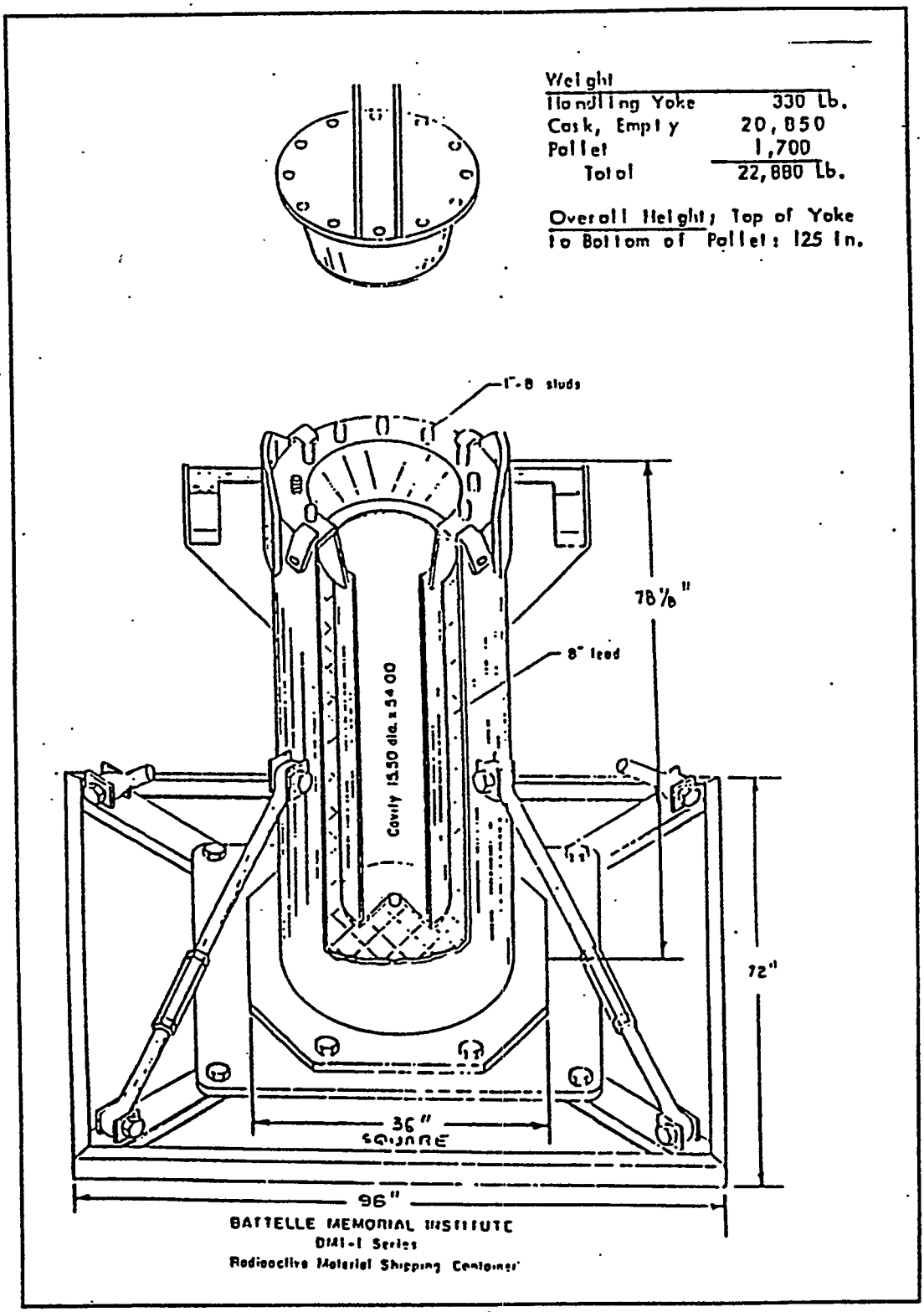


Figure 2 BMI-1 Shipping Cask perspective

A. Certificate of Compliance (COC) (No. 5957, Rev. 21)

The COC for the BMI-1 Cask (Appendix E) was reviewed by the Reactor Administrator and Assistant to the Director prior to the shipping date to determine requirements that needed to be met. Satisfaction of COC requirements relevant to shipment of spent HEU fuel are addressed individually below. All references to the COC or parts thereof in these procedures will be to COC No. 5957, Rev. 21, unless otherwise noted.

The package contents to be shipped are described by COC 5(b)(1)(i). All spent fuel assemblies to be shipped are intact MTR-type fuel assemblies, each containing less than 200 grams of U-235 at a nominal 93% (93.5% allowed) enrichment prior to irradiation; most assemblies, after significant burn-up (see Appendix A), contain much less than 200 grams of U-235. In all cases, the active fuel length is less than 25 inches; shorter active fuel lengths are preferable over longer ones because inter-assembly shielding of neutrons by boron-containing neutron-absorbing plates in the Texas A&M basket container will be more effective.

COC 5(b)(2) requires a minimum 90-day cooling time of each fuel assembly, maximum decay heat generation per package not to exceed 1.5 kW, and the external dose rate not to exceed 10 mrem/hr 3 feet from the external surface of the cask. Reactor Facility fuel records shall be reviewed prior to shipment to assure that the 90-day cooling period requirement is satisfied for each assembly shipped. The heat generation rate shall be demonstrated to be in compliance by calculation and comparison to the allowed value. External dose-rate measurements will be made with a calibrated survey instrument at the time of shipment to assure that the external dose-rate limit is not exceeded.

The maximum allowable quantity per package of the material type described above is set by COC 5(b)(2)(i) as twelve (12) assemblies, when the product container specified in COC 5(a)(4)(v) is used. This product container is commonly called the "Texas A&M basket," and it is physically impossible to load more than twelve intact fuel assemblies into it.

COC 7 requires that package contents of type 5(b)(1)(i) be

shipped dry. This condition will be satisfied by performance of a pre-use (post-loading) pressure and liquid test, using a test manifold equivalent to one described in 7.4 Appendix to the BMI-1 SARP (Rev A 3-28-80) and a procedure (see Section III.E of these procedures) derived from the procedures included in the SARP. This will ensure that, after loading and closure, the cask is not pressurized and does not contain a significant quantity of sensible water.

As required by COC 11, the presence and effectiveness of neutron absorber plates in the Texas A&M Basket must be verified with neutron measurements prior to first use and records maintained of such verification. Verification must be remade before each subsequent use. This requirement will be satisfied by performance of a procedure entitled "Verification of Neutron Absorber Plates in the Texas A&M Basket." The procedure includes a data log and checklist, which, upon completion, will satisfy the record-keeping requirement and permit quantification of the effectiveness of the center-cross basket plates as neutron absorbers (see Appendix D).

COC 14 requires that contents must be securely confined in the cask to preclude secondary impacts during accident conditions of transport. The contents will be closely and securely confined in the cask in all horizontal directions by the plates comprising the basket, which, itself, fits closely into the cask cavity. Because of the length of the assemblies to be shipped (between 34 and 38 inches), relative to the effective basket height (38 inches), there will be very little vertical movement of assemblies possible in the event of an accident involving the cask. Therefore, it is believed that this requirement is met without necessity for special actions.

COC 15 requires that, prior to each use, adequacy of the containment vessel (cask) must be demonstrated by performance of the leak test described in Section 7.1.1.1 of the application for the COC by Battelle Columbus Laboratories. The same procedure followed to satisfy COC 7 will assure that the cask is free of leaks within a reasonable observable limit before shipment.

B. Personnel Assignments:

Personnel assignments for the shipment operation may be found in Appendix B to these procedures. The Reactor Staff and Health Physics personnel are assigned to this operation. Reactor Staff may perform duties normally attended to by Health Physics personnel, given appropriate knowledge, training, and experience. All personnel not directly involved in the operation and the general public will be excluded from those areas of the facility where fuel handling and heavy equipment operating activities are underway. To the extent that truck driver(s) and auxiliary crane operator(s) will be on-site and issued self-reading dosimetry devices, they are included in the operation personnel. They do not need to be intimately familiar with all of these procedures, however, as their actions will be directed and monitored by Reactor Staff.

C. Radiation and Contamination Monitoring

The personnel involved in this operation shall be issued self-reading dosimeters in addition to film badges. The constant air monitor shall be in operation in the reactor room during all operations. Portable survey instruments shall be located in the reactor room and the transfer area. Health Physics personnel will be on-site during fuel transfer operations to provide continual assessment of radiation hazards, in addition to assisting in completing the attached DOT / 49 (Appendix F) and Personnel Exposure Record. The Health Physicist shall keep a record of individual exposure. Protective clothing will be worn by personnel as appropriate.

D. Notification

The UVA Police Chief will be notified that a shipment is to take place several days prior to the loading of the cask and after the shipment leaves UVA, although police presence at the UVAR Facility is not required. Other notification requirements are enumerated in a checklist in these procedures and will be made in timely fashion by the Reactor Administrator or Director.

UVA Administrators will be notified of an imminent fuel

shipment, however, the exact date will not be divulged. The administration will be notified upon successful completion of a fuel shipment. At the administration's discretion, public disclosure, in the form of a press release, may be made 10 days following the completion of a shipment or series of shipments.

E. Auxiliary Water Tank and Bridge Preparation

The auxiliary tank will be cleaned, checked and filled with tap water to a level approximately 1.5 feet below its top several days before the planned shipment. The tank is 12 feet in diameter, 12 feet tall, and the steel wall and bottom thicknesses are 1/4 inch.

$Volume_{(water)}$ = 8883 gallons $weight_{(water)}$ = 73995 lbs.

The maximum mass, cask, contents, and water, that will be in the auxiliary water tank at any time during fuel transfer operations is approximately 100,000 pounds.

The auxiliary wooden bridge with railings used during previous spent fuel shipments will be raised into place atop the auxiliary water tank.

F. Fork Lift Truck

The Reactor Facility fork lift truck will be operationally checked-out and fueled before needed for fuel shipments. It will be used to move a single fuel assembly transfer cask between the UVAR pool and auxiliary water tank.

G. 5-Ton UVAR Room Polar Crane

The 5-ton polar crane located in the UVAR Room will be used to manipulate the single assembly transfer cask in the Reactor Room. This will facilitate transfer of single assemblies from storage locations in the pool.

H. Auxiliary Crane and BMI-1 Shipping Cask

An auxiliary crane will be hired locally to manipulate the BMI-1 cask, the single assembly transfer cask, and related components outside of the reactor building. Verification will be obtained that the auxiliary crane is certified to handle more than maximum weight required, which is calculated below, in Table I, as the sum of the weights of the greatest number of components to be handled concurrently.

Table I. Individual and Combined Weights to be Lifted by Auxiliary Crane.

Component	Weight (lb)
Empty BMI-1 cask body (without lid)	*19,750
BMI-1 cask lid	*1,100
BMI-1 cask skid	*1,700
BMI-1 handling yoke (from Figure 2)	330
Product Container specified in COC 5(a)(4)(v) (est)	210
12 of the heaviest fuel element assembly type (conservative assumption of 12 lb/assembly)	144
Cask volume of water (about 7 cubic feet)	450
Total of Component Weights	23,684
Certified Rated Load of Crane to be supplied and operated by a local contractor	50,000

(* measured data from BMI-1 SARP REV. A., 3-28-80)

I. UVAR Single Fuel Assembly Transfer Cask

The UVAR Facility possesses a lead and steel cask fabricated especially for transport of individual fuel assemblies from the reactor pool to the auxiliary water tank. As shown in Figure 3, this cask is cylindrical in shape, with a central square hole to accommodate a fuel assembly. The original lid for this cask has been replaced with a lead cylinder, approximately 4 inches tall and 8 inches in diameter. The cask weight is approximately 2.5 tons, which is 1/2 the rated capacity of the overhead polar crane in the UVAR room.

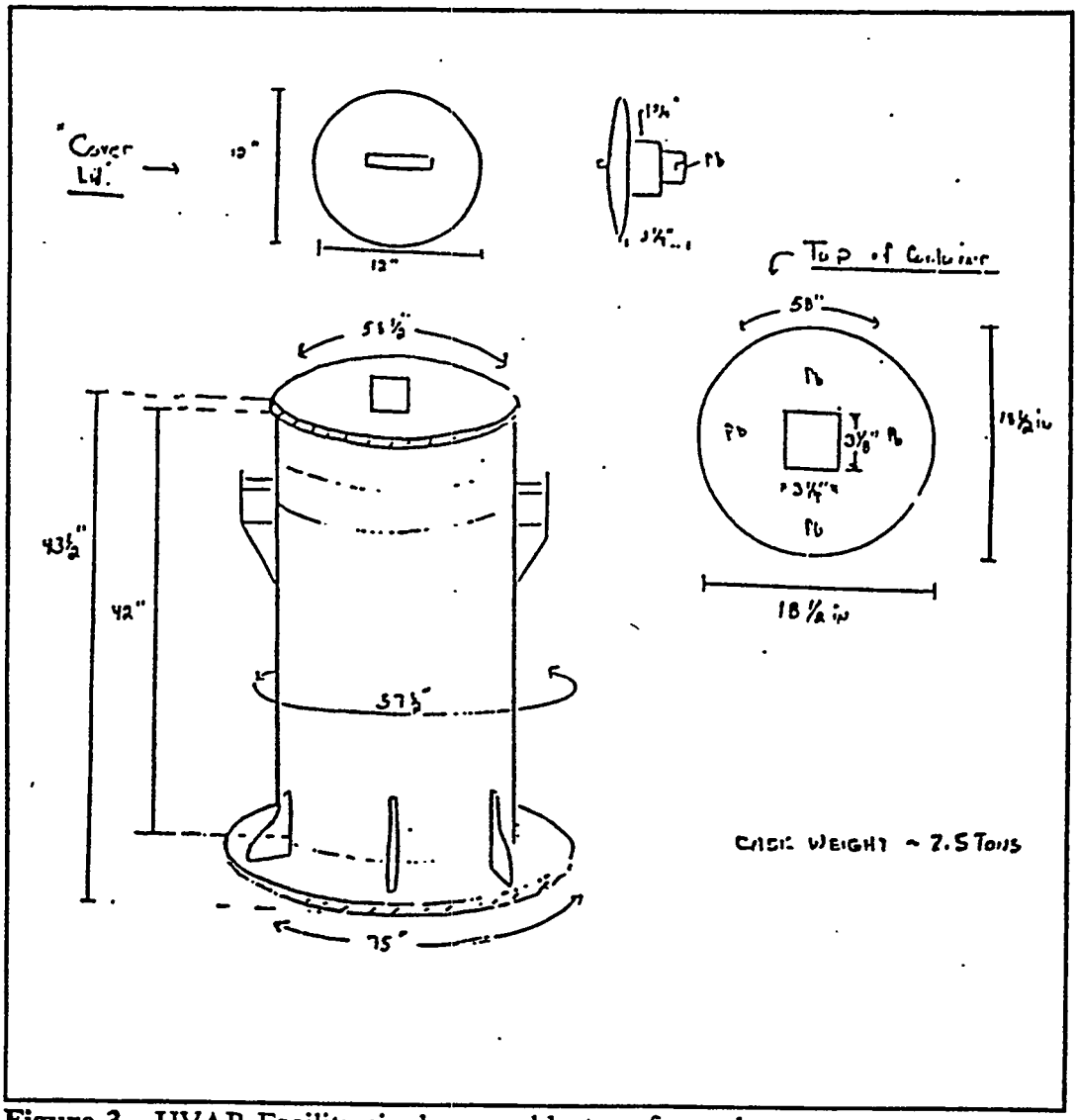


Figure 3. UVAR Facility single assembly transfer cask

J. Criticality Control

Criticality controls are not required by the BMI-1 Cask Certificate of Compliance for the type and quantity of material to be shipped, nor by Federal regulations or the Facility's SOP's. Only 12 assemblies, with an as-manufactured total U-235 mass of less than 2.4 Kg will be loaded, a number of assemblies insufficient for criticality to occur, assuming a water-flooded cask and taking no credit for boron in the basket dividers. Therefore, no subcritical multiplication measurements or calculations will be required with these fuel shipments. The cask is certified for 4.8 kg (24 assemblies contained in two baskets) of U-235 in irradiated MTR fuel form loaded in boron-containing baskets.

K. Emergency Planning

The UVAR Facility Emergency Plan does not specifically address incidents involving reactor fuel outside of the pool. However, should an accident involving spent fuel occur during shipment activities, the Reactor Staff and Health Physics personnel will be capable of responding quickly and appropriately according to the Emergency Plan Implementing Procedures, which have general applicability.

L. Documentation

All documentation related to the shipment of spent fuel will be maintained at least ten years after cancellation of the University of Virginia Nuclear Liability Insurance Policy or the life of the BMI-1 cask, whichever is longer, in the files of the Reactor Facility and the EH&S Office. They will be available during that time for NRC audits [10 CFR 71]. These procedures have been developed by the Reactor Facility Staff in cooperation with UVA Health Physics personnel. The Reactor Facility supervisors have applied the Facility's QA/QC program in the review of these procedures. [10 CFR 71.12 (b), 10 CFR 71.103 through 137] [10 CFR 71.87 and 10 CFR 71.91 (c)] [10 CFR 71.135] [10 CFR, subpart H] [NRC Reg. Guide 7.10]. Personnel training for implementation of these procedures will be conducted and documented as required by the QA/QC program and applicable regulations.

II. OPERATIONAL CHECKLISTS

A. Pre-Shipment Documentation and Notification Checklist

All portions of this checklist shall be completed by the Reactor Administrator prior to the shipment described here: **(date and time to be completed only after shipment departure, as this information is safeguarded)**

Shipment Date _____ Time Leaving UVA _____

This checklist, or a similar and RSC-approved checklist must completed for each shipment of spent fuel from the University of Virginia. Important addresses, phone and FAX numbers of personnel to be notified are located in Appendix H to these procedures.

Prior to each use of the cask, the following shall be done or verified:

_____ 1. Current BMI-1 Cask Certificate of Compliance obtained [BMI-1 COC No. USA/5957/Rev. 19].

_____ 2. NRC approval for use of cask obtained [10 CFR 71.12(c)(3)].

_____ 3. Savannah River approval for shipment obtained.

_____ 4. Notification of impending shipment mailed to NRC. 10 CFR 73.72 (a) requires that written notice be sent to the Division of Safeguards and Transportation, U.S. Nuclear Regulatory Commission, Washington, D.C. 20555. **This notice must be received at least ten days before transport of the shipment commences at the shipping facility.**

_____ 5. As required by 10 CFR 73.72 (a)(4), the Division of Safeguards and Transportation has been notified at least 10 days before the shipment commences at the

shipping facility by telephone [(301) 504-2458] that an advance notification of shipment has been sent, as above.

_____ 6. Notification of impending shipment mailed to VA, NC, and SC Governors' Designees.

_____ 7. UVA Police Chief notified of impending shipment.

_____ 8. NRC Form 741 complete for forwarding to Oak Ridge National Laboratory.

_____ 9. Record of annual cask inspection within the previous 12 months is on file.

_____ 10. Record of satisfactory biennial cask inspection and/or repairs within the previous 24 months is/are on file.

_____ 11. Record of satisfactory five-year lifting yoke inspection/test within the previous 60 months is on file.

_____ 12. Contents meet requirements concerning material type, form, total mass, fissile material content, and decay heat.

_____ 13. The planned weight of cask contents, including the basket, do not exceed 1800 pounds (see Table I).

_____ 14. The cask lid gasket has been replaced within 12 months of the shipping date.

_____ 15. Certification of chokers to lift single assembly transfer cask obtained (tag attached to chokers).

_____ 16. Certification of sufficient auxiliary crane rated load obtained.

_____ 17. NRC route approval for shipment obtained.

_____ 18. Savannah River acknowledgment of receipt of security seal type and number detail is received.

Seal Numbers _____ (lid), _____ (drain), _____ (upper port)

Additional detail: _____

_____

_____ 19. Commonwealth of Virginia approval for shipment obtained.

_____ 20. RSC approval of these shipping procedures obtained.

_____ 21. Certification of training of truck driver(s) for duty obtained.

_____ 22. Letter from employer or other verification of crane operator's industry-standard certification for duty obtained.

_____ 23. Written instructions delivered to truck driver(s).

B. Minimum Tools and Equipment Needed for Fuel Shipment

_____ 1. Step ladder for accessing top of cask when on ground

_____ 2. 5 gallon bucket and 1/2 gallon jug for BMI-1 cask water sample collection and disposal

_____ 3. Extension hose for UVAR room demineralizer system to reach auxiliary water tank

_____ 4. SNOOP for bubble test

_____ 5. Identification tags with strings

_____ 6. Hose clamp to close test manifold sample collection tube

_____ 7. Water trap and HEPA filter for venting cask

_____ 8. Torque Wrench calibrated at 50 foot-lb

_____ 9. Scaffolding by auxiliary water tank installed and leveled

_____ 10. UVAR Room demineralizer system is operational

_____ 11. Chains to secure single assembly cask to forklift

_____ 12. Wrench for loosening cask tie-down turnbuckles

_____ 13. Wrench for removing cask lifting eye covers

_____ 14. Wrench for removing cask lid bolts

_____ 15. Wrench for removing cask plugs

_____ 16. Teflon tape pipe sealant

_____ 17. Two 3-ton choker cables (to arrive with crane)

_____ 18. Cask air sample collection device

_____ 19. Pressure Leak Test manifold assembly finished and tested

_____ 20. Pressurized air line with 50 psi regulator

_____ 21. Water hose for decontamination operations

_____ 22. Gloves, coveralls, shoe covers, blotting paper

_____ 23. Portable survey instruments, swipe survey supplies

_____ 24. Grease pencil for marking lid orientation on cask and cask orientation on skid

_____ 25. Rope and stanchions for staging area isolation

_____ 26. Restricted area signs

_____ 27. Saw horses for blocking roads from lower Reactor Facility parking area

_____ 28. Lubricant for cask bolt threads

_____ 29. Spare placards for truck

_____ 30. Drain hose for purging cask

C. Preparation for Fuel Transfer Operations Checklist

All items on this checklist shall be addressed as far in advance of the fuel shipment as practical. However, this checklist should be performed just prior to fuel transfer activities. The purpose is to ensure that preparations for fuel transfer operations have been successfully completed, to ensure personnel safety and readiness, and to encourage a comprehensive overview of the staging area and planned activities prior to initiation of fuel-transfer activities.

_____ 1. All personnel have had BMI-1 Operational Training. They have read and understood these procedures and understand their general assignments.

_____ 2. Auxiliary water tank is cleaned and filled with tap water to within approximately 1.5 feet from its top.

_____ 3. Personnel bridge placed and secured over auxiliary tank in a position that allows for insertion and removal of the BMI-1 cask.

_____ 4. Fork lift truck is gassed-up and determined to be operational.

_____ 5. The presence and effectiveness of neutron absorbing plates in the Texas A&M basket has been verified according to these procedures.

_____ 6. Copy of Auxiliary Crane certification for handling of weights greater than the total mass of components to be lifted has been reviewed and filed.

_____ 7. All personnel actively participating in fuel transfer operations have been issued self-reading and film badge dosimetry and initial data have been entered in the Personnel Exposure Record.

_____ 8. UVAR Room Constant Air Monitor is in operation.

_____ 9. Portable survey meters are in operation and located for use in the reactor room and the outside operations area.

_____ 10. The UVAR is secured and tagged "Out of Operation" for the duration of fuel shipment activities.

D. Receiving and Preparation of Cask for Loading

This procedure is to be used for a BMI-1 shipping cask, when the cask arrives at the Reactor Facility. The Reactor Director has the authority, given by the Reactor Safety Committee, to alter any of the these shipping procedures as deemed necessary, provided their intent is not altered. Such changes to the procedures shall be reported to the Reactor Safety Committee after the shipments. A copy of these procedures is included in the training documents distributed to all personnel prior to the fuel shipments; exceptions to this are the auxiliary crane operator and truck driver, who will be directed as needed by trained personnel.

E. Placement of Truck with Cask

_____ 1. Direct delivery carrier to position truck with cask along the upper-level facility parking area, near the auxiliary water tank.

_____ 2. Walk around truck to check for visible damage incurred during transit and unusual objects on the cask and/or vehicle.

_____ 3. Direct auxiliary crane operator to position the crane conveniently between the truck bed and the auxiliary tank.

_____ 4. Cordon-off the roadways leading to and from the upper-level parking area to create a temporary restricted area until shipment is completed.

F. Initial Equipment Inventory and Radiation and Contamination Surveys

1. Check that the following items are on truck.

_____ a. BMI-1 cask body

_____ b. BMI-1 cask lid

_____ c. BMI-1 cask tool box

_____ d. BMI-1 cask lifting yoke (may be in tool box)

_____ e. BMI-1 Shipping Basket **(BMI #'s BCL-000-500, Rev. A as modified by BCL-000-236, Rev. c and BCL-000-502, Rev. B (modification for individual support of 12 MTR fuel elements -- for Texas A&M)** This basket will only be on the truck if it has not already been delivered early, as expected.

_____ 2. Make notes here on observations of any equipment missing or out of order, e.g., cask lid bolts damaged or missing, bent, loose, or missing turnbuckle assemblies. Items checked should include but not be limited to the cask drain, vent, and protective shrouds. Report any problems to the Director. Necessary maintenance must be performed and adequately documented.

_____

_____

_____

_____

IMPORTANT NOTE: It is required by 10 CFR 71.95 that the licensee report any instance in which there is significant reduction in the effectiveness of authorized packaging during use, details of defects with safety significance, and means used to repair such defects to prevent their recurrence. No attempt shall be made to effect repairs without written approval and procedures from DOE.

3. Health Physics personnel shall perform a survey of radiation dose-rates upon receipt of the truck, cask, and associated equipment. The Director's approval of survey results shall be obtained before continuing with these procedures. Record below maximum observed radiation dose-rates at the locations specified.

	on Contact (mrem/h)	at Distance (mrem/h)	Distance (feet)
a) Cask, side	_____	_____	_____
b) Cask, top	_____	_____	_____
c) Truck, under cask	_____	_____	_____
d) Skid	_____	_____	_____
e) Handling Yoke	_____	_____	_____
f) Tool box exterior	_____	_____	_____
e) Truck bed	_____	_____	_____
f) Basket, if not in cask (data from prior receipt of basket acceptable)	_____	_____	_____

Data Collected by: _____

Meter Model: _____ Serial Number: _____

Calibration Due Date: _____

Director's Approval: _____ (Director)

Date: _____

4. Health Physics personnel shall perform radioactive contamination swipe surveys on 300 cm^2 areas of the cask exterior, skid, handling yoke, cask tool box exterior, truck bed, and basket, if the basket is not in the cask upon arrival.

If contamination greater than acceptable is determined to exist, the Director shall be notified before proceeding with decontamination and the remainder of this procedure. The Director's approval shall be obtained before continuing with these procedures. Record the following maximum levels of equipment contamination observed:

	Beta-Gamma (dpm per 1 cm^2 based on swiping a 300 cm^2 area)	Alpha
a) Cask outside	_____	_____
b) Skid	_____	_____
c) Handling Yoke	_____	_____
d) Tool box exterior	_____	_____
e) Truck bed	_____	_____
f) Truck bed (under cask)	_____	_____
g) Basket if not in cask (data from prior receipt of basket acceptable)	_____	_____

Data Collected by: _____ Analyzed by: _____

Instrument Model: _____ Serial Number: _____

Calibration Due Date: _____

Director's Approval: _____ Date: _____

_____ 5. Immediate notification of the delivery carrier and the NRC Regional (II) Office shall be made if removable contamination exceeds 0.01 microcurie (22,000 dpm) per 100 cm^2 [10 CFR 20.205(b)(2)] and/or if radiation dose rates of greater than 200 mrem/h at the package surface, or 10 mrem/h at 3 feet are observed [10 CFR 20.205(c)(2)]. The NRC is to be notified by telephone and by FAX [phone: (404) 331-4503]. The delivery carrier, if notified verbally, will initial below, to confirm receipt of information regarding contamination above the limit stated here.

Reactor Staff: _____

Delivery Carrier: _____

_____ 6. If it is determined that clean-up of any of the items surveyed above is necessary, an area for contaminated tools and dry solid waste shall be established before proceeding with decontamination by standard health physics methods and the remainder of these procedures.

Note: The Director may give preliminary authorization for continuance of these procedures in the following step if, at a minimum, the above survey results are acceptable. The swipe survey of the truck bed, under cask, must be performed after unloading of the cask, in Section III, at which time, these data may be entered above and the Director may give firm authorization to continue.

7. The Director authorizes implementation of the remainder of these procedures, with or without discretionary changes to the procedure sections clearly noted below, by placing his initials on the line provided here. Procedural modifications shall be included either in the text (substitution of pages) of this procedure or as attachments to this procedure. Notes:

_____

_____

_____

_____

_____

No. of pages _____ attached

(enter number or indicate N/A above).

Copies of modified procedure pages and/or copies of attachments defining procedural changes distributed to all involved personnel (see Appendix G, Distribution List)

Sign-off when done or indicate N/A _____.

Director's Signature: _____ for Preliminary Authorization to continue

Director's Signature: _____ for Firm Authorization to continue, given results of contamination survey of truck bed under incoming cask location.

III. BMI-1 CASK OPERATING PROCEDURES

Introduction.

These BMI-1 operating procedures have been based on previous UVAR Facility spent fuel shipping procedures. They represent an adaptation of the procedures applicable to "handling the BMI-1 Cask during loading of the package at Battelle-Columbus Hot Laboratory at West Jefferson, Ohio," as recommended in Revision A (3-28-80) of the BMI-1 Cask SARP. A Controlled Copy of the SARP was obtained from the Los Alamos National Laboratory in December of 1992.

These operating procedures cover BMI-1 Cask operations of receipt and initial inspection, internal pressure and liquid testing, opening, loading, closing, leak testing, and final preparation for shipment.

In addition to these procedures, Health Physics personnel have developed a DOT/49 Checklist to assure that final preparations for shipping are in accordance with all applicable regulations.

A. Internal Cask Pressure and Liquid Test

Scope:

This procedure applies to testing the BMI-1 cask before opening for internal pressure and undocumented liquid content.

Purpose:

The purpose of this procedure is to ensure that cask pressure restraint devices are not defeated if pressure above atmospheric pressure exists in the cask. It is also intended to eliminate contamination of the cask exterior, other equipment, and the environment because of an unplanned release of undocumented liquid that may be in the cask upon arrival or after loading.

Application:

This procedure is to be followed upon receipt of the BMI-1 cask

before the lid is removed and any of the cask valves are opened and before any of the cask plugs are removed.

General Considerations:

In the event that any liquid enters the manifold and passes through the filter, in-line filter element shall be replaced after the pressure and liquid check to ensure the integrity of the manifold filter during subsequent tests.

If any liquid is found in the cask cavity, it shall be collected and disposed of in a manner judged appropriate by Health Physics personnel.

Procedure:

_____ 1. Re-verify that auxiliary crane is certified to handle all weight associated with the cask and contents (23,684 lb, with lid, basket, fuel, water, and lifting yoke) [49 CFR 173.411(d)].

Auxiliary Crane certified for _____ lb.

_____ 2. Verify that the Director has given firm authorization to continue with these procedures, in light of all contamination survey results.

_____ 3. Remove, label, and store the cask drain valve and gauge housings.

_____ 4. Observe the cask pressure gauge indication and record it.

_____psig

_____ 5. After assuring that all cask valves and both manifold valves are fully closed, remove the cask drain valve plug. Store it appropriately.

_____ 6. Attach the test manifold, assembled according to Appendix C, with all cask and manifold valves closed, to the cask drain valve.

_____ 7. Attach one end of a flexible tubing to the open end of the manifold and hold or secure the opposite end of the tubing to a suitable collection container for radioactive liquid. Also attach second flexible tubing to the sight glass bottom and secure the loose end as the first.

_____ 8. Slowly open the cask drain valve and observe the sight glass for the presence of any liquid. Excessive liquid may be released from the sight glass and collected.

_____ 9. When the cask drain valve is fully open, slowly open Valve 1 and note the maximum pressure observed at the manifold pressure gauge:

_____psig

_____ 10. Slowly open Valve 2, while monitoring collection of any liquid that passes through the manifold assembly and being careful not to cause it to be splashed. Collected liquid may be tapped off from thesight glass.

_____ 11. Continue venting and draining the cask until it is clear that the cask is not pressurized and that all liquid that may have been contained has been removed. Record the final pressure indicated by the cask pressure gauge.

_____ psig

_____ 12. Close the cask drain valve.

_____ 13. Clamp or tape shut the collection container end of the flexible tubing attached to the manifold end. Also clamp shut or tape the end of the sight glass vent tubing.

_____ 14. Close Valve 1 and Close Valve 2.

_____ 15. Remove the manifold from the cask drain valve, being careful to blot up any liquid that may have been trapped in the sight glass or between the sight glass and the cask valve.

_____ 16. Label the manifold appropriately (as possibly internally contaminated). It is to be reused for other shipment operations, so all liquid should be drained from it and disposed of in accordance with normal OEHS procedures. The absolute filter element should be replaced. Then, after reassembly of the filter stage, it should be pressure tested as described in Appendix C and stored appropriately until needed for the next planned shipment. This step may be performed concurrently with steps below.

Note: The cask drain plug is in storage after this section.

B. Opening the Cask

General:

Health Physics personnel should carefully monitor all activities described below to identify radiological hazards that may exist, particularly when removing the cask lid, sampling cask water, and surveying interior surfaces.

Procedure:

_____ 1. The Director shall verify that the cask is not pressurized before opening and that liquid that may have been contained in it upon receipt has been removed and is being properly disposed of.

_____ 2. Remove stainless steel fill valve plug from cask and store with drain valve plug (attach identification tag) for use during reassembly. Open fill valve.

_____ 3. Inspect the drain and fill valves for damage. Check the valves to insure normal operation. Leave the fill valve fully open and the drain value fully closed.

_____ 4. Mark Position of cask lid with grease pencil or other means if no marks exist. Note below the method of lid position identification used.

Note: Figure 2, page 3, may be used as a diagram basis for this step, if desired.

_____

_____

_____ 5. Describe below an appropriate lid hole numbering and parts storage scheme implemented to ensure that cask bolts and washers may be returned to their original lid locations upon cask closure. This step should involve preparation of numbered envelopes, bins, or other appropriate storage containers.

Note: Figure 2, page 3, may be used as a diagram basis for this step, if desired.

_____

_____

_____

_____

_____ 6. Remove cask lid bolts and washers. Inspect them for worn threads or other damage. Store bolts and flat washers as indicated above to prevent loss, damage, or contamination. The bolts are required for reassembly. The Director shall be notified if any damage is noted.

_____ 7. Using the auxiliary crane, remove the cask lid with auxiliary crane hook in cask lid loop.

CAUTION: USE A CALIBRATED PORTABLE SURVEY INSTRUMENT TO MONITOR CASK LID REMOVAL. A REACTOR SUPERVISOR MUST BE PRESENT DURING LID REMOVAL. [10 CFR 20.205]

_____ 8. Conduct a survey of direct radiation from cask interior.

Max. dose rate at surface _____ mrem/hr

Max. dose rate at 3 ft. _____ mrem/hr

Meter Model: _____ Serial #: _____

Calibration Due Date _____

By: _____

_____ 9. Inspect the lid gasket (O-ring) and gasket sealing surface under lid for breaks, deformities, rust, dirt, or other damage. Clean components as necessary, under Health Physics supervision, and report any damage to the Director. Ensure that the O-ring is properly seated in the lid groove but DO NOT REMOVE THE O-RING FROM ITS GROOVE UNLESS IT MUST BE REPLACED.

_____ 10. If the O-ring is found to be inadequate, it shall be replaced with an equivalent O-ring meeting applicable QA/QC standards. Indicate N/A or identify replacement O-ring below.

_____

_____ 11. Inspect the cask cavity for the presence of foreign material. If any foreign material is found, notify the Director, who will authorize appropriate corrective procedures.

_____ 12. Hose down cask cavity with approximately 5 gallons of water, collecting a sample for radioactive material analysis through the cask drain valve. Report results to Director and Health Physics personnel. Keep results of analysis for the record. Ensure that all water is disposed of properly. Leave drain valve fully open after this operation.

C. Loading the Cask

_____ 1. Verify that cask drain and fill valves are fully open.

_____ 2. Check dimensions of cask and loading area, location of basket and personnel bridge, crane travel, etc., to ensure that loading operations can be performed as planned.

_____ 2.a Remove and temporarily store cask lifting eye covers.

_____ 2.b Disconnect and remove each of four sets of tie-down cables from the shipping cask.

_____ 3. Loosen and disconnect each of the 4 turnbuckle tie-down devices at cask ends.

_____ 4. Remove the 8 one-inch bolts securing the cask to the skid.

_____ 5. Attach cask lifting yoke to auxiliary crane and move cask into position over the water-filled auxiliary water tank.

_____ 5.a Perform a swipe survey for radioactive material contamination on the truck bed where the cask was located, and enter these data above in Section II.F.4.

_____ 6. Hose down cask with water. This is to avoid or reduce surface contamination of cask by tank water.

_____ 7. Lower cask into position at bottom of the auxiliary water tank, next to basket, hosing down lifting yoke with water as convenient.

_____ 8. Remove lifting yoke from cask, decontaminate using water hose-down while it is positioned above the auxiliary tank, and then store on truck bed on blotting paper.

_____ 9. Use the auxiliary crane and basket handling tool to position the Texas A&M basket at the bottom of the cask cavity and indicate basket orientation with respect to fill valve location on the BMI-1 Loading Diagram below (Figure 4, page 38).

_____ 10. In Steps III.C.12 though III.C.24 below, enter required information in the numbered space(s), beginning with Number 1 and proceeding in order corresponding to shipping cask basket position being loaded. One of the lower activity assemblies should be loaded first to gain "experience."

These steps should not be signed-off until all required information has been entered.

Important Note: Upon each repetition of the above-noted steps, verify that the same radiation monitoring instrument is used, or make clear notes to identify substitution(s).

_____ 11. Before lowering the single assembly transfer cask into the UVAR pool for the first time, suspend the cask over pool with overhead crane and hose off the cask with demineralized water. This is done to reduce or eliminate contamination by pool, and later, auxiliary tank water.

12.a. Remove lid from single assembly transfer cask and lower cask into UVAR pool with UVAR crane, and, using a fuel handling tool, insert first fuel assembly to be shipped.

Note: This operation must be supervised by a licensed Senior Reactor Operator.

12.b. Verify the number of the assembly using binoculars and portable light.

12.c Record operation in the UVAR Log Book and the assembly number below.

1._____ 2._____ 3._____ 4._____ 5._____ 6._____

7._____ 8._____ 9._____ 10._____ 11._____ 12._____

_____ 13. Withdraw the single assembly transfer cask with fuel assembly to near the top of the pool. Monitor dose rate at surface with a portable monitor and enter maximum dose rate observed with the cask top about at 1. ft. below surface.

1._____ 2._____ 3._____ 4._____ 5._____ 6._____

7._____ 8._____ 9._____ 10._____ 11._____ 12._____

Meter Model: _____ Serial #: _____

Calibration Due Date: _____

By: _____

_____ 14. Replace and secure lid on cask as it is withdrawn from the pool, completely out of water. Add additional lead brick shielding on top of the cask if necessary. Enter initials below.

1._____ 2._____ 3._____ 4._____ 5._____ 6._____

7._____ 8._____ 9._____ 10._____ 11._____ 12._____

_____ 15. Measure dose rates on outside and top of single assembly transfer cask. If dose rates exceed 75 mrem/hr at 1 foot, consult Health Physics personnel before proceeding. Enter below maximum dose rate at 1 ft.

1._____ 2._____ 3._____ 4._____ 5._____ 6._____

7._____ 8._____ 9._____ 10._____ 11._____ 12._____

Meter Model: _____ Serial #: _____

Calibration Due Date: _____

By: _____

_____ 16. Hose down single assembly transfer cask with demineralized water to remove possible surface contamination, move cask to side of reactor pool, quickly remove excess water, and lower onto the fork lift truck. Enter initials below when actions completed.

1._____ 2._____ 3._____ 4._____ 5._____ 6._____

7._____ 8._____ 9._____ 10._____ 11._____ 12._____

_____ 17. Chain the single assembly transfer cask to the forklift and move it next to auxiliary water tank located outside of the UVAR building. Enter initials below.

1._____ 2._____ 3._____ 4._____ 5._____ 6._____

7._____ 8._____ 9._____ 10._____ 11._____ 12._____

_____ 18. Unchain single assembly transfer cask, and, using auxiliary crane, raise it from the fork lift truck, then lower it into the auxiliary tank to a position about one foot under surface of water. Enter initials below.

1._____ 2._____ 3._____ 4._____ 5._____ 6._____

7._____ 8._____ 9._____ 10._____ 11._____ 12._____

_____ 19. Remove all the personnel from the immediate tank area except for the personnel situated at top of the tank to handle the fuel and others that may be needed to help. Enter initials below.

1._____ 2._____ 3._____ 4._____ 5._____ 6._____

7._____ 8._____ 9._____ 10._____ 11._____ 12._____

_____ 20. Remove the top from the single assembly transfer cask and lower the cask into the tank, beside the shipping cask. Enter initials below.

1._____ 2._____ 3._____ 4._____ 5._____ 6._____

7._____ 8._____ 9._____ 10._____ 11._____ 12._____

_____ 21. Transfer fuel assembly from single assembly transfer cask to shipping cask.

CAUTION: DO NOT FORCE ASSEMBLY INTO SHIPPING BASKET.

If assembly will not fit easily, leave that position empty. Health Physics personnel should monitor radiation levels at top of tank during transfer. Monitor outside of tank at ground level and at top after transfer is completed. If dose rate exceeds 75 mrem/hr at 1 foot from tank, consult with Health Physics personnel before proceeding. Enter below maximum dose rate.

At top of tank:

1._____ 2._____ 3._____ 4._____ 5._____ 6._____

7._____ 8._____ 9._____ 10._____ 11._____ 12._____

Meter Model: _____ Serial #: _____

Calibration Due Date: _____

By: _____

Outside tank at ground level and 1 foot from tank:

1._____ 2._____ 3._____ 4._____ 5._____ 6._____

7._____ 8._____ 9._____ 10._____ 11._____ 12._____

Meter Model: _____ Serial #: _____

Calibration Due Date: _____

By: _____

_____ 22. Enter the assembly identification characters and loading order number on BMI-1 Cask Loading Diagram below. **This actual loading diagram is required by the consignee.**

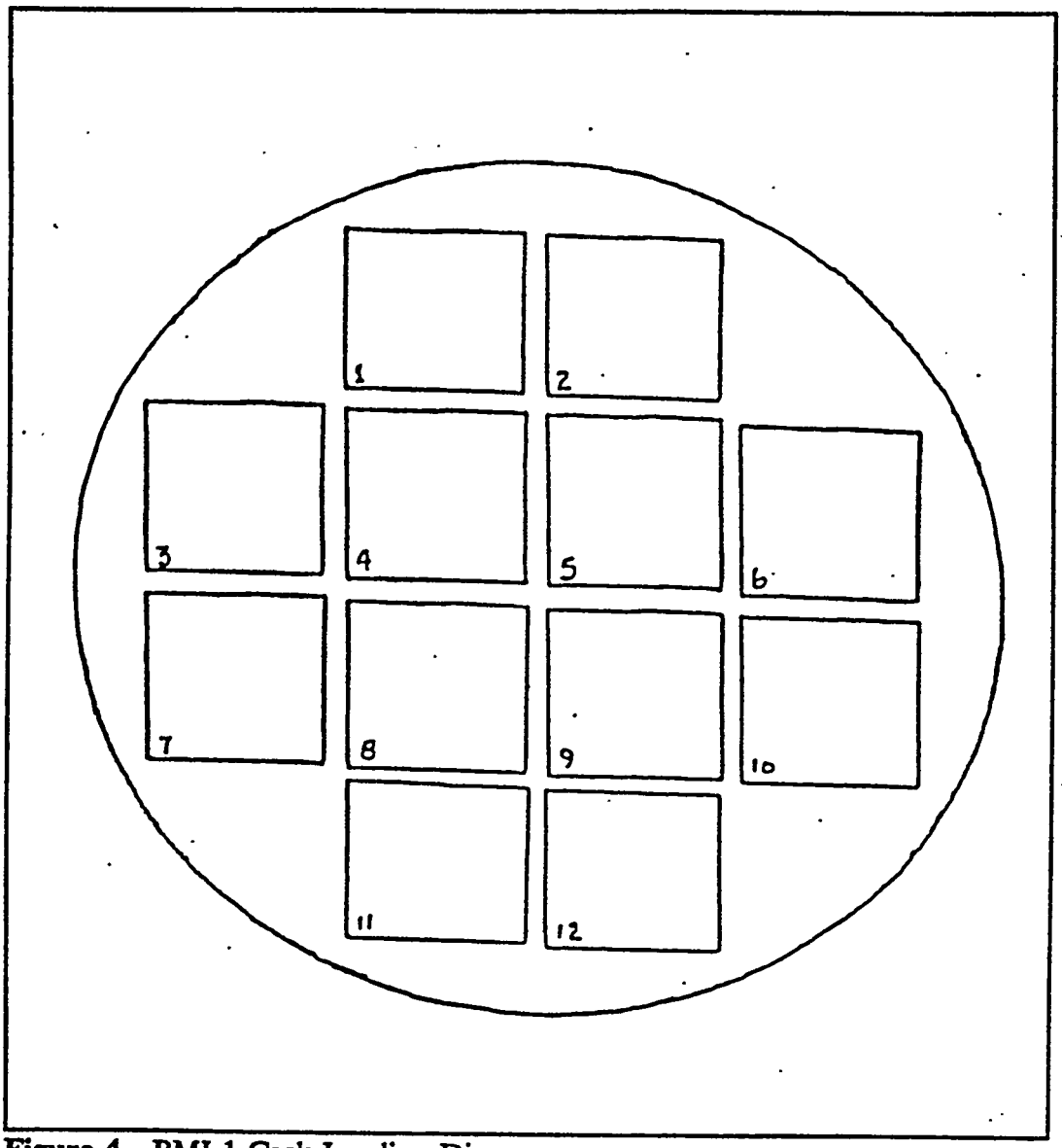


Figure 4. BMI-1 Cask Loading Diagram

_____ 23. Using auxiliary crane, withdraw the single assembly transfer cask to the top of tank. Hose down cask while above tank to remove possible contamination. Enter initials below.

1._____ 2._____ 3._____ 4._____ 5._____ 6._____

7._____ 8._____ 9._____ 10._____ 11._____ 12._____

_____ 24. Lower single assembly transfer cask onto fork lift truck, secure the cask with chains, and move to reactor room beside pool. Read personnel dosimeters and record on Table 2, the Personnel Exposure Record. Enter initials below.

1._____ 2._____ 3._____ 4._____ 5._____ 6._____

7._____ 8._____ 9._____ 10._____ 11._____ 12._____

Fuel Assembly Transfer From UVAR Pool To Shipping Cask

Date: _____

Assembly Number																
Reading		Initial													Final	Tota
Personnel	Dosimeter															
Robert U. Mulder																
J.P. Farrar																
Thomas E. Doyle																
Paul Benneche																
B. Hosticka																
Don Krause																
Lisa Scheid																
J.S. Baber																
Neil Wilson																
Rick Piccolo																
Jim Gilchrist																
Deborah P. Steva																
Scott Garver																

Note: Enter dosimeter readings initially, after transfer of each assembly, and after completion of all operations. Be sure to include additional personnel data, as for truck and crane drivers, in this record. Enter "NP" in the "Dosimeter" column to indicate listed personnel who are not present.

_____ 25. Repeat Steps III.C.12 though III.C.24 until the shipping cask is fully loaded. Reactor Administrator shall initial here when all assemblies have been successfully transferred as planned for the shipment.

Note:

Should a situation develop preventing the cask from being shipped in a timely fashion, the Director may order the fuel assemblies returned to reactor pool storage, one at a time, by reverse order of Steps III.C.12 though III.C.24. Appropriate notification is to be made to NRC, Savannah River, State Agencies and Tri-State Motors. Required notification is listed in 10 CFR, Part 71.97 and 10 CFR Part 73.37.F

D. Securing the Cask

_____ 1. Check that all fuel assemblies in the cask are located below the projecting lifting lugs of basket.

_____ 2. Using auxiliary crane, remove cask lid from truck bed and slowly lower lid onto top of cask. Align the lid on the cask using the two guidepins, cask lid pilot holes, and alignment notes made in Step III.B.4.

_____ 3. Using auxiliary crane and lifting yoke, lift the cask so that it's top is accessible, slightly above water level, for the following steps.

_____ 4. Monitor direct radiation levels. If dose rate exceeds 75 mrem/hr at 1 foot from the cask while it is completely or partially in air, consult with Health Physics personnel before proceeding. Enter below the maximum radiation level observed and the location.

Max: _____ mrem/h Location: _____

_____

_____ 5. Lubricate at least 2 cover bolts and install them, with washers, in their original locations. Tighten bolts loosely with the cask elevated slightly above water level.

_____ 6. Lubricate remaining cover bolts and install them with washers on the lid, tightening to 50 foot-pounds torque in a star pattern by approximately 10 ft-lb increments.

_____ 7. Use auxiliary crane and cask lifting yoke to slowly remove shipping cask from tank and hold its bottom approximately 6 inches above the water level. Monitor direct radiation level and record the highest measurement at 1 foot here.

Dose rate: _____ mrem/hr at 1 foot

Meter Model: _____ Serial #: _____

Calibration Due Date: _____

By: _____

_____ 8. Obtain a sample of cask water for radioactive material analysis as water exits cask drain valve. Close the drain valve when it appears that most water has drained from the cask.

Note: Results of this analysis must remain with the Reactor Administrator. One copy must be attached to shipping documents and another given to the Health Physicist for filing.

_____ 9. Hose down yoke and cask to remove possible surface contamination.

E. Pre-Shipment Cask Pressure Leak Test

The pre-shipment pressure leak test shall be performed immediately after the cask is loaded for a shipment. After the cask lid is secured in place, the cask will be purged of residual water and subjected to a 50 psig minimum pressure (not to exceed 55 psig) test.

The purpose of the pressure leak test is to establish that the seal of the cask has been accomplished and meets its specification. The maximum permissible leak rate for the BMI-1 cask is 9.24×10^{-3} atm-cc/sec. According to ANSI Standard N-14.5, the required sensitivity of a leak test to detect this degree of leak is 4.62×10^{-3} atm-cc/sec. The soap bubble type leak test procedure below has a sensitivity of 1×10^{-3} atm-cc/sec and, therefore, meets the requirements.

_____ 1. Connect a drain hose to the cask drain valve.

_____ 2. Connect a regulated air supply to the fill valve. Insure that both the fill and drain valves are open.

_____ 3. Lift the cask and move back to just above the auxiliary tank and position the drain hose so that its loose end is under water.

_____ 4. Remove residual water from the cask by opening the drain valve and applying a maximum of 15 psig air pressure. Monitor dose rate around cask as it is emptied of water. If dose rate exceeds 75 mrem/hr at 1 foot or 10 mrem/hr at 3 feet from cask, consult with Health Physics personnel before proceeding.

Max. Dose Rate (at 1 ft) _____ mrem/hr

Max. Dose Rate (at 3 ft) _____ mrem/hr

Meter Model: _____ Serial #: _____

Calibration Due Date: _____

By: _____

_____ 5. Once the cask is empty of water, shut off the air supply. Measure and record maximum dose rates on contact and at 1 and 3 ft. If any of these dose rates exceed the allowable limits of 200 mrem/h on contact, 75 mrem/h at 1 foot, and 10 mrem/h at 3 feet, stop. Consult the Director and Health Physicist to determine appropriate actions.

Max. Dose Rate (contact) _____ mrem/hr

Max. Dose Rate (at 1 ft) _____ mrem/hr

Max. Dose Rate (at 3 ft) _____ mrem/hr

Meter Model: _____ Serial #: _____

Calibration Due Date: _____

By: _____

_____ 6. Shut the drain valve and disconnect drain hose. Place drain hose on blotter paper.

_____ 7. Hose off lifting yoke and allow it to hang over the auxiliary water tank. Return cask to truck bed after drying.

_____ 8. Open the air supply regulator and slowly pressurize the cask to 50 $\pm$ 5 psig. DO NOT EXCEED 55 PSIG. Hold this pressure for at least 15 minutes.

Start time _____ End time _____ Observation time _____

_____ 9. Shut the fill valve and disconnect air supply. Check air hose connector for contamination. Clean if contaminated.

_____ 10. Apply a soapy (leak detection) solution to all pressure boundaries. Reapply as necessary to maintain a heavy film over these regions.

_____ 11. Observe cask seal regions for a minimum of 2 minutes, looking for bubbles that may indicate a leak. If leak-indicating bubbles are observed, corrective action must be taken. These may include re-torquing the lid bolts and/or replacing the cask O-ring. If no bubbles are observed, the cask has passed the leak test. Continue with these procedures only it the leak test has been passed. Notify the Director of test result. The director will authorize corrective actions, if required.

Start time _____ End time _____ Observation time _____

Test Result (Pass / Fail) _____

Director notified of test results _____

Director notified of test results _____

Corrective Actions Authorized (N/A or detail) _____

_____

Note: If corrective actions are required, the pressure test must be repeated. Appropriate documentation should be attached to these procedures.

Additional Documentation Attached (N/A or detail) _____

_____

_____ 12. The cask must now be vented. Attach hose to fill valve to vent air through water trap and HEPA filter. Open fill valve to vent cask. When cask is vented, close fill valve. Check filter for activity and dispose of as radioactive waste, if required. If activity is found in filter, consult with Health Physics personnel and Reactor Director.

F. Preparation of Cask for Shipping

_____ 1. Verify that cask is properly aligned on skid and that excess water has been removed.

_____ 2. Perform direct radiation and contamination surveys of yoke and cask external surfaces. If surface contamination exceeds 22 dpm per cm^2 (β,γ) or 2.2 dpm per cm^2 (α) based on swiping a 300 cm^2 area or if direct radiation exceeds 200 mrem/hr on contact or 10 mrem/hr at 3 ft. from surface, halt operations and notify Health Physics personnel. Check results of cask water sample. If radioactive material content is found, consult with Health Physics personnel and Reactor Director. [49 CFR 173.475(i), 49 CFR 173.441, 49 CFR 173.443 and 10 CFR 71.87 (i) and (j)]

Direct Radiation:

Max. Dose Rate (contact) _____ mrem/hr

Max. Dose Rate (at 1 ft) _____ mrem/hr

Max. Dose Rate (at 3 ft) _____ mrem/hr
[49 CFR 173.403(b)(2)]

Meter Model: _____ Serial #: _____

Calibration Due Date: _____

By: _____

Contamination:

Max. ($\beta;\gamma$) _____ dpm/cm^2 Max (α) _____ dpm/cm^2

Instrument Model: _____ Serial #: _____

Calibration Due Date: _____

By: _____

Fission Products in Cask Water: Yes / No _____

Activity _____ Ci/l

Instrument Model: _____ Serial #: _____

Calibration Due Date: _____

By: _____

_____ 3. Replace bolts at cask base and secure turnbuckle tie-down devices at cask and pallet ends. Apply lubricant to machine threads. Assure that the cask is firmly bolted to its pallet and that turnbuckle anchors are secure.

_____ 4. Check that the fill and drain valves are shut. Apply teflon tape pipe sealant to the two stainless steel plugs that were removed from the fill and drain valves when the cask arrived. Install and tighten them appropriately.

_____ 5. Place Radiation labels with appropriate information on cask, on each of two opposite sides. [49 CFR 172.403 through 406] [49 CFR 172, subpart E]

_____ 6. Attach three security seals to the cask in holes provided at the cask lid, drain line cover, and upper pressure port cover. Record seal numbers here.

Seal Numbers _____ (lid), _____ (drain), _____ (upper port)

_____ 7. Verify with the Reactor Administrator that the numbers on these seals correspond with information previously supplied to Savannah River and that the numbers are clearly written on shipping papers.

_____ 8. Reinstall cask valve cover housings and lifting eye covers.

_____ 9. Reinstall each of four tie-down cable systems for cask on truck bed so that the cask is secured in place for travel. Consult truck drivers (if present), any available written information on these restraints, and any other individuals who may have been involved in loosening them.

_____ 10. Attach "Radioactive" placards on square background on four sides of vehicle [49 CFR 172, subpart F].

_____ 11. Health Physics personnel should perform final survey of vehicle using the following criteria:

a) The maximum radiation level at any point on the vertical planes projected from the outer edges of the vehicle cannot exceed 200 mrem/hr. This includes area under truck bed.

Max. Dose Rate _____ mrem/hr

@ Location: _____

Meter Model: _____ Serial #: _____

Calibration Due Date: _____

By: _____

b) The maximum radiation level at any point 2 meters (6.6 feet) from the vertical planes projected from the outer edges of the vehicle cannot exceed 10 mrem/hr.

Max. Dose Rate _____ mrem/hr

@ Location: _____

Meter Model: _____ Serial #: _____

Calibration Due Date: _____

By: _____

c) The maximum smearable contamination on exterior of package and vehicle cannot exceed 22 dpm per cm^2 (β,γ) or 2.2 dpm per cm^2 (α). [49 CFR 173.475 (i) and 10 CFR 71.87 (i) and (j)]

Vehicle:

Max. (β,γ) _____ dpm/cm^2 Max (α) _____ dpm/cm^2

@ Location: _____

Instrument Model: _____ Serial Number: _____

Calibration Due Date _____

By: _____

Package:

Max. (β,γ) _____ dpm/cm^2 Max (α) _____ dpm/cm^2

@Location: _____

Instrument Model: _____ Serial Number: _____

Calibration Due Date _____

By: _____

Occupied Vehicle Positions:

d) The maximum radiation level in any occupied position of the vehicle cannot exceed 2 mrem/hr.

Max. Dose Rate _____ mrem/hr

@Location: _____

Meter Model: _____ Serial #: _____

Calibration Due Date: _____

By: _____

Note: If all of the above criteria are met, continue with these procedures. If any of the above criteria are not met, the Director should be notified, and appropriate corrective actions must be taken to decontaminate the cask or other equipment, or to reduce direct radiation levels.

_____ 13. Ask drivers for certification of training documents to make photocopies for records. These records are to be retained by the Reactor Administrator.

_____ 14. Check that drivers have dosimetry devices to monitor exposure during shipment. Collect and read self-reading dosimeters issued to drivers of truck and crane. These data must be recorded in the Personnel Exposure Record and filed by the Health Physicist.

_____ 15. Check that truck drivers have spare placards to replace those that might be lost or destroyed during shipment.

_____ 16. Verify shipment route with drivers. Provide written instructions for exclusive use shipment controls. [49 CFR 173.441 (c) and 49 CFR 173.425 (b)(4)]. Instruct drivers to report to DOT and UVA any incident that might occur, in which as a direct result of the radioactive material; any person is killed; receives injury requiring hospitalization; property damage exceeds $50K; or fire, breakage, spillage, or suspected radioactive contamination occurs [49 CFR 171, 15 and 49 CFR 171.16]; or of an attempt at theft or diversion.

_____ 17. Check that shipping paper description specifies one package and includes relevant information, including shipper's certificate for restricted articles/dangerous goods [49 CFR 172, Subpart C] [10 CFR 20.311].

_____ 18. Make copies of the completed bill of lading and shipping papers, then deliver originals to drivers.

_____ 19. Verify that all appropriate paperwork has been completed, i.e., complete Procedural Reviews section of these procedures.

_____ 20. A Reactor Facility Supervisor or his designee makes a final check to insure integrity of the tamper-indicating security seal affixed to the cask.

_____ 21. Reactor Facility Director will release the truck for shipment, and send off crane operators, when ready.

Comments: _____

_____

_____

_____

_____

_____

_____

22. Make the following notifications immediately after departure of the cask on truck. As appropriate, notification should include an indication of the shipment timeliness, in accordance with advance notifications sent.

_____ a. NRC Division of Safeguards and Transportation

_____ b. Savannah River consignee

_____ c. Armed escort in VA

_____ d. Armed escort in NC

_____ e. Armed escort in SC

_____ f. UVA Police Chief

_____ g. UVA Office of EH&S

_____ 23. Health Physics personnel will next swipe areas of the reactor room which were involved in the fuel transfer and the staff will clean up if normal action levels (greater than 250 dpm/100 cm^2) are exceeded.

_____ 24. Reactor Facility Staff will collect and correctly dispose of all dry solid wastes (gloves, blotting paper, etc.) with assistance from Health Physics personnel.

_____ 25. Reactor Facility Staff will collect possibly contaminated tools & instruments. These will be radiation-surveyed and decontaminated as indicated before release.

_____ 26. Health Physics personnel will collect all self-reading personnel dosimetry for final reporting in the Personnel Exposure Record. They may make a copy of this record. The original shall be attached to this procedure and remain with the Reactor Administrator.

_____ 27. Health Physics personnel will collect a sample of water from the auxiliary tank to analyze by γ-spectroscopy and determine method for final disposition of water.

IV. CANCELLATION OF SHIPMENT

In the event that a shipment is canceled, notifications are to be made in accordance with 10 CFR 71.97 and 10 CFR 73.37.F. All personnel and organizations previously notified of the impending shipment must be promptly notified of its cancellation. Those requiring notification are enumerated in Operational Checklist II.A.

V. SAFEGUARDS

A. Shipment Dates

Fuel shipment schedules and itineraries are safeguarded information and shall not be divulged to non-personnel or discussed in public areas. Such information regarding a completed shipment (or series of shipments) may be divulged 10 days following shipment arrival at destination [10 CFR 73.21(b)(2)(ii)].

B. Unaccounted Shipment

If the shipment does not arrive at its destination by the estimated time of arrival, the UVA reactor staff shall initiate a trace investigation. If shipment has been lost, the NRC Operations Center is to be notified within one hour of the investigation's determination of loss, and subsequently, of shipment recovery or accounting. These notifications are to be made via the commercial telephone number of the NRC Operations Center: (301) 951-0550. A written report of the trace investigation is to be filed with the NRC within 15 days [10 CFR 73.71(a)].

If a change in shipment itinerary or other change to a written advance NRC notification should be necessary, the Division of Safeguards and Transportation shall be notified by telephone at 301-492-3365 [10 CFR 73.74].

C. Safeguards Events

The UVA Reactor Staff must notify the NRC Operations Center within one hour of any safeguards event, which may include but is not limited to, an attempt being made or believed to have been made to commit a diversion of SNM [10 CFR 73.71(b)]. This notification must be made in the same manner as notification of an unaccounted shipment above. A current log of such events must be maintained, and a detailed written report shall be submitted to the NRC within 30 days.

VI. PROCEDURAL REVIEWS

This procedural review, to be completed by the Reactor Administrator and Director, with final concurrences by a Reactor Supervisor and Health Physicist shall be evidence that Reactor Safety Committee approval was obtained for these procedures, that these procedures were properly followed, that Director-authorized procedural modifications will be properly reviewed, that shipping documents required by transportation regulations and consignee request are in order, and that shipment records are complete.

The persons indicated below shall sign above their titles to indicate completion of items.

_____ Reactor Director	(1)	Procedures were reviewed by RSC and approved on _____.
_____ Reactor Administrator	(2)	Copy of cask water isotopic analysis has been attached to shipping documents.
_____ Reactor Administrator	(3)	Copy of actual assembly loading has been attached to shipping documents.
_____ Reactor Administrator	(4)	Security Seal Numbers (3 seals) are listed on shipping papers.
_____ Reactor Administrator	(5)	Irradiation and decay history of the shipped assemblies has been attached to the shipment papers and records [10 CFR 71.91 (ii)].
_____ Reactor Administrator	(6)	Shipping Documentation requested by consignee has been transmitted to drivers.

C. Safeguards Events

_____ (7) Verify that the EH&S-generated, RSC-approved DOT/49 Checklist has been properly completed.
Reactor Director

_____ (8) Ask all personnel on the distribution list of these procedures, who subsequently were active participants in fuel transfer operations, if they are aware of any actions that have not been properly and completely performed.
Reactor Director

_____ (9) Revision of procedures authorized by Reactor Director during shipment will be sent ASAP to the Reactor Safety Committee for review.
Reactor Administrator

_____ (10) These procedures are properly completed.
Reactor Director

_____ Date _____
Reactor Supervisor

_____ Date _____
Reactor Health Physicist

APPENDIX A

UVAR HEU Fuel Assembly Inventory

This Appendix A contains burn-up history and exposure-rate data for the assemblies being shipped in the first fuel shipment prior to LEU conversion. It also contains recent burn-up data for the remaining HEU inventory to be shipped following LEU conversion. These data will be updated prior to each shipment in the second series of shipments planned.

Table A.1 is a summary of the HEU UVAR fuel inventory being shipped by these procedures to Savannah River in Shipment No. 1. The original U-235 content of each assembly is given in the column immediately to the right of the number identifying that assembly. The current contents of U-235, U-236, and then Total U, as determined by calculations of burn-up through 9-30-92, are given in the remaining three columns.

Table A.2 is a summary of exposure-rate measurements recently obtained on the 12 assemblies of Shipment No. 1 at the request of Savannah River. All of these assemblies have cooled for more than 90 days, as required by COC 5(b)(2), and radiation exposure rates have been measured under-water, as per agreement with Ms. Sachiko MacAlhany [(803) 715-5535] at Savannah River. The values for exposure rates in air, derived from measurements in water, are given in Table A.2.

Table A.3 is a burn-up data summary for HEU UVAR fuel that will be shipped in the remaining three shipments in the second series of shipments. The information in this table is in the same format as that in Table A.1. Many of these assemblies are loaded in the UVAR as of April 1993. The groups of assemblies to be shipped in the remaining shipments have not been determined, nor have exposure-rate measurements recently been made of the remaining inventory. Burn-up history through 9-30-92 is reflected.

Table A.1 UVAR Fuel Assemblies to be Sent to Savannah River in Shipment No. 1

Assembly #	Original U-235 (g)	Current U-235 (g)	Current U-236 (g)	Current Total U (g)
TC-31	98.11	69.68	5.80	82.67
T-6	191.07	153.78	7.40	175.72
T-15	191.28	152.88	7.56	175.00
T-16	193.16	144.81	8.94	168.46
T-19	193.16	145.72	8.90	169.32
T-20	193.16	155.87	7.43	178.01
T-29	195.18	150.91	8.41	173.61
VC-19	97.36	69.45	5.21	81.84
VC-23	97.34	97.26	0.01	104.45
V-007	194.78	192.17	0.54	207.03
V-012	194.78	191.66	0.48	206.51
1-RP	192.57	192.57	0.00+	206.64
Totals	2,031.95	1,716.76	60.68	1,929.26

Table A.2 UVAR Fuel Assembly Exposure Rates in Shipment No. 1

	Assembly Number	Exposure Rate @ 1' in air on 3-17-93 (R/h)	Exposure Rate @ 3' in air on 3-17-93 (R/h)
7	TC-31	1112.4	123.6
1	T-6	43.2	4.8
2	T-15	939.6	104.4
3	T-16	356.4	39.6
4	T-19	259.2	28.8
5	T-20	345.6	38.4
6	T-29	432.0	48.0
11	VC-19	313.2	34.8
10	VC-23	334.8	37.2
8	V-007	32.4	3.6
9	V-012	475.2	52.8
	1-RP	0.0025 (measured on contact, in air, on 4-19-93)	0.0 (measured in air on 4-19-93)

Note: It is suggested that loading of less active assemblies be done first to gain on-the-spot experience.

Table A.3 UVAR Fuel Assemblies to be Shipped to Savannah River in the Second Series of Shipments

Assembly Number	Original U-235 (g)	Current U-235 (g)	Current U-236 (g)	Current Total U (g)
TC-32	98.11	76.67	4.47	88.32
T-7	191.07	133.63	10.25	158.42
T-8	191.07	162.34	6.23	183.12
T-9	191.07	128.16	11.17	153.87
T-10	191.07	142.97	9.18	166.69
T-13	191.07	136.20	10.01	160.75
T-14	191.07	135.04	10.12	159.69
T-18	193.16	134.30	10.55	159.56
T-21	193.54	137.13	10.15	162.05
T-24	195.18	141.68	9.69	165.66
T-30	195.18	136.39	10.56	161.24
T-3P	97.77	76.26	4.45	87.88
T-4P	96.77	85.37	2.77	95.70
VC-18	97.31	65.43	5.49	78.11
VC-19	97.36	69.45	5.21	81.84
VC-20	97.38	96.13	0.19	103.53
VC-21	97.34	95.42	0.30	102.92
VC-24	97.34	97.34	0.00+	104.53
VC-25	97.35	95.83	0.24	103.26
VC-26	97.45	96.40	0.16	103.73
V-001	194.80	176.59	4.35	195.27
V-002	194.73	176.27	4.82	195.47
V-003	194.73	178.12	2.94	195.42
V-004	194.79	180.38	2.65	197.40
V-005	194.80	182.01	2.39	198.72
V-006	194.84	179.71	2.43	196.46
V-008	194.79	177.39	3.02	194.75
V-009	194.76	184.85	1.65	200.87
V-010	194.83	184.65	1.56	200.51
V-011	194.79	186.03	1.35	201.75
V-013	194.78	194.78	0.00+	209.13
V-014	194.71	171.32	5.52	191.23
V-027	194.94	172.75	5.35	192.366
Totals	5,429.95	4,586.99	159.22	5,150.22

APPENDIX B

Personnel Assignments

Name	Qualification	Function
Robert U. Mulder	R. Director	Overall Administration
J.P. Farrar	R. Administrator	QA/QC & Documentation
Thomas E. Doyle	R. Director's Assistant	General Support
Paul Benneche	R. Supervisor	Fuel Loading Supervisor
B. Hosticka	Research Scientist	UVAR Pool Operations
Don Krause	SRO	UVAR Pool Operations
Lisa Scheid	SRO	Health Physics Coverage
J.S. Baber	R. Mach. Shop Super.	Fork Lift Operation
Neil Wilson	RO Trainee	Equipment Procurement
Rick Piccolo	Rad. Safety Officer	Health Physics Coverage
Jim Gilchrist	EH&S Assist. Director	Health Physics Coverage
Deborah P. Steva	R. Health Physicist	Health Physics Coverage
Scott Garver	Rad. Safety Specialist	Health Physics Coverage

Other personnel may be assigned to this operation at the discretion of the Reactor Director. Qualification requirements for additional personnel will be determined by the Director. Any additional personnel authorized to work in the vicinity of fuel transfer operations must be issued a self-reading dosimetry device, and their names must be added to the Personnel Exposure Record.

Entries will be made in the Personnel Exposure Record for each person as they come on-shift, indicating their dosimeter number and the initial reading. A current dosimetry reading entries will be made for each person on-shift after the completion of each fuel assembly transfer.

APPENDIX C

Assembly and Test of a Pressure, Leak, and Liquid Test Manifold

A pressure and liquid check manifold must be assembled and tested prior to cask arrival, so that an internal pressure and liquid leak test may be performed on the cask with quality assurance at the appropriate times. This assembly procedure has been developed in accordance with the Cintichem pre-use test procedure. The following are among the components that shall be procured for this purpose:

_____ 1. One (1) 1/4" pipe nipple (4" minimum length) -- to be attached to the cask drain valve during the check procedure.

_____ 2. One (1) absolute in-line filter

_____ 3. One (1) pressure gauge (0-50 psig minimum range) approved for pneumatic and hydraulic use

_____ 4. Two (2) 1/4" globe-type valves

_____ 5. One (1) pressurized air fitting to mate with hose that can be brought from the electronics shop air supply

_____ 6. Sufficient heavy wall tygon tubing, or equivalent, to reach from the cask to a contamination control area

_____ 7. One (1) Site bowl, type ERNST E-57-0, or equivalent.

_____ 8. Sufficient pipe fittings and teflon tape, as necessary, to complete assembly of the manifold.

_____ 9. One (1) 1/4" pipe cap for performance of manifold Q/A

The manifold must be carefully assembled and tested as follows:

Manifold Assembly:

Beginning with the 1/4" nipple, assemble the above components in this order (and note how the valves have been numbered, for future reference):

1/4" pipe nipple
Sight bowl
Valve 1
Absolute filter
Value 2
Pressure Gauge
Valve
Male Air pressure quick-disconnect fitting

Manifold Test:

_____ 1. Using teflon tape, install a 1/4" pipe cap on the cask end (that end with the 1/4" nipple) of the manifold assembled as above.

_____ 2. Open Valve 1 completely and Close Valve 2 completely.

_____ 3. Attach the quick-disconnected of the manifold to the air supply.

_____ 4. Slowly Open Valve 2 until at least 50 psig registers on the manifold pressure gauge.

_____ 5. Close Valve 2 Completely again and remove the air supply.

Note the Pressure Gauge indication here: _____ psig

_____ 6. Flood all manifold joints and other likely leak locations with a soap bubble detection liquid, e.g., SNOOP, and observe for the formation of bubbles that indicate a leak for at least two minutes, applying more liquid as necessary to maintain coverage.

_____ 7. If any leaks are found, release air pressure from the manifold by opening Valves 1 and 2, and assuring that the pressure gauge indicates Zero pressure. Then, tighten joints or take other appropriate actions to ensure that the manifold assembly is leak free. Retest, as necessary, by repeating the steps above.

_____ 8. When the manifold is demonstrably leak free and stored in a location that will protect it from damage until it is needed, initial here.

_____ 9. Return the air hose to the electronics shop and place a highly visible tag in the vicinity indicating that the air hose and supply system should not be tampered with until further notice, as it is required for spent fuel shipment operations.

APPENDIX D

Verification of Neutron Absorber Plates in the Texas A&M Basket

This method should be followed at a convenient time, given the Director's approval, before initiation of fuel assembly transfer from the UVAR pool to the BMI-1 shipping cask. The purpose is to assure the presence and effectiveness of neutron absorber plates in the Texas A&M basket, as required by BMI-1 COC 11. Health Physics personnel should monitor the work area to quantify neutron and gamma-ray fields during such times as the neutron source is in use to verify that 10 CFR 20 dose and dose-rate limits are not exceeded. Unnecessary personnel should be held at a safe distance at those times.

Evidence of the presence of neutron absorbing material in the central cruciform of the basket can be obtained in three ways. B-Al alloy material is non-magnetic, as are the stainless steel basket-divider leg plates it is secured between. Hence, the basket dividers may be tested with a permanent magnet for the presence of magnetic media in the plates, which are not expected to be present. Secondly, the dimensions of the basket assembly, and especially the dividers, may be compared with drawings on-file to provide more evidence of authenticity. As a third and most definitive test, a neutron source and BF-3 detector will be used underwater to verify that the basket dividers are significantly more effective in attenuating thermal neutrons than a steel plate of similar thickness and substantial cross-sectional area.

Revision 1 (7-22-93)

Equipment Required:

Record model and serial number of equipment or other information, as specified, on the line by each item below. Record initials to the left.

_____ 1. NIM Bin _____

_____ 2. with: HVPS _____;

_____ 3. Amplifier _____;

_____ 4. SCA _____;

_____ 5. Counter _____;

_____ 6. Scaler _____.

_____ 7. Oscilloscope _____

_____ 8. Detector pre-amp _____

_____ 9. Sufficient cable for connections

_____ 10. BF-3 tube detector about 1" in diameter

_____ 11. Electrical tape

_____ 12. A nominally 1 or 5 Ci Pu-Be source

(Source Inventory No.) _____

_____ 13. Strong string for support of Pu-Be source

_____ 14. Aluminum test rig capable of holding the BF-3 tube and neutron source at a constant separation distance of approximately 5"

_____ 15. A stainless steel plate, approximately the thickness of a cruciform leg and large cross-sectional area relative to detector size.

(Dimensions) _____

_____ 16. Texas A&M Basket and basket handling tool

_____ 17. UVAR polar crane

_____ 18. Nalgene bucket

_____ 19. Permanent magnet

_____ 20. Texas A&M Basket drawings

_____ 21. Micrometer and tape measure

Procedure:

_____ 1. Verify that dimensions of the basket in possession are in satisfactory conformance with drawings on file of the Texas A&M basket.

_____ 2. Test locations on the basket (with a permanent magnet) that should be non-magnetic and boron containing.

Note: If either of the above two tests are failed, i.e., significant dimensional discrepancies or magnetic response are noted, consult the Reactor Director.

_____ 3. Line the bucket with a plastic bag or equivalent to prevent contamination and fill to about an inch below the inner, top lip with demineralized water.

Note: Water level may be adjusted as necessary for the counting configurations required below. Potentially contaminated water should be disposed of in Liquid Waste Tank #1.

_____ 4. Set up counting equipment in a convenient location near the bucket.

_____ 5. Retrieve a 1 or 5 Ci Pu-Be source from the Source Storage Room and bring it in its shield to the experimental area.

_____ 6. Place detector in a source shield hole to obtain a source of thermal neutrons. Adjust counting equipment so that amplifier output is acceptable and most counts obtained are from thermal neutrons.

_____ 7. The Director shall initial here to authorize implementation of this method.

_____ 8. Identify Health Physics personnel now conducting radiation monitoring.

_____

_____

_____ 9. Identify monitoring meters:

Meter 1 _____

Calibration Due Date _____

Meter 2 _____

Calibration Due Date _____

_____ 10. Hang the test rig from the UVAR crane near the bucket.

_____ 11. Install the BF-3 tube, with signal cable and pre-amp attached, in the longer of the two wells in the test rig. Tape the cable connection at the BF-3 tube to impede water damage or electrical shorting, should the detector inadvertently come in contact with water.

_____ 12. Lower the test rig by attached wire so that the two wells hang vertically in open water and their tops are about one inch above the water line.

_____ 13. Verify that no unnecessary personnel are in the vicinity, and that if there are any, directed them to leave.

_____ 14. While Health Physics personnel monitor radiation levels and note working times in the vicinity of the source handler, remove the Pu-Be source from its shield and lower it into the shorter test rig well.

_____ 15. Adjust counting equipment again so that at least 10,000 counts from thermal neutrons are obtained (1% statistics or better). Record the counts obtained, and counting time here, then calculate the counting rate observed with the test rig in open water.

Ct. Time _____ Gross Ct. _____ Gross Ct. Rate _____

_____ 16. Return the Pu-Be source to its shield and take a background (BG) count. Record the BG counting time and count here.

BG Ct. Time _____ BG Ct. _____ BG Ct. Rate _____

_____ 17. Calculate and record here the Net counting rate (Gross Ct. Rate - BG Ct. Rate = Net Ct. Rate). Record Net Ct. Rate in open water in the Data Summary below and sign off here when complete.

Net Ct. Rate in Open Water _____

_____ 18. Lift test rig sufficiently for attachment of stainless steel plate between sourced and detector wells. Attach the plate.

_____ 19. Lower the test rig with plate and dectector again to just

above water level.

_____ 20. Take a background count with test rig straddling steel for the same amount of time as for the open water background count.

BG Ct. Time _____ BG Ct. _____ BG Ct. Rate _____BG

_____ 21. Install the Pu-Be source in the test rig and count for the same amount of time as for the open water gross count. Record data here.

Ct. Time _____ Gross Ct. _____ Gross Ct. Rate _____
(Test rig Straddling steel plate)

_____ 22. Calculate the Net Ct. Rate for the test rig straddling steel, enter this datum in the Neutron Data Summary and sign off here when done.

Net Ct. Rate (steel) _____

_____ 23. Return the Pu-Be source to its shield.

_____ 24. Dry off and appropriately store the stainless steel plate.

_____ 25. Remove test rig from crane, dry it, and set it aside.

_____ 26. Pick up the basket by crane and hang it so that cruciform top is just above water level.

_____ 27. Install the test rig so that it straddles one of the central four basket-divider legs near basket center. Make a sketch below to indicate how the legs of the central basket cross can be identified and this initial position of the test rig. This initial position will be called position number one. Identify three other positions that straddle the other dividing legs as No. 2, 3, and 4.

Sketch:

_____ 28. Obtain a background count with the test rig in each of the four locations. Then, return the neutron source to the test rig and obtain a gross count in each location, counting in each instance for the same amount of time as necessary in open water. Record these data in the Neutron Data Summary.

_____ 29. Return the neutron source to its shield and the Source Storage Room.

_____ 30. Lift the basket and allow it to drip-dry above bucket. Store it appropriately until use in the BMI-1 cask.

_____ 31. Direct the auxiliary crane operator to rest the basket on the auxiliary tank bottom, away from where the BMI-1 Cask will be placed.

_____ 32. Dismantle and put away counting equipment.

_____ 33. Properly dispose of potentially contaminated bucket liner and water.

_____ 34. Health Physics personnel will verify here that this operation has been safely completed and documented.

Health Physics Personnel Notes:

Neutron Data Summary

Net Ct. Rate in Open Water _____

Net Ct. Rate Straddling Steel Plate _____

Position 1

Gross Time _____ Gross Cts. _____ Gross Ct. Rate _____

BG Time _____ BG Cts. _____ BG Ct. Rate _____

Net Ct. Rate in Basket Position # 1 _____

Position 2

Gross Time _____ Gross Cts. _____ Gross Ct. Rate _____

BG Time _____ BG Cts. _____ BG Ct. Rate _____

Net Ct. Rate in Basket Position # 2 _____

Position 3

Gross Time _____ Gross Cts. _____ Gross Ct. Rate _____

BG Time _____ BG Cts. _____ BG Ct. Rate _____

Net Ct. Rate in Basket Position # 3 _____

Position 4

Gross Time _____ Gross Cts. _____ Gross Ct. Rate _____

BG Time _____ BG Cts. _____ BG Ct. Rate _____

Net Ct. Rate in Basket Position # 4 _____

35. The Director shall sign here to assure that the presence and effectiveness of neutron-absorbing plates in the Texas A&M Basket has been verified via magnetism test, dimensional conformity, and effective attenuation of thermal neutrons, and that this operation has been carried out safely.

(Reactor Director) _____

APPENDIX E

BMI-1 Certificate of Compliance

No. 5957, Revision No. 21

Package Identification Number USA/5957/B( )F

Revised 10.6.94

UNITED STATES
NUCLEAR REGULATORY COMMISSION
WASHINGTON, D.C. 20555-0001

STSB:NLO
71-5957

MAY 24 1994

Department of Energy
ATTN: Mr. Michael E. Wangler
Transportation and Packaging
Safety Division, EH-332
Washington, DC 20585

Dear Mr. Wangler:

As requested by your application dated September 16, 1993, as supplemented March 2, 1994, and May 2, 1994, enclosed is Certificate of Compliance No. 5957, Revision No. 21, for the Model No. BMI-1 package. This certificate supersedes, in its entirety, Certificate of Compliance No. 5957, Revision No. 20, dated November 17, 1993.

Changes made to the enclosed certificate are indicated by vertical lines in the margin.

Those on the attached list have been registered as users of the package under the general license provisions of 10 CFR §71.12 or 49 CFR §173.471.

The approval constitutes authority to use the package for shipment of radioactive material and for the package to be shipped in accordance with the provisions of 49 CFR §173.471.

Sincerely,
Original Signed By
Cass R. Chappell

Cass R. Chappell, Section Leader
Cask Certification Section
Storage and Transport Systems Branch
Division of Industrial and
Medical Nuclear Safety, NMSS

Enclosures:
1. Certificate of Compliance
No. 5957, Rev. No. 21
2. Approval Record

cc w/encl:
Mr. James K. O'Steen
Department of Transportation

Registered Users

UNITED STATES
NUCLEAR REGULATORY COMMISSION
WASHINGTON, D.C. 20555-0001

APPROVAL RECORD
Model No. BMI-1 Package
Certificate of Compliance No. 5957
Revision No. 21

By application dated September 16, 1993, as supplemented March 2, 1994, and May 2, 1994, Department of Energy requested an amendment to Certificate of Compliance No. 5957, for the Model No. BMI-1 package. The request was to include High Flux Beam Reactor (HFBR) irradiated fuel as authorized contents, and to include a basket design for the HFBR fuel as an authorized product container.

The HFBR fuel is in the form of MTR-type fuel assemblies. Each assembly weighs approximately 9.9 lbs and contains 351 grams of U-235 prior to irradiation. The maximum fuel assembly burnup at discharge is approximately 130 MWD/assembly, and the minimum cooling time is 470 days.

The basket assembly is composed of two stainless steel baskets, stacked axially. The baskets are separated by a 3/8-inch thick stainless steel spacer plate. Each basket holds 10 fuel assemblies, for a total of 20 fuel assemblies per shipment. Only a full load (20 assemblies) is authorized. The basket is almost identical to the configuration previously approved for shipment of 20 HFBR fuel assemblies in the Model No. GE-700 package. The basket is manufactured in accordance with ASME Code Section III, Subsection NG, consistent with recommendations in NUREG/CR-3854, "Fabrication Criteria for Shipping Containers."

STRUCTURAL

The basket is fabricated from 3/16-inch thick and 1/4-inch thick 304 stainless steel plates. The steel plates form 10 rectangular fuel compartments with a length of 25-3/8 inches. Fuel assemblies are supported at the bottom of each compartment by 3/16-inch thick and 1-inch wide plates welded to the fuel compartment plates. The total weight of the fuel assemblies, fuel baskets and spacer plate is 586 lbs, which is less than the allowable maximum contents weight of 1,800 lbs.

In the structural analysis, the applicant considered bottom, top, side, and corner drop orientations for the 30 foot drop test. The g loads for each orientation were applied to the fuel basket. The maximum g loads were 375, 680, 500, and 128, for the bottom, top, side, and corner drop orientations. The design of the fuel basket was shown to have acceptable margins of safety. The fuel basket will provide structural support, and will maintain the separation between fuel assemblies under normal conditions of transport and under hypothetical accident conditions.

CRITICALITY

To demonstrate the criticality safety of the package the applicant submitted previous criticality analyses performed for the HFBR fuel in the GE-700 package. The criticality analyses used the KENO IV computer code and the 27GROUPNDF4 cross section set.

The normal condition analysis considered an array of two packages side-by side. The applicant assumed that each package was filled with mist at a density of 8.8×10^{-5} g/cm^3, representing saturated air at 120°F and one atmosphere. The array was reflected with 12 inches of water on all sides. The calculated k_{eff} was 0.30094 ± 0.00319.

The accident conditions analysis considered one package. The applicant analyzed two models for accident conditions, the first with the two baskets (each basket containing 10 fuel assemblies) inside the cask and the other with the two baskets located outside the cask, positioned side by side. Both models assumed full density water moderation and full reflection. The calculated values of k_{eff} were 0.91561 ± 0.00479 and 0.84505 ± 0.00499.

The NRC staff performed an independent criticality analysis using the KENO Va computer code in the SCALE system. The 27GROUPNDF4 cross section set was used for staff calculations. The staff modeled the fuel assembly, basket, and package explicitly. The staff result for the accident case was a k_{eff} of 0.8202 ± 0.0029. The staff's results confirm that the package meets the criticality requirements of 10 CFR Part 71 for fissile material packages.

SHIELDING

The applicant performed a shielding analysis to show that the package meets the external radiation standards of 10 CFR Part 71. The ORIGEN2 computer code was used to calculate the shielding source term. The basis of the source term calculation was 93.5 percent enriched MTR fuel assemblies with a core burnup of 3600 MWD (60 days at 60 MW) and a minimum 470 day cool time. The design basis source term consisted of 20 MTR fuel assemblies.

The applicant used the MICROSHIELD computer code to perform the shielding analysis. The applicant's shielding model consisted of a cylindrical source surrounded by concentric rings of stainless steel and lead. For the radial dose rate calculations, the uranium, aluminum and stainless steel of the fuel and basket were homogenized in the source region. The applicant did not perform axial shielding calculations, but the lid and cask bottom contain similar thicknesses of lead shielding as the radial shield. The applicant used the most abundant fission products as the radiation source term.

The applicant provided the ORIGEN2 output which showed that the neutron dose rate from the fuel is negligible, because the fuel is high enriched. The staff agrees that the neutron dose rate is negligible.

The NRC staff performed calculations to confirm the applicant's results. Staff used the ORIGEN-S code in the SCALE system to generate the radiation source terms. The shielding calculations utilized this source term with the MICROSHIELD computer code. The staff calculated dose rates for normal conditions. The staff's analysis did not take credit for shielding of the aluminum in the fuel assemblies or the spacer plate between the two baskets. In addition, the staff's model used discreet energy groups and their associated activity from the ORIGEN-S output.

The dose rates calculated by the staff were consistent with those presented in the application. The results of the applicant's analysis, as confirmed by the staff, demonstrate that the BMI-1 package with the HFBR fuel meets the external radiation standards of 10 CFR Part 71, as shown below.

	Dose Rates (millirem/hr)		
Location	Applicant	NRC	Limit
Radial Surface	18.4	22.4	200
Radial - 1 meter from package	5.0	6.2	1000
Radial - 2 meters from package	2.2	2.7	10

CONTAINMENT

The fuel cladding provides containment of the fuel and fission products under normal and accident conditions of transport. The cladding integrity is tested for all HFBR fuel assemblies prior to shipment. Leaking fuel assemblies are not authorized for transport. The package is soap bubble leak tested prior to each shipment. The leak test has a sensitivity of approximately 10^{-3} atm-cm^3/sec.

The total inventory of fission gas (krypton-85) in 20 fuel assemblies is 942 curies. Therefore, in the event all of the cladding failed under accident conditions, less that 10,000 curies of krypton-85 would be available for release. The package, with 20 HFBR fuel assemblies meets the requirements of 10 CFR §71.51 for both normal and hypothetical accident conditions of transport.

THERMAL

The applicant assumed a 60 day burn time at 60 MW for a full core of HFBR fuel assemblies and a cool down time of 470 days. The resulting decay heat load of the 20 HFBR fuel assemblies was 1.01 kW, which is below the limit of 1.5 kW given in the certificate, and below the 1.02 kW value used in previous thermal analysis for MTR type fuel. The package temperatures will be bounded by temperatures calculated in the application.

The staff performed an independent thermal analysis which confirmed the applicant's results. The staff agrees with the applicant's conclusion that the package heat load is bounded by previous analyses.

SUMMARY

The Certificate of Compliance has been revised to include the HFBR fuel assemblies as authorized contents, and to include the HFBR basket assembly as a product container. These changes do not affect the ability of the package to meet the requirements of 10 CFR Part 71.

Cass R. Chappell

Cass R. Chappell, Section Leader
Cask Certification Section
Storage and Transport Systems Branch
Division of Industrial and
Medical Nuclear Safety, NMSS

MAY 24 1994

Date_____

NRC FORM 618
(8-85)
10 CFR 71

U.S. NUCLEAR REGULATORY COMMISSION

CERTIFICATE OF COMPLIANCE
FOR RADIOACTIVE MATERIALS PACKAGES

1.a. CERTIFICATE NUMBER	b. REVISION NUMBER	c. PACKAGE IDENTIFICATION NUMBER	d. PAGE NUMBER	e. TOTAL NUMBER PAGES
5957	21	USA/5957/B( )F	1	8

2. PREAMBLE

a. This certificate is issued to certify that the packaging and contents described in Item 5 below, meets the applicable safety standards set forth in Title 10, Code of Federal Regulations, Part 71, "Packaging and Transportation of Radioactive Material."

b. This certificate does not relieve the consignor from compliance with any requirement of the regulations of the U.S. Department of Transportation or other applicable regulatory agencies, including the government of any country through or into which the package will be transported.

3. THIS CERTIFICATE IS ISSUED ON THE BASIS OF A SAFETY ANALYSIS REPORT OF THE PACKAGE DESIGN OR APPLICATION

a. ISSUED TO *(Name and Address)*

Department of Energy
Transportation & Packaging
Safety Div., EH-33.2
Washington, DC 20585

b. TITLE AND IDENTIFICATION OF REPORT OR APPLICATION:

Battelle Columbus Laboratories application dated June 20, 1985, as supplemented.

c. DOCKET NUMBER 71-5957

4. CONDITIONS

This certificate is conditional upon fulfilling the requirements of 10 CFR Part 71, as applicable, and the conditions specified below.

5.

(a) Packaging

(1) Model No.: BMI-1

(2) Description

A steel-encased lead shielded shipping cask. The basic cask body is a cylinder 33.37 inches in diameter by 73.37 inches high formed by two concentric stainless steel shells whose annular region is filled with lead. The outer 1/2-inch thick shell has a 0.12-inch thick plate spot welded to it, providing a 0.06-inch thick air gap insulator. The inner shell is 15.5 inches inside diameter by 54 inches inside length. The cask lid is a stainless steel weldment having 7.75 inches of lead shielding. The cask lid is secured to the cask by twelve steel studs which are welded to the cask body. The cask is provided with a drain line with needle valve and plug, pressure gauge, and a pressure relief valve. The total cask weight, including maximum contents of 1,800 lbs, is 23,660 lbs.

(3) Drawings

The cask is constructed in accordance with the following Battelle Memorial Institute (BMI) Drawing Nos.: 43-6704-0001, Rev. B; and 41-4409-0003, Rev. B.

5. (a) Packaging (continued)

(4) Product Containers

The various authorized product containers are constructed in accordance with the following Drawing Nos.:

(i) Inner can assembly as shown in BMI Drawing No. 00-000-421, Rev. C.

(ii) Basket Assembly as shown in BMI Drawing Nos. BCL-000-500, Rev. A; BCL-000-501, Rev. A; and 0048, Rev. A.

(iii) Fermi Fuel Element copper casting assembly as shown in BMI Drawing No. K5928-5 0049D, Rev. to May 12, 1966.

(iv) Basket Assembly as shown in BMI Drawing No. 1020, Rev. B (or with alternate spacer shown in CI Drawing No. 334D2193) or GA Drawing No. 9590001, Rev. A. Failed fuel assemblies must be seal welded in aluminum or stainless steel tubes with wall and end cap thicknesses of at least 0.015 inch.

(v) Basket Assembly defined by BMI Drawing No. BCL-000-500, Rev. A, as modified by BMI Drawing Nos. 00-000-236, Rev. C, and BCL-000-502, Rev. B.

(vi) Basket Assembly and storage can defined by BMI Drawing No. 00-000-391, Rev. C, and Atomic International Drawing No. AIHL, S8DR 0019-01, Rev. A, respectively.

(vii) Inner can assembly as shown in Union Carbide Corporation Drawing No. 101501, Rev. A.

(viii) Basket Assembly as shown in University of Missouri Research Reactor (MURR) Drawing No. 2234, Sheets 1 through 5, Revision 0.

(ix) HFBR assembly basket and spacer plate as shown in Brookhaven National Laboratory Drawing Nos.: BNL 93-001, Sheets 1, 2, and 3, Rev. 2, and BNL 93-002, Sheet 1, Rev. 2.

(b) Contents

(1) Type and form of material

(i) Intact irradiated MTR- or BRR-type fuel assemblies containing not more than 200 grams U-235 per assembly prior to irradiation. Uranium may be enriched to a maximum 93.5 w/o in the U-235 isotope. Active fuel length shall be approximately 25 inches.

5. (b) Contents (Continued)

(1) Type and form of material (Continued)

(ii) Intact irradiated Enrico Fermi Core. A fuel assembly containing not more than 4.77 kgs U-235 prior to irradiation. Uranium may be enriched to 25.6 w/o in the U-235 isotope.

(iii) Greater than Type A quantity of radioactive material which may include uranium enriched in the U-235 isotope, U-233, plutonium, as metal, oxides, or compounds which are thermally stable up to 600°F. Plutonium in excess of twenty (20) curies per package must be in the form of metal, metal alloy, or reactor elements.

(iv) Greater than Type A quantity of byproduct material meeting the requirements of special form radioactive material.

(v) Greater than Type A quantity of byproduct material in normal form as metal, oxides, or compounds which are thermally stable up to 600°F.

(vi) Irradiated Triga Type fuel assemblies described in Section 6.6 of the application (pp. 6-23 through 6-27).

(vii) Irradiated S8DR fuel elements 0.56-inch OD by 18.7 inches long by 0.010-inch wall thickness of Hastelloy-N. The fuel material is UZrH fully enriched in U-235.

(viii) Intact irradiate CP-5 fuel assemblies containing not more than 176 grams U-235 per assembly prior to irradiation. Uranium may be enriched to a maximum 93 w/o in the U-235 isotope. Active fuel length shall be 28.5 inches.

(ix) Solid nonfissile irradiated hardware which may contain encapsulated fission monitors.

(x) Irradiated uranium oxide waste enriched in the U-235 isotope up to a nominal 93 w/o which is thermally stable up to 800°F.

(xi) Irradiated uranium enriched in the U-235 isotope meeting the requirements of special form radioactive material.

(xii) Intact irradiated MURR fuel assemblies containing not more than 775 grams of U-235 per assembly prior to irradiation. Uranium may be enriched to a maximum 93.5 w/o in the U-235 isotope. Active fuel length shall be 24 inches.

5. (b) Contents (Continued)

(1) Type and form of material (Continued)

(xiii) Intact irradiated MITR-II fuel assemblies containing not more than a nominal 510 grams of U-235 per assembly prior to irradiation. Uranium may be enriched to a maximum 93.5 w/o in the U-235 isotope. Active fuel length shall be approximately 24 inches.

(xiv) Intact irradiated High Flux Beam Reactor (HFBR) fuel assemblies containing not more than a nominal 351 grams of U-235 per assembly prior to irradiation. Uranium may be enriched to a maximum of 93.5 w/o in the U-235 isotope. Active fuel length shall be nominal 24 inches.

(2) Maximum quantity of material per package

The minimum cooling time of each fuel assembly and rod is 90 days, maximum decay heat generation per package not to exceed 1.5 kw, and the external dose rate not to exceed 10 mrem/hr 3 feet from the external surface of the cask and:

(i) For the contents described in 5(b)(1)(i):

Twenty-four (24) fuel assemblies as contained in product containers specified in 5(a)(4)(ii) or 12 fuel assemblies as contained in product containers specified in 5(a)(4)(v).

(ii) For the contents described in 5(b)(1)(ii):

One (1) fuel assembly as contained in product container specified in 5(a)(4)(iii).

(iii) For the contents described in 5(b)(1)(iii):

480 grams U-233 or 480 grams Pu-239 or 800 grams U-235 as contained in product container specified in 5(a)(4)(i).

(iv) For the contents described in 5(b)(1)(iv):

Gamma sources securely confined in the cask cavity to preclude secondary impacts during accident conditions of transport. Thermal heat generation rate is limited to 200 watts.

(v) For the contents described in 5(b)(1)(v):

Contained in product containers specified in 5(a)(4)(i) and limited to 200 thermal watts.

Page 5 - Certificate No. 5957 - Revision No. 21 - Docket No. 71-5957

5. (b) Contents (Continued)

(2) Maximum quantity of material per package (Continued)

(vi) For the contents described in 5(b)(1)(vi):

Thirty-eight (38) fuel assemblies as contained in product containers specified in 5(a)(4)(iv). Fuel assemblies with an initial enrichment (U-235 in U) of greater than 70 w/o U-235 are limited to 19 assemblies per product container. Shipments of less than 19 assemblies with a U-235 enrichment greater than 70 w/o may be combined with assemblies of 70 w/o U-235 or less provided: $x/38 + y/19 \leq 1$; x = no. assy's $\leq$ 70 w/o U-235, y = no. assy's $>$ 70 w/o U-235.

(vii) For the contents described in 5(b)(1)(vii):

Twenty-four (24) fuel elements per can and six sealed cans per basket as described in 5(a)(4)(vi). Each of the six cans may contain up to 818 g U-235 and 158 g hydrogen. The cask is limited to 4.908 kg U-235.

(viii) For the contents described in 5(b)(1)(viii):

Twelve (12) fuel assemblies.

(ix) For the contents described in 5(b)(1)(ix):

Thermal heat generation rate is limited to 200 watts.

(x) For the contents described in 5(b)(1)(x):

Twenty-four (24) containers each limited to 352 grams U-235 as contained in product containers specified in 5(a)(4)(vii). The decay heat per container is limited to 20 watts. The containers must be leak tested in accordance with Union Carbide Corporation letter dated November 17, 1980.

(xi) For the contents described in 5(b)(1)(xi):

Twenty-four (24) capsules each limited to 100 grams U-235.

(xii) For the contents described in 5(b)(1)(xii):

Eight (8) fuel assemblies as contained in the product container specified in 5(a)(4)(viii). The maximum burnup is 150 MWD/Assembly and the minimum cooling time of each fuel assembly is 150 days. The maximum radiation source term is 400,000 curies.

5. (b) Contents (Continued)

(2) Maximum quantity of material per package (Continued)

(xiii) For the contents described in 5(b)(1)(xiii):

Eight (8) fuel assemblies, contained in the product container specified in 5(a)(4)(viii). The maximum decay heat per package is 200 watts.

(xiv) For the contents described in 5(b)(1)(xiv):

Twenty (20) fuel assemblies contained in two baskets separated by a spacer plate as specified in 5(a)(4)(ix). Each shipment must contain twenty fuel assemblies. The maximum burnup is approximately 130 MWD/assembly, and the minimum cooling time is 470 days.

(c) Fissile Class	I and III
(1) Class I	For the contents specified in 5(b)(1)(iii) and limited in 5(b)(2)(iii).
(2) Maximum number of packages per shipment as Fissile Class III	For the contents specified in 5(b)(1)(i), 5(b)(1)(ii), 5(b)(1)(vi), 5(b)(1)(vii), 5(b)(1)(viii), 5(b)(1)(x), 5(b)(1)(xi), 5(b)(1)(xii), 5(b)(1)(xiii), and 5(b)(1)(xiv), and limited in 5(b)(2)(i), 5(b)(2)(ii), 5(b)(2)(vi), 5(b)(2)(vii), 5(b)(2)(viii), 5(b)(2)(x), 5(b)(2)(xi), 5(b)(2)(xii), 5(b)(2)(xiii), and 5(b)(2)(xiv): One (1) package.

6. For Item 5(b)(1)(iii), mixtures of fissile material are authorized, provided the following equation is satisfied:

$$\frac{X}{480} + \frac{Y}{480} + \frac{Z}{800} \leq 1, \text{ where}$$

X = Grams U-233 to be shipped
Y = Grams Pu-239 to be shipped
Z = Grams U-235 to be shipped

7. Except for the contents described in 5(b)(1)(ii), 5(b)(1)(iv) and 5(b)(1)(xii); and limited in 5(b)(2)(ii), 5(b)(2)(iv) and 5(b)(2)(xii), the cask must be shipped dry.

8. If the cask contents of 5(b)(1)(ii), 5(b)(1)(iv) or 5(b)(1)(xii) are shipped wet, the licensee must confirm that the pressure relief valve is operable (set pressure - 75 psig). When needed, sufficient antifreeze in the cask must be used to prevent damage of any component of the package by freezing.

9. Loading and unloading operations of the contents described in 5(b)(1)(iii) and limited in 5(b)(2)(iii) must preclude contact of water with the contents.

10. When the contents of 5(b)(1)(vi) are loaded wet, the optional 0.5-inch diameter drain hole must be present in the primary basket lower plate to assure proper draining of the basket.

11. The presence and effectiveness of the Boral poison plate in the Basket Assemblies as shown in BMI Drawing Nos. BCL-000-500, Rev, A; 0048, Rev. A; and 00-000-236, Rev. C, must be verified by neutron measurements prior to first use and records maintained of such verification. Verification of the presence of the Boral must be made in each subsequent use.

12. Contents 5(b)(1)(i) and 5(b)(1)(x) may be mixed provided the sum of the product containers and fuel assemblies does not exceed 24.

13. Axial movement of fuel assemblies must be limited so that the active fuel region will remain correctly positioned with respect to the poisoned section of the basket. Removable spacers may be used in each section of the basket to limit axial movement of the assemblies.

14. Contents must be securely confined in the cask cavity to minimize movement.

15. Prior to each use, adequacy of containment vessel must be demonstrated by performance of the leak test described in Section 7.1.1.1 of the application.

16. Gaskets and seals (cask and fuel canister) must be replaced at least every 12 months or earlier if visible degradation occurs.

17. In addition to the requirements of Subpart G of 10 CFR Part 71:

    (a) The package shall be prepared for shipment and operated in accordance with the Operating Procedures of Chapter 7 of the application.

    (b) The packaging must meet the Acceptance Tests and Maintenance Program of Chapter 8 of the application.

18. The package authorized by this certificate is hereby approved for use under the general license provisions of 10 CFR §71.12.

19. Expiration date: May 31, 1995.

REFERENCES

Battelle Columbus Laboratories consolidated application dated June 20, 1985.

Cintichem Inc. supplements dated December 14, 1987; May 30, July 15 and September 28, 1988; and April 17, 1990.

University of Missouri Research Reactor letters dated April 18, June 7, June 11, June 13, and August 8, 1990.

Massachusetts Institute of Technology Nuclear Reactor Laboratory letters dated October 19, 1992, and January 11, 1993.

Department of Energy supplements dated: July 15 and September 16, 1993; and March 2 and May 2, 1994.

FOR THE U.S. NUCLEAR REGULATORY COMMISSION

Cass R. Chappell

Cass R. Chappell, Section Leader
Cask Certification Section
Storage and Transport Systems Branch
Division of Industrial and
Medical Nuclear Safety, NMSS

Date: MAY 2 6 1994

LIST OF USERS FOR CERTIFICATE - 5957

FOR MODEL - BMI-1

BABCOCK & WILCOX CO.
ATTN: MR. CHARLIE C. BOYD, JR.
P.O.BOX 11165
LYNCHBURG VA 24506

BATTELLE COLUMBUS LABORATORY
ATTN: MR. RICHARD J. BURIAN
505 KING AVENUE
COLUMBUS OH 43201

CHEM-NUCLEAR SYSTEMS, INC.
ATTN: MS. SUSAN KINTNER
140 STONERIDGE DRIVE
COLUMBIA SC 29210

CINTICHEM INC.
ATTN: MR. ROBERT A. STRACK
P. O. BOX 816
TUXEDO NY 10987

FLORIDA POWER & LIGHT CO.
ATTN: MR. J. H. GOLDBERG
P. O. BOX 14000
JUNO BEACH FL 334080420

GENERAL ATOMICS
ATTN: DR. KEITH E. ASMUSSEN
P.O.BOX 85608
SAN DIEGO CA 92138

GENERAL ELECTRIC COMPANY
ATTN: MR. T. E. INGELLS
7555 EAST COLLINS ROAD
MORRIS IL 60450

GPU NUCLEAR CORPORATION
ATTN: MR. THOMAS SNIDER
P.O. BOX 388
FORKED RIVER NJ 08731

KANSAS STATE UNIVERSITY
ATTN: MR. RICHARD E. FAW, DIRE
DEPT. OF NUCLEAR ENGINEERING
MANHATTEN KS 66506

MASS. INSTITUTE OF TECH.
ATTN: ARA B. SANENTZ
138 ALBANY STREET
CAMBRIDGE MA 02139

LIST OF USERS FOR CERTIFICATE - 5957

FOR MODEL - BMI-1

MICHIGAN STATE UNIVERSITY, COLLEGE OF ENGINEERING
ATTN: MR. BRUCE W. WILKINSON
DIVISION OF ENGINEERING RESEARCH
EAST LANSING MI 488241326

N.C. STATE UNIV. AT RALEIGH
ATTN: MR. K. V. MANI
P.O. BOX 7909
RALIEGH NC 27695

NIAGARA MOHAWK POWER CORP.
ATTN: MR. JACK TORBITT, JR.
P. O. BOX 32
LYCOMING NY 13093

NORTHEAST NUCLEAR ENERGY COMPANY
ATTN: MR. E. J. MROCZKA
P. O. BOX 270
HARTFORD CT 061410270

NORTHERN STATES POWER CO.
ATTN: MR. THOMAS PARKER
512 NICOLLET MALL
MINNEAPOLIS MN 55402

RHODE ISLAND ATOMIC ENERGY COMMISSION
ATTN: MR. TERRANCE TEHAN
SOUTH FERRY ROAD
NARRAGANSETT RI 028821197

U. S. DEPARTMENT OF ENERGY
ATTN MR. MICHAEL E. WANGLER
TRANSPORTATION AND PACKAGING SAFETY DIV., EH-33.3
WASHINGTON DC 20585

UNIVERSITY OF CA, BERKELEY
ATTN: MR. T. H. LIM
COLLEGE OF ENGINEERING
BERKELEY CA 94720

UNIVERSITY OF MICHIGAN
ATTN: MR. GARY COOK
PHOENIX MEMORIAL LAB.
ANN ARBOR MI 48109

UNIVERSITY OF MISSOURI
ATTN DR. ROLAND A. HULTSCH
ROOM 402 RESEARCH REACTOR FACILITY
COLUMBIA MO 65211

LIST OF USERS FOR CERTIFICATE - 5957

FOR MODEL - BMI-1

UNIVERSITY OF VIRGINIA, NUCLEAR REACTOR FACILITY
ATTN: MR. J.P. FARRAR
DEPT. OF NUCLEAR ENGINEERING
CHARLOTTESVILLE VA 229032442

VIRGINIA ELECTRIC AND POWER COMPANY
ATTN: V.P.-NUCLEAR OPERATIONS
5000 DOMINION BOULEVARD
GLEN ALLEN VA 23060

WESTINGHOUSE ELEC. CORPORATION
ATTN: MR. A. J. NARDI
P.O. BOX 355
PITTSBURGH PA 15230

APPENDIX F

DOT / 49 CFR Quality Assurance Checklist

NOTES

DOT - 49 CFR Quality Assurance Checklist — Cover Sheet

Fissile Radioactive Material Shipment Number:

Date:

To:

Transport vehicle designation: exclusive nonexclusive
(circle one)

NOTES

DOT - 49 CFR Quality Assurance Checklist

The following is a quality assurance checklist designed to ensure compliance with Department of Transportation regulations governing the transportation of fissile radioactive material over public roads. The users of this checklist, by initialling the space to the right of the listed item, are providing a "yes" response to the action required by the item. An entry of "NA" into this space indicates that the item is not applicable to this shipment.

10CFR71.87

I. Cask Receipt

The level of non-fixed contamination does not exceed the limits described in item VIIA. below. _____

49CFR173.475

Quality Control Requirements - shipper has ensured by examination or appropriate tests that quality control requirements as specified in 173.475 are met. _____

10CFR71.87

The package is in unimpaired physical condition except for superficial defects such as marks or dents. _____

49CFR173.416-417

Shipper has on file a copy of the package certification showing package meets requirements of 173.416 - 417. _____

49CFR173.471

Any shipper of a Type B, Type B(U), Type B(M) or fissile material package that has been approved by USNRC in accordance with 10CFR Part 71 shall be registered with the USNRC as a party to the approval, and shipment must be made in compliance with the terms of the approval. _____

49CFR subpart D
172.300-310
172.400-450

II. Marking and Labeling

49CFR172.304

Markings are durable, printed on or affixed to the surface of the package (or over-pack) or on a label, tag or sign. The sign or tag is displayed on a background of sharply contrasting color and is unobscured by labels or attachments. All markings and labellings must be located away from other markings that could substantially reduce its effectiveness. _____

172.301

The package is marked with the proper shipping name and the appropriate UN number (not applicable if exculsive use) _____

The package is marked with consignee's or consignor's name and address. _____

172.310

The package gross weight (if in excess of 110 lbs. (50 kg)) is plainly and durably marked on the outside of the package. _____

NOTES

49CFR172.310

The package type (e.g. A or B) is marked on the outside of the container in letters at least $\frac{1}{2}$ inch high. _____

Outside of package durably and legibly marked with package identification marking indicated in USNRC or DOT approval. _____

The proper RADIOACTIVE labels are affixed in accordance with the following criteria: _____

172.403
172.406

A. Two labels must be affixed to opposite sides of the container near the marked proper shipping name and near the closure. The following information must be entered on the labels using a durable weather resistant means of marking.

1. contents of package (i.e., name of radionuclide. For mixtures of radionuclides, list the most restrictive radionuclide(s) on the basis of radiotoxicity). ___
2. activity of contents in appropriate Curie units. For fissile material, the weight (in grams or kg) of the fissile radioisotopes also may be inserted. ___
3. transportation index. ___
4. classification of hazardous material (e.g. radioactive). ___
5. category of label (e.g. Yellow III). ___

49CFR172.403(c) Footnote

B. Highway route controlled quantities (HRCQ) must be labelled as a Yellow III. _____

49CFR172.436-440

C. Labels must be as described in 49CRR172.436-440 _____

49CFR172.101

III. Reportable Quantity (RQ) Determination

Use the attached Appendix to 49CFR172.101 to determine if the quantity of radioactive material being shipped is considered an RQ. Use the following table to make the RQ determination.

Radionuclide	Quantity (Ci)	RQ Value (Ci)	Ratio (Quantity/RQ)

Sum of Ratios = _____

If total of ratios is greater than 1, proceed as follows; otherwise continue with the next section.

NOTES

49CFR172.203

A. Identify the RQ radionuclides on the shipping papers. The RQ should be written before the proper shipping name, e.g. RQ, Radioactive Material, Fissile, n.o.s. _____

172.324

B. The letters "RQ" are marked on the package in association with the proper shipping name. _____

NOTE: If the Facility is involved in a release of a reportable quantity, notification must be made immediately to the National Response Center, phone number 800-424-8802.

IV. Placarding

49CFR172.500-519

172.504

If a vehicle contains a package with a radioactive Yellow III label, it must be placarded.

172.506

"Radioactive" placards are placed on each end and each side of the motor vehicle. Shipper shall provide motor carrier with required placards unless carrier's motor vehicle is already placarded for material as required. _____

172.507

For HRCQ shipments, the "radioactive" placards must be placed on a square background as described in 172.527 _____

172.516

Placards are securely attached, away from dirt or water wheel spray points and not reduced in effectiveness by proximity to any other markings, and in any case at least 3 inches away from such markings. _____

172.556

Placards are as described in 49CFR172.556, Appendices B&C. _____

V. Shipping Papers/Manifests

49CFR172.200-205

Shipping papers/manifests contain:

172.201

A. Hazardous material must be identified by the entry of an "X" placed before the proper shipping name in a column captioned "HM'. (The "X" may be replaced by "RQ" if appropriate). _____

NOTES

49CFR172.202

B. A description of the hazardous material, printed legibly in English, with no codes or abbreviations. For HRCQ shipments, the words "Highway Route Controlled Quantity" must be entered in association with the basic description. _____

The description of hazardous material must include:

172.203

1. The name, address and telephone number of the shipper. _____
2. The proper shipping name (Radioactive Material, Fissile, n.o.s.). _____
3. The hazardous material classification ((7) for RAM) _____
4. The UN number (2918 for Radioactive Material Fissile, n.o.s.). _____
5. If the quantity of radioactive material is a reportable quantity, the letters RQ must be entered before or after the basic description, e.g. RQ, Radioactive Material Fissile, n.o.s. _____
6. The total quantity (by net or gross mass, capacity or as otherwise appropriate. _____
7. The name of each radionuclide (in this case "MFP" for Mixed Fission Products) and activity of each radionuclide contained in the package. _____
8. The total activity per package (in appropriate Curie units). _____
9. A description of the physical and chemical form. _____
10. The category of label (e.g. Yellow III). _____
11. The transportation index. _____
12. The fissile class of each package as determined by 173.455. _____

Note: For Fissile Class III, the shipping papers contain the additional notation: "Warning - Fissile Class III Shipment. Do not load more than _____ package per vehicle. In loading and storage areas, keep at least 20 feet (6 meters) from other packages bearing radioactive labels".

172.203
172.471

13. The type of packaging or notation of the package identification markings as prescribed in the applicable DOE or USNRC approval.

172.201
172.600

14. Emergency Response telephone number provided. _____

NOTES

49CFR172.204

15. Certification by the shipper that the transported materials are properly classified, described, packaged, marked, and labeled and are in proper condition for transportation according to the applicable regulation of the DOT and the NRC. _____

16. Signature of shipper. _____

49CFR172 Subpart G
172.600-604

17. Emergency response information provided to carrier _____

18. A copy of the shipping papers/manifest is delivered to the waste collector who provides a signed acknowledgement.

10CFR71.47
49CFR173.441

VI. Radiation Level Limits

A. General Requirements

The radiation level limit is 2 mrem/hr in any normally occupied position in the transport vehicle, unless the motor carrier personnel are operating under a radiation protection program and wear monitoring devices. If the latter is the case, dosimeter possession will be verified and noted on this form under "comments" _____

49CFR177.842

B. For a shipment containing more than one package, the sum of the T.I.'s does not exceed 50. (This does not apply to exclusive use shipments described in 173.441(b), 173.457, 173.425.) _____

49CFR173.441
10CFR71.47

C. Non-Exclusive Use Vehicle

The radiation level does not exceed 200 mrem/hr at any point on the external surface of the package, and the transport index does not exceed 10.

D. Exclusive Use Vehicles

If radiation level limits specified in C. above are exceeded then the package shall be transported by exclusive use shipment only and radiation levels for such shipments must not exceed the following during transportation:

173.441

1. 200 mrem/hr on the package surface for open transport vehicles. _____

2. 1000 mrem/hr on the package surface for a closed transport vehicle and following conditions met: _____

   a. package secured within vehicle so that package position remains fixed during transportation and no loading or unloading operations between beginning and end of the transportation. _____

NOTES

49CFR173.441
10CFR71.47

3. Dose rates are less than or equal to 200 mrem/hr at any point on the outer vehicle surface, or in the case of an open transport vehicle, at any point on the vertical planes projected from the outer edges of the transport vehicle, on the upper surface of the load, and on the lower external surface of the transport vehicle. This includes the top and underside of the transport vehicle or load. _____

4. Dose rates are 10 mrem/hr or less 2 meters from the above described vertical planes. _____

5. For sole use shipments, the shipper has provided written instructions for maintenance of the exclusive use shipment controls tot he carrier. The instructions are included with the shipping paper information. These instructions will not cause unnecessary delays or radiation exposures. _____

6. The carrier is instructed that no loading or unloading operations between the beginning and the end of the transport will be made. _____

49CFR173.443

VII. Contamination Control

A. The level of non-fixed contamination on external surfaces of each package is kept ALARA. The level of nonfixed radioactive contamination may be determined by wiping an area of 300 square centimeters of the surface concerned with an absorbent material, using moderate pressure and measuring the activity on the wiping material. Sufficient measurements shall be taken in the most appropriate location to yield a representative assessment of the non-fixed contamination levels.

10CFR71.89

10CFR71.97

The amount of activity measured on any single wiping material at any time during transport does not exceed the following limits: _____

1. For beta-gamma emitting radionuclides: 22 dpm/cm^2
2. All alpha-emitting radionuclides: 2.2 dpm/cm^2

B. Exclusive Use Vehicle

1. If the transport vehicle is for exclusive use only, the removable (non-fixed) radioactive contamination on any package at any time during transportation shall not exceed ten times the preceding limit. The levels at the beginning of transport shall not exceed paragraph A. of this section. Survey results are retained in file. _____

NOTES

2. A transport vehicle used for the transportation of RAM as an exculsive use shipment shall not be returned to service until the radiation dose rate at each accessible surface is 0.5 mrem/hr or less and there is no significant removable (non-fixed) radioactive surface contamination as specified in paragraph A _____

49CFR177.825

VIII. For shipment of HRCQ, copy of written route plan provided by carrier to driver and shipper before departure as per 177.825. _____

49CFR173.475
10CFR71.87

IX. Package and its contents satisfies applicable regulations of 10CFR71.87 and 49CFR173.475

A. Each closure device of the packing, including any required gasket, is properly installed and secured and free of defects _____

B. Any system for containing liquid is adequately sealed and has adequate space or other specific provision for expansion of the liquid. _____

49CFR173.448
177.842

X. The package or shipment is secured in order to prevent prevent shifting during normal transportation conditions. _____

10CFR71.89

XI. Advanced Notification: The licensee has ensured that any special package opening instructions have been sent to the consignee. _____

10CFR71.97

XII. Advanced Notification . See Appendix 2 check list. _____

49CFR173.22

XIII. Prior to shipment of fissile material or HRCQ packages of RAM, shipper shall notify consignee of dates of shipment and expected arrival, special loading , unloading instructions and provide for any shipments of irradiated reactor fuel, physical protection in compliance with a plan established under requirements prescribed by USNRC. _____

49CFR173.451

XIV. Except as provided in173.453, each package containing fissile radioactive material complies with 49CFR173.451 through 173.459. _____

XV. Loading and unloading of RAM into or from a motor vehicle shall comply with requirements of 177.842 _____

XVI. Copy of this completed checklist given to Reactor Supervisor or Reactor Director. _____

XVII. Present to Radiation Safety Officer (or designee) for approval. _____

XVIII. Comments

Appendix to §172.101 - List of Hazardous Substances and Reportable Quantities

1. This appendix lists materials and their corresponding reportable quantities (RQs) which are listed or designated as "hazardous substances" under section 101(14) of the Comprehensive Environmental Response, Compensation, and Liability Act (CERCLA; Pub. L. 96-510). This appendix is divided into 2 tables which are entitled "Table 1—Hazardous Substances Other Than Radionuclides" and "Table 2—Radionuclides". A material in this appendix is regulated as a hazardous material and a hazardous substance under this subchapter if it meets the definition of a hazardous substance in §171.8 of this subchapter.

2. The procedure for selecting a proper shipping name for a hazardous substance is set forth in §172.101(c)(9).

3. Column 1 of Table 1, entitled *"Hazardous substance"*, contains the names of those elements and compounds which are hazardous substances. Following the listing of elements and compounds is a listing of waste streams. These waste streams appear on the list in numerical sequence and are referenced by the appropriate "F" or "K" numbers. Column 2 of Table 1, entitled *"Synonyms"*, contains the names of synonyms for certain elements and compounds listed in Column 1. No synonyms are listed for waste streams. Synonyms are useful in identifying hazardous substances and in identifying proper shipping names. Column 3 of Table 1, entitled *"Reportable quantity (RQ)"*, contains the reportable quantity (RQ), in pounds and kilograms, for each hazardous substance listed in Column 1 of Table 1.

4. A series of notes are used throughout Table 1 and Table 2 to provide additional information concerning certain hazardous substances. These notes are explained at the end of each Table.

5. Table 2 lists radionuclides which are hazardous substances and their corresponding RQs. The RQs in Table 2 for radionuclides are expressed in units of curies and terabecquerels, whereas those in Table 1 are expressed in units of pounds. If a material is listed in both Table 1 and Table 2, the lowest RQ shall apply. Radionuclides are listed in alphabetical order. The RQs for radionuclides are given in the radiological unit of measure of curie, abbreviated "Ci", followed, in parentheses, by an equivalent unit measured in terabecquerels, abbreviated "TBq".

6. For mixtures of radionuclides, the following determinations shall be used in determining if a package contains an RQ of a hazardous substance: (i) If the identity and quantity (in curies or terabecquerels) of each radionuclide in a mixture or solution is known, the ratio between the quantity per package (in curies or terabecquerels) and the RQ for the radionuclide must be determined for each radionuclide. A package contains an RQ of a hazardous substance when the sum of the ratios for the radionuclides in the mixture or solution is equal to or greater than one; (ii) if the identity of each radionuclide in a mixture or solution is known but the quantity per package (in curies or terabecquerels) of one or more of the radionuclides is unknown, an RQ of a hazardous substance is present in a package when the total quantity (in curies or terabecquerels) of the mixture or solution is equal to or greater than the lowest RQ of any individual radionuclide in the mixture or solution; and (iii) if the identity of one or more radionuclides in a mixture or solution is unknown (or if the identity of a radionuclide by itself is unknown), an RQ of a hazardous substance is present when the total quantity (in curies or terabecquerels) in a package is equal to or greater than either one curie or the lowest RQ of any known individual radionuclide in the mixture or solution, whichever is lower.

Table 1—Hazardous Substances Other Than Radionuclides

Hazardous Substances	Synonyms	Reportable Quantity (RQ) Pounds (Kilograms)
Acenaphthene		100 (45.4)
Acenaphthylene		5000 (2270)
Acetaldehyde*	Ethanal	1000 (454)
Acetaldehyde, chloro-	Chlorooacetaldehyde	1000 (454)
Acetaldehyde, trichloro-	Chloral	5000 (2270)
Acetamide, N-(aminothioxomethyl)-	1-Acetyl-2-thiourea	1000 (454)
Acetamide, N-(4-ethoxyphenyl)-	Phenacetin	100 (45.4)
Acetamide, N-fluoren-2-yl-	2-Acetylaminofluorene	1 (0.454)
Acetamide, 2-fluoro-	Fluoroacetamide	100 (45.4)
Acetic acid*		5000 (2270)
Acetic acid (2,4-dichlorophenoxy)-	2,4-D, salts and esters	100 (45.4)
	2,4-D acid	
Acetic acid, ethyl ester	Ethyl acetate*	5000 (2270)
Acetic acid, fluoro-, sodium salt	Fluoroacetic acid, sodium salt	10 (4.54)
Acetic acid, lead (2+)salt	Lead acetate	5000 (2270)
Acetic acid, thallium(i+) salt	Thallium(I) acetate	100 (45.4)
Acetic acid, (2,4,5-trichlorophenoxy)	2,4,5-T*	1000 (454)
	2,4,5-T acid	
Acetic anhydride*		5000 (2270)
Acetone*	2-Propanone	5000 (2270)
Acetone cyanohydrin*	Propanenitrile, 2-hydroxy-2-methyl-	10 (4.54)
	2-Methyllactonitrile	
Acetonitrile*	Ethanenitrile	5000 (2270)
Acetophenone	Ethanone, 1-phenyl-	5000 (2270)
2-Acetylaminofluorene	Acetamide, N-fluoren-2-yl-	1 (0.454)
Acetyl bromide*		5000 (2270)
Acetyl chloride*	Ethanoyl chloride	5000 (2270)

Table 2—Radionuclides, Continued

(1)—Radionuclides	(2)—Atomic number	(3)—Reportable quantity (RQ) Ci (TBq)
Uranium-232	92	0.01 (.00037)
Uranium-233	92	0.1 (.0037)
Uranium-234**	92	0.1 (.0037)
Uranium-235**	92	0.1 (.0037)
Uranium-236	92	0.1 (.0037)
Uranium-237	92	100 (3.7)
Uranium-238**	92	0.1 (.0037)
Uranium-239	92	1000 (37)
Uranium-240	92	1000 (37)
Vanadium-47	23	1000 (37)
Vanadium-48	23	10 (.37)
Vanadium-49	23	1000 (37)
Xenon-120	54	100 (3.7)
Xenon-121	54	10 (.37)
Xenon-122	54	100 (3.7)
Xenon-123	54	10 (.37)
Xenon-125	54	100 (3.7)
Xenon-127	54	100 (3.7)
Xenon-129m	54	1000 (37)
Xenon-131m	54	1000 (37)
Xenon-133	54	1000 (37)
Xenon-133m	54	1000 (37)
Xenon-135	54	100 (3.7)
Xenon-135m	54	10 (.37)
Xenon-138	54	10 (.37)
Ytterbium-162	70	1000 (37)
Ytterbium-166	70	10 (.37)
Ytterbium-167	70	1000 (37)
Ytterbium-169	70	10 (.37)
Ytterbium-175	70	100 (3.7)
Ytterbium-177	70	1000 (37)
Ytterbium-178	70	1000 (37)
Yttrium-86	39	10 (.37)
Yttrium-86m	39	1000 (37)
Yttrium-87	39	10 (.37)
Yttrium-88	39	10 (.37)
Yttrium-90	39	10 (.37)
Yttrium-90m	39	100 (3.7)
Yttrium-91	39	10 (.37)
Yttrium-91m	39	1000 (37)
Yttrium-92	39	100 (3.7)
Yttrium-93	39	100 (3.7)
Yttrium-94	39	1000 (37)
Yttrium-95	39	1000 (37)
Zinc-62	30	100 (3.7)
Zinc-63	30	1000 (37)
Zinc-65	30	10 (.37)
Zinc-69	30	1000 (37)
Zinc-69m	30	100 (3.7)
Zinc-71m	30	100 (3.7)
Zinc-72	30	100 (3.7)
Zirconium-86	40	100 (3.7)
Zirconium-88	40	10 (.37)
Zirconium-89	40	100 (3.7)
Zirconium-93	40	1 (.037)
Zirconium-95	40	10 (.37)
Zirconium-97	40	10 (.37)

§ The RQs for all radionuclides apply to chemical compounds containing the radionuclides and elemental forms regardless of the diameter of pieces of solid material.

† The RQ of one curie applies to all radionuclides not otherwise listed. Whenever the RQs in TABLE 1—HAZARDOUS SUBSTANCES OTHER THAN RADIONUCLIDES and this table conflict, the lowest RQ shall apply. For example, uranyl acetate and uranyl nitrate have RQs shown in TABLE 1 of 100 pounds, equivalent to about one-tenth the RQ level for uranium-238 in this table.

** The method to determine the RQs for mixtures or solutions of radionuclides can be found in paragraph 6 of the note preceding TABLE 1 of this Appendix. RQs for the following four common radionuclide mixtures are provided: radium-226 in secular equilibrium with its daughters (0.053 curie); natural uranium (0.1 curie); natural uranium in secular equilibrium with its daughters (0.052 curie); and natural thorium in secular equilibrium with its daughters (0.011 curie).

*** Indicates that the name was added by RSPA because it appears in the list of radionuclides in 49 CFR 173.435. The reportable quantity (RQ), if not specifically listed elsewhere in this Appendix, shall be determined in accordance with the procedures in Paragraph 6 of this Appendix.

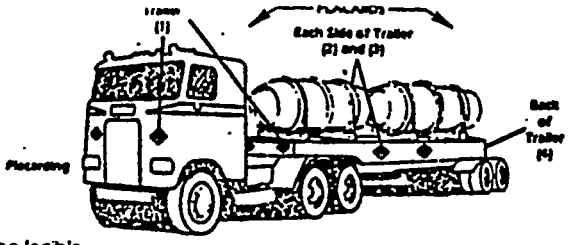
Symbol of radionuclide	Element and atomic number	A_1(Ci) (Special form)	A_2(Ci) (normal form)
^{153}Gd	Gadolinium (64)	200	100
^{159}Gd		300	20
^{68}Ge	Germanium (32)	20	10
^{71}Ge		1000	1000
^{3}H	Hydrogen (1) See T-Tritium		
^{181}Hf	Hafnium (72)	30	25
^{197m}Hg	Mercury (80)	200	200
^{197}Hg		200	200
^{203}Hg		60	25
^{166}Ho	Holmium (67)	30	30
^{123}I	Iodine (53)	50	50
^{125}I		1000	70
^{126}I		40	10
^{129}I		1000	2
^{131}I		40	10
^{132}I		7	7
^{133}I		30	10
^{134}I		8	8
^{135}I		10	10
^{111}In	Indium (49)	30	25
^{113m}In		60	60
^{114m}In		30	20
^{115m}In		100	20
^{190}Ir	Iridium (77)	10	10
^{192}Ir		20	10
^{194}Ir		10	10
^{42}K	Potassium (19)	10	10
^{43}K		20	10
^{85m}Kr (uncompressed)	Krypton (36)	100	100
^{85m}Kr (compressed)		3	3
^{85}Kr (uncompressed)		1000	1000
^{85}Kr (compressed)		5	5
^{87}Kr (uncompressed)		20	20
^{87}Kr (compressed)		0.6	0.6
^{140}La	Lanthanum (57)	30	30
LSA	Low specific activity material-see §173.403		
^{177}Lu	Lutetium (71)	300	25
MFP	Mixed fission products	10	0.4
^{28}Mg	Magnesium (12)	6	6
^{52}Mn	Manganese (25)	5	5
^{54}Mn		20	20
^{56}Mn		5	5
^{99}Mo	Molybdenum (42)	100	20
^{13}N	Nitrogen (7)	20	10
^{22}Na	Sodium (11)	8	8
^{24}Na		5	5
^{93m}Nb	Niobium (41)	1000	200
^{95}Nb		20	20
^{97}Nb		20	20
^{147}Nd	Neodymium (60)	100	20
^{149}Nd		30	20
^{59}Ni	Nickel (28)	1000	900
^{63}Ni		1000	100
^{65}Ni		10	10
^{237}Np	Neptunium (93)	5	0.005
^{239}Np		200	25
^{185}Os	Osmium (76)	20	20
^{191}Os		600	200
^{191m}Os		200	200
^{193}Os		100	20
^{32}P	Phosphorus (15)	30	30
^{230}Pa	Protactinium (91)	20	0.8
^{231}Pa		2	0.002
^{233}Pa		100	100
^{201}Pb	Lead (82)	20	20
^{210}Pb		100	0.2

Symbol of radionculide	Element and atomic number	A_1(Ci) (Special form)	A_2(Ci) (normal form)
^{96}Tc		6	6
^{97m}Tc		1000	200
^{97}Tc		1000	400
^{99m}Tc		100	100
^{99}Tc		1000	25
^{125m}Te	Tellurium (52)	1000	
^{127m}Te		300	20
^{127}Te		300	20
^{129m}Te		30	10
^{129}Te		100	20
^{131m}Te		10	10
^{132}Te		7	7
^{227}Th	Thorium (90)	200	0.2
^{228}Th		6	0.008
^{230}Th		3	0.003
^{231}Th		1000	25
^{232}Th		Unlimited	Unlimited
^{234}Th		10	10
Th (natural)		Unlimited	Unlimited
Th (irradiated)[2]			
^{200}Tl	Thallium (81)	20	20
^{201}Tl		200	200
^{202}Tl		40	40
^{204}Tl		300	10
^{170}Tm	Thulium (69)	300	10
^{171}Tm		1000	100
^{230}U	Uranium (92)	100	0.1
^{232}U		30	0.03
^{233}U		100	0.1
^{234}U		100	0.1
^{235}U		100	0.2
^{236}U		200	0.2
^{238}U		Unlimited	Unlimited
U (natural)		Unlimited	Unlimited
U (enriched) <20%		Unlimited	Unlimited
20% or greater		100	0.1
U (depleted)		Unlimited	Unlimited
U (irradiated)[3]			
^{48}V	Vanadium (23)	6	6
^{181}W	Tungsten (74)	200	100
^{185}W		1000	25
^{187}W		40	20
^{127}Xe (uncompressed)	Xenon (54)	70	70
^{127}Xe (compressed)		5	5
^{131m}Xe (compressed)		10	10
^{131m}Xe (uncompressed		100	100
^{133}Xe (uncompressed)		1000	1000
^{133}Xe (compressed)		5	5
^{135}Xe (uncompressed)		70	70
^{135}Xe (compressed)		2	2
^{87}Y	Yttrium (39)	20	20
^{90}Y		10	10
^{91m}Y		30	30
^{91}Y		30	30
^{92}Y		10	10
^{93}Y		10	10
^{169}Yb	Ytteblum (70)	80	80
^{175}Yb		400	25
^{65}Zn	Zinc (30)	30	30
^{69m}Zn		40	20
^{69}Zn		300	20
^{93}Zr	Zirconium (40)	1000	200
^{95}Zr		20	20
^{97}Zr		20	20

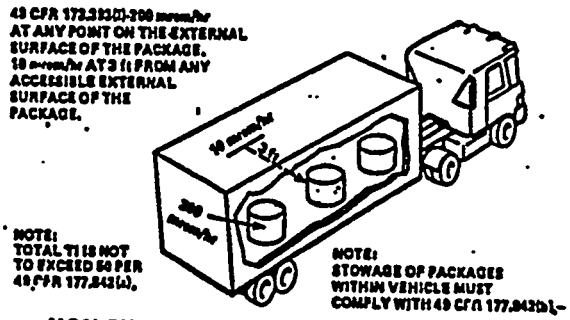
[1]For shipments solely within the United States the A_1 value is 20 curies for americium and plutonium contained in Am-Be or Pu-Be neutron sources or in nuclear-powered pacemakers.

[2]The values of A_1 and A_2 must be calculated in accordance with the procedure specified in §173.433 of this subchapter, taking into account the activity of the fission products and of the uranium-233 in addition to that of the thorium.

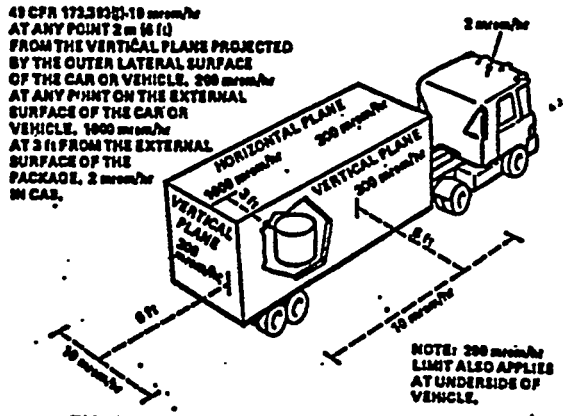
[3]The values of A_1 and A_2 must be calculated in accordance with the procedure specified in §173.433 of this subchapter, taking into account the activity of the fission products and plutonium isotopes in addition to that of the uranium.



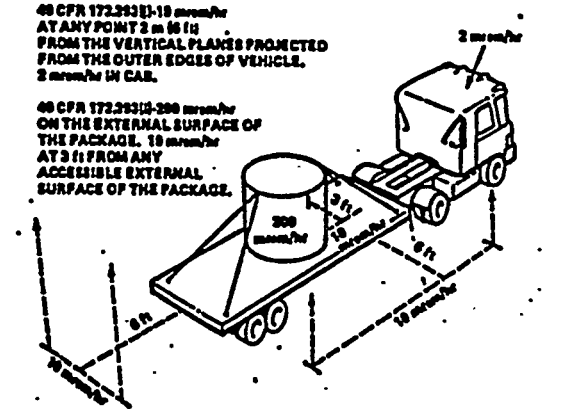
- Placards must be legible.
- Placards must be visible from the direction they face.
- Placards must be located in a position that is clear of obstructions.
- Placards must be placed at least 3 inches away from any marking or advertising that could reduce their effectiveness.
- Placards must be secured so that the words or identification numbers appear horizontally and read from left to right.



NON-EXCLUSIVE-USE OPEN OR CLOSED TRANSPORT



EXCLUSIVE-USE CLOSED TRANSPORT



EXCLUSIVE-USE OPEN TRANSPORT

APPENDIX G

Distribution List

All personnel shall acknowledge below, by initialling, that they have read and understood these procedures, including their general assignments. If on-the-spot changes are made to these procedures, all personnel shall indicate receipt of such changes (notes identifying such changes to be added as need be below) by initialling again.

Name	Initials	Initials	Initials	Initials
Robert U. Mulder				
J.P. Farrar				
Thomas E. Doyle				
Paul Benneche				
B. Hosticka				
Don Krause				
Lisa Scheid				
J.S. Baber				
Neil Wilson				
Rick Piccolo				
Jim Gilchrist				
Deborah P. Steva				
Scott Garver				

APPENDIX H

Notification Addresses, Phone and FAX Numbers

Savannah River Approval

Matt Beckum work phone: 803-557-8773
Westinghouse Savannah River Company
Bldg. 244-H
Savannah River Site
Aiken, SC 29808

Mr. Nazir Khalil
Nuclear Materials Management and Staff Support Office
Building 703-A, Room E-144

phone: (803) 725-5535

Sachiko McAlhany
Dept. of Energy at Savannah River
P.O. Box A
Aiken, S.C. 29802

Phone: (803) 725-5572

NRC Route Approval

U.S. Nuclear Regulatory Commission
Attn: Ms. Gloria Bennington
NMSS: SGTB
Mail Stop WF-4E4
Washington, D.C. 20555

phone: (301) 504-2381, (301) 504-2461

Safeguards and Transportation contact: John R. Cook (ph.: 301-504-2458)

State of Virginia

Michael M. Cline, Director of Operations
Department of Emergency Services
Commonwealth of Virginia
310 Turner Road
Richmond, VA 23225

phone: (804) 674-2400

State of North Carolina

Major Walter K. Chapman, Director, Administrative Services
North Carolina Highway Patrol Headquarters
P.O. Box 27687
Raleigh, NC 27611

phone:
(919) 733-7952
after hours (919) 733-3861, or 1-800-662-7956 (in state)

FAX: 919-733-6593

State of South Carolina

Heyward G. Shealy, Chief, Bureau of Radiological Health
Virgil Autry, Director
South Carolina Dept. of Health and Environmental Control
2600 Bull Street
Columbia, SC 29201

phone:
(803) 734-4632
after hours: (803) 253-6497

George Snyder, Emergency Preparedness Division

phone: (803) 734-8020

Fuel Transport Carrier

Tri-State Motor Transit Co.
P.O. Box 113
Joplin, MO 64802
Attn: Mr. Don Ritchie

phone: 1-800-846-8768

Roanoke Escort

Charles W. (Bill) Mayo
36 Frances Drive N.W.
Roanoke, VA 24017

phone:
703-375-3095 (office)
703-342-4972 (home)

Charlotte, N.C. Escort

Commander J.I. Pendergraph
% Mecklenburg County Police Department
618 North College Street
Charlotte, NC 28202

phone:
Work: (704) 336-2846 (24 hours)
Home: (704) 588-4585

Columbia, S.C. Escort

Lt. Durwood Barton
Richland County Sheriff's Office
1400 Huger Street
Columbia, SC 29201

phone:
Work: (803) 343-3950
After hours: (803) 3433956
Home: (803)892-2037

D.O.E. Contact to Arrange BMI-1 Cask

Dr. William Wilkes
U.S.D.O.E.
Isotope Production & Distribution Office
Forrestall Building
Washington, D.C. 20585

Phone: (301) 903-5161

Mr. Keith Brown
U.S.D.O.E.
ST-511
Forrestall Building, Room 3F-043
Washington, D.C. 20585

phone: (202) 586-3904 or (202) 585-8949?
FAX: (202) 586-0019

DISTRIBUTION LIST

1 - 2	Ms. Barbara J. Jackson Environmental Acquisitions Branch, AD-423 U. S. Department of Energy P.O. Box 2001 Oak Ridge, TN 37831-8758
3 - 4	R. U. Mulder
5	R. D. Flack
*	Postaward Research Administration
6 - 7	H. Earnhardt, Clark Hall
8	SEAS Preaward Administration Files

* Cover Letter Only

JO#5999:pa